

# Birla Central Library

PILANI (Rajasthan)

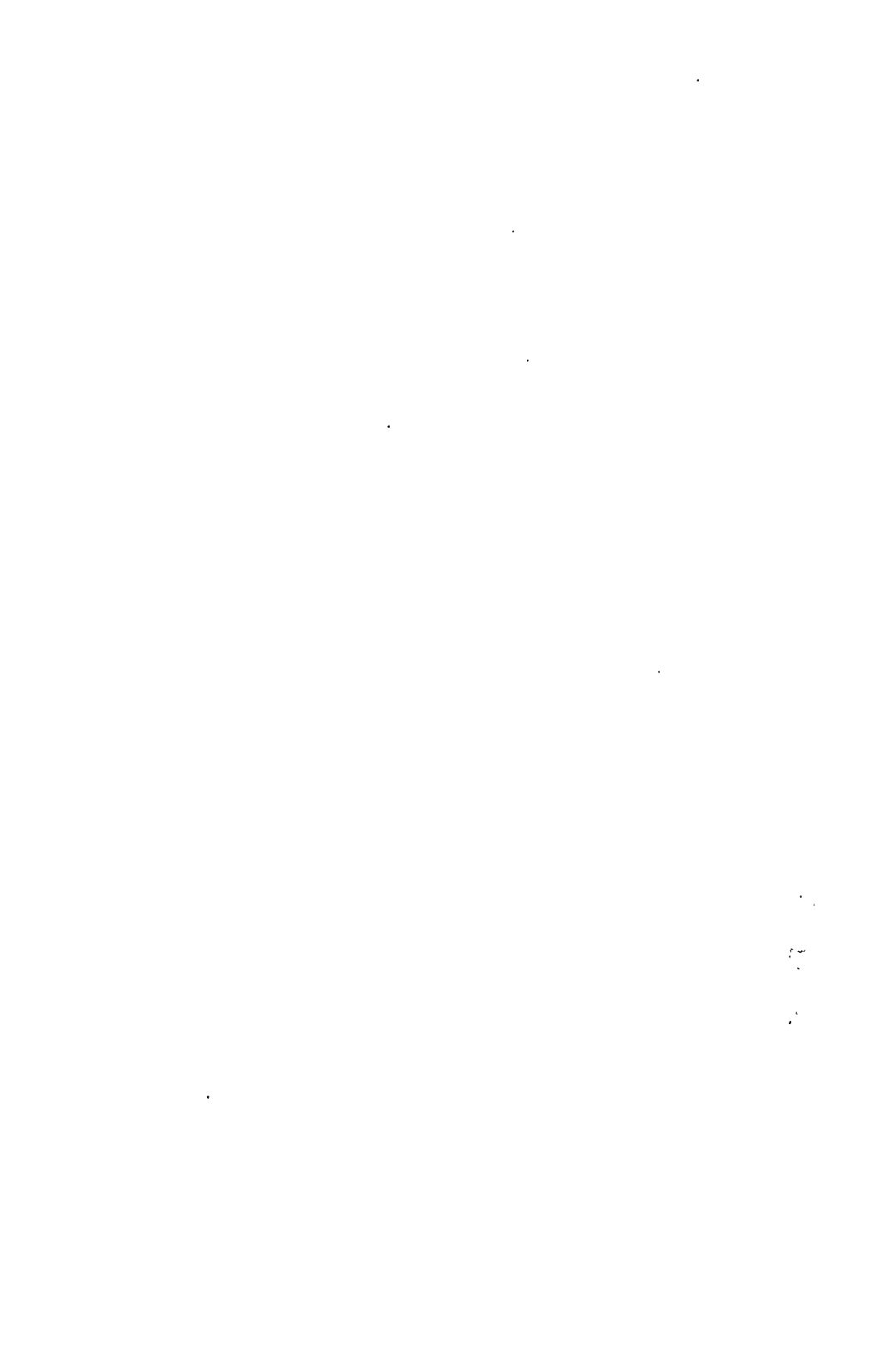
Class No :- 621.3841531

Book No :- R292V-V2

Accession No :- 38225







**VERY HIGH-FREQUENCY TECHNIQUES**

**VOLUME II**



# VERY HIGH-FREQUENCY TECHNIQUES

COMPILED BY THE STAFF OF THE  
RADIO RESEARCH LABORATORY  
HARVARD UNIVERSITY

*Office of Scientific Research and Development  
National Defense Research Committee  
Division of Radio Coordination*

UNDER THE EDITORIAL DIRECTION OF  
*Herbert J. Reich, Editor  
Louise S. McDowell, Asst. Editor  
Andrew Alford, Robert R. Buss, John F. Byrne  
Arthur Dorne, William G. Dow, John D. Kraus  
Joseph M. Pettit, Edwin A. Yunker*

Volume II

FIRST EDITION  
THIRD IMPRESSION

---

*McGraw-Hill Book Company, Inc.*  
NEW YORK AND LONDON · 1947

VERY HIGH-FREQUENCY TECHNIQUES ,

COPYRIGHT, 1947, BY THE

McGraw-Hill Book Company, Inc.

PRINTED IN THE UNITED STATES OF AMERICA

*All rights reserved. This book, or  
parts thereof, may not be reproduced  
in any form without permission of  
the publishers.*

# CONTENTS

## Volume II

	PAGE
PREFACE . . . . .	v
FOREWORD . . . . .	vii
Chapter 23. EXTERNALLY TUNED MAGNETRON OSCILLATORS . . . . .	555
<i>by Herbert J. Reich</i>	
Externally Tuned Magnetron Oscillator Circuits—Types of Tube—Performance—Tube Life—Modulation—Load Coupling—Mode Jumping—Frequency Pulling—Frequency Pushing—Pulsing—Modulation by Filament Field.	
Chapter 24. POWER-MEASURING DEVICES FOR ULTRAHIGH FREQUENCIES. . . . .	569
<i>by Edwin A. Yunker, Harold C. Early, Gunnar Hok, and Glendon R. Bridgeford</i>	
Introduction—Dummy Loads—Determination of Power from Current or Voltage and Resistance—Thermocouple in Coaxial Line—Disk Resistor with Voltmeter—Photometric Systems—Gas-filled Load Lamps—Calorimeter Wattmeters—Oil-immersed Dummy Load—Air Calorimeters—Lossy-coaxial-cable Calorimeter Wattmeter—Coaxial Line with Resistive Center Conductor—Coaxial Line with Water Dielectric—Salt-water Loads—Calorimeter Load for Waveguide—Quick-response Calorimeter for Large Waveguide—Sloping-guide Water-load Calorimeter—Slotted Coaxial Lines—Notched Coaxial Lines—The Thermistor—The Bolometer Bridge—Directional Couplers—Capacitive-loop Directional Coupler—Two-hole Directional Coupler—Bethe Hole Directional Coupler—A Broad-band Monitoring-type Wattmeter for Waveguides—Output Indicators—Spectrum Analyzers—Cold Analysis of Resonant Systems—Constants and Parameters of Resonant Systems—Equivalent Circuits—Measurements—Methods for Calculation of the Parameters—Analytical Foundations of Methods I to V.	
Chapter 25. RECEIVERS—GENERAL CONSIDERATIONS . . . . .	627
<i>by Joseph M. Pettit</i>	
Design Objectives—Direct-detection Receivers—Superheterodyne Receivers—Definition and Measurements of Receiver Performance—Receiver Sensitivity—Noise Figure—Minimum Gain Requirement: Standard Noise Output—Signal Amplification: Standard Output—Combined Sensitivity Figure—Voltage Sensitivity vs. Power Sensitivity—Receiver Selectivity—Receiver Fidelity—Receiver Power Output Capability.	

	PAGE
Chapter 26. PRINCIPLES OF TRANSMISSION-LINE FILTER DESIGN . . . . .	648
<i>by Seymour Cohn</i>	
Fundamental Filter Relations—Calculation of the Image Impedance and Transfer Constant from the Short- and Open-circuit Impedances—Symmetrical-section Parameters in Terms of the Half-section Parameters—The Equivalent-circuit Method of Filter Analysis—Exact Equivalent-circuit Method of Filter Analysis—The Fundamental Analysis Method—Filter Insertion Loss—Filter Pass-band Response—Methods of Reducing Pass-band Insertion Loss—Transforming End Sections—Filter Stop-band Response—Pass-band Loss of a Filter with Improper Termination—Maximum Possible Insertion Loss of a Mismatched Filter—Line-loss Correction for Standing-wave Ratio—Waveguide as a Circuit Element in Filters—Properties of Ridge Waveguide—Higher Mode Cutoff Frequencies in Ridge Waveguide—Attenuation in Ridge Waveguide—Experimental Verification of the Ridge-waveguide Design Curves—Applications for Ridge Waveguide.	
Chapter 27. DESIGN OF TRANSMISSION-LINE FILTERS . . . . .	685
<i>by Seymour Cohn</i>	
The Complete Filter—Short-line Filter Types—Short-line Low-pass Filter—Exact Design of the Varying-impedance Low-pass Filter—Design of a Typical Low-pass Filter—Short-line High-pass Filter— <i>M</i> -derived Terminating Half Sections for Low- and High-pass Filters—Short-line Band-pass Filters—Resonant-line Filter Types—Type 3-1, Band-pass and High-pass Filter—Type 3-2, Band-pass and High-pass Filter—Type 3-3, High-pass Filter—Type 3-4, Band-pass and High-pass Filter—Type 3-5, Low-pass Filter—Type 3-6, <i>M</i> -derived Band-pass Filter—The Filters of Tables 27-4 and 27-5—Mechanical Construction—Dielectric Materials—Effect of Physical Discontinuities—Specific Design—The Design of Simple Broadband Waveguide-to-coaxial-line Junctions for Use with Waveguide Filters and Transmission Systems—The Basic Junction—The Transforming Junction—A Junction for Ridge Waveguide—Tapered-ridge Junction—Method of Testing the Waveguide-to-coaxial-line Junctions—Waveguide High-pass Filters—The Varying-impedance Band-pass Waveguide Filter—Test Methods for High-frequency Filters.	
Chapter 28. TUNERS FOR MICROWAVE RECEIVERS. . . . .	741
<i>by Seymour Cohn, Robert A. Soderman, Samuel J. Griffin, and Raymond O. Petrich</i>	
General Requirements for Receiver Tuners—The General Theory of Narrow-band Coupled-circuit Tuners—Losses in Radio-frequency Tuners—The Single-circuit Tuner—Two Coupled Circuits—Three Coupled Circuits—Butterfly Resonators: General Description—Butterfly Design—Butterflies as Tuners—Selectivity and Pass-band Loss—Coupling Methods—Spurious Responses—Examples of Butterfly Tuner Design—Double Butterfly—Mechanical Design—The Coaxial Cavity as a Tuner—Coupling Problems in a Coaxial Cavity—Coupling-loop Construction—Short-circuiting Devices—The Metal-to-metal Joint—Low-impedance Joint—The Choke Joint—Spurious Responses in Coaxial Cavities—Coupling between Coaxial Cavities—Design of Single-cavity Coaxial Tuners—Design of Two-cavity Coaxial Tuners—Design of Three-cavity Coaxial Tuners—Rectangular-waveguide Cavity—"Loaded" Waveguide Cavity—Rotary-tuned	

Coaxial Cavity—Rotary-tuned Waveguide Cavity—Movable-slug Coaxial Tuners.

Chapter 29. DETECTORS AND MIXERS . . . . . 796

*by Robert A. Soderman*

Introduction—Types of Mixers and Detectors—Crystal Rectifiers—Crystal-mixer Circuits—Crystal-mixer Characteristics—Radio-frequency Impedance Considerations—Effect of Changes in the Local-oscillator Power Input on Mixer Performance—Local-oscillator Coupling Problems—Termination of Waveguide in Broad-band Untuned Waveguide Mixers—Crystal Characteristics Affecting Conversion Loss at High Frequencies—The Optimum Intermediate Frequency from Noise Considerations—Effect of Bias on Crystal-mixer Performance—Harmonic Mixing—Diode Mixers—Examples of Crystal and Diode Mixers—Low-level Direct Detection at High Frequencies—Diode and Crystal Low-level Detectors—Equivalent Circuit of a Low-level Crystal Detector—Noise in Low-level Crystal Detectors—Direct-detector Receiver Sensitivity—Input Impedance of a Low-level Detector—Examples of Wide-band Direct Detectors—Second Detectors—Crystals as Measuring Devices.

Chapter 30. LOCAL OSCILLATORS. I. GENERAL CONSIDERATIONS AND BUTTERFLY OSCILLATORS . . . . . 824

*by Robert A. Soderman, William H. Huggins, and Frederick J. Kamphoefner*

General Requirements—Survey of Oscillator Types—Butterflies as Resonators for Wide-range Oscillators—Oscillator Circuits—Butterfly Design—Grid-blocking Capacitor and Resistor Considerations—Plate-supply Connections—Sources of Holes—Effect of Cathode-lead Inductance—High-frequency Limitations—Stability—Output-coupling Methods—Butterfly Oscillator Efficiency—Oscillator Tubes—Examples of Butterfly Local Oscillators—Mechanical Tracking of Oscillator with Preselector and Dial.

Chapter 31. LOCAL OSCILLATORS. II. REFLEX-KLYSTRON OSCILLATORS . . . 849

*by William H. Huggins, Raymond O. Petrich, and Joseph W. Kearney*

Introduction—The Electronic Admittance—Power Stability—Frequency Stability—The Resonator Admittance—Electronic Tuning—Oscilloscopic Techniques—Electronic Multiple Transits and Hysteresis—Harmonic-frequency Generation—Effect of Parasitic Resonances—Power-supply Requirements—Repeller-voltage Tracking Systems.

Chapter 32. LOCAL OSCILLATORS. III. WIDE-BAND COAXIAL-LINE RESONATORS. . . . . 878

*by William H. Huggins, Howard M. Zeidler, and Laurence A. Manning*

Introductory Summary—Circular Coaxial Resonators—Summary of Basic Wave Types—Transverse Electromagnetic (*TEM*) Mode—Transverse Electric (*TE*) Modes—Transverse Magnetic (*TM*) Modes—Adaptation of Coaxial Resonators to Typical Reflex Tubes—Conditions for Oscillation—Equivalent Corner Length—Effect of Inductive and Capacitive Corner Terminations—Physical Realizability of  $\lambda$ -D Tuning Characteristic—Effect of Cavity Dimensions—Effect of Plunger Reactance—Repeller-voltage-vs.-cavity-length Tuning Characteristics—*TEM*-mode Interference—Desirable Modes and Ranges—Elimination of *TEM*-mode Interference—



General Analysis of *TEM*-mode Suppressor—Design of the  $k = 1$  Mode-suppressor Section—Parasitic Circumferential Resonances of the Suppressor Section—Parasitic *TE* and *TM* Modes—*TE* Parasitic Resonances—*TM* Parasitic Resonances—Output-coupling Methods—Optimum Position of a Fixed Loop in  $\frac{3}{4}$ -wavelength Resonator—Combination Loop-probe Methods—General Consideration of Noncontacting Plunger Design—Compound-line Section—Basic Noncontacting Plunger Types: Capacitance Plunger—Choke and Bucket Plungers—*S* and *Z* Plungers—Measurement of Plunger Reactance—Internal Power Loss of Plunger—Total Power Loss of Plunger—Permissible Plunger Loss in Reflex Oscillators—Parasitic Resonances in a Noncontacting Plunger.

**Chapter 33. INTERMEDIATE-FREQUENCY AMPLIFIERS. . . . . 940**

*by Matthew T. Lebenbaum*

Introduction—Choice of Intermediate Frequency—Band Width and Selectivity Characteristics—Noise in Intermediate-frequency Amplifiers—Input Admittance of Vacuum Tubes—Gain—General Serviceability and Tube-constant Variations—Interstage Coupling Methods—Single-tuned Coupling—Multituned Coupling Networks—Stagger Tuning—Design of a Stagger-tuned Amplifier—Regeneration—Gain Control—Automatic Gain Control.

**Chapter 34. RECEIVER OUTPUT CIRCUITS. . . . . 977**

*by Robert R. Buss, Jerre D. Noe, C. Bruce Clark, and Horace E. Overacker*

Video Output—Band Width of Video Amplifiers—Control of Gain in Video Amplifiers—Measurement Problems—Video Output-coupling Circuits—Pulse Stretchers—Panoramic Presentation—Spurious Responses—Marker Signals for Frequency Indication—Phase and Amplitude Response of the Video and Deflection Amplifiers—Pulse Stretching and Trace Intensification—Recording Circuits and Equipment—Pulse Analysis—Oscilloscopic Measurement of Pulse Length—Meter Indication of Pulse Length—Oscilloscopic Measurement of Pulse-repetition Frequency—Meter Indication of Pulse-repetition Frequency.

**Chapter 35. MEASURING EQUIPMENT FOR RECEIVERS . . . . . 1008**

*by W. Bruce Wholey*

Test Equipment—Signal Sources—Components of Signal Sources—Radio-frequency Oscillators—Modulators—Pulse Modulation of Radio-frequency Oscillators: Lighthouse Tubes, Reflex Klystrons—Output Systems—Piston Attenuators—Attenuation Pads—Output Calibration—Power Measurement—Shielding—Auxiliary Output Systems—Ultrahigh-frequency Sweep Oscillator—Heterodyne Frequency Meters.

**Bibliography. SUPPLEMENTARY BIBLIOGRAPHY OF RECENT ARTICLES IN THE FIELD . . . . . 1033**

**INDEX . . . . . 1037**

## CHAPTER 23

### EXTERNALLY TUNED MAGNETRON OSCILLATORS

By H. J. REICH

In the types of magnetron oscillators that have been discussed in Chaps. 20, 21, and 22, the tank circuit forms an integral part of the tube. Tuning over wide frequency ranges is therefore inherently difficult. Wide tuning range may be achieved by the use of an external tank circuit in conjunction with a split-anode magnetron tube. Oscillators of this type will be discussed in the present chapter.

**23-1. Externally Tuned Magnetron Oscillator Circuits.**—In its simplest form the split-anode magnetron consists of a straight-wire

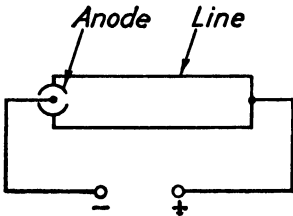


FIG. 23-1.—Basic circuit of parallel-line magnetron oscillator.

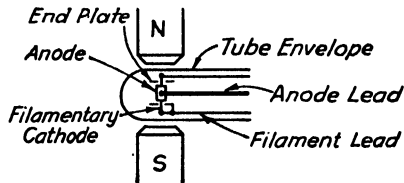


FIG. 23-2.—Method of mounting split-anode magnetron in magnetic field.

cathode surrounded by a coaxial cylindrical electrode, which is split longitudinally to form two semicylindrical anodes. The tank circuit, which is usually a parallel-line resonator one or more quarter wavelengths long, is connected to the anodes, as shown in Fig. 23-1. The tube is mounted between the pole pieces of a magnet, in such a manner that the anode-cathode region is in a magnetic field that is parallel to the axis and of essentially uniform density, as illustrated in Fig. 23-2. Direct voltage is applied between the cathode and the anodes.

Electronically, the behavior of the split-anode magnetrons discussed in this chapter appears to be in most respects similar to that of multicavity magnetrons (see Sec. 20-5). Except at frequencies considerably lower than those at which the tubes are normally operated, it does not seem to depend upon static negative resistance,<sup>1</sup> nor is it apparently

<sup>1</sup> BRAINERD *et al.*, "Ultra-high-frequency Techniques," Sec. 10-11, D. Van Nostrand Company, Inc., New York, 1942.

related to the radial transit time of electrons in the cathode-anode space.<sup>1</sup>

The tank circuit of an externally tuned magnetron oscillator may consist of either a lumped-constant parallel  $LC$  circuit shunted between the anodes, or a parallel-line resonator. In practice, however, the lumped-constant oscillator usually tends to oscillate at a frequency much higher than that of the  $LC$  circuit. The reason for this phenomenon is that lumped capacitance serves as an effective short circuit at frequencies

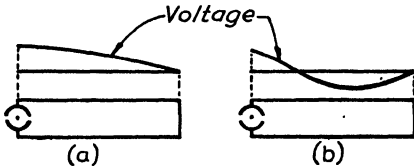


FIG. 23-3.—Voltage distribution in parallel-line oscillator in the  $\lambda/4$  and  $3\lambda/4$  modes of oscillation.

considerably higher than the resonant frequency of the lumped-constant tank. In conjunction with the anode leads, therefore, it provides a quarter-wave parallel-line resonator that may act as an alternative tank circuit. Which type of oscillation takes place depends upon the relative values of loaded  $Q$  of the two tank circuits. The remainder of this chapter will be devoted to parallel-line oscillators.

Oscillations in parallel-line oscillators may take place at any resonant frequency of the resonator, provided that the electrodes are at or near a voltage antinode of the resonator. In Fig. 23-1, the anode segments are connected to the open end of a parallel-wire line short-circuited at the other end. When unloaded, this circuit normally oscillates at the fundamental resonant frequency of the line. At this frequency of oscillation the anodes are at a voltage antinode, and there is a single voltage node, which is at the short-circuited end of the line. Because the length of the line is approximately  $\frac{1}{4}$  wavelength, this mode of oscillation is called the  $\lambda/4$  mode. The voltage distribution in the  $\lambda/4$  mode of oscillation is shown in Fig. 23-3a. The next higher mode of oscillation is one for which the electrical length of the line is  $\frac{3}{4}$  wavelength and there is a second voltage node between the anodes and the short-circuited end of the line, as shown in Fig. 23-3b. In general, oscillation is possible at any frequency for which the electrical length of the line is  $(2n - 1)\lambda/4$ , where  $n$  is any integer and  $\lambda$  is the line wavelength corresponding to the frequency. Because the lumped capacitance of the anodes is across the open end of the line, the physical length of the line is somewhat less than  $(2n - 1)\lambda/4$ . Factors that determine the mode in which oscillation takes place will be discussed in Sec. 23-7.

The circuit of Fig. 23-1 is ordinarily tuned by means of an adjustable short-circuiting bar, which may be moved along the line. The highest frequency of oscillation is obtained when the short-circuiting

<sup>1</sup> BRAINERD *et al.*, *op. cit.*, Sec. 10-12.

bar is adjacent to the tube envelope. Design considerations limit the extent to which the length of the anode leads within the tube may be reduced, and in tubes designed to deliver an output of 150 watts or more, the maximum frequency obtainable in the  $\lambda/4$  mode with the circuit of Fig. 23-1 is of the order of 400 Mc.

Higher frequency may be obtained by using within the tube envelope an additional short-circuiting loop, called a *back-loop*, as shown in Fig. 23-4. The higher frequency results both because of the shorter length of line and because the interelectrode capacitance is in effect divided between the two halves of the line. As in the circuit of Fig. 23-1, tuning is accomplished by means of a movable short-circuiting bridge on the external portion of the line. Oscillation may occur at any frequency for which the electrical length of the line is  $n\lambda/2$ , where  $n$  is an integer and  $\lambda$  is the wave-length. The anodes should, however, preferably be at or near a voltage antinode. An unloaded, or lightly loaded, symmetrical circuit normally oscillates in the  $\lambda/2$  mode.

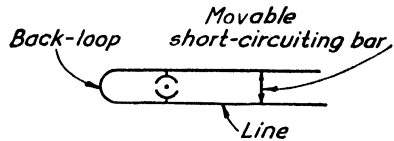


FIG. 23-4.—Double-ended parallel-line oscillator.

**23-2. Types of Tube.**—Figure 23-5a shows the structure of a single-ended magnetron designed for use in the single-ended circuit of Fig. 23-1. The anodes of this tube are cooled by water fed through the lines, as shown in Fig. 23-7. In order to afford circulation, the water is brought in through a small tube inside each line and flows out through the line.

The highest frequency at which useful output may be obtained with the 5J30 tube shown in Fig. 23-5a is approximately 385 Mc. The lowest usable frequency of oscillation is determined by tube failure resulting from electron bombardment of the glass in the vicinity of the anode seals. Electrons that escape from the interaction space through the anode gaps spiral around the anode leads, moving toward the seals. The direction of motion is, however, reversed between half cycles. At high frequency the length of a half period is insufficient to enable electrons to escape from the interaction space and reach the seals. As the frequency is reduced, a value is reached at which sufficient bombardment of the glass occurs to result in strains in the glass and rapid failure. Tube failure from this cause has been eliminated in recent tube models by the use of improved shielding baffles at the gaps between the anode segments and of electrically floating shields on the anode leads near the seals (see Fig. 23-5a).

Aside from tube failure resulting from electron bombardment of the glass, the lower frequency limit of oscillation appears to be determined by the length of line that can be conveniently used. The physical length of the line at a given frequency can be reduced by the use of lumped

capacitance across the line at the anode terminals, but such capacitance is likely to result in operation in a higher mode, since the capacitance provides a low-impedance shunt across the line and thus tends to produce a voltage node at that point. The amount of capacitance that can be used is therefore limited.

Figure 23-5*b* shows the structure of the 5J29, a tube with an internal back-loop designed for the circuit of Fig. 23-4. Cooling of such a tube is simplified by the fact that the back-loop makes it possible to carry water in through one line and out through the other. The maximum frequency of oscillation of the 5J29 tube is approximately 800 Mc, although power cannot be coupled out efficiently above about 770 Mc.

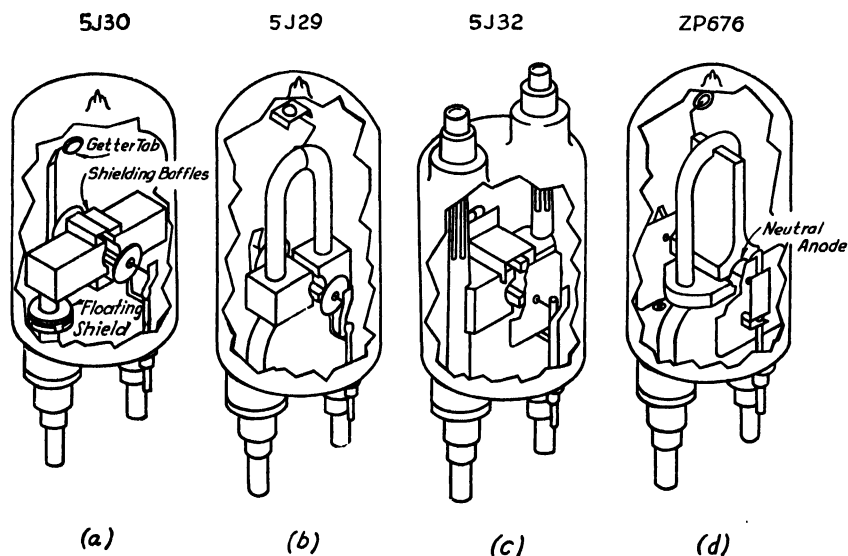


FIG. 23-5.—Typical glass split-anode magnetrons.

In order that a high upper frequency limit may be attained, the back-loop must be made short. It is evident, therefore, that only when the movable external short-circuiting bar is near the anode terminals of the tube will the anodes be near the mid-point of the line. As the frequency is reduced by lengthening the external line, the position of the anodes departs more and more from that of the voltage antinode. Finally, a position is reached for which the anodes are in a more favorable position in the  $\lambda$  mode than in the  $\lambda/2$  mode of oscillation. Operation therefore jumps abruptly to the  $\lambda$  mode, with a corresponding increase of frequency. Further lengthening of the line again causes reduction of frequency until conditions are more favorable to the  $3\lambda/2$  mode than to the  $\lambda$  mode. The frequency then again jumps to approximately the same

value as in the preceding jump. It is apparent that this phenomenon limits the frequency range at the low-frequency end.

Mode jumping of the type just discussed can be prevented by the use of the double-ended tube shown in Fig. 23-5c. With this tube both sections of the line may be adjusted in length and the anodes thus kept near the voltage antinode at the center of the line. This tube may also be used in a single-ended line. In single-ended-line operation, a capacitor may be shunted across the "back" terminals (those to which the line is not connected). Lower frequencies may thus be obtained without the tendency toward mode jumping that is observed when the capacitor is connected between the line terminals of the anodes.

Another type of tube is the *neutral-anode tube* or *neutrode* illustrated in Figs. 23-5d and 20-2. In this tube the anode is divided into three segments, one of which connects to the mid-point of the internal loop. The latter segment covers 180 deg or more of the total anode circumference, and each of the others covers 90 deg or less. Since the mid-point of the loop is a voltage node, the r-f potential of the large anode is neutral relative to the other two. The electronic behavior of the tube resembles that of a multicavity magnetron even more closely than does the two-anode type. Operation appears to be more stable, and a higher frequency limit is obtained than in the two-anode type. The neutrode is, however, more adversely affected by unbalanced loading (see Sec. 23-6), since unbalanced loading displaces the voltage node from the mid-point of the internal loop.

**23-3. Performance.**—Outputs in excess of 1 kw at efficiencies ranging up to 70 per cent have been obtained with tubes of the type shown in Fig. 23-5 and tubes of similar structure. A production model of a transmitter using interchangeable 5J29 and 5J30 tubes to cover the frequency range from 150 to 585 Mc gives a power output in excess of 180 watts in the range from 150 to 700 Mc. The output falls approximately linearly to 50 watts as the frequency is increased from 700 Mc to 785 Mc. Figure 23-6 shows curves of power output and efficiency of an oscillator using a ZP599 tube. Operating data for 10 types of split-anode magnetrons are listed in Table 23-1.

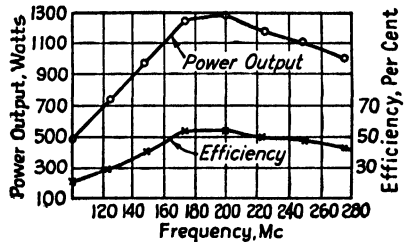


FIG. 23-6.—Curves of power output and efficiency of a ZP599 magnetron used in a single-dial parallel-line oscillator.

In order to prevent undesirable radiation from the tube and the lines, the system must be shielded. A satisfactory type of shielded oscillator is shown in Fig. 23-7.

Typical curves of direct anode voltage as a function of direct anode

current at fixed filament current and wavelength at three values of magnetic flux are shown in Fig. 23-8a. Throughout the ranges in which the curves are dotted, the oscillation is unstable (see Sec. 23-10). Figure 23-8b shows the manner in which the form of the current-voltage curves is affected by filament current. Reduction of frequency affects the form of the anode current-voltage curves at low values of anode current in a similar manner to reduction of filament current. The small slope of the current-voltage curves at low filament current is in part the result of *back-heating*, which is the heating of the cathode by electrons that return to the cathode with increased kinetic energy.

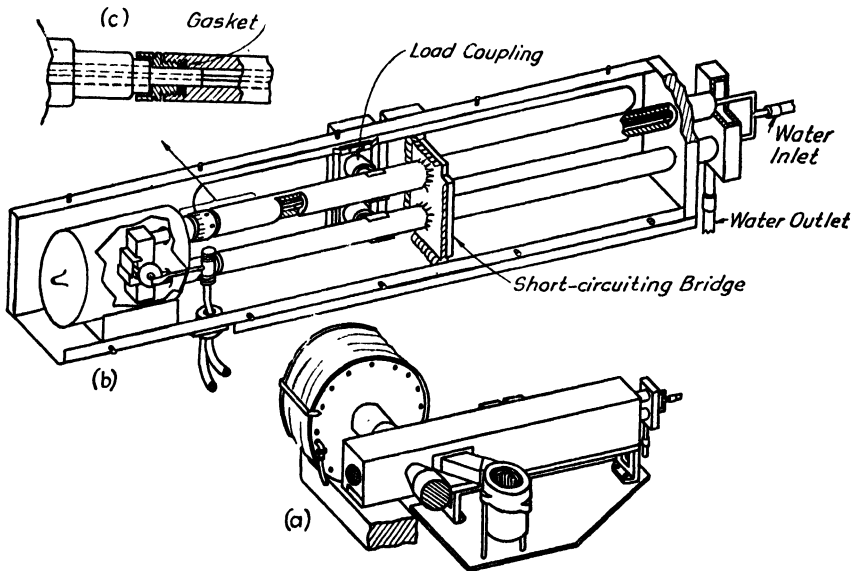


FIG. 23-7.—Structure of a practical parallel-line split-anode magnetron oscillator.

As the anode voltage is increased from a low value, very little anode current flows until the voltage reaches the value corresponding to the voltage intercept of the anode current-voltage curve. Because of the reduction of voltage with increase of current at low values of anode current, particularly at low frequency, the current then jumps abruptly to a higher value, which depends upon the resistance of the power supply and the shape of the current-voltage curve. If the dotted portion of the curve covers a considerable range of anode voltage, if the slope of the curve at higher currents is low, and if the impedance of the power supply is small, the anode current may jump to such a high value as to result in damage to the tube. For this reason it is usually necessary to provide some means of limiting the anode current.

The anode current may be stabilized by (1) the use of an anode power supply having high internal resistance; (2) the use of a constant-current network in the a-c line of the power supply; (3) the use of a constant-direct-current device, such as a pentode, in series with the anode power supply; (4) the use of the direct anode current to excite the electromagnet that supplies the magnetic flux; and (5) the automatic reduction of filament current with increase of anode current. In the fourth method

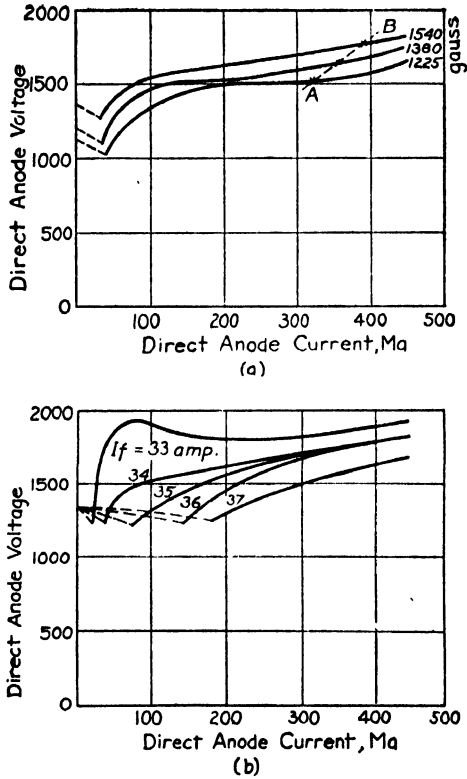


FIG. 23-8.—Anode current-voltage curves of a 5J30 magnetron at a frequency of 250 Mc: (a) at a filament current of 34 amp and (b) at a flux density of 1540 gauss.

the effect of making the magnetic flux proportional to the anode current is to increase the slope of the anode current-voltage characteristic. Thus, if the electromagnet is designed to produce a flux density of 1540 gauss at an anode current of 400 ma, flux densities of 1380 and 1225 gauss will be obtained at approximately 358 and 318 ma, respectively. The resultant curve is shown by the dashed line A-B in Fig. 23-8a. In the fifth system, the anode current is limited by limiting the cathode emission. This method is useful in partly compensating for the effect of back-heating, but will obviously fail if the back-heating is more than



sufficient to supply the necessary emission. In some high-power tubes the back-heating is great enough so that the filament heating current may be turned off when the tube is oscillating.

Because of the extreme complexity of the problem, no complete theoretical analysis of performance has so far been made. A number of useful approximate relations have been derived, however. Slater has shown that oscillation cannot take place unless the magnetic flux density exceeds a minimum value which depends upon the number of anode gaps and the wavelength. For a two-segment split-anode magnetron the minimum required flux density is given by the relation

$$\lambda \mathfrak{B} > 31,800 \quad (23-1)$$

in which  $\lambda$  is the wavelength and  $\mathfrak{B}$  the flux density.

Hartree has shown that oscillation cannot start spontaneously unless the anode voltage exceeds a minimum value. For a two-segment split-anode magnetron the minimum voltage is given by the equation

$$2 \frac{e}{m} \left( \frac{\lambda}{2\pi c} \right)^2 \frac{E_b}{r_a^2} = \frac{e}{m} \frac{\lambda}{2\pi c} \mathfrak{B} \left[ 1 - \left( \frac{r_c}{r_a} \right)^2 \right] - 1 \quad (23-2)$$

where  $E_b$  is the anode voltage;  $\mathfrak{B}$  the flux density in gauss;  $\lambda$  the wavelength in centimeters;  $r_c$  and  $r_a$  the cathode and anode radii, respectively, in centimeters;  $c$  the velocity of light in centimeters per second; and  $e$  and  $m$  the charge and mass, respectively, of an electron.

The voltage at which most efficient operation should be expected has been derived by Slater. For a two-segment split-anode magnetron the relation for best operation is

$$r_a = 0.0345 \sqrt{\frac{\lambda E_b}{\mathfrak{B} - \frac{10,600}{\lambda}}} \quad (23-3)$$

In the derivation of Eq. (23-3) the assumption was made that the ratio of the anode radius to the cathode radius has a theoretical optimum value.

It has also been shown theoretically that oscillation should cease when the anode current exceeds a certain maximum value. This phenomenon is observed experimentally.

**23-4. Tube Life.**—At the time of writing, the tube life of this series of magnetrons has not been long. Thirty hours represents a typical life expectancy, and many tubes fail much earlier.<sup>1</sup> Tube life is greatly shortened by no-load operation and by nonuniform cooling of the envelope. Unless the filament is destroyed by a rapid increase of anode current and resulting back-heating, the tubes invariably fail by cracking as the result of strains set up in the glass. A contributing factor to

<sup>1</sup>Satisfactory tube life can be achieved by the use of a cylindrical shields surrounding the electrode structure.

failure appears to be the tungsten that is deposited on the inside of the envelope. It is possible that this coating causes excessive losses and localized heating of the glass. In order to conserve tube life, the filament should be operated at as low a temperature as is consistent with required power output and with ease of starting of oscillation.

Not only must the anodes of split-anode magnetrons be water-cooled, but the filament leads and the entire envelope must be cooled by air. It is important to cool the envelope as uniformly as possible. In order to ensure proper circulation of water within the anodes of tubes not having an internal loop, the inner tubes that carry the water into the anodes must extend as far into the anodes as possible. If this precaution is not observed, boiling may take place within the anodes.

**23-5. Modulation.**—Figure 23-9 shows a circuit that has been found satisfactory in modulating split-anode magnetrons. Anode-current modulation is produced by varying the grid voltage, and hence the plate current, of the series pentodes. The pentodes serve the additional function of stabilizing the anode current, as discussed in Sec. 23-3. The peaking coil  $L$  partly compensates for the stray capacitance of the modulating circuit, which would otherwise affect the response adversely at high modulation frequencies. The effective load resistance of the modulator tubes is approximately equal to the average slope of the anode voltage-current curve of the magnetron in the operating range. From the point of view of fidelity, the output of this type of modulated oscillator is not very satisfactory, since the amplitude of oscillation does not in general vary linearly with anode current. Moreover, amplitude modulation is accompanied by appreciable frequency modulation.

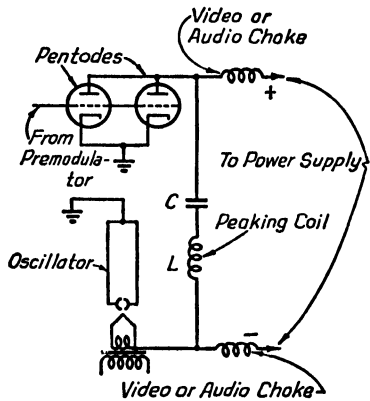


FIG. 23-9.—Amplitude-modulation circuit for split-anode magnetron oscillator.

If the frequency of oscillation is increased at constant anode current and flux density, it is found that the anode voltage rises. In order to make possible the maintenance of the correct operating voltage of the series pentodes, therefore, the power supply must be provided with means for varying the anode supply voltage.

The attainable band width increases with the tightness of load coupling, because of the reduced value of  $Q$ .

**23-6. Load Coupling.**<sup>1</sup>—The simplest method of coupling out power from a parallel-wire magnetron oscillator is by direct connection to one

<sup>1</sup> See also Chap. 16.

side of the line near the movable short-circuiting bridge, as shown in Fig. 16-10a. The tap connects to the center conductor of a coaxial cable, the outer conductor of which is connected to the shield surrounding the parallel-wire resonator. A disadvantage of this type of coupling is that it unbalances the oscillatory circuit with respect to ground and thus tends to reduce the efficiency of operation. For normal requirements, however, this effect is not serious, provided that both the outer conductor of the output line and the short-circuiting bar are solidly grounded to the shield by good low-impedance connections.

Theoretically, in order to achieve single-dial tuning with optimum coupling over the entire frequency range of the oscillator, the mechanical coupling mechanism between the short-circuiting bar and the load tap should be such that the distance between the bar and the tap is automatically reduced as the frequency is increased. In practice, however, it is found that this refinement is not justified, since the load is seldom perfectly matched and the oscillator is, moreover, rather tolerant of mismatch. The effects of lead inductances and other frequency-sensitive portions of the circuit must also be considered. By careful attention to details, it is possible to achieve a condition in which the optimum distance from the short-circuiting bar to the load tap is approximately constant when the load is matched. The oscillator of Fig. 23-7 employs this type of output coupling and has two controls. The frequency control moves both the short-circuiting bar and the coupling tap; the coupling control moves only the coupling tap. With a matched load, this oscillator is capable of operating over a range of 150 or 200 Mc with single-dial control with only a slight reduction of output and efficiency.

The unbalancing resulting from the use of a single coupling tap can be avoided by tapping both lines and connecting to the output cable by means of a balun (see Secs. 3-13 to 3-16). The limitations and complications introduced by this arrangement may, however, outweigh its advantage.

Figure 16-12a shows a system of coupling that is advantageous when operation is desired at the highest possible frequency. The load impedance is transformed by means of matching networks to a very low value and is in effect inserted in series between one side of the resonator line and the short-circuiting bar. Since no space is required ahead of the bar for coupling purposes, useful power may be obtained with the bar right at the tube seals. This method of coupling has the added advantage that it does not require separate coupling adjustments.

Another method that avoids the need of a separate coupling adjustment is to couple the load to the oscillator by means of a second parallel-wire line which is close to the oscillator lines, and the length of which is adjusted simultaneously with that of the oscillator lines, as shown in

Fig. 16-6a. By comparatively small adjustments in the relative positions of the two short-circuiting bridges, the tracking can be made sufficiently good over the entire frequency range so that a single tuning control suffices. Figure 23-6 shows curves of power output and efficiency of a single-control oscillator using this type of coupling.

**23-7. Mode Jumping.**—Figure 23-10 shows typical experimentally determined curves of minimum ratio of anode voltage to flux density at which oscillation starts, plotted as a function of frequency. Curves of this type vary with tube structure and with flux density [see Eq. (23-2)] and to some extent with load. After oscillation starts, operation is possible over a range of  $E_b/\mathfrak{B}$  that may in general extend on either side

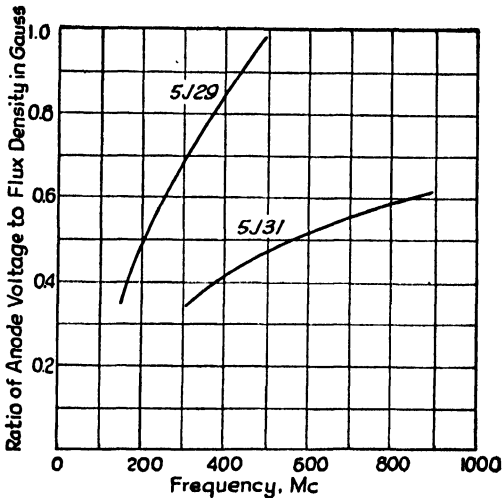


FIG. 23-10.—Minimum ratio of anode voltage to flux density for oscillation of type 5J29 and 5J31 tubes.

of the starting value. The curves shown in Fig. 23-10 were plotted from data obtained in  $\lambda/4$ ,  $3\lambda/4$ , and  $5\lambda/4$  operation and are, therefore, applicable to at least these three modes.

From a curve of the type shown in Fig. 23-10, it is possible to determine in which modes oscillation is possible. Suppose, for instance, that the frequency of the resonant line used with a type 5J29 tube is 150 Mc in the  $\lambda/4$  mode. The frequency in the  $3\lambda/4$  mode is then approximately 450 Mc. Oscillation is possible in the  $\lambda/4$  mode if  $E_b/\mathfrak{B}$  exceeds 0.35. If  $E_b/\mathfrak{B}$  exceeds 0.92, oscillation may take place in either the  $\lambda/4$  mode at 150 Mc or in the  $3\lambda/4$  mode at 450 Mc. If the loaded  $Q$  in the two modes is the same, oscillation will normally occur in the  $\lambda/4$  mode, since  $E_b/\mathfrak{B}$  exceeds the value required for the  $\lambda/4$  mode by a much greater amount than it does the value required for the  $3\lambda/4$  mode. This is merely another way of saying that at the lower frequency the

conditions are more favorable to the transfer of energy to the resonator from the source of direct voltage by electrons in the anode-cathode space. Any oscillator capable of oscillating in more than one mode will, however, tend to oscillate in the mode in which its loaded  $Q$  is highest if other operating parameters are such as to allow oscillation in that mode. In effect, the oscillator always tries to shed its load if that is possible. If the load is coupled to a parallel-line magnetron oscillator at a point on the line at which a voltage node exists in a higher mode, the loaded  $Q$  may be greater in the higher mode than in the fundamental mode. Hence, as the load is gradually increased, a value is reached at which the oscillation will jump to the higher mode if  $E_b/\mathcal{B}$  is sufficiently great to support oscillation. Such an abrupt change from one mode to another is called *mode jumping*.

Mode jumping may also be influenced by the facts that the flux density required to sustain oscillation increases with frequency [see Eq. (23-1)] and that there is a maximum value of anode current at which oscillation is possible. Under operating conditions normally used, however, the ratio  $E_b/\mathcal{B}$ , rather than the values of flux density and anode current, determines whether oscillation can jump to a higher mode.

Mode jumping may take place at constant load if the oscillator is modulated. If the load and the operating value of  $E_b/\mathcal{B}$  are such as to cause operation in the  $3\lambda/4$  or a higher mode when the oscillator is loaded, modulation may cause  $E_b/\mathcal{B}$  to fall to a value so low that oscillation is not possible in this mode, or that efficiency of electronic energy transfer is so low that operation shifts to a lower mode in spite of its lower loaded  $Q$ . Mode jumping as the result of modulation is obviously highly undesirable in ordinary applications of a modulated oscillator.

The tendency toward mode jumping in a parallel-line oscillator may be reduced by lowering the impedance of the load. This fact may be explained as follows. In order to maintain the load constant, the coupling point must be moved closer to the short-circuiting bridge as the load impedance is decreased. The closer the coupling point is to the short-circuiting bar, however, the higher is the mode of oscillation at which the coupling point is at or near a voltage node. Since the values of  $\mathcal{B}$  and  $E_b/\mathcal{B}$  are insufficient to sustain high-order-mode oscillation, there is less tendency for mode jumping.

The tendency toward mode jumping may also be reduced by the use of a form of coupling circuit in which the coupling is not made at a single point along the line. The coupling methods illustrated in Figs. 16-6a and 16-12a are therefore preferable from the point of view of avoidance of mode jumping.

**23-8. Frequency Pulling.**—Like other self-excited oscillators, split-anode parallel-line oscillators exhibit frequency pulling, or change in

frequency with load impedance (see Sec. 21-6), and are subject to the long-line effect. The long-line effect is the presence of frequency discontinuities over the tuning range of the oscillator and is observed if the load is tightly coupled to the oscillator through a long transmission line that is not matched to the load (see Sec. 21-8). The long-line effect is merely an example of the frequency discontinuities that may be observed over the tuning range of any oscillator having two or more tightly coupled oscillatory circuits. The transmission line acts as one oscillatory circuit. When the load cannot be matched to the coupling line throughout the entire frequency range, frequency jumping may be prevented by making the transmission line so short that it cannot resonate within the tuning range of the oscillator, or by coupling the transmission line loosely to the oscillator. When frequency jumping does exist, the frequencies at which jumping occurs may be shifted away from a desired portion of the tuning range by means of a line-stretcher inserted in series with the transmission line.

**23-9. Frequency Pushing.**—Frequency pushing, or change in frequency with direct anode current, is observed in split-anode magnetron oscillators. It is caused by change of impedance presented to the tank circuit at the anodes as the result of electronic action within the tube (see Sec. 21-4). Frequency pushing causes amplitude modulation to be accompanied by frequency modulation.

**23-10. Pulsing.**—Under certain conditions of operation, particularly at low values of anode current, the amplitude of oscillation of split-anode magnetrons jumps periodically between two values, one of which may be zero. This action is called *pulsing*. The pulsing frequency may be changed from the order of once a second to as much as 1 Mc per sec by variation of the circuit constants of the power supply. It is not prevented by the use of a constant-current supply. In at least some types of split-anode magnetrons, pulsing does not occur at high values of anode current, but to date no way has been found to ensure that it will not occur at low currents. Pulsing therefore limits the usefulness of this type of oscillator as a generator of amplitude-modulated waves when large percentages of modulation are desired, unless the modulation introduced by the pulsing is not objectionable.

Pulsing is probably explained by the presence of regions of the anode current-voltage diagram in which the anode current-voltage curves have a negative slope, the action in some respects resembling that of a glow-tube relaxation oscillator. It is of interest to note that pulsing is not ordinarily encountered in multicavity magnetrons.

**23-11. Modulation by Filament Field.**—Split-anode magnetrons now available make use of single-wire filamentary cathodes. Computation of the magnetic flux produced by the filament current discloses that the

density of the flux at the surface of the cathode is of the order of one-tenth that of the main applied magnetic flux. Although the flux produced by the filament current in a straight filament is normal to the main flux, it does affect the electron paths. When the filament current is alternating, as is usually true, the effect of the filament-current flux is to modulate the oscillation at twice the supply frequency. This effect, which is very objectionable in the generation of modulated waves for communication purposes, can be prevented by the use of direct heating current or of tubes having bifilar reversed-helix filaments or filaments resembling a short-circuited length of coaxial cable. Such tubes are not at present available, but tests have shown that they are feasible.

TABLE 23-1

Developmental number	Type number	Frequency, Mc	Power output, watts	Efficiency, per cent	Direct anode voltage	Direct anode current, ma	Flux density, gauss	Filament volts	Filament amp	Structure
ZP579	5J29	350-770	75-150	..	2500	450max	1500	2.2	35	Internal loop
ZP584	5J31	700-1200	75-150	..	2500	450 max	2640	2.5	40	Internal loop
ZP590	5J30	150-385	75-150	50	2500	450 max	1500	2.2	35	Single-ended
ZP599	....	90-300	750 min	..	2300	1000	1750	7	32	Single-ended
ZP646	5J32	90-450	80-150	..	2500	450 max	1500	2.2	35	Double-ended
ZP647	....	225-500	1000	50	2300	1000	1200-1500	10	32	Neutrode
ZP675	....	425-775	> 150	50	1500	400	.....	.....	..	Neutrode
ZP676	5J33	750-1150	200	40	1800	400	1500	2.2	35	Neutrode
ZP677	....	1100-1650	> 200	50	....	.....	.....	7	32	Neutrode-tropotron*
ZP685	....	450-700	1000	50	2300	1000	1500	7	32	Tropotron*
RCA A-133	....	700-1050	1000	50	2500	1000	1500	7	32	Tropotron*

\* The tropotron is a recently developed multisegment tube in which the resonant line makes one or more complete turns about the anode structure, the various segments being connected to the line in such a manner that the tube behaves like a multicavity magnetron.

## CHAPTER 24

### POWER-MEASURING DEVICES FOR ULTRAHIGH FREQUENCIES

BY E. A. YUNKER, H. C. EARLY, G. HOK, AND G. R. BRIDGEFORD

**24-1. Introduction.**—The measurement of power at very high frequencies presents a number of problems not encountered at low radio frequencies. At the lower frequencies, currents and voltages may be quite accurately measured. Also the reactances of resistors are not importantly large. As a result, power may be calculated from current, voltage, and resistance measurements. At very high frequencies, however, these measurements ordinarily cannot be made accurately, and in any case special devices are required. Thus, an ordinary thermoammeter cannot be connected into a coaxial cable to measure current, nor can it be applied to waveguide-current measurement. Because of the difficulty of making power measurements at high radio frequencies, a great many devices have been developed for the purpose. A number of these will be described in this chapter.

These devices may be divided into several fairly definite categories. Probably the most important of these are the calorimeter wattmeters. Here the r-f power is absorbed and converted into heat in a resistive load in some form of calorimeter. The heat is then either calculated from measurements of mass, temperature, specific heat, and time, or a comparison is made with d-c or low-frequency a-c power. Such power-measuring devices give absolute readings and tend to read low because some power is invariably lost in places where it cannot be accounted for. Calorimeter wattmeters are, however, in general the most accurate.

Another type of r-f wattmeter depends upon the conversion of r-f energy into optical radiation, as by a lamp filament. The light flux through a fixed solid angle is measured by optical means such as a photronic or photoelectric cell, optical pyrometer, or photometer.

Some r-f wattmeters utilize the change in electrical resistance of an element that carries all, or a known fraction, of the power to be measured. The resistance measurements may be made by an ohmmeter or a bridge. This group includes gas-filled load lamps, bolometers, and thermistor bridges. The load lamp in this case may or may not operate in the optical temperature range.

There are also a number of sampling devices and relative-power indicators. In these a fraction of the total power is taken off and rectified



and a relative indication presented on a d-c milliammeter. Probes in slotted lines and coaxial cables, unidirectional couplers, and indicators that take a fraction of the power radiated from an antenna are included in this group.

Special devices have been developed for measuring the current in a coaxial line without spoiling the impedance continuity of the line. Such a device permits power to be calculated from the relation  $P = I^2R$  when the resistance of the load is known.

An ideal r-f wattmeter should be instantaneous in reading, indicate absolute values, present a pure resistance load to the source at all frequencies, require no tuning, and be accurate. One type of wattmeter may be superior to others in one or more of these characteristics; another may be better in some other respect. This further accounts for the multiplicity of wattmeters that have been devised. In general, one device is suitable over only limited ranges of frequency and power.

An impedance mismatch into the load will not necessarily cause an error in the reading of the power-measuring device, since the device measures whatever power reaches it. Such mismatches may, however, cause the transmitter to deliver less than its maximum output to the load because of the reflections back into the transmitter. The amount of power reflected may be measured by using a slotted line between transmitter and power meter and applying the formula

$$\text{Per cent reflected power} = \left( \frac{\sigma - 1}{\sigma + 1} \right)^2 \times 100$$

where  $\sigma$  is the ratio of the voltage maximum to the voltage minimum of the standing waves along the slotted line.

**24-2. Dummy Loads.**—A *dummy load*, as applied to radio transmitters, is a device for dissipating r-f power in the form of heat or light rather than by radiation from an antenna. Such devices are useful when operation of a transmitter is desired without radiation. More often, in high-frequency practice, dummy loads are used to absorb r-f power that is being measured. The load itself may form the dissipation element of the wattmeter, as in the calorimetric wattmeters and load lamps; or it may be incidental to the measurement, as in the thermocouple types. Ideally, the impedance of a dummy load should match that of the device driving it and be resistive at all frequencies, without tuning.

**“Lossy” Line.**—Probably the closest approach to these characteristics is exhibited by an unterminated coaxial cable long enough so that, at the operating frequency, the loss is, say, 10 db to the open-circuited end. The reflected wave then suffers an equal attenuation, giving 20 db total loss back to the input so that the effect of reflections is no longer objectionable. By choosing high-loss cable, such as those using polyethylene

dielectric for ultrahigh frequencies, or rubber insulation for the lower, the required attenuation may be obtained in a reasonable length. The loss is preferably produced in the dielectric rather than in the center conductor, because the heat generated is then more readily dissipated by conduction in the cable. If desired, a disk resistor (Sec. 24-5) may be used to terminate the line so that less lossy cable is required.

Since the current in a line terminated in its characteristic impedance decreases exponentially, the greatest loss, and therefore insert the greatest heating, occurs at the input end of the cable. The size of cable used should thus be chosen to transmit the total power. However, smaller sizes of cable, having higher attenuations and therefore requiring less total length, may be used after the initial current has been attenuated down to where the smaller cable can transmit it without causing the dielectric to melt and the cable to short-circuit. Forced air may be used to cool the cable if necessary. The use of lossy cable and other dummy loads is taken up in subsequent sections in connection with the wattmeters in which they are used.

*Resistor Star.*—A load that is satisfactory for frequencies up to 500 Mc, if carefully made, consists of a star of metallized resistors connected between the center and outer conductors at the end of a coaxial cable. By making the center conductor longer than the outer, the several resistors may be arranged cylindrically with a minimum length of leads. The resistors should, of course, be chosen to give a resistance equal to the characteristic impedance of the line when they are connected in parallel. The power-dissipating ability of this load may be greatly increased by immersing it in oil that is kept in circulation and cooled. It is well to check the impedance match of such a resistor load by examining the standing waves on a slotted line. If oil is to be used, the slotted-line measurements should be made with the resistor in oil because of capacitance effects. Considerable improvement in impedance match may often be made by carefully selecting resistors.

*Gas-cooled Resistors.*—A noninductive resistor in a gas-filled bulb such as the Ohmite D-100 is very satisfactory for frequencies up to about 25 Mc. It has the advantages of compactness and portability. Other types of gas-filled load lamps for higher frequencies are discussed in Sec. 24-7 in connection with power measurements.

*Sloping-guide Water Load.*—A simple waveguide water load suitable for use in the power range from a few milliwatts to perhaps 100 kw is shown in Fig. 24-1. It consists simply of a piece of rectangular waveguide, with a watertight plate on one end, mounted on a slight tilt and filled with water. The wide dimension of the guide is horizontal so that the electric field is nearly perpendicular to the surface of the water. For a low standing-wave ratio the length of the load should be at least six

times the width of the guide. Under these conditions a voltage standing-wave ratio of less than 1.05:1 may be expected.

For outdoor use at high power levels the heat may be carried away by the steam that escapes through holes in the top side, while for indoor use the water may be circulated through a heat exchanger.

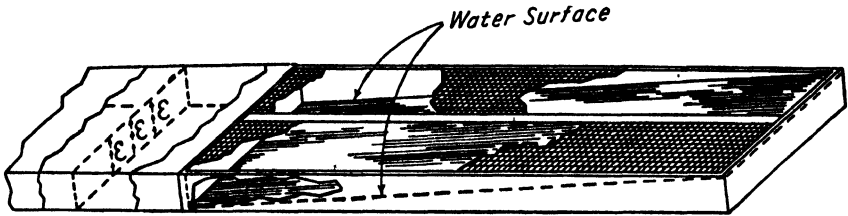


FIG. 24-1.—A simple waveguide water load.

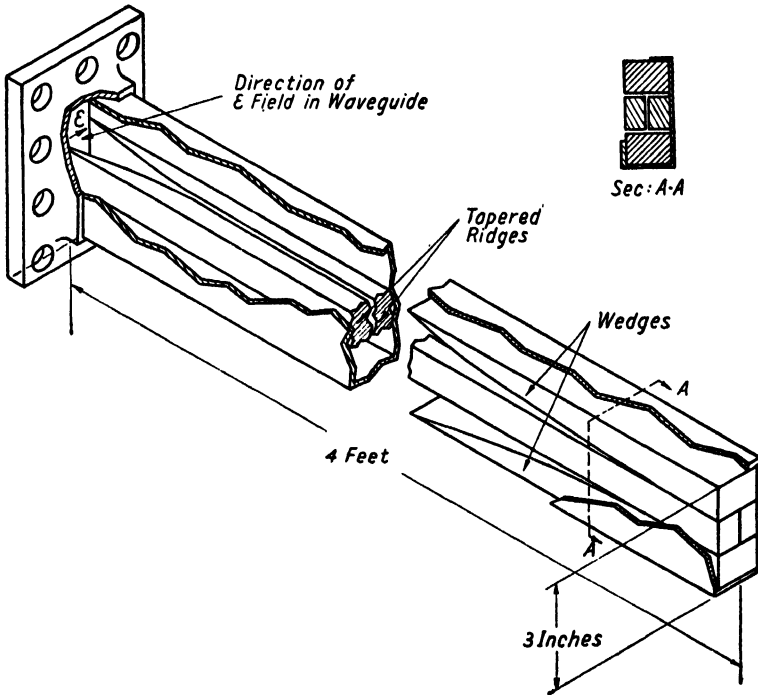


FIG. 24-2.—A dummy load designed to dissipate 1 kw, of power at wavelengths of 8 to 12 cm.

*All-metal Waveguide Load.*—Figure 24-2 shows a dummy load designed to dissipate 1 kw of power at wavelengths of 8 to 12 cm. It is not adapted to power measurement. For use where mechanical ruggedness is important, the all-metal type is superior to types employing lossy dielectrics such as sand or transite. The high attenuation in this device

is produced by the tapered steel ridges that serve to load the guide and to reduce the impedance in order that the currents may be large. These steel ridges are fastened to the inside walls of a 4-ft section of 1½-by 3-in. waveguide by means of machine screws. This 4-ft length of guide has enough surface area to dissipate a kilowatt of power without the use of cooling fins or forced air circulation. If cooling fins are used, the over-all length can be reduced.

The spacing between the ridges is about 0.035 in. except at the front end of the load where the ridges are tapered in a manner that resembles an exponential curve. The design of this curve is important if the standing-wave ratio is to be kept low over a wide frequency range.

In order to distribute the heat evenly along the length of the load and to avoid local overheating, it is necessary that the attenuation near the terminal end of the load be much greater than it is near the middle. This increase in the rate of attenuation is obtained by decreasing the wide dimension of the guide (the dimension that is perpendicular to the electric field). In ridge waveguide this dimension can be reduced greatly without reaching the cutoff frequency. The two metal wedges are used to taper this dimension gradually until the cutoff frequency is reached and the attenuation approaches infinity.

It is important that the ridges be made from steel that has good magnetic properties. The skin depth of the currents in the metal is proportional to  $\sqrt{\rho/\mu f}$ , where  $\rho$  is the resistivity,  $\mu$  the permeability, and  $f$  the frequency. Thus the higher the value of  $\mu$ , the greater the attenuation. The steel should be of low carbon content and, if it has been cold-rolled, should be annealed. There may be a magnetic type of stainless steel, having a high resistivity, which would be advantageous for this application, but this possibility has not been investigated.

The standing-wave ratio for the foregoing load has been tested at various frequencies. When the load is dissipating a kilowatt of power the standing-wave ratio does not exceed 1.15:1 over the wavelength range from 8 to 12 cm. Measurements taken with low-power test equipment when the load is at room temperature show a somewhat higher standing-wave ratio.

*Antennas.*—An antenna giving a low standing-wave ratio makes a good load for test purposes except for the fact that the radiation may be objectionable. If an antenna is used as a load for measuring purposes, it must be borne in mind that the impedance of an antenna depends upon its location with respect to ground and near-by objects. Its impedance must be determined usually by measuring-line methods, for conditions under which it will be used. This is especially true for the very high frequencies where even a hand placed near by causes appreciable reflection that changes the input impedance of the antenna.

Several other types of dummy loads such as water-filled waveguides and coaxial lines are discussed in subsequent sections in connection with complete wattmeters. These may also be used for simple dummy loads.

**24-3. Determination of Power from Current or Voltage and Resistance.**—Probably the most satisfactory method for determining power at comparatively low radio frequencies, say below 50 Mc, consists in measuring the rms current into, or voltage across, a dummy load of known resistance and calculating the power from  $I^2R$  or  $E^2/R$ . Any dummy load or antenna is satisfactory for this purpose provided that the resistance at the point where the current or voltage measurements are made is known for the operating conditions. A thermocouple r-f ammeter may be used to measure the current; vacuum-tube voltmeters or oscilloscopes are suitable for voltage measurements. As the frequency of the r-f power is increased, errors in measurement and uncertainties in resistance values increase so that above perhaps 50 Mc special devices such as calorimeters are more satisfactory.

**24-4. Thermocouple in Coaxial Line.**—The principal limitation to the use of the ordinary type of r-f ammeter, which consists of one or more thermocouple elements and a d-c milliammeter in a case, or a thermo-

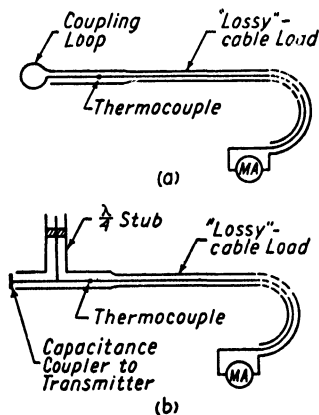


FIG. 24-3.—A coaxial-line thermocouple wattmeter: (a) schematic diagram; (b) quarter-wave stub used with capacitance-type output coupling system.

couple unit with external meter, is that it is so large that it must be used with open-wire lines and that, particularly at very high frequencies, it causes a large impedance discontinuity in the line in which it is used. This difficulty may be surmounted by making the thermoelement part of the center conductor of a coaxial line used to transmit power to a load. The meter used to measure the d-c output of the thermoelement is then placed outside the r-f system as, for example, at the terminal end of a lossy line used as a dummy load. Such an arrangement, developed to meet some special needs, is shown schematically in Fig. 24-3a. The thermoelement may be conveniently mounted as the center conductor of a short section of coaxial line between two cable fittings, as shown in Fig. 24-4. If a capacitance type of output coupling system is used on the transmitter, a quarter-wave stub, or similar high-impedance shunting device, must be used in order to complete the d-c circuit to the meter. This is shown in Fig. 24-3b.

With proper care the device can be used at frequencies up to 2500

Mc and for powers up to 500 watts. It is rugged, quick-reading, and simple to operate. It may be calibrated with an absolute-reading wattmeter, such as those described in Sec. 24-8, or on low-frequency power with theoretical corrections for skin effects in the thermocouple. Since the impedance of the thermocouple is very low, a microammeter of low resistance and high sensitivity should be used.

Thermocouples may be made by welding together two wires of different metals or of one metal and an alloy of that metal. The problems of thermoelectric power and mechanical properties are the same as for ordinary thermocouples used for temperature measurements. The ends of the wire may be spot-welded, or a flame weld may be used. An r-f arc is convenient and satisfactory as a welding heat source. In this case the ends of the wires to be welded are twisted together and then placed in two close-fitting capillary tubes made by drawing a larger glass tube down to fit the wires.

The twisted ends of the wires should project a short distance beyond the glass. By bringing these wire ends close to the tank of an r-f oscillator, an arc may be drawn to the wires, which causes them to fuse. After they have been welded, the wires should be pulled out collinearly. As little as possible of the wire should be fused, so as not to make a large globule of metal at the joint. A butt joint between the ends of the wires is the most desirable form of weld because the corrections for skin effect, which are based on a circular wire of uniform diameter, apply more closely to such a joint than to one of indeterminate shape, but such a joint is difficult to make on small wires.

The sensitivity of a thermocouple depends on the metals used and upon the diameter of the wires and their length, the latter two factors involving cooling effects. The shorter the wire, the less is the impedance discontinuity to the line in which it is used. A copper-constantan couple  $\frac{3}{16}$  to  $\frac{1}{4}$  in. long made of wires 0.003 to 0.005 in. in diameter is suitable for powers up to about 50 watts. Silver with bismuth gives greater sensitivity and about the same power rating.

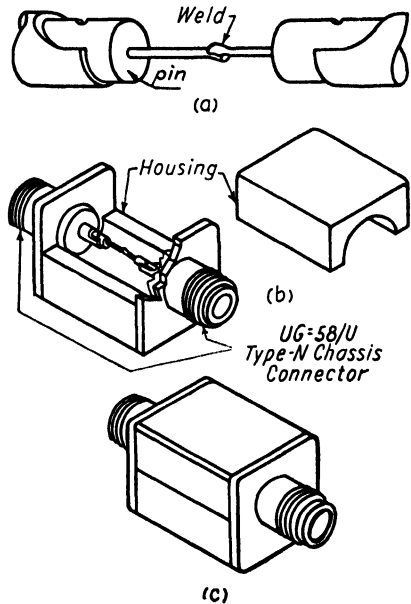


FIG. 24-4.—Thermocouple mounted as center conductor of short coaxial line.

Thermocouples that are geometrically ideal from the standpoint of corrections for skin effect may be made by silver-plating a constantan wire for one-half its length. Plated couples, however, for reasons not investigated, lose their calibration if overheated.

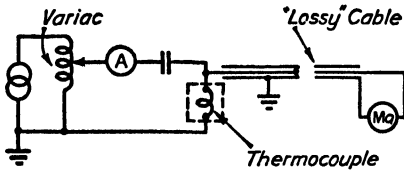


FIG. 24-5.—Circuit for calibrating thermocouples.

Thermocouple-type r-f power-measuring devices may be calibrated by comparison with an absolute power-measuring device such as a calorimetric wattmeter (Sec. 24-8) or on low-frequency alternating current, as shown in Fig. 24-5. In the second case, correction must be made for skin effect in the thermocouple. This may be done in accordance with the following analysis:

Let  $R_1$  = d-c resistance of the wire of the first metal of the thermocouple

$R_2$  = d-c resistance of the wire of the second metal of the thermocouple

$R_1'$  = a-c resistance of the first wire

$R_2'$  = a-c resistance of the second wire

$P_{dc}$  = d-c power consumed in the couple

$P_{ac}$  = a-c power consumed in the couple

$I$  = current through the couple

Then

$$P_{dc} = I^2(R_1 + R_2) \quad (24-1)$$

$$P_{ac} = I^2(R_1' + R_2') \quad (24-2)$$

$$R_1' = K_1R_1 \quad (24-3)$$

$$R_2' = K_2R_2 \quad (24-4)$$

where  $K_1$  and  $K_2$  are functions of frequency. Then

$$P_{ac} = I^2(K_1R_1 + K_2R_2) \quad (24-5)$$

and, if we write

$$R_2 = \alpha R_1 \quad (24-6)$$

$$P_{ac} = I^2(K_1R_1 + K_2\alpha R_1) \\ = I^2R_1(K_1 + K_2\alpha) \quad (24-7)$$

$$P_{dc} = I^2R_1(1 + \alpha) \quad (24-8)$$

Then

$$\frac{P_{ac}}{P_{dc}} = \frac{K_1 + \alpha K_2}{1 + \alpha} \quad (24-9)$$

or

$$P_{ac} = P_{dc} \frac{(K_1 + \alpha K_2)}{1 + \alpha} \quad (24-10)$$

Equation (24-10) provides a means of conversion between the calibrating d-c power and the a-c power corresponding to the same thermocouple temperatures. Ratios of  $R_{ac}$  to  $R_{dc}$  are given by Terman.<sup>1</sup>

Because of the small diameter of the thermocouple, it is not feasible to make the impedance of the coaxial line, of which the thermocouple is the center conductor, low enough to match standard coaxial cables. The couple, therefore, presents an impedance discontinuity in the line. This corresponds to a voltage standing-wave ratio of about 2:1 at 500 Mc for the average thermocouple unit. If this amount of reflection cannot be taken care of by the transmitter output tuning system, a tuning stub, such as that shown in Figs. 24-3*b* and 24-9, should be used. As in any device that indicates power by voltage or current measurements at a single point in a transmission line, standing waves on the line will introduce errors depending upon where the indicator happens to be on the standing wave (see Secs. 24-22 and 24-27). The load should therefore be sufficiently good to make the fraction of power reflected consistent with the accuracy desired.



FIG. 24-5.—Arrangement of parallel thermocouples to prevent impedance discontinuity in the coaxial line.

The impedance discontinuity in the line caused by the small diameter of the thermocouple wire may be largely prevented by using a number of thermocouples in parallel arranged around the circumference of a circle in the manner of wires in a cage antenna, as shown in Fig. 24-6. The diameter of the circle should, of course, be equal to that of the center conductor of the coaxial-cable section. For a given power rating, the wires used for the couple must then be smaller than for a single-element thermocouple, or the thermoelectric power of the metals used must be greater. Multielement couples of this type must be calibrated against a standard r-f power-measuring unit because of the uncertainty of the current distribution among the parallel elements of the multielement system.

**24-5. Disk Resistor with Voltmeter.**—Small amounts of power, say up to 25 watts, may be dissipated in an air-cooled disk resistor used as a termination to a coaxial line. The disk will ordinarily be larger in diameter than the cable and may be attached to the cable by means of a tapered coaxial section. If the disk resistor has a resistance that properly matches the line, a constant-impedance taper is used. If not, the taper may be made to effect the necessary match. By building a suitable nonreactive voltmeter across, and integral with, the disk resistor, measurements of power may be made. Such an arrangement is shown schematically in Fig. 24-7. The carbon resistor was designed for 50-ohm

<sup>1</sup>TERMAN, F. E., "Radio Engineers' Handbook," p. 31, McGraw-Hill Book Company, Inc., New York, 1943.



termination. Its impedance, measured in the mounting shown, is  $49 + j5$  ohms at 1100 Mc. The center electrode of the disk resistor should be relatively large, because otherwise the current density at the inner conductor may be so high as to cause breakdown in the resistor. In the unit shown, the center conductor was  $\frac{3}{4}$  in. in diameter. The disk was capable of dissipating 30 watts when cooled by air from a 7500-rpm 2-in. fan. Resistors of this type have also been made of germanium. A disk-type diode such as the GL559, should be used because tubes having conventional leads

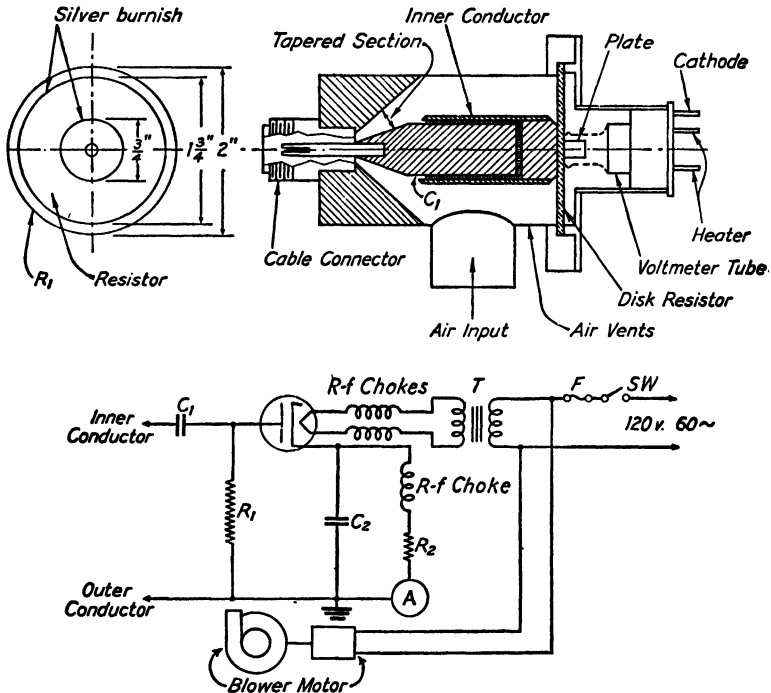


FIG. 24-7.—Wattmeter using a disk-resistor voltmeter.

would introduce serious reactances. The capacitance  $C_2$ , which is built into the tube, is large enough to cause the diode voltmeter, of which it is a part, to read peak volts.

The power-measuring device of Fig. 24-7 is compact, quick- and direct-reading, rugged, and does not require tuning. It is usable as described for frequencies up to 1200 Mc. However, considerable inaccuracy may occur because the voltmeter reads peak volts. Readings are therefore a function of wave form, and it cannot be used to measure the power in a modulated wave. Improvement of the disk resistors would be desirable, since those used change value with age because of loss of the coating material and possibly breakdown near the center conductor.

**24-6. Photometric Systems.**—The photometric power-measuring system is essentially a load lamp of some sort, usually incandescent, coupled to the source. The r-f energy lights the lamp, and the radiant energy is measured by some means such as a light meter, a photoelectric cell and amplifier, or an optical pyrometer. The lamp must be tuned for each frequency. Usually a  $\lambda/4$  line is coupled to it for this purpose, but a  $\lambda/2$  line may also be convenient as an aid in matching lamp impedances. Depending upon the size of lamp and the light-measuring equipment, powers of 1 mw to 20 or 30 watts may be measured. The lower powers can be measured with fair accuracy by this method, but errors of over 5 per cent are obtained at the higher powers, such as 1 to 30 watts. Above 800 Mc the errors due to losses in the glass seals become so great that the method should not be used.

Lamps are normally calibrated by using an a-c or d-c power source. For the most accurate measurement a comparison method is used by which the low-frequency and high-frequency powers are put on the lamp alternately so as to eliminate any danger of error due to aging or other calibration change.

It is important that the r-f current be constant along the filament; otherwise there will be hot spots that cause errors in calibration. This is so because the luminous efficiency of an incandescent lamp increases with temperature so that a given amount of r-f power expended in a section where the temperature is high will produce a greater effect on the photometric device than will the same amount of d-c or low-frequency power expended uniformly along the wire in calibrating the lamp. Non-uniformity of current is caused by standing waves. These are not easy to prevent, since the impedance of the filament is a function of temperature and thus complicates the problem of matching the load to the line. The effect of current nonuniformity may be almost entirely avoided by using lamps with very short filaments such as, for example, those used in automobile headlights. Since most lamps of this type are gas-filled, excessive voltage will cause a gaseous arc within the lamp. This arc is less likely to occur if the lamp selected for the load is one in which the parallel wires ordinarily used to support the filament are bent away from each other at the ends where the filament is attached rather than bent inward. Other sources of error are heating losses in the leads to the lamp, in the tuning device, and in the glass, since heat thus developed will not cause a response in the photometric indicator. Darkening of the lamp bulb between calibration and use, caused by a deposit of tungsten, is also a source of error.

Advantages of photometric systems lie mainly in their small size and rapidity of reading. Completely portable units, very light in weight, can be made for measuring the range of powers above 1 watt or so.

Below this, power supplies for amplifier systems necessarily increase the size of the units. If accuracy is sacrificed for simplicity, a very rugged and portable unit consisting of 3- to 50-candlepower bulbs on tunable Lecher wires with a shielded light meter of the photographic type can be made up quickly. These provide sufficiently good measurements for many types of use.

A "grease-spot" photometer is very useful for temporary use or in cases where more convenient devices are not available. A translucent spot is made on a sheet of paper with oil, grease, or varnish and is illuminated on one side by the load lamp. An ordinary lamp, the brilliance of which is controlled by a variac, is placed on the other side of the paper and adjusted for disappearance of the spot.

**24-7. Gas-filled Load Lamps.**—Ordinary high-vacuum single-filament lamps are found to have fairly desirable properties as load lamps except that the heat-dissipating ability is low. By filling the lamp with a gas, such as hydrogen, the dissipation capability is raised by a factor of the order of 20. Measurements with these lamps at frequencies up to 1200 Mc are very accurate and check well with calorimetric measurements. Above 1200 Mc the load lamp can still be used



FIG. 24-8.—Gas-filled load lamp for ultrahigh frequencies.

with good results up to frequencies of the order of 3000 Mc, although the accuracy is less. Available lamps of this type are suitable for measuring powers in the range from 1 to 50 watts. A gas-filled lamp having a shape adapted to use at ultrahigh frequencies is shown in Fig. 24-8.

The errors likely to be encountered in the use of gas-filled load lamps are the same as those discussed in the preceding section. It has been shown experimentally and mathematically that, if the length of wire is kept below  $\frac{1}{4}$  wavelength, standing-wave effects, and the difference between d-c and r-f resistance, are small or negligible. Table 24-1 shows the error due to length of filament.

TABLE 24-1

Length of filament.....	0	$\lambda/16$	$\lambda/8$	$3\lambda/16$	$\lambda/4$
Ratio of a-c to d-c power.....	1.000	1.002	1.037	1.185	1.500

Although the lamps are made to fit into holders that go into coaxial lines, they are not ordinarily good terminations. Furthermore, the resistance of the lamp is a function of the power dissipated. For example, the cold resistance of a particular lamp of the type shown in Fig. 24-8 is about 8 ohms, while for 15-watt dissipation the resistance is 75 ohms. Tuning can be accomplished by a single variable plunger behind the lamp,

a double-stub tuner preceding the lamp, or a combination of both, as shown in Fig. 24-9. These tuning stubs should be adjusted so that the hot section of the filament is in the middle because, if it is near the end, errors will occur owing to the cooling effect of leads and seals in the tube.

Gas-filled load lamps may be calibrated on direct current by measuring the voltage across the lamp for various currents through it. From these data the corresponding resistances and power dissipations are calculated and a curve of power as a function of resistance is plotted. Radio-frequency measurements may then be made, with the circuit shown in Fig. 24-9, by noting the resistance of the filament while it is dissipating the power to be measured and reading the power from the curve. The power used in determining the d-c resistance is, of course, negligibly small.

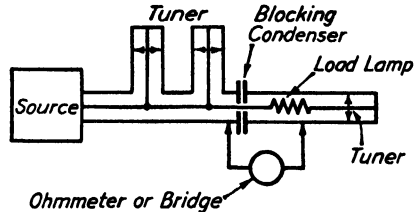


FIG. 24-9.—Circuit of gas-filled load-lamp wattmeter.

**24-8. Calorimeter Wattmeters.**—A calorimeter wattmeter is a device in which power is measured in terms of a rise in temperature in a mass of substance of known thermal capacity. It consists essentially of a dummy load by which the power is dissipated into a medium such as water or oil and means for measuring the mass of the substance and its rise in temperature. Since heat energy is measured by the product of mass of substance, specific heat, and rise in temperature, and since power is a rate of flow of energy, calorimetric measurement of power is made either by rise in temperature of a fluid flowing at a fixed rate or by the rate of rise of temperature in a fixed quantity of a substance such as a mass of water. Examples of both types are described in the following sections.

**24-9. Oil-immersed Dummy Load.**—One of the simplest calorimetric wattmeters consists of a vessel of oil into which is immersed the dummy load in which the r-f power is dissipated. The oil is kept in circulation by means of a small motor and impeller so that the temperature throughout the mass of oil is essentially uniform. The power may then be calculated in terms of time, mass, specific heat, and temperature rise. Usually, however, a given mass of oil is calibrated by dissipating d-c or low-frequency a-c power in either the same dummy load, or in a separate heating element, and plotting temperature as a function of time for different power inputs, or power as a function of rate of rise of temperature. An accuracy of 5 per cent is attainable.

A dummy load suitable for this type of calorimeter consists of a number of small metallized resistors, say 2-watt, arranged radially between the center and outer conductors of a coaxial cable, as discussed in Sec. 24-2. The cooling effect of the oil will, of course, increase the power rating of

the resistors. The upper frequency limit for a wattmeter of this type depends upon the excellence of the dummy load and is in the neighborhood of 500 Mc. Disk types of resistors (Sec. 24-5) are good to considerably higher frequencies.

**24-10. Air Calorimeters.**—Air, in place of a liquid, may be used for absorbing the heat dissipated in the dummy load of a calorimetric wattmeter. An advantage over liquid cooling is that the time required for the calorimeter to reach equilibrium may be reduced. Whether this advantage obtains in practice or not depends upon the thermal capacity

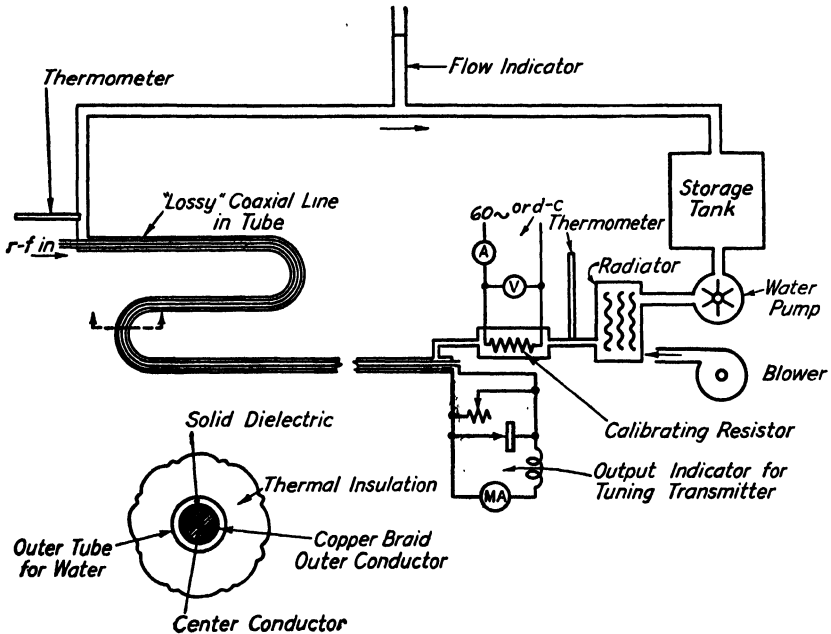


FIG. 24-10.—Wattmeter using a lossy-coaxial-cable calorimeter.

of the load used. Essentially the air calorimeter consists of a load resistor cooled by a blast of air and a differential thermocouple, or thermometer, arranged to read the rise in temperature of the air. If thermocouples or mercury thermometers are used, care must be taken to shield them from the r-f fields. The sensitivity of the thermocouple system may be increased by the use of thermopiles, or multiple thermocouples.

Several types of resistor loads are applicable. One consists of a tubular resistor used as the center conductor of a coaxial line. Tapered coaxial lines are used to connect the load to the coaxial cable used to transmit the power. Air is forced through the resistor, out through holes in the end opposite the blower and back between the resistor and the outer conductor of the coaxial line of which it is a part. Such loads have been

built that were good up to 1000 Mc, a frequency at which the standing-wave ratio was 2:1. The power dissipated was 100 watts. Another type of load uses a length of lossy solid-dielectric coaxial cable with the outer waterproof covering stripped off, arranged in a grid or coil so as to give a large exposure to the air forced past it. This resistor gives a better termination than the coaxial resistor and is useful up to several thousand megacycles but is bulkier and slower heating. In general, air-calorimeter wattmeters are not so satisfactory as water-calorimeter wattmeters because they are less accurate and, on account of limitations in the load resistors, are not much faster. The lower accuracy is caused by the difficulty of avoiding losses in heat.

**24-11. Lossy-coaxial-cable Calorimeter Wattmeter.**—A calorimeter wattmeter that takes advantage of the simplicity, convenience, and good terminating characteristics of lossy coaxial lines is shown in Fig. 24-10. It consists essentially of a length of solid-dielectric coaxial cable, with the protective covering removed, inside a copper, vinyl, or similar tube, a water pump, a radiator, a water-flow indicator, a blower, and thermometers to indicate the temperatures of the water going into and flowing out of the tube surrounding the lossy-cable load. A heating element to be used on direct current or low-frequency alternating current is included in the system for calibrating purposes. An output indicator consisting of a rectifying crystal and milliammeter (Sec. 24-27) is connected to the low r-f end of the lossy cable for convenience in tuning transmitters not provided with such an indicator.

The length of lossy cable used in the load should be such as to give about 10-db attenuation at the operating frequency. Since the end of the cable farthest from the transmitter is open-circuited, reflections will occur and another 10-db attenuation will result before the wave reaches the transmitter. Since the length of cable required is dictated by the lowest frequency at which it is to be used, the cable will always be longer than necessary for the higher frequencies. The principal objection to excessive lengths of lossy cable is that the amount of water required for the system is increased, thus increasing the time required for a reading. For frequencies in the 500- to 2500-Mc range, RG-8/U cable is good; at lower frequencies RG-38/U, which has a higher loss dielectric, may be used in order to reduce the length required. If the power level, as well as the frequency, is low, the percentage error may be expected to increase because of losses of heat along the cable and its covering. The flow of water may be adjusted so as to give a conveniently readable temperature rise for a given power input. Care should be taken to ensure that the system is closed so that no air is forced through it, losses in cables external to it should be held to a minimum and, if thermocouples are used, they should be shielded from the r-f fields.

This wattmeter is suitable for powers in the range from 5 to 500 watts and for frequencies up to 3000 Mc. The lower frequency limit is imposed by the relatively great length of cable required to produce the necessary attenuation. Thus, at 100 Mc, 333 ft of RG-8/U would be required for 20-db attenuation. The whole system should be given a stabilization period of 30 min before readings are taken. For accurate measurements after larger power-level changes, 10 min should be allowed; small changes in power require less time for equilibrium to be established. Accuracies within 5 per cent are to be expected. Some of the advantages of the lossy-coaxial-line calorimeter wattmeter are broad frequency band, with freedom from tuning, good impedance termination, wide power range, and low per cent error. On the other hand, it is slow in reading, bulky, and heavy.

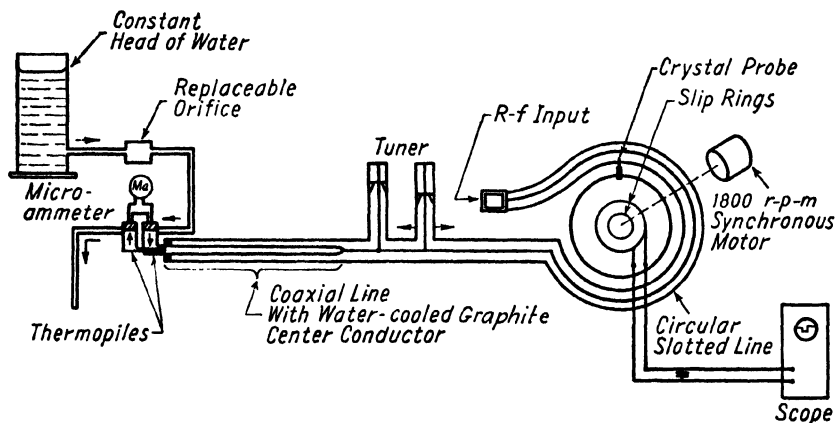


FIG. 24-11.—Schematic diagram of wattmeter with coaxial-line water calorimeter.

**24-12. Coaxial Line with Resistive Center Conductor.**—A coaxial-line water-calorimeter wattmeter designed for operation in the frequency range 300 to 3000 Mc at powers in the range 5 to 300 watts is shown schematically in Fig. 24-11.

The r-f load consists of an 11-in. section of a 50-ohm coaxial line short-circuited at the terminal end. The conductor is a copper tube covered with a  $\frac{1}{16}$ -in. layer of graphite held on by a pyrex-glass tube. The water flow is down the inside of the copper tube and back through an axial glass tube within the copper tube.

The rise in temperature of the water is measured by differential thermopiles. One pile, consisting of three copper-constantan thermocouples, is located in the water-inlet pipe; an identical one is located in the outlet. Copper-screen baffles to mix the water are used to ensure uniformity of water temperature in the region surrounding the thermopiles. The flow system consists of a storage tank, a pump, a standpipe

open to the atmosphere on the top to ensure constant pressure head, a control orifice, and a radiator. The rate of flow is changed by changing orifices.

Because of the wide range in frequency over which the single coaxial load is used, some form of tuning is necessary. A double-stub tuner in which the stub nearest the load is fixed and the other movable along a 6-in. slot is used for this purpose. A slotted line, made in the form of a circle, with a rotating probe and cathode-ray-oscilloscope presentation, is used to determine when the load is properly matched to the line. This arrangement is shown in Fig. 24-12.

The accuracy of this calorimeter is estimated to be within 5 per cent, the inaccuracies being caused by stray heat losses and errors in reading temperature rise and in variation in rate of flow of water.

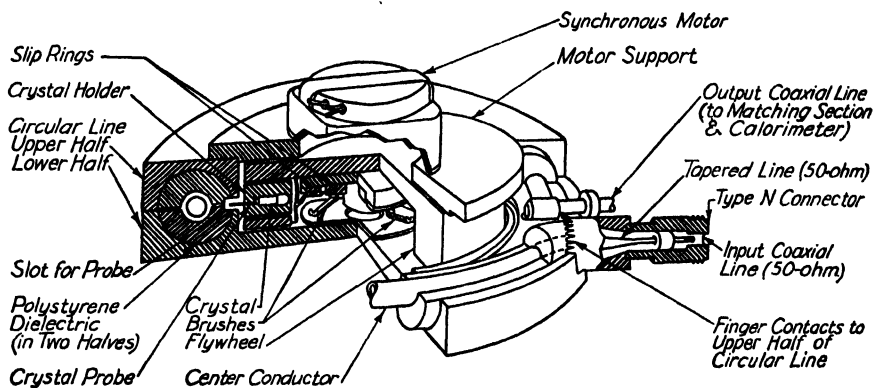


Fig. 24-12.—Slotted-line rotating-probe standing-wave indicator.

**24-13. Coaxial Line with Water Dielectric.**—The calorimeter wattmeter shown schematically in Fig. 24-13 is similar to the one described above. It has, however, certain features that make possible operation over the frequency band from 1000 to 3000 Mc with an accuracy of 8 to 10 per cent without the necessity for tuning. If tuning, by stubs, for example, is used so as to reduce the voltage standing-wave ratio, this error may be reduced to 5 per cent. It has also the advantage, over most of the calorimeter wattmeters, of being rapid in reading, as only 10 to 25 sec are required. The maximum power that can be measured is 150 watts.

The load consists of a 9-in. section of coaxial line with a 50-mil Cromax-wire center conductor and water dielectric, short-circuited at the terminal end. The water flows between the inner and outer conductors and serves to carry away the heat and to indicate the quantity of heat in terms of temperature rise. Attenuation in power is produced by ohmic losses in the center conductor and by dielectric losses in the water.



Since the dielectric constant of water is very high, the electrical length of the 9-in. section of line is much greater than its physical length. Thus, although the loss per wavelength is small in the water, the number of wavelengths is sufficient to produce the total attenuation required. The high dielectric constant of water would require a conductor-diameter ratio of 1800:1 for a 50-ohm line. Since this is impractical, a 6-in. exponential dielectric taper of titanium dioxide fired to the same dielectric constant as water is used to effect a transformation from the 50-ohm impedance of input line to that of the water-dielectric line. The exponential taper is such as to provide a constant change in impedance per wavelength. In order to correct for the variation in the dielectric constant of water with temperature, another taper, 2 in. long, extends into the water from the point of maximum diameter of the first taper, *i.e.*,

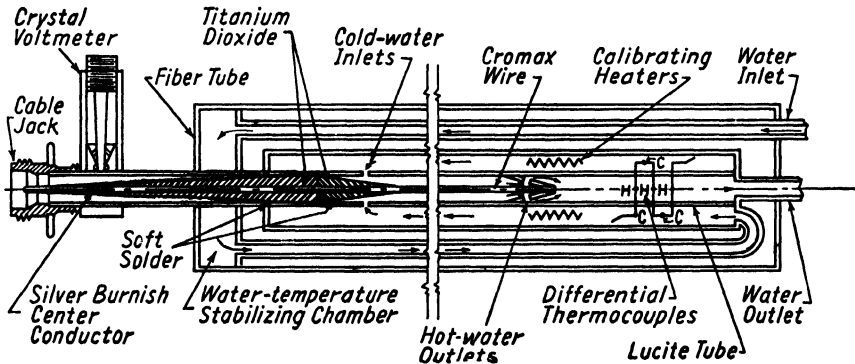


FIG. 24-13.—Wattmeter, with coaxial-line water-dielectric calorimeter.

the inner diameter of the outer conductor, to the diameter of the Cromax center conductor (see Fig. 24-13). Connections to the titanium dioxide that are both watertight and electrically good are made by applying a silver burnish to the oxide and soft-soldering to it. Silver burnish also serves for the center conductor inside the titanium dioxide tapers.

A closed water-circulating system with a pump, radiator, and flow indicator is used. A differential thermocouple having three hot and three cold junctions is used with a microammeter to measure the temperature rise in the water. A calibrating unit operating on 110-volt 60-cycle power is built into the system. To facilitate tuning the transmitter, a crystal voltmeter is incorporated in the input r-f section of the wattmeter. This device gives instantaneous readings of relative power.

Titanium dioxide, after it is fired, has a hardness of the order of 9 on the Brinnell scale, which makes fashioning difficult. The tapers for the wattmeter should, therefore, be shaped while the substance is in the chalky prefired state, allowances being made for shrinkage. The

mixture used for making the tapers for this wattmeter was prepared by the Laboratory for Insulation Research at the Massachusetts Institute of Technology, and firing was done there. It was found impractical to mold the center conductor inside the titanium dioxide, so instead a hole of the proper size was formed in the extruding operation. This was then silvered by drawing silver paste through it and baking. Figure 24-14.

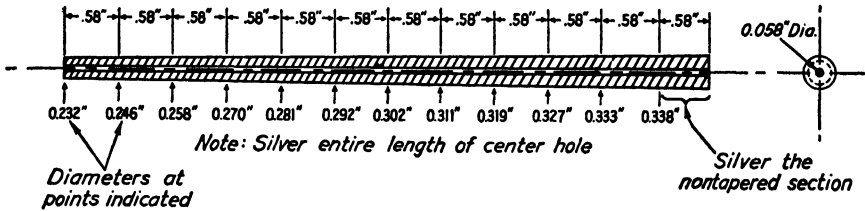


FIG. 24-14.—Titanium dioxide taper (dimensioned) for use with wattmeter of Fig. 24-13.

gives the dimensions, before firing, of a taper that, when used in a cylindrical outer conductor having an inner diameter equal to the maximum diameter of the tapered section, gives a constant change in impedance per wavelength.

Another calorimeter wattmeter suitable for powers between 25 and 1500 watts in the frequency band 250 to 800 Mc is shown in Fig. 24-15. The reading time is about 45 sec, accuracy 10 per cent, and weight 25 lb. Calibration is made on 60-cycle power. A crystal voltmeter (Sec. 24-27)

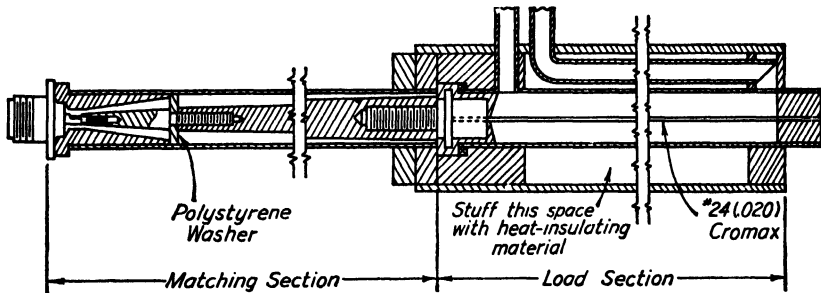


FIG. 24-15.—Wattmeter, with coaxial-line water calorimeter.

may be added to give instantaneous readings of relative power output as a convenience in tuning. The wattmeter is rugged, quick-reading, and fairly accurate.

The power-dissipating element consists of a 34-in. length of attenuating coaxial line short-circuited on the terminal end. The outer conductor is a brass tube 1 in. in diameter, the inner conductor a No. 24 Cromax wire. Water flowing between the two conductors forms the dielectric and also serves to measure the power dissipated. The attenuation per wavelength is about 1 db but, because of the high dielectric constant of

water and the resulting number of wavelengths in the given physical length, the total attenuation one way is more than 10 db at 500 Mc. Under these conditions the imaginary component of the characteristic impedance of the line is negligible and the input impedance essentially real and constant over the required frequency range. A taper is used to match the impedance of the water-filled coaxial line, 10 ohms, to the 50-ohm input cable.

**24-14. Salt-water Loads.**—The coaxial calorimeter wattmeter shown in Fig. 24-16 will dissipate 1 or 2 kw of power at frequencies of a few

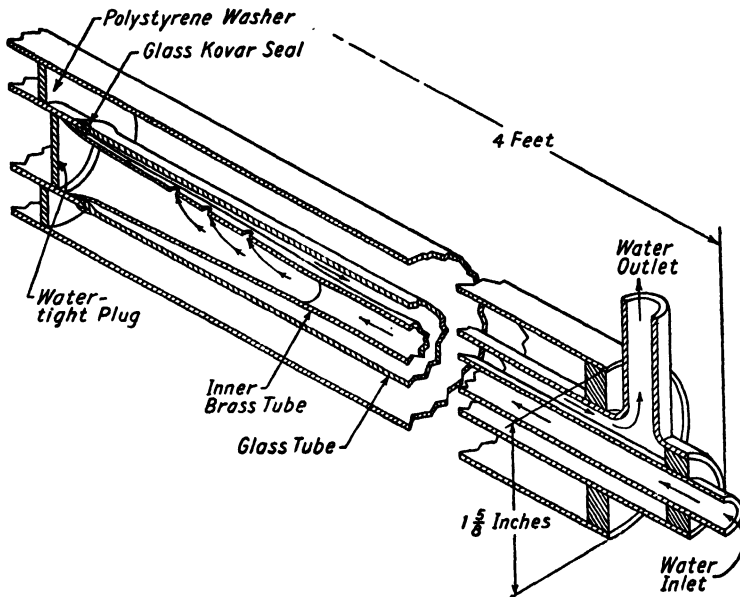


FIG. 24-16.—Wattmeter with a 2-kw salt-water calorimeter.

hundred megacycles. The power is absorbed by the salt water that enters through the hollow center conductor and, in the vicinity of the glass-Kovar seal, passes out through holes to the outer water jacket and returns through the space between the center conductor and the glass tube to the end from which it started. This load gives a low standing-wave ratio over a very broad frequency band without requiring tuning adjustment. It is probably capable of handling considerably more power than 2 kw.

A type of salt-water load that is very convenient for measuring the power output of parallel-line oscillators is shown in Fig. 24-17. The load consists of the salt water contained in a short length of glass tubing. Connection is made to the lines through conducting terminals sealed to

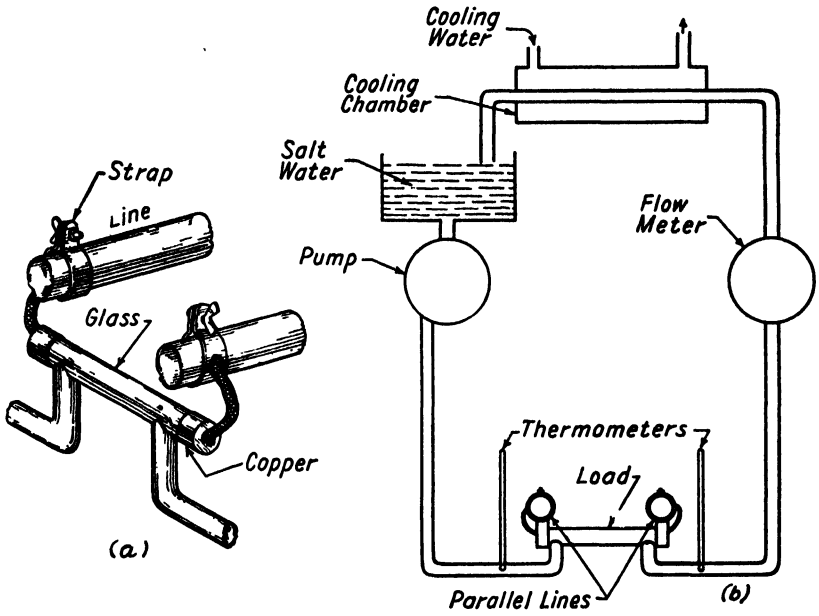


FIG. 24-17.—Salt-water load for parallel-line oscillators.

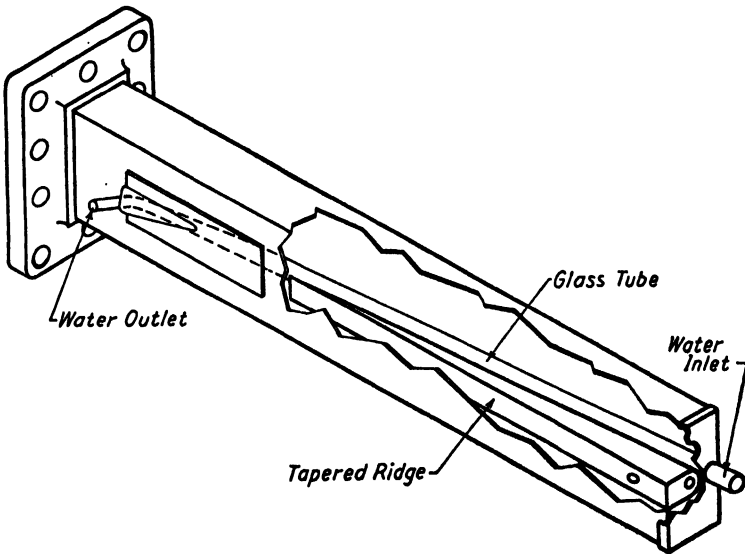


FIG. 24-18.—Wide-band calorimeter load for waveguide.

the tube by means of metal-to-glass seals. The salt water is circulated through the load, a flow meter, and a cooling coil by means of a circulating pump. At a known rate of salt-water flow the power dissipated in the load is measured by the temperature difference of the water on the two sides of the load. Calibration is accomplished either by dissipating known amounts of low-frequency or d-c power in the load, or by substituting for the load another tube containing a resistance coil in which measured amounts of low-frequency or d-c power may be dissipated.

**24-15. Calorimeter Load for Waveguide.**—The device shown in Fig. 24-18 was designed at the Radiation Laboratory for use in the 3000-Mc region. It consists of a piece of  $1\frac{1}{2}$ - by 3-in. waveguide about 20 in. long closed at the end opposite the source of power. A glass tube enters through the middle of the 3-in. side and passes obliquely through the guide and out at the end. The power is carried off by the water in this tube. A metal ramp or ridge is placed between the glass tube and one wall of the guide. This ridge tapers the impedance of the guide to a lower value and at the same time concentrates the field in the vicinity of the water. This effect produces sufficient attenuation so that ordinary city water can be used and the standing-wave ratio will not exceed about 1.1:1 over the band from 8 to 11 cm. If the load is used with a circulating water system, the performance can be improved by adding a little salt to the water. Since the volume of water in the glass tube is quite small, it will respond very quickly to changes in power level.

**24-16. Quick-response Calorimeter for Large Waveguide.**—The load and calorimeter shown in Fig. 24-19 were designed for use in large waveguides at frequencies at which the calorimeter type of water load described above would have excessive size and thermal capacity. It will measure kilowatts of power, and the response is very rapid. The guide has a cross section 6 by 15 in. The glass tube that carries the salt water is about 1 in. in diameter and can be moved back and forth with respect to the end plate on the waveguide. If the salt-water conductivity is properly adjusted, the load will approximately match the guide impedance when the glass tube is a quarter of a guide wavelength from the end plate. In general, however, if a good match is desired, the load must be tuned by means of the plunger whenever the frequency or the water temperature is changed.

A modification of this device, which will handle a more limited amount of power, consists of a Globar resistor inside the glass tube. These resistors are made in the form of a tube from a ceramic type of material. The Globar resistor is slightly smaller than the glass tube, so that the water cools both the inner and outer surfaces, and should be at least as long as the portion of the glass tube inside the guide. Since the water serves merely as a cooling medium, the salt is no longer needed. Elimina-

tion of the salt solution simplifies the system, since tap water may then be used and the water pump and heat exchanger eliminated.

It was found that when the resistor was placed in the center of the guide, as in the case of the salt-water tube in Fig. 24-19, a good match could not be obtained unless a great deal of compensation was applied by means of the tuning plunger. This was because the available types of Globar tubes did not have a resistance high enough to match the impedance of the waveguide. To avoid using compensation from the tuner, which was very frequency sensitive, means were provided for moving the resistor from the center toward the edge of the guide where a more broadband match could be obtained.

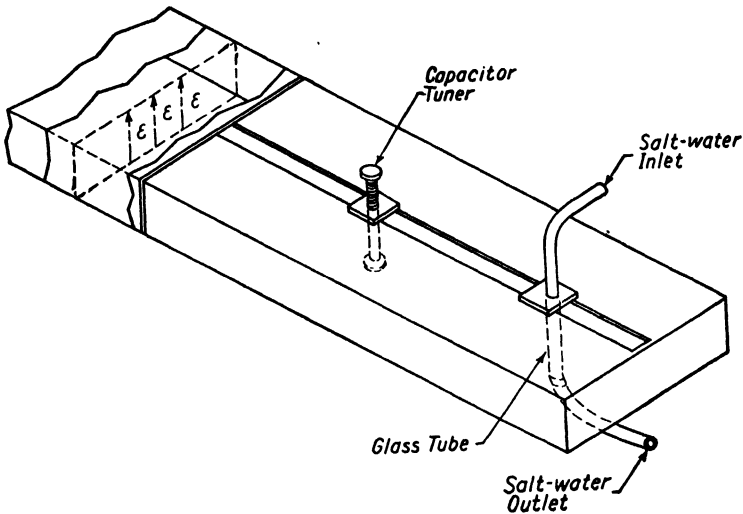


FIG. 24-19.—Tunable water-load assembly for large waveguide.

**24-17. Sloping-guide Water-load Calorimeter.**—Satisfactory power measurements may be made by placing thermometers and a flow gauge in the water-circulating system of the dummy load shown in Fig. 24-1. The reading time is long, since considerable time is required for the water to reach thermal equilibrium. In calibrating a wattmeter or bolometer, this time lag is not objectionable, but the device would not be satisfactory as an indicator for tuning an oscillator. This calorimeter is best suited to high power levels because of the relatively large amount of water used.

**24-18. Slotted Coaxial Lines.**—A slotted coaxial transmission line, such as is used for making measurements of standing-wave ratios, may be used for measuring relative power transmitted along the line. Any amount of power may be monitored, and very little power is lost in the

process. It can be shown that the power transmitted through a coaxial transmission line is

$$P = \frac{E_{\max}E_{\min}}{Z_0} \quad (24-11)$$

in which  $P$  is the power in watts,  $Z_0$  the characteristic impedance of the line, and  $E_{\max}$  and  $E_{\min}$  are the maximum and minimum voltages across the line, expressed in rms volts. Since the probe in the slotted line indicates voltages proportional to the actual line voltages, Eq. (24-11) becomes, for a given line,

$$P = KE_{\max}E_{\min} \quad (24-12)$$

where  $K$  is a constant.

If a square-law crystal is used with a current meter for indicating the maximum and minimum voltages along the line, the power is

$$P = K'(I_{\max}I_{\min})^{1/2} \quad (24-13)$$

where  $K'$  is a constant and  $I_{\max}$  and  $I_{\min}$  are crystal currents. In order to read actual power it is then necessary to determine the values of  $K$  or  $K'$  for the particular apparatus used. This may be done by comparison with an r-f power meter, such as one of the calorimeter types reading power in absolute units.

The errors inherent in slotted-line measurements of power may amount to about 10 per cent and are caused mainly by aging of rectifier crystals, inaccuracies of tuning of probe systems, variation of response of probe and detector with frequency, and setting errors between calibration and use.

**24-19. Notched Coaxial Lines.**—A notched coaxial cable is a cheap and easily made substitute for a slotted line and is satisfactory for measurements not requiring great accuracy. It is made by notching or cutting through the outer covering, outer conductor, and dielectric of a solid-dielectric coaxial cable so as to expose the inner conductor. The protective covering should also be removed around each notch to expose the braided outer conductor. There should be about 10 notches per wavelength in the cable.

Voltage measurements may be conveniently made by means of a "pin stick" or r-f voltmeter, shown in Fig. 24-20, applied to the notches in succession. The telescopic line of the pin stick should be adjusted for maximum impedance at the open end of the telescoping line. This may be most satisfactorily done by holding the probe or open end of the line near a source of r-f power at the operating frequency and adjusting the line for maximum meter deflection. This source may be the field near an antenna or the tank circuit of an oscillator. If the source is too weak, the probe may be adjusted on the notched line itself. The center pin of

the probe is pressed against the center conductor of the line, and the outer-conductor contact clips against the outer braid of the notched line. When the telescoping coaxial line of the probe is properly adjusted, the deflection of the meter will be the same when the probe is very close to the center conductor of the notched coaxial line as when it is actually in contact. By very close is meant distances of the order of a millimeter for a cable transmitting about 5 watts of power.

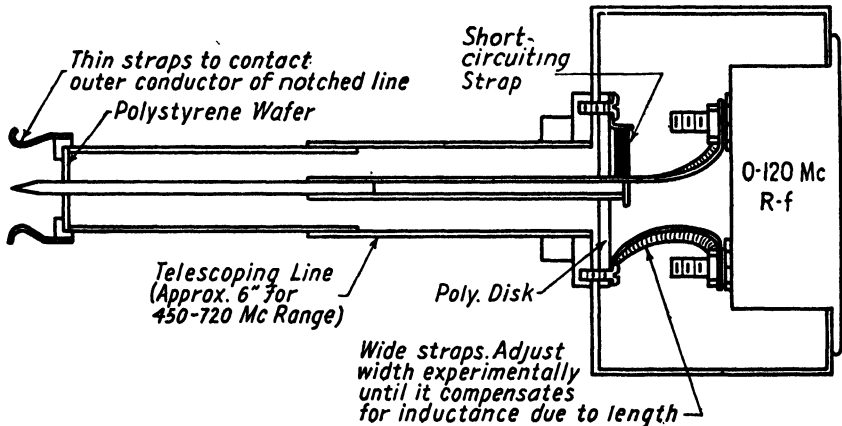


FIG. 24-20.—R-f voltmeter with "pin-stick" probe.

**24-20. The Thermistor.**—A thermistor unit ordinarily consists of a small hard bead composed of certain oxides and resins, supported between two small leads or terminals. This unit may be used as an r-f load to dissipate small amounts of power. The resulting rise in temperature causes a change in the resistance of the unit, usually in the negative direction, which may be used as a measure of the power dissipated. The change in resistance may be measured by a bridge, one leg of which includes the thermistor bead. A description of the thermistor bridge and a discussion of its use may be found in Sec. 35-11.

Since the amount of power that may be dissipated in a thermistor bead is of the order of milliwatts, some sampling device, such as a directional coupler (Sec. 24-22) or an attenuator of known characteristics, *e.g.*, a length of lossy cable, must be used when large amounts of power are to be measured. The thermistor bridge is particularly useful for measurements on microwaves at low power levels because of the very small dimensions possible in the unit. It is stable, rugged, convenient, and accurate.

**24-21. The Bolometer Bridges.**—A typical r-f bolometer consists of a resistance element, often a Littelfuse, in which the r-f power to be measured is dissipated, arranged as one arm of a bridge. The change in resistance of this element is then a measure of the r-f power.



Since the resistance element may be small and can be incorporated as part of an r-f system, the r-f bolometer is a very satisfactory device for use on microwaves as well as for lower frequencies. The response is linear in power, and the device itself may be made rugged, stable, accurate, and reasonably sensitive. Like the thermistor bridge (Sec. 24-20) it must be used with a sampling system or a power attenuator. The bolometer bridge is discussed in Sec. 35-11.

**24-22. Directional Couplers.**—A directional coupler is a device which, when attached to a waveguide or a coaxial line, gives indications of the power flowing in one direction regardless of the presence of power flowing in the opposite direction. Thus the response is independent of standing waves caused by reflections from the termination of the guide or line. This feature, which enables it to distinguish between the power that is flowing away from a transmitter and the power that has been reflected back, has led to a number of important applications.

The most important advantage of a directional coupler in the measurement of power is due to the fact that its response is independent of its position with respect to the maximums and minimums of the standing-

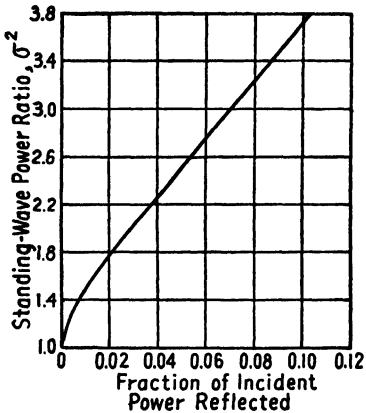


FIG. 24-21.—Effect of reflection of incident power on power measurements.

wave pattern in the guide. In making power measurements with an ordinary type of probe that does not have directional characteristics, a slotted section is usually necessary in order to obtain the maximum and minimum readings. This is often very inconvenient and may also lead to errors. The curve of Fig. 24-21 shows how a low-power reflected wave in the transmission line can result in a large variation in the power picked up by the ordinary type of probe. For instance, a reflected wave that represents only 1 per cent of the power transmitted can set up a standing wave so large that the ordinary type of capacitance probe will pick up 50 per cent more power

when it is near a maximum than when it is near a minimum. When a directional coupler is used in the same situation, the presence of this 1 per cent reflected power will produce an error of only 1 per cent.

Spectrum-analyzer measurements usually require some means of obtaining a small sample of power from a transmission line. The purpose of spectrum analyses is to determine the relative power distribution over a band of frequencies, and the sample taken from the transmission line should have the same distribution as the power being delivered to a load

or antenna. With the ordinary nondirectional pickup, this sample is apt to be quite misleading, because the positions of the maximums and minimums change rapidly with frequency. This is especially important if the line is long in terms of wavelengths. Thus for some frequencies in the spectrum the probe may be at a standing-wave maximum, and for other frequencies it may be at a minimum. When a directional coupler is used for spectrum measurements, there is no error due to the frequency sensitivity of the transmission line.

A directional coupler is also useful for matching a load to a transmission line. If it is oriented so as to respond only to the reflected power, it is easy to "tune" the load or to adjust the impedance until the reflection is a minimum. This arrangement can also be used to operate a warning device or an interlock to protect an oscillator tube from damage when the reflected power is too large.

Unidirectional couplers do not measure power from the guide or coaxial line directly. They take a portion of the total power which may be used as a measure of the magnitude of the total power flowing in one direction in the guide or line. It is therefore necessary to calibrate the device by means of a calorimeter wattmeter or other absolute power-measuring system. Furthermore, the power flow in each direction must be measured in order to determine the net power going into the load.

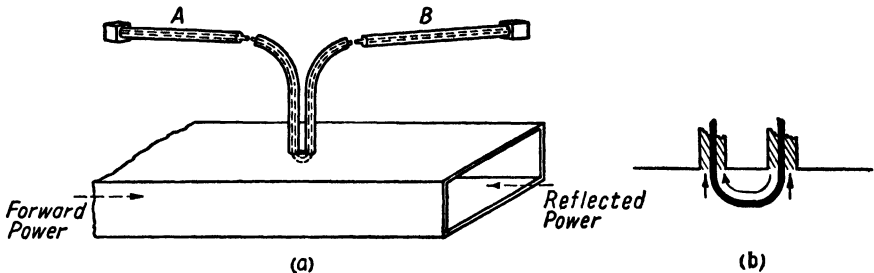


FIG. 24-22.—Capacitive-loop directional coupler.

**24-23. Capacitive-loop Directional Coupler.**—This type of coupler was designed to operate over a relatively wide frequency band. It consists of a small loop projecting into a waveguide, as shown in Fig. 24-22. Each end of the loop is connected to a length of 50-ohm lossy cable which has enough attenuation so that its input impedance is essentially a pure resistance. When the device is in operation, the current in cable *A* is caused by the wave that is traveling toward the right in the transmission line and that in cable *B* by a wave, such as a reflection from the load, traveling to the left.

This type of coupler is directive because the loop is acted upon by both the electric and the magnetic field of the wave in the guide. The

current due to the electric field has the same phase in both cables, while that due to the magnetic field is always in the opposite direction in cable *A* from that in cable *B*. Thus, for a wave traveling to the right in the guide, the currents add in cable *A* and subtract in cable *B*, as shown in Fig. 24-22*b*. If the current produced by the electric field is equal to that produced by the magnetic field, cancellation will result in cable *B*. For a wave traveling to the left in the guide, the cancellation will be in cable *A*.

For satisfactory directional properties, the following relations must obtain:

1. The loop must be small compared with  $\frac{1}{4}$  wavelength.
2. The reactance of the loop due to its uncoupled self-inductance should be small compared with the characteristic impedance of the cables.
3. The geometry of the loop must be such that the current caused by the electric field has the proper magnitude and phase with respect to that caused by the magnetic field.
4. The ends of the loop must each be terminated in a pure resistance (such as a length of lossy cable).

A more detailed explanation of the directional effect in the loop may be gained from the vector diagram and equivalent circuits of Figs. 24-23 and 24-24. This is a linear system and can be analyzed on the basis of superposition. The two voltage sources and their equivalent circuits can each be considered separately and then superimposed to find the resulting effect. When a traveling wave passes the loop, the maximum of the  $\mathcal{E}$  and  $\mathcal{H}$  fields occur simultaneously, but the voltage due to  $d\mathcal{H}/dt$  is 90 deg out of phase with the voltage of the  $\mathcal{E}$  field. This phase difference would seem to prevent effective cancellation of the currents in one or the other of the cables. However, this is not necessarily true.

Figure 24-23 is an equivalent circuit and vector diagram for the currents due to the  $\mathcal{H}$  field. This circuit contains a generator giving a voltage proportional to  $d\mathcal{H}/dt$  and having an internal impedance  $X_L$  which is caused by the self-inductance of the loop. The resistances  $R_a$  and  $R_b$  represent the characteristic impedances of the two cables which are in series as far as this circuit is concerned. The principal impedance in this circuit is resistive, because of the lossy cable, and the current is nearly in phase with the generator voltage, or nearly 90 deg ahead of the voltage in the waveguide. The angle  $\alpha$  is caused by the self-inductance of the loop. The dotted vector  $I_b$  is included to indicate that the currents induced in the two cables will be in opposite directions.

Figure 24-24 shows the circuit for the electric field. The generator in this circuit produces a voltage proportional to the electric field in the guide. The capacitance between the loop and the opposite wall of the

guide is represented by  $C_1$ , while  $C_2$  represents the capacitance between the loop and the adjacent wall of the guide. In this circuit, the two resistances  $R_a$  and  $R_b$  are in parallel. Since the impedance of  $C_1$  is very much higher than the other impedances in the circuit, the current  $I'_0$  will be nearly 90 deg ahead of the generator voltage. The angle  $\alpha'$  between  $I'_0$  and  $I'_a$  is caused by the shunting effect of the capacitance  $C_2$ .

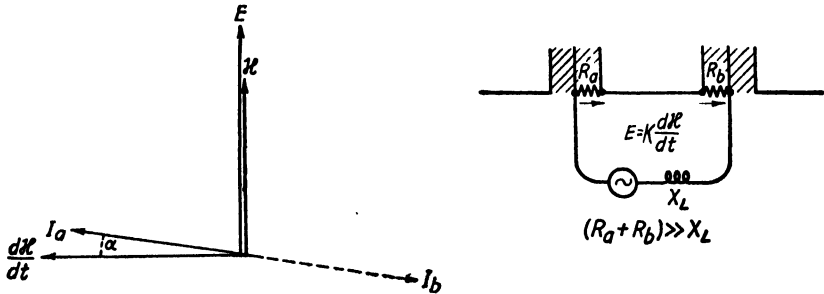


FIG. 24-23.—Equivalent circuit and vector diagram for currents due to magnetic field.

From these two vector diagrams it can be seen that the currents in  $R_a$  caused by the two generators will be approximately either in phase or 180 deg out of phase. The same is true for  $R_b$ . Thus, for a wave traveling a given direction there will be cancellation in one of the cables if the magnitudes are equal and opposite. These relative magnitudes can be adjusted by changing the area or shape of the loop or by adjusting

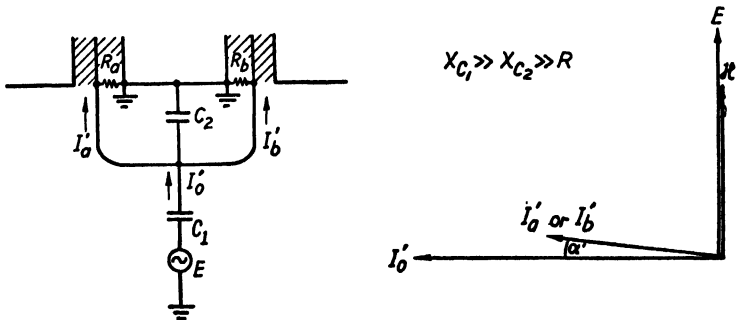


FIG. 24-24.—Equivalent circuit and vector diagram for currents due to electric field.

the width of the conductor from which the loop is made. Then the angles  $\alpha$  and  $\alpha'$  can be made equal by adjusting the value of  $C_2$ .

Satisfactory operation of this coupler requires that the ratio of the transverse components of the  $\mathcal{E}$  and  $\mathcal{H}$  fields remain substantially constant. When the coupler is used with ordinary rectangular waveguide, the band width is limited by the variation in guide impedance. This guide impedance varies rapidly at frequencies near cutoff, but at frequencies remote from cutoff it approaches a constant value. The cutoff

frequency can be reduced to less than one-third of the normal value by placing a tapered ridge inside the waveguide, as in Fig. 24-25. If the taper of this ridge is properly designed, it will not introduce appreciable reflections. At the crest of the ridge, where the coupler is located, the guide wavelength and the impedance are nearly the same as in free space, and the variation in impedance is insignificant over a considerable fre-

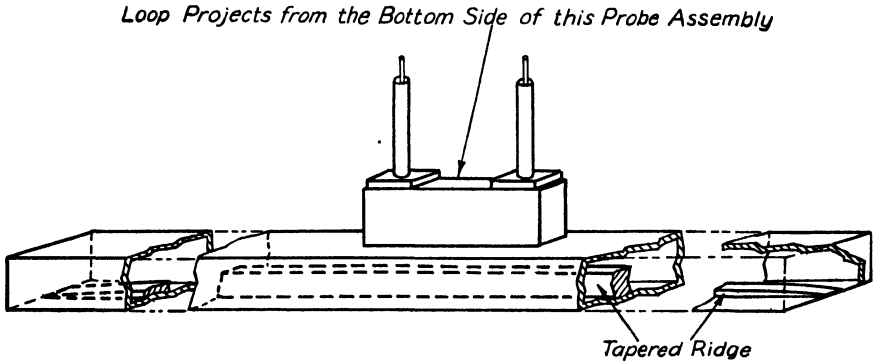


FIG. 24-25.—Waveguide with tapered ridge.

quency range. The probe does not need to be centered with respect to the width of the guide and can be moved toward the edge to keep it clear of the ridge.

The vector relations of Figs. 24-23 and 24-24 are not sensitive to frequency changes. The requirement that  $X_{c1}$  be large compared with the parallel resistance of the two cables is not hard to meet, since  $X_{c1}$  will be of the order of 3000 ohms while  $R_a$  and  $R_b$  in parallel are 25 ohms. In Fig. 24-23, the angle  $\alpha = \tan^{-1} \omega L / (R_a + R_b)$ , and in Fig. 24-24 the angle  $\alpha' = \tan^{-1} (R_a \omega C_2) / 2$ . Both of these angles increase with frequency at the same rate so that if they are equal at one frequency they will be equal at other frequencies. This is also true in regard to the magnitudes of the vectors, since the voltages caused by both the  $\mathcal{E}$  and  $\mathcal{J}C$  generators

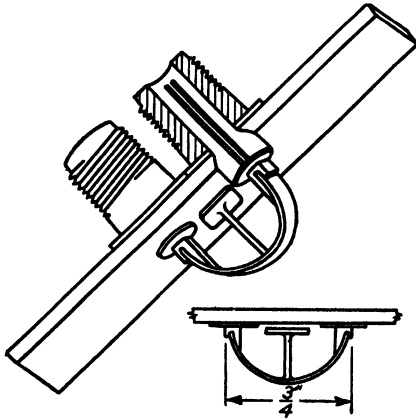


FIG. 24-26.—Directional coupler suitable for operation at 500 Mc in very large waveguide.

increase with frequency at the same rate and the requirements for cancellation are maintained. Although the directional properties do not change with frequency, the voltage output does change. This is not

objectionable for many purposes, but if necessary the change in attenuation of the lossy cables can be adjusted to compensate for the change in probe response, so that the voltage at the end of the cables does not change by more than  $\pm 0.25$  db over a frequency range of 2 to 1.

A coupling loop suitable for operation at 500 Mc is shown in Fig. 24-26. It was used in a waveguide that had a cross section of 6 by 15 in. The cables are attached to the two type-N chassis connectors that also support the loop. A loop suitable for operation at 3000 Mc was used as part of a wattmeter to monitor the power output of a c-w magnetron that had a tuning range of 8 to 12 cm. Type-N fittings could not be used in this model because they introduced reflections at certain frequencies.

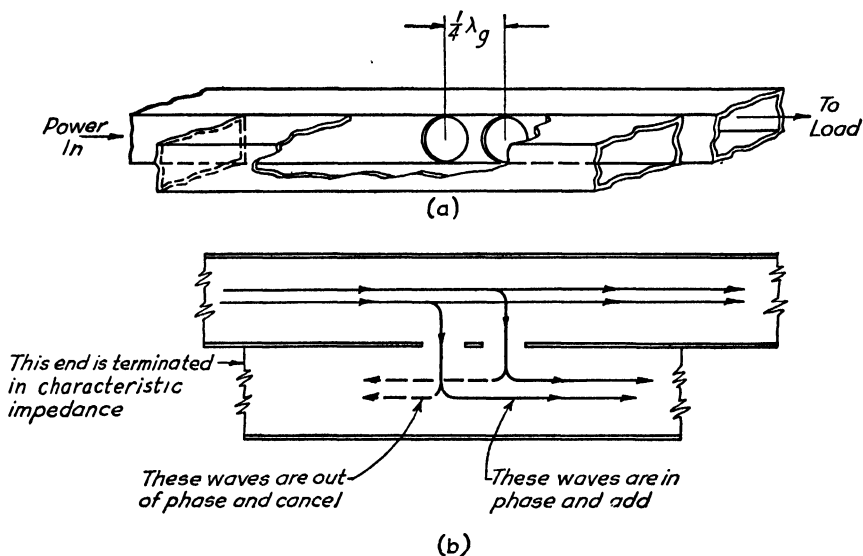


FIG. 24-27.—Two-hole directional coupler.

The cables were therefore not detachable from the coupler assembly, and the loop was soldered directly to the center conductors so that there were no electrical discontinuities. The ends of the loop were bent inward so as to increase their capacitance to the surrounding metal surface.

**24-24. Two-hole Directional Coupler.**—This type of directional coupler, which was developed at the Bell Laboratories, is shown attached to a waveguide transmission line in Fig. 24-27a. The principle may, however, also be applied to a coaxial line. The auxiliary section of guide is coupled to the main section by two holes that are spaced a quarter of a guide wavelength apart. The magnetic field in the main guide fringes out through these two holes and sets up waves in the auxiliary section of guide. The waves in the auxiliary section of guide will travel in the same direction as in the main section for the following reason. The waves

that follow the paths shown by the solid lines in Fig. 24-27*b* travel the same distance and are in phase, whereas the waves that travel the paths shown by the dotted lines are 180 deg out of phase because one of them has traveled  $\frac{1}{2}$  wavelength farther than the other. Since they have the same magnitude, they will cancel each other.

If there is a reflected wave in the main guide, it will travel toward the left in the auxiliary section. For most applications, one end or the other of this auxiliary section will be connected to some measuring apparatus. It is necessary to terminate the opposite end in its characteristic impedance to prevent reflections that would destroy the directional properties.

This type of coupler is ordinarily satisfactory for frequency ranges of the order of 10 per cent. By using three or more holes instead of two, the band width can be increased. The power in the auxiliary section of guide is at least 18 to 20 db down from the power in the main guide.

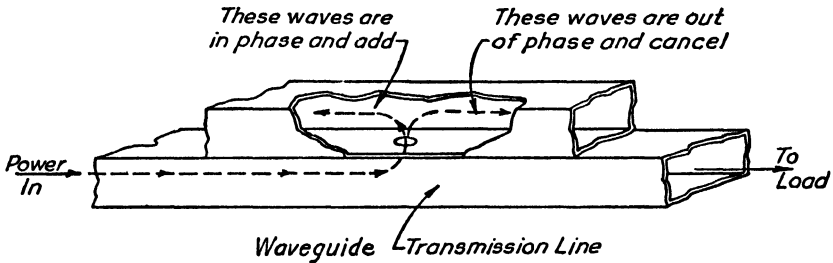


FIG. 24-28.—Bethe hole directional coupler.

**24-25. Bethe Hole Directional Coupler.**—This type of directional coupler shown in Fig. 24-28 is a development of the Radiation Laboratory. The lower piece of waveguide is the transmission line carrying r-f power. The upper, or auxiliary, section of guide is electrically coupled to the lower one by a hole in the middle of the wide face. When power is flowing through the transmission line, a small amount leaks out through the hole and sets up waves in the auxiliary section of waveguide. The waves that are set up in this auxiliary section, however, tend to travel in the opposite direction from those in the transmission line.

In order to understand this effect, assume a forward wave in the transmission line from the generator on the left to the load on the right. It may also be assumed that coupling between the guide transmitting the power and the auxiliary guide is produced by both the electric field and the magnetic field and that each gives rise to a wave traveling to the right and another to the left in the auxiliary guide. If the strength of the electric coupling is properly related in magnitude to that of the magnetic coupling, the electric components of the two waves will be equal, as will the magnetic components. The directions of the two fields fringing from

the lower guide into the upper, or auxiliary, guide are such that the two waves propagated to the left in the auxiliary guide will add, while those to the right subtract, or cancel each other if they are of equal strengths. Thus, for a wave transmitted to the right in the primary guide the combined coupling results in a wave to the left in the auxiliary guide, but none to the right. For a wave directed to the left in the lower guide, caused possibly by reflections from the load on the right-hand end, the effect in the auxiliary guide is reversed. The same conclusion may be reached by representing by a Poynting vector the direction of propagation of a wave produced by the combined electric and magnetic fields in the auxiliary guide near the hole. It will be found that, in the example given, the relative directions of the two fields are such as to cause a flow of

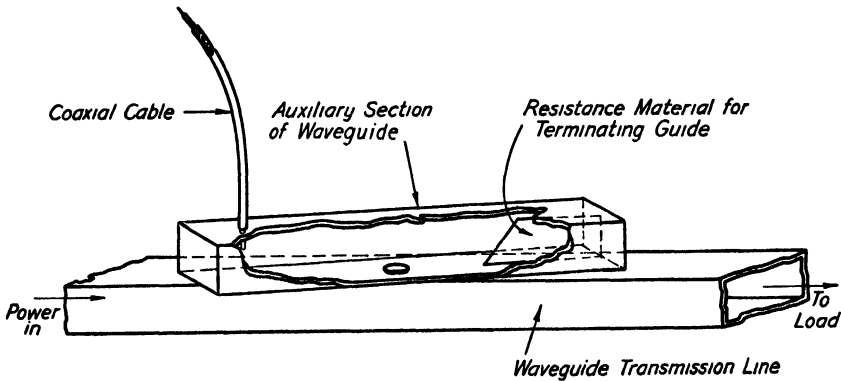


FIG. 24-29.—Bethe hole coupler with rotatable auxiliary section of waveguide.

energy only to the left for a wave directed to the right in the lower guide, provided that the strengths of the two fields are properly related.

The relative magnitudes of magnetic and electric coupling can be adjusted in several different ways, but these magnitudes change with frequency and the adjustment is limited in band width. The geometry shown in Fig. 24-28 produces complete cancellation of the wave in one direction only when the free-space wavelength is  $\sqrt{2}$  times the width of the guide, but it is easy to alter this geometry to obtain cancellation at other wavelengths. One method is to rotate the auxiliary section of guide with respect to the main section, as in Fig. 24-29. This changes the coupling due to the transverse component of the magnetic field without changing the coupling due to the electric field. Other possible methods are to change the shape of the hole or to change the dimensions of either section of waveguide.

Figure 24-29 also shows the arrangement that is ordinarily used for connecting a coaxial cable to the output of this coupler. It is necessary



that the end of the auxiliary section of guide opposite the end to which the cable is connected be terminated in its characteristic impedance, otherwise there will be reflections that will destroy the directional properties of the coupler. This reflectionless termination is obtained by means of a piece of carbon-impregnated resistance material that resembles cardboard. The size of this terminating strip is rather critical and depends on the frequency at which it is to operate. The coupling between the waveguide and the coaxial cable is by means of a capacitance probe. This probe should be designed so as to match the impedance of the cable to that of the waveguide. This matching is desirable because the measuring apparatus will seldom match the impedance of the cable, so that in general there will be standing waves present on the cable. These standing waves will not disturb the measurements, provided the cable is matched at the waveguide end. If the cable is not matched at either end, there are reflections from both ends and the cable becomes a resonant system. A slight change in frequency may then produce a large difference in the voltage at the output end of the cable. An alternative to matching the cable to the waveguide is to use a length of lossy cable that has enough attenuation to prevent multiple reflections. However, the lossy line introduces about a 15-db attenuation into the system, and inasmuch as the output of the coupler is already down about 25 db from the power in the transmission line, the resultant output is too low for many purposes.

#### **24-26. A Broad-band Monitoring-type Wattmeter for Waveguides.**

The directional coupler described in Sec. 24-23 may be used as the basis of a direct-reading wattmeter. This wattmeter is of the monitoring type, which measures the power being delivered to the antenna, and is to be distinguished from the dummy-load type, which measures the power that is absorbed. The unit shown in Fig. 24-30 was used with a 1-kw magnetron transmitter that had a tuning range of 8 to 12 cm. Over this range the calibration of the wattmeter was substantially flat.

The advantages of a directional coupler for power-measuring applications were discussed in Sec. 24-22. It was pointed out that difficulties due to maximums and minimums of the standing-wave pattern are greatly reduced if only the power in the forward direction is measured. As long as the standing-wave ratio is reasonably low, the power flowing in the forward direction is approximately the same as the power delivered to the load, and the power in the reflected wave can be neglected. For instance, if the voltage standing-wave ratio is 1.2:1, the error caused by neglecting the reflected power is less than 1 per cent. If the standing-wave ratio is 1.5:1, the error is 4 per cent. Probably this amount of error can be tolerated in most applications, but if the error becomes too large it is possible to arrange an automatic compensation.

The wattmeter shown in Fig. 24-30 was designed to make this compensation by subtracting the reflected power from the power flowing toward the load. This is accomplished by means of two thermocouples. The heating of one of these thermocouples is caused by the power in the forward wave in the transmission line, while the heating of the other is due to the power in the reflected wave. The d-c output voltages of these thermocouples are made to subtract. The resulting voltage is then proportional to the net power delivered to the antenna. Figure 24-30 shows also how the thermocouple junctions are soldered across the ends of the cables. The d-c blocking capacitor is built into the outer conductor of the cable in such a manner as not to disturb the r-f circuit. It is, of

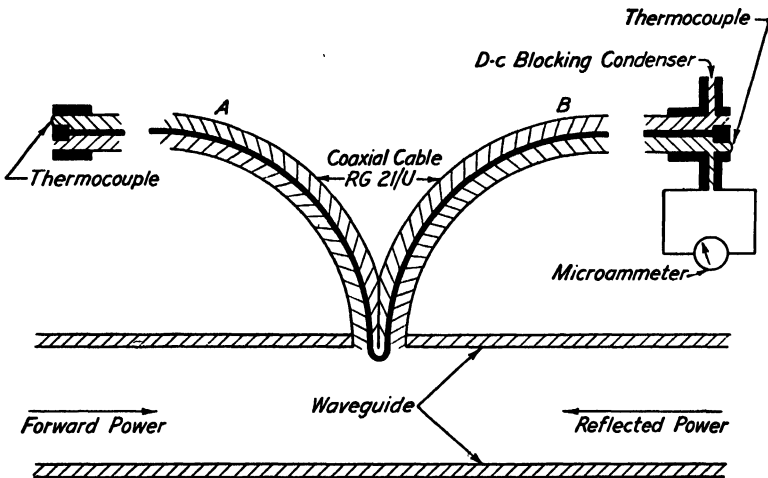


FIG. 24-30.—Broad-band monitor-type wattmeter for waveguides.

course, desirable that the two thermocouples have the same sensitivity. Otherwise one of them must be shunted with a choke-and-resistance combination.

In many applications for which this wattmeter was used, the standing-wave ratio was low enough so that the use of the thermocouple on cable B resulted in no significant increase in accuracy, and it was omitted in the interest of simplicity. Since the d-c blocking capacitor was then no longer needed, the microammeter was connected across the end of cable B. Although the u-h-f attenuation of the cables used was approximately 15 db, the d-c resistance was only a few ohms and did not interfere with the d-c currents. There was never enough u-h-f current at the end of the cable to disturb the microammeter.

It is desirable that the meter be calibrated in terms of watts per division and that this calibration be independent of frequency over the required range. To make the calibration independent of frequency,

there must be compensation for the effect of frequency upon (1) voltage picked up by a probe or loop, (2) attenuation of the solid dielectric cable, (3) guide impedance, (4) inductive reactance of the wires forming the thermocouple, and (5) skin depth and r-f resistance of the thermocouples.

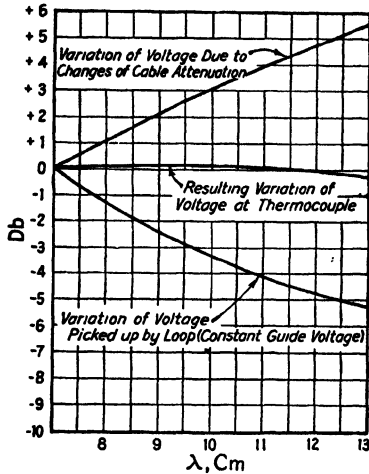


FIG. 24-31.—Frequency compensation produced by proper length of cable.

The first two effects oppose each other and by proper choice of length of cable good compensation can be secured over a fairly wide frequency range. Figure 24-31 shows the effectiveness of 15 ft of RG-21/U cable in providing this compensation over the wavelength range from 7 to 13 cm. The lower curve shows the variation with frequency of the voltage picked up by the loop of the directional coupler when the field strength in the waveguide is held constant. The top curve shows the frequency variation of the voltage at the thermocouple end of the cable if the voltage at the input end of the cable is held constant. The center curve shows the effective way in which these two

variables compensate one another. The slope of the upper curve is determined by the length of the cable. In this particular application a 15-ft length of RG-21/U cable produced the right slope for the best compensation.

Changes in guide impedance tend to affect not only the field strength but also the directional properties of the coupler. These effects may be

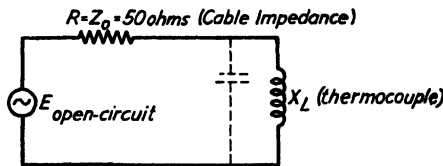


FIG. 24-32.—Equivalent circuit of cable and thermocouple.

minimized by means of the tapered section of ridge waveguide, as discussed in Sec. 24-23.

The thermocouple consists of a spot-welded junction between a piece of nichrome wire 0.001 in. in diameter and a piece of constantan wire of the same size. One end of this junction is soldered to the center conductor of the coaxial conductor and the other end to a brass ring that is attached to the outer conductor. These two supports for the thermocouple are about  $\frac{1}{16}$  in. apart so that the inductive reactance is of the

order of 25 ohms. The frequency sensitivity of this arrangement can be analyzed from the equivalent circuit of Fig. 24-32, based on Thevenin's theorem. Inasmuch as the resistance of the thermocouple is less than 10 per cent of the reactance, it can be neglected. When the reactance is small enough compared with 50 ohms, it too can be neglected, but at frequencies over 3000 Mc it begins to produce a noticeable effect and should be compensated. The dotted capacitor in Fig. 24-32 represents the capacitance of the two supports of the thermocouple. If this capacitance is adjusted to the proper value, it will greatly reduce any frequency sensitivity caused by inductive effects.

Skin effect does not cause trouble if the distance of penetration of the current into the wires forming the thermocouple junction is large compared with the radius of the wire. In the thermojunction described above, which has a wire diameter of 0.001 in., a certain amount of skin effect is present at 3000 Mc, as shown by a tendency toward a slightly greater sensitivity at the high-frequency end of the range. However, the inductance tends to reduce the high-frequency response, and a good compensation is not hard to obtain.

The wattmeter described above can be expected to be accurate within 2 per cent, when carefully calibrated against a calorimeter wattmeter.

The type of thermocouple described in connection with Fig. 24-30 may develop a larger emf than is required to produce full-scale deflection of 100  $\mu$ a on a microammeter with a resistance of 100 ohms, but the emf may be adjusted to a suitable value by changing the location of the directional probe with respect to the center of the waveguide. Moving it away from the center toward the edge decreases the pickup without affecting the directional properties. However, the plane of the loop must be kept parallel to the longitudinal axis of the guide.

There are several ways in which the sensitivity of the thermocouples may be increased for measuring power levels lower than those described, without resorting to bridge circuits or vacuum tubes. One possibility is the use of vacuum thermocouples. Although this would increase the thermal emf for a given level of r-f power, the objection is that the meter calibration would no longer be linear. The heat dissipation from a vacuum thermocouple is principally by radiation, and the relation between r-f power and d-c current is not so linear as it is for air-cooled couples. For this reason, vacuum thermocouples would not be suitable in the arrangement of Fig. 24-30, in which the reflected power is subtracted from the incident power.

Another way to increase the meter current is to place the thermocouple near the coupler end of the cable instead of at the opposite end. This can be done by placing the thermocouple in series with the center conductor, as shown in Fig. 24-33. The shunt capacitances are used to

compensate for the inductance of the thermocouple. If the proper adjustments are made, the series inductance and two shunt capacitances form a low-pass  $\pi$ -section filter which will have the same characteristic impedance as the cable over a limited frequency range. Of course, placing the thermocouple near the probe

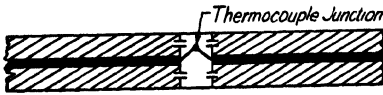


FIG. 24-33.—Thermocouple mounted in series with center conductor.

destroys the frequency-compensating effect produced by the cable attenuation. This filter-section arrangement for a thermocouple was used at a frequency of 500 Mc and was very satisfactory. The cutoff frequency of the filter section was about 3000 Mc, so that the variation of characteristic impedance with frequency was not too rapid at the operating frequency. The arrangement could presumably be scaled down for use at much shorter wavelengths.

**24-27. Output Indicators.**—Devices designed to indicate r-f or video voltage at some convenient point in the output are a desirable feature of any transmitter system. The purpose of an output indicator is to give a nearly instantaneous indication of relative power output so that the transmitter can be tuned for optimum performance. It is also useful as a monitor on the operation of the transmitter. The device can be useful even if the indication varies with frequency, since the important consideration is relative power output.

The mere presence of r-f voltage in an outgoing transmission line near the transmitter does not necessarily mean that any appreciable power is being delivered to a load. Hence devices that indicate voltage at the load or in the field of an antenna are obviously to be preferred whenever they can be used; at least they eliminate all doubt as to the condition of the transmission line.

Output indicators located in a transmission line are frequency sensitive, not only because the degree of coupling to the line varies with frequency, but because of the usual presence of some standing wave, which shifts past the indicating point in the line as the frequency changes. Indicators located in the field of an antenna may also be frequency sensitive because there is inevitably some change in voltage at a given point in the near-zone of an antenna as the frequency changes. Moreover, the presence of any reflecting bodies (of dimensions comparable to  $\lambda/4$ ) near the antenna and pickup probe will cause a further and unpredictable variation in the indication of r-f output.

One simple output-indicating device consists of a small rectifying crystal, shunted by a milliammeter, capacitively coupled into the line. Another uses, in a similar manner, a small incandescent lamp in series with a variable capacitor. These are indicated schematically in Figs.

24-34a and b. The crystal system requires less power for operation than does the lamp and has the further advantage that, if a square-law crystal is used, readings are proportional to power.

In some cases, such as for lossy-line loads, errors caused by standing waves on the line may be avoided by installing the crystal monitoring system of Fig. 24-34a at the load end of the transmission line.

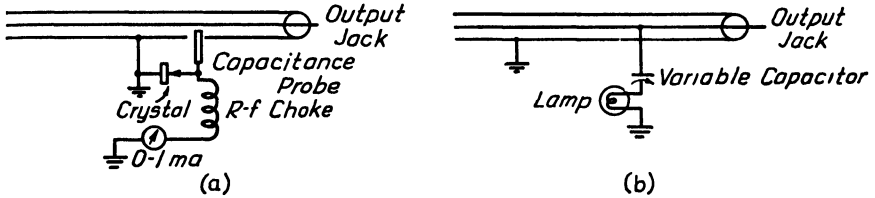


FIG. 24-34.—Schematic diagrams of output-indicating devices: (a) with rectifying crystal; (b) with incandescent lamp.

A method of indicating flow of power through waveguides is to mount a long neon tube on the guide, as indicated in Fig. 24-35. The starting voltage can be controlled by the length of the striking wire extending down into the guide. The length of the discharge column is proportional to peak power and can be read to  $\pm 1\frac{1}{2}$  mm. Thus by the addition of a

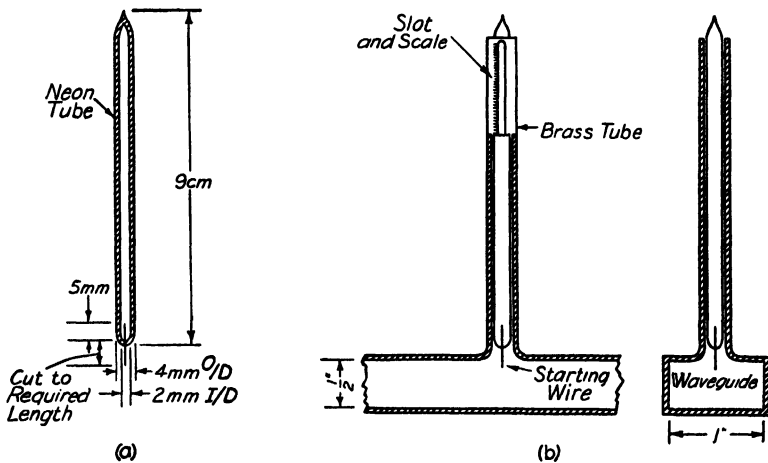


FIG. 24-35.—Neon-tube power-indicator in waveguide.

scale along the neon tube the device may be calibrated to monitor power flow or, if movable in a slot along the guide, as a standing-wave indicator.

Several of the power-measuring systems, such as unidirectional couplers, slotted lines, and photometric devices, discussed in Secs. 24-18 to 24-25 are suitable for use as power monitors. In order to be useful for tuning or adjusting transmitters, an output monitor should be instan-

taneous in reading and should not in itself require adjustments. Linearity of reading is desirable but not necessary.

In general, the most desirable type of output indicator is one that operates from the radiated field. Thus the transmitter, coupling system, antenna cables and fittings, and the antenna are simultaneously monitored. Probably the simplest of these devices consists of a small antenna, or probe, placed near the transmitting antenna, a crystal rectifier, and a meter, as shown in Fig. 24-36. The probe antenna should be placed near the transmitting antenna in a region free from reflecting objects that might set up standing waves in the space near the probe and thus make the indicating system frequency sensitive. If the probe is made small and placed near the antenna, the measuring system will respond to the monitored antenna only, yet the crystal rectifier will not be overloaded.

A diode may be used in place of the crystal rectifier, as shown in Fig. 24-37. However, this necessitates the use of additional conductors in the cable between the probe antenna and rectifier, which must be located near the transmitting antenna, and the indicating meter, which would be

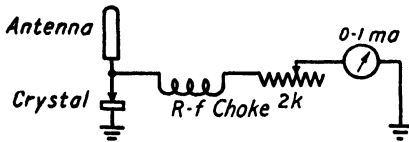


FIG. 24-36.—Output indicator with probe antenna and crystal rectifier.

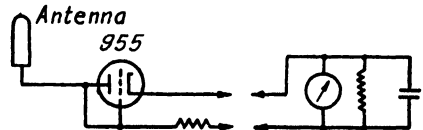


FIG. 24-37.—Output indicator with probe antenna and diode rectifier.

located near the transmitter. The crystal has the further advantage that it is operable at higher frequencies than the diode.

The Littelfuse bolometer, described in Sec. 35-11, used with a pickup, or probe, antenna is a good output indicator in that its response is directly proportional to power. It is also more stable than either the crystal or diode indicator because the fuses used in the bolometer arms do not change their characteristics with age. It is more complicated, however, than the devices previously discussed.

A very simple and useful power-output indicator consists of a 2-volt 60-ma flashlight bulb in the middle of a dipole antenna made by soldering wires, each approximately  $\frac{1}{4}$  wavelength long, directly to the lamp terminals.

**24-28. Spectrum Analyzers.**—In the construction and testing of transmitters, it is desirable to have some method for studying the final spectrum of the transmitter under modulation. Such devices for studying spectra are called *spectrum analyzers*. Two devices commonly used for this purpose are absorption wavemeters and receivers.

*Absorption Wavemeters as Spectrum Analyzers.*—Coaxial-line and cavity-type wavemeters can be readily employed as spectrum analyzers.

The band widths of such devices are very small because of their inherently high  $Q$ , so that power in a very narrow portion of the spectrum may be measured. If the crystal detector is not overloaded, *i.e.*, if it is operating in the square-law portion of its curve, the crystal-detector meter reading will be directly proportional to the power in the frequency band of the coaxial line or cavity. When the transmitter is modulated with "noise" or some other type of signal that has a uniform distribution of energy over a frequency spectrum, a graph of the spectrum in power as a function of frequency can be constructed by tuning the wavemeter through the spectrum of the transmitter and recording at frequent intervals the crystal-detector meter reading.

*Receivers as Spectrum Analyzers.*—Narrow-band heterodyne receivers can also be used as spectrum analyzers. A voltmeter is placed across the second detector to measure the i-f output voltage, the avc is removed, and a voltmeter is connected across the i-f gain-control potentiometer. A calibrated signal generator is then connected to the receiver for purposes of calibration. With the output voltage kept at a constant level, the voltage developed across the gain control is calibrated against the input voltage. It is then possible to measure the relative voltages of the portions of the spectrum being studied and to construct a db-vs.-frequency curve of the spectrum.

Special heterodyne receivers have been constructed for use as spectrum analyzers. A very convenient and useful type is the panoramic spectrum analyzer which is designed to show on the screen of an oscilloscope the Fourier analysis of the output of a transmitter. It is essentially a narrow-band superheterodyne receiver, the local oscillator of which is frequency-modulated with a low-frequency sweep. The output voltage of the receiver is applied to the vertical plates of a cathode-ray oscilloscope, the horizontal plates of which are supplied with the same low-frequency sweep used to frequency modulate the local oscillator.

The operation of a panoramic spectrum analyzer can be seen more clearly by referring to the block diagram of Fig. 24-38. This particular analyzer will cover a frequency range from 70 to 1000 Mc and has a resolving power of 100 kc. One added feature is that the spectrum can be accurately measured in decibels by means of a bolometer circuit and a vacuum-tube voltmeter. The tuning capacitor of the sweeping oscillator may be either motor- or hand-driven throughout a range of either 20 Mc or 5 Mc. The motor drive provides panoramic presentation, whereas the hand drive is used to obtain bolometer measurements in decibels, as indicated by a vacuum-tube voltmeter.

Any desired 20-Mc band of incoming signals may be selected by combining the incoming signals with the output of the local oscillator in the crystal mixer and impressing the difference-frequency band upon the



input of the 20- to 40-Mc i-f amplifier. The i-f output is then heterodyned with that of the sweeping oscillator. The latter sweeps either from 20 to 40 Mc or from 27.5 to 32.5 Mc, the range being selected by a panel switch. The resulting output, after rectification, is passed through a 5- to 50-kc video amplifier and applied either to the plates of an oscilloscope, or to a bolometer circuit, the output of which furnishes a-v-c voltage for the i-f amplifier. The a-v-c voltage is proportional to the logarithm of the input signal voltage and therefore reads the input level in decibels. The scope is calibrated to read frequency in megacycles.

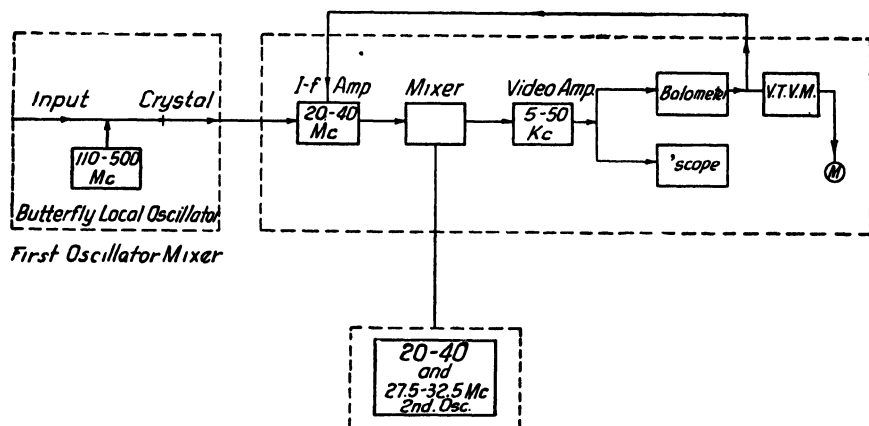


FIG. 24-38.—Block diagram of panoramic spectrum analyzer.

**24-29. Cold Analysis of Resonant Systems.**—In microwave work there are many applications where a cavity resonator is coupled to a coaxial line or waveguide, and where it is desirable to measure and express in a few figures some properties of the combination such as, for instance, band width or impedance of the cavity as termination of the line. Wavemeters, echo boxes, and TR boxes are common examples, but the most frequent and important application is the tank circuit of a vacuum-tube amplifier or oscillator. Magnetrons, klystrons, resonators, etc., may all have tank circuits consisting of cavity resonators built into the evacuated shell. In Chaps. 18 to 22, where some of these tubes have been described and their operation analyzed, it has been shown how the operation of the resonators can be illustrated by means of equivalent circuits and discussed quantitatively by means of concepts and terms borrowed from the theory of circuits with lumped constants, even though the resonators actually are distributed-constant systems.

The purpose of the following sections is to outline some methods of measuring and calculating the constants and parameters of the equivalent circuits. Other subjects to be discussed are the approximations involved and the conditions that should be satisfied in order that the equivalent

circuit and the calculated values of its constants and parameters accurately represent the resonant system within the band of frequencies of interest to the problem.

**24-30. Constants and Parameters of Resonant Systems.**—The following discussion has been written chiefly with vacuum-tube tank circuits in mind, as "cold tests" of tubes with internal resonators is at present the most important application of the methods of measurement and calculation outlined. The treatment of these problems is general enough to cover other arrangements of similar nature.

In order to start from as general a point of view as possible, a four-terminal resonant system is considered as a combination of an input coupling, a resonator proper, and an output coupling. A resonator generally has a number of different resonance modes. The discussion will be limited to a narrow frequency band at each resonance, and a set of at least five parameters will be associated with each mode. These are

1. The resonance frequency  $f_0$  of the resonator proper
2. The loaded  $Q$ ,  $Q_L$
3. The unloaded  $Q$ ,  $Q_0$
4. An input-network parameter
5. An output-network parameter

These parameters are all independent in the sense that none of them can be determined from known values of the other four.

The loaded  $Q$  is the parameter that expresses the band width of the system when a load is applied. More specifically,  $Q_L$  is defined conventionally for matched load on the output line. The loaded  $Q$  derives its significance chiefly from the information it gives about the transmission losses in the resonator and, in combination with  $Q_0$ , about the circuit efficiency.

The choice of input and output parameters allows a certain freedom. In the general case both these parameters are complex and each of them would be given by two constants, an impedance constant and a transmission constant. The output-network parameter will be specified by the characteristic impedance  $Z_0$  of the output line and a certain equivalent length of line, as shown below in connection with the equivalent circuit. The input-network parameter will be specified as an impedance  $Z_0/k_s^2$  where  $k_s$  is the turns ratio of a certain ideal transformer in the equivalent network of the four-terminal resonator. In the type of network involved here, the equivalent length of line on the input side is always zero, because the input-coupling network, which has been assumed in the general case, actually is nonexistent in the vacuum tubes we have in mind. The resonator proper is a parallel-resonant circuit connected directly

between the input terminals represented by the interaction space in the tube.

All these parameters have a definite meaning, regardless of whether the system has lumped or distributed constants. A certain ambiguity arises, however, when input and output terminals are of different kinds, one a waveguide connection, for instance, because of the fact that the characteristic impedance of a waveguide can be expressed in ohms according to several different conventions: as the wave impedance, as  $E^2/W$ , as  $E/I$ , or as  $W/I^2$ . This difficulty is purely formal, of course, and is in every case removed by stating which definition of  $Z_0$  is used.

Note that in this section "input" and "output" will consistently refer to the *normal* operation of the system, even when, for the purpose of measurement, the flow of energy is reversed and power is fed to the system through the output terminals. In the circuit diagrams, however, the direction of transmission of power *during the measurements* will be from the left to the right. The normal output terminals in the diagrams will thus appear to the left of the normal input terminals.

**24-31. Equivalent Circuits.**—Suppose that it is desired to determine as many as possible of the parameters of a resonant system when it is excited in a particular mode and that the output terminals constitute the only channel through which the properties of the system can be observed. This is the problem of "cold tests" of vacuum tubes, in which the normal input circuit is the stream of electrons and the tank circuit is inside the vacuum envelope. The object is to express the relations between the impedance at the output terminals and the parameters by equations that are at least approximately accurate for the largest possible number of cases likely to be encountered in practice. The first step is to make some general assumptions regarding the relative order of magnitude of some of the quantities involved. This will make it possible to simplify the equivalent circuit of the system and to discuss the approximations involved.

The system is considered to be made up of the resonator proper and a coupling network (Fig. 24-39a). The output terminals are at *A*; the generator, line, and standing-wave indicator shown to the left constitute the impedance-measuring equipment. Since the resonator proper is a two-terminal network, the input circuit, if shown, would also be connected to the terminals at *B*.

The methods for calculating the parameters of resonant systems that are presented in this section are based on the following assumptions:

1. The loaded  $Q$  of the resonator is relatively high, so that the total band width does not exceed a few per cent of the resonance frequency.
2. No elements or combinations of elements in the coupling network resonate in the vicinity of the resonance frequency of the resonator. If the coupling

network has filter properties, all cutoff frequencies must also be far removed from the resonance frequency.

3. The coupling network has negligible losses, so that its circuit constants can be considered as pure reactances, which, as a consequence of the two previous assumptions, are approximately constant within the frequency band of the system.

4. The resonance frequencies of different modes are far enough apart so that the resonator behaves as a simple resonant circuit within the frequency band of each mode.

The equivalent circuits are shown in Fig. 24-39. In all of them the resonator is represented by a simple resonant circuit. Generally, the solution of Maxwell's equations for any resonator will include an infinite number of resonance modes, each represented by its own parallel-resonant circuit in the equivalent circuit, and all of them connected in series (see Chap. 20, Fig. 20-10c). The assumptions made above, however, make it possible to consider each mode separately while neglecting all the others. The coupling network is represented by a  $\pi$ -network in Fig. 24-39b, by a series reactance and an ideal transformer in Fig. 24-39c, or by a section of transmission line and an ideal transformer in Fig. 24-39e. The constants of the resonator proper ( $Z_r$ ,  $Z_r'$ , and  $Z_r''$ ) are not exactly the same in the three cases. The difference can be shown as a comparatively small susceptance.

Let us now consider our parameters in the light of the equivalent circuit of Fig. 24-39e, which is the most useful one for this purpose. If  $Z_0$  is the output impedance constant and  $Z_0/k_3^2$  the input impedance constant, both real numbers, it is evident that one more parameter is needed to determine the system completely, *i.e.*, the equivalent length  $\Delta l$  of the coupling network. A more general equivalent circuit would be obtained by attributing to input and output each a length of line  $\Delta l_i$ ,  $\Delta l_o$ , respectively, as shown in Fig. 24-40, but for the vacuum-tube applica-

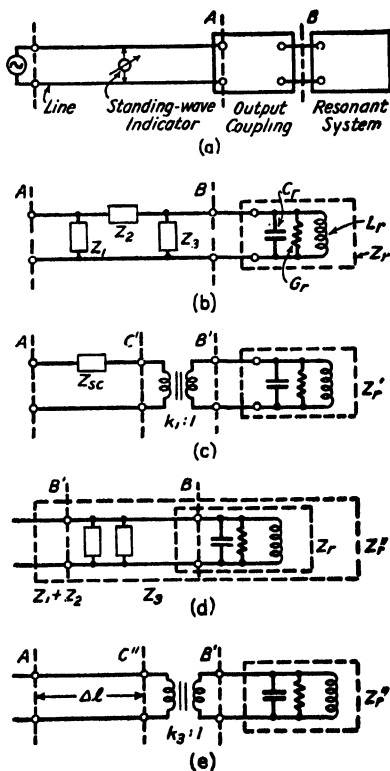


FIG. 24-39.—Equivalent network of a resonator coupled to a transmission line.

tion considered here  $\Delta l_i$  is always zero. The loaded and unloaded  $Q$  have been defined in previous chapters; the unloaded  $Q$ ,  $Q_0$ , is the  $Q$  of the resonator without any load applied, *i.e.*, determined by the losses in the resonator itself, while the loaded  $Q$ ,  $Q_L$ , is the  $Q$  of the system including load, which by convention is assumed to be matched to the output line.

Other constants and parameters that can be derived from the fundamental parameters are the following:

$$\text{External } Q, \text{ given by } \frac{1}{Q_E} = \frac{1}{Q_L} - \frac{1}{Q_0} \quad (24-14)$$

$$\text{Circuit efficiency } \eta_c = \frac{Q_L}{Q_E} = 1 - \frac{Q_L}{Q_0} \quad (24-15)$$

Input admittance for matched load ( $Z_L = Z_0$ ) at resonance

$$Y_i = \frac{k_s^2}{Z_0} + \frac{1}{Z_r''} = \frac{k_s^2}{Z_0} + \frac{1}{Q_0} \sqrt{\frac{C}{L}} = \frac{k_s^2}{\eta_c Z_0} \quad (24-16)$$

When  $\Delta l$  is known, this formula can easily be modified to give the input conductance and susceptance for any load.

Perhaps we should here recognize the fact that the identity

$$Q = \frac{\omega L}{R} = \frac{f_0}{f_1 - f_2} \quad (24-17)$$

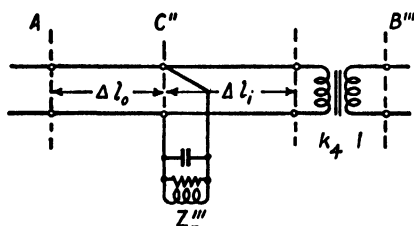


FIG. 24-40.—Equivalent network of a four-terminal resonant system.

where  $f_1$  and  $f_2$  are the half-power frequencies, is an identity for lumped constant systems only. For systems with distributed constants the two expressions for  $Q$  will differ by a factor determined by the geometry. In this section we use  $Q$  defined by variation of impedance with frequency. In either case Eq. (24-16) above can be made

quantitatively correct by assigning the proper value to the turns ratio  $k_s$  of the ideal transformer.

**24-32. Measurements.**—The method of measuring impedances at ultrahigh frequencies by observing the standing waves on a transmission line terminated by the impedance to be measured is well known. Here this technique will be used to find the parameters of a resonant system by measuring the “cold” impedance, looking into the output terminals, as a function of the frequency. For this purpose an oscillator is connected to these terminals by means of a transmission line provided with a stand-

ing-wave indicator. The frequency of the oscillator is varied within a small range on both sides of resonance, and the standing-wave ratio  $\sigma$  and the position of the minimum are plotted vs. frequency-meter dial reading, as shown in Fig. 24-41. The position of the minimum should be measured from the output terminals and expressed as a fraction of a wavelength  $l/\lambda$ . This plot, which will be called the *standing-wave diagram*, provides the basis for most of the methods for calculating the circuit parameters, as outlined below.

It may seem a waste of time and work to take data for a complete standing-wave diagram when, theoretically, two or three judiciously chosen observations are sufficient to determine the parameters of the system. Actually, several of the methods of computation given below can be—and have been—made the basis of such simplified procedures. In most cases, however, the reliability of such spot measurements is subject to some doubt. The equivalent circuit on which the calculations are based is only approximately equivalent, and even very loosely coupled spurious resonant systems may cause large errors. The standing-wave diagram reveals any anomalies, which can then be accounted for. Furthermore, the curves are, of course, more accurate than the individual observations.

Figure 24-41 shows a typical standing-wave diagram, *i.e.*, a plot of the standing-wave ratio and the position of the minimum vs. frequency, for a resonant system free from spurious resonances and with  $\Delta l = 0$ . The lowest standing-wave ratio  $\sigma_0$  occurs at the resonance frequency  $f_0$ . At this frequency, the first minimum occurs  $\frac{1}{4}$  wavelength from the terminals and, as the frequency increases or decreases, the minimum approaches asymptotically zero and a distance of  $\frac{1}{2}$  wavelength from the terminals, respectively. This is the appearance of the standing-wave diagram for high-efficiency systems, where the circuit efficiency  $\eta_c > 50$  per cent or  $Q_0 > 2Q_L$ .

Figure 24-42 gives the curves of  $l/\lambda_0$  for  $Q_0 = 1.5 Q_L$ ,  $2 Q_L$ , and  $3 Q_L$ , respectively. Since only high-efficiency systems ( $Q_0 > 2Q_L$ ) are of any practical importance, mainly systems of this kind will be discussed in this section. The formulas in Sec. 24-35 apply to low-efficiency as well as high-efficiency systems, however.

When  $\Delta l$  is not zero, the ordinate axis should be readjusted so that the center of antisymmetry falls at  $l/\lambda_0 = 0.25$ ; this operation is equivalent

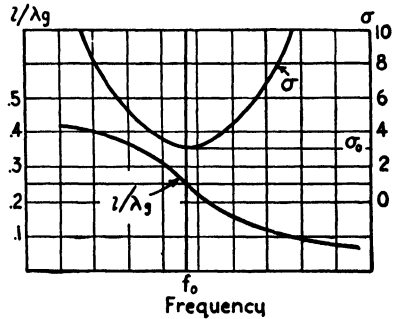


FIG. 24-41.—Standing-wave data of resonant system.

to using the point  $C''$  of Fig. 24-39e, instead of  $A$ , as the point of reference in determining the position of the minimum.

If a wavemeter is used, instead of a frequency meter, and wavelengths or corresponding dial readings are plotted along the horizontal axis, the diagram will be reversed from left to right, otherwise the shape of the curves will remain the same.

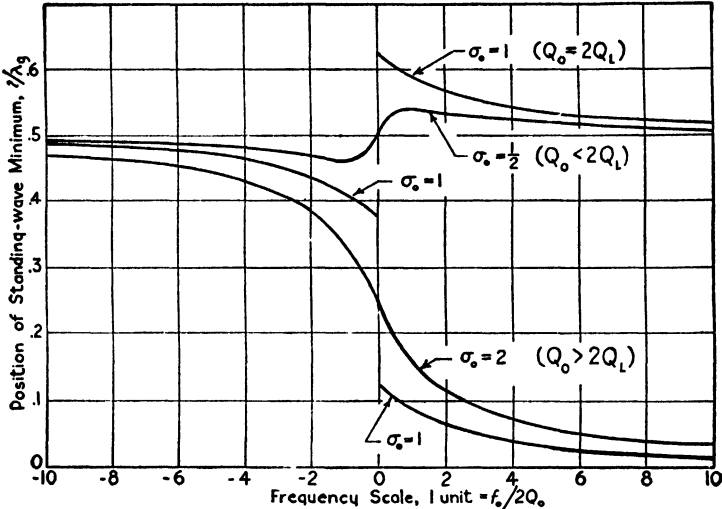


FIG. 24-42.—Position of standing-wave minimum  $l/\lambda_0$  for resonant system with three different load impedances.

Some of the sources of errors that should be watched during these measurements are as follows:

1. Reflections from the line joints between the output terminals of the system and the standing-wave section
2. Reflections from the probe
3. Insufficient shielding
4. Drift or instability of the oscillator or the receiver
5. Oscillator harmonics
6. Insufficient accuracy in measuring frequency increments
7. Unwanted modes in the transmission line

Since the standing-wave indicator necessarily absorbs some power from the line, it is impossible entirely to avoid reflections from the probe, especially where the standing-wave ratio is high. If a minute probe is used with a very sensitive receiver or a powerful oscillator, in order to minimize these errors, then the shielding becomes particularly critical. To decrease the effect of inaccuracy in measuring frequency increments, the abscissas of the standing-wave-ratio curve should be the actual vernier-dial readings, and backlash should be eliminated by moving the

dial continuously in the same direction. The seventh source of error, unwanted modes in the transmission, occurs particularly in waveguides where asymmetric excitation or loading may produce interfering transmission modes with different phase velocity.

It is evident that measurements from the output terminals only cannot give any parameters that contain the factor  $k_3$ , as for instance, the input impedance and  $\sqrt{L/C}$  for the resonator. These constants are, however, of interest only in connection with tube design; the engineer using the tube for power generation has no need to measure them.

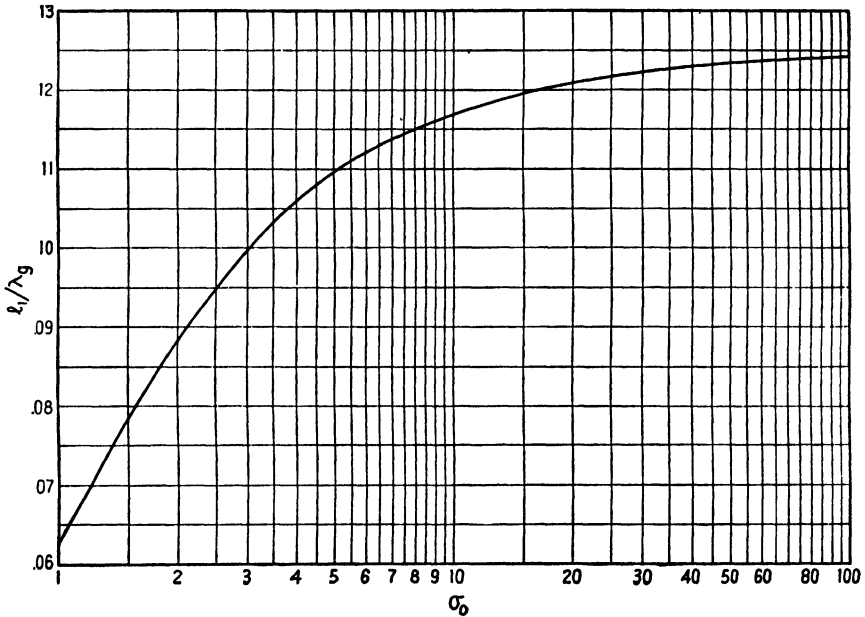


FIG. 24-43.—Graph for determination of  $Q_L$ .

**24-33. Methods for Calculation of the Parameters. Method I.** In this section and Sec. 24-34 methods for calculating the parameters of the equivalent circuits will be discussed. The mathematical justification of these methods will be given in Sec. 24-35.

The conventional method for determining the  $Q$  of a circuit formed by lumped elements is to measure the frequencies at the half-power points. For the loaded  $Q$  these points can be found from the curve of Fig. 24-43. The minimum standing-wave ratio  $\sigma_0$  is taken from the standing-wave diagram, and the corresponding value of  $l_1/\lambda_g$  is read from the curve in Fig. 24-43. By antisymmetry, the other value is  $l_2/\lambda_g = \frac{1}{2} - l_1/\lambda_g$ . Finally the half-power frequencies  $f_1$  and  $f_2$  are obtained by locating the points  $l_1/\lambda_g$  and  $l_2/\lambda_g$  on the curve in the standing-wave diagram. Figure



24-44 and the curve of the standing-wave ratio can also be used in the same fashion to find  $f_1$  and  $f_2$ , but the accuracy is in general lower. Sometimes  $\sigma_0$ ,  $f_1$ , and  $f_2$  are measured directly and no standing-wave diagram is plotted. The accuracy and dependability of the result is then considerably reduced. The results are

$$f_0 = \text{abscissa for center of antisymmetry} \quad (24-18)$$

$$Q_L = \frac{f_0}{f_1 - f_2} = \frac{\lambda_0}{\lambda_2 - \lambda_1} \quad (24-19)$$

$$Q_0 = (1 + \sigma_0)Q_L \quad (24-20)$$

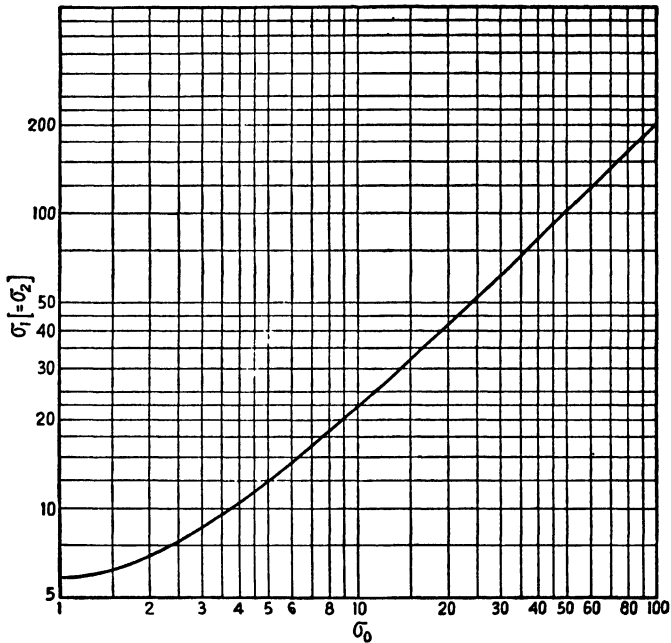


FIG. 24-44.—Graph for determination of  $Q_L$ .

Of the remaining parameters,  $Z_0$  is known,  $\Delta l/\lambda_0$  is equal to the vertical displacement required to place the center of antisymmetry at  $l/\lambda_0 = 0.25$ , and  $k_3$  cannot be determined from the standing-wave data alone.

*Method II.*—The unloaded half-power points  $f_1'$  and  $f_2'$  can be determined in the same way by use of the Figs. 24-45 and 24-46 in combination with the standing-wave diagram. The results are

$$f_0 = \text{abscissa for center of antisymmetry} \quad (24-21)$$

$$Q_L = \frac{1}{1 + \sigma_0} Q_0 \quad (24-22)$$

$$Q_0 = \frac{f_0}{f_1' - f_2'} = \frac{\lambda_0}{\lambda_2' - \lambda_1'} \quad (24-23)$$

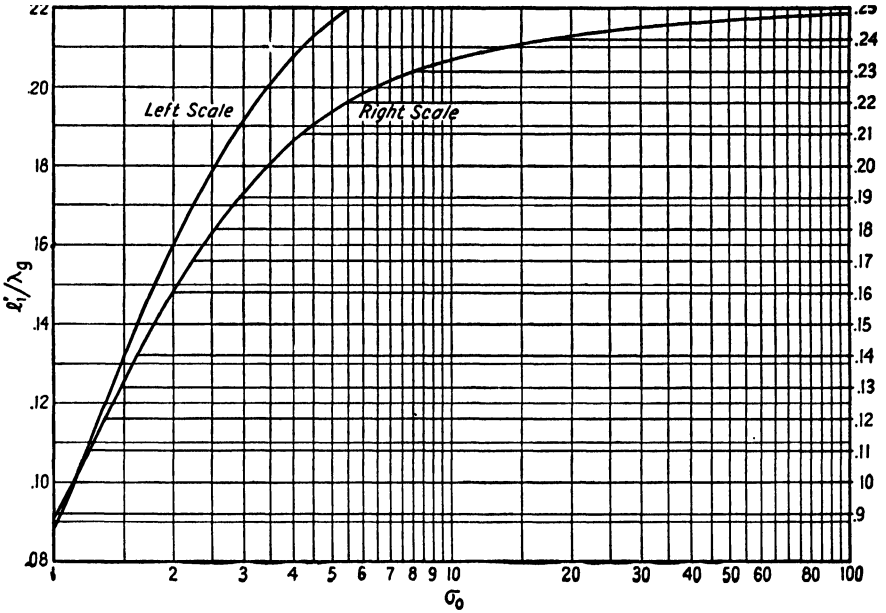


FIG. 24-45.—Graph for determination of  $Q_0$ .

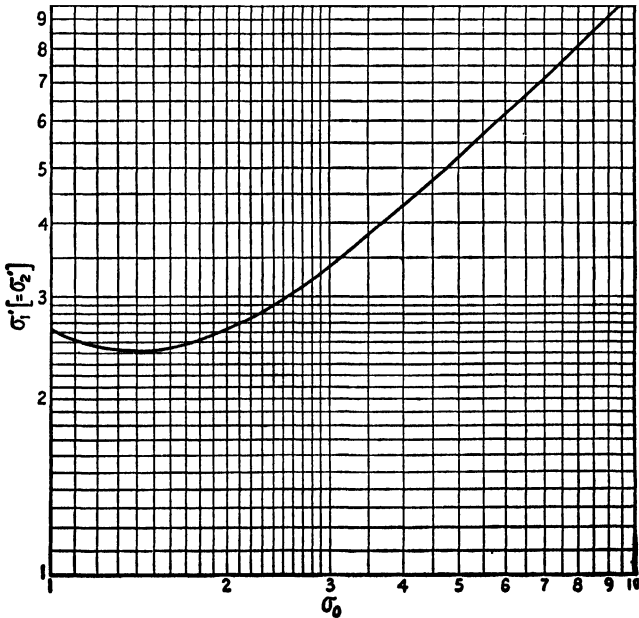


FIG. 24-46.—Graph for determination of  $Q_0$ .

*Method III.*—The maximum slope of the  $l/\lambda_g$  curve occurs at the resonance point and is a function of  $Q_L$  and  $Q_0$ . We define  $S_0$  as the actual slope of the  $l/\lambda_g$  curve at this point, expressed in the coordinates of the diagram, divided by the relative frequency (or wavelength) change per degree of the frequency meter. The results are

$$f_0 = \text{abscissa for center of antisymmetry} \quad (24-24)$$

$$Q_L = \pi S_0 \frac{\sigma_0 - 1}{\sigma_0} \quad (24-25)$$

$$Q_0 = (1 + \sigma_0)Q_L \quad (24-26)$$

*Method IV.*—If we calculate the quantity  $y$  defined by the relation

$$y = (\sigma - \sigma_0) \tan \frac{2\pi l}{\lambda_g} \quad (24-27)$$

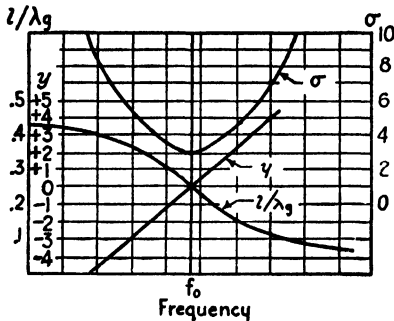


FIG. 24-47.—Graphs used in Method IV.

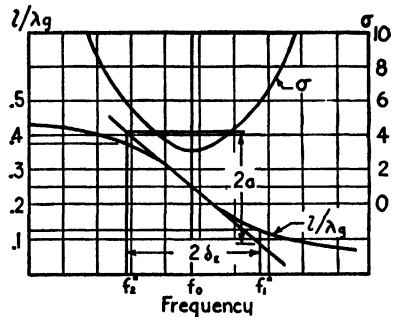


FIG. 24-48.—Graphs used in Method V.

for a number of points and plot it as a function of frequency, we obtain a straight line, as shown in Fig. 24-47. The unloaded  $Q$  is half the slope of this line. Before  $y$  is calculated, the zero point on the ordinate axis for  $l/\lambda_g$  must be adjusted so that the center of antisymmetry falls at 0.25. The results are

$$f_0 = \text{abscissa for center of antisymmetry} \quad (24-28)$$

$$Q_0 = \frac{1}{2} S_y = \frac{1}{2} \frac{d}{df} \left[ (\sigma - \sigma_0) \tan \frac{2\pi l}{\lambda_g} \right] \quad \text{for } f = f_0 \quad (24-29)$$

$$Q_L = \frac{1}{\sigma_0 + 1} Q_0 \quad (24-30)$$

*Method V.*—As both curves in the standing-wave diagram depend on  $Q_L$  as well as  $Q_0$ , these parameters can be determined even if only one of these curves is known. The following method offers a way of finding the answer from the  $l/\lambda_g$  curve.

The procedure is illustrated in Fig. 24-48. Draw a tangent to the curve through the center of antisymmetry ( $l/\lambda_g = 0.25$ ). Find the points

of the curve with the ordinates 0.125 and 0.375. Draw vertical lines through these points. Determine the difference  $2a$  between the ordinates of the intersections of these lines with the tangent. The corresponding frequencies are  $f_1''$  and  $f_2''$ . From these quantities,  $Q_E$  and  $\sigma_0$  can be calculated as follows:

$$Q_E = \frac{f_0}{f_1'' - f_2''} \cdot \frac{1}{2\pi a} \quad (24-31)$$

$$\sigma_0 = \frac{2\pi a}{\sqrt{(2\pi a)^2 - 1}} \quad (24-32)$$

According to the author's experience,  $\sigma_0$  is not obtained very accurately by this method, as the denominator contains a difference between two quantities that in general are approximately equal. On the other hand, this method of determining  $Q_E$  has the advantage of requiring no graph and still being easy to remember and apply.

From the point of view of design,  $Q_E$  is more significant than  $Q_L$ , since it depends on the geometry only and not on conductivity, surface conditions, etc. The latter factors, on the other hand, determine  $Q_0$ .  $Q_L$  and  $Q_0$  are related to  $Q_E$  as follows:

$$f_0 = \text{abscissa for center of antisymmetry} \quad (24-33)$$

$$Q_L = \frac{\sigma_0}{1 + \sigma_0} Q_E \quad (24-34)$$

$$Q_0 = \sigma_0 Q_E \quad (24-35)$$

**24-34. Other Methods for Calculation of Parameters.**—A number of other methods, graphical as well as algebraical, have been devised. When it is important to make the most of incomplete data or data that are distorted by minor parasitic resonances, it is often helpful to plot the impedance circle of the resonant system. The work involved can be reduced to a minimum by using one of the graph papers mentioned in Chap. 21 (Figs. 21-6 and 21-7), with coordinate systems of standing-wave ratio vs. position of minimum  $l/\lambda_g$ . The process of fitting a circle to the points plotted allows the best possible use to be made of the information contained in the experimental data.

Figure 24-49 shows an impedance circle drawn in a circular diagram, the Smith chart. Instead of the standing-wave ratios  $\sigma$  and  $\sigma_0$ , the corresponding values of the reflection coefficient  $\rho$  and  $\rho_0$  are shown in the figure. The point  $D$  represents resonance, and  $A$  and  $B$  represent the half-power points of the loaded system. When a graph paper with coordinates of  $\sigma$  and  $l/\lambda_g$  is used  $\sigma_0$ ,  $\sigma$ , and  $l_1/\lambda_g$  can be read directly from the graph. The corresponding frequencies will still have to be found from the standing-wave diagram of Fig. 24-41, *i.e.*,  $\sigma$  and  $l/\lambda_g$  vs. frequency.

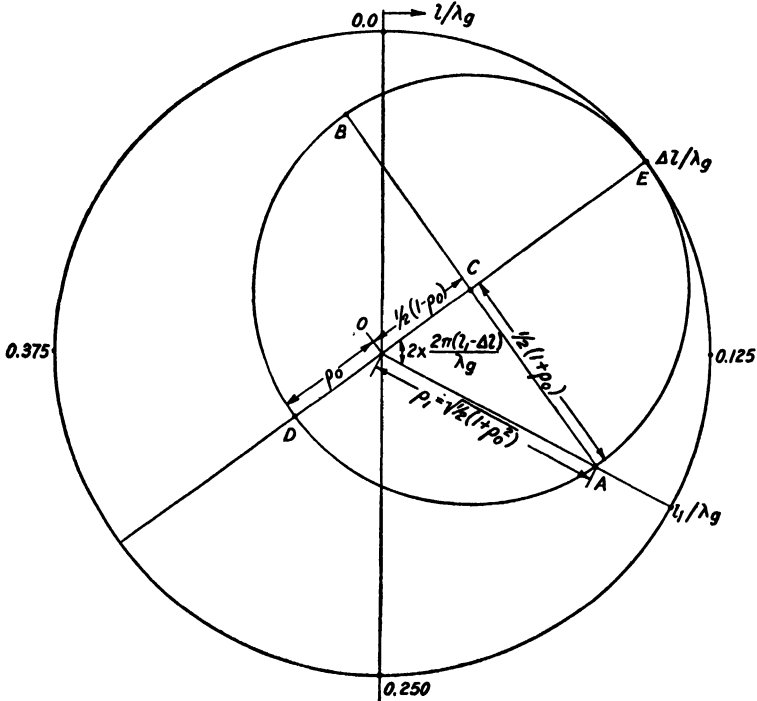


FIG. 24-49.—Smith chart showing impedance circle of resonant system.

**24-35. Analytical Foundations of Methods I to V.**—If a transmission line with negligible losses is terminated by an impedance  $Z$ , the impedance at a distance  $l$  from the termination, looking in the direction of the termination, is

$$Z_l = Z_0 \frac{Z \cos \frac{2\pi l}{\lambda_g} + jZ_0 \sin \frac{2\pi l}{\lambda_g}}{Z_0 \cos \frac{2\pi l}{\lambda_g} + jZ \sin \frac{2\pi l}{\lambda_g}} \tag{24-36}$$

Introducing small letters for normalized impedance ( $z = Z/Z_0$ ) and defining  $\alpha = \tan \frac{2\pi l}{\lambda_g}$ , we get

$$z_l = \frac{z + j\alpha}{1 + jz\alpha} \tag{24-37}$$

Now letting  $l$  represent the distance from the termination to a voltage minimum on the line makes  $z_l$  real and equal to the reciprocal of the standing-wave ratio  $\sigma$ . This leads to the following relations between the normalized resistance  $r$  and reactance  $x$  of the termination impedance and the standing-wave data  $\sigma$  and  $\alpha$ .

$$\left\{ \begin{aligned} \sigma &= \frac{r^2 + x^2 + 1}{2r} \left[ \pm \sqrt{1 - \frac{4r^2}{(r^2 + x^2 + 1)^2} + 1} \right] \\ \alpha &= -\frac{r^2 + x^2 - 1}{2x} \left[ \pm \sqrt{1 + \frac{4x^2}{(r^2 + x^2 - 1)^2} + 1} \right] \end{aligned} \right. \quad (24-38)$$

$$\left\{ \begin{aligned} \sigma &= \frac{r^2 + x^2 + 1}{2r} \left[ \pm \sqrt{1 - \frac{4r^2}{(r^2 + x^2 + 1)^2} + 1} \right] \\ \alpha &= -\frac{r^2 + x^2 - 1}{2x} \left[ \pm \sqrt{1 + \frac{4x^2}{(r^2 + x^2 - 1)^2} + 1} \right] \end{aligned} \right. \quad (24-39)$$

or

$$r = \sigma \frac{\alpha^2 + 1}{\alpha^2 + \sigma^2} \quad (24-40)$$

$$x = \alpha \frac{\sigma^2 - 1}{\alpha^2 + \sigma^2} \quad (24-41)$$

The equivalent circuit of Fig. 24-39e is used, and for simplicity  $C''$  instead of  $A$  is considered to be the terminating point of the line. The factor  $k_3$  cannot be determined, and for convenience we write  $k_3 = 1$ . In other words, all impedances are referred to the left-hand side of the ideal transformer. For application of the equations derived above, the line is terminated as shown in Fig. 24-50, and the following expressions are obtained:

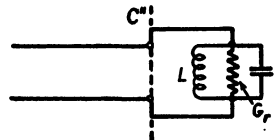
$$r \approx \frac{r'}{\frac{1}{Q_0^2} + 4\delta^2} \quad (24-42)$$

$$x \approx \frac{2\delta\omega L'}{\frac{1}{Q_0^2} + 4\delta^2} \quad (24-43)$$

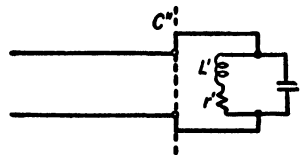
where

$$\delta = \frac{\omega - \omega_0}{\omega} \quad (24-44)$$

$$Q_0 = \frac{\omega_0 L'}{r'} \quad (24-45)$$



(a)



(b)

FIG. 24-50.—Equivalent circuit of resonator proper.

Let us first assume that the resonance impedance is greater than  $Z_0$ , as is usually the case. The first minimum then occurs  $\frac{1}{4}$  wavelength from the end at resonance.

Thus at resonance

$$\alpha = \infty \quad (24-46)$$

$$r = \sigma_0 = Q_0^2 r' = Q_0 \omega L' = \frac{Q_0}{Q_R} \quad (24-47)$$

$$x = 0 \quad (24-48)$$

Introducing

$$y = 2\delta Q_0 \quad (24-49)$$

we can write

$$r = \frac{\sigma_0}{1 + y^2} \quad (24-50)$$

$$x = \frac{\sigma_0 y}{1 + y^2} \quad (24-51)$$

Substituting these expressions for  $r$  and  $x$  in Eqs. (24-38) and (24-39), we obtain

$$\sigma = \frac{1 + y^2 + \sigma_0^2}{2\sigma_0} \left[ \pm \sqrt{1 - \frac{4\sigma_0^2}{(1 + y^2 + \sigma_0^2)^2} + 1} \right] \quad (24-52)$$

$$\alpha = \tan \frac{2\pi l}{\lambda_g} = -\frac{1 + y^2 - \sigma_0^2}{2\sigma_0 y} \left[ \pm \sqrt{1 + \frac{4\sigma_0^2 y^2}{(1 + y^2 - \sigma_0^2)^2} + 1} \right] \quad (24-53)$$

These equations represent the two curves in our standing-wave diagram. Considering the frequency as the independent variable, we see that the curves have two independent parameters. The factor  $2Q_0/f_0$  according to the definition of  $y$  determines the scale along the frequency axis, and  $\sigma_0$  or  $Q_0/Q_E$  determines the shape of the curves.

To calculate the loaded  $Q$  at unity standing-wave ratio, a load resistance equal to  $Z_0$  is added in parallel with the resonant system. Then

$$\frac{1}{Q_L} = \frac{1}{Q_0} + \frac{\omega_0 L'}{1} = \frac{1}{Q_0} + \frac{1}{Q_E} \quad (24-54)$$

$$\omega_0 L' = \frac{\sigma_0}{Q_0} \quad (24-55)$$

$$Q_0 = (1 + \sigma_0)Q_L \quad (24-56)$$

To find the points on the curves for  $\sigma$  and  $l/\lambda_g$  that determine the loaded  $Q$ , we set

$$y = \pm \frac{Q_0}{Q_L} = \pm (1 + \sigma_0) \quad (24-57)$$

and to find the unloaded  $Q$

$$y = \pm 1 \quad (24-58)$$

This leads to the final expressions from which Figs. 24-43 to 24-46 have been plotted:

$$Q_L = \frac{f_0}{f_1 - f_2} \quad (24-59)$$

$$\sigma_1 = \sigma_2 = \frac{1 + \sigma_0 + \sigma_0^2}{\sigma_0} \left[ \sqrt{1 - \frac{\sigma_0^2}{(1 + \sigma_0 + \sigma_0^2)^2} + 1} \right] \quad (24-60)$$

$$\frac{l_1}{\lambda_g} = \frac{1}{4\pi} \tan^{-1} \sigma_0 \quad (24-61)$$

$$\frac{l_2}{\lambda_g} = \frac{1}{2} - \frac{l_1}{\lambda_g} \quad (24-62)$$

$$Q_0 = \frac{f_0}{f_1' - f_2'} \quad (24-63)$$

$$\sigma_1' = \sigma_2' = \frac{\sigma_0^2 + 2}{2\sigma_0} \left[ \sqrt{1 - \frac{4\sigma_0^2}{(\sigma_0^2 + 2)^2} + 1} \right] \quad (24-64)$$

$$\left. \begin{aligned} \frac{l_1'}{\lambda_g} &= \frac{1}{4\pi} \tan^{-1} \frac{2\sigma_0}{\sigma_0^2 - 2} \\ \frac{l_2'}{\lambda_g} &= \frac{1}{2} - \frac{l_1'}{\lambda_g} \end{aligned} \right\} \quad (24-65)$$

It can easily be verified that the two pairs of roots of Eqs. (24-38) and (24-39) are related as follows:

$$\sigma'' = \frac{1}{\sigma'} \quad (24-66)$$

$$\alpha'' = -\frac{1}{\alpha'} \left( \text{or } \frac{l''}{\lambda_g} = \frac{1}{4} + \frac{l'}{\lambda_g} \right) \quad (24-67)$$

The second pair of roots ( $\sigma''$  and  $\alpha''$ ) would apply if the position of the maximum instead of the minimum voltage on the line were to be plotted. If we have a case where  $Q_0 < 2Q_L$  (curve  $\sigma_0 = \frac{1}{2}$  in Fig. 24-42),  $\sigma''$  and  $\alpha''$  will give the correct answer if  $\sigma_0$  is replaced by  $1/\sigma_0$  ( $< 1$ ). In the impedance diagram the circle is too small to reach the point 1.0 on the horizontal axis. In other words, the terminating impedance is for all frequencies smaller than the characteristic impedance of the line. This is often the case, for instance, with loosely coupled spurious resonant systems.

In order to find the slope of the  $l/\lambda_g$  curve at resonance, which is utilized in Methods III and V, it is necessary to derive the limiting value of  $d(l/\lambda_g)/d\delta$  as the frequency approaches  $f_0$ ,  $\alpha$  approaches infinity, and  $y$  approaches zero.

$$\begin{aligned} \frac{d\alpha}{dy} &= \frac{2\pi}{2Q_0} \times \frac{1}{\left(\cos \frac{2\pi l}{\lambda_g}\right)^2} \times \frac{d}{d\delta} \left(\frac{l}{\lambda_g}\right) \\ &= \frac{\pi}{Q_0} S_0(1 + \alpha^2) \end{aligned} \quad (24-68)$$

By differentiating Eqs. (24-53) and approaching the limit we obtain

$$S_0 = \frac{Q_0}{\pi} \times \frac{\sigma_0}{\sigma_0^2 - 1} \quad (24-69)$$



or

$$Q_0 = \frac{\pi S_0}{\sigma_0} (\sigma_0^2 - 1) \quad (24-70)$$

$$Q_L = \frac{\pi S_0}{\sigma_0} (\sigma_0 - 1) \quad (24-71)$$

To verify the results obtained by Method V, we transform Eq. (24-53) into

$$\sigma_0^2 + \sigma_0 y (\frac{1}{2} - \alpha) = 1 + y^2 \quad (24-72)$$

By introducing  $S_0$  from Eq. (24-69) we obtain

$$\begin{aligned} \frac{Q_E}{\pi S_0} &= \frac{\sigma_0^2 - 1}{\sigma_0} = -\frac{y}{\sigma_0} \left( \alpha - \frac{1}{\alpha} \right) + \frac{y^2}{\sigma_0^2} \\ &= Q_E \times 2\delta \left( \alpha - \frac{1}{\alpha} \right) + Q_E^2 \times (2\delta)^2 \end{aligned} \quad (24-73)$$

$$Q_E = \frac{1}{2\delta} \left( \frac{1}{2\delta S_0 \pi} + \tan \frac{2\pi l}{\lambda_g} - \cot \frac{2\pi l}{\lambda_g} \right) \quad (24-74)$$

If we apply this equation when  $\alpha = 1$ , we get  $l/\lambda_g = \frac{1}{8}$  and (see Fig. 24-48)  $2\delta S_0 = 2a$

$$Q_E = \frac{1}{2\delta_E} \times \frac{1}{2\pi a} \quad (24-75)$$

$$\sigma_0 = \frac{2\pi a}{(2\pi a)^2 - 1} \quad (24-76)$$

The relation used to get Eq. (24-27) in Method IV is obtained from Eqs. (24-52) and (24-53) by eliminating  $y^2$ ,  $\alpha^2$ , and  $\sigma^2$ .

$$y = \alpha(\sigma - \sigma_0) \quad (24-77)$$

which should be compared with the definition

$$y = 2\delta Q_0 \quad (24-49)$$

The properties of the impedance circle in the Smith chart mentioned in Sec. 24-34 are easily verified. In Fig. 24-49 we see that  $OC = \frac{1}{2}(1 - \rho_0)$ ,  $AC = \frac{1}{2}(1 + \rho_0)$ , and consequently  $\rho_1 = AO = \sqrt{\frac{1}{2}(1 + \rho_0^2)}$ . The angle  $AOC = 2 \times 2\pi \frac{l_1 - \Delta l}{\lambda_g}$ . If we introduce the relation

$$\rho = \frac{\sigma - 1}{\sigma + 1} \quad (24-78)$$

and shift the zero of the angular coordinates  $\Delta l/\lambda_g$  to the right, we obtain the same expression for  $\sigma_1$  and  $l_1/\lambda_g$  as in the Eqs. (24-60) to (24-62).

## CHAPTER 25

### RECEIVERS—GENERAL CONSIDERATIONS

By J. M. PETTIT

**25-1. Design Objectives.**—Since the receiving equipment for which design principles will be discussed was developed under wartime conditions, and for a somewhat specialized type of service, it is necessary at the outset to define the requirements for the equipment. Although most of the techniques described will be useful in fields outside the specific military applications for which they were originally intended, the reader may not find design or performance data for the application of most interest to him, such as, *e.g.*, television or frequency-modulation reception. The presentation will, however, be as general as possible.

*Type of Signal.*—The receiving equipment to be described was intended principally for monitoring a frequency range of approximately 50 to 11,000 Mc. The receivers were to provide continuous coverage of the frequency spectrum, emphasis being placed upon achieving as wide a tuning range as possible for a given unit, such as a 2:1 or 3:1 ratio of high- to low-frequency limits. The requirement of such a wide tuning range has generally not been encountered in radar or special communications equipment in this frequency range, and hence many of the new techniques treated in this chapter have to do with the wide-range problem. Its solution is achieved usually at some expense in performance or simplicity of design. Although similar problems have been dealt with in the past for conventional broadcast and “all-wave” receivers, techniques suitable there, such as bending of condenser plates to assist in tracking, are not adaptable to the higher frequencies.

The primary use of the receivers has been the reception of radar transmissions, characterized generally by pulse modulation, in which high peak powers are present for relatively short intervals. The low-duty cycle and consequent low average power in the signal call for special consideration. One factor that must be considered is that an a-v-c circuit designed for normal operation on sine-wave amplitude-modulated signals, in which considerable carrier power is present, will not function on radar signals of even large amplitude. Furthermore, if the receiver is to reproduce the modulation envelope with reasonable fidelity, with pulses having a duration of 1  $\mu$ sec or less, it must be able to handle side bands and video-modulation components extending into the megacycles. Per-

haps the most important consideration is that comparative sensitivity measurements on receivers for pulse service cannot reliably be made with conventional sine-wave amplitude-modulation techniques.

The nature of the radar transmission has implications concerning the sensitivity requirements of the receiver. A receiver of relatively low sensitivity is entirely adequate, for instance, to be carried in an airplane to detect the signal from a radar that is observing the airplane. The reason for this is, of course, the fact that high beam power, directed at the airplane, is necessary in order that the proportionately low-power echo from the airplane shall be detectable at the radar receiver. For general-purpose work, on the other hand, in order to provide for detection of the radar when its highly directive transmission is not beamed exactly in the direction of the receiver, or when the receiver is at a great distance from the radar, it is desirable to have as high sensitivity as possible. Hence, the more important techniques described in this chapter are concerned with high-performance superheterodynes having sensitivities approaching more nearly the limits imposed by thermal noise.

*Types of Information to Be Obtained.*—In contrast to radar service itself, where accurate measurement of range requires precise timing and presentation circuits, or to television service, where the video modulation is presented as a picture, the type of information to be obtained from the receivers under consideration here is of a simpler sort. Basically, the objective has been measurement of the characteristics of pulse signals, *viz.*, the carrier frequency, the pulse-recurrence frequency, the pulse length, and the general pulse shape. Measurement of carrier frequency to an accuracy of  $\frac{1}{2}$  to 1 per cent has generally been satisfactory, while 5 per cent has been adequate for pulse length and recurrence frequency. Observation of pulse shape has been entirely qualitative, an oscilloscope display with a pulse-triggered time base being employed. These measurements have not required a high degree of r-f precision or stability, nor a high-fidelity video presentation.

One special type of measurement for which a receiver has been adapted is the determination of the relative energy distribution in the spectrum produced by a wide-band modulated signal, but here, too, high precision was not required.

It is the object of the following sections to present several examples of receivers that provide the type of service described in this section, and, in so doing, to show the need for the various receiver elements that will be discussed in the chapters to follow.

**25-2. Direct-detection Receivers.**—The simplest type of receiver is one in which a detector is connected to the antenna and the output of the detector is amplified to a suitable level for earphone use. Selectivity is provided by means of either a tunable or a fixed-frequency r-f filter

inserted between the antenna and the detector. Such a receiver has relatively low selectivity and sensitivity compared, for instance, with a superheterodyne. The low sensitivity results in part from the poor rectification efficiency of vacuum-tube or crystal detectors at low signal levels. Nevertheless, as was pointed out in the preceding section, there are applications where even a low-sensitivity receiver can provide useful service. Two examples may be cited. One is a receiver intended for providing crude monitoring of a particular frequency band, an indication being given when a signal appears anywhere within the band. The indication does not tell the exact frequency of the signal within the band, nor the number of signals present if there are more than one. A block

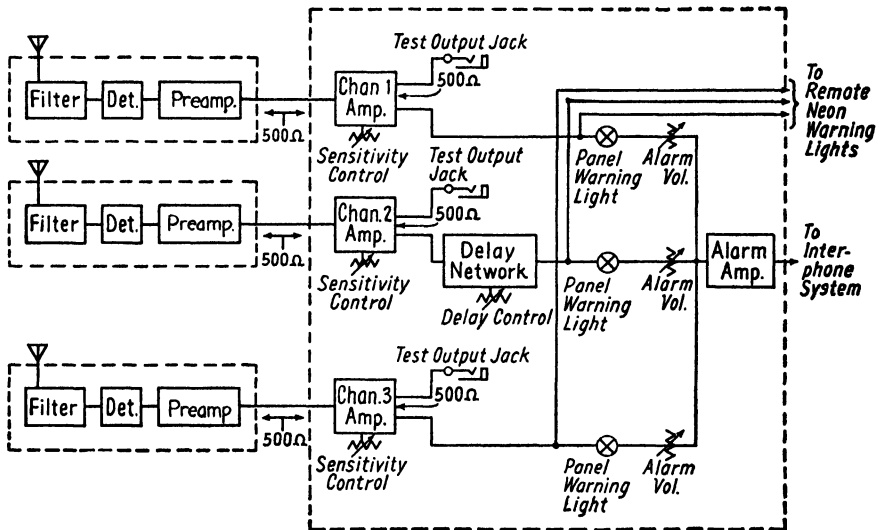


FIG. 25-1.—Direct-detection receiver for untuned monitoring of three separate r-f channels.

diagram of such a receiver is shown in Fig. 25-1. It will be seen that three bands are provided, each with separate antenna, r-f filter, and indicator. One of the channels happens to be provided with a delay network in order that an indication on this channel shall not occur until some desired interval after the signal appears.

A problem arises in direct-detection receivers because of the high gain, of the order of 100 db, that is often required in the audio or video amplifier. If the antenna is located at some distance from the receiver, the r-f filter and detector may be placed at the antenna, with an audio transmission line to the receiver amplifier. This is a low-level line, followed by the high-gain amplifier, and hence is extremely susceptible to noise pickup, particularly in airplanes having 400-cycle a-c power systems. Another possibility is to transmit the r-f energy to the receiver

by means of coaxial line or waveguide. There are two objections to this. One arises from the fact that it is virtually impossible for such a line to be perfectly matched over a wide frequency range, by either the antenna at one end or the filter and detector at the other end. Hence resonance

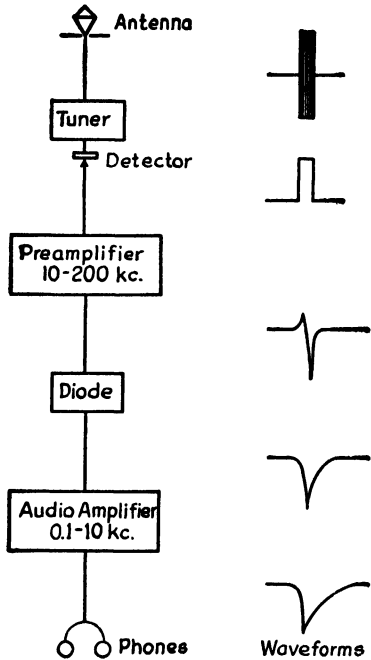


FIG. 25-2.—Tunable direct-detection receiver for pulsed signals.

phenomena occur on the line, and these will vary for different installations if the line lengths are not identical. It is therefore impossible to guarantee the behavior of the receiver over a wide frequency range, the resonances sometimes permitting transmission at some point in the normal rejection band. The second objection to the r-f line is that the attenuation for a given line length is higher than when audio frequencies are used. Since this loss is introduced ahead of the detector, the signal-to-noise ratio is correspondingly impaired, and hence r-f loss cannot be compensated by additional amplification after detection. The solution to this problem, as exemplified by the receiver under discussion, is to place the r-f filter, and the detector, together with a preamplifier, at the antenna,

followed then by an audio transmission line in which the signal level is relatively high with respect to induced hum or noise. An alternate method, applicable only to the reception of pulse signals, has been employed in a receiver to be described in the following paragraph.

It is sometimes feasible to use a low-sensitivity tunable receiver for monitoring a wide frequency band when (1) the signals are few and well-separated, (2) the signals are relatively strong, (3) only crude information, such as approximate carrier frequency, is desired, and (4) signals are pulse-modulated, or at least have many high-frequency modulation components. If these conditions are acceptable, it is possible to provide a direct-detection receiver that has much to offer in simplicity, small size, and low weight. In Fig. 25-2 are shown the essential elements of such a receiver. The r-f tuner and detector are of a type to be described in detail in Chaps. 28 and 29. The principal feature to be noted is the combination of a preamplifier and a second diode rectifier. For pulse signals the modulation envelope comprises a spectrum of harmonics of the recurrence frequency, and in order to reproduce the pulse shape

accurately, a receiver would have to transmit these components up to several megacycles. For the simple objective of producing an audible signal, however, considerable liberty can be taken with these components. In the receiver of Fig. 25-2 the preamplifier passes only the components between 10 and 200 kc. The audible components are restored by cross modulation in the second diode. The net result is a wave form of pulse type, but very rounded and with a large overshoot. The advantage lies in the fact that the total effective gain can be made very large, and yet the low-level circuits in the preamplifier will not pass the unwanted noise and hum pickup. Furthermore, by splitting the total gain between audio amplifiers and preamplifiers, problems of oscillation are reduced, an important factor when compact construction necessitates close spacing of components. The complete receiver including a-c power supply, is illustrated in Fig. 25-3.

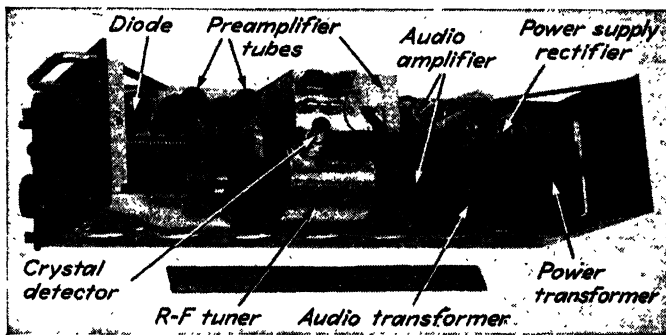


Fig. 25-3.—Photograph of the direct-detection receiver of Fig. 25-2.

**25-3. Superheterodyne Receivers.**—For general-purpose reception, the superheterodyne has proved to be the best type. Its advantages in the frequency range under consideration are similar to those at lower frequencies. First is its sensitivity. A detector can generally function at higher efficiency as a frequency converter than as a low-level detector. Second is its selectivity, determined by a series of fixed band-pass circuits in the i-f amplifier, which can be made to provide a satisfactorily uniform response over a desired band width, with sharp rejection outside this band. Furthermore, this selectivity will not vary over the receiver tuning range (under the assumption that the i-f band is narrower than that of the r-f circuits), as is true with tunable r-f amplifiers and detectors. Finally, distortion of the signal modulation is less in a superheterodyne because the second detector receives a relatively large voltage from the i-f amplifier, and hence a linear diode detector can be used to full advantage. The principal disadvantage of the superheterodyne, especially at higher frequencies, is its susceptibility to spurious responses, *i.e.*,

signals appearing in the tuning range at dial settings that do not correspond to their actual frequencies. These spurious responses are normally eliminated by the use of r-f preselection *ahead of the mixer* in the form of tuned antenna circuits and r-f amplifiers. Limitations on available high-frequency tubes, together with the problems of tracking and certain arbitrary restrictions on physical space, have thus far precluded the use of tuned r-f amplifiers. Among the available tubes for r-f amplifiers at the higher frequencies, the most promising was the GL446 lighthouse tube, but when this tube is used as an amplifier above 1500 Mc, it actually decreases the signal-to-noise ratio of the receiver, even though it provides r-f gain. Hence it has been the practice to provide r-f preselection only by means of tunable filters and antenna or mixer circuits, designed to have as low insertion loss in the pass band as possible. In

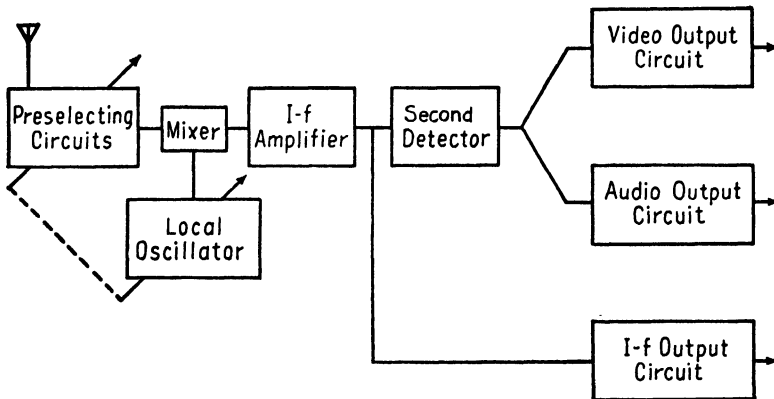


FIG. 25-4.—Block diagram of major components in a wide-range tunable superheterodyne receiver.

some receivers, r-f preselection has been omitted entirely; the operator is left to determine the signal frequency from the oscillator dial readings at the points where the two images are received. The operator must also decide from the frequency separation of the images whether he is working with the fundamental of the oscillator and the signal frequency, or with multiples of either or both.

The essential components of the superheterodyne receiver are shown in Fig. 25-4. It will be noted that it is possible to obtain three sorts of output from a superheterodyne: (1) video output, in which the pulse modulation is reproduced with adequate fidelity for purposes of analysis; (2) audio output, in which the audible components are emphasized, sometimes by deliberately distorting the pulse shape; and (3) i-f output, for analysis and panoramic presentation of the pass band of the i-f amplifier.

It should also be noted that the local oscillator is shown ganged to the preselecting circuits. This is essential if spurious responses are to be eliminated, but at least one early receiver did not incorporate this feature, and, as stated before, one other receiver did not even include the preselecting circuits.

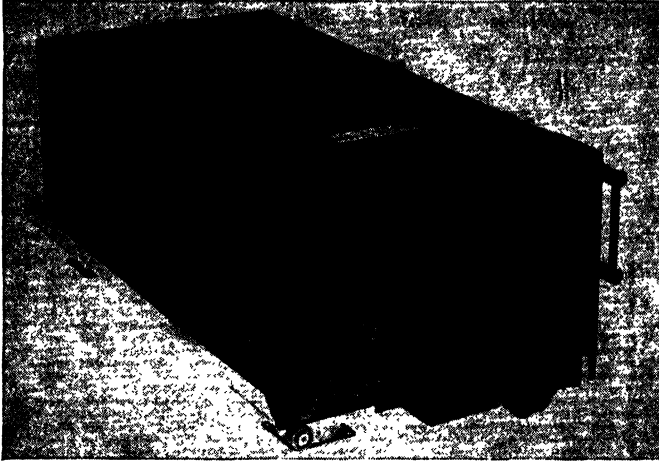


FIG. 25-5.—External view of typical wide-tuning-range wide-band superheterodyne receiver for aircraft service.

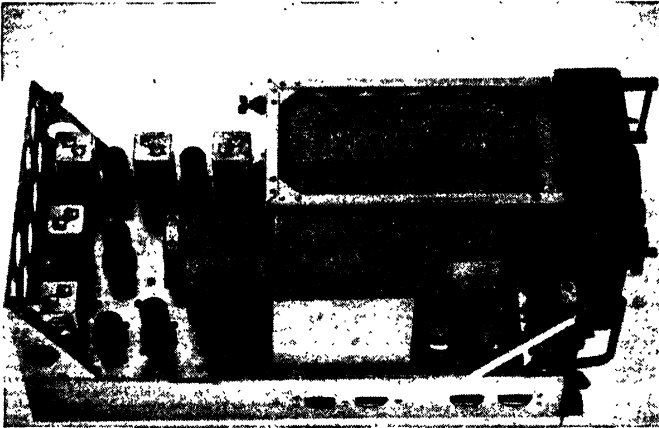


FIG. 25-6.—View of the receiver of Fig. 25-5 with dust cover removed.

A typical example of superheterodyne receiver intended for airborne use is illustrated in Figs. 25-5, 25-6, and 25-7. The first figure shows the external appearance, together with the layout of the controls. The over-all size is about 8 by 10 by 21 in., and, in spite of very rugged construction, the weight is only 40 lb.



In order to obtain maximum use of the basic i-f amplifier and the circuits that follow it, the r-f circuits are provided in the form of a series of plug-in tuning units. An interior view of the basic i-f and video unit is shown in Fig. 25-6, while an interior view of one of the tuners is presented in Fig. 25-7. Four tuners provide coverage from 38 to 3400 Mc, each covering at least a 2 to 1 frequency range.

Although detailed discussion of each of the elements in this and other superheterodynes will be presented in later chapters, several salient and unique features should be pointed out at this time. Single-dial control is provided, and tuning is accomplished either by manual operation of the knob, or by automatic traversing of the frequency range (or any desired

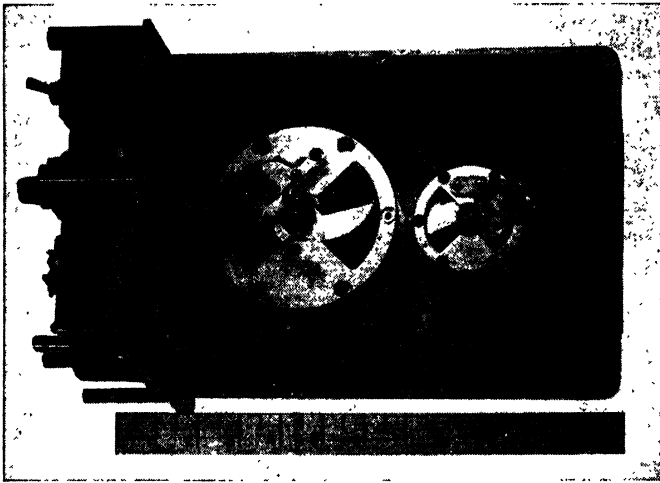


FIG. 25-7.—Interior view of 300 to 1000-Mc tuning unit for receiver of Fig. 25-5.

sector thereof) by means of a small motor coupled to the tuning mechanism through a magnetic clutch that operates when a panel switch is thrown to the AUTOSWEEP position. A mechanical tracking system couples the oscillator and antenna butterfly circuits. The five-stage i-f amplifier has a band width of 4 Mc, centered at 30 Mc, although a front-panel switch enables reduction of the band width to  $\frac{1}{2}$  Mc whenever a narrower band is desirable for separating adjacent signals or for more accurate carrier-frequency measurement. Gain control is provided both in the i-f amplifier and in the audio-video amplifier following the second detector. The i-f gain control is a tap switch, designed for 6-db voltage steps, and thus can be used for determinations of relative signal strength. Output jacks are provided for audio, video, and i-f voltages, the last being labeled PAN because of its use with a panoramic display unit known as a *panoramoscope*. A "heterotone" oscillator, serving the same purpose

as the better-known heterodyne oscillator, provides an audible tone in the presence of unmodulated carriers. A d-c panel meter connected in the diode, second-detector circuit, functions as a volume-level indicator.

The power supply is a separate subassembly and is a dual unit, supplying separate d-c sources for the tuner and for the rest of the receiver. It is designed for a-c operation from a 60- to 2600-cycle source, at either 80 or 115 volts.

The receiver can be used with a variety of antennas and output indicators such as pulse analyzers, panoramic-presentation units, and recorders, all of which will be discussed in Chap. 34.

**25-4. Definition and Measurements of Receiver Performance.**— Chapters to follow, describing the elements that comprise complete receivers, will include discussions of appropriate testing methods for these individual components. These methods stem from the more general problem of defining and testing the performance of the complete receiver itself.

Certain factors for describing receiver performance have been generally adopted. For receivers of the type under consideration in this book, these factors must be reexamined and their significance reevaluated. The most important performance factors may be listed as follows:

1. Sensitivity, which involves
  - a. Noise limitations imposed by the r-f and i-f sections of the receiver
  - b. Adequacy of over-all receiver gain to amplify weak signals, as weak as the noise threshold itself, to a useful level at the output
  - c. Amount of signal required to produce some arbitrary output level
2. Selectivity, which involves
  - a. Adjacent-channel rejection
  - b. Spurious responses due to image frequencies, i-f break-through, and high-order intermodulation in the mixer
3. Fidelity, or ability of the receiver to detect and present, without distortion, the information transmitted in the signal
4. Power-delivering capability, which involves
  - a. Dynamic range of input level which depends upon a-v-c effectiveness
  - b. Maximum attainable output without overload

There are, of course, additional performance details of more specialized nature which it will not be possible to discuss here.

Another type of performance test determines, in terms of arbitrary performance standards, the general suitability of a receiver for a given type of service. An example of such a test procedure is seen in broadcast practice, where the I.R.E. standards<sup>1</sup> specify completely the type of

<sup>1</sup> "Standard on Radio Receivers," pp. 14-15, Institute of Radio Engineers, Inc., New York, 1938.

modulated signal to be supplied by the signal generator, the dummy antenna through which the generator is connected to the receiver, the gain and tone-control settings, and an arbitrary "normal test output." No such standardization exists for the type of receivers described in this book. In fact, there is even lack of agreement upon the methods for comparing two similar receivers with respect to a single performance characteristic such as sensitivity. Therefore the discussion to follow will be directed primarily toward outlining and attempting to evaluate the relative merits of the factors involved in specifying and measuring receiver performance.

**25-5. Receiver Sensitivity.**—The subject of the sensitivity of receivers for the u-h-f and higher ranges has received considerable attention in the current literature,<sup>1</sup> mostly with respect to the influence of thermal-agitation noise in the receiver input circuits. This has resulted from the greater importance that must be assigned to such noise in these frequency ranges, particularly in high-gain wide-range receivers, as compared with the broadcast range. In the latter range, sensitivity is defined<sup>2</sup> solely in terms of signal input required to produce an arbitrary output power. This corresponds to rating the sensitivity of a d-c ammeter only in terms of the current to produce full-scale deflection, the assumption being that the meter will be useful for low currents producing only very small deflections, *e.g.*, one-tenth full scale. Carrying the analogy to the u-h-f case, we may find that one meter reads half of full scale *without any current applied*, while another meter of equal full-scale sensitivity has only one-tenth full-scale residual deflection. The second meter is obviously superior, since it is the only one of the two that can detect relatively weak currents. Therefore when the sensitivity of a receiver, which in a broad sense is a measuring instrument, is described, both "full-scale" sensitivity and noise threshold must be specified. The first is dependent only upon over-all receiver gain, while the second depends basically upon the noise sources and signal-handling efficiency of the receiver input circuits. Nevertheless, it must be emphatically pointed out that it is valueless to build a receiver with a low noise threshold if the over-all gain is inadequate to amplify this noise to a level where it appears at the receiver presentation. This rather obvious requirement has at times actually been overlooked. One example was a receiver for aircraft use, which, merely because of inadequate audio gain, was incapable of amplifying the noise threshold to a level where it could be heard above the

<sup>1</sup> NORTH, D. O., The Absolute Sensitivity of Radio Receivers, *RCA Rev.*, **6**, 332 (1942); HEROLD, E. W., Some Aspects of Radio Reception at Ultra-high-frequency, Part III, The Signal-to-noise Ratio of Radio Receivers, *Proc. I.R.E.*, **31**, 501 (1943).

<sup>2</sup> "Standards on Radio Receivers," Definition 1R36, p. 3, Institute of Radio Engineers, Inc., New York, 1938.

acoustic noise present in the aircraft. Yet in the laboratory this receiver was perfectly capable of detecting exceedingly weak signals.

Thus, although the noise limitation of receivers has come to be defined in terms of a noise figure, which relates only to the theoretical input noise of an ideal receiver, without regard to total gain, the total gain must also be evaluated in over-all testing of the complete receiver. The gain to be specified, in turn, depends upon the exact service for which the receiver is intended, and hence the need for arbitrary standards seems unavoidable.

Actually, two values of gain must be considered, one the minimum gain required to amplify the receiver noise to the point where the noise output is perceptible above the room noise, and the other an arbitrary gain to provide adequate signal output. To whatever extent the receiver transmits differently the noise and the signal, both gains have to be specified and tested independently. Receiver sensitivity can be tested and described in at least two ways. One is to determine independently the quantities described above; the other is to obtain a single figure that combines all of them.

**25-6. Noise Figure.**—The term *noise figure* refers to a figure of merit that compares the actual noise threshold of a receiver with that of a hypothetical noise-free receiver having the same band width. Much has been written on this subject, and only the basic relationships will be introduced here. For purposes of the over-all receiver test, it is most convenient to refer all noise to the input terminals of the receiver. Since the theoretically perfect receiver is defined as one that does not introduce additional noise, the only noise to be considered is that which comes to it from the signal source, *i.e.*, the antenna and transmission circuits. These circuits are treated together, since these tests regard the receiver as an entity in itself, designed to operate from a specified source impedance. Thus, considerations of antenna and transmission efficiency are excluded from this discussion. Consider, therefore, a receiver designed to operate from a voltage source of internal resistance  $R$ . The thermal noise voltage developed in the resistance  $R$ , which is the theoretical minimum noise of the receiver, can be regarded as an equivalent constant-voltage generator in series with  $R$ , as shown in Fig. 25-8. The rms voltage  $E_n$  of this generator is given by the relation

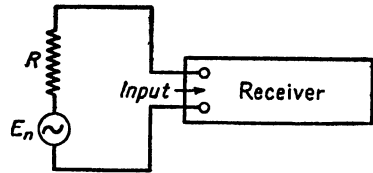


FIG. 25-8.—Equivalent circuit for noise voltage  $E_n$  generated in a resistance  $R$  connected across the input terminals of a receiver. The resistance  $R$  may be the internal resistance of the signal source normally used with the receiver.

$$E_n^2 = 4kTR \Delta f \quad (25-1)$$

where  $k$  = Boltzman's constant,  $1.37 \times 10^{-23}$  joule per deg K

$T$  = temperature of the resistance, degrees Kelvin (usually taken to be room temperature,  $300^\circ\text{K}$ )

$\Delta f$  = receiver-noise band width (precise definition to be given later)

Let  $E_n'$  be the *actual* noise of the receiver, including the theoretical noise, referred back to the voltage source at the input. This is again an equivalent noise voltage in series with the resistance  $R$ , replacing  $E_n$  in Fig. 25-8. Then the noise figure may be defined as

$$F = \left( \frac{E_n'}{E_n} \right)^2 \quad (25-2)$$

This is essentially a power ratio, although, of course, the measurement of  $E_n'$  can be made from either voltage or power. The ratio is usually expressed in decibels, typical figures for microwave receivers ranging from 8 to 30 db.

There are two methods of measuring  $E_n'$ . In either case the test generator must present the specified source impedance for which the receiver is intended. In one case the test generator provides noise of adjustable power and known amount having a uniform frequency spectrum over the receiver pass band. Up to moderately high frequencies such a generator can use as the noise source a temperature-limited diode for which the noise component of the plate current is proportional to the direct current through the diode. This relation has been shown to be<sup>1</sup>

$$I_n^2 = 2eI_{dc} \Delta f \quad (25-3)$$

where  $e$  = charge on the electron,  $1.59 \times 10^{-19}$  coulomb

$I_{dc}$  = direct current in the diode, amperes

$\Delta f$  = band width for which  $I_n$  is the rms noise current

To measure  $E_n'$ , the noise generator, an example<sup>2</sup> of which is shown in Fig. 25-9, is connected to the receiver through the proper source impedance. Noise from the generator is increased from zero until the output noise of the receiver is doubled. The added noise is then equal to the

<sup>1</sup> This is rigorously true only for pure metal filaments. Oxide-coated cathodes have additional noise known as *flicker effect*.

<sup>2</sup> The necessary requirements for use of this circuit are that the diode have a high impedance compared with the desired source resistance  $R$  and that the connections to the receiver be very short. If these conditions are met, Eqs. (25-4) and (25-5) can be used for the measurements. The coupling capacitor  $C_c$  must have essentially zero impedance at the desired noise frequencies. The r-f filter is basically a low-pass filter. It must have no shunt paths for the direct current  $I_{dc}$  and must present to the diode a high impedance at the noise frequencies.

actual receiver noise, referred to the input, plus the thermal noise from the source resistance  $R$ . In measuring the output noise, the principal requirement is that all the significant noise sources be included. Usually noise generated in the receiver beyond the first i-f amplifier stages is ineffective, inasmuch as the signal has assumed such large proportions compared with this noise. Hence the output noise can be measured at any point following these first stages. The indicator must correctly add the rms noise of the receiver and that from the noise generator.

If a 3-db attenuator can be inserted just ahead of the detector at the time the noise from the test generator is added, the requirements for the output indicator can be simplified. The noise generator is connected to the input terminals, and the output from the generator is set at zero. The actual receiver output noise, without the attenuator in the circuit, is then observed on the indicator. The attenuator is next inserted and the output of the noise generator increased until the indicator gives the same reading as before. The added noise is then equal to the original noise, provided that insertion of the attenuator in no way influences the band-pass or gain characteristic of the receiver. It is not necessary for the indicating meter to read linearly in rms values, since the meter receives the same current in both readings. Furthermore, if the receiver has a gain control calibrated with sufficient accuracy, and if changes in the gain do not change the input noise of the receiver (a reasonable approximation if the gain control does not act on a high-gain first i-f stage), then the need for the 3-db attenuator is obviated, and the second detector of the receiver can be used directly as the indicator.

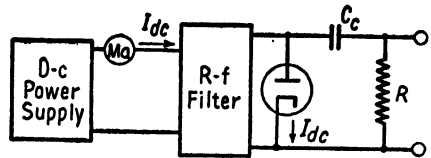


FIG. 25-9.—A simple form of noise generator.

The most useful feature of the noise-generator method arises from the fact that the noise (power, or current squared) produced by the generator is directly proportional to  $\Delta f$ , as indicated by the equation

$$(E_n')^2 = (I_n R)^2 = 2eI_{dc}R^2 \Delta f \tag{25-4}$$

Since the receiver noise figure  $F = (E_n'/E_n)^2$  and  $E_n^2 = 4kTR \Delta f$

$$F = \frac{eI_{dc}R}{2kT} \tag{25-5}$$

It will be noted that  $\Delta f$  has dropped out of the determination. This is a decided help, for it is not easy to measure  $\Delta f$ . Hence receivers of differing band-pass characteristics can be compared more readily by means of the noise-generator method.

The alternative method of measuring the actual receiver noise, referred to the input terminals, is to use a c-w signal generator to supply sufficient energy to double the receiver output indication due to the noise voltage  $E_n'$ . The basic requirement is that the output indicator respond identically to the summation of c-w plus noise energy as it does to noise alone. This requirement necessitates the use of an rms or power type of indicator, including thermocouples, bolometers, etc. The expression for the noise figure is then

$$F = \frac{E_s^2}{4kTR \Delta f} \quad (25-6)$$

where  $E_s$  is the c-w signal voltage applied in series with  $R$  to double the output indication due to the actual receiver noise  $E_n'$ . The quantity  $\Delta f$  is obtained from the selectivity characteristic of the receiver. It is defined by the relation

$$\Delta f = \int_0^\infty \frac{A^2 df}{A_0^2} \quad (25-7)$$

where  $A$  is the voltage amplification at the frequency  $f$  and  $A_0$  the amplification at the reference frequency  $f_0$ . The reference frequency  $f_0$  may be either the center frequency of the pass band or the frequency of maximum gain. In any event  $A_0$  must be the amplification for the frequency at which the c-w signal generator is set during the noise-figure test. It is usually more convenient to use the frequency of maximum gain, which is more easily located in a test.

One difficulty in using the c-w signal generator lies in the measurement of the low input power required. For instance, a typical microwave receiver may have  $F = 15$  db, or a voltage ratio of 4.65 above the theoretical limit of thermal noise from the signal source. For this receiver, if supplied from a 50-ohm antenna, the theoretical noise voltage given by Eq. (25-1) for a typical band width of 4 Mc is

$$E_n = \sqrt{4kTR \Delta f} = \sqrt{4 \times 1.37 \times 10^{-23} \times 300 \times 50 \times 4 \times 10^6} = 1.81 \times 10^{-6} \text{ volt}$$

Hence the actual noise voltage is  $4.65 \times 1.81 \times 10^{-6}$  volt, or only 8.4  $\mu$ v.

**25-7. Minimum Gain Requirement: Standard Noise Output.**—As stated earlier, a receiver that is able to detect weak signals to the limit imposed only by noise must be able to amplify this input noise to a readily observable level at the presentation. Where the conditions of service are accurately known, it is possible to require that a specified minimum noise voltage or power shall be delivered to the receiver output with the receiver gain control set at maximum. For every type of service and for each method of presenting the output, there can be specified a *standard noise output* that defines this minimum noise at the presentation.

For instance, a useful figure for a receiver intended for aural presentation in aircraft installations is 0.5 mw in a 600-ohm noninductive resistor, the power to be measured with an rms meter accurate at frequencies up to 10 kc. The 600-ohm load is an arbitrary one, based upon standard military headphones. For cathode-ray presentation, standard noise level may be defined in terms of a "grass" height equal to, say, one-half of full deflection. Such a standard is, unfortunately, not completely objective, since, if the noise is not clipped, the grass height is purely nominal and can only be estimated. The measurement for intensity-modulated cathode-ray presentations is even more obscure and will not be considered here.

**25-8. Signal Amplification : Standard Output.**—The amount of signal required to produce an arbitrary output at the presentation is usually designated as *standard output*. This is usually a mean value somewhere between the noise threshold and the maximum output that the receiver is capable of delivering without overloading. The important consideration is that the gain thus measured be strictly a signal gain, free of noise considerations and within the linear range of the receiver. As an example, consider again the airborne receiver, for which 0.5 mw can be proposed as a suitable standard noise output. Tests by the Psycho-Acoustic Laboratory at Harvard have shown that, for voice communication, an average speech power of 100 mw at the headphones is required in an airplane at an altitude of 35,000 ft; hence a good receiver must be able to deliver a maximum power of at least this value. A suitable standard output for purposes of sensitivity measurement could then be 10 mw. For military-headphone use this power would be measured with an rms or average meter using a 600-ohm load. If cathode-ray presentation only is to be used, the standard output would be defined as some suitable mean deflection.

The setting of the gain control is a problem. At broadcast frequencies the thermal noise is negligible, and the gain is usually set at maximum. For a high-gain noisy receiver it is not possible to do this and still have standard output represent mostly signal with negligible noise. It therefore becomes impossible to dissociate sensitivity related to signal gain and sensitivity related to noise. A proposal for correlating these sensitivities into a combined figure of merit is presented in the next section.

A basic requirement for measuring the sensitivity for standard output is that the signal be typical of the service intended. In broadcast practice this has been standardized at 30 per cent amplitude modulation with a 400-cycle sine wave. For radar reception, whether with aural or visual presentation, pulse modulation must be used. One standard pulse, based on present radar characteristics, that has been found useful is 2  $\mu$ s in length with a repetition frequency of 1000 cps. Because of



convenience in using conventional signal generators the temptation has been to use sine-wave modulation in testing receivers with aural presentation, even though they were intended for pulse reception. The results thus obtained are quite misleading, since the average audio power in pulse modulation is very low compared with that for sine-wave modulation of the same r-f carrier. Furthermore, if the receiver contains special pulse-stretching circuits to increase this audio power, the only possible way of properly evaluating their effectiveness is through the use of a pulsed signal.

**25-9. Combined Sensitivity Figure.**—In order to provide a single figure whereby receivers intended for the same type of service may be directly compared, the concept of *standard gain setting* is introduced. This is the setting of the gain control that provides delivery of standard noise output. The test procedure consists first of connecting a signal generator of proper source impedance and of specified modulation suitable for the intended service. Then, with zero signal delivered by the generator, the receiver is adjusted for standard gain setting, *i.e.*, for standard noise output. If standard noise output is not achieved, even at maximum gain, then maximum gain is used in lieu of standard gain. The output of the signal generator is then advanced until standard output is obtained at the presentation. The amount of this signal from the generator is then defined as the sensitivity of the receiver.

It is interesting to note how the various design variables show up in such a figure for sensitivity. Consider, for instance, two receivers that have the same maximum gain, but one of which has greater noise, due either to unnecessarily large band width or to poor design of the input circuits. Standard gain for this second receiver will be lower, and thus a larger signal will be required to produce standard output. Of course, if greater band width achieves a certain advantage from some other operating standpoint, this must be weighed separately against the poorer sensitivity. If these two receivers do have comparable input design, the difference being only in band width, they will then be found to have equal noise figures, as defined in Sec. 25-6. That is, *when compared with hypothetical noise-free receivers of the same band width*, they are equally good. Yet, from a practical standpoint, they are not equally good *when compared for the same type of service*. Thus noise figure alone is not an adequate sensitivity specification.

If one of two receivers having the same input noise has insufficient gain to deliver standard noise output, this receiver will require a larger signal to produce standard output and will thus be rated as a poorer receiver for the intended service.

**25-10. Voltage Sensitivity vs. Power Sensitivity.**—Traditionally, in radio-engineering circles at least, the sensitivity of a receiver has been

specified in volts, or microvolts, rather than in watts. Furthermore, for an established service like standard broadcasting, voltage levels of "distant," "local," etc., signals induced in a typical antenna are well-known and appear in the published standards of the Institute of Radio Engineers. On the other hand, in the microwave radar art which has grown up during the war, power measurements are used almost exclusively. For the benefit of those whose work encompasses receivers in the entire range of frequencies extending from the traditional communication bands up through the microwave regions, it is useful to correlate voltage sensitivity and power sensitivity and to point out their relative merits. Each has its field of utility, and the radio engineer should be conversant with both. It is probable that no essential value would be gained by attempting to standardize on either voltage or power for the entire frequency range.

At the lower frequencies, where propagation is primarily ground-wave transmission, the voltage induced in a receiving antenna is calculated as the product of the electric field strength of the wave and the "effective height" of the antenna. It is perfectly convenient to treat the problem thus simply, inasmuch as noise figure, antenna gain, transmission-line loss, etc., usually do not have to be considered. As one moves to higher frequencies, however, particularly in passing into the u-h-f range, these other factors do enter, and in such a way as to make it more convenient to handle all the calculations on a power basis.

Before discussing the use of power in receiver measurements it is necessary to introduce the concept of *maximum available power*. First it should be pointed out that in all standard receiver measurements the signal generator is connected, not to the receiver terminals directly, but in series with an impedance so chosen as to typify the normal source impedance presented by the antenna or transmission line. How much of the energy thus provided by the signal generator is actually absorbed by the receiver is not known unless the exact receiver input impedance is known. Since it is the problem of the receiver designer to utilize this available energy most efficiently, his degree of success will show up in the sensitivity attained. Thus the input voltage or power in any receiver test is actually only a measure of the energy *available* to the receiver. The energy may be expressed in terms of either the voltage that is applied in series with the source impedance, or the *maximum power available*, *i.e.*, that power which would be delivered to the receiver if it were carefully

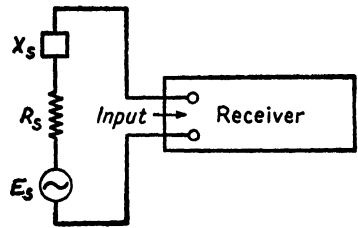


FIG. 25-10.—Equivalent circuit of a signal source connected to receiver input terminals.

matched to the source impedance. The relation between applied voltage and maximum available power is as follows (see Fig. 25-10):

$$P_{\max} = \frac{E_s^2}{4R_s} \quad (25-8)$$

where  $P_{\max}$  = maximum available power

$E_s$  = rms voltage from signal generator

$R_s$  = resistive component of source impedance (including both dummy antenna and signal generator)<sup>1</sup>

In order to illustrate the relative magnitudes of corresponding power and voltage figures, Table 25-1 is presented for the familiar broadcast situation.

TABLE 25-1

Signal	Rms voltage in series with antenna * $E_s$ , volts	Maximum available power † $P_{\max}$ , watts
Distant.....	$50 \times 10^{-6}$ (50 $\mu$ v)	$25 \times 10^{-12}$ (25 $\mu$ $\mu$ w)
Mean.....	$5 \times 10^{-3}$ (5 mv)	$0.25 \times 10^{-6}$ (0.25 $\mu$ w)
Local.....	$100 \times 10^{-3}$ (100 mv)	$100 \times 10^{-6}$ (100 $\mu$ w)
Strong.....	2	$40 \times 10^{-3}$ (40 mw)

\* Listed in "Standards on Radio Receivers," p. 14, Institute of Radio Engineers, 1938.

† For a frequency of 1 Mc, where  $R_s$  for the standard dummy antenna is 25 ohms. The impedance of the signal generator is assumed to be included.

The first reason for defining sensitivity in terms of power rather than voltage as the higher frequencies are reached is the types of measuring instrument available. Signal generators up to 50 Mc may use vacuum-tube voltmeters to measure the r-f voltage, but such voltmeters are not generally used at higher frequencies. The next step is a crystal-type voltmeter, which is used in signal generators up to 1000 Mc. Beyond 1000 Mc, however, it has proved more expedient to use devices such as thermistors and bolometers, which are basically power devices since their operation depends upon a heating phenomenon. Use of such devices to measure directly the maximum available power will be discussed in Chap. 35.

Another reason for defining sensitivity in terms of power is that power is the natural measure of noise. If the equation for thermal noise [Eq. (25-1)] is converted to express maximum available power, it becomes

$$P_n = \frac{E_n^2}{4R} = kT \Delta f \quad (25-9)$$

It is thus seen that the available noise power is independent of the impedance level,  $\Delta f$  being the prime consideration.

<sup>1</sup> The reactance  $X_s$  of the signal source does not enter into the equation.

Finally, high-frequency propagation and transmission are calculated more easily on a power basis. With high-gain antennas, particularly those using reflectors, it is more convenient to talk of intercept areas, rather than effective heights, and thus to talk of fields in terms of watts per square meter rather than volts per meter.

**25-11. Receiver Selectivity.**—Selectivity for receivers of the type discussed in this book has no significant difference from that for conventional receivers, particularly superheterodyne receivers, at the lower frequencies. Such differences as there are reside principally in the difficulty of defining adjacent-channel selectivity when there is no formal assignment of channels as such (see Sec. 33-3). The other difference lies in the realm of spurious responses, where the fundamental principles are no different from superheterodynes in general, but where design limitations make spurious responses a more serious problem than at lower frequencies.

Adjacent-channel selectivity is determined in the usual manner by obtaining curves of relative signal input for a constant receiver output as the frequency of the generator is varied. Here it is acceptable to use a c-w signal, or low-frequency sine-wave modulation, although in broadcast practice it is customary to use the same standard modulation as in the sensitivity test. As the carrier frequency becomes high with respect to the i-f band width, oscillator instability or inadequate precision of resettability—both in the signal generator and in the local oscillator—may preclude measurement of the selectivity curve at the receiver input terminals. Since the r-f circuits usually have much greater band width than the i-f amplifier, it is acceptable and, in fact, preferable to measure the frequency response of the i-f amplifier alone, by using an i-f signal generator connected to the input of the first stage.

The measurement of spurious responses consists in determining the sensitivity of the receiver at one or more arbitrary frequencies within the normal tuning range and for each of these determining the sensitivity for spurious signals by then tuning the signal generator to the appropriate spurious frequencies. The ratio of sensitivity for undesired to that of desired signals, expressed in decibels, is defined as the rejection for each particular type of spurious response. The most serious of these spurious signals is usually the image, *viz.*, the signal whose frequency differs from that of the local oscillator by an amount equal to the intermediate frequency, but whose frequency appears in the spectrum on the opposite side of the local oscillator frequency from the desired signal. The difficulty of obtaining good image rejection makes its determination an important test for receivers intended to indicate a given signal at only one spot on the dial.

The same difficulty of building good r-f preselection to remove the

image makes it necessary to test u-h-f and microwave receivers for spurious responses of other sorts, principally those involving multiples of the local oscillator frequency and of the signal frequency. These are commonly referred to as *harmonic responses*. Even though the receiver oscillator voltage and the signal voltage may initially be devoid of harmonics, both of these r-f voltages are applied to the mixer, which is a nonlinear circuit element. In the output of such a nonlinear circuit there appear frequencies comprising differences (and also sums) of multiples of the original frequencies. When the difference frequency of any pair of multiples is equal to the intermediate frequency of the receiver, the following formulas tell where the signal generator should be set in order to measure each of these harmonic responses.

For receivers in which the local oscillator is tracked at a frequency *higher* than the signal frequency,

$$f = \frac{m}{n} f_{\text{dial}} + \frac{f_i}{n} (m \pm 1) \quad (25-10)$$

where  $f$  = signal-generator setting where spurious response will be found

$n$  = integer (2, 3, etc.) indicating the order of the multiple of signal-generator frequency

$m$  = integer representing the order of the multiple of local-oscillator frequency

$f_{\text{dial}}$  = indicated frequency on the receiver dial

$f_i$  = intermediate frequency of receiver

For receivers whose local-oscillator frequency is *lower* than the signal frequency,

$$f = \frac{m}{n} f_{\text{dial}} - \frac{f_i}{n} (m \pm 1) \quad (25-11)$$

The only other spurious response to be tested is *i-f break-through*, *viz.*, the response due to a strong signal at intermediate frequency reaching the i-f amplifier in spite of the selectivity and shielding in the r-f circuits. The test consists simply in applying a signal of intermediate frequency to the receiver input and comparing the sensitivity thus measured with that for a signal to which the receiver is tuned.

**25-12. Receiver Fidelity.**—Tests for the ability of a receiver to handle properly the type of modulation for which it is intended are as diverse as the varieties of modulation themselves. The choice as to whether one tests with actual modulation of the intended type, and then examines the result on the intended presentation, or whether one synthesizes that modulation by means of sine waves or square waves, depends upon the degree to which objective measurements are desired and realizable and upon the capabilities of available equipment.

**25-13. Receiver Power-output Capability.**—Two power considerations can be specified, one depending primarily on the effectiveness of the a-v-c action in preventing i-f overloading and the other on the power capabilities of the output circuits.

The a-v-c effectiveness should be measured under conditions of standard gain. If the receiver has both i-f and audio (or video) gain controls, the total gain should be apportioned between them, one possible specification being that the audio gain be set at half maximum setting. The signal-generator power is varied from the minimum detectable level to such a level that the output no longer increases. From a curve of output vs. input, the input variation is found that results in an output variation of  $\pm 5$  db from the point on the curve corresponding to standard output. As an example, the superheterodyne receiver described in the introductory section will handle a 60-db input variation for 10-db output variation.

*Maximum output* is a measure of the saturation limits of the high-level circuits of the receiver and is measured with the audio or video gain set at maximum and the i-f gain control retarded to, say, one-half maximum setting. A curve of output power vs. input is then prepared, and from this the maximum is determined. Note that this is not the maximum *undistorted* power output. Although specification and measurement of allowable distortion is a well-established procedure for broadcast service, it is more difficult to specify for pulse or other nonsinusoidal modulation. For aural presentation, the objective being merely the detection of the signal, there is virtually no limit to the tolerable distortion. For video presentation, the purpose being, for instance, measurement of the pulse length, more attention must be paid to overloading. Since the transient response is never perfect, the pulse length at the base line is greater than at the top. Hence, if the output is advanced beyond the overload point, this longer portion of the pulse appears as the complete pulse, and length measurements become erroneous. Distortion of the pulse from the radar standpoint, where precise ranging is the objective, must be held to even closer and more carefully defined limits. Similarly, allowable distortion for television service is another specialized problem and is outside the scope of this book.

## CHAPTER 26

### PRINCIPLES OF TRANSMISSION-LINE FILTER DESIGN

BY S. B. COHN

General filter theory has already been highly developed. Applications of this theory have been made in great detail in the design of a large variety of filters having lumped-impedance elements. Above about 200 Mc it becomes difficult to construct practical high- $Q$  lumped inductances, while above about 2000 Mc it becomes difficult to construct practical lumped capacitances. Cavity resonators and sections of transmission line can, however, be used with success in place of lumped inductances and capacitances.<sup>1</sup> This chapter and the next will present considerable new material on transmission-line filter design based on classical filter theory. Chapter 28 will present design data for narrow-band receiver tuners, which are based on coupled-resonant-circuit theory.

Transmission-line elements have much higher values of  $Q$  than the usual low-frequency inductance. The dissipation can therefore be neglected in all types of transmission-line filters except those having band widths less than about 5 per cent. Hence, the emphasis in this chapter and the next will be on dissipationless structures. Chapter 28 will take account of dissipation in narrow-band tuners.

**26-1. Fundamental Filter Relations.**—In the following discussion it is assumed that the reader has an elementary knowledge of transmission-line, network, and filter theory.<sup>2</sup> All elements are assumed to be linear, and the networks to be passive.

Any linear passive two-terminal-pair network,<sup>3</sup> no matter how complex, obeys the following simple voltage-current relations:

<sup>1</sup> MASON, W. P., and R. A., SYKES The Use of Coaxial and Balanced Transmission Lines in Filters and Wide-band Transformers for High Radio Frequencies, *Bell System Tech. J.*, **16**, 275 (1937). MASON, W. P., "Electromechanical Transducers and Wave Filters," pp. 58-79, D. Van Nostrand Company, Inc., New York, 1942.

<sup>2</sup> The following references may be consulted for an introduction to basic filter theory: GUILLEMIN, E. A., "Communication Networks," Vol. II, Chap. 4, John Wiley & Sons, Inc., New York, 1935; STARR, A. T., "Electrical Circuits and Wave Filters," Chap. 6, Sir Isaac Pitman & Sons, Ltd., London, 1934.

<sup>3</sup> This is often called a four-terminal network, but since of the four, two are always designated as input and two as output terminals, the term *two-terminal-pair* is more accurate.

$$\begin{cases} E_1 = AE_2 + BI_2 \\ I_1 = CE_2 + DI_2 \end{cases} \tag{26-1}$$

As shown in Fig. 26-1,  $E_1$  and  $I_1$  are the input voltage and current, while  $E_2$  and  $I_2$  are the output voltage and current. The parameters  $A$ ,  $B$ ,  $C$ , and  $D$  are functions both of the network structure and of the frequency. They are independent of the voltage and the current and the external impedances presented to the network terminals. Any three of these

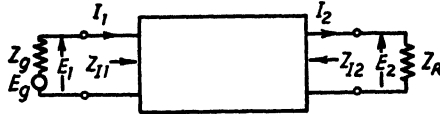


FIG. 26-1.—Two-terminal-pair network.

four parameters are sufficient to describe the network fully, since  $A$ ,  $B$ ,  $C$ , and  $D$  are related by the identity<sup>1</sup>

$$AD - BC \equiv 1 \tag{26-2}$$

The performance of the network may also be determined from the *image transfer constant*  $\Theta$ , the *input image impedance*  $Z_{I1}$ , and the *output image impedance*  $Z_{I2}$ . In terms of  $A$ ,  $B$ ,  $C$ , and  $D$ , these are

$$\cosh \Theta = \sqrt{AD} \tag{26-3}$$

$$Z_{I1} = \sqrt{\frac{BA}{CD}} \tag{26-4}$$

$$Z_{I2} = \sqrt{\frac{BD}{CA}} \tag{26-5}$$

In these equations, and in similar ones to follow, a plus sign is used before the radical if  $Z_{I1}$ ,  $Z_{I2}$ , or  $\Theta$  is real. For imaginary values of these quantities, the sign is chosen so that the rate of change of  $Z_{I1}$ ,  $Z_{I2}$ , or  $\Theta$  with frequency is positive.

If the network is *symmetrical*,  $A = D$  and therefore

$$Z_{I1} = Z_{I2} = Z_I = \sqrt{\frac{B}{C}} \tag{26-6}$$

$$\cosh \Theta = A = D \tag{26-7}$$

$\Theta$  is in general a complex number  $\alpha + j\beta$ , where the attenuation constant  $\alpha$  and the phase constant  $\beta$  are both real numbers. If the network is nondissipative,  $\Theta = j\beta$  in pass bands, and  $\Theta = \alpha$  in stop bands. Another way of stating this is that pass bands exist only in ranges of frequencies in

<sup>1</sup> This identity is valid for any network for which the *reciprocity theorem* is valid. This includes all linear passive networks that have no *unidirectional* elements such as vacuum tubes.



which  $\cosh \Theta$  lies between  $-1$  and  $+1$ . Also, for nondissipative networks  $Z_I$  is a real number in pass bands and purely imaginary in stop bands.

Solution of Eqs. (26-2) to (26-5) for  $A$ ,  $B$ ,  $C$ , and  $D$  gives the following relations

$$\left. \begin{aligned} A &= \sqrt{\frac{Z_{I1}}{Z_{I2}}} \cosh \Theta & B &= \sqrt{Z_{I1}Z_{I2}} \sinh \Theta \\ C &= \frac{1}{\sqrt{Z_{I1}Z_{I2}}} \sinh \Theta & D &= \sqrt{\frac{Z_{I2}}{Z_{I1}}} \cosh \Theta \end{aligned} \right\} \quad (26-8)$$

Therefore, with the aid of Eq. (26-1), the voltage-current equations for any linear passive two-terminal-pair network may be written

$$\left. \begin{aligned} E_1 &= \left( \sqrt{\frac{Z_{I1}}{Z_{I2}}} \cosh \Theta \right) E_2 + \left( \sqrt{Z_{I1}Z_{I2}} \sinh \Theta \right) I_2 \\ I_1 &= \left( \frac{1}{\sqrt{Z_{I1}Z_{I2}}} \sinh \Theta \right) E_2 + \left( \sqrt{\frac{Z_{I2}}{Z_{I1}}} \cosh \Theta \right) I_2 \end{aligned} \right\} \quad (26-9)$$

The *input impedance* of the network is  $Z_s = E_1/I_1$ . The *load impedance* of the network is  $Z_R = E_2/I_2$ . In terms of these quantities, Eq. (26-9) may be written

$$Z_s = Z_{I1} \frac{Z_R + Z_{I2} \tanh \Theta}{Z_{I2} + Z_R \tanh \Theta} \quad (26-10)$$

If the network is symmetrical,  $Z_{I1} = Z_{I2} = Z_I$ , and Eq. (26-10) becomes

$$Z_s = Z_I \frac{Z_R + Z_I \tanh \Theta}{Z_I + Z_R \tanh \Theta} \quad (26-11)$$

And for a nondissipative symmetrical network in a pass band

$$Z_s = Z_I \frac{Z_R + jZ_I \tan \beta}{Z_I + jZ_R \tan \beta} \quad (26-12)$$

For the important special case of a symmetrical nondissipative two-terminal-pair network consisting simply of a length of uniform nondissipative transmission line, a different image impedance and image phase constant will be defined to avoid confusion. The *characteristic impedance* symbol  $Z_0$  will be used in place of  $Z_I$ , and the *phase-length* symbol  $\theta$  will be used in place of  $\beta$ . Equations (26-8), (26-9), and (26-12) are written below for a nondissipative transmission line of length  $\theta$ .

$$\left. \begin{aligned} A &= \cos \theta & B &= jZ_0 \sin \theta \\ C &= \frac{j}{Z_0} \sin \theta & D &= \cos \theta \end{aligned} \right\} \quad (26-13)$$

$$\left. \begin{aligned} E_1 &= E_2 \cos \theta + jE_2 Z_0 \sin \theta \\ I_1 &= j \frac{E_2}{Z_0} \sin \theta + I_2 \cos \theta \end{aligned} \right\} \quad (26-14)$$

$$Z_s = Z_0 \frac{Z_R + jZ_0 \tan \theta}{Z_0 + jZ_R \tan \theta} \quad (26-15)$$

$\theta$  is related to the physical length of the line and to frequency by the formula

$$\theta = \frac{2\pi l}{\lambda} = \frac{\omega l}{v} \quad (26-16)$$

where  $l$  = line length, cm

$\lambda$  = wavelength on the line, cm

$\omega$  = angular frequency =  $2\pi f$ ,  $2\pi \times$  cps

$v$  = velocity of propagation along the line, cm per sec

For air dielectric in a simple transmission line,  $v = 3 \times 10^{10}$  cm per sec. For dielectric constant  $\epsilon$ ,  $v = 3 \times 10^{10} \sqrt{\epsilon}$  cm per sec.

It should be pointed out that, since a symmetrical filter network of image impedance  $Z_I$  and image phase constant  $\beta$  is mathematically equivalent to a uniform transmission line of characteristic impedance  $Z_0 = Z_I$  and phase length  $\theta = \beta$ , all equations, line charts, and concepts derived for transmission lines apply equally to symmetrical filters, and vice versa.

**26-2. Calculation of the Image Impedance and Transfer Constant from the Short- and Open-circuit Impedances.**—In the design of transmission-line filters it is often easy to obtain design equations giving the desired cutoff frequencies, but the image-impedance and transfer-constant equations may be so complex as to discourage their use. In such cases these parameters may be calculated from the impedances  $Z_{sc1}$  and  $Z_{oc1}$  measured at the number-one pair of terminals when the number-two pair are short-circuited and open-circuited, respectively. These *short-circuit* and *open-circuit* impedances are usually quite easy to calculate for a given filter section by means of a transmission-line circle-diagram chart. The Smith chart (see Sec. 2-2) is particularly useful for this purpose. Since the filter section undergoing calculation is assumed to be non-dissipative, all impedances will be pure reactances, and therefore all points will fall on the outer rim of the Smith chart.

Equation (26-1) shows that  $Z_{sc1} = B/D$  and  $Z_{oc1} = A/C$ . With the aid of Eqs. (26-2), (26-3), and (26-4), it is easily shown that

$$Z_{I1} = \sqrt{Z_{sc1} Z_{oc1}} \quad (26-17)$$

$$\tanh \Theta = \sqrt{\frac{Z_{sc1}}{Z_{oc1}}} \quad (26-18)$$

**26-3. Symmetrical-section Parameters in Terms of the Half-section Parameters.**—Any symmetrical filter section may be split (at least on paper) into two equal half sections, as shown in Fig. 26-2. All the properties of the full section may be calculated from one of the half sections. The labor involved in such a procedure is usually less than that for analysis of the full section by the relations of Sec. 26-1. The half section itself is in general an unsymmetrical network, and it must be treated as such. Consider the half section at the left in Fig. 26-2. The image impedance at the No. 1 terminals is easily shown to be the same for a half section as for a full section. The image transfer constant is one-

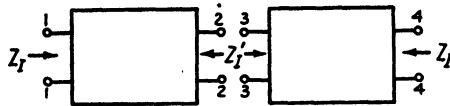


FIG. 26-2.—A symmetrical filter section divided into two equal half sections.

half that for a full section. In terms of the coefficient parameters  $A'$ ,  $B'$ ,  $C'$ ,  $D'$  for the half-section, and  $\Theta$  for the symmetrical section,

$$Z_i = \sqrt{\frac{B'A'}{C'D'}} \tag{26-19}$$

$$\cosh\left(\frac{\Theta}{2}\right) = \sqrt{A'D'} \tag{26-20}$$

and therefore

$$\cosh \Theta = A'D' + B'C' = 2A'D' - 1 = 1 + 2B'C' \tag{26-21}$$

Since the edges of the pass band are given by  $\cosh \Theta = \pm 1$ , they are also given by

$$A'D' = 0 \quad \text{or} \quad B'C' = 0 \tag{26-22}$$

The image impedance and transfer constant may also be calculated from the short-circuit and open-circuit impedances of the half section. Let these impedances be  $Z_{sc1}'$  and  $Z_{oc1}'$  as measured at terminals No. 1 when terminals No. 2 are short-circuited and open-circuited, respectively. Then

$$Z_i = \sqrt{Z_{sc1}'Z_{oc1}'} \tag{26-23}$$

$$\tanh \frac{\Theta}{2} = \sqrt{\frac{Z_{sc1}'}{Z_{oc1}'}} \tag{26-24}$$

If, in Fig. 26-2, terminal pairs 1 and 4 are joined together, a new, though similar, type of symmetrical section will result which has pairs 2 and 3 as input and output terminals. The image transfer constant is still given by Eq. (26-21) or Eq. (26-24), and therefore the cutoff frequencies, the image phase constant, and the image attenuation con-

stant are the same as for the original section. The image impedance at the new outer terminals is different, however, and is given by the relation

$$Z_i' = \sqrt{\frac{B'D'}{C'A'}} \tag{26-25}$$

where  $A'$ ,  $B'$ ,  $C'$ , and  $D'$  for the half section are the same as before.

**26-4. The Equivalent-circuit Method of Filter Analysis.**—Filter structures having distributed-constant elements may be analyzed in a variety of ways ranging from very simple and approximate methods to complicated and exact ones. Analysis methods that have been found useful are described in this section and in Secs. 26-5 and 26-6.

The easiest method of designing a transmission-line filter is to use short lengths of line as lumped inductances and capacitances in standard lumped-constant filter circuits.<sup>1</sup> A length of line may be replaced at

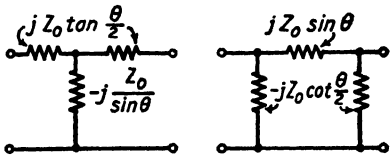


FIG. 26-3.—Exact equivalent circuits for a nondissipative transmission line of phase length  $\theta$  and characteristic impedance  $Z_0$ .

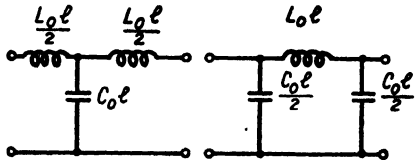


FIG. 26-4.—Approximate equivalent circuits for a nondissipative transmission line of physical length  $l$ , inductance per unit length  $L_0$ , and capacitance per unit length  $C_0$ , where  $l$  is less than  $\frac{1}{8}$  wavelength.

one frequency by a T-network or by a  $\pi$ -network, as shown in Fig. 26-3. If the line length  $l$  is less than  $\frac{1}{8}$  wavelength, the series and shunt arms may be approximated by constant inductances and capacitances, as shown in Fig. 26-4.  $L_0$  is the series inductance, and  $C_0$  is the shunt capacitance per unit length of line. For a coaxial line,

$$Z_0 = \frac{60}{\sqrt{\epsilon}} \ln \frac{b}{a} \quad \text{ohms} \tag{26-26}$$

$$L_0 = 2(10)^{-9} \ln \frac{b}{a} = \frac{Z_0}{v} \quad \text{henrys per cm} \tag{26-27}$$

$$C_0 = \frac{0.556\epsilon}{\ln \frac{b}{a}} (10)^{-12} = \frac{1}{Z_0 v} \quad \text{farads per cm} \tag{26-28}$$

where  $Z_0$  = characteristic impedance of the transmission line  
 $b$  = inner radius of the outer conductor of the line  
 $a$  = outer radius of the inner conductor of the line

<sup>1</sup> MASON, *loc. cit.*

$\epsilon$  = dielectric constant of the insulating material filling the space between the inner and outer conductors ( $\epsilon = 1$  for empty space)

$v$  = velocity of propagation of energy in the line, centimeters per second

For very short lengths of line, a still simpler approximation may be made. For example, a short length of line terminated by an impedance several times smaller than its characteristic impedance acts very nearly like a series inductance. Equation (26-15) may be written

$$Z_s = \frac{Z_0[Z_R Z_0(1 + \tan^2 \theta) + j \tan \theta(Z_0^2 - Z_R^2)]}{Z_0^2 + Z_R^2 \tan^2 \theta} \quad (26-29)$$

If  $Z_R \ll Z_0$  (say  $Z_R \leq Z_0/4$ ) and  $\theta \ll \pi/2$  (say  $\theta \leq 1/2$  radian), then  $\tan \theta \approx \theta \approx \omega l/v = 2\pi l/\lambda$ , and  $Z_s$  has the approximate value given by the relation

$$Z_s \approx Z_R(1 + \tan^2 \theta) + j \frac{lZ_0}{v} \omega \approx Z_R + j \frac{lZ_0}{v} \omega \quad (26-30)$$

where  $l$  is the line length in centimeters. Therefore  $Z_s$  is given approximately by the series circuit of the load impedance  $Z_R$  and an equivalent inductance  $lZ_0/v$ . The latter is shown by Eq. (26-27) to be merely the total series inductance  $L_0 l$  of the line.

In a similar fashion, it may be shown that if  $Z_R \gg Z_0$  (say  $Z_R \geq 4Z_0$ ) and  $\theta$  is restricted as before, the input impedance is given approximately by the parallel circuit of the load impedance  $Z_R$  shunted by the capacitance  $C_0 x = l/Z_0 v$ .

In particular, a short-circuited line shorter than about  $1/12$  wavelength acts almost like a pure lumped inductance, *i.e.*, its input reactance is proportional to frequency, while an open line shorter than about  $1/12$  wavelength acts almost like a pure lumped capacitance, *i.e.*, its input reactance is inversely proportional to frequency. Use can be made of these properties in determining the approximate equivalent circuit of a transmission-line filter composed of short lines. For examples, see Tables 27-1 and 27-2.

A more exact equivalent circuit is obtained by using the T- or  $\pi$ -section of Fig. 26-4.<sup>1</sup> In this case, the shunt capacitances in the T- or  $\pi$ -section are lumped where possible with actual capacitances already present in the filter. For still greater accuracy, the exact T- or  $\pi$ -network of Fig. 26-3 may be used instead of Fig. 26-4.

*Example:* The approximate design equations for the filter of Fig. 26-5a will be derived by the use of Fig. 26-4. In Fig. 26-5b is shown the exact circuit representation of the physical structure of Fig. 26-5a. Any number of these

<sup>1</sup> MASON, *loc. cit.*

sections may be connected in cascade, in the usual manner. The circuit representation for a transmission line as used here and in later sections is a rectangular box with a pair of input terminals and a pair of output terminals. The length and characteristic impedance of the line are noted in the rectangle as  $Z_{02}$ ,  $l_2$ , etc.

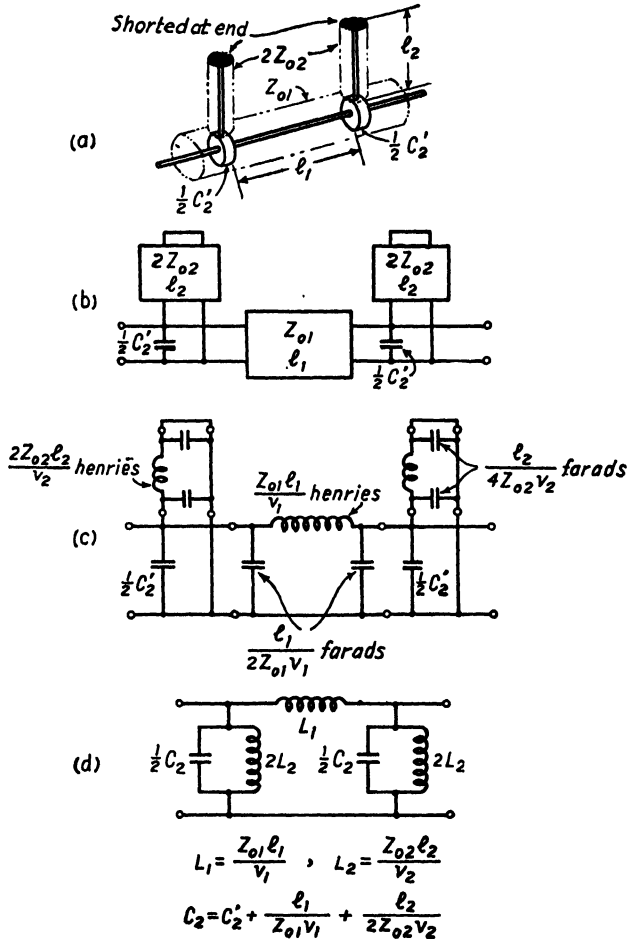


FIG. 26-5.—Example showing the development of the approximate circuit for a transmission-line filter: (a) the filter; (b) the exact circuit representation of (a); (c) and (d) the approximate equivalent circuit.

Connections between boxes are assumed to have zero length. Figure 26-5 shows the approximate equivalent circuit arrived at by the use of the transmission-line approximation of Fig. 26-4. In Fig. 26-5d, the shunt capacitances are grouped together. The last circuit is seen to be that of a standard lumped-element band-pass filter section, having the following design equations:<sup>1</sup>

<sup>1</sup>TERMAN, F. E., "Radio Engineers' Handbook," p. 231, McGraw-Hill Book Company, Inc., 1943.

$$L_1 = \frac{R}{\pi(f_1 + f_2)}, \quad L_2 = \frac{(f_2 - f_1)R}{4\pi f_1^2}, \quad C_2 = \frac{1}{\pi(f_2 - f_1)R} \quad (26-31)$$

where  $R$  is the load resistance that may be used with the filter,  $f_1$  is the lower cutoff frequency, and  $f_2$  is the upper cutoff frequency.

Upon introduction of the values for  $L_1$ ,  $L_2$ , and  $C_2$  from Fig. 26-5*d*, the approximate design equations for the short-length transmission-line filter of Fig. 26-5*a* are found to be

$$\left. \begin{aligned} Z_{01}l_1 &= \frac{vR}{\pi(f_1 + f_2)} \\ Z_{02}l_2 &= \frac{v(f_2 - f_1)R}{4\pi f_1^2} \\ C_2' &= \frac{1}{\pi(f_2 - f_1)R} - \frac{l_1}{Z_{01}v} - \frac{l_2}{2Z_{02}v} \end{aligned} \right\} \quad (26-32)$$

These approximate design equations will hold quite well as long as  $l_1$  and  $l_2$  are not longer than about  $\frac{1}{4}$  wavelength at the upper cutoff frequency,  $f_2$ .

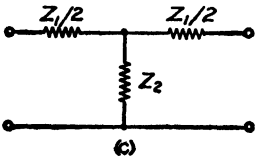
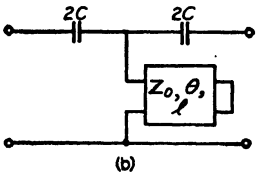
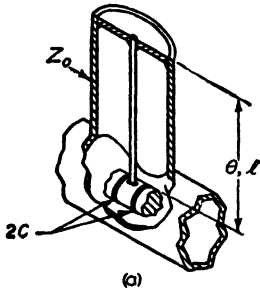


FIG. 26-6.—(a) A transmission-line filter section; (b) its circuit representation; and (c) the standard T-section form to which it corresponds.

**26-5. Exact Equivalent-circuit Method of Filter Analysis.**—There are several types of transmission-line filters that have lumped series capacitances and a shunt transmission-line structure, *e.g.*, types 1-2, 1-4, and 4-3 in Tables 27-1 and 27-4. Such a structure has an exact T or  $\pi$  counterpart; hence the standard filter analysis in terms of lumped shunt-arm and series-arm impedances may be used.

A number of other types that have shunt structures at the end and a length of line in the middle, *e.g.*, the type of Fig. 26-5, can be analyzed exactly in this manner, since when this line is replaced by its exact equivalent  $\pi$ -section, a circuit having the form of a  $\pi$ -section filter will result.

*Example:* The transmission-line filter of Fig. 26-6*a* will be analyzed by the method of this section. Figure 26-6*b* shows the exact circuit representation of Fig. 26-6*a*. This is seen to have the form of the ordinary T-section shown in 26-6*c*. For the filter section under consideration, the series-impedance and shunt-impedance arms have the values

$$Z_1 = \frac{1}{j\omega C}, \quad Z_2 = jZ_0 \tan \theta \quad (26-33)$$

where  $Z_2$  is calculated from Eq. (26-15), with  $Z_R = 0$ . The image impedance and the image transfer constant for any T-section are given by the equations<sup>1</sup>

<sup>1</sup> TERMAN, *op. cit.*, p. 226.

$$Z_I = \sqrt{Z_1 Z_2 + \frac{1}{4} Z_1^2} \tag{26-34}$$

$$\cosh \Theta = 1 + \frac{Z_1}{2Z_2} \tag{26-35}$$

Substituting the values for  $Z_1$  and  $Z_2$  in Eqs. (26-34) and (26-35), we obtain

$$Z_I = \sqrt{\frac{Z_0}{\omega C} \left( \tan \theta - \frac{1}{4\omega C Z_0} \right)} \tag{26-36}$$

$$\cosh \Theta = 1 - \frac{1}{2\omega C Z_0 \tan \theta} \tag{26-37}$$

Boundaries between stop bands and pass bands occur at frequencies for which  $Z_I$  changes from an imaginary quantity to a real quantity. Inspection of Eq. (26-36) shows that for low frequencies  $Z_I$  is imaginary, and hence a stop band exists.  $Z_I$  changes from imaginary to real at all values of  $\theta$  for which  $\tan \theta = 1/(4\omega C Z_0)$ , and back to imaginary for  $\theta$  an odd multiple of  $\pi/2$  radians. Therefore, pass bands exist between corresponding values of  $\theta = \tan^{-1} [1/(4\omega C Z_0)]$

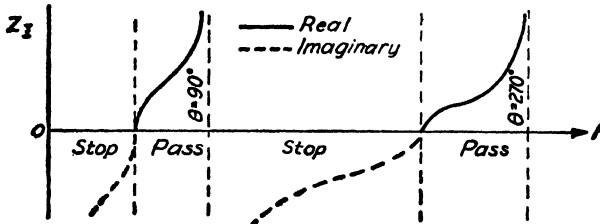


FIG. 26-7.—The image impedance function for the filter of Fig. 26-6 with the location of stop bands and pass bands noted.

and  $\theta = n\pi/2$ , where  $n$  is odd. The image impedance is sketched in Fig. 26-7 for the first few stop and pass bands. The filter is seen to be of a multiple-band-pass type.

If the lower cutoff frequency of the first pass band is  $f_1$  and the upper is  $f_2$ , the following equations are valid:

$$\theta_2 = \frac{2\pi f_2 l}{v} = \frac{\pi}{2} \tag{26-38}$$

$$2\pi f_1 \tan \left( \frac{2\pi f_1 l}{v} \right) = \frac{1}{4CZ_0} \tag{26-39}$$

The design equations are, therefore,

$$l = \frac{v}{4f_2} = \frac{\lambda_2}{4} \tag{26-40}$$

$$CZ_0 = \frac{1}{8\pi f_1 \tan \left( \frac{2\pi f_1 l}{v} \right)} \tag{26-41}$$

The image-impedance function of Eq. (26-36) may now be written as follows:

$$Z_I = \sqrt{\frac{Z_0}{C} \left( \frac{f \tan \theta - f_1 \tan \theta_1}{2\pi f^2} \right)} \tag{26-42}$$



where  $\theta = 2\pi fl/v$  and  $\theta_1 = 2\pi f_1 l/v$ . A change in the value of the ratio  $Z_0/C$  does not change the cutoff frequencies, as long as the product  $CZ_0$  satisfies Eq. (26-41). This ratio should be chosen so that in the pass band the image-impedance function of Eq. (26-42) will approximate the constant load resistance  $R$  of the filter as closely as possible. This kind of choice is always possible with filter networks and will be considered in Sec. 26-8.

The multiplicity of pass bands found for the filter section of Fig. 26-6 is characteristic of transmission-line filters. Pass bands will usually occur at or near the frequencies for which the various line elements in the filter are either odd or even multiples of  $1/4$  wavelength, or both.

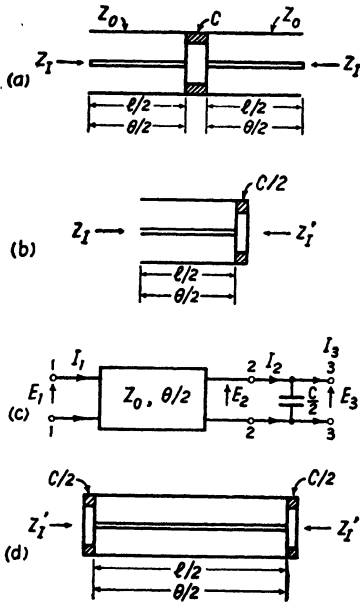


FIG. 26-8.—(a) A transmission-line filter section; (b) its half section; (c) the circuit representation of the half section; (d) a second filter type that may be analyzed by means of the same half section.

26-6. The Fundamental Analysis Method.—In the general case it is often not possible to use the methods given above. A method that is always applicable is to solve the filter circuit for the voltage-current equations of the form of Eq. (26-1).<sup>1</sup> The image-transfer constant  $\Theta$  and the image impedance  $Z_I$  are then determined from the coefficients of the voltage-current equations by means of Eqs. (26-3) and (26-6). The location of stop bands and pass bands and the optimum terminating resistance may then be determined from  $\Theta$  and  $Z_I$ . For  $\Theta$  real and  $Z_I$  imaginary, a stop band exists. For  $Z_I$  real and  $\Theta$  imaginary, a pass band exists. The optimum terminating resistance may be chosen as indicated in Sec. 26-8.

It is usually simpler to calculate the image impedance and transfer constant from the coefficients  $A', B', C',$  and  $D'$  for the half section than for the whole symmetrical filter section.  $Z_I$  and  $\Theta$  are then calculated by means of Eqs. (26-19) and (26-21). Cutoff frequencies may be obtained from the relations of Eq. (26-22). These relations show that a cutoff frequency occurs whenever any one of the coefficients  $A', B', C',$  or  $D'$  is zero, as long as the corresponding quantity  $D', C', B',$  or  $A',$  respectively, is not infinite.<sup>2</sup>

<sup>1</sup> MASON and SYKES, *op. cit.* Examples are worked out in this paper.

<sup>2</sup> RICHARDS, P. I., The Application of Matrix Algebra to Filter Theory, *Proc. I.R.E.*, 34, 145 (1946).

*Example:* The filter section of Fig. 26-8a will be analyzed by the last method. The half section for this filter is shown in Fig. 26-8b, and its circuit representation in Fig. 26-8c. It is necessary to calculate the coefficients  $A'$ ,  $B'$ ,  $C'$ , and  $D'$  from the following relations that connect the input voltage and current with the output voltage and current of the half section:

$$\left. \begin{aligned} E_1 &= A'E_3 + B'I_3 \\ I_1 &= C'E_3 + D'I_3 \end{aligned} \right\} \quad (26-43)$$

In order to set up these relations, the voltage-current relations for each element of the filter must first be written. For the capacitance

$$\left. \begin{aligned} E_2 &= E_3 \\ I_2 &= \frac{j\omega C}{2} E_3 + I_3 \end{aligned} \right\} \quad (26-44)$$

and for the length of transmission line

$$\left. \begin{aligned} E_1 &= E_2 \cos \frac{\theta}{2} + jI_2 Z_0 \sin \frac{\theta}{2} \\ I_1 &= j \frac{E_2}{Z_0} \sin \frac{\theta}{2} + I_2 \cos \frac{\theta}{2} \end{aligned} \right\} \quad (26-45)$$

Equations (26-44) and (26-45) are then combined so as to eliminate the intermediate voltage and current,  $E_2$  and  $I_2$ . The resulting relations have the form of Eq. (26-43), and the coefficients are found to be

$$\left. \begin{aligned} A' &= \cos \frac{\theta}{2} - \frac{\omega C Z_0}{2} \sin \frac{\theta}{2}, & B' &= j Z_0 \sin \frac{\theta}{2} \\ C' &= j \left( \frac{\sin \frac{\theta}{2}}{Z_0} + \frac{\omega C}{2} \cos \frac{\theta}{2} \right), & D' &= \cos \frac{\theta}{2} \end{aligned} \right\} \quad (26-46)$$

The image impedance and transfer constant can now be written with the aid of Eqs. (26-19) and (26-21) and are

$$Z_I = \sqrt{\frac{\left( Z_0 \sin \frac{\theta}{2} \right) \left( \cos \frac{\theta}{2} - \frac{\omega C Z_0}{2} \sin \frac{\theta}{2} \right)}{\left( \frac{\sin \frac{\theta}{2}}{Z_0} + \frac{\omega C}{2} \cos \frac{\theta}{2} \right) \left( \cos \frac{\theta}{2} \right)} \quad (26-47)$$

$$\cosh \Theta = 2 \left( \cos \frac{\theta}{2} \right) \left( \cos \frac{\theta}{2} - \frac{\omega C Z_0}{2} \sin \frac{\theta}{2} \right) - 1 \quad (26-48)$$

Examination of Eq. (26-47) shows that the image impedance is real between zero frequency and the frequency at which  $C' = 0$ . Therefore, the filter of Fig. 26-8a is a low-pass type. Further examination shows that higher pass bands exist above the first attenuation band. These have a relatively narrow band width.

The image impedance of the filter of Fig. 26-8d may be written at once with the aid of Eq. (26-25) and is

$$Z_i' = \sqrt{\frac{\left(Z_0 \sin \frac{\theta}{2}\right) \left(\cos \frac{\theta}{2}\right)}{\left(\frac{\sin \frac{\theta}{2}}{Z_0} + \frac{\omega C}{2} \cos \frac{\theta}{2}\right) \left(\cos \frac{\theta}{2} - \frac{\omega C Z_0}{2} \sin \frac{\theta}{2}\right)} \quad (26-49)$$

The image-transfer constant for Fig. 26-8d is the same as for Fig. 26-8a, and is given by Eq. (26-48). Therefore, the filter section of Fig. 26-8d is a low-pass type having the same cutoff frequency as the one of Fig. 26-8a.

Equation (26-1) for a given filter can be calculated as in the preceding example or by means of matrix algebra. The work is considerably shortened and chances for errors are greatly reduced, if elementary matrix algebra is used.<sup>1</sup> With matrix algebra, only the coefficients of the various voltage-current equations are handled, and these are handled in a systematic way that reduces the analysis to a bare minimum.

**26-7. Filter Insertion Loss.**<sup>2</sup>—*Insertion loss* of a network is defined as the decibel loss in power delivered to the load when the network is inserted between the generator and load as compared with the power delivered when the generator and load are connected directly. In terms of the fundamental voltage-current-equation coefficients, the general insertion-loss equation may be written as follows:

$$L = 10 \log_{10} \left| \frac{AZ_i + DZ_g + B + CZ_g Z_i}{Z_g + Z_i} \right|^2 \quad \text{db} \quad (26-50)$$

where  $Z_g$  and  $Z_i$  are the generator and load impedances. If  $Z_g = Z_i = R$  (real) and the network is symmetrical and nondissipative,

$$L = 10 \log_{10} \left[ 1 + \frac{1}{4} \left( \frac{B}{jR} - \frac{C}{j} R \right)^2 \right] \quad (26-51)$$

These formulas can be rewritten in numerous ways for special cases. For example, if  $Z_g = Z_i = R$  (real) and the network is a symmetrical  $n$ -section nondissipative filter, then in the *pass band*  $Z_i$  will be real and

$$L = 10 \log_{10} \left[ 1 + \frac{1}{4} \left( \frac{Z_i}{R} - \frac{R}{Z_i} \right)^2 \sin^2 n\beta \right] \quad \text{db} \quad (26-52)$$

In the *stop band*,  $Z_i = 0 + jX_i$ , and

$$L = 10 \log_{10} \left[ 1 + \frac{1}{4} \left( \frac{X_i}{R} + \frac{R}{X_i} \right)^2 \sinh^2 n\alpha \right] \quad \text{db} \quad (26-53)$$

<sup>1</sup> PIPES, L. A., Matrix Theory of Four-terminal Networks, *Phil. Mag.*, **30**, 370 (1940); GUILLEMIN, E. A., "Communication Networks," Vol. II, p. 140, John Wiley & Sons, Inc., New York, 1935; RICHARDS, *op. cit.*

<sup>2</sup> See RICHARDS, *op. cit.*

These equations are extremely useful in predicting the response of a filter of given design and in choosing the optimum load resistance for particular image-impedance and phase-shift functions. Figures 26-9 and 26-10 express Eqs. (26-52) and (26-53) in nomogram form, thus making their use very simple. A straightedge intersecting any two variables on these nomograms will also intersect the third variable. In Fig. 26-9,

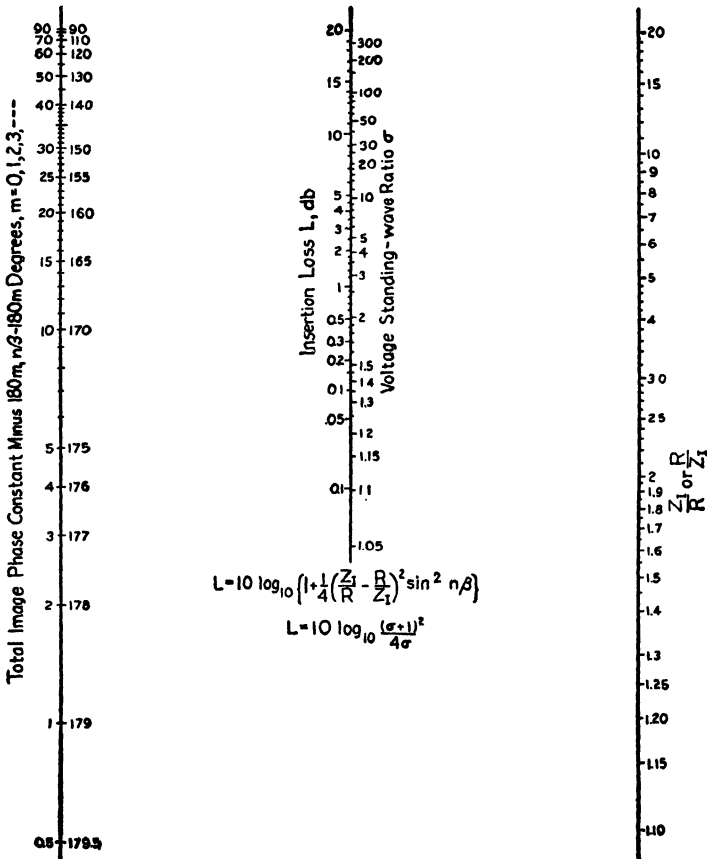


FIG. 26-9.—Pass-band insertion loss and standing-wave ratio for a symmetrical nondissipative filter.

a voltage standing-wave-ratio scale is plotted on the insertion-loss scale. This scale gives the filter-input voltage standing-wave ratio that would be measured on a line of characteristic impedance  $R$  if the filter-output terminals were loaded by a resistance equal to  $R$ .

Equations (26-52) and (26-53) apply also to a filter composed of dissimilar sections as long as the image impedances of the sections are matched throughout (as is true in  $M$ -derived terminated filters) and as

long as the image impedances at the extreme terminals are equal. In such a filter, the sum of the phase constants for each section or half section is used in place of  $n\beta$ , and the sum of the attenuation constants in place of  $n\alpha$ . The image impedance to be used in Eqs. (26-52) and (26-53) is the image impedance at the terminals of the first and last section or half section.

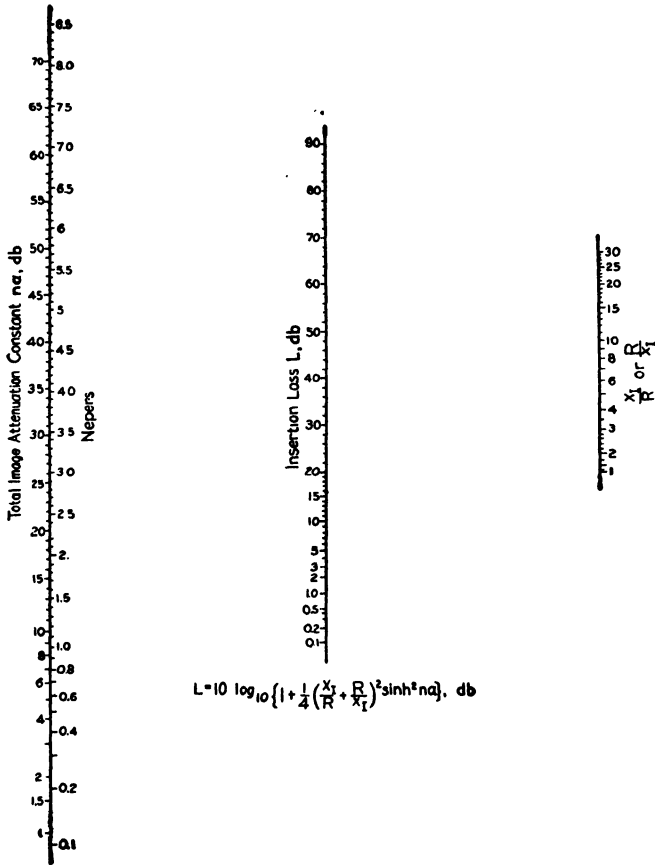


FIG. 26-10.—Stop-band insertion loss for a nondissipative symmetrical filter.

**26-8. Filter Pass-band Response.**—Equation (26-52) shows that the insertion loss of a filter will be zero everywhere in a pass band only if  $Z_I = R$  in the pass band. It is necessary, however, for  $Z_I$  to approach infinity or zero at the cutoff frequency of a filter, and hence there must always be some mismatch between  $Z_I$  and  $R$  near cutoff. For  $Z_I$  not equal to  $R$ , a *loss peak* will occur very near every frequency for which the total image phase constant  $n\beta$  is an odd multiple of 90 deg, while zero loss

will occur at every frequency for which  $n\beta$  is any multiple of 180 deg. This phenomenon is illustrated by Figs. 26-11 and 26-12 for a low-pass filter having five sections.

In a particular filter, the size of the loss peaks will, of course, depend on the degree of mismatch between  $Z_I$  and  $R$ . With careful design, this mismatch may be made small over the pass band except very near cutoff. A brief inspection of Fig. 26-9 shows the permissible mismatch before an assumed insertion loss is exceeded. For example, with the worst possible value for  $n\beta$ , *i.e.*, an odd multiple of 90 deg,  $\frac{1}{2}$ -db loss results for  $Z_I/R$  or  $R/Z_I$  equal to 1.4, 1 db for a ratio of 1.62, 2 db for a ratio of 2.0, and 3 db for a ratio of 2.4.

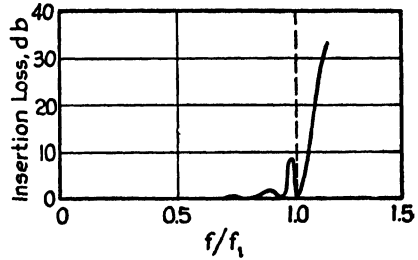


FIG. 26-11.—Calculated pass-band response of a five-section low-pass filter (for  $Z_{I0} = R$ ).

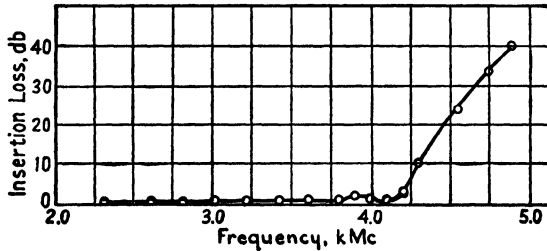


FIG. 26-12.—Measured response of a five-section low-pass filter having  $Z_{I0} = R$ .

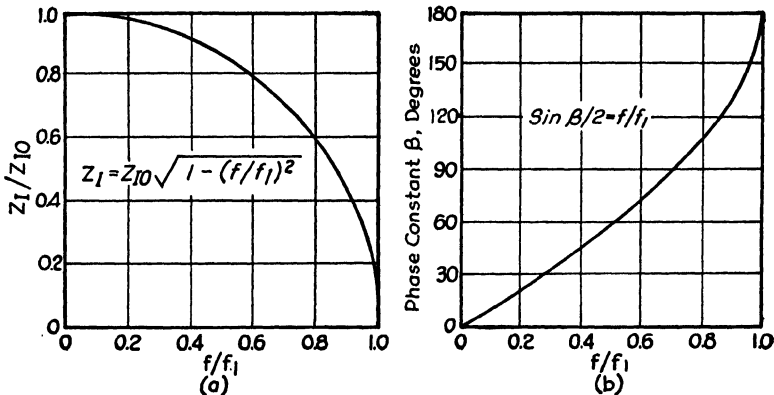


FIG. 26-13.—Image impedance and phase constant for a constant- $k$  low-pass filter T-section having a cutoff frequency equal to  $f_1$ .

**Example:** The pass-band loss peaks will be determined for a five-section low-pass filter (type 1-1 of Table 27-1). As will be pointed out in Chap. 27, the image-impedance and phase-constant functions for this transmission-line filter

section are very nearly the same as that for the lumped-element constant- $k$  low-pass section. These functions for the latter are plotted in Fig. 26-13. Note that the ordinate in Fig. 26-13a is  $Z_I/Z_{I0}$ , where  $Z_{I0}$  is the value of image impedance at zero frequency.

Loss peaks will occur near  $n\beta = 90, 270, 450, 630,$  and  $810$  deg. For  $n$  equal to five, these values of  $n\beta$  correspond to  $\beta = 18, 54, 90, 126,$  and  $162$  deg. Figure 26-13b gives the value of  $f/f_1$  corresponding to these values of  $\beta$ , and Fig. 26-13a gives the values of  $Z_I/Z_{I0}$  for these values of  $f/f_1$ . Finally, from the  $Z_I/Z_{I0}$  values, the insertion loss at these loss peaks may be obtained from Fig. 26-9. The calculation is given in Table 26-1 for  $Z_{I0}$  set equal to  $R$ .

TABLE 26-1

$n\beta^\circ$	$\beta^\circ$	$f/f_1$	$Z_I/R$	$R/Z_I$	$L_{db}$
90	18	0.155	0.99	1.01	< 0.01
270	54	0.45	0.89	1.12	0.05
450	90	0.707	0.707	1.41	0.50
630	126	0.88	0.47	2.13	2.2
810	162	0.985	0.17	5.88	9.5

The approximate pass-band response for this filter is sketched from these data in Fig. 26-11. The last peak and dip are so sharp that they will often not be found when an actual filter is being tested. Also, slight irregularities and slight filter dissipation will tend to round them off. The measured response for a five-section transmission-line low-pass filter, the image impedance and phase constant of which are very nearly those of the example, is given in Fig. 26-12. Except very near cutoff, the measured response checks the calculated response fairly well.

It is apparent that for a filter consisting of  $n$  identical sections, where  $n$  may be any integer, loss peaks may occur at virtually any frequency. The envelope of all possible loss peaks for a given type of filter is of interest since it places an upper bound on the pass-band loss of the filter. This envelope may be quickly obtained from the image-impedance curve of the filter and the nomogram of Fig. 26-9. The total phase constant should be assumed equal to an odd multiple of  $90$  deg at all frequencies. In order to perform this calculation, a relation between the image-

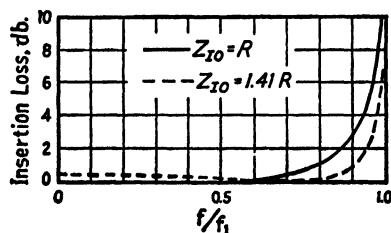


FIG. 26-14.—Loss envelopes for an  $n$ -section low-pass filter.

impedance curve and the constant load resistance  $R$  must be assumed. Figure 26-14 shows two maximum-pass-band-loss envelopes for the low-pass filter of the last example. For one envelope,  $Z_{I0}$  is assumed equal to  $R$ . For the other envelope,  $Z_{I0}$  is assumed equal to  $1.41R$ .

**26-9. Methods of Reducing Pass-band Insertion Loss.**—Several methods of reducing pass-band insertion loss now suggest themselves:

1. If the band (or bands) of frequencies to be passed is not close to the band (or bands) of frequencies to be rejected, the cutoff frequencies of the filter should be located sufficiently far from the frequencies to be passed so that any excessive pass-band peaks are outside the useful frequency band. In this case, with reference to the design data in Tables 27-1 and 27-2, the extreme values  $Z_{I0}$  should be set equal to  $R$ . If, at the frequency where the mismatch first becomes excessive, one chooses a number of sections  $n$  such that  $n\beta$  is a multiple of 180 deg, the filter may be made to have low loss still closer to the cutoff frequency.

2. If optimum response is desired over the entire pass band right up to the cutoff frequency,  $m$ -derived half-section terminations (see Tables 27-1 and 27-2) should be used, where possible. The constancy of image impedance with these terminations, except very near cutoff, will provide an extremely flat response curve, while, in addition, the very sharp rejection characteristic associated with  $m$ -derived terminations will be attained. The more complicated construction and adjustment of this type of filter make it difficult to build for use over 1000 or 2000 Mc, and even below this the use of simpler constructions is recommended if they can be made to satisfy the specifications.

3. With filters having a more rounded image-impedance curve than that obtained with  $m$ -derived half-section terminations, improved response over the pass band will result from a judicious choice of the load-resistance for a given image-impedance curve. As an example, consider the constant- $k$  T-section low-pass filter. The envelopes of Fig. 26-14 for  $R = Z_{I0}$  and  $R = Z_{I0}/1.41$  show that a considerable improvement near cutoff is obtained for the lower value of  $R$  at the expense of a very slight increase of maximum possible loss at low frequencies.

In general, filters the image impedance of which approaches zero at their cutoff points will have their over-all response improved by making  $Z_{I0}$  approximately equal to  $1.414R$ . Filters the image impedance of which approaches infinity at their cutoff points will have their over-all response improved by making  $Z_{I0}$  approximately equal to  $R/1.41$  ( $Z_{I0}$  is the maximum image impedance in the pass band in the first case, and the minimum in the second). If a particular filter has an image impedance that is zero at one cutoff and infinite at another, the designer must use a little more judgment in choosing the load resistance.

In the general case, the most foolproof way of ensuring a good match is to calculate and plot the image-impedance function, and then choose the load resistance so that it will approximate the  $Z_I$  curve as well as possible.

A good match will usually result if the value of  $Z_I$  at the frequency for which  $\cosh \Theta = 0$  (i.e.,  $\beta = \pm 90$  deg) is made equal to  $R$ . It is often easier to derive design equations based on this criterion than on any



other. The design equations in Tables 27-3, 27-4, and 27-5 use this criterion.

If  $\beta = \pm 90$  deg for a full section, the phase constant is  $\pm 45$  deg for a half section. Equation (26-12) shows therefore, that for a half section  $Z_I = |Z_{oc1}| = |Z_{sc1}|$  when  $\cosh \Theta = 0$ . It is often simpler to use this relation to calculate  $Z_I$  for  $\cosh \Theta = 0$ , than to evaluate  $Z_I$  from the image-impedance equation.

**26-10. Transforming End Sections.**—Of the methods thus far described for obtaining low pass-band loss, the use of  $m$ -derived terminating half sections gives the best results. As pointed out, however, the construction and adjustment of  $m$ -derived sections becomes difficult at the higher frequencies. A method of obtaining a greatly improved pass-band response without the use of  $m$ -derived half-sections will be described in the following paragraphs.

In this method, the same type of filter section is used throughout. The end sections, however, have a different cutoff frequency from the internal sections. These *transforming end sections* are designed so that they improve the impedance match between the constant load resistance  $R$  and the variable image impedance  $Z_I$  of the internal sections. The principle underlying this method will now be described for a low-pass filter of the type shown in Figs. 26-8 and 27-3.

The image impedance and phase constant for the low-pass filter

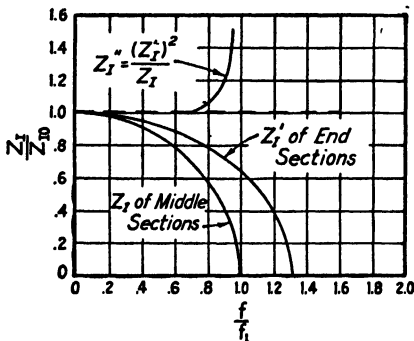


FIG. 26-15.—The various image impedances involved in a low-pass filter having transforming end sections. The significance of  $Z_I''$  is explained in the text.

section under consideration are shown in Fig. 26-13. The image phase constant is seen to be equal to 90 deg and the image impedance to  $0.707 Z_{I0}$  at  $0.707$  times the cutoff frequency  $f_1$ . A single section, therefore, is equivalent at  $0.707f_1$  to a  $1/4$ -wavelength transmission line of characteristic impedance  $0.707Z_{I0}$  (see Sec. 26-1). At this frequency, then, the image impedance of a section is the geometric mean of the load impedance terminating the section and the input impedance. In the vicinity of this

frequency, this relation will hold approximately, the error becoming greater as the departure from 90 deg is increased and as the ratio between the image impedance and the load impedance is increased.

Figure 26-15 shows the image impedance  $Z_I$  of the internal sections, and  $Z_I'$  of the end sections. The 90-deg point for the end section should be located at or slightly below the cutoff frequency  $f_1$  of the middle

sections. For the case of Fig. 26-15 this point corresponds to  $0.93f_1$ . It will be noted that the  $Z_I'$  curve falls between the  $Z_I$  curve and the constant-resistance line  $Z_{I0}$ . The end sections will therefore transform points on the  $Z_I$  curve up toward the  $Z_{I0}$  line. The curve  $Z_I''$  is the transformed-impedance curve under the assumption that the phase constant of the end sections is 90 deg at all frequencies. This curve is seen to be very nearly equal to the constant value  $Z_{I0}$  over a large part of the pass band. The end sections act as transformers only in the vicinity of  $0.93f_1$ . Below this frequency, the transforming action becomes less perfect, but at the same time the mismatch between the various impedances involved also becomes less. On the whole, therefore, very little mismatch occurs in the pass band except very close to cutoff.

Figure 26-16 gives the maximum-pass-band-loss envelope for a low-pass filter having transforming end sections and having the image-impedance functions and cutoff frequencies shown in Fig. 26-15.  $Z_{I0}$  is assumed equal to the load resistance  $R$ . The actual filter insertion loss will fall between zero and this curve, depending upon the total phase constant of the internal sections. This envelope is seen to give a response greatly improved over the envelopes in Fig. 26-14.

The envelope curve of Fig. 26-16 was calculated exactly by a rather laborious process. An approximate curve may be calculated in a relatively simple manner, however, by assuming the image impedance of the over-all filter to be equal to  $Z_I''$ , and using the nomogram of Fig. 26-9 with the phase constant set equal to 90 deg. For the case considered above, the approximate envelope checked the exact envelope within  $\pm 0.2$  db up to at least  $0.98f_1$ . It must be pointed out, however, that although  $Z_I''$  may be considered to be approximately equal to the filter image impedance in calculating the maximum-insertion-loss envelope, the actual image impedance is really radically different from  $Z_I''$ . In fact, the image impedance will have imaginary values at a number of places in the pass band, depending upon the number of internal sections. The apparent paradox is explained by the fact that at frequencies at which the image impedance is imaginary the attenuation constant of the filter is negligible, and at frequencies at which the image impedance is real but greatly different from  $Z_I''$  the phase constant is very nearly a multiple of 180 deg. The insertion-loss nomograms of Figs. 26-9 and 26-10 show that under these conditions the filter insertion loss can be

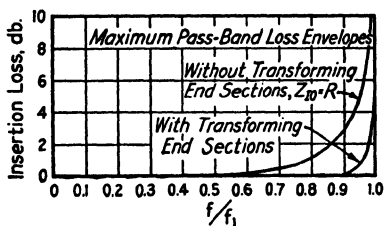


FIG. 26-16.—The maximum-pass-band loss envelopes for a low-pass filter having transforming end sections as compared with the envelope for a low-pass filter without transforming end sections.

very low. Since the insertion loss rather than the image impedance is usually of primary concern in the use of a filter, this interesting phenomenon is usually of no importance and may be neglected. Figures 26-17 and 27-2b show the measured response of two low-pass filters having transforming end sections.

If a termination of the  $\pi$ -type is used (Figs. 26-8d and 27-3b), the same design procedure applies. In this case, the image-impedance curves will be the reciprocal of the corresponding curves in Fig. 26-15, while the envelope curve in Fig. 26-16 will apply exactly.

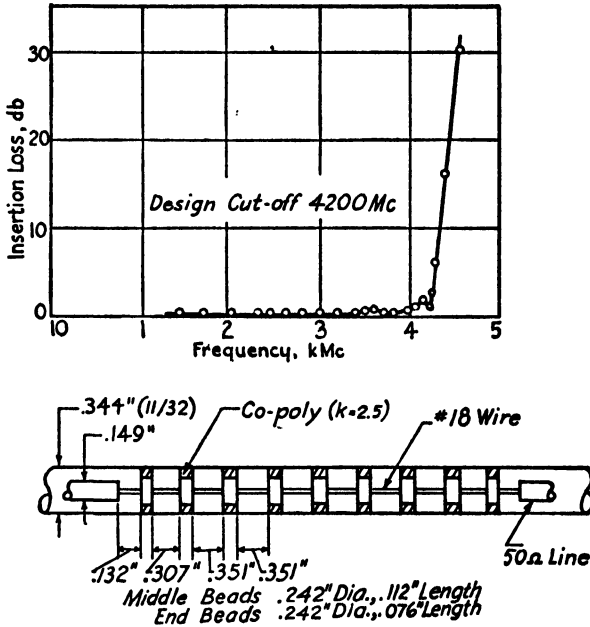


FIG. 26-17.—The measured response and construction of a low-pass filter having transforming end sections.

This type of termination is just as easily applied to high-pass filters. The constant- $k$  lumped-element high-pass filter section, which the transmission-line filter of Fig. 26-6 resembles, has the same image-impedance and phase-shift function as the low-pass section except that  $f_1/f$  is substituted everywhere for  $f/f_1$ , where  $f_1$  is the cutoff frequency. Consequently, a high-pass section has a 90-deg phase constant at 1.41 times the cutoff frequency. The end sections should therefore have their cutoff frequency at or slightly higher than 0.707 times the cutoff frequency of the internal sections. The envelopes of Fig. 26-16 apply if the reciprocals of the  $f/f_1$  scale are used for the abscissas.

The transforming end-section design may also be used with band-pass filters that have rounded image-impedance curves. Figure 26-18 shows

how it may be applied to a filter having zero image impedance at the cutoff frequencies. For the end sections, a type having the same sort of image-impedance function as the inside sections and having a phase-constant variation from  $-180$  deg to  $+180$  deg is required. The cutoff points of this section are located so that the plus and minus  $90$ -deg phase-constant points are at or just inside the edges of the filter pass band. The maximum pass-band image impedances  $Z_{I0}$  of the inner and outer sections are made equal to the terminating resistance  $R$ . Figure 26-18 shows that the *approximate* over-all filter impedance  $Z_I''$  is far more nearly constant over the pass band with the matching sections than without. As for the low-pass filter,  $Z_I''$  is not the true over-all filter image impedance, but it may be used in calculating a good approximation of the maximum-loss envelope.

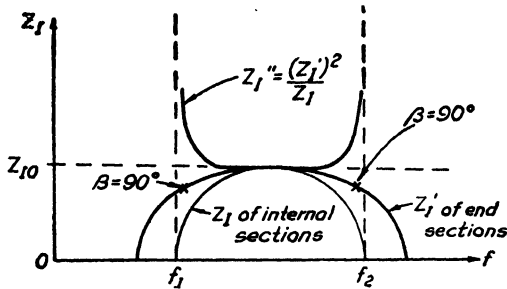


FIG. 26-18.—The image impedances involved in a band-pass filter having transforming end sections.

All the filter sections in Table 27-2 are suitable for use as internal sections, but only type 2-3 has a suitable phase-constant function for end-section use. The construction of type 2-3 is more complicated, however, than that of the others, and it is therefore not usable at the higher frequencies. The simpler constructions have a phase-constant variation of only  $180$  deg, and hence a single such section provides only one transforming frequency, while two are required. If, however, two such sections are used at each end of the filter, the phase-constant variation will be  $360$  deg, and the two necessary transforming points (at  $90$  and  $270$  deg) will be obtained.

**26-11. Filter Stop-band Response.**—Examination of Eq. (26-53) and Fig. 26-10 reveals a number of useful facts concerning insertion loss in the stop band of a filter terminated by a constant resistance  $R$ :

1. If  $X_I/R$  is infinite or zero within a stop band, the insertion loss at that frequency is infinite, even though  $n\alpha$  may be finite. ( $jX_I$  is the image impedance, a pure reactance in the stop band, and  $n\alpha$  is the attenuation constant of the filter.) Such points occur in many kinds of filter sections, e.g., in types 3-2, 3-3, and 3-4 of Table 27-3. This fact shows that the stop-band response of a filter cannot

be judged merely from its attenuation-constant curve and that a filter which may appear inadequate from the attenuation-constant standpoint may actually provide an excellent insertion-loss response.

2. The insertion loss of a filter cannot be less than the total attenuation-constant  $n\alpha$  by more than 6 db. It will be 6 db less only for  $X_I/R$  equal to 1, and only when  $n\alpha$  is greater than about 12 db.

3. For  $X_I/R$  in the neighborhood of 1, and for  $n\alpha$  small, the insertion loss will be very small. For  $X_I/R$  equal to 1 and for  $n\alpha$  equal to 4 db, the insertion loss is less than 1 db. This property makes some types of filters transmit freely in a stop band. An example is the high-pass filter 2-1 of Table 27-2. This subject will be treated in detail in Sec. 27-6.

**26-12. Pass-band Loss of a Filter with Improper Termination.**—In practical use, especially with wide-range receivers, the load and generator impedances presented to a filter may be considerably different from the load resistance  $R$  for which the filter is designed. In such cases, the loss of the filter in the pass band may be considerably greater than that measured for the filter when properly loaded. The maximum limits of these variations will now be considered.

The material in this section is particularly applicable to the case of a receiver r-f transmission line with filters inserted, but may be used for any kind of transmission system. For the sake of simplicity it will be assumed, as in other sections of this chapter, that (1) the filters are non-dissipative, (2) operation in the pass band only is considered, and (3) transmission lines are not long enough to introduce appreciable dissipation. In Sec. 26-14, however, a correction equation will be given for line loss. The filter may consist of two or more different types of filter sections in series, as long as they are all operating in their pass bands.

*Mismatch loss*  $M$  in a transmission system is the decibel gain obtained when a perfect matching section is introduced anywhere in the transmission line. The *insertion loss*  $L$  of a filter is defined, as before, to be the decibel reduction in transmitted power when the filter is inserted at a particular point in a particular transmission line. *Standing-wave ratio*  $\sigma$  of a device is defined as the ratio of maximum voltage to minimum voltage on a transmission line (generally of 50-ohm characteristic impedance) feeding the device in question as a load. A transmission line is said to be *matched* when the impedance in either direction at any point on the line is equal to the characteristic impedance of the line.

Even when terminated at both ends by the optimum fixed resistance, (generally chosen to be 50 ohms), any filter must have insertion loss somewhere in the pass band. With carefully designed filters, the loss is small everywhere in the pass band except near the theoretical cutoff. If, however, the transmission lines are not matched (*i.e.*, if the terminations on these lines are not 50 ohms), the insertion loss of a filter will not

be negligible and will vary considerably with line length, even if the filter insertion loss is zero in a matched line. Also, if several types of filters have identical insertion loss in matched lines, they may differ greatly among themselves when inserted in the same mismatched line. In both cases, insertion *gains* will often result.

Without extensive complicated calculations [see Eq. (26-50)], the insertion loss for a given filter under a given condition of mismatch cannot be determined. If, however, the standing-wave ratios of the antenna and the receiver in the absence of a filter and the matched-line insertion loss of the filter are known, the *maximum possible* and *minimum possible insertion loss* may be easily determined.

*Mismatched Line without Filter.*—1. If one end of the line is matched while the other is connected to a device having a standing-wave ratio  $\sigma_0$ , the mismatch loss in decibels will always be

$$M = 10 \log_{10} \frac{(\sigma_0 + 1)^2}{4\sigma_0} \quad (26-54)$$

This is the basic loss equation, which will be used repeatedly in the more complicated cases to follow. Equation (26-54) is plotted on the center scale of the nomogram of Fig. 26-9.

2. If both ends of the line are mismatched with respective standing-wave ratios  $\sigma_1$  and  $\sigma_2$ , the maximum possible mismatch loss is given by Eq. (26-54) with

$$\sigma_0 = \sigma_1 \sigma_2 \quad (26-55)$$

The least possible loss is given by Eq. (26-54) with

$$\sigma_0 = \frac{\sigma_1}{\sigma_2} \quad \text{or} \quad \sigma_0 = \frac{\sigma_2}{\sigma_1} \quad (26-56)$$

In these cases and in all that follow, the appropriate value of  $\sigma_0$  may be used with Fig. 26-9. For example, if  $\sigma_1 = 2$ , and  $\sigma_2 = 3$ , the maximum possible mismatch loss occurs for  $\sigma_0 = 2 \times 3 = 6$  and, by Fig. 26-9, is equal to 3.1 db.

*Mismatched Line with Filter.*—1. If the filter has zero insertion loss in a matched line, the maximum possible total mismatch loss in an unmatched line is given by the combination of Eqs. (26-54) and (26-55) and the minimum possible by Eqs. (26-54) and (26-56). Note that the effect of inserting such a filter is the same as though it were a length of 50-ohm line.

2. If the filter has an insertion loss  $L_0$  in a matched line, the maximum possible mismatch loss is given by Eq. (26-54) with

$$\sigma_0 = \sigma_1 \sigma_2 \sigma_3 \quad (26-57)$$

where  $\sigma_1$  and  $\sigma_2$  are the termination standing-wave ratios, and  $\sigma_3$  is the

value of the equivalent standing-wave ratio given by Eq. (26-54) with  $M = L_0$ . This value is easily obtained from Fig. 26-9.

For example, if  $L_0 = 3$  db, then according to Fig. 26-9,  $\sigma_s = 5.8$ . Now if  $\sigma_1 = 2$  and  $\sigma_2 = 3$ , then  $\sigma_0 = 34.8$ . Figure 26-9 indicates that the maximum possible mismatch loss is 9.7 db.

**26-13. Maximum Possible Insertion Loss of a Mismatched Filter.**

The maximum possible insertion loss  $L_{max}$  for a given coordination of filter, line, and terminations is equal to the loss in Eqs. 26-54 and 26-57 minus the loss in Eqs. (26-54) and (26-56). For the example considered above ( $\sigma_1 = 2, \sigma_2 = 3, L_0 = 3$  db), the maximum possible insertion loss is therefore

$$L_{max} = 9.7 - 0.2 = 9.5 \quad \text{db}$$

Note that this maximum possible insertion loss is considerably greater than the sum of  $L_0$  and the maximum possible mismatch loss without the filter ( $3.0 + 3.1 = 6.1$  db).

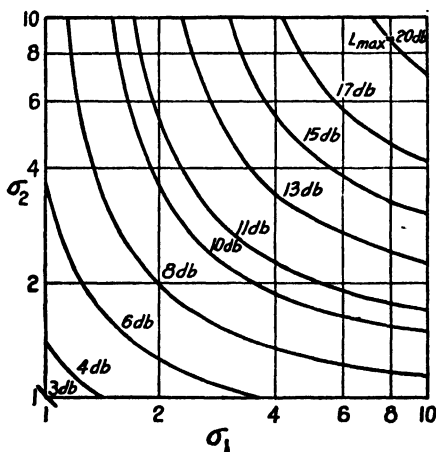


FIG. 26-19.—Maximum insertion loss  $L_{max}$ , of a filter operating in its pass band when placed between loads of standing-wave ratio  $\sigma_1$  and  $\sigma_2$ .  $L_0$  is assumed to be 3 db.

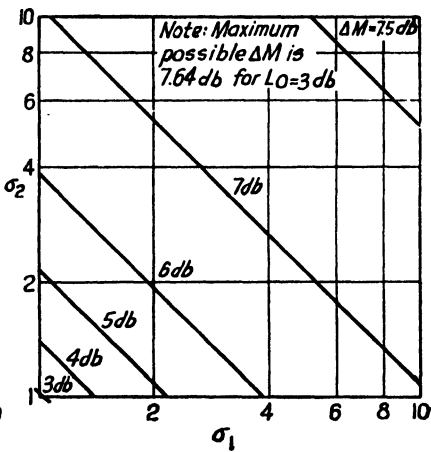


FIG. 26-20.—Difference between maximum mismatch loss in pass band with and without the filter. Loads having standing-wave ratios  $\sigma_1$  and  $\sigma_2$ ; filter  $L_0 = 3$  db.

Combining Eqs. (26-54), (26-56), and (26-57) gives

$$L_{max} = 10 \log_{10} \frac{(\sigma_1 \sigma_2 \sigma_3 + 1)^2}{\sigma_3 (\sigma_1 + \sigma_2)^2} \tag{26-58}$$

$L_{max}$  is plotted in Fig. 26-19 as a function of  $\sigma_1$  and  $\sigma_2$  for the case of  $L_0 = 3$  db.

*Increase in Maximum Possible Mismatch Loss upon Insertion of a Filter.*—Equation (26-58) gives the worst insertion loss possible. In order to attain this high loss, the line without the filter must by chance have exactly the right length at that frequency to result in the minimum

possible loss given by Eqs. (26-54) and (26-56). Also, the filter must have just the right properties at that frequency to be capable of transforming the system into the worst possible case given by Eqs. (26-54) and (26-57). The line without the filter might just as well have been in the worst possible condition, and, therefore, in sensitivity measurements on a receiver the least possible sensitivity as found by means of a line stretcher ought to be considered the standard sensitivity of the receiver. If the minimum sensitivity is taken as the standard, the maximum possible decrease in standard sensitivity upon insertion of a filter will be a more useful criterion of filter performance than the maximum possible insertion loss. This loss quantity  $\Delta M$  is given by Eqs. (26-57) and (26-54) minus Eqs. (26-55) and (26-54). It may be expressed as

$$\Delta M = 10 \log_{10} \frac{(\sigma_1 \sigma_2 \sigma_3 + 1)^2}{\sigma_3 (\sigma_1 \sigma_2 + 1)^2} \tag{26-59}$$

Equation (26-59) is plotted in Fig. 26-20 as a function of  $\sigma_1$  and  $\sigma_2$  for the case of  $L_0 = 3$  db. It should be remembered, however, that Eq. (26-59) assumes the extreme case of the filter parameters causing the worst possible loss. In general, insertion gains as well as losses can result.

For the case of  $\sigma_1 = 2$ ,  $\sigma_2 = 3$ ,  $L_0 = 3$  db,  $\Delta M = 9.7 - 3.1 = 6.6$  db, a value that is much less than  $L_{max}$ , but still considerably exceeds  $L_0$ .

As the mismatch is increased,  $\Delta M$  rapidly approaches the limiting value given by

$$\lim_{(\sigma_1 \sigma_2 \rightarrow \infty)} \Delta M = 10 \log_{10} \sigma_3 \tag{26-60}$$

For  $L_0 = 3$  db, this limiting value is 7.64 db. Figure 26-20 and the foregoing example indicate that this value is approached for relatively small values of  $\sigma_1$  and  $\sigma_2$ .

*Effects in the Filter Stop Band.*—In the stop band, similar changes in attenuation will be noted when the filters are mismatched. The problem is more complex than pass-band attenuation and will not be considered here. Severe decreases of attenuation, however, are not likely unless the mismatch is extremely large.

**26-14. Line-loss Correction for Standing-wave Ratio.**—The effect of line loss is to make the standing-wave ratio at the point of measurement on a line less than the standing-wave ratio of the termination. The input voltage standing-wave ratio  $\sigma_{in}$  of a line as a function of the standing-wave ratio  $\sigma_L$  of the load impedance, the line length  $l$  in meters, and the attenuation  $\alpha$  in decibels per meter is given by the relation

$$\sigma_{in} = \frac{\sigma_L + \tanh\left(\frac{\alpha l}{8.686}\right)}{1 + \sigma_L \tanh\left(\frac{\alpha l}{8.686}\right)} \tag{26-61}$$



Insertion-loss and mismatch values for a filter inserted in a given transmission line can be calculated accurately by using antenna and receiver standing-wave-ratio values corrected by Eq. (26-61).

**26-15. Waveguide as a Circuit Element in Filters.**—Above 1000 or 2000 Mc, the construction of coaxial high-pass and band-pass filters becomes difficult because of the small dimensions and tolerances involved. Because of the simple shape and construction of waveguide and its relatively large cross section, waveguide can provide practical structures at a much higher frequency than can coaxial line. In addition, the increased cross section gives a higher  $Q$ , an important consideration in narrow-band filters. A waveguide filter may be used in a waveguide transmission-line system, or it may be combined with two waveguide-to-coax junctions and used in a coaxial-line system.

It is well known that waveguide behaves much like an ordinary transmission line.<sup>1</sup> It has been shown that reflection at an abrupt change in cross-sectional shape in a waveguide may be calculated by means of ordinary transmission-line formulas by using a properly defined *waveguide characteristic impedance* on each side of the discontinuity and including a lumped shunt reactance at the point of discontinuity.

An impedance function for waveguide may be defined in several ways. In the following treatment  $TE_{1,0}$  propagation is assumed, and impedance at a point along the waveguide line is defined as the electric field strength at the center of the cross section times the height  $b$  divided by the total component of current in the longitudinal direction on the top side (length  $a$ ) of the waveguide. If there is no reflected wave, *i.e.*, if the waveguide is terminated perfectly, this impedance is constant along the waveguide and is defined to be the characteristic impedance of the waveguide. The characteristic impedance for rectangular waveguide in the  $TE_{1,0}$  mode is<sup>2</sup>

$$Z_0 = \frac{60\pi^2 b}{\sqrt{\epsilon} a} \frac{1}{\sqrt{1 - \left(\frac{f_c}{f}\right)^2}} = \frac{Z_{0\infty}}{\sqrt{1 - \left(\frac{f_c}{f}\right)^2}} \quad (26-62)$$

where  $b$  and  $a$  are the cross-sectional dimensions (see Fig. 26-21),  $f$  is the frequency of calculation,  $f_c$  the cutoff frequency of the guide,  $\epsilon$  the dielectric constant ( $\epsilon = 1$  for free space), and  $Z_{0\infty} = (60\pi^2/\sqrt{\epsilon})(b/a)$  is the characteristic impedance at infinite frequency. The ratio  $Z_0/Z_{0\infty}$  is plotted in Fig. 26-22. Another important relation is

<sup>1</sup> SCHELKUNOFF, S. A., "Electromagnetic Waves," pp. 319-320, 490-494, D. Van Nostrand Company, Inc., New York, 1943.

<sup>2</sup> SCHELKUNOFF, *op. cit.*, p. 319.

$$\frac{\lambda_g}{\lambda} = \frac{1}{\sqrt{1 - \left(\frac{f_c}{f}\right)^2}} = \frac{1}{\sqrt{1 - \left(\frac{\lambda}{\lambda_c}\right)^2}} \tag{26-63}$$

where  $\lambda$  is the wavelength in unbounded medium of dielectric constant  $\epsilon$  and is equal to  $1/\sqrt{\epsilon}$  times the space wavelength,  $\lambda_g$  the *guide wavelength* (i.e., the longitudinal distance at a given instant between points of equal phase), and  $\lambda_c$  the cutoff wavelength of the guide ( $\lambda = \lambda_c$  at  $f = f_c$ ). For rectangular waveguide

$$\lambda_c = 2a \sqrt{\epsilon} \tag{26-64}$$

Equation (26-63) is also plotted in Fig. 26-22.

Equations (26-62) and (26-63) are used extensively in the design of waveguide filters, along with the usual transmission-line equations

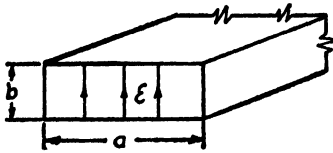


FIG. 26-21.—Cross-sectional dimensions for rectangular waveguide.

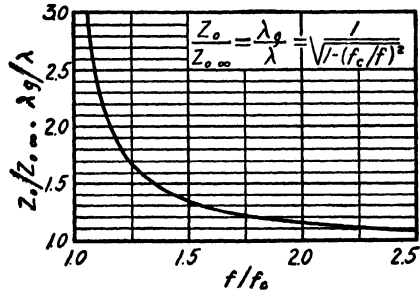


FIG. 26-22.—Waveguide characteristic impedance and wavelength as a function of frequency.

e.g., Eqs. (26-14) and (26-15), and circle diagrams. It is important to remember in applying these transmission-line relations that  $Z_0$  is a function of frequency and that the electrical phase length  $\theta$  is equal to  $2\pi l/\lambda_g$  and not to  $2\pi l/\lambda$ . Equation (26-15) may be written as follows for waveguide:

$$Z_0 = \left[ \frac{Z_{0\infty}}{\sqrt{1 - \left(\frac{f_c}{f}\right)^2}} \right] \left\{ \frac{Z_R + \frac{jZ_{0\infty}}{\sqrt{1 - \left(\frac{f_c}{f}\right)^2}} \tan \left[ \frac{2\pi l}{\lambda} \sqrt{1 - \left(\frac{f_c}{f}\right)^2} \right]}{\frac{Z_{0\infty}}{\sqrt{1 - \left(\frac{f_c}{f}\right)^2}} + jZ_R \tan \left[ \frac{2\pi l}{\lambda} \sqrt{1 - \left(\frac{f_c}{f}\right)^2} \right]} \right\} \tag{26-65}$$

At abrupt changes in cross section such as those shown in Fig. 26-23, or at thin irises such as those shown in Fig. 26-24, the effect of the local field disturbances may be accurately accounted for by assuming a lumped

shunt reactance at the point of discontinuity. Figure 26-25 shows the exact circuit representation for two lengths of waveguide joined with a discontinuity. Once a circuit representation such as this has been found for a waveguide configuration, the configuration may be treated as an ordinary circuit problem.

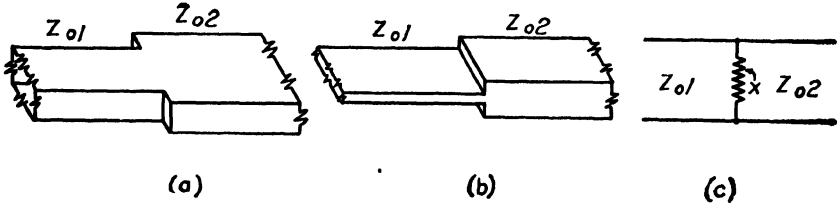


FIG. 26-23.—Two important types of junctions between rectangular waveguides having unequal cross sections; (c) the equivalent circuit.  $X$  is inductive for (a), capacitive for (b).

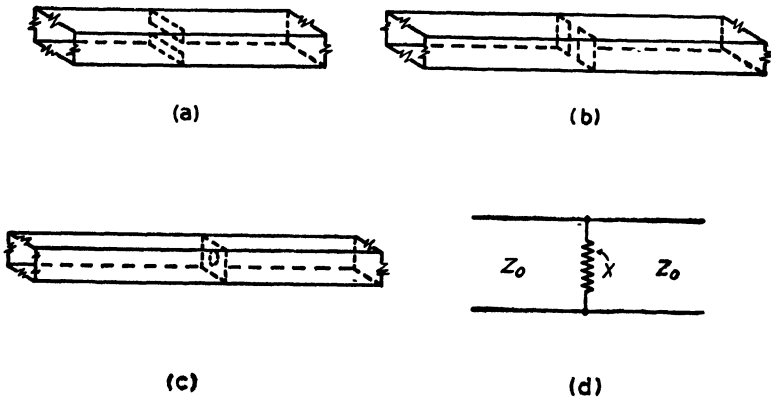


FIG. 26-24.—A few types of waveguide irises; (d) the equivalent circuit for an extremely thin iris.  $X$  is capacitive for (a), inductive for (b) and (c).

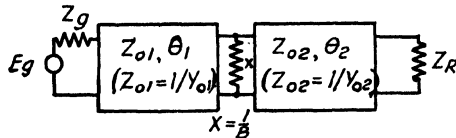


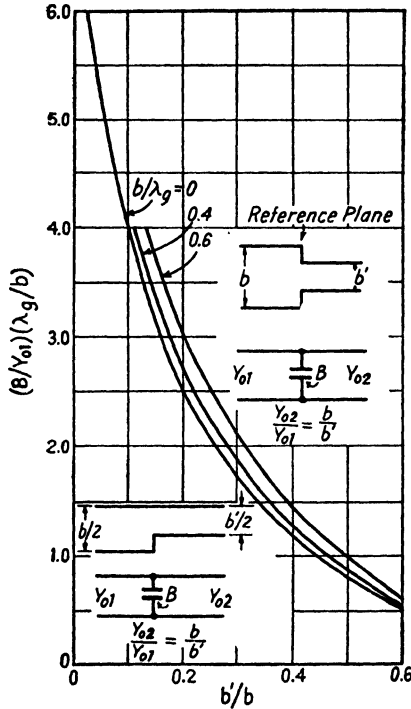
FIG. 26-25.—Complete circuit representation for a discontinuity of the type shown in Figs. 26-23 and 26-24.  $Z_{01}$  and  $\theta_1$  are the characteristic impedance and phase length of the waveguide to the left of the discontinuity, and  $Z_{02}$  and  $\theta_2$  to the right.  $X$  is the equivalent discontinuity reactance,  $Z_g$  the equivalent generator impedance,  $Z_R$  the equivalent load impedance.

The shunt susceptance has been calculated and plotted for several types of discontinuities.<sup>1</sup> The equivalent shunt susceptance at a change in height of a waveguide is particularly useful. It is given by the curves in Fig. 26-26.<sup>1</sup> This lumped susceptance becomes small and may often

<sup>1</sup> MARCUVITZ, N., "Waveguide Handbook," Radiation Laboratory Series, Vol. 10, McGraw-Hill Book Company Inc., New York (in press).

be neglected when the maximum height  $b$  is much less than the width  $a$ , *i.e.*, if  $\lambda_g/b$  is large. It should be noted that if successive discontinuities are very close to each other, their interaction effect must be considered.

*Attenuation below Cutoff in Waveguide.*—For frequencies less than  $f_c$  in waveguide, the characteristic impedance is purely imaginary, as shown by Eq. (26-62). The guide wavelength is also imaginary, as



$$\text{For } b/\lambda_g \leq .3 \text{ and } b'/b \leq \frac{1}{4}, B/Y_{01} = \frac{2b}{\lambda_g} \left\{ \log_e \frac{b}{4b'} + 1 \right\},$$

(within 4%)

FIG. 26-26.—Equivalent shunt susceptance at a change of height of a rectangular waveguide.

shown by Eq. (26-63), and the image transfer constant per centimeter ( $\Theta = 0 + j2\pi l/\lambda_g$ ) is a positive real quantity. Below cutoff, therefore, a length of waveguide is analogous to a filter in a stop band, and the attenuation constant per centimeter is given by the relation

$$\alpha = (8.686) \frac{2\pi}{\lambda_c} \sqrt{1 - \left(\frac{f}{f_c}\right)^2} \quad \text{db per cm} \quad (26-66)$$

Equation (26-66) is plotted in Fig. 26-27.

The analogy between a length of waveguide and a high-pass filter is now apparent. A waveguide high-pass filter may be simply a short

length of waveguide having a cutoff frequency equal to the desired cutoff frequency for the filter. This length of waveguide may be inserted directly into a freely transmitting waveguide transmission line, or it may have broad-band waveguide-to-coaxial junctions at each end. In either

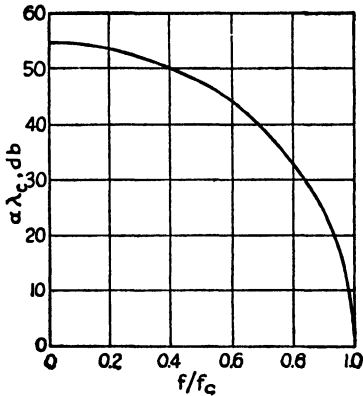


FIG. 26-27.—Waveguide attenuation below the cutoff frequency.  $\alpha$  is the db attenuation per cm of length;  $\lambda_c$ , the cutoff wavelength in cm;  $f/f_c$ , the ratio of frequency to cutoff frequency.

case, the insertion-loss curve below and above cutoff differs somewhat from the attenuation-constant curve, and the remarks of Secs. 26-7 to 26-11 apply. In particular, the insertion loss is infinite at zero frequency, although the attenuation constant is finite. In Chap. 27, the design of high-pass and band-pass waveguide filters that make use of the waveguide cutoff will be described.

**26-16. Properties of Ridge Waveguide.**<sup>1</sup>—In this section equations and curves are presented giving cutoff frequency and characteristic impedance for rectangular waveguide having a rectangular ridge projecting inward from one or both sides, as shown in Fig. 26-28. The lowered cutoff frequency, lowered impedance, and wide band width free from

higher mode interference obtainable with *ridge waveguide* make it a particularly useful element in waveguide filters, or in waveguide-to-coax junctions for use with these filters. A number of other uses are listed at the end of this section.

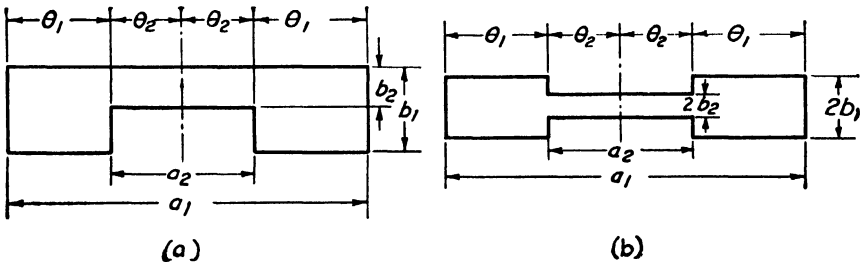


FIG. 26-28.—Cross-sectional shape of (a) single-ridge, and (b) double-ridge waveguide.

**Design Curves ( $TE_{1,0}$  Mode).**—Figures 26-29 and 26-30 give cutoff and impedance values for single-ridge waveguide as a function of the cross-sectional dimensions. Figure 26-29 is specifically for  $b_1/a_1 = 0.136$  (“toll-ticket” waveguide,  $2\frac{3}{4} \times \frac{3}{8}$  in.), while Fig. 26-30 is for  $b_1/a_1 = 0.5$ .

<sup>1</sup> COHN, S. B., Properties of Ridge Waveguide, accepted for publication in *Proc. I.R.E.*

The ordinate  $\lambda_c'/2a_1 = \lambda_c'/\lambda_c = f_c/f_c'$  is the ratio of cutoff wavelength with the ridge to that without the ridge, or cutoff frequency without the ridge to that with the ridge. The abscissa  $a_2/a_1$  is the ratio of ridge width to guide width. Each solid curve corresponds to a constant value of  $b_2/b_1$ . For example, if a particular ridge waveguide has  $b_1/a_1 = 0.5$ ,  $a_2/a_1 = 0.4$ , and  $b_2/b_1 = 0.1$ , then from Fig. 26-30,  $\lambda_c'/\lambda_c = f_c/f_c' = 2.85$ . If the cutoff frequency without the ridge is 2850 Mc, the cutoff frequency with the ridge will be 1000 Mc.

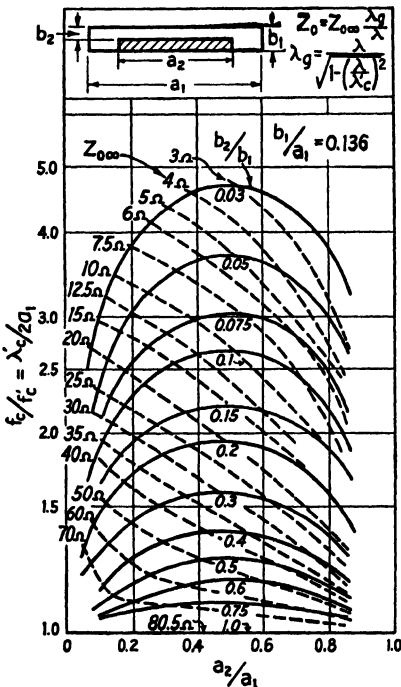


FIG. 26-29.—Characteristic impedance and cutoff wavelength of ridge waveguide. ( $b_1/a_1 = 0.136$ .)

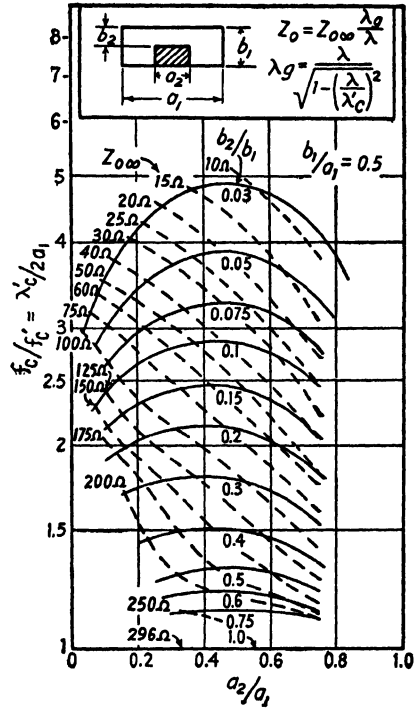


FIG. 26-30.—Characteristic impedance and cutoff wavelength of ridge waveguide. ( $b_1/a_1 = 0.5$ .)

On comparing Fig. 26-29 with Fig. 26-30, it will be seen that there is not a great deal of difference between the corresponding constant- $b_2/b_1$  curves. If  $b_1/a_1$  has a value different from 0.136, or 0.5, Figs. 26-29 and 26-30 may still be used with little error. Figure 26-29 should be used for values of  $b_1/a_1$  between zero and about one-third, and Fig. 26-30 should be used for values of  $b_1/a_1$  in the vicinity of 0.5.

Each dashed curve corresponds to a value of characteristic impedance at infinite frequency ( $Z_{0\infty}$ ). With  $Z_{0\infty}$  and the cutoff frequency  $f_c'$  known, the characteristic impedance at any frequency  $f$  is obtained by

multiplying  $Z_{0\infty}$  by the right-hand side of

$$\frac{Z_0}{Z_{0\infty}} = \frac{\lambda_c}{\lambda} = \frac{1}{\sqrt{1 - \left(\frac{f_c'}{f}\right)^2}} \quad (26-67)$$

The guide wavelength at frequency  $f$  is obtained by multiplying the space wavelength by the same factor. Equation (26-67) is plotted in Fig. 26-22.

In the example cited above, the impedance of a waveguide having  $b_1/a_1 = 0.5$ ,  $a_2/a_1 = 0.4$ ,  $b_2/b_1 = 0.1$ , and  $\lambda_c'/\lambda_c = 2.85$  would be 47 ohms at infinite frequency. At one and one-half times the cutoff frequency, the impedance is greater than that at infinite frequency by the factor 1.34 found from Fig. 26-22, *i.e.*,  $Z_0 = 47 \times 1.34 = 63$  ohms.

If  $b_1/a_1$  is not equal to 0.136 or 0.5,  $Z_{0\infty}$  may still be determined very closely from Figs. 26-29 and 26-30. For values of  $b_1/a_1$  between about zero and one-third, values of  $Z_{0\infty}$  on Fig. 26-29 should be multiplied by the scale factor  $(b_1/a_1)/0.136$ . For values of  $b_1/a_1$  between about one-third and two-thirds, values in Fig. 26-30 should be multiplied by  $(b_1/a_1)/0.5$ . For example, if  $b_1/a_1 = 0.2$ ,  $b_2/b_1 = 0.3$ , and  $a_2/a_1 = 0.5$ , Fig. 26-29 gives  $Z_{0\infty} = 28$  ohms for  $b_1/a_1 = 0.136$ . Therefore, for  $b_1/a_1 = 0.2$ ,  $Z_{0\infty} = 28 \times 0.2/0.136 = 41.1$  ohms. The characteristic impedance was checked experimentally for a cross section having  $b_1/a_1 = 1/4$  and was found to be very close to the value calculated by the foregoing method.

Because of approximations made in the derivation of the formulas, the values in Figs. 26-29 and 26-30 are truly accurate only if  $b_1/a_1$  is small. Errors in cutoff frequency values are fairly small in both figures. However, while errors in impedance are small in Fig. 26-29, they are quite appreciable in Fig. 26-30. For instance, Fig. 26-30 shows that for  $a_2/a_1 = 0.36$  a ratio of 0.095 for  $b_2/b_1$  is called for to give an impedance  $Z_{0\infty} = 50$  ohms. Experimentally, however,  $b_2/b_1$  had to be increased to about 0.13 in order to give this impedance. But even for  $b_1/a_1 = 0.5$ , the impedance curves give a useful approximation and a good starting point in design work.

The formulas and curves for a single ridge in a waveguide are directly applicable to the *double-ridge* cross section shown in Fig. 26-28*b*. In this case, the total height of the guide is  $2b_1$  and the total spacing is  $2b_2$ . Thus, if the width is  $2\frac{3}{4}$  in. and the height is  $\frac{3}{4}$  in., then  $b_1/a_1 = 0.136$  and the cutoff curves in Fig. 26-29 apply exactly. The characteristic-impedance curves apply also, but their values must be doubled. Hence for a double-ridge guide in which  $b_1/a_1 = 0.136$ ,  $a_2/a_1 = 0.35$ , and  $b_2/b_1 = 0.2$ , the cutoff wavelength ratio is  $\lambda_c'/\lambda_c = 1.9$ , and the infinite-

frequency characteristic impedance is  $Z_{0\infty} = 2 \times 26 = 52$  ohms, according to Fig. 26-30.

*Design Equations.*—The design equations used to plot the curves of Figs. 26-29 and 26-30 use the notation of Fig. 26-28.  $a_1$ ,  $a_2$ ,  $b_1$ , and  $b_2$  are inside dimensions in centimeters.  $\theta_1$  and  $\theta_2$  are the electrical phase lengths of portions of the cross sections (see Fig. 26-28) in terms of the cutoff wavelength in free space, e.g.,  $\theta_2 = 360(a_2/2)/\lambda_c'$  deg where  $\lambda_c'$  is the wavelength in free space at the ridge-guide cutoff frequency.

The cutoff of the  $TE_{1,0}$  mode occurs at the frequency for which the following equation is satisfied by the first pair of  $\theta_1$  and  $\theta_2$  values:

$$\frac{b_1}{b_2} = \frac{\cot \theta_1 - \frac{B}{Y_0}}{\tan \theta_2} \quad (26-68)$$

$(B/Y_0)$  may be obtained from Fig. 26-26. In evaluating  $(B/Y_0)$  from that graph,  $\lambda_c$  is made equal to  $\lambda_c'$ ,  $b$  to  $2b$ , and  $b'/b$  to  $b_2/b_1$ . Equation (26-68) is very accurate so long as  $(a_1 - a_2)/2 > b_1$ .

In terms of  $\theta_1$  and  $\theta_2$ ,  $\lambda_c'$  is given by

$$\lambda_c' = \left( \frac{90^\circ}{\theta_1 + \theta_2} \right) \lambda_c \quad (26-69)$$

where  $\lambda_c = 2a_1$  is the cutoff wavelength of the guide without the ridge, and where  $\theta_1$  and  $\theta_2$  are values satisfying Eq. (26-68).

The characteristic impedance at infinite frequency for the  $TE_{1,0}$  mode in single-ridge waveguide is given by

$$Z_{0\infty} = \frac{120\pi^2 b_2}{\lambda_c' \left( \sin \theta_2 + \frac{b_2}{b_1} \cos \theta_2 \tan \frac{\theta_1}{2} \right)} \quad \text{ohms} \quad (26-70)$$

Equation (26-70) does not take the discontinuity susceptance fully into account, and consequently it is truly accurate only if  $b_1/a_1$  is small. In addition to this, it has the same restrictions as Eq. (26-68). For double-ridge waveguide, the impedance is twice that given by Eq. (26-70).

**26-17. Higher Mode Cutoff Frequencies in Ridge Waveguide.**—The cutoff frequencies of the higher propagation modes are of importance since the operating range of a piece of apparatus containing a waveguide section is often limited to the range between the  $TE_{1,0}$  cutoff and the cutoff frequency of one of the higher modes. This point will be discussed further in Sec. 27-22. It is generally desirable, therefore, in waveguide for broad-band equipment to separate the  $TE_{1,0}$  and the higher cutoff frequencies as much as possible. One of the advantages of ridge wave-



guide is that it can provide a separation considerably greater than ordinary rectangular waveguide.

Because of the presence of the ridge (or ridges), the two higher modes next to the  $TE_{1,0}$  in ridge waveguide are usually the  $TE_{2,0}$  and  $TE_{3,0}$  modes. For ordinary rectangular waveguide, the  $TE_{2,0}$  cutoff frequency ( $f_{c2}$ ) occurs at exactly twice the  $TE_{1,0}$  cutoff frequency, and the  $TE_{3,0}$  cutoff ( $f_{c3}$ ) at exactly three times the  $TE_{1,0}$  cutoff. The cutoff frequencies of the  $TE_{2,0}$  and  $TE_{3,0}$  modes for single- and double-ridge waveguide ( $f_{c2}'$  and  $f_{c3}'$ ) are plotted in Fig. 26-31 as a function of the cross-sectional dimensions. The ordinates give the ratio of the cutoff frequency in ridge waveguide of the mode in question to the corresponding cutoff frequency of ordinary rectangular waveguide having the same width,  $a_1$ . The abscissas give the ratio of ridge width to guide width.

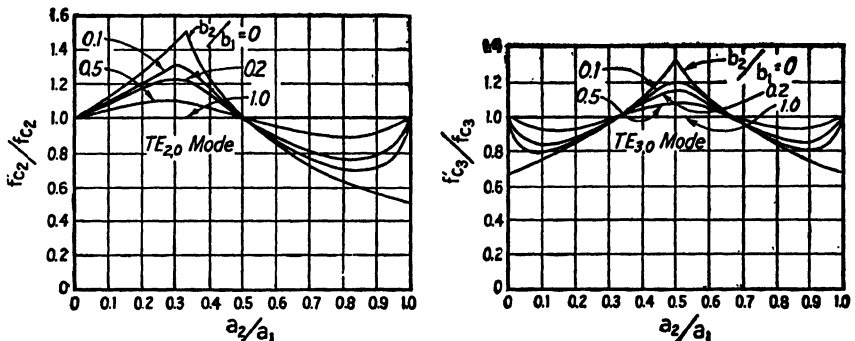


FIG. 26-31.—Cutoff-frequency ratios for the  $TE_{2,0}$  and  $TE_{3,0}$  modes in single- and double-ridge waveguide.

The maximum value of  $f_{c2}'/f_{c2}$  occurs for  $a_2/a_1$  between one-fourth and one-third, depending upon  $b_2/b_1$ . As  $b_2/b_1$  is made vanishingly small, the maximum value of  $f_{c2}'/f_{c2}$  approaches  $\frac{3}{2}$  at  $a_2/a_1 = \frac{1}{3}$ .

$f_{c3}'/f_{c3}$  is a maximum when  $a_2/a_1$  is one-half. For this value of  $a_2/a_1$ , the greatest separation of the  $TE_{1,0}$  and  $TE_{3,0}$  cutoff frequencies is obtained. It is easily shown that when  $a_2/a_1 = \frac{1}{2}$ ,  $f_{c3}'/f_{c3}$  increases as  $b_2/b_1$  decreases, and in the limit approaches  $\frac{4}{3}$ .

Figures 26-29, 26-30, and 26-31 show that when a wide frequency band free from  $TE_{2,0}$  and  $TE_{3,0}$  modes is desired, the ridge width should be between about one-third and one-half of the total guide width.

The curves in Fig. 26-31 are exact only for extremely thin waveguide. They are quite good, however, for ordinary ratios of  $b_1/a_1$ , subject to all the restrictions mentioned above for the  $TE_{1,0}$  cutoff curves.

**26-18. Attenuation in Ridge Waveguide.**—The attenuation constant in decibels per meter for copper single-ridge waveguide in the transmission range may be calculated fairly closely from the following approximate formula:

$$\alpha = 6.01(10)^{-7} K \sqrt{f} \left[ \frac{1}{a_1} + \frac{2}{b_1} \left( \frac{f_c}{f} \right)^2 \right] \left[ \frac{60\pi^2 \left( \frac{b_1}{a_1} \right)}{Z_{0\infty}} \right] \text{ db per m} \quad (26-71)$$

where  $a_1$  and  $b_1$  are in centimeters,  $f$  is in cycles per second, and  $K$  is a correction constant a little larger than unity, which takes account of the fact that the current distribution in ridge waveguide is more crowded than in plain waveguide. If  $a_2/a_1$  is larger than about one-third, this term is probably not greater than 1.5.

For double-ridge waveguide,  $b_1$  should be replaced by the total guide height  $2b_1$ . If any other metal besides copper is used,  $\alpha$  is proportional to  $\sqrt{\mu/\sigma}$ , where  $\mu$  is the permeability and  $\sigma$  the conductivity.

**26-19. Experimental Verification of the Ridge-waveguide Design**

**Curves.**—A 3-ft length of ridge waveguide having the cross-sectional dimensions shown in Fig. 26-32 has been tested. For this symmetrical cross section, the parameters are  $b_1/a_1 = 0.136$ ,  $b_2/b_1 = 0.35$ , and  $a_2/a_1 = 0.40$ . Without the ridges, the cutoff wavelength would be  $2 \times 2.36 \times 2.54 = 12.0$  cm, and the cutoff frequency would be

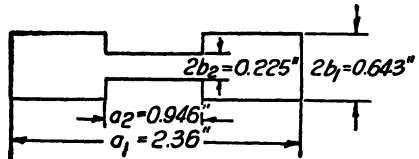


FIG. 26-32.—A double-ridge waveguide cross section. Experimental data for this cross section are given in Table 26-1.

$$\frac{30,000}{12.0} = 2500 \text{ Mc}$$

Figure 26-29 gives  $f_c/f_c' = 1.50$  and  $Z_{0\infty}/2 = 37$  ohms. Therefore,  $f_c' = 1670$  Mc and  $Z_{0\infty} = 74$  ohms. Figure 26-31 gives approximately  $f_{c2}'/f_{c2} = 1.10$  and  $f_{c3}'/f_{c3} = 1.06$ . Hence,

$$\begin{aligned} f_{c2}' &= 2 \times 2500 \times 1.10 = 5500 \text{ Mc} \\ f_{c3}' &= 3 \times 2500 \times 1.06 = 7950 \text{ Mc} \end{aligned}$$

The calculated and measured cutoff frequencies are tabulated in Table 26-2.

TABLE 26-2.—MODE CUTOFFS

Mode	Calculated, Mc	Measured, Mc
$TE_{1,0}$	1670	1675
$TE_{2,0}$	5500	5200
$TE_{3,0}$	7950	7900

Ridge waveguide has been used for elements in wide-band junctions between waveguide and coaxial line. These waveguide-to-coax junctions are described in Chap. 27, and experimental verification of the characteristic-impedance curves for ridge waveguide are given there.

**26-20. Applications for Ridge Waveguide.**—It has already been stated that ridge-waveguide sections are useful in the design of waveguide-to-coax junctions and waveguide filters. Ridge waveguide has several other applications, some of which are described below:

1. Ridge waveguide is useful as transmission waveguide when a wide frequency range must be covered and when only the fundamental mode can be tolerated. A frequency range of 4 to 1 or more can be easily obtained between the cutoff frequencies of the  $TE_{1,0}$  and  $TE_{2,0}$  modes, and 6 to 1 or more between those of the  $TE_{1,0}$  and  $TE_{3,0}$  modes. The attenuation is several times as great as that for ordinary waveguide, but it is still much less than that for ordinary coaxial cable. In addition, the reduced cutoff frequency of ridge waveguide permits a compact cross section.

2. The attenuation formula for ridge waveguide [Eq. (26-71)] shows that the attenuation may be made very high by making  $a_1$  and  $Z_{0w}$  as small as possible. If the guide, or just the ridges, is made of steel instead of copper, the attenuation may be made about one thousand times greater than that for ordinary copper waveguide without ridges. A length of such waveguide tapered to standard  $3 \times 1\frac{1}{2}$ -in. waveguide has been used successfully in the design of a broad-band matched load (see Sec. 24-2). The total length of the load and taper is only 4 ft.

3. Another application is in a wide-band directional pickup and wattmeter in which a waveguide having nearly constant impedance over a wide band is required (see Sec. 24-26). The variation in characteristic impedance with frequency is shown in Fig. 26-22. For transmission use, rectangular waveguide usually operates at about 1.5 times its cutoff frequency. The figure shows that the characteristic impedance varies rapidly in this range. Ridge waveguide having the same outer dimensions as the rectangular waveguide will have a much lower cutoff frequency and, hence, will be operating in a range at several times the ridge-waveguide cutoff. Figure 26-22 shows that the impedance in this range is nearly constant. This length of ridge waveguide may be smoothly joined to the ordinary rectangular waveguide by a transition length having gradually tapering ridges. Although the constancy of impedance could also have been obtained by widening the rectangular waveguide and thus lowering its cutoff frequency, this expedient has several disadvantages compared with the use of ridge waveguide. (1) The widened rectangular waveguide can transmit higher modes which may cause trouble, and (2) its construction is more cumbersome.

## CHAPTER 27

### DESIGN OF TRANSMISSION-LINE FILTERS

By S. B. COHN

This chapter will present design data for *coaxial* and *waveguide transmission-line filters*. The coaxial filters will be classified as follows: (1) *short-line* types, with line elements sufficiently short to approximate inductances or capacitances; (2) *resonant-line* types, the line elements of which are resonant in or near the principal pass band. The sections on waveguide high-pass and band-pass filters will be preceded by a section on the design of *wide-band waveguide-to-coax junctions* suitable for use with waveguide filters. These junctions might also be used to provide coaxial terminations for waveguide transmission systems.

**27-1. The Complete Filter.**—The design equations presented in this chapter give the physical parameters for single *filter sections*. A filter section is defined as the simplest symmetrical unit that embodies the principal properties of the filter. A *complete filter* will consist of one or more sections of one or more different types connected in cascade, with an available pair of terminals at each end. One filter section by itself will rarely give a satisfactory frequency response. A combination of sections in cascade, however, can be made to provide almost any kind of response that may be desired.

If the filter is composed of a number of identical sections, its response may be readily predicted through the use of the insertion-loss nomograms of Figs. 26-9 and 26-10. If the sections are not identical, but the image impedances in both directions are equal, *i.e.*, matched, at every junction between the sections, these nomograms may still be used. If a filter consists of dissimilar sections with unmatched image impedances, however, those nomograms do not apply, and the exact calculation of the insertion-loss response is quite laborious. The recommended design procedure is then to make the image impedances of all the sections approximate the terminal load resistance as closely as possible throughout the pass band, and to hope for the best.

Although it is relatively easy to construct high-pass and low-pass sections in the microwave range, it is difficult to construct broad-band band-pass filter sections. A group of high-pass sections may, however, be combined with a group of low-pass sections to form the band-pass filter.

**27-2. Short-line-filter Types.**—Short-line filters, *i.e.*, filters composed of lengths of line small compared with  $\frac{1}{4}$  wavelength, are useful for the following reasons: (1) They are physically smaller than resonant-line filters, and therefore less bulky at lower frequencies. (2) In general transmission-line low-pass and band-pass filter sections have pass bands above the lowest (or principal) pass band, and high-pass sections have stop bands above the lowest pass band (see Sec. 26-6). These spurious responses and rejections are, however, much higher in frequency for short-line filters than for resonant-line filters. They are also generally narrower in short-line filters. (3) Short-line filters can be closely patterned after standard lumped-element types.

Tables 27-1 and 27-2 show the characteristics and design equations for a number of short-line filters.<sup>1</sup> The band-pass types cannot be constructed for very narrow bands, because impractically high characteristic impedances are required.

Information on the design of a filter for optimum performance with a given terminal resistance has been given in Secs. 26-8 and 26-9. Lumped-capacitance formulas, discontinuity-capacitance curves, and suggestions on practical construction will be given in Sec. 27-15.

**27-3. Short-line Low-pass Filter.**—Type 1-1, shown in Table 27-1, is an easily constructed and efficient low-pass type of filter. The approximate equivalent circuit given in the table shows this filter section to be very similar to the lumped-element constant- $k$  type. Exact calculations have shown the image impedance, phase constant  $\beta$ , and attenuation constant  $\alpha$  to be within a few per cent of those for the lumped-element analogues, for values of  $\theta_1$  up to at least 1 radian, or about 60 deg (Fig. 27-1). ( $\theta_1$  is an arbitrary design parameter.) In design considerations, therefore, or in pass-band response calculations, the image impedance and phase constant for the lumped-element type may be used.

The type 1-1 filter can be built to cut off at frequencies up to at least 10,000 Mc. Anywhere from 1 to 15 sections have been used in low-pass filters, depending on the sharpness of cutoff desired. Response curves for several filters are given in Figs. 26-12 and 27-2.

The design equations in Table 27-1 are exact as long as  $C$  is a pure lumped capacitance. Although  $\theta_1$  may have any value up to 180 deg ( $\pi$  radians), it should be as small as possible in order to separate and make narrower the spurious responses, and in order to maximize the stop-band attenuation. A value of  $\theta_1$  between about 30 and 60 deg would be proper

<sup>1</sup> The design equations and properties of several other configurations are given in MASON, W. P., and R. A. SYKES, *The Use of Coaxial and Balanced Transmission Lines in Filters and Wide-band Transformers for High Radio Frequencies*, *Bell System Tech. J.*, **16**, 275 (1937); and W. P. MASON, "Electromechanical Transducers and Wave Filters," p. 69, D. Van Nostrand Company, Inc., New York, 1942.

in most cases. Spurious responses for this filter occur near frequencies for which  $l$  is equal to, or a multiple of, a half wavelength.  $\theta_1$  should be chosen so that the spurious responses will fall where they will cause no harm. By constructing a filter with two groups of sections having different values of  $\theta_1$ , but the same cutoff frequency, the spurious responses

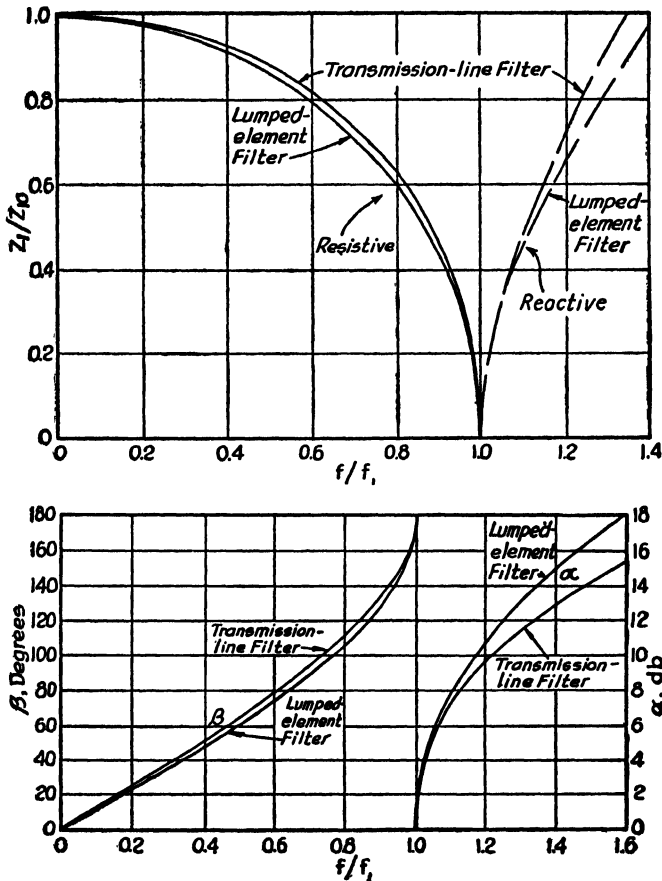


FIG. 27-1.—Image impedance and transfer constant for the varying-impedance filter as compared with that of the constant- $k$  low-pass filter. Attenuation constant  $\alpha$ , phase constant  $\beta$  ( $\theta_{1c} = 50$  deg,  $\theta_{2c} = 25$  deg,  $B_c = 0$ ).

of each group can be made to fall in the stop bands of the other group, with the result that all spurious responses will be highly attenuated.

The reader should refer to Secs. 26-8 and 26-9 for information on the best ratio of zero-frequency image impedance  $Z_{i0}$  to terminating resistance  $R$  and for methods of improving the response of the low-pass filter.

**27-4. Exact Design of the Varying-impedance Low-pass Filter.**—The practical construction of the transmission-line low-pass filter requires

capacitance disks of fairly great length. At frequencies above about 1500 Mc the capacitance can no longer be considered lumped and, for exact design, the disk must be treated as a length of transmission line, with the discontinuity capacitance at the ends of the disk taken into

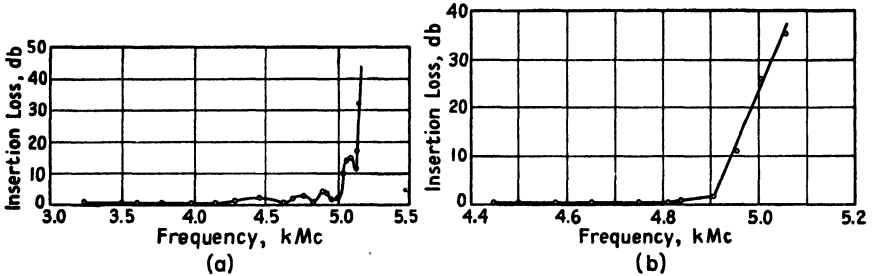


FIG. 27-2.—Measured frequency response of two 15-section low-pass filters: (a) is for identical sections throughout; (b) is for the same filter redesigned for transforming-end-section termination (13 inner sections plus 2 end sections).

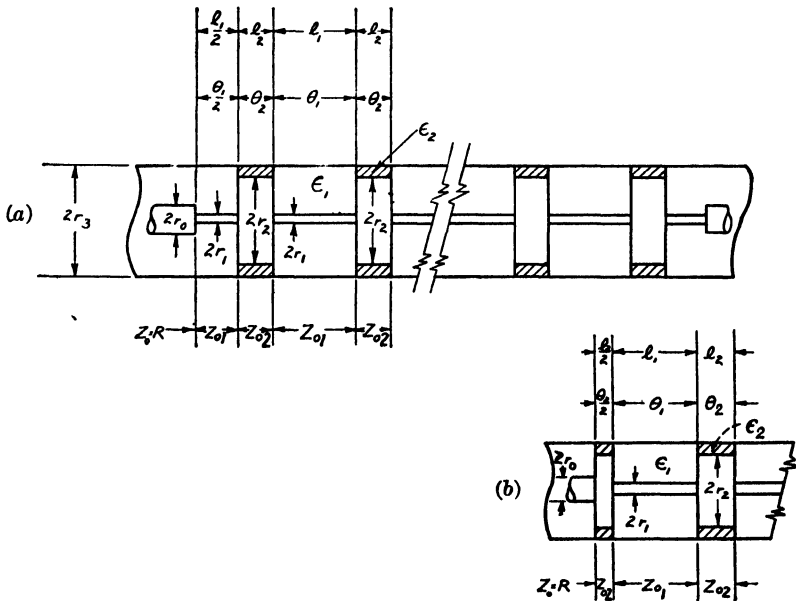


FIG. 27-3.—Construction of the varying-impedance low-pass filter (a) with mid- $\theta_1$  termination, and (b) with mid- $\theta_2$  termination.

account. The filter therefore consists of a succession of high- and low-impedance transmission-line lengths. The exact design procedure for this *varying-impedance low-pass filter* is described in the following paragraphs and is very easily carried out through the use of graphs. With this design method, the actual cutoff frequency will in practice fall within

about 2 per cent of the design cutoff frequency, if the filter parts are machined with good precision.

In designing a low-pass filter to cut off at a given frequency  $f_1$ , the first step is to choose values of cutoff electrical length  $\theta_{1c}$  and  $\theta_{2c}$  (Fig. 27-3)

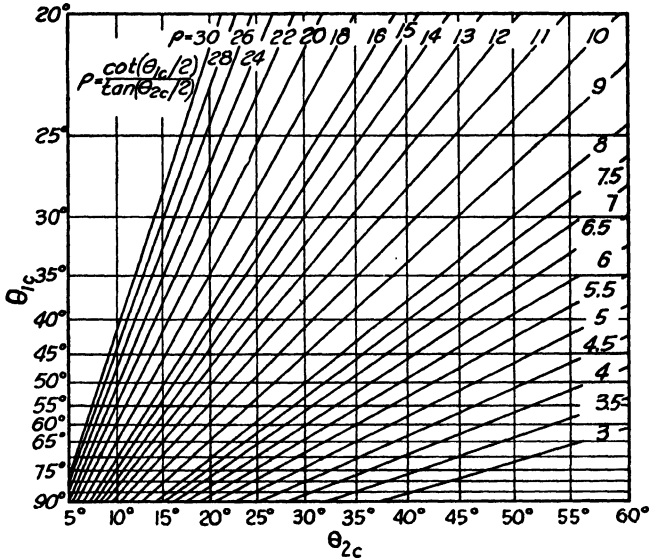


Fig. 27-4.—Design curves for the varying-impedance filter.

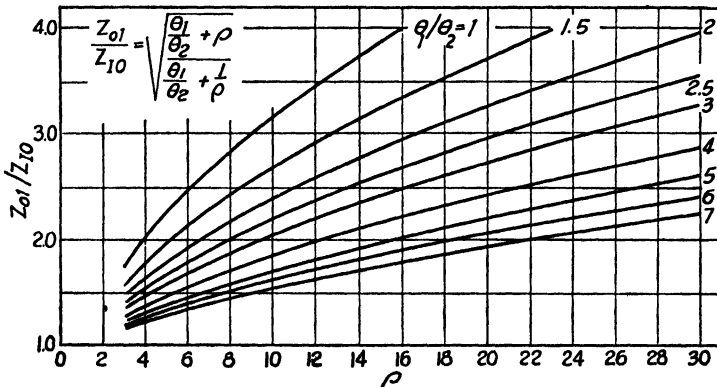


Fig. 27-5.—Design curves for the varying-impedance filter.

so that spurious responses will fall where they will do no harm. For  $\theta_1$  greater than  $\theta_2$ , a narrow spurious response occurs for  $\theta_1$  near  $n\pi$ , where  $n$  is an integer, and a wide response occurs for  $\theta_2$  equal to  $n\pi$ . The narrow responses are very sharp, usually less than  $\frac{1}{2} f_1$  in width if  $\theta_1/\theta_2$  is greater than about 2 to 1. The wide response is twice  $f_1$ , if  $\theta_1/\theta_2$  is an integer.



Of course  $\theta_{1c}$  and  $\theta_{2c}$  must have values within the ranges in which it is possible to meet mechanical tolerances.

The next step is to determine  $Z_{01}/Z_{02} = \rho$  from Fig. 27-4.  $Z_{01}$  is the higher characteristic impedance and  $Z_{02}$  the lower (Fig. 27-3). The value of  $\theta_{2c}$  used in Fig. 27-4 is a tentative value that is correct only if the discontinuity capacitance is zero. The actual value of  $\theta_{2c}$ ,  $\bar{\theta}_{2c}$ , will be given below.

A value of zero-frequency characteristic impedance  $Z_{10}$  is chosen as discussed in Sec. 26-9, and then  $Z_{01}$  is found from Fig. 27-5. In this graph, the tentative uncorrected value of  $\theta_{2c}$  should be used.

$Z_{02}$  is then easily obtained from  $Z_{01}$  by use of the relation  $Z_{02} = Z_{01}/\rho$ .

The conductor diameters (Fig. 27-3) are obtained from the impedance formula for a coaxial line, Eq. (26-26).

The corrected value of  $\theta_{2c}$  is calculated from the equation

$$\bar{\theta}_{2c} = 2 \tan^{-1} \left( \tan \frac{\theta_{2c}}{2} - B_c Z_{02} \right) \quad (27-1)$$

where  $B_c$  is the discontinuity susceptance at the change in inner-conductor diameter. To calculate  $B_c$ , the discontinuity capacitance curves of Fig. 27-28 are used. In terms of  $C_{d1}'(\alpha, \tau)$  obtained from these curves,

$$B_c Z_{02} = 5.00 f_1 D C_{d1}'(\alpha, \tau) Z_{02} (10)^{-5} \quad (27-2)$$

where  $f_1$  is the cutoff frequency in megacycles,  $C_{d1}'(\alpha, \tau)$  is in micro-microfarads per centimeter of circumference, and  $D = 2r_3$  is the outer diameter in inches. Figure 27-28 and Eq. (27-2) assume  $\epsilon_1 = 1$ , but  $\epsilon_2$  may have any value.  $l_1$  and  $l_2$  are calculated from  $\theta_{1c}$  and  $\bar{\theta}_{2c}$  through the use of Eq. (26-16).

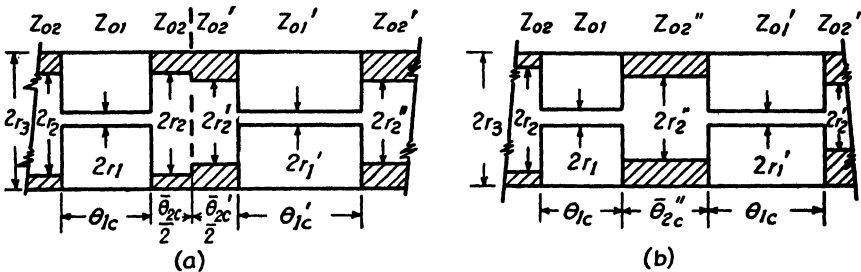
Either a mid- $\theta_1$  or mid- $\theta_2$  termination may be used (Fig. 27-3). All the above design equations apply equally well to both.

Figure 27-28 is accurate only if the successive discontinuities are far apart. Very good results should be obtained for  $l_2 \geq 2(r_3 - r_2)$  and  $l_1 \geq 2(r_3 - r_1)$ . The first condition is generally satisfied without difficulty. The second places a definite restriction on the largest allowable outer radius  $r_3$ . It is good practice at microwave frequencies to make  $r_3$  as small as possible, *e.g.*,  $2r_3 = 0.25$  in., since this not only reduces the error in  $B_c$ , but also reduces  $B_c$  itself. The number of sections necessary to attain a given sharpness of cutoff may be roughly estimated from the sample performance curves of Figs. 27-2 and 26-12.

If the spurious responses of the low-pass filter are likely to cause trouble, they may be eliminated, as mentioned above, by using two dissimilar groups of sections in the filter. The simplest method of joining the dissimilar groups is to join them at a low-impedance point, as

shown in Fig. 27-6a. It is generally more convenient to substitute a plain line for the stepped low-impedance line, as shown in Fig. 27-6b.  $Z_{o2}''$  and  $\theta_{2c}''$  are given by the equations in Fig. 27-6. These equations are very close for  $\bar{\theta}_{2c}$  and  $\bar{\theta}_{2c}'$  less than 40 deg, as is generally the case, and fairly close when these values are somewhat larger.

For improved pass-band response at microwave frequencies, the transforming-end-section design described in Sec. 26-9 should be used. A low-pass filter having this type of design is shown in Fig. 26-17 with its measured response. The response of another such filter is shown in Fig. 27-2b. The latter should be compared with the response curve in Fig. 27-2a, which is for a similar filter without transforming end sections.



$$Z_{o2}'' = Z_{o2} \sqrt{\frac{\bar{\theta}_{2c}/\bar{\theta}_{2c}' + Z_{o2}'/Z_{o2}}{\bar{\theta}_{2c}/\bar{\theta}_{2c}' + Z_{o2}/Z_{o2}'}} , \quad \bar{\theta}_{2c}'' = \frac{\bar{\theta}_{2c}}{2} \frac{Z_{o2}''}{Z_{o2}} + \frac{\bar{\theta}_{2c}'}{2} \frac{Z_{o2}}{Z_{o2}''}$$

FIG. 27-6.—(a) Junction between two groups of dissimilar low-pass filter sections; (b) equivalent low-impedance line length with the step eliminated. The characteristic impedance and the length of this equivalent line are given by the equations.

**27-5. Design of a Typical Low-pass Filter.**—The design procedure discussed in the preceding section will be illustrated by the design of a filter having the following requirements:

1. Pass band up to 3450 Mc
2. Greater than 30 db attenuation above 4050 Mc
3. Terminations 40 ohms ( $R = 40$  ohms)
4. No spurious responses below 10,000 Mc or near 24,000 Mc

A cutoff frequency of 3550 Mc will provide some tolerance. Six sections should be ample.

With  $\theta_{1c} = 40$  deg and  $\theta_{2c}$  about 20 deg, a narrow response can exist at  $180 \text{ deg}/40 \text{ deg} \times 3550 \text{ Mc} = 16,000 \text{ Mc}$ , and a wide one at 32,000 Mc. These do not violate the specifications.

In order that  $\bar{\theta}_{2c}$  shall be near 20 deg, assume an uncorrected value of 25 deg. Then Fig. 27-4 shows  $\rho$  to be 12.4, and Fig. 27-5 shows that  $Z_{o1}/Z_{10} = 2.88$ .

In order to obtain a flatter response with mid- $\theta_{1c}$  terminations, let  $Z_{10} = 1.41R = 1.41 \times 40 = 57$  ohms. Therefore,  $Z_{01} = 165$  ohms, and  $Z_{02} = 165/\rho = 13.3$  ohms. The ratio of diameters may now be calculated from Eq. (26-25). For the high-impedance lengths, air dielectric will be used ( $\epsilon = 1$ ). For the low-impedance lengths, polystyrene dielectric will be used ( $\epsilon = 2.5$ ). Then

$$\frac{r_3}{r_1} = e^{165/60} = 15.6$$

$$\frac{r_3}{r_2} = e^{\frac{13.3\sqrt{2.5}}{60}} = 1.419$$

Let  $2r_3 = \frac{5}{16}$  in. (0.3125 in. diam.). Then  $2r_1 = 0.020$  in. and  $2r_2 = 0.220$  in.

The discontinuity susceptance  $B_c$  is calculated by means of Fig. 27-28. The parameters used with Fig. 27-28 are

$$\alpha = \frac{r_3 - r_2}{r_3 - r_1} = \frac{\frac{1}{2}(0.3125 - 0.220)}{\frac{1}{2}(0.3125 - 0.020)} = 0.316$$

and

$$\tau = \frac{r_3}{r_1} = \frac{\frac{1}{2}(0.3125)}{\frac{1}{2}(0.020)} = 15.6$$

Then by Fig. 27-28,  $C_{d1}'(\alpha, \tau) = 0.052 \mu\text{mf}$  per cm. By Eq. (27-2),  $B_c Z_{02} = 5 \times 3550 \times 0.3125 \times 0.052 \times 13.3(10)^{-6} = 0.0384$ .

The corrected  $\bar{\theta}_{2c}$  may now be calculated by Eq. (27-1)

$$\begin{aligned}\bar{\theta}_{2c} &= 2 \tan^{-1} \left( \tan \frac{25 \text{ deg}}{2} - 0.0384 \right) \\ &= 2 \tan^{-1} (.221 - 0.0384) \\ &= 2 \times 10.4 \text{ deg} = 20.8 \text{ deg}\end{aligned}$$

The last dimensions to be calculated are  $l_1$  and  $l_2$ . By Eq. (26-16) with the cutoff wavelength  $\lambda_1 = \frac{30,000}{3550 \sqrt{\epsilon}} = \frac{8.45}{\sqrt{\epsilon}}$  cm.

$$\begin{aligned}l &= \frac{\theta \text{ deg}}{360 \text{ deg}} \lambda_1 \\ l_1 &= \frac{40 \text{ deg}}{360 \text{ deg}} \times 8.45 \text{ cm} = 0.939 \text{ cm} \\ l_2 &= \frac{20.8}{360} \times \frac{8.45}{\sqrt{2.50}} = 0.308 \text{ cm}\end{aligned}$$

or in inches,  $l_1 = 0.370$  in. and  $l_2 = 0.122$  in.

**27-6. Short-line High-pass Filter.**—The simplest high-pass type of filter for use below about 1200 Mc is type 1-2. of Table 27-1. Its

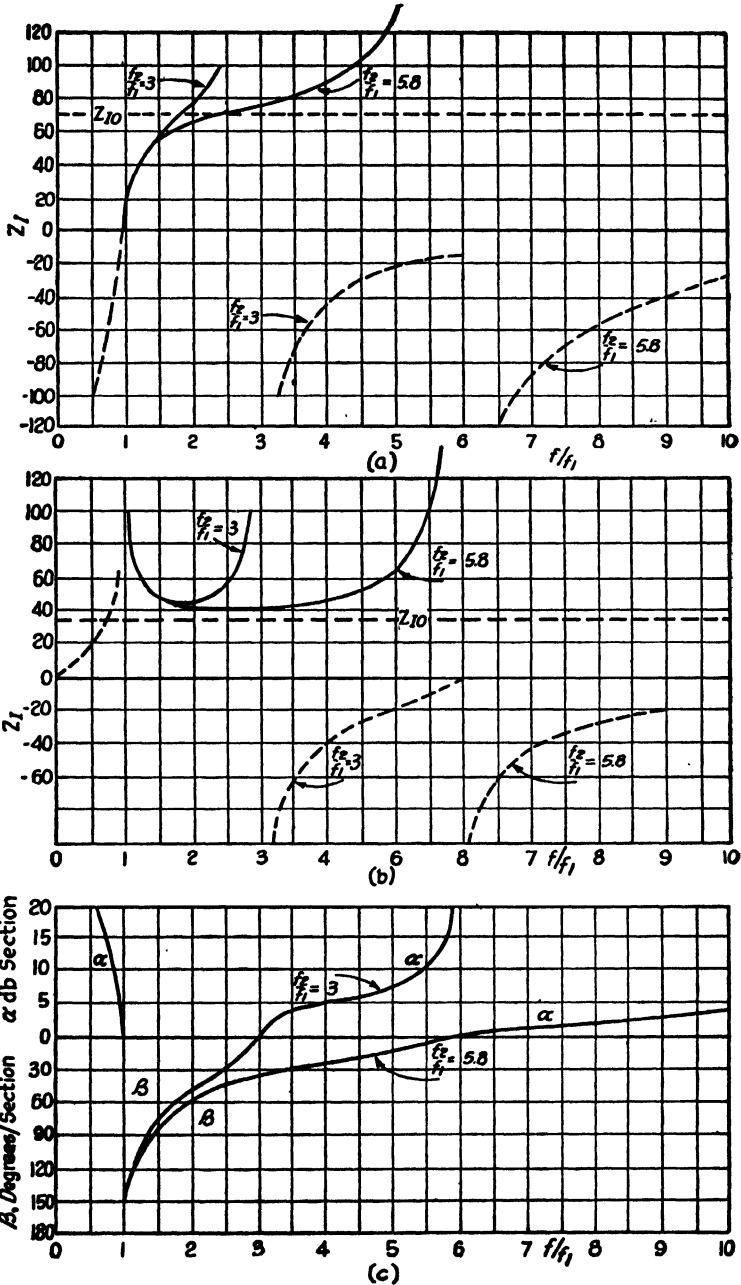


FIG. 27-7.—Image-impedance and transfer-constant curves for the type 1-2 high-pass filter; (a) for a T-section; (b) for a  $\pi$ -section. The attenuation constant  $\alpha$  and phase constant  $\beta$  for both (a) and (b) are given in (c). Unbroken lines represent resistance and dashed lines reactance.

approximate equivalent circuit is that of the simple constant- $k$  lumped-element high-pass filter. The image impedance, attenuation constant, and phase constant for the transmission-line type are similar to the corresponding functions for the lumped-element type, but only up to the frequency for which the electrical length of the short-circuited shunt line is approximately  $\frac{1}{8}$  wavelength. The exact equations for the image impedance and transfer constant of this filter are derived in Sec. 26-5. Curves plotted from these equations for several values of  $\theta_1$  are given in Fig. 27-7. This figure shows that the  $\pi$ -termination image impedance is

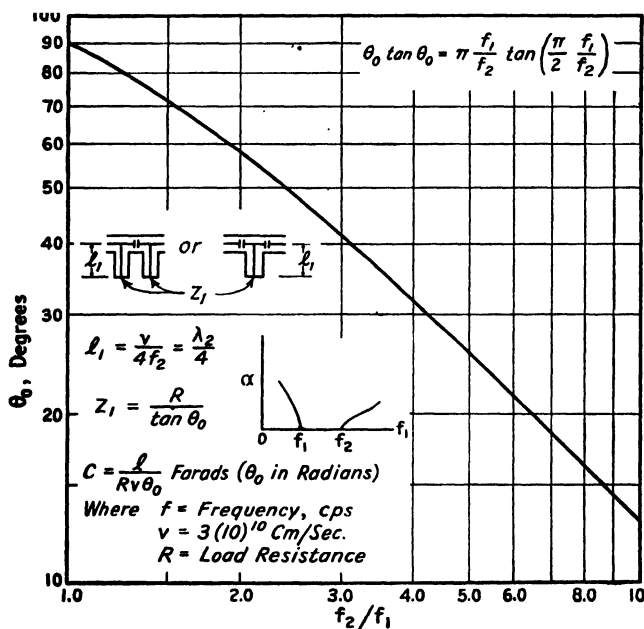


FIG. 27-8.—Exact design relations for the type 1-2 filter. The parameter  $\theta_0$  is obtained from the graph.

a good match to the load resistance over a much broader band than is the T-termination image impedance. The latter is usually easier to construct, however, since one less shunt line is required for the same number of sections, and since the characteristic impedance of all the shunt lines may be made equal.

The design equations of Table 27-1 for the high-pass filter are approximations that assume  $\theta_1$  to be very small and the line connecting the sections to be of zero length. For  $\theta_1$  equal to  $\frac{1}{3}$  radian, the error in cutoff frequency due to the design equation approximations is about 2 per cent, which should be less than the error caused by the uncertainty in the various physical discontinuities in this type. Figure 27-7 shows that the high-pass filter pass band exists only up to the frequency for which  $\theta$

is equal to 90 deg, *i.e.*, the length of the shunt line is  $\frac{1}{4}$  wavelength. Above this frequency there is a theoretical stop band. If  $f_2/f_1$  is large, however, the attenuation constant rises very slowly for a considerable distance into the stop band above  $f_2$ . As an example, for a two-section filter in which  $f_2/f_1$  is equal to 6, the calculated insertion loss is only 2 db

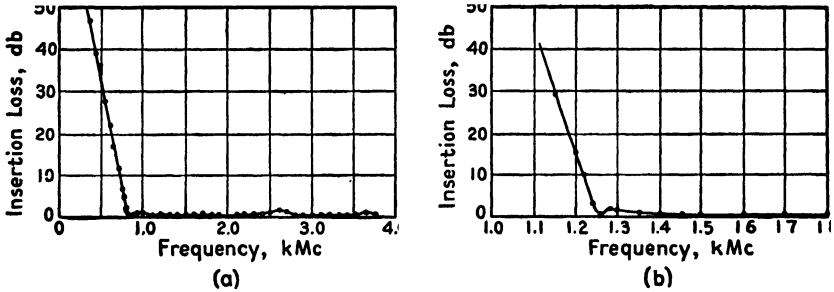


FIG. 27-9.—Measured response of two high-pass filters composed of type 1-2 T-sections. Curve (a) is for a two-section filter and (b) for a five-section filter.

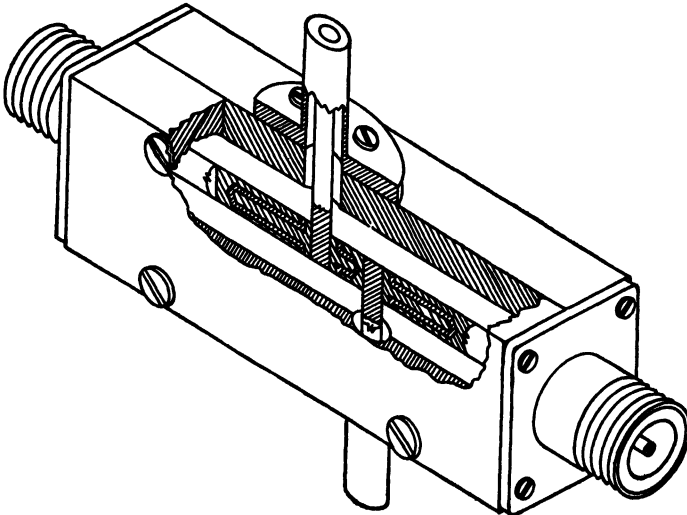


FIG. 27-10.—Construction of a two-section high-pass filter measured response curve. It is shown in Fig 27-9a

at a frequency 50 per cent above the upper cutoff frequency  $f_2$ . This type of filter may be used, therefore, with fairly low loss considerably beyond the theoretical upper cutoff frequency.

Figure 27-8 gives exact design relations for a stub length of any value up to  $\frac{1}{4}$  wavelength, when the connecting lines between sections are very short.  $\theta_0$  is a design parameter that is a function of  $f_2/f_1$  only and that is not closely related to any physical dimension in the filter.

Through the use of the  $\theta_0$  curve given in Fig. 27-8, the filter parameters may be calculated very easily. It must be pointed out that in the design equations of Fig. 27-8 the load resistance  $R$  is set equal to the image-impedance value at the frequency for which  $\beta$  is equal to  $-90$  deg. This frequency is very nearly 41 per cent higher than  $f_1$ , and the crossover point between the  $Z_i$  curve and the constant-load line  $R$  is almost exactly the same as that recommended for general use in Sec. 26-9, part 3.

Examination of the design equations shows that, as the pass-band ratio  $f_2/f_1$  is increased, the shunt-line characteristic impedance must also be increased. For  $f_2/f_1$  equal to 10 and for a load resistance  $R = 50$  ohms, a shunt-line impedance of 224 ohms is required. This is about the practical limit of construction.

Figure 27-9 gives the measured response curves of two high-pass filters, the construction of which is shown in Figs. 27-10 and 27-29. The characteristic pass-band bumps near cutoff should be noted. These are explained in Sec. 26-9. Various methods of minimizing these insertion-loss bumps are given in Secs. 26-8 and 26-9.

**27-7.  $M$ -derived Half Sections for Terminating Low- and High-pass Filters.**—In low-frequency lumped-element filter work, the use of  $m$ -derived full sections and half sections is widespread. The theory and properties of this class of filter sections are covered in any textbook on filters<sup>1</sup> and will, therefore, not be considered in detail here.

$M$ -derived half sections are useful as terminations for constant- $k$  filter types. Filter 1-3 of Table 27-1 is a low-pass filter termination. This is intended for use with the filter of type 1-1a. The type 1-4 filter is a high-pass filter termination for use with the filter of type 1-2a. Figures 27-11 and 27-12 show two complete filter structures with their measured response.

$M$ -derived terminations are advantageous for the following reasons: (1) They provide a much flatter terminal image impedance for the filter than do the simpler constant- $k$  structures. For this reason, the pass-band insertion loss is generally less for a filter having  $m$ -derived terminations than for one in which these terminations are omitted. (2) They provide an extremely sharp cutoff with an extremely high rejection point at a frequency a short distance within the stop band from the cutoff frequency. Farther within the stop band, however, the attenuation constant for an  $m$ -derived filter section or half section decreases, and, therefore, a filter composed purely of  $m$ -derived sections may not have sufficiently high insertion loss throughout the stop band. (3) At one pair of terminals an  $m$ -derived half section has the flat image-impedance

<sup>1</sup> For example, see T. E. SHEA, "Transmission Networks and Wave Filters," p. 244, D. Van Nostrand Company, Inc., 1929. Image-impedance and attenuation-constant curves for  $m$ -derived low-pass and high-pass sections are given in that text.

curve mentioned above, while at the other pair of terminals the image impedance is the same as that for the constant- $k$  type from which it is derived. For this reason, a filter may be constructed of a number of constant- $k$  sections with an  $m$ -derived terminating half section at each end. Such a filter has its internal image impedances matched throughout, and, as a consequence, the terminal image impedance will be the flat  $m$ -derived image impedance already mentioned. In this way, the flat pass-band response, the sharp cutoff characteristic, and the frequency

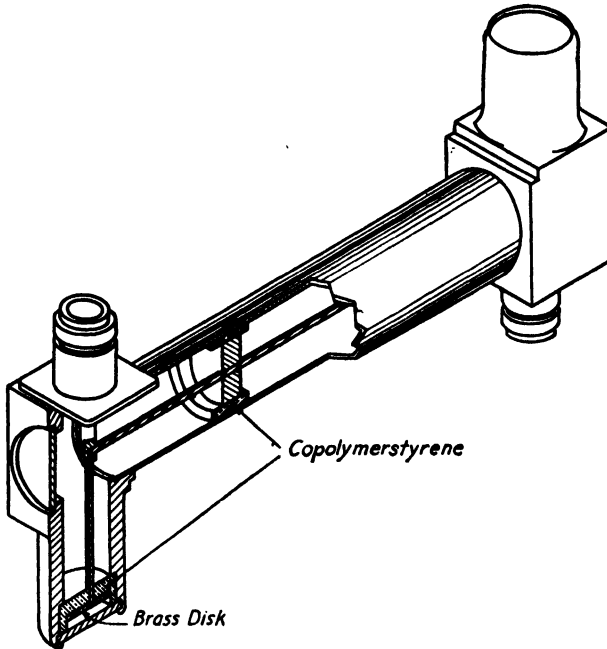


FIG. 27-11.—A low-pass filter with  $m$ -derived terminations. Frequency response shown in Fig 27-12.

of high attenuation near the cutoff frequency provided by the  $m$ -derived half sections are combined with the high increasing attenuation far into the stop band provided by the constant- $k$  sections.

The design equations given in Table 27-1 for the transmission-line  $m$ -derived half sections are approximate ones that hold fairly well if the line lengths are made as small as possible. In designing a composite low-pass or high-pass filter having internal sections of type 1-1a or 1-2a, and  $m$ -derived terminating half sections of type 1-3 or 1-4, the image-impedance value  $Z_{10}$  should be made equal to  $R$ .

The shape of the image-impedance curve is a function of the parameter  $m$ . For optimum flatness,  $m$  should be equal to about 0.6. A text on



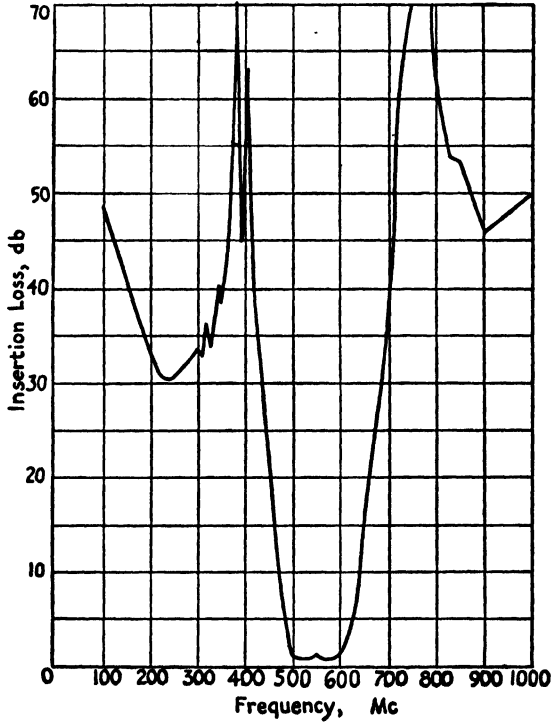
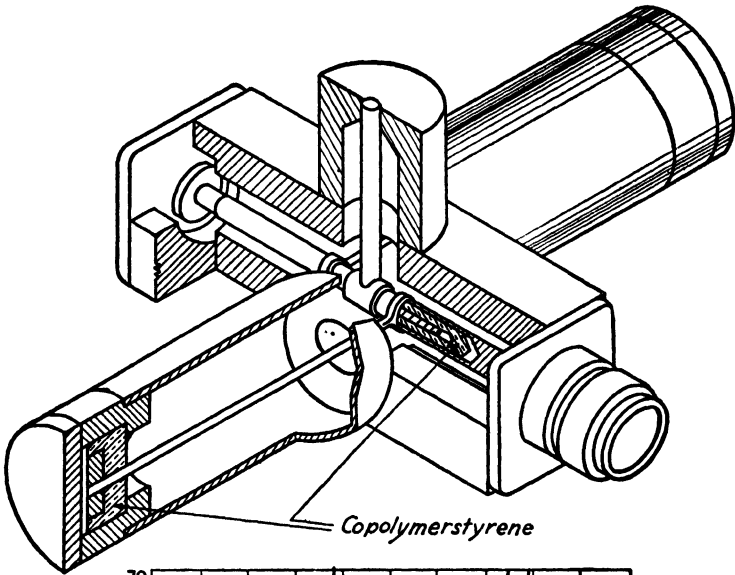
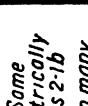
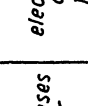
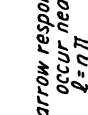
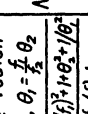

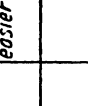
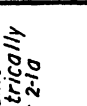
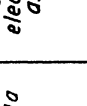


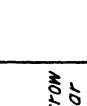
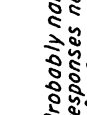


FIG. 27-12.—(a) A high-pass filter with  $m$ -derived terminations. (b) Frequency response for filters of Figs. 27-11 and 27-12a connected in cascade.

TABLE 27-1 SHORT-LINE FILTER SECTIONS - LOW-PASS AND HIGH-PASS		$v = 3 (10)^{10} / \sqrt{\epsilon}$ cm/sec, $\omega = 2\pi f$		Other Remarks	
Structure	Appr Equiv Circuit	Image Impedance	Transfer Constant	Design Equations	Spurious Responses
<p>1-1</p> <p>(a) </p> <p>(b) </p> <p>L.P.F.</p>	 			$\ell = \theta_1 \frac{v}{\omega_1}$ $Z_0 = Z_{10} \sqrt{1 + \frac{\cot^2(\theta/2)}{\theta_1/2}}$ $C = \frac{2 \cot(\theta/2)}{Z_0 \omega_1}$	<p>Narrow responses occur near <math>\ell = \frac{1}{2} \lambda, \lambda, \frac{3}{2} \lambda, \text{etc.}</math> or <math>\theta = \pi, 2\pi, 3\pi, \text{etc}</math> See text for exact design equations</p>
<p>1-2</p> <p>(a) </p> <p>(b) </p> <p>H.P.F.</p>	 			<p>for <math>\theta_1 \leq \frac{1}{2}</math>  <math>\ell = \theta_1 \frac{v}{\omega_1}</math>  <math>Z_0 = \frac{Z_{10}}{2\theta_1}</math>  <math>C = \frac{1}{2\omega_1 Z_{10}}</math> </p>	<p>High attenuation bands around <math>\ell = \frac{\pi}{2} \lambda</math></p> <p><math>\theta</math> preferably less than <math>\frac{1}{4}</math> for wide band width. See Fig. 27-8 for exact design equations</p>
<p>1-3</p> <p></p> <p><math>Z_0 = R = \frac{Z_1}{2}</math></p> <p>M-derived L.P.F. - <math>\frac{1}{2}</math> section</p>				<p>for <math>\theta_1 \leq \frac{1}{2}, \theta_2 \leq \frac{1}{2}</math>  <math>\ell_1 = \theta_1 \frac{v}{\omega_1}, \ell_2 = \theta_2 \frac{v}{\omega_2}</math>  <math>Z_{01} = \frac{2mR}{\theta_1}, C_2 = \frac{m}{\pi f R}</math>  <math>Z_{02} = \frac{(1-m^2)R}{2m\theta_2}</math> </p>	<p><math>\frac{f_{\infty}}{f_1} = \frac{1}{\sqrt{1-m^2}}</math>  <math>Z_1</math> is flattest for <math>m</math> approximately equal to 0.6</p>
<p>1-4</p> <p></p> <p><math>Z_0 = R</math></p> <p>M-derived H.P.F. - <math>\frac{1}{2}</math> section</p>				<p>for <math>\theta_2 \leq \frac{1}{2}</math>  <math>\ell_2 = \theta_2 \frac{v}{\omega_2}</math>  <math>Z_{02} = \frac{2mR}{2m\theta_2}</math>  <math>C_1 = \frac{4\pi f R m}{4\pi f R}</math>  <math>C_2 = \frac{1}{(1-m^2) 4\pi f R}</math> </p>	<p><math>\frac{f_{\infty}}{f_1} = \frac{1}{\sqrt{1-m^2}}</math>  <math>Z_1</math> is flattest for <math>m</math> approximately equal to 0.6</p>

TABLE 27-2 SHORT-LINE FILTER SECTIONS, BAND-PASS  $v = 3(10)^{10}/4\pi$  cm/sec.,  $\omega = 2\pi f$

Structure	Appr. Equiv. Circuit	Image Impedance	Transfer Constant	Design Equations	Spurious Responses	Other Remarks
 <p>2-1a</p>				for $\theta_2 \leq \frac{1}{2}$ radian $\ell = 2\theta_2 \frac{v}{\omega_2}$ , $\theta_1 = \frac{1}{2} \theta_2$ $Z_0 = Z_{10} \sqrt{\frac{(\frac{f_2}{f_1})^2 + \theta_2^2}{(\frac{f_2}{f_1})^2 - 1}}$ $C_1 = \frac{1}{\omega_1 \theta_2 Z_0}$ , $C_2 = \frac{2C_1}{(\frac{f_2}{f_1})^2 - 1}$	Narrow responses occur near $\theta = n\pi$	Same electrically as 2-1b. In many instances 2-1b is easier to construct.
 <p>2-1b</p>		same as 2-1a	same as 2-1a	for $\theta_2 \leq \frac{1}{2}$ $\ell$ , $Z_0$ , and $\theta$ , as in 2-1a $C_A = \frac{1}{\omega_1 \theta_2 Z_0} \left( \frac{f_1}{f_2} \right)$ $C_B = \frac{1}{2\omega_1 \theta_1 Z_0} \left\{ 1 - \left( \frac{f_1}{f_2} \right)^2 \right\}$	same as 2-1a	Same electrically as 2-1a
 <p>2-2</p>		same as 2-1a		$\theta_2 \leq \frac{1}{2}$ and $\theta_2' \leq \frac{1}{2}$ $Z_{01} = \frac{Z_{10}}{\theta_2} \left( \frac{f_1}{f_2} \right)$ , $\ell_1 = \frac{2\theta_2 v}{\omega_2}$ $Z_{02} = \frac{Z_{10}}{2\theta_2'} \left( \frac{f_1 + f_2}{f_1} \right)$ , $\ell_2 = \theta_2' \frac{v}{\omega_2}$ $C_1 = \frac{1}{4\pi Z_{10}} \left( \frac{f_2 - f_1}{f_1 f_2} \right)$	Probably narrow responses near $\ell_j = n\pi$	
 <p>2-3</p>		same as 2-1a		$\theta_2 \leq \frac{1}{2}$ and $\theta_2' \leq \frac{1}{2}$ $\ell_1$ , $\ell_2$ , $C_1$ , as in 4 $Z_{01} = \frac{Z_{10}}{\theta_2} \left( \frac{f_2}{f_1} \right)$ $Z_{02} = \frac{Z_{10}}{2\theta_2'} \left( \frac{f_2 - f_1}{f_1} \right)$ $C_2 = \frac{1}{\pi} \left( \frac{f_2 - f_1}{f_1} \right) \frac{1}{Z_{10}}$	same as 2-2	$\pi$ -section construction is also possible

filters should be consulted for image-impedance curves for this and other values of  $m$ .

**27-8. Short-line Band-pass Filters.**—The design equations and properties of several short-line band-pass filter types are presented in Table 27-2. Each one is seen to have as an equivalent circuit a well-known lumped-element type. Therefore, in the frequency range far from line resonance, the image impedance and transfer constant for the short-line filters will be closely similar to the corresponding functions for the lumped-element type.

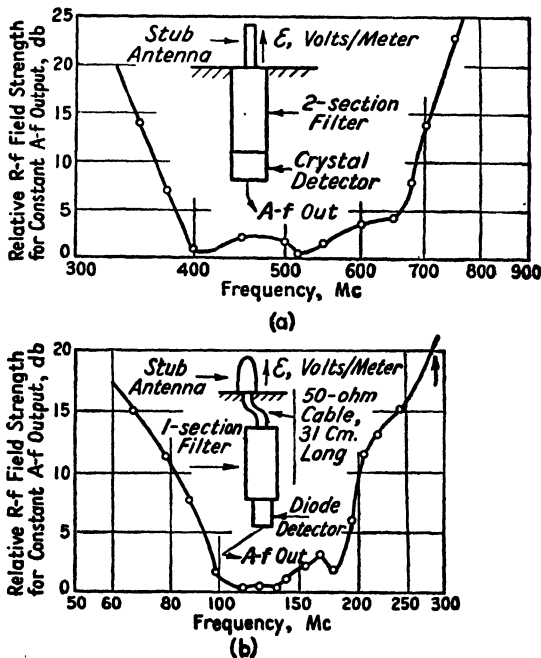


FIG. 27-13.—Over-all frequency response of two type 2-1a filters used with a broadband stub antenna and a detector termination. The filters themselves would, of course, have a somewhat flatter insertion-loss response in the pass band.

These filters cannot be designed for a narrow band width. For a load resistance of  $R = Z_{l0} = 50$  ohms, the narrowest band width for type 2-1 is about a 2:1 frequency ratio; for type 2-2, a 1.5:1 ratio; and for type 2-3, a 2:1 ratio. Filter types 2-1a, 2-2, and 2-3 are difficult to construct at frequencies much over 1000 Mc. Type 2-1b, however, can be designed with an upper cutoff of at least 2000 Mc.

The filter types in Table 27-2 have similar image-impedance functions. The maximum image impedance in the pass band for these types occurs near the geometric mean of the two cutoff frequencies. As pointed out

in Sec. 26-8, the flattest over-all pass-band response would result for  $Z_{i0} = 1.414 R$ . As this value of  $Z_{i0}$  would in most cases require impractically high line impedances,  $Z_{i0}$  may be made equal to  $R$ , or as much higher than  $R$  as possible, up to  $1.414R$ .

Types 2-1a and 2-1b have been used more than the other short-line band-pass types at the Radio Research Laboratory. Figure 27-13 shows some typical response curves.

Type 2-1 has narrow spurious responses at frequencies for which  $l$  is  $\frac{1}{2}$  wavelength or a multiple thereof. The spurious responses for the other types in Table 27-2 have not been worked out, but they are also likely to occur near frequencies for which  $l_1$  and  $l_2$  are each  $\frac{1}{2}$  wavelength or a multiple thereof. All these spurious responses will be narrow and may be eliminated by the method suggested for low-pass filters.

**27-9. Resonant-line Filter Types.**<sup>1</sup>—As frequencies are increased, the dimensions of the short-line filter types become very small. The larger dimensions of resonant-section types make them most useful in this range of about 1000 Mc and higher.

Besides the difference in size, there are other differences between short-line types and resonant-line types. (1) The former have spurious responses that are widely separated from the principal pass band by a nonintegral ratio that may be varied at will, while the latter have higher pass bands that are fairly close to the lowest pass band, the first one occurring generally at two or three times the lowest pass-band frequency. (2) In the former, the large separation of the spurious responses and the action of the lumped shunt capacitances generally cause the spurious responses to be narrower than the principal pass band, while in the latter the higher pass bands are equal to or wider than the principal pass band.

Tables 27-3, 27-4, and 27-5 give design information for a large number of filter sections having resonant-line elements. The filters of Table 27-3 are the types that were found most useful at the Radio Research Laboratory. Some of the others have not had much use, and some are more difficult to build, but many may prove to be desirable types in specific instances.

**27-10. Type 3-1 Band-pass and High-pass Filter.**—Filter 3-1 of Table 27-3 has the same structure as 1-2, and the same design equations are valid. In this case, however, the use of the structure as a narrow-band band-pass filter will be considered. In the earlier discussion of this filter as a high-pass type,  $f_2/f_1$  was made as large as was practicable. Under this condition it was shown that the attenuation rise above  $f_2$  was extremely gradual compared with that below  $f_1$ . As  $f_2/f_1$  is reduced, the attenuation slope above  $f_2$  becomes greater and, for  $f_2/f_1$  less than 1.5,

<sup>1</sup> The resonant-line-filter design equations are from an unpublished report by P. I. Richards.

the attenuation slope above  $f_2$  is almost as great as that below  $f_1$ . Filter 3-1 is therefore a practical narrow-band filter.

The design equations of Fig. 27-8 may be used for filter 3-1, or, for  $f_2/f_1$  less than or equal to 1.5, the approximate equations of Table 27-3 are accurate within 3 per cent. Examination of the design equations shows that for  $f_2/f_1$  less than about 1.15, and for a load resistance of 50 ohms, the characteristic impedance of the shunt line becomes so small that construction becomes difficult. In addition, very narrow band widths require large capacitances, which make construction even more difficult. The practical band-width ratios for this narrow-band filter, therefore, lie between about 1.15 and 1.50. It must be pointed out, however, that the spurious pass bands are wider than  $f_2 - f_1$ , and each successive spurious pass band is wider than the preceding one.

The characteristic impedance of the connecting line between sections should be made equal to  $R$ , and as short as possible.

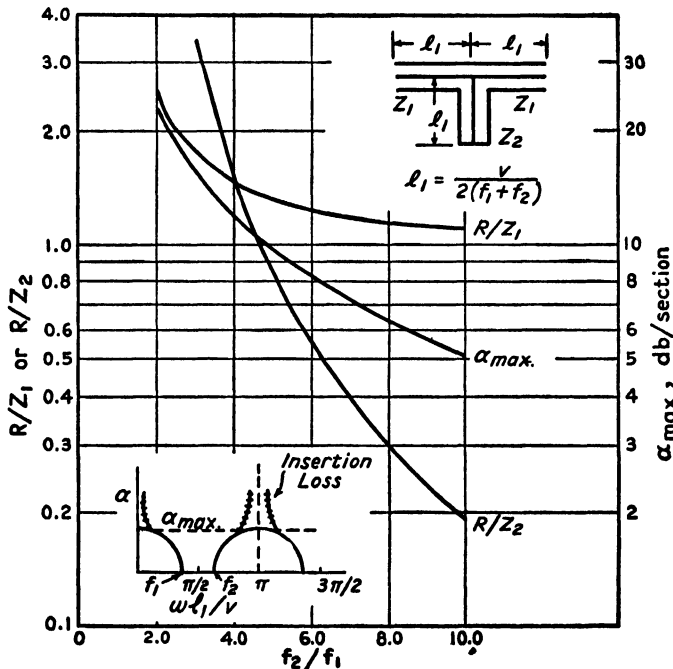


FIG. 27-14—Design relations for the type 3-2 filter.

**27-11. Type 3-2 Band-pass and High-pass Filter.**—The exact design equations for filter 3-2 are given in Table 27-3 and are plotted in Fig. 27-14. Inspection of this figure shows that the practical band-width design range for  $R = 50$  ohms is that in which  $f_2/f_1$  lies between about 2 and 9. With such large band widths, the higher pass bands are very

close to the first pass band, and therefore this filter is not very useful as a band-pass filter, except in special cases or in conjunction with another filter that eliminates the higher pass bands. Filter 3-2 is most useful as a high-pass filter or as a band-rejection filter. In both cases,  $f_2/f_1$  should be made as large as is practicable. When used as a rejection

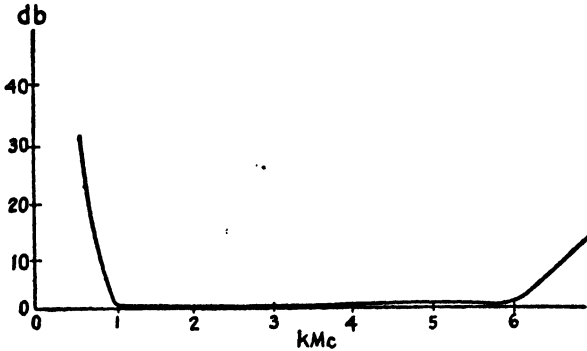


FIG. 27-15.—Measured response of a type 3-2 filter with seven sections.  $f_2/f_1 = 6$ ,  $R = 50$  ohms. The construction is shown in Fig. 27-30.

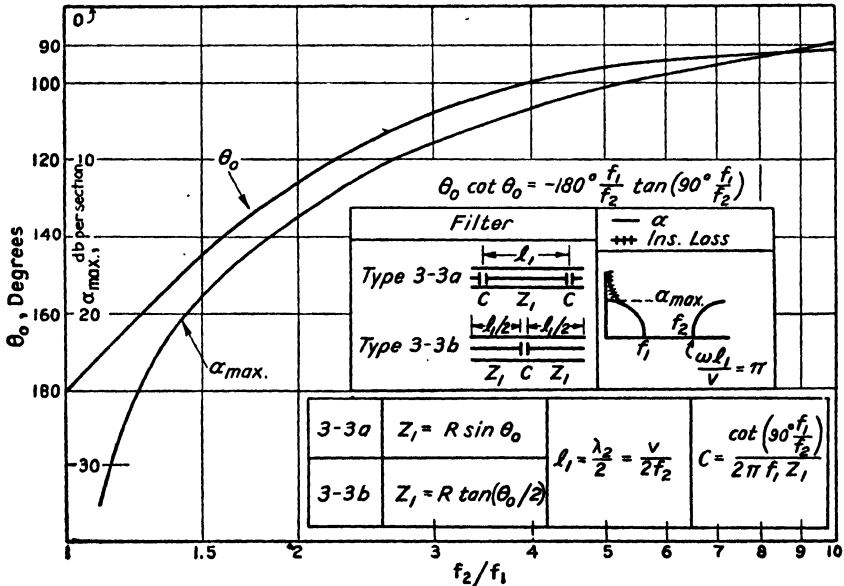


FIG. 27-16.—Design data for the type 3-3 filter.

filter,  $l_1$  should be made equal to or an integral multiple of  $\frac{1}{2}$  wavelength at the frequency to be rejected. Although the attenuation constant for this filter section is finite at this frequency and at zero frequency, the insertion loss is obviously infinite at these frequencies, due to the short-circuiting action of the shunt lines (see Sec. 26-11).

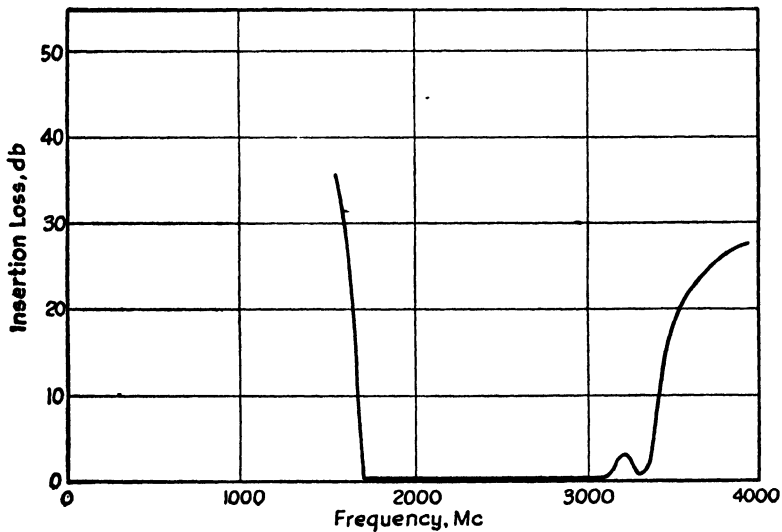
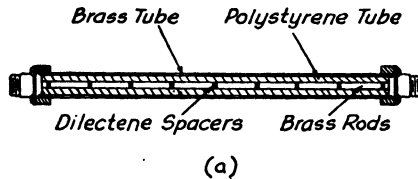
TABLE 27-3 RESONANT-LINE FILTER SECTIONS  $v = 3(10)^{10}/\sqrt{\epsilon}$  cm/sec.  $\omega = 2\pi f$

Filter	 $\alpha$ vs $\omega/v$ Loss			$\cosh(\alpha/2)$ (dB)	$\theta_1$	$Z_1$	$Z_2$	Others	Remarks
3-1			$2 \sec^2 \frac{\pi f}{f_1 + f_2} - 1$	$\frac{v}{4f_2} = \frac{\lambda_2}{4}$ For $f_2/f_1 \approx 1.5$ $R f_2 \cot(\frac{\pi}{2} \frac{f}{f_2})$	$R \cot \left[ \frac{1}{2} \cos^{-1} \left\{ -\sin^2 \left( \frac{\pi f}{f_1 + f_2} \right) \right\} \right]$	$\frac{Z_1}{2 \tan^2 \left( \frac{\pi f}{f_1 + f_2} \right)}$	$c = \frac{2\ell}{\pi R v}$	1 Pass bands on odd harmonics $Z_1 = R$ at $\beta = -90^\circ$	
3-2			$1 + \pi \frac{f}{f_2} \tan \left( \frac{\pi f}{2f_2} \right)$	$\frac{v}{2(f_1 + f_2)}$	$R \sin \theta_0$ $R \tan \frac{\theta_0}{2}$	$\frac{Z_1}{2 \tan^2 \left( \frac{\pi f}{f_1 + f_2} \right)}$	$c = \frac{\cot \left( \frac{\pi}{2} \frac{f}{f_2} \right)}{2\pi f_1 Z_1}$	1 Pass bands on odd harmonics 2 $\theta_0$ occurs at $\omega_0/\nu = \pi$ 3 See Fig 27-14 4 $Z_1 = R$ at $\cos \beta = 0$	
3-3			$1 + \frac{Z_L}{Z_2}$	$\frac{v}{2(f_1 + f_2)}$	$R \tan \left[ \frac{1}{2} \cos^{-1} \left\{ -\sin^2 \left( \frac{\pi f}{f_1 + f_2} \right) \right\} \right]$	$2Z_1 \tan^2 \left( \frac{\pi f}{f_1 + f_2} \right)$		1 Spurious pass bands on odd harmonics 2 See Fig 27-18 3 $Z_1 = R$ at $\cos \beta = 0$	
3-4			$1 + 2 \cot^2 \omega_0 \ell_1 / v$	If $f_m$ is not important make $\theta_1$ as small as possible	$R \sin^2 \left( \omega_0 \ell_1 / v \right)$	$2R \cos^2 \left( \omega_0 \ell_1 / v \right)$		1 Pass bands centered at $\omega_0/\nu = \pi$ 2 $\theta_0$ occurs for $\omega_0/\nu = (2n+1)\pi/2$	
3-5					See Text			1 Pass bands and "infinite" att points odd harmonically related 2 $\theta_0$ occurs for $\omega_0/\nu = \pi$ 3 $\theta_m > \theta_0$ 4 $\frac{3}{4}$ of the frag. $f_1, f_2, f_m$ from can be specified	
3-6									



Figure 27-15 shows the measured insertion-loss response for the seven-section filter of Fig. 27-30, having  $f_2/f_1 = 6$  and intended for high-pass use. It is seen to give an extremely flat pass band usable over a wider range than type 1-2, but more sections of 3-2 and a greater over-all length are required for the same insertion-loss slope in the stop band below  $f_1$ .

**27-12. Type 3-3 High-pass Filter.**—Filter 3-3 is really a band-pass type, but with a gradual upper cutoff and with close, wide higher pass



(b)

FIG. 27-17.—The construction and measured response of a type 3-3 filter. Eight sections;  $f_2/f_1 = 2$ ;  $R = 50$  ohms.

bands. It is in general, therefore, not useful as a band-pass filter, but it makes an excellent high-pass filter, especially in the range from about 1200 to 3000 Mc where type 1-2 becomes hard to build. Design data are given in Table 27-3 and Fig. 27-16. It will usually be found that sharpness of cutoff is determined more by physical length of a multiple-section filter of this type than by choice of  $f_2/f_1$ . That is, if  $f_2$  is doubled, then  $l_1$  is halved, but twice as many sections are needed for the same

sharpness of cutoff. If anything, cutoff for a given over-all length seems a little sharper for smaller values of  $f_2/f_1$ .

Figure 27-17a shows the construction of an eight-section filter of type 3-3a, and Fig. 27-17b gives the measured response of this filter. The manner in which the internal parts are suspended inside a polystyrene rod should be noted.

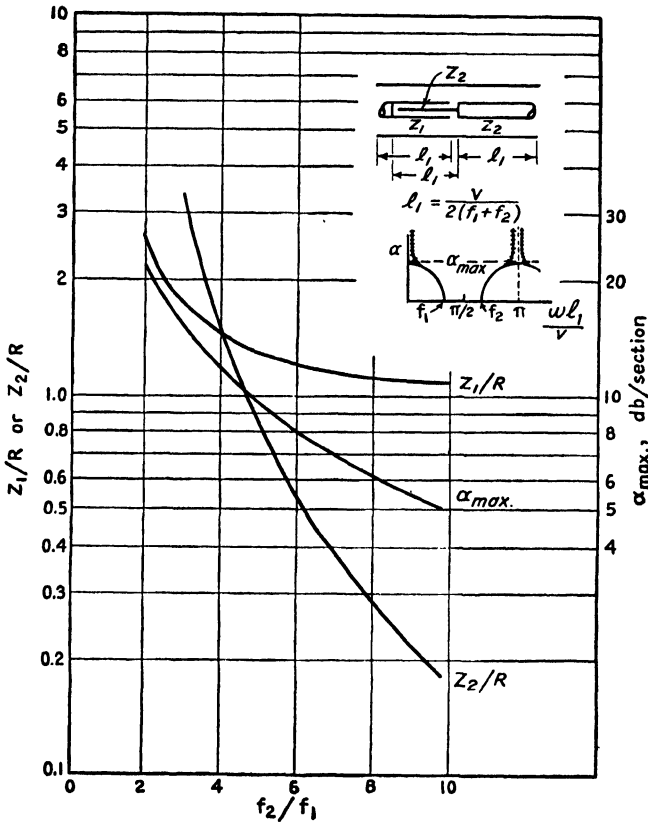


FIG. 27-18.—Design data for the type 3-4 filter.

**27-13. Type 3-4, Band-pass and High-pass Filter.**—Filter 3-4 is characterized by equally sharp cutoff at each end of the pass band. This type may be used, therefore, as a band-pass filter wherever the repeating higher pass bands will either cause no interference or will be eliminated in some other manner. The design data of Table 27-3 and Fig. 27-18 show that the practical range of  $f_2/f_1$  is from about 3 to 10. This filter type also makes an excellent high-pass filter. An infinite insertion-loss point occurs at zero frequency and at the center of each higher stop band.

**27-14. Type 3-5, Low-pass Filter.**—Filter 3-5 is a low-pass filter that provides an infinite insertion-loss at a frequency within the stop band, as indicated in Table 27-3. Multiple-section filters using this type of section can be constructed quite easily. By making  $l_1$  as small as possible compared with a wavelength, the spurious pass bands can be raised considerably in frequency, as with filter 1-1. The spurious pass bands of filter 3-5 are, however, all equal to  $2f_1$  in width, while for filter 1-1, they are generally less than half of  $f_1$ .

Filter 3-5 might in some instances be useful as a rejection filter. In this case,  $l_1$  would be made  $\frac{1}{4}$  wavelength at the frequency to be rejected and  $f_1$  would be made as nearly equal to this frequency as is practicable.

**27-15. Type 3-6 “M-derived” Band-pass Filter.**—The type of response obtained with filter 3-6 is shown in Table 27-3. This filter is similar to an  $m$ -derived lumped-constant structure in that it has two

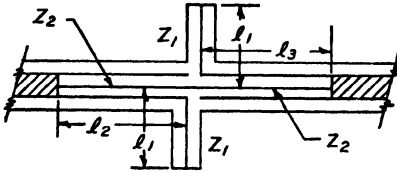


FIG. 27-19.—The type 3-6 band-pass filter.

“infinite” attenuation peaks near the edges of the pass band, and as these peaks are moved nearer the cutoff points, the attenuation far off the band drops lower. It is possible, however, to specify only three of the four key frequencies  $f_1, f_2, f_{1\infty}, f_{2\infty}$ . The image-impedance function

in the pass band has not been studied for filter 3-6, and consequently it is not known at present whether this filter also exhibits the flat image-impedance characteristic of the true  $m$ -derived section. A detailed sketch of this filter is shown in Fig. 27-19.

Since the design procedure for this filter is more complicated than for the others, it will be described in detail. The transfer constant  $\Theta$ , which will be used as a check, is given by the relation

$$\cosh \Theta = 1 + 2\rho \frac{1 + \cos 2\theta_1}{\cos 2\theta_1 + \cos 2a\theta_1} \quad (= -1 \text{ for cutoff frequencies}) \tag{27-3}$$

where

$$\rho = \frac{Z_2}{Z_1} \tag{27-4}$$

$$a = \frac{l_2 - l_3}{2l_1} = \frac{f_{2\infty} - f_{1\infty}}{f_{2\infty} + f_{1\infty}} < 1 \tag{27-5}$$

The design equations (exact) are found to be

$$l_2 = \frac{v}{4f_{1\infty}} = \frac{\lambda_{1\infty}}{4} \tag{27-6}$$

$$l_3 = \frac{v}{4f_{2\infty}} = \frac{\lambda_{2\infty}}{4} \tag{27-7}$$

$$l_1 = \frac{1}{2}(l_2 + l_3) \quad (27-8)$$

$$-\frac{1}{\rho} = \frac{1 + \cos 2\theta_{10}}{\cos 2\theta_{10} + \cos 2a\theta_{10}} \quad (27-9)$$

where

$$v = 3(10)^{10} / \sqrt{\epsilon} \text{ cm per sec}$$

$$\theta_{10} = \omega_0 l_1 / v$$

$\omega_0 = a$  a desired angular cutoff frequency (upper or lower)

$a$  is given in Eq. (27-5)

Cosh  $\Theta$  should then be checked by Eq. (27-3) to see that it is between  $-1$  and  $+1$  near the other desired cutoff frequency. If not, the other cutoff frequency should be used in Eq. (27-9). Finally

$$Z_1 = R \frac{\sqrt{1 - \cos \pi a}}{2\rho}; \quad Z_2 = \rho Z_1 \quad (27-10)$$

If it is desired to specify the two cutoff frequencies, and one infinite attenuation frequency, say  $f_{1\infty}$ , then  $l_2$  is found by Eq. (27-6). If  $\omega_1$  and  $\omega_2$  are the angular cutoff frequencies,  $l_1$  is found by solving the equation

$$\left( \frac{\cos \frac{\omega_1 l_1}{v}}{\cos \frac{\omega_2 l_1}{v}} \right)^2 = \frac{\cos \frac{\omega_1 l_2}{v} \cos \left( \frac{2\omega_1 l_1}{v} - \frac{\omega_1 l_2}{v} \right)}{\cos \frac{\omega_2 l_2}{v} \cos \left( \frac{2\omega_2 l_1}{v} - \frac{\omega_2 l_2}{v} \right)} \quad (27-11)$$

The root of Eq. (27-11) will generally be extremely close to the value

$$l_1 \approx \frac{\lambda_1 + \lambda_2}{8} = \frac{v}{8} \left( \frac{1}{f_1} + \frac{1}{f_2} \right) \quad (27-12)$$

The remaining components are found by Eqs. (27-7) to (27-10).

In practice it is best to set the stubs back about  $\frac{1}{8}$  wavelength (at center frequency) from the center gap in order to avoid distributed capacitances that tend to detune the series sections.

**27-16. The Filters of Tables 27-4 and 27-5.**—Tables 27-4 and 27-5 give design equations for a number of additional types of filter section. Since less experience has been obtained with these than with the ones previously described, they will not be given much space. This does not mean, however, that the filters of Tables 27-4 and 27-5 are necessarily less useful than other types. It should be noted from the tables that these additional filters offer a considerable variety of insertion-loss curves, many of them having infinite-rejection points. Specific design problems where such characteristics are required are often encountered.

TABLE 27-4		RESONANT-LINE FILTER SECTIONS					$v = 3(10)^{10} \sqrt{\epsilon}$ cm/sec, $\omega = 2\pi f$
Filter	Type of Attenuation $\frac{1}{\omega} \text{ vs } \frac{\omega}{V}$ -----Ins. Loss	$\cosh \left( \frac{\alpha}{2} \right)$ $\frac{\alpha}{2}$	$\ell_1$	$Z_1$	$Z_2$	Others	Remarks
4-1			$\sec \frac{\pi f}{f_1 + f_2}$	$R$	$\frac{R}{\sec \left( \frac{\pi f}{f_1 + f_2} \right) - 1}$		1. Pass band on odd harmonics 2. $\alpha_1$ occurs for $\omega \ell_1 / v = n\pi$ ( $n = 0, 1, 2, 3, \dots$ )
4-2			$1 + \frac{\theta}{\pi^2 \left( \frac{f_2}{f_1} - 1 \right)}$ $\frac{v/4f_1}{\lambda_1/4}$ or $\lambda_1/4$	$Z_2 \frac{\pi^2}{\theta} \left( \frac{f_2}{f_1} - 1 \right)$	$R \sqrt{1 + \frac{1}{\theta_{1m}^2}}$	$\ell_2 = \frac{\theta_{1m} v}{\pi \left( \frac{f_1}{f_2} + 1 \right)}$	1. Narrow pass bands on odd harmonics 2. $f_1/f_2 \approx .685$ 3. $\theta_{1m} \leq \frac{1}{2}$ , otherwise arbitrary
4-3			$1 - \frac{2\omega \ell_1}{v \tan \frac{\omega \ell_1}{v}}$ $\frac{\lambda_2}{2} = \frac{\lambda_{1,00}}{4}$ or $\frac{v}{2f_2} = 4f_{1,00}$	$-R \frac{\tan \omega_1 \ell_1}{v}$			1. Pass bands on odd harmonics 2. $\alpha_1$ occurs for $\omega = 0$ 3. $f_2 = 2f_{1,00}$
4-4			$1 + 2 \cot^2 \left( \frac{\omega \ell_1}{v} \right)$ If $f_m$ is unimportant make $\ell_1$ as small as possible	$\frac{R}{\sin^2 \left( \frac{\omega_1 \ell_1}{v} \right)}$	$\frac{R}{2 \cos^2 \left( \frac{\omega_1 \ell_1}{v} \right)}$		1. Pass bands at $\omega \ell_1 / v = n\pi$ 2. $\alpha_1$ occurs for $\omega \ell_1 / v = (2K+1)\pi/2$ ( $K = 0, 1, 2, 3, \dots$ )

TABLE 27-5  
RESONANT-LINE FILTER SECTIONS

		v = 3(10 <sup>10</sup> )/λ√ε cm/sec					Remarks
Filter	Q vs ω/V ----- Ins. Loss +++++ Loss	cosh $\frac{Q(\omega)}{886}$	ℓ <sub>1</sub>	Z <sub>1</sub>	Z <sub>2</sub>	Others	
5-1 		1 + 2ρ	$\frac{v}{2(f_1 + f_2)}$ or $\frac{\lambda_1 \lambda_2}{2(\lambda_1 + \lambda_2)}$	$\rho Z_2$	$\frac{R}{\sqrt{1+2\rho}}$	$2/\rho = \sec(\pi \frac{f_2 - f_1}{f_2 + f_1}) - 1$ or $\sec(\pi \frac{\lambda_1 - \lambda_2}{\lambda_1 + \lambda_2}) - 1$	1. Pass band on odd harmonics 2. α <sub>1</sub> occurs at ωℓ <sub>1</sub> /v = nπ 3. Z <sub>1</sub> = R at cos β = 0
5-2 		α <sub>1</sub> = 15.3 db/sctn.	$\lambda_1/4 - 217 \ell_2 - Z_1 C_2 v$ (ℓ <sub>0</sub> < 0.5 ℓ <sub>1</sub> )	$\frac{R}{2 \cdot 31}$	To obtain eff. ε = 4 with proper Z <sub>1</sub> use laminated structure $\log_{10} \frac{b}{a} = \frac{R}{160}$ $\log_{10} \frac{a}{b} = \frac{R}{160}$ $(\frac{1}{4} - \frac{\epsilon_1}{\epsilon_2}) \frac{R}{(\epsilon_1 - \epsilon_2) 160}$		1. C <sub>0</sub> will usually be small and may be estimated 2. Make ℓ <sub>0</sub> as small as possible, consistent with low stray capacitance
5-3 		α = 15.3 db/sctn.	$\frac{v}{4f_1} = \frac{\lambda_1}{4}$	2 · 31 R			3. Spurious pass bands from 3f <sub>1</sub> to 5f <sub>1</sub> , from 7f <sub>1</sub> to 9f <sub>1</sub> , etc

**27-17. Mechanical Construction.**—Changes in characteristic impedance in a line are accomplished by changing the diameter of the inner or outer conductor (Fig. 27-20), the dielectric constant in the line, or both, as indicated by Eq. (26-25).

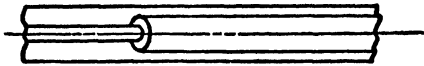


FIG. 27-20.—Junction between a high- and a low-impedance coaxial line.

The maximum practical coaxial characteristic impedance obtainable is about 230 ohms, with a ratio of outer to inner conductor diameter of about 50. The minimum practical impedance is about 2 ohms with

polystyrene dielectric and a ratio of outer to inner conductor diameter of about 1.05. Figure 27-21 shows how a shunt line is connected to the main line. Figure 27-22 shows how a line may be added in series with the outer conductor, and Fig. 27-23 with the inner conductor.

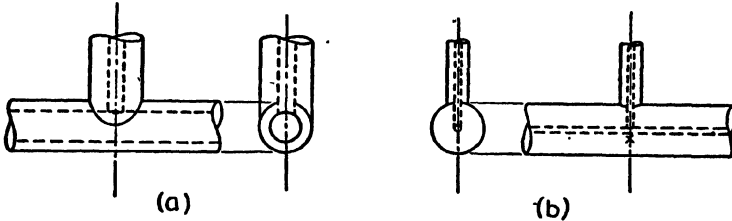


FIG. 27-21.—Shunt connection of one line to another.



FIG. 27-22.—A short-circuited line in series with the outer conductor of a coaxial line.

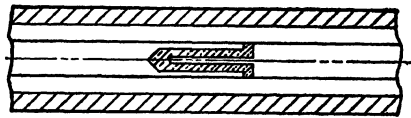
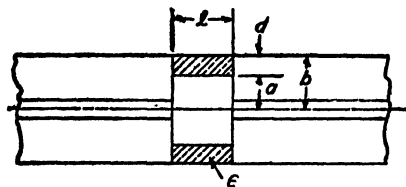


FIG. 27-23.—An open line in series with the inner conductor of a coaxial line.

Figure 27-24 shows the structure of a shunt capacitance. Such a capacitance is in reality a short length of very low-impedance line. In order that this construction may simulate a lumped capacitance, the length of the line should be less (preferably much less) than  $\frac{1}{8}$  wavelength at the highest important operating frequency. Figure 27-25 shows several ways in which series capacitances may be built into the end of a short-circuited line. Figure



$$\text{for } l \ll \frac{\lambda}{4}, C = \frac{0.555\epsilon}{\log_e \left(\frac{b}{a}\right)} l \mu\text{mf}$$

or,

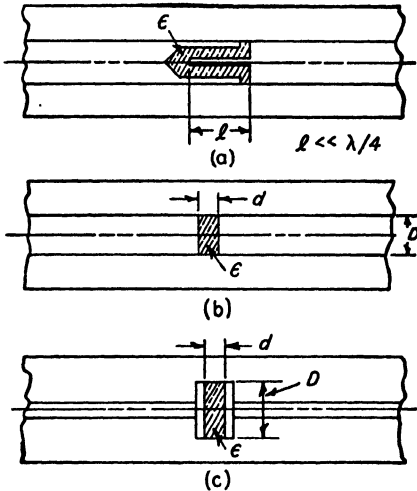
$$l = \frac{C \mu\text{mf}}{1.41\epsilon \left(\frac{b}{a} - \frac{1}{2} + \dots\right)} \text{ inches}$$

(less than 1% error for  $\frac{b}{a} > 4$ )

FIG. 27-24.—A shunt capacitance in a coaxial line. The capacitance formula neglects the discontinuity capacitance.

series capacitances may be constructed, and Fig. 27-26 shows how a series capacitance may be built into the end of a short-circuited line. Figure

27-27 shows the manner in which small ceramic capacitors may be used as shunt and series capacitances at low frequencies. The thin conducting disk reduces the inductance of the capacitor leads. This sort of construction has been used successfully up to 300 Mc in the type 2-1a filter (Table 27-2).



$$D = \sqrt{\frac{Cd}{0.176\epsilon}}, \quad d = \frac{0.176\epsilon D^2}{C}$$

FIG. 27-25.—A series capacitance in a coaxial line. The formula applies to (b) and (c). The discontinuity capacitance around the edges of the faces is neglected. *D* = diameter, inches; *C* = capacitance, μmf; *d* = separation, inches; ε = dielectric constant.

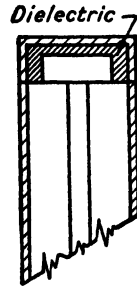


FIG. 27-26.—A capacitive termination for a coaxial line.

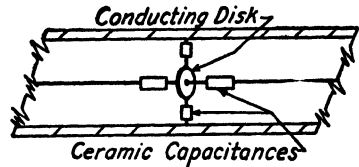


FIG. 27-27.—A coaxial structure having series and shunt ceramic capacitances. This type of construction can be used below about 300 Mc.

**27-18. Dielectric Materials.**—Dielectric material is used in filters in order to provide high capacitances or low characteristic impedances, and in order to provide mechanical support for various physical parts. The requirements for dielectric material in r-f filters are low loss, ease of fabrication, and adequate strength. In addition, its properties should not be affected by humidity or temperature variation. Dielectric materials that have been found useful are polystyrene (ε = 2.5), co-polymerstyrene (ε = 2.5), Dilectene No. 100 (ε = 3.4), Teflon, also known as poly F-1114 (ε = 2.1), and titanium dioxide (ε may be made almost any value up to about 100).<sup>1</sup>

**27-19. Effect of Physical Discontinuities.**—The field disturbances at the junction between various transmission-line-filter elements are gener-

<sup>1</sup> The dielectric constants given for these materials may vary somewhat with the manufacturer, with frequency, etc. Where extreme accuracy is required, the manufacturer's data should be consulted.



ally so complicated that it is usually necessary to neglect them in order to obtain any usable filter design solution at all.

One common type of discontinuity that has been analyzed exactly is that which occurs when lines of different impedance are butted together, as in Fig. 27-20. Such construction results in a *lumped capacitance* effectively in shunt at the point of the discontinuity. The magnitude

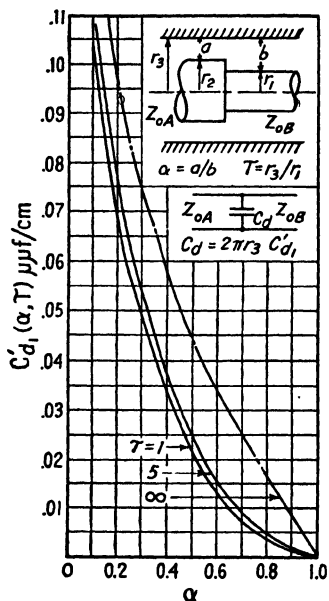


FIG. 27-28.—Discontinuity capacitance curves at a change in diameter of the inner conductor in a coaxial line. For  $\tau$  up to at least 20, use  $\tau = 5$  curve. Analysis has shown the error to be negligible. [By permission, from article by J. R. Whinnery, H. W. Jamieson, and T. E. Robbins, *Proc. I.R.E.*, **32**, 695 (1944).]

such as those of Fig. 27-21 this rule can be quite inaccurate, and a certain amount of intuitive judgment must be exercised.

It goes without saying that, in designing the structure of filters, sharp points, edges, undesired proximities, and other discontinuities must be avoided as much as possible, except where they are taken into account, as by Fig. 27-28.

<sup>1</sup> Figure 27-28 is taken from a paper by J. R. Whinnery, H. W. Jamieson, and T. E. Robbins, *Coaxial-line Discontinuities*, *Proc. I.R.E.*, **32**, 695 (1944). Reference should also be made to N. Marcuvitz, "Waveguide Handbook," Vol. 10, Radiation Laboratory Series McGraw-Hill Book Company, Inc., New York (in press), which will cover this and many other types of discontinuities.

of this discontinuity capacitance is given by Fig. 27-28.<sup>1</sup> Other curves in the paper from which Fig. 27-28 was taken give the effective discontinuity capacitance for changes in outer conductor diameter and a few additional cases.

A common construction having considerably discontinuity effect is a shunt line, or stub, on a coaxial line. The question arises as to just how the electrical length of the shunt line should be measured. The part of the shunt-line center conductor extending into the main line has, certainly, a greater inductance per unit length than the remainder. Thus, the equivalent length of the shunt line is somewhat greater than that of its center conductor. How much greater it is depends obviously on the type of configuration. In Fig. 27-21a, the effective length is probably very nearly that of the center conductor. In Fig. 27-21b, however, the effective length should probably be measured from the neighborhood of the point marked X. A fairly general rule of thumb is to measure from the center of the central conductor of the main line, but in extreme cases

It may sometimes be impossible to build a filter so that the sections can be joined directly together (*e.g.*, type 1-2). In such cases the sections must be joined by short lengths of line, the characteristic impedance of which may be made equal to the filter load resistance. These lengths will, however, have a greater effect than might at first be imagined, and every effort should be made to keep them as short as possible—certainly less than  $\lambda/8$  throughout the pass band. If electrical requirements are stringent or if a large number of sections is to be used, the filter should be reanalyzed and the design equations altered to take account of the effects of the added line sections.

**27-20. Specific Design.**—Permissible mechanical tolerances to be allowed depend on the allowable electrical tolerance. In general, how-

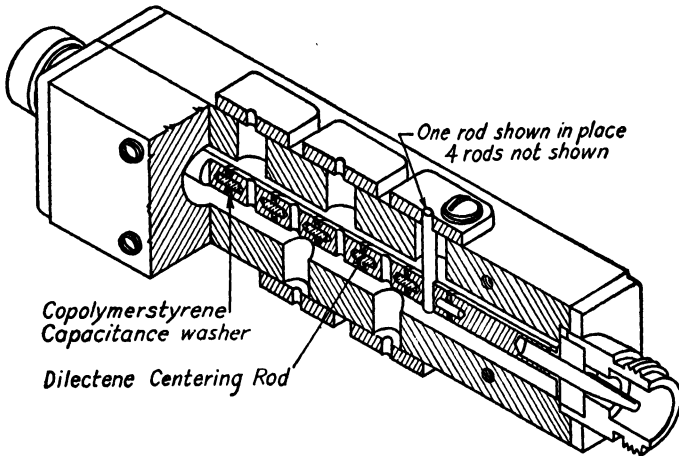


FIG. 27-29.—An example of split-block construction. A five-section high-pass filter of type 1-2. The measured response of this filter is given in Fig. 27-9b.

ever, even when close frequency tolerances are not needed, the usual requirement of low insertion loss in the pass band calls for rather tight mechanical tolerances (of the order of 1 to 5 per cent). A tolerance of  $\pm 0.0005$  in. is about the ultimate that can be specified without requiring special tools or hand-finishing.

One general type of construction that has met with considerable success is the "split-block" type. In this method, the filter as a whole is split in such a way that one-half of the outer conductor is formed by a half-round groove in each block, as shown in Figs. 27-29 and 27-30. The internal assembly can therefore be made "in the open." The assembly is completed by bolting the blocks together. The grooves in the blocks can be roughed out with a half-round milling cutter and then worked up to size by preassembling the blocks and reaming. In many cases it may be

found advisable to split dielectric fillers in the same way, as shown in Fig. 27-30.

The input and output connectors must be attached to the filter with great care, so that discontinuities are eliminated or minimized if possible. Solder fillets and possible residues of soldering flux must be avoided. If practical, construction should be such as to avoid any possible misalignment. Center conductors of small-diameter wire are particularly prone to bend and stretch. Very often, pressure of the screws holding the split blocks together may crumble dielectric pieces unless tolerances are watched closely. Whenever positioning of the parts depends on press fits, drawings should be annotated to indicate the importance of a proper fit and correct assembly. If metal cylinders must be pressed into dielec-

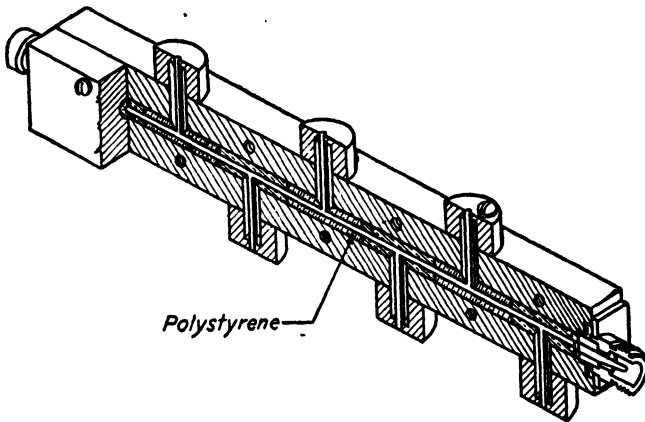


FIG. 27-30.—A split-block filter with split-dielectric fillers. This is a seven-section filter of type 3-2. The measured response of this filter is given in Fig. 27-15.

tric pieces, they may gather chips off the walls. If these can cause any trouble, the machinist should be warned about them. It goes without saying that no metal filings or dust, however fine, should be left in the assembly.

Brass and duralumin have proved to be satisfactory conducting materials. Silver plating of metal parts is, of course, to be recommended but is often not necessary. In some structures, moreover, it is difficult to remove the plating fluid completely. In such structures, it is wise to forego plating. *Wide-band* filters made with unplated brass have been found to measure up in every respect to their silver-plated counterparts.

Finally, certain constructions may require drilling a long, accurate hole in a piece of dielectric. Inasmuch as most dielectrics are difficult to machine (they either melt easily or crumble readily), it is best to cut such a piece into several smaller pieces and specify accurate butt joints at the junctions. These joints should occur, when possible, in the middle of

a line section so that there will be no chance of adding further discontinuity effects at a junction already heavily encumbered by them.

**27-21. The Design of Simple Broad-band Waveguide-to-coaxial Junctions for Use with Waveguide Filters and Transmission Systems.**—A few specific types of waveguide-to-coaxial junctions will be described in the following sections.<sup>1</sup> In all these the coaxial outer conductor will terminate on the top surface of the waveguide, and the center conductor on the lower. Only physical configurations that lead to a simple equivalent circuit will be considered. For a discussion of waveguide as a circuit element, see Sec. 26-15.

**27-22. The Basic Junction.**—Figure 27-31 shows the simplest junction of the type considered in this section. At the center frequency, the

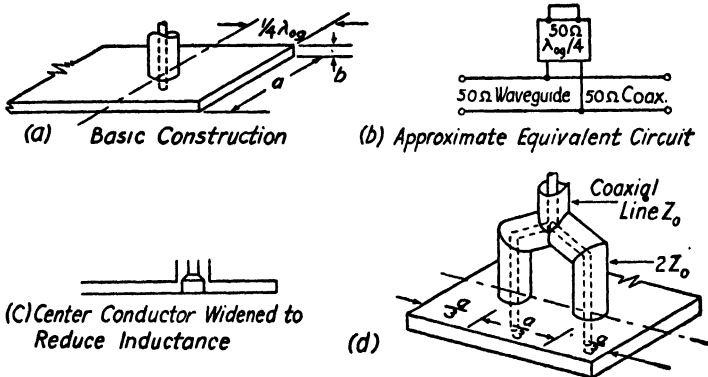


FIG. 27-31.—Simple matched junction: (a) basic construction; (b) approximate equivalent circuit; (c) center conductor widened to reduce inductance; (d) balanced coaxial connection.

waveguide characteristic impedance should be equal to the coaxial-line impedance, and the waveguide short-circuiting block should be a quarter of a guide wavelength ( $\lambda_g/4$ ) from the point of junction. For example, for 50-ohm coaxial line, the waveguide must have a 50-ohm characteristic impedance at the center ( $f_0$ ) of the frequency band. Equation (26-62) shows that the ratio of guide width to height  $a/b$  will be about 16:1, depending upon the ratio  $f_0/f_c$ .

The approximate equivalent circuit is shown in Fig. 27-31b. A more exact circuit would show an inductance in series with the coaxial line at the point of junction. This is the inductance of the short length of coaxial-line center conductor inside the guide. If its diameter is small compared with the width of the guide, its inductive reactance will cause considerable mismatch, despite the fact that it is extremely short in the 50-ohm guide. An idea of the magnitude of this reactance may be

<sup>1</sup>CONN, S. B., Design of Simple Waveguide-to-coaxial-line Junctions, accepted for publication in *Proc. I.R.E.*

obtained from the analysis of a cylindrical post contacting the top and bottom of a waveguide.<sup>1</sup> The waveguide-to-coaxial-line coupling differs mainly in that a 50-ohm load resistance must be considered in series with the post. A cylindrical post can be shown to be equivalent to a T-network consisting of a shunt inductance and series capacitances, all of whose reactances are much less than 50 ohms if the post diameter has an optimum value of about 0.15 times the width  $a$  of the waveguide. In all wide-band junctions of this type, therefore, the center conductor should

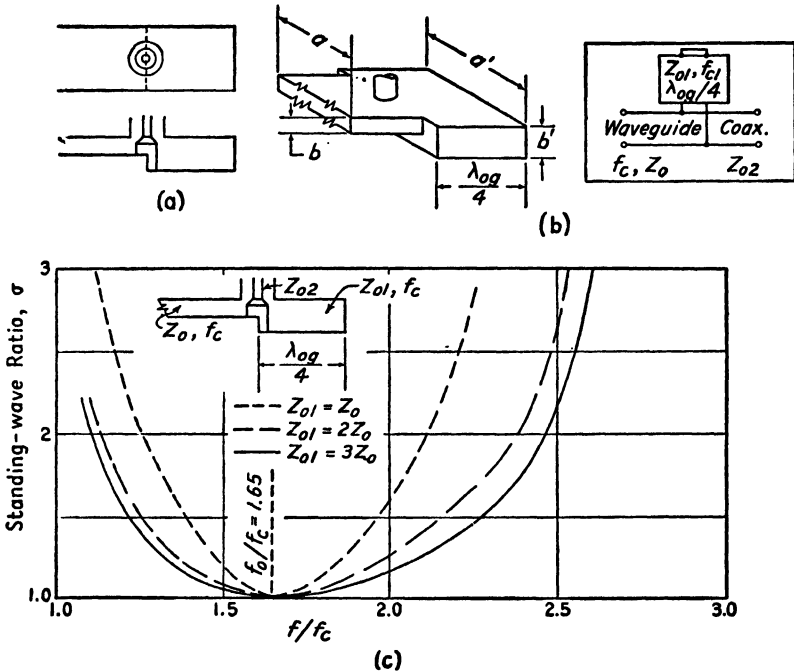


FIG. 27-32.—Generalized matched junction: (a) construction with high-impedance end-section; (b) construction with high-impedance and low cutoff-frequency end section; (c) calculated response for junction of (a).

be about 0.15 $a$  inside the guide. A practical compromise construction is shown in Fig. 27-31c.

The circuit shows this junction to be equivalent to a continuous length of 50-ohm transmission line with a short-circuited length of 50-ohm line shunted across it. So long as the shunt line has a reactance large compared with 50 ohms, the voltage standing-wave ratio  $\sigma$  of the junction will be low. The voltage standing-wave ratio is also affected by the fact that the waveguide characteristic impedance can be 50 ohms at only one frequency. This effect is most detrimental at the low-frequency end of

<sup>1</sup> MARCUVITZ, N., "Waveguide Handbook," Vol. 10, Radiation Laboratory Series, McGraw-Hill Book Company, Inc., New York (in press).

the band, and complete mismatch results at the guide cutoff frequency, for which the characteristic impedance is infinite.

By increasing the characteristic impedance of the short-circuited shunt line, its reactance may be kept high compared with 50 ohms over a wider band (Fig. 27-32a). The most generalized design of the basic junction is shown in Fig. 27-32b.

In calculating the standing-wave-ratio characteristic of these junctions, the equivalent circuits are solved by transmission-line formulas and charts. At each frequency, the proper guide wavelength and characteristic impedance given by Eqs. (26-62) and (26-63) must be used. The values of  $\sigma$  may be read directly from many types of transmission-line charts once the input impedance of the junction has been computed.

Figure 27-32c shows the calculated curve of  $\sigma$  as a function of  $f/f_c$  for the junction of Fig. 27-32a for several values of characteristic impedance of the short-circuited shunt waveguide. Even for  $Z_{01}$  equal to  $Z_0 = 50$  ohms, the band width is 1.65 to 1 for a 2:1 voltage standing-wave ratio. For  $Z_{01} = 3Z_0 = 150$  ohms, the band width is 2.2 to 1.

These thin waveguide junctions are particularly useful for waveguide filters requiring coaxial terminations, since such filters can, and often must, be constructed with thin waveguide.

The junctions described in this section will not excite the  $TE_{2,0}$  mode, since the coaxial line connects to a point of zero electric field for that mode. Except for the junction described in the next paragraph, those described in this chapter are generally not usable at frequencies above the  $TE_{3,0}$  cutoff frequency, which occurs at three times the  $TE_{1,0}$  cutoff in rectangular waveguide. Since the junctions freely set up the  $TE_{3,0}$  mode above its cutoff frequency, both the  $TE_{1,0}$  and  $TE_{3,0}$  modes are present at once in this region. Since the guide wavelength for the two modes is different, especially near the  $TE_{3,0}$  cutoff, the phase relation between the modes will vary with frequency, causing corresponding loss variations.

One type of junction for rectangular waveguide that will theoretically not excite the  $TE_{3,0}$  mode is shown in Fig. 27-31d. The coaxial line (assumed to be 50-ohm) is split into two 100-ohm lines, which join the waveguide one-third of the distance in from each side. This is a point of zero electric field for the  $TE_{3,0}$  mode, and consequently this mode should not be set up. Since the two junction points are driven in phase, the  $TE_{2,0}$  and  $TE_{4,0}$  modes should not be set up either. A good match into the  $TE_{1,0}$  mode is at the same time easily obtainable. This design requires very accurate locating of the junction points and careful design of the coaxial Y-connection in order to reduce discontinuity effects. Although this junction will theoretically not set up the  $TE_{2,0}$ ,  $TE_{3,0}$ , and  $TE_{4,0}$  modes, discontinuities in a waveguide line such as twists and

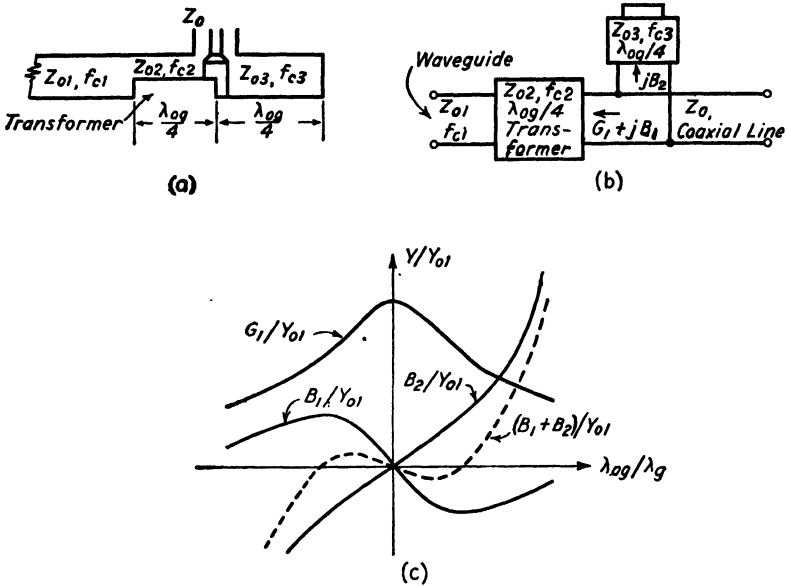


FIG. 27-33.—Transforming type of junction: (a) structure; (b) approximate equivalent circuit; (c) admittance curves for  $f_{c1} = f_{c2} = f_{c3}$ .

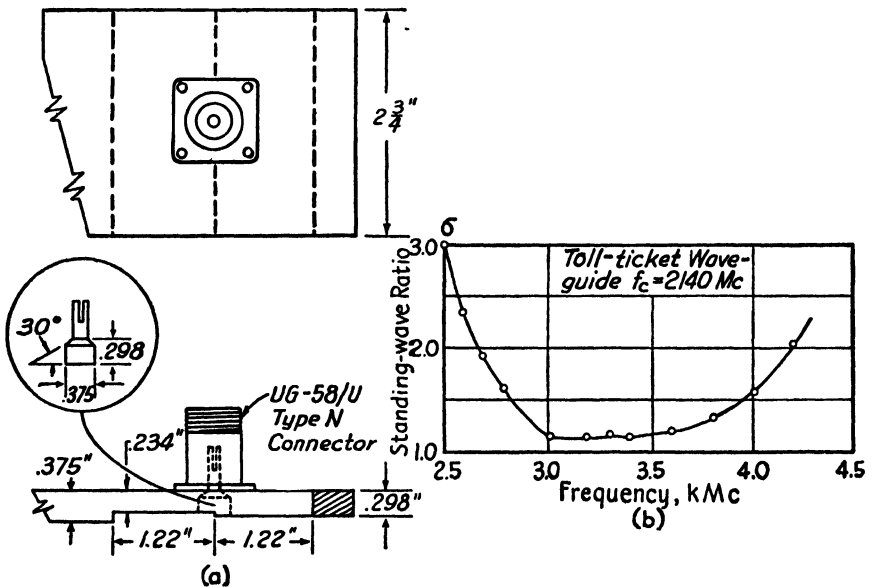


FIG. 27-34.—Transforming junction matched at center frequency of 3200 Mc: (a) construction; (b) frequency response.

bends can do so, with consequent irregularities in the over-all transmission loss. Whether or not these modes will be set up to a serious degree has not yet been fully investigated.

**27-23. The Transforming Junction.**—The junctions of Figs. 27-31 and 27-32 can be used with guide having a higher characteristic impedance than the coaxial line only if a sufficiently long taper, either in the guide or the coaxial line, is used to transform the coaxial-line impedance to the guide impedance. An exponential taper about one guide wave-

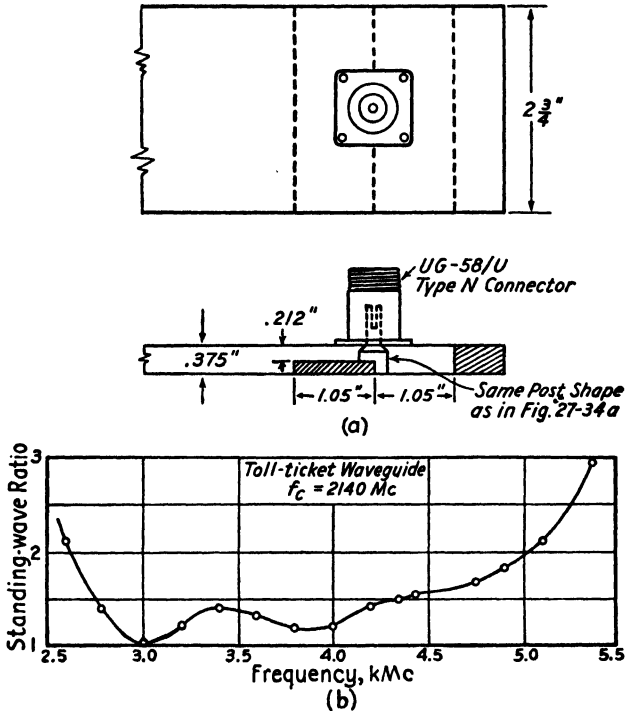


FIG. 27-35.—Transforming junction designed to have  $\sigma = 1.5$  at center frequency of 3550 Mc: (a) construction; (b) frequency response.

length long at the lowest frequency desired will suffice for many purposes. A particular design of this type will be described in a later section.

For guide impedance not over about three times the coaxial-line impedance, a good broad-band match may be obtained by means of a  $\lambda_{0g}/4$  transformer in the guide (Fig. 27-33a). Besides providing an impedance match at the center frequency, the transforming junction has the advantage that the susceptance introduced by the  $\lambda_{0g}/4$  transformer at frequencies other than the center frequency is of opposite sign from the susceptance of the  $\lambda_{0g}/4$  short-circuited shunt line. By choosing the optimum characteristic impedance ( $Z_{0s}$ ) for the latter element, a



cancellation of susceptance is made possible over a wide band. This is illustrated by Fig. 27-33c. Note that the abscissa is plotted in terms of  $\lambda_{0g}/\lambda_g$ , which in waveguide is not proportional to frequency. The ordinate is in terms of  $Y_{01}$ , which is not constant. ( $Y_{01}$  is the characteristic admittance of the waveguide,  $1/Z_{01}$ .) When actual mismatch values at a particular frequency are desired, points from Fig. 27-33c must be transformed by Eqs. (26-62) and (26-63).

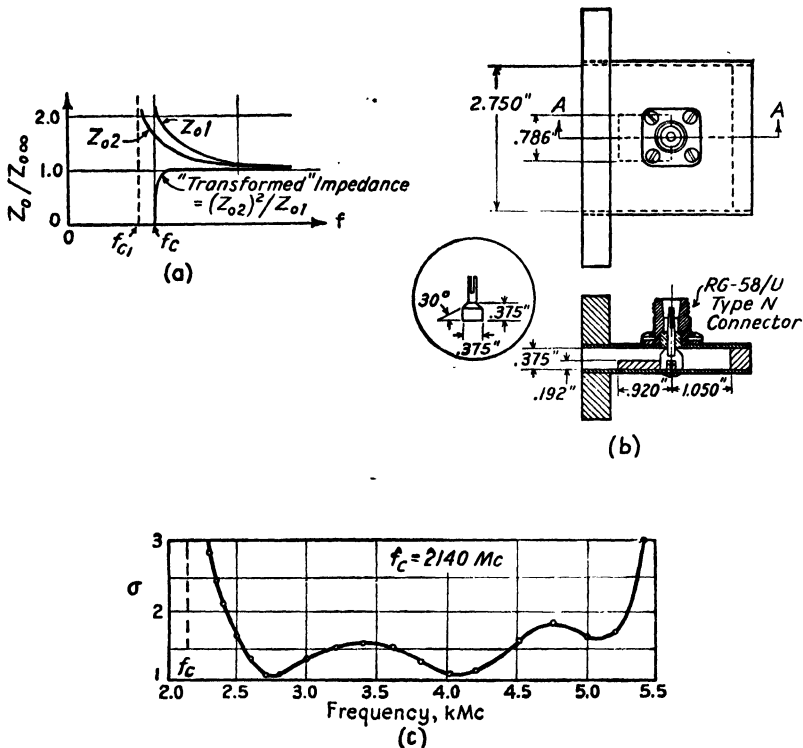


FIG. 27-36.—Ridge-block transforming junction: (a) "transformed" impedance; (b) frequency response.

Figure 27-34a shows the dimensions of a junction designed for a perfect match at a center frequency of 3200 Mc. The measured voltage standing-wave ratio is given in Fig. 27-34b.

By purposely transforming the guide impedance to less than 50 ohms, a wider band width may be obtained. This is illustrated by the junction of Fig. 27-35a and its measured response, Fig. 27-35b. This junction was designed to transform to 33 ohms at a center frequency of 3530 Mc. This value of resistance gives a theoretical midband voltage standing-wave ratio equal to 1.5:1.

In the notation of Fig. 27-33a, the junctions of Figs. 27-34 and

27-35 were designed with  $f_{c1} = f_{c2} = f_{c3}$ . By making  $f_{c2}$  about  $0.8 f_{c1}$  and  $f_{c3} = f_{c1}$ , a large improvement near the guide cutoff is obtained. This is so because the electrical length of the transformer does not become zero at  $f_{c1}$ , and because the *transformed impedance* looking from the point of junction through the transformer toward the properly terminated waveguide is almost constant, except very near  $f_{c1}$ . The transformed impedance is plotted and compared with the characteristic impedances  $Z_{01}$  and  $Z_{02}$  in Fig. 27-36a. Note that the function plotted is not the true input impedance of the transformer, but rather the input impedance

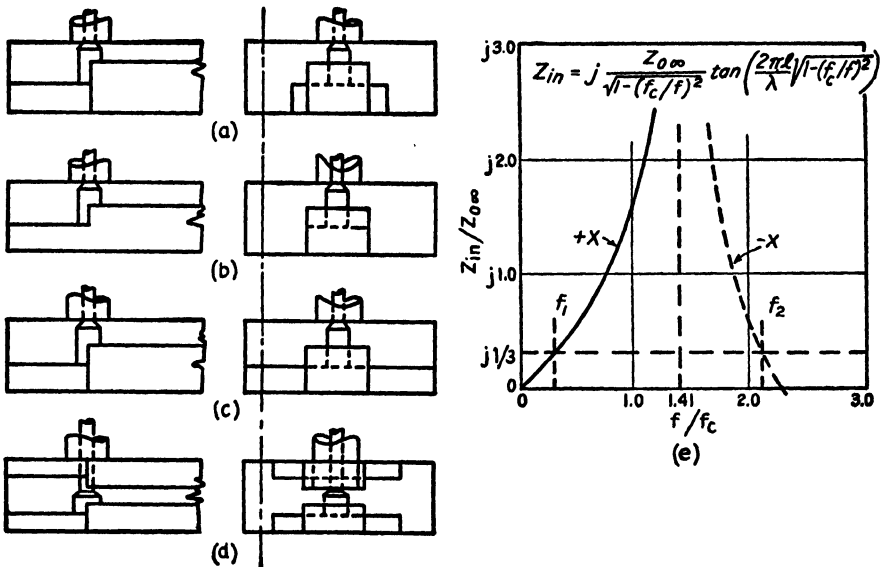


FIG. 27-37.—A waveguide-to-coaxial-line junction for ridge waveguide: (a) generalized structure; (b) and (c) two easily constructed designs; (d) a construction for double-ridge guide; and (e) the input impedance of the short-circuited section of waveguide.

of a hypothetical transformer that is a quarter of a guide wavelength long at all frequencies. The curve does, however, give an idea of the improvement in match made possible by this reduction in  $f_{c2}$ .

The reduction in  $f_{c2}$  may be obtained by widening the transformer portion of the waveguide. A better method is to use a length of *ridge waveguide* (see Sec. 26-16). This type of waveguide has a lower cutoff frequency and a lower characteristic impedance than ordinary rectangular waveguide having the same width and maximum height. The curves in Sec. 26-16 give the impedance and cutoff frequency as functions of the physical parameters, thus making a selection of dimensions to suit a particular problem very simple.

Figure 27-36b shows the dimensions of a ridge-transformer junction between a 2.75- by 0.375-in. guide and 50-ohm cable. The calculated

ridge-guide cutoff frequency is 1620 Mc, and the characteristic impedance at center frequency  $f_0 = 3540$  Mc is 58 ohms. This should give a transformed impedance at  $f_0$  of 33 ohms, corresponding to a calculated 1.5:1 voltage-standing-wave ratio. The measured curve, shown in Fig. 27-36c, is seen to check closely the calculated voltage-standing-wave ratio at  $f_0$ . The improvement in low-frequency response is evident, and the over-all band-width ratio is seen to be  $5300/2400 = 2.2:1$ .

**27-24. A Junction for Ridge Waveguide.**—As mentioned in Sec. 27-22, the higher modes in waveguide can seriously interfere with transmission of the  $TE_{1,0}$  mode. The usable frequency range, which is limited by the higher modes, can be extended by the use of ridge waveguide in place of ordinary rectangular waveguide in the transmission system or waveguide filter. In Sec. 26-16, it is shown that the ratio between the cutoff frequencies of the  $TE_{1,0}$  and  $TE_{2,0}$  modes in ridge waveguide can easily be made as high as about 4:1 or 7:1, or even higher, as compared with the 2:1 ratio for ordinary rectangular waveguide. Between the  $TE_{1,0}$  and  $TE_{3,0}$  cutoffs, the ratio can be about 6:1 or 10:1, as compared with 3:1 for ordinary rectangular waveguide.

The construction of a ridge-waveguide junction is shown in Fig. 27-37. Figure 27-37a shows the generalized structure in which the short-circuited back cavity is of ridge waveguide that may have any shape, characteristic impedance, and cutoff frequency. Figures 27-37b and c show two easily constructed specific designs. In both, the cutoff frequency and characteristic impedance of the back cavity are higher than that of the ridge waveguide fed by the junction. The approximate circuit of Fig. 27-32b applies to this junction and shows that the junction acts as though the equivalent waveguide line of characteristic impedance  $Z_0$  were connected directly to the coaxial line of impedance  $Z_{02}$ , with a reactance  $X$  due to the short-circuited back cavity shunted across the point of junction. The standing-wave-ratio response may be calculated from this circuit.

The junction of Fig. 27-37 differs from the previously described junctions principally in that the cutoff frequency of the back cavity of the former occurs *within* the operating range of the junction. Although the wavelength in waveguide approaches infinity as the frequency is lowered toward cutoff, the waveguide characteristic impedance also approaches infinity, and the result is that the input impedance of the back cavity is greater than zero and is actually finite. The theoretical input impedance may be calculated from Eq. (26-65). This has been done for a short-circuited length of waveguide that is a quarter of a guide wavelength long at 1.414 times the cutoff frequency, and the results are plotted in Fig. 27-37e. If the characteristic impedance of the back-cavity section at infinite frequency is made to be three times the coaxial-

line characteristic impedance, as indicated on this graph, the input reactance is greater than the coaxial-line impedance between  $f_1$  and  $f_2$ , by about a 6-to-1 frequency range. If the cutoff frequency of the ridge waveguide fed by the junction is made to come at  $f_1$ , the junction will work well from almost  $f_1$  to  $f_2$ . Other values for the various parameters involved might give a still greater band width. This design may be used with any other form of loaded waveguide as well as with ridge waveguide.

**27-25. Tapered-ridge Junction.**—The most common waveguide shape for signal transmission is a rectangular cross section with about a 2:1 ratio of width to height. A flatter cross section is generally more practical for filter construction, but since a very simple class of broadband junctions for the 2:1 cross section can be designed by the methods given above, they will be discussed in this section.

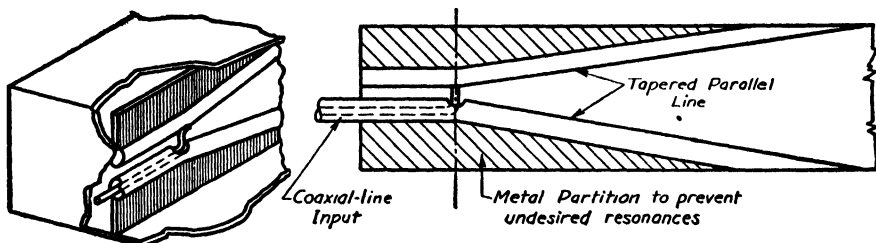


FIG. 27-38.—A junction using a length of tapered "loaded" waveguide as a transition element.

A transforming junction like those in Fig. 27-33 would not give a very great band width for this shape of waveguide, but any of the earlier junctions may be used with a sufficiently long tapered section of waveguide to transform gradually the low impedance at the junction to the high impedance of the 2:1 cross-section waveguide. Loaded waveguide, such as ridge waveguide, is particularly suitable for this taper, since its lowered cutoff frequency causes its impedance and wavelength to remain finite at the cutoff frequency of the main guide. An early form of junction having this general design is shown in Fig. 27-38. The junction consists essentially of a parallel-conductor transmission line tapered from the 50-ohm impedance of the coaxial input line to the waveguide impedance. The coaxial connection to this balanced line is made at a point that is  $\frac{1}{4}$  wavelength from the short-circuited end of the balanced line at some intermediate frequency in the operating range. This junction has a measured voltage-standing-wave ratio varying between 1.3:1 and 2.3:1 over a 2.15:1 frequency range. Impedance measurements showed that the reactance remains close to zero, and that the resistance is high, around 100 ohms at the low-frequency end of the band, and around 60 ohms at the high-frequency end of the band. By

bringing the tubes closer together, the balanced-line impedance at the junction point could be made more nearly equal to 50 ohms, and the standing-wave ratio would be improved over a large part of the frequency range.

Ridge waveguide is especially well suited for such a junction, because it affords simple construction and can be designed so that its  $TE_{3,0}$  cutoff frequency is equal to or greater than that for rectangular waveguide having the same width (see Sec. 26-16).

A junction using tapered-ridge waveguide is shown in Fig. 27-39. It consists of a short length of ridge waveguide tapered from the main guide impedance to 50 ohms at the point of junction with the 50-ohm

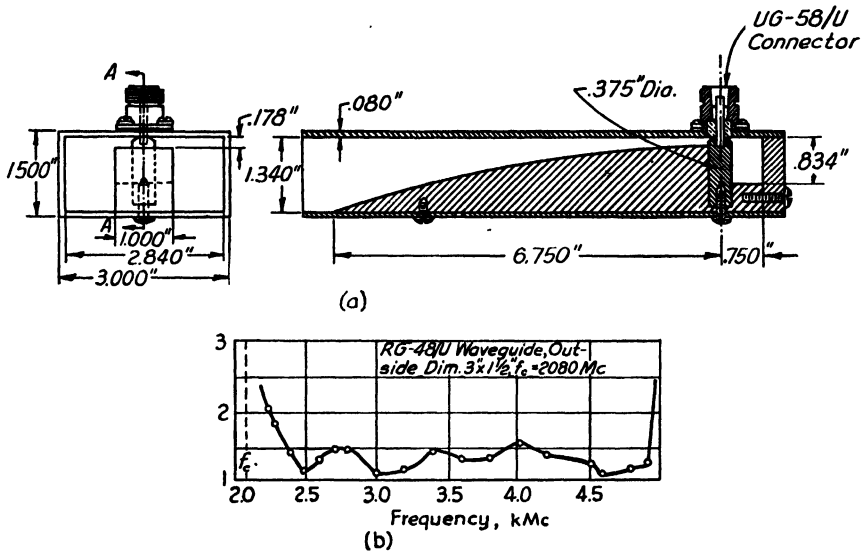


FIG. 27-39.—Tapered-ridge junction: (a) construction of junction; (b) frequency response.

coaxial line. Beyond this point is a length of 150-ohm ridge guide short-circuited at the end. This length is  $\frac{1}{4}$  wavelength long at some point in the operating range. The operation of this junction is similar to that of Fig. 27-32b.

The cross-sectional shape of the ridge for a 50-ohm impedance was taken from the ridge waveguide curves in Sec. 26-16. Experimentally, it was found that these dimensions actually gave an impedance of about 35 ohms, the error being due to the small ratio of width to height of the waveguide, as explained in Sec. 26-16. The dimensions shown in Fig. 27-39a give an impedance of about 50 ohms. They were found experimentally by a brief cut-and-try process. The ridge was given an approximately exponential taper, with the change in guide wavelength along the

ridge taken into account. The frequency response appears in Fig. 27-39b. Figure 27-40 shows the dimensions and response of another junction of the same type scaled down for 1.5- by 0.75-in. waveguide.

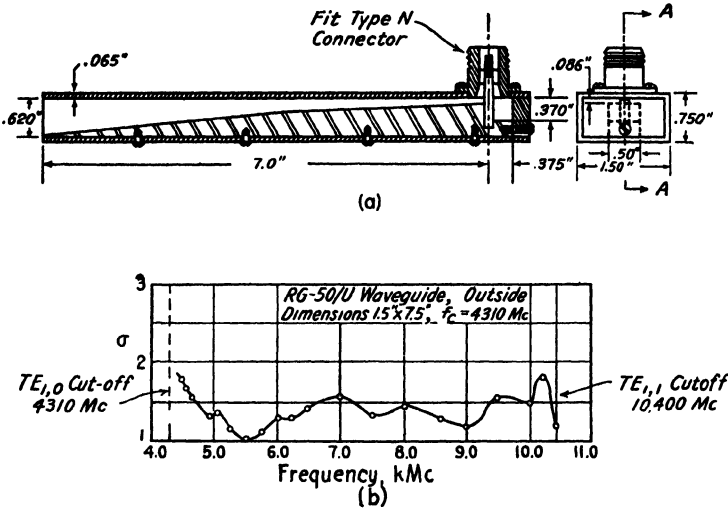


FIG. 27-40.—Tapered-ridge junction: (a) construction of junction; (b) frequency response.

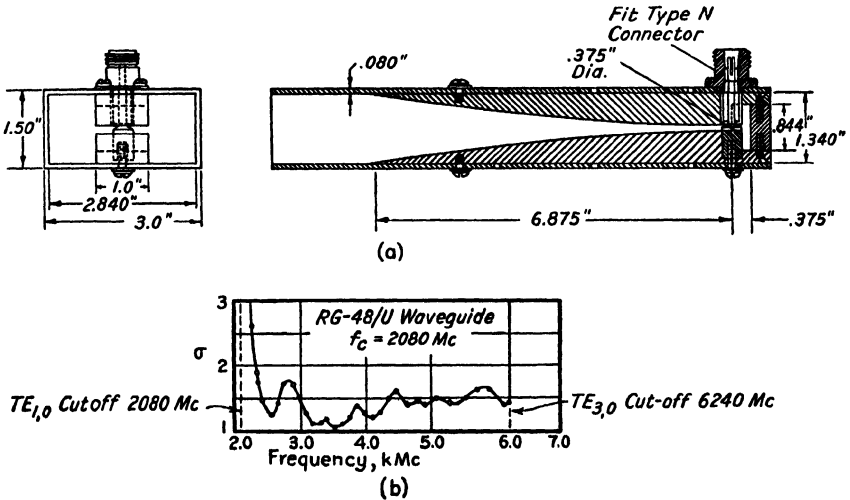


FIG. 27-41.—Double-ridge junction: (a) construction; (b) frequency response.

This second junction works much closer to cutoff than the first because its tapered-ridge section is in proportion twice as long.

The sharp increase in standing-wave ratio at the upper limit in both ridge junctions is due to the  $TE_{1,1}$  and/or  $TM_{1,1}$  modes, the cutoff fre-

quencies of which are, respectively, 4900 Mc in the large guide and 10,400 Mc in the small. With a symmetrical double-ridge taper these modes will not be excited. A thin conducting sheet in the center of the guide perpendicular to the  $\mathcal{E}$  field will also suppress these modes. With such a construction, good performance up to the  $TE_{3,0}$  cutoff frequency (6240 Mc in 3- by 1½-in. waveguide) is possible.

The dimensions of a double-ridge junction are given in Fig. 27-41 along with the measured curve of voltage standing-wave ratio vs. frequency. It is seen that a low standing-wave ratio is obtained from slightly above the  $TE_{1,0}$  cutoff up to the  $TE_{3,0}$  cutoff. The band-width ratio is 2.7:1 for a standing-wave ratio of less than 2:1. If a longer ridge taper were used, a band-width ratio of very nearly 3:1 could be obtained. The 50-ohm double-ridge cross section was obtained directly from the curves in Sec. 26-16, the cut-and-try process being unnecessary in this case, *i.e.*, for  $b_1/a_1 \approx 0.25$ .

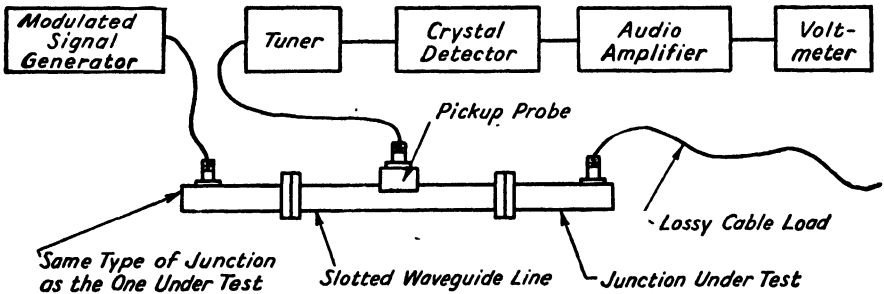


Fig. 27-42.—Setup used for testing waveguide-to-coaxial-line junctions.

**27-26. Method of Testing the Waveguide-to-coaxial-line Junctions.** The test setup is shown in Fig. 27-42. The over-all calibration of crystal detector, amplifier, and voltmeter was carefully checked throughout the test range. Except for Fig. 27-40b, all curves were taken using for a load over 20 db of RG-21A/U lossy cable with a UG-18/U type-N connector. For Fig. 27-40b, a 100-ft length of RG-8/U cable was used with a UG-21 B/U connector. It must be remembered that the connectors have a considerable effect on the over-all standing-wave ratio.

**27-27. Waveguide High-pass Filters.**—As shown in Sec. 26-15, waveguide will freely pass all signals above the waveguide cutoff frequency  $f_c$  and will rapidly attenuate all signals below this frequency. The cutoff frequency is a function of the particular propagation mode and the cross-sectional dimensions of the waveguide. Only the  $TE_{1,0}$  mode will be considered. For rectangular waveguide, the  $TE_{1,0}$  cutoff frequency occurs for  $f = f_c = 3(10)^{10}/\lambda_c = 3(10)^{10}/2a \sqrt{\epsilon}$ , where  $a$  is the guide width in centimeters, and  $\epsilon$  is the dielectric constant. Any of the wide-band junctions of the preceding sections may be used at the ends

of a length of waveguide to provide a high-pass filter with coaxial terminations. The more useful combinations will be described in the present section.

The rate of cutoff in the stop band depends upon the length of the waveguide between the junctions. The attenuation constant for waveguide is given by Eq. (26-66) and is seen to be proportional to the length

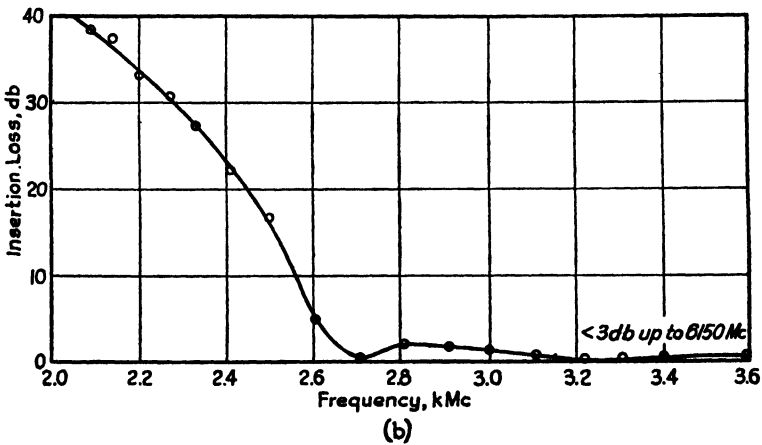
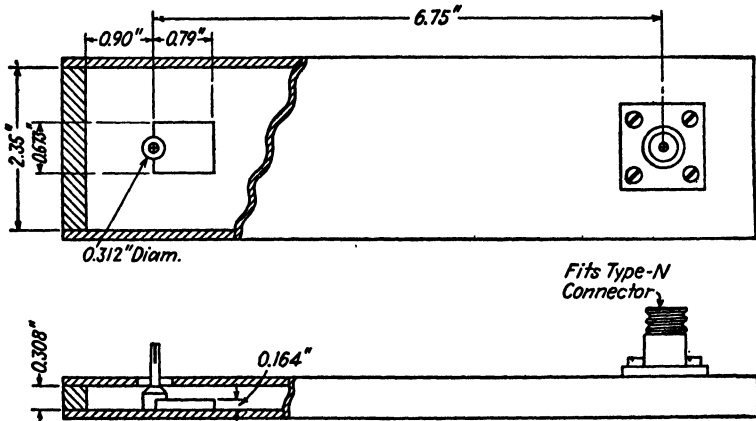


FIG. 27-43.—The construction and measured insertion loss of a waveguide high-pass filter. ( $R = 50$  ohms)

of the guide. The insertion loss of a waveguide filter is somewhat different from the total attenuation constant, because of the effect of the waveguide-to-coaxial-line junctions and the constant terminating resistance of the coaxial line. For instance, the insertion loss at zero frequency is infinite, while the field attenuation is finite. The field-attenuation formula, however, provides a useful guide. The measured



insertion-loss curves that follow furnish an additional guide in the design of a filter that must have a particular sharpness of cutoff.

The junctions of Figs. 27-31, 27-32, 27-33, and 27-36 appear to be the most useful types for waveguide-filter termination. It should be remembered that the junctions and waveguide can be filled with dielectric, if desired, in order to reduce the filter size at low frequencies. The filter may be reduced in size in this manner by approximately the ratio  $1/\sqrt{\epsilon}$ . If a junction and filter have already been designed for  $\epsilon = 1$ , and it is desired to change the design to a dielectric-filled one with the same cutoff

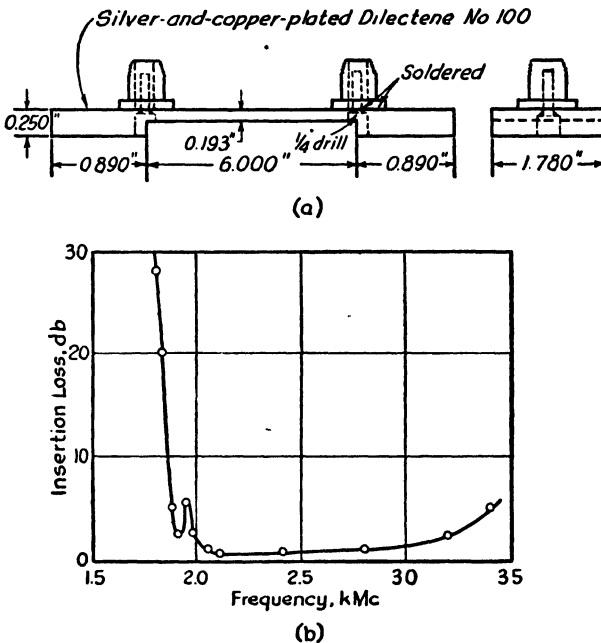


FIG. 27-44.—(a) A dilectene-filled-waveguide high-pass filter; (b) its measured frequency response.

frequency, it will be found (at least to a first approximation) that all width dimensions (in the  $a$  direction) and all length dimensions must be scaled by the factor  $1/\sqrt{\epsilon}$ , while all height dimensions remain unchanged.

Figure 27-43 shows the construction and measured response of a high-pass filter type that has had wide use at the Radio Research Laboratory. This filter uses the junction of Fig. 27-36. Figure 27-44 shows the construction and measured response of an experimental filter having a dielectric filler of Dilectene No. 100 ( $\epsilon = 3.4$ ). The junctions are of the type shown in Fig. 27-32a. The filter consists of a machined slab of Dilectene having a thin deposit of silver on the surface. Over the silver is plated several thousandths of an inch of copper. The type-N

fittings are soldered onto this copper plating. (The plating on the Dilectene between the inner and outer conductor of the type-N connectors is, of course, removed.) This filter would have had considerably better response if the characteristic impedance of the short-circuited end sections had been higher. This would have required a thicker slab of Dilectene, which was not available at the time. A filter having the junctions of Fig. 27-36 could also be easily made out of plated dielectric.

The filters described thus far are usable up to not over three times the waveguide cutoff frequency. At three times the  $TE_{1,0}$ -mode cutoff, the  $TE_{3,0}$  cutoff occurs in rectangular waveguide. Since the junctions set up the  $TE_{3,0}$  mode freely above its cutoff frequency, both the  $TE_{1,0}$  and the  $TE_{3,0}$  modes are present at once in this region. The guide wavelength for the two modes is different, especially near the  $TE_{3,0}$  cutoff, and, consequently, the phase relation between the modes will vary with frequency, causing corresponding loss variations. It is possible, of course, that in a particular filter careful design may make the filter usable somewhat above the  $TE_{3,0}$  cutoff frequency.

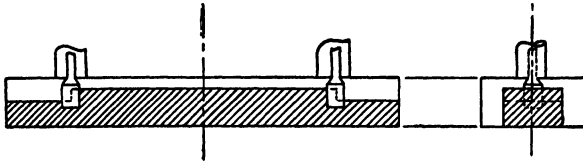


FIG. 27-45.—A ridge-waveguide high-pass filter.

The frequency-range limitation discussed above can be raised considerably through the use of ridge waveguide in place of ordinary rectangular waveguide. A ridge-waveguide high-pass filter design is shown in Fig. 27-45. In Sec. 26-16, it is shown that the ratio between the cutoff frequencies of the  $TE_{1,0}$  and  $TE_{3,0}$  modes can be easily made as high as about 6:1 or 10:1, or even higher, as compared with the 3:1 ratio for ordinary rectangular waveguide. A high-pass filter constructed of ridge waveguide can, therefore, be used over this 6:1 or so range, provided that the coaxial-line-to-waveguide junctions used with it are efficient over this range. An easily constructed junction for ridge waveguide was described in Sec. 27-22 and is shown in Fig. 27-37. The cross-sectional dimensions for a given cutoff frequency may be obtained from the curves in Sec. 26-16.

**27-28. The Varying-impedance Band-pass Waveguide Filter.**—Since waveguide has a natural high-pass cutoff, it is necessary only to combine a length of waveguide with some sort of low-pass structure to make a band-pass filter. This band-pass filter can be used in a waveguide transmission line, or it can be used with a pair of broad-band junctions to provide a band-pass filter with coaxial-line terminations. The simplest

combination would be a waveguide high-pass filter and a coaxial low-pass filter in cascade. Such combinations have been used with success in the microwave range. The low-pass structure can, however, be built directly into the waveguide. Several such types are possible, and the one found most useful thus far will now be discussed.

Section 27-4 describes a type of low-pass filter consisting of alternate lengths of high- and low-impedance transmission line. Although that section considers only coaxial low-pass filters, the theory can be easily applied to waveguide filters. Equation (26-62) shows that the waveguide characteristic impedance  $Z_0$  is easily controlled in two ways: (1) by varying  $\epsilon$ , and (2) by varying  $b/a$ . With everything else held

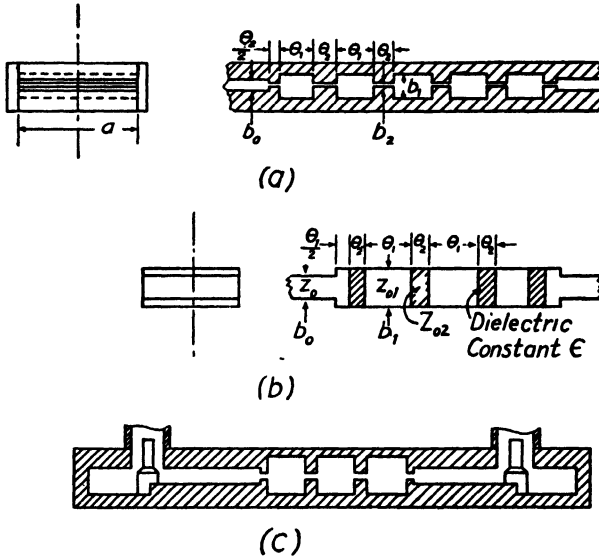


FIG. 27-46.—Two types of varying-impedance low-pass structure for waveguide band-pass filters. The waveguide filter may be combined with a pair of waveguide junctions as shown in (c).

constant  $Z_0$  is proportional to the dimension  $b$ . The dependence of  $Z_0$  upon  $\epsilon$  is more complicated, since the guide wavelength  $\lambda_g$  is also a function of  $\epsilon$ . Figure 27-46a shows a waveguide filter structure in which  $b$  alone is varied, and Fig. 27-46b shows a structure in which  $\epsilon$  alone is varied. Figure 27-46c shows a structure combined with waveguide-to-coaxial-line junctions of the type shown in Fig. 27-32.

In designing the low-pass structure, the design equations and graphs of Sec. 27-4 are used as they stand.  $B_c/Y_{02}$  may be obtained from the curves in Fig. 26-26. It should be remembered that the discontinuity-susceptance curves given by this figure are accurate only if the length of each section of the waveguide line is equal to or greater than the height  $b$  of this particular section. This places a definite restriction on

the permissible maximum height  $b_1$ . This condition will generally be met if the filter is designed for 50-ohm terminations. Once  $\theta_{1c}$ ,  $\bar{\theta}_{2c}$ ,  $Z_{01}$ ,  $Z_{02}$  have been calculated, the physical dimensions of the filter may be calculated from Eqs. (26-62) and (26-63) with  $\theta = 2\pi l/\lambda_0$ .

The image impedance of a waveguide filter measured at the end of the low-pass structure (mid- $\theta_1$  termination) is equal to the product of the waveguide characteristic impedance  $Z_{10}/\sqrt{1 - (f_c/f)^2}$  given in Fig. 26-22, ( $Z_{0\infty} = Z_{10}$ ) and the ratio of  $Z_1/Z_{10}$  of the low-pass filter given in Fig. 26-13. Figure 27-47 shows the image impedance for mid- $\theta_2$  termination and for mid- $\theta_1$  termination. The former is seen to have a shape that can be well matched over a greater portion of the pass band than can the latter. It must be pointed out, however, that when lengths of waveguide are incorporated between the end of the low-pass structure and the

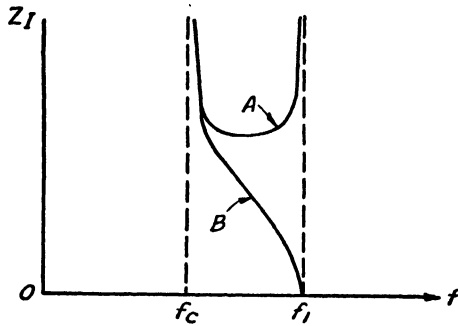


FIG. 27-47.—The image impedance of a waveguide band-pass filter. A is for mid- $\theta_2$  termination, and B is for mid- $\theta_1$  termination.

waveguide-to-coaxial-line junction (as in Fig. 27-46c) the *over-all* image impedance as seen from the *point of junction* can be considerably different from that shown in Fig. 27-47. For example, if this length is made a quarter of a guide wavelength at the low-pass cutoff frequency, the over-all image impedance for a mid- $\theta_1$ -terminated filter will be similar to curve A of Fig. 27-47. In practical design, it is usually desirable to have these added lengths between the end of the low-pass structure and the point of junction in order to provide additional high-pass cutoff sharpness, and in order to permit the field disturbances in the vicinity of the junction to die out before the wave front reaches the low-pass structure. In general, therefore, these added lengths should be at least equal to the width  $a$  of the waveguide and should be chosen so that an over-all image-impedance curve similar to curve A will result. The characteristic impedance  $Z_0$  of these added lengths at or near the center of the pass band should generally be made equal to the characteristic impedance of the coaxial line that connects to the waveguide-to-coaxial-line junction. This value should also be made equal to the image impedance of the waveguide

filter at this frequency. Reference should be made to Secs. 26-8 and 26-9 for further information and for other possibilities.

Figure 27-48 shows a waveguide band-pass filter with its measured response. In measuring the insertion-loss response, the filter was connected at each end to a matching length of tapered waveguide and a wide-band waveguide-to-coaxial junction. The insertion loss of this entire combination was the quantity measured.

The varying-impedance-waveguide band-pass filter has spurious responses near frequencies for which the various line lengths are multiples

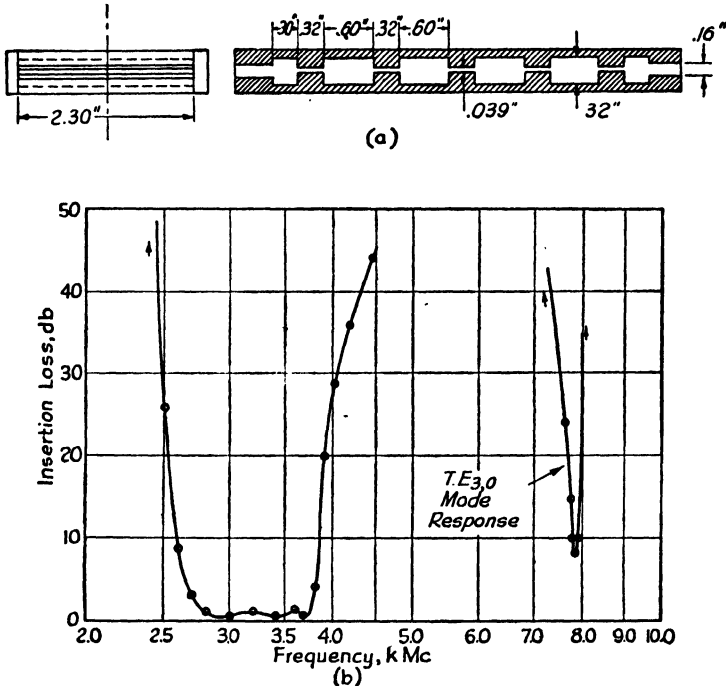


FIG. 27-48.—A waveguide band-pass filter, 2700 to 3800 Mc: (a) physical dimensions; (b) measured response in conjunction with a pair of tapers and waveguide-to-coaxial-line junctions.

of a half guide wavelength (see Sec. 27-4). These may be eliminated by combining two or more groups of sections as in Sec. 27-4. In addition to these responses, there will also be relatively sharp responses for the higher waveguide propagation modes occurring just above their cutoff frequencies. With the usual waveguide-to-coaxial junctions, the *even*  $TE_{m,0}$  modes will not be set up, and therefore these responses will not be passed by the complete filter. The *odd*  $TE_{m,0}$  modes, however, are set up by the usual junction, and these responses will therefore be passed (Fig. 27-48). The higher mode responses may be eliminated by using

two or more groups of sections having different high-pass cutoff frequencies, *i.e.*, different widths  $a$ , as in Fig. 27-49. The low-pass cutoff frequencies of the groups of sections are of course made to be the same. The groups of sections may be so designed as to eliminate both of the types of spurious responses mentioned above. Their image impedances should be made equal at some frequency near the center of the pass band.

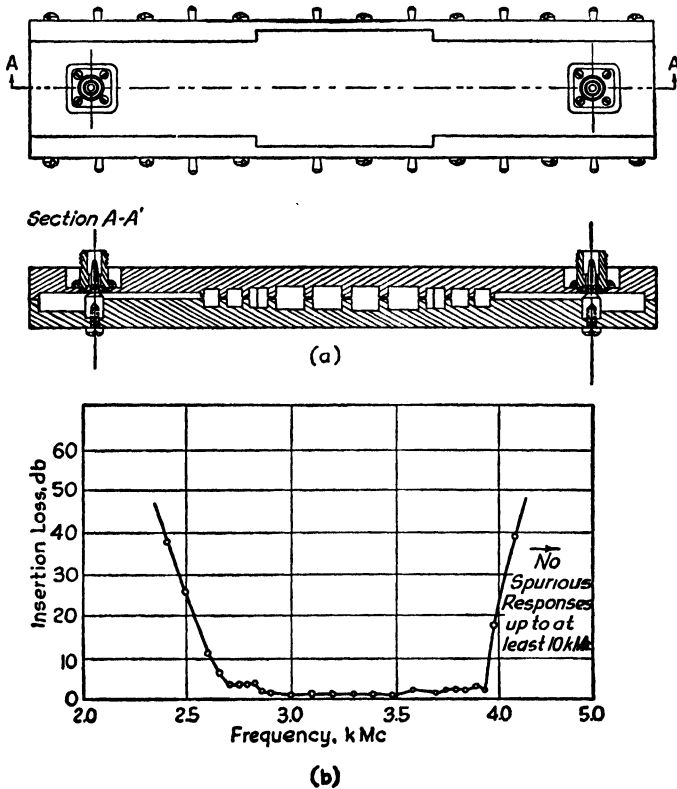


FIG. 27-49.—(a) Method of constructing a waveguide band-pass filter with two different types of section in order to eliminate spurious responses; (b) measured frequency response of this filter.

For the dielectric-slab type of filter, a dielectric material having a very high dielectric constant should be used. Titanium dioxide-base ceramics can be made with a dielectric constant ranging up to about 100. This material has low loss, is easily procured, and can be fired and ground to close tolerances. If the slab thickness first calculated is too thin for easy manufacture, the  $\theta_2$  dimension may be made the long one and the  $\theta_1$  dimension the short one. The design data in Sec. 27-4 may be used for this case as well as for the case of  $\theta_2$  less than  $\theta_1$  that has been

considered thus far. The discontinuity susceptance is zero in the dielectric slab filter, and hence  $\theta_{2c} = \theta_{2c}$ .

It is sometimes advantageous to construct a varying-impedance waveguide band-pass filter in ridge waveguide (Fig. 27-50) in order to separate the  $TE_{3,0}$  mode response from the main pass band. The cutoff frequency and characteristic-impedance curves for ridge waveguide given in Sec. 26-16 should be used in designing such a filter. Since the discontinuity-susceptance correction cannot be determined accurately at present, it is necessary to estimate its value.

The ridge-waveguide band-pass filter is similar to the dielectric-slab type in that the cutoff frequency of the low-impedance lengths is lower than the cutoff frequency of the high-impedance lengths. For both cases, it can be shown by analysis that the lower cutoff frequency of the band-pass filter is not equal to the waveguide cutoff frequency of either set of lengths, but actually falls at some frequency between these two waveguide cutoff frequencies. This actual cutoff frequency will usually be at

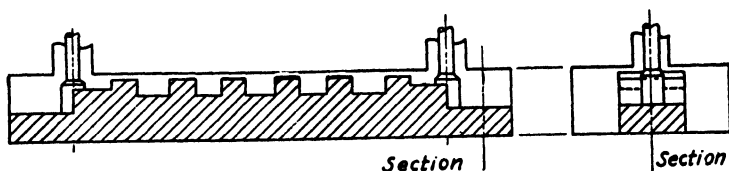


FIG. 27-50.—A varying-impedance ridge-waveguide band-pass filter.

a lower frequency than the waveguide cutoff frequency of the terminating lengths of waveguide for a ridge-waveguide filter of the type shown in Fig. 27-50. The over-all high-pass cutoff, therefore, must be provided entirely by these added lengths.

**27-29. Test Methods for High-frequency Filters.**—After a filter has been designed and constructed, it must be tested in order to determine whether its characteristics are actually within the specified performance tolerances. If the tolerances are not met, the test will indicate what sort of changes in design are required.

The most significant property of a filter is usually its insertion loss. Several methods of measuring the curve of insertion-loss vs. frequency for a filter will be described. First, however, it is important to point out that the insertion-loss measurements are meaningless unless the impedances  $Z_o$  and  $Z_R$  looking toward the generator and toward the load, respectively, at the point of insertion are specified. In particular, the resulting insertion-loss curve is generally most useful if these impedances are equal to the load resistance  $R$  for which the filter was designed. In a test setup, therefore, it is necessary to be very certain that the impedances viewed in both directions by the filter are equal to  $R$ .

Figure 27-51a and b show two test setups that have been found useful for filters having coaxial terminations. Both consist essentially of some sort of signal source, a detector, an indicator, and some means of measuring the decibel difference in level produced when the filter is inserted between the cables at (I). In both circuits, lossy coaxial lines provide isolation from the signal source and the detector, and provide impedance  $Z_o$  and  $Z_R$  very nearly equal to the characteristic impedance of the lossy cable, which in turn is chosen equal to the load resistance of the filter to be tested. This load resistance value has been almost universally made equal to 50 ohms at the Radio Research Laboratory. It should be noted that an attenuating transmission line in general has a reactive characteristic-impedance component. This, however, is usually small enough to be neglected. RG-21A/U cable has been found to be

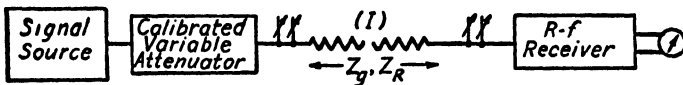
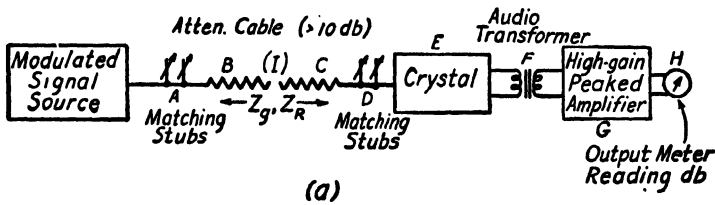


FIG. 27-51.—Two test setups useful for measuring insertion-loss curves of filters.

quite satisfactory. Instead of lossy cables, it is possible to use attenuators that have a terminal resistance equal to  $R$ .

The length of lossy cable required on each side of the filter may be determined from Eq. (26-61). This equation gives the input voltage-standing-wave ratio  $\sigma_{in}$  as a function of the decibel attenuation of the cable  $al$  and of the terminating voltage-standing-wave ratio  $\sigma_L$ . Under the worst condition, that of  $\sigma_L = \infty$ , Eq. (26-61) may be written

$$\sigma_{in} = \coth \frac{al}{8.686} \tag{27-13}$$

For  $al$  equal to 10 db,  $\sigma_{in}$  equal to 1.22. For  $al$  equal to 15 db,  $\sigma_{in}$  is equal to 1.07. These voltage-standing-wave ratios assure a good approximation of  $Z_o$  and  $Z_R$  to  $R$ . It is recommended that for *pass-band* measurements the cable attenuation on each side of the filter be at least 15 db. For *stop-band* measurements, the cable attenuation may be reduced to 10 db, if necessary. When insufficient signal power is available, it may, however, be necessary to compromise on these values. The matching



stubs shown in Fig. 27-51 should then be peaked with great care, and for best results they should be combined with a line stretcher in order to assure perfect matching between the generator and detector and the cable. In any case, it must be remembered that an oscillator may be affected in a nonlinear fashion by the impedance into which it works. If, therefore, sufficient attenuation isolation is not provided between the oscillator and the filter, the actual oscillator level may change when the filter is inserted. For this reason, it is recommended that at least 10-db attenuation always be provided between the oscillator and the point of insertion. If attenuators are used in place of attenuating cables, the same rules apply regarding required total attenuation.

The test setup in Fig. 27-51a requires a modulated signal source (sine-wave, square-wave, etc.). The crystal  $E$  operates as a low-level detector, and the resulting audio signal is fed into the audio amplifier. The transformer  $F$  provides a low-resistance d-c return path for the crystal. This feature is essential to ensure that the crystal act as an accurate square-law device. In addition, care must be taken to keep the r-f power level at the crystal as low as practicable. Several crystals operating under these conditions have been tested at spot frequencies in the range 100 to 10,000 Mc and the square-law agreement has been found to be very good over the range of power used. If there is doubt about a particular crystal, however, it is recommended that this characteristic be checked for that crystal.

Under the square-law assumption, one-half the difference in decibels in the output meter  $H$  readings under any two conditions gives the decibel difference in r-f power level at the crystal. If desired, meter  $H$  may be calibrated to read r-f decibels directly. The amplifier  $G$  must have as great a *dynamic range* (signal output at overload vs. noise-and-hum output at same gain setting) as possible; a range of somewhat over 80 db is required to measure conveniently attenuations of 40 db. This requirement necessitates an amplifier peaked at the signal-generator modulation frequency rather than a broad-band amplifier. A separate plate supply and d-c filament voltage are recommended.

The test procedure is as follows: The lines are joined at  $I$  (filter out), the signal generator is set on frequency, and stubs  $A$  and  $D$  are tuned. The stubs will be independent in adjustment if cables  $B$  and  $C$  have the proper attenuation. The gain of amplifier  $G$  is then set to give a convenient reading on meter  $H$ . Care must be taken to ensure that the amplifier is never overloaded at this point. The filter is then inserted at  $I$ . One-half the audio-decibel difference between the readings of the meter  $H$  with and without the filter inserted gives the filter attenuation in decibels.

If it is desired to measure insertion losses greater than those allowed by the dynamic range of the amplifier, the procedure may be somewhat modified by the use of a length of attenuating cable of the same type as cables *B*, *C*, the attenuation of which is known. (This can be measured by the same method as above since, under this condition of measurement, the cable attenuation is equal to its insertion loss.) The previous procedure is then altered in the following respects: (1) The initial tuning and gain adjustments are made with the cable of known attenuation inserted at *I*; (2) this cable is then removed and the filter inserted in its place; (3) the filter insertion loss is given by one-half the decibel difference in meter readings *plus* the known attenuation of the added cable.

Several further precautions may be added. (1) It must be remembered that the attenuation of cable is a function of frequency. Hence, if measurements are made over a wide frequency band, cables *B* and *C* will have to be changed several times to ensure that the attenuation of each is sufficiently high. For the same reason, the attenuation of the supplementary cable in the modified procedure of the last paragraph must be known at each frequency. (2) Great care must be taken in selecting male and female fittings to keep the number of r-f cable connectors near *I* at a minimum. Very few of the present types of connectors are well matched above 3000 Mc, and a large number of these can seriously affect the accuracy of measurement.

Oscillator harmonics can cause considerable trouble in testing high-pass filters. If a point in the stop band of such a filter is being tested and oscillator harmonics are 30 db below the fundamental, the filter will *apparently* have no more than 30-db attenuation at this point, even though the actual loss for the fundamental frequency may be much greater. Extreme care must therefore be taken to eliminate oscillator harmonics during such tests. This may be done by placing a low-pass filter between *A* and *B* of Fig. 27-51a. (If the filter is placed *before* the tuning stubs at *A*, it will not be working between the proper impedances and may not give the desired effect.)

The test setup of Fig. 27-51b involves the use of a reliable r-f attenuator of the variable type. In this case, components *E*, *F*, *G*, and *H* of Fig. 27-51a are replaced by an r-f receiver. The attenuator is placed somewhere before cable *B* and is often built into the oscillator. The receiver is used merely to indicate a standard output; the difference between attenuator readings with filter out and filter in for this standard output then gives the filter attenuation. The other steps in the procedure remain the same. The attenuator should be checked, however, since many models have been found unreliable at 3000 Mc and higher frequencies. It should be noted that if a superheterodyne receiver is tuned

to the signal-generator fundamental, it will not pick up its harmonics. Variations and combinations of these two methods may be desirable to suit particular conditions or available equipment.

In the case of filters for transmitter systems, the pass-band standing-wave ratio may be of more interest than the pass-band insertion loss. The standing-wave ratio of a coaxial or waveguide filter may be measured with a slotted line of characteristic impedance equal to the load resistance  $R$  and a traveling pickup probe (Fig. 27-52). The load end of the filter

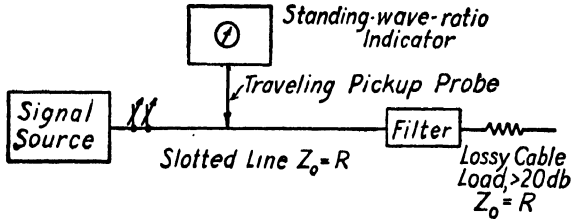


FIG. 27-52.—A test setup for measuring the input standing-wave ratio of either a coaxial or waveguide filter. In the former case, a slotted coaxial line is used, in the latter a slotted waveguide.

should be terminated by the load resistance  $R$ . This load may be 20 db or so of lossy cable of characteristic impedance  $Z_0 = R$ . Since tests of this sort are described in detail in Chap. 2, a complete discussion will be omitted here. It should be noted that, if the filter dissipation is zero, the insertion loss and voltage standing-wave ratio of the filter are related by Eq. (26-54), which is plotted on the center scale in Fig. 26-9. This scale shows that the voltage standing-wave ratio is extremely high for an insertion loss greater than 10 db, and therefore this method is not useful for measuring stop-band response.

## CHAPTER 28

### TUNERS FOR MICROWAVE RECEIVERS

BY S. B. COHN, R. A. SODERMAN, S. J. GRIFFIN, AND R. O. PETRICH

**28-1. General Requirements for Receiver Tuners.**—A narrow-band filter is required at the input of a receiver in order to separate the desired signal from signals of other frequencies. Unless the receiver is intended for use at just one frequency, the filter must generally be capable of easy tuning over a wide frequency range. It must provide adequate selectivity and low pass-band loss over the entire range. The design of such tunable filters, called *r-f tuners*,<sup>1</sup> will be described in this chapter.

The best type of tuner for a given receiver depends upon the receiver, the frequency range, and the required rejection of undesired signals. In any case, the tuning should be noiseless, the pass-band loss low, and the tuning should follow a simple smooth curve.

For a *direct-detection* type of receiver, the response curve should be very sharp, *i.e.*, the pass band should be very narrow and should have only one peak. Signals inside the tuning range should be passed by the tuner at only one point on the dial, and no signal outside the tuning range should be passed at all.

The antenna-input-circuit tuner of a superheterodyne receiver must have a band width at least as great as the i-f band width, with enough extra to provide for oscillator tracking tolerance. The requirements concerning spurious tuner pass bands are less stringent than for direct-detection receivers, since a superheterodyne receiver is capable of responding to only a few scattered frequencies in addition to the desired one (see Sec. 25-11). At these undesired frequencies, the tuner must provide a high insertion loss. The tune may be permitted to have spurious pass bands as long as they are well separated from any undesired frequencies that can be received by the superheterodyne receiver. The undesired frequency response that is the closest to the desired signal frequency, and hence is the most difficult to eliminate, is the image frequency. The frequency separation between the signal and its image is twice the i-f amplifier frequency.

<sup>1</sup> In this and following chapters the term *tuner* will be applied to tunable resonant circuits. The term *preselector* will be applied to the entire tunable filter, which may include one or more tubes.

A single-resonant-circuit tuner does not usually give adequate image rejection in receivers at very high frequencies. Greater rejection for a given band width may be obtained through the use of two or more resonant circuits loosely coupled together. The number of coupled resonant circuits required in the tuner depends upon the percentage separation of the signal and its image, upon the required tuner band width, and upon the desired image rejection. In the next section this problem will be considered quantitatively.

**28-2. General Theory of Narrow-band Coupled-circuit Tuners.**—The tuners described in this chapter differ from the filters of Chaps. 26 and 27 in the following ways: (1) the tuners always have a narrow band width; (2) in most cases their analysis is only approximate and is based on coupled-circuit considerations; (3) their pass band is tunable over a wide frequency range.

*A Generalization Concerning Different Types of Resonant Circuits.* Figure 28-1 shows a symmetrical series of resonant four-terminal elements coupled together by other nonresonant four-terminal elements.

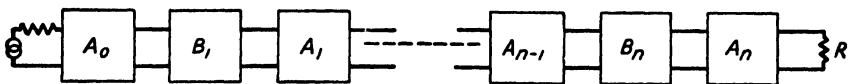


FIG. 28-1.—The generalized coupled-circuit filter having any number of resonant circuits, with structure symmetrical about the center.  $A_i$  are nonresonant reactive coupling elements;  $B_i$  are resonant elements.

The resonant elements may be series- or parallel-resonant  $LC$  circuits, resonant transmission lines, waveguides, cavity resonators, etc. The nonresonant coupling elements may be series or shunt inductances or capacitances, T- or  $\pi$ -sections, coupling loops, irises, apertures, probes, etc. In any case, it can be shown that the curve of insertion-loss vs. frequency is independent of the type of nonresonant coupling and is a function only of the number of resonant cavities and the degree of coupling, as long as the width of the pass band is not more than a few per cent of the mean pass-band frequency.<sup>1</sup>

*A Generalization Concerning the Effect of Coupling Variation.*—Consider a narrow-band tuner consisting of any number of nondissipative coupled resonant circuits in cascade, all tuned to the same frequency. If the end couplings are held constant, and the intermediate ones are increased from zero, the response curve starts as a narrow single peak and widens and flattens. Except for a single resonant circuit, there is a certain degree of intermediate coupling corresponding to a given degree of end coupling, for which the response curve will attain its maximum degree of flatness. This condition is known as *critical coupling*. For

<sup>1</sup> RICHARDS, P. I., Universal Optimum-response Curves for Arbitrarily Coupled Resonators, *Proc. I.R.E.*, **34**, 624 (1946).

lower intermediate couplings, the tuner is said to be *undercoupled*. Further increase of the intermediate couplings will widen the pass band still further, but will introduce transmission dips and peaks in the pass band

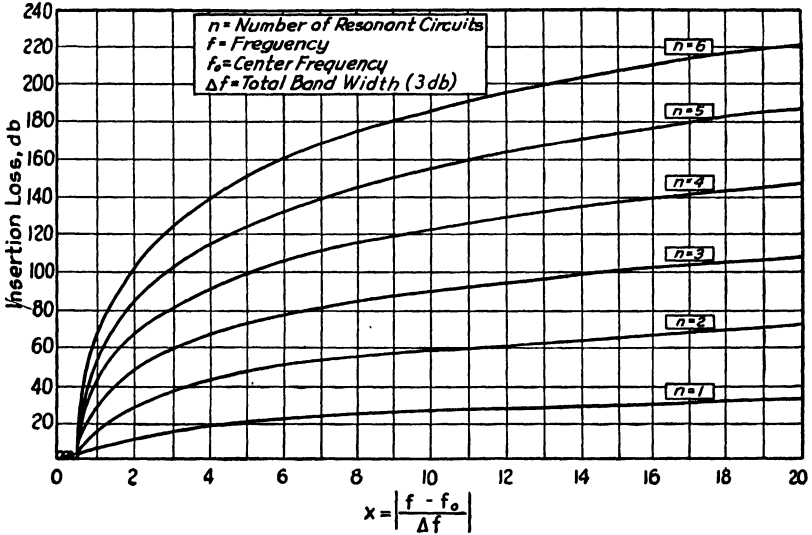


FIG. 28-2.—Universal off-band response for narrow-band coupled-circuit tuners. Curves are shown for tuners having one to six resonant circuits.

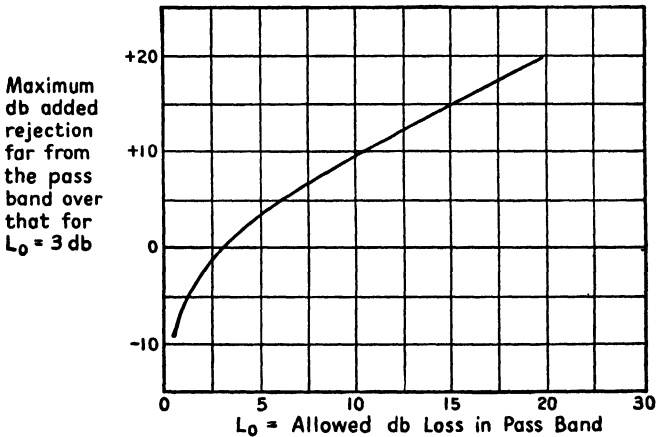


FIG. 28-3.—Correction curve for Fig. 28-2. With the aid of this curve, the off-band rejection of a coupled-circuit tuner having any number of resonant circuits may be determined when the band width is measured between insertion-loss points  $L_0$  other than 3 db.

(Figs. 28-5 and 28-6). This condition is known as *overcoupling*. Two resonant circuits will introduce one dip (two peaks), three resonant circuits will introduce two dips (three peaks), etc., *i.e.*, the number of transmission peaks will equal the number of resonant circuits.

*Universal Off-band Response Curves.*—For a sufficiently narrow band, the entire frequency response of an overcoupled tuner is fully determined if the number of resonant circuits, the band width, and the insertion loss at the pass-band transmission dips are specified. Figure 28-2 gives the universal response curves for one to six coupled circuits.<sup>1</sup> The band width is measured at the points at which the response is 3 db down, and the couplings are adjusted so that all pass-band loss peaks are equal to 3 db. The response differs only very slightly if the loss peaks are other than 3 db, provided that the band width is still measured at the 3-db points and provided that the degree of coupling is critical or greater. If it is desired to measure the band width at an insertion-loss level  $L_0$  not equal to 3 db, the correction curve of Fig. 28-3 may be applied to insertion-loss values taken from Fig. 28-2. The correction curve assumes that all transmission dips are equal to  $L_0$ , and the curve is accurate only for values far from the pass band.

**28-3. Losses in Radio-frequency Tuners.**—Losses in r-f tuners are of two kinds—*mismatch* and *dissipation*. A tuner is generally a two-terminal-pair network, one pair of terminals connecting to the antenna line and the other pair to the detector, mixer, or amplifier. Mismatch losses occur whenever the impedances looking in both directions at each terminal pair are not exact conjugate matches. In other words, a receiver tuner must not only provide the desired frequency response, but it must also act as a matching transformer between the antenna and detector impedances.

The mismatch-loss considerations of Chap. 26 do not apply exactly to r-f tuners because of their appreciable dissipation loss. Nevertheless, the curves in Sec. 26-12 for mismatched filters will give a good, though rough, idea of the magnitude of tuner mismatch loss.

Dissipation (or resistive) loss is an important factor in narrow-band tuner design, because of the relatively high values of operating  $Q$  required for narrow pass bands. For a distributed-constant resonant circuit, the well known lumped-element-circuit definition of  $Q = \omega L/R$  is not applicable. The  $Q$  of a resonant circuit may, however, be defined as the ratio of the mean pass-band frequency to the 3-db band width ( $f/\Delta f$ ) for the resonant circuit used as a single-circuit tuner. For multiple-circuit tuners, the  $Q$  of each circuit considered alone will generally be somewhat higher than the over-all value of  $f/\Delta f$ , but will be of the same order of magnitude. The  $Q$  is also equal to  $2\pi f$  times the energy stored in a resonant circuit divided by the average power dissipated.

$$Q = 2\pi f \frac{\text{stored energy}}{\text{average dissipated power}} \quad (28-1)$$

<sup>1</sup> RICHARDS, *op. cit.*

The dissipated power is lost internally in the resonant circuit itself, and also externally in the equivalent resistances coupled into the circuit from the external input and output circuits (antenna and detector). The loss in the coupling reactances is generally negligible. In order that the power-transmission efficiency shall be high, the internal losses must be a small fraction of the external losses.

The pass-band insertion loss due to dissipation alone for a single resonant circuit is given by

$$D = 20 \log_{10} \left( \frac{Q'}{Q' - Q} \right) \quad \text{db} \quad (28-2)$$

where  $Q'$  is the  $Q$  for the unloaded (or isolated) circuit, and  $Q$  is that for the circuit loaded by the antenna and detector impedances. In a multiple-circuit tuner, the dissipation insertion loss is given by the sum of the individual losses for each circuit as calculated by Eq. (28-2). If the loaded and unloaded  $Q$ 's are the same for each circuit in an  $n$ -circuit tuner, as will generally be assumed, the dissipation insertion loss is given by

$$D = 20n \log_{10} \left( \frac{Q'}{Q' - Q} \right) \quad \text{db} \quad (28-3)$$

Equation (28-3) shows, for example, that for  $Q' = 10Q$  the loss is 0.92 db per circuit. Since  $Q$  is of the order of magnitude of  $f/\Delta f$ , where  $\Delta f$  is the band width, a  $Q'$  of at least 1000 in a three-circuit tuner having a 1 per cent band must be provided in order to limit the dissipation loss to less than 3 db. More specific information on the loaded  $Q$  required for a given band width in two- and three-circuit tuners will be given in later sections.

**28-4. The Single-circuit Tuner.**—The frequency response of all single-circuit configurations having the same loaded  $Q$  is identical so long as the band width is less than a few per cent. A universal response curve for a single resonant circuit is given in Fig. 28-4. The 3-db band-width ratio  $\Delta f/f$  for the single tuned circuit is seen to be exactly equal to  $1/Q$ . The response farther from resonance can be read from Fig. 28-2.

**28-5. Two Coupled Circuits.**—As can be seen from the universal-loss curves of Fig. 28-2, considerably more off-band rejection is offered by two coupled circuits than by one. For some receiver purposes, one tuned circuit provides sufficient selectivity, but for adequate rejection of images and other undesired responses, greater selectivity is usually required in a tuner than that provided by one circuit. As a consequence, tuners have been developed consisting of two and three coupled circuits whose tuning motions are ganged together.



As an example of the increased selectivity provided by two coupled circuits instead of one, consider a receiver having its image frequency separated by 150 Mc from its signal frequency and requiring a tuner band

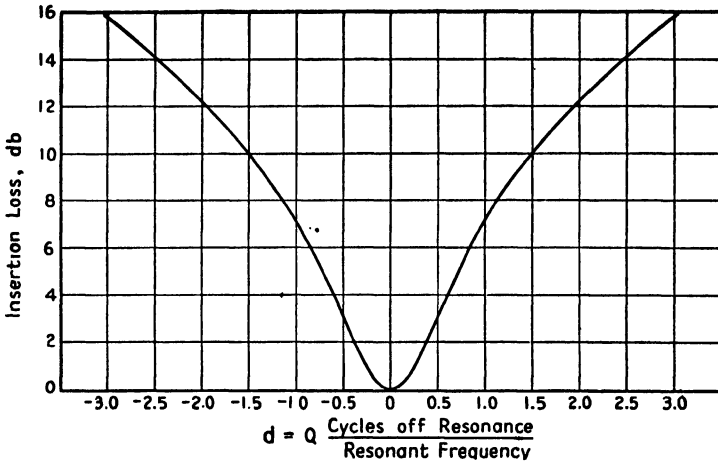


FIG. 28-4.—Universal response for one resonant circuit.

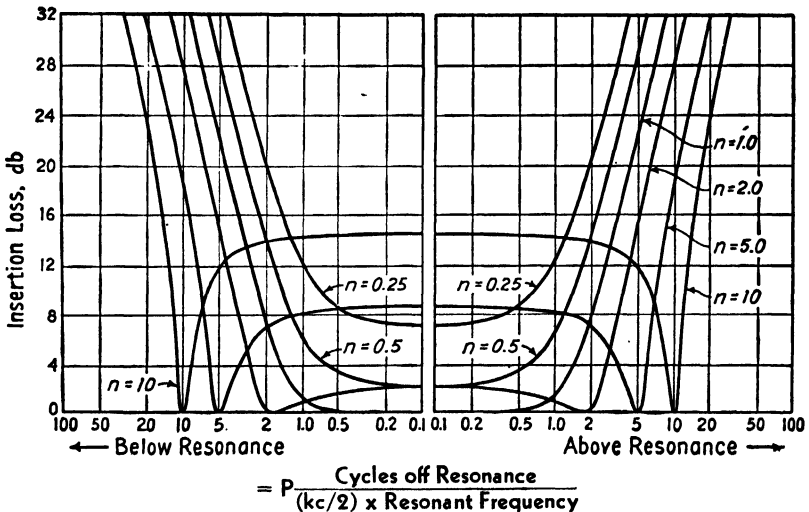


FIG. 28-5.—Universal response curve for two coupled resonant circuits.  $n$  is the ratio of the actual coupling coefficient  $k$  to critical coupling  $k_c$ .  $k_c = 1/Q$ . (From F. E. Terman, "Radio Engineers' Handbook," Fig. 22a, p. 160.)

width of 50 Mc. Figure 28-2 shows that a single-circuit tuner provides only 16-db image rejection (which is entirely inadequate), while a two-circuit tuner provides 37-db rejection.

Universal pass-band-response curves for two coupled circuits are given

in Fig. 28-5.<sup>1</sup> The  $Q$  referred to in this figure is that for the first tuned circuit as loaded by the input circuit alone and that for the second tuned circuit as loaded by the output circuit alone. These two  $Q$ 's are assumed to be equal.

**28-6. Three Coupled Circuits.**—For many receiver designs, two coupled circuits offer sufficient rejection of images and other undesired responses. But in some receivers, especially in microwave receivers in which the percentage difference between the signal and its image is small, sharper rejection is required. In such cases, a three-circuit tuner may be used. In the example given in the last section for a receiver in which the

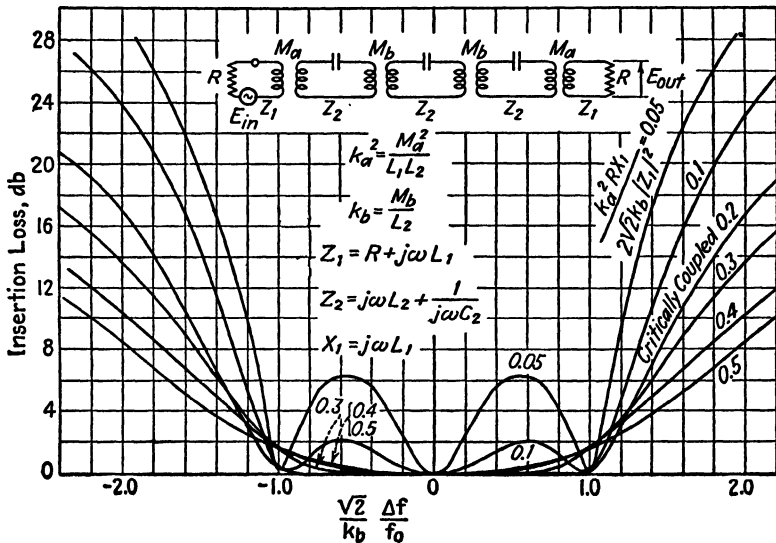


FIG. 28-6.—Universal response curve for three coupled resonant circuits. The tuner is assumed to be dissipationless.

image frequency is separated by 150 Mc from the signal frequency and which requires a tuner having a 50-Mc band width, Fig. 28-2 shows that a three-circuit tuner provides about 58-db rejection, while a two-circuit tuner provides only 37-db rejection. For many receiver uses, 37-db rejection will not suffice.

A three-circuit tuner is capable of better image rejection than the two-circuit tuner, but on the other hand, it is harder to design and build, is more critical as to tolerances, and has approximately 50 per cent more dissipation loss in the pass band for the same band width. By increasing the band width of the three-circuit tuner 50 per cent, however, its pass-

<sup>1</sup> TERMAN, F. E., "Radio Engineer's Handbook," p. 160, McGraw-Hill Book Company, Inc., New York, 1943. This reference gives a brief theoretical treatment of two coupled circuits.

band loss will be about the same as that of the two-circuit tuner, while the off-band rejection of the former will still be considerably greater than that of the latter.

Universal pass-band response curves for three coupled circuits are given in Fig. 28-6.<sup>1</sup> These curves assume the circuits to be identical, nondissipative, and all tuned to the same frequency. Note that in this idealized case the center peak is lossless, even for less than critical coupling. For coupling greater than critical, three distinct peaks develop, the outer two also being virtually lossless.

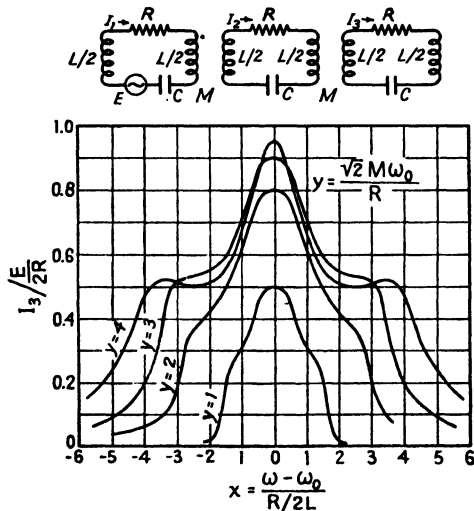


FIG. 28-7.—Universal response curve for three coupled resonant circuits. The load is assumed to be equally distributed among the three circuits. (By permission of E. A. Guillemin, "Communication Networks," Vol. 1, Fig. 122, p. 338, John Wiley & Sons, Inc., 1931.)

In practice, the resonant circuits will have some dissipation loss. The usual effect of this is to introduce additional insertion loss at all frequencies, but particularly at the response peaks, the loss being greater for the outer peaks than for the center one. Figure 28-7<sup>2</sup> shows some calculated output-voltage curves for the case of a three-circuit tuner loaded by its dissipation alone. The dissipation is assumed identical in each circuit. Experiment has shown the response of a three-circuit tuner to lie somewhere between the extremes of Figs. 28-6 and 28-7, depending upon the measured minimum insertion loss. For the usual losses of not

<sup>1</sup> SPANGENBERG, K. R., The Universal Characteristics of Triple-resonant-circuit Band-pass Filters, *Proc. I.R.E.*, **34**, 629 (1946).

<sup>2</sup> Figure 28-7 is taken from E. A. Guillemin, "Communication Networks," Vol. 1, p. 338, John Wiley & Sons, Inc., New York, 1931.

more than a few decibels the response will resemble that of Fig. 28-6 more than the other.

Figure 28-6 gives relations between the parameters of the circuit for each response curve. By the use of these relations, a three-circuit tuner may be designed to have the desired band width and pass-band shape. All the three-circuit tuners described in this chapter may be shown to have an equivalent circuit the same as that in Fig. 28-6. In an actual design problem, however, the couplings have to be adjusted semi-empirically, but Fig. 28-6 nevertheless provides a valuable guide.

**28-7. Butterfly Resonators.**—The *butterfly* type of lumped-constant tunable resonant circuit,<sup>1</sup> developed by Karplus, Sinclair, and Peterson, overcomes some of the difficulties encountered in the use of lumped-constant elements in conventional resonators at frequencies between about 100 and 1000 Mc. In this frequency range, the self-inductance present in conventional variable capacitors is detrimental when the capacitors are used in conventional parallel-resonant circuits. No matter how small an external inductance is used, the self-inductance of a capacitor limits the highest obtainable resonant frequency of the circuit to the natural resonant frequency of the capacitor and its self-inductance. It also reduces the resonant impedance developed across the capacitor terminals to a value that is very low at frequencies near the natural resonant frequency.

In well-designed variable capacitors the effect of the inductance at frequencies up to about 100 Mc is relatively small, but at higher frequencies its effect increases rapidly, and a satisfactory resonant circuit becomes increasingly harder to obtain. Furthermore, conventional variable capacitors usually have relatively large losses at frequencies above about 100 Mc because of the relatively high current concentrations produced in sections of the capacitor plates and terminals as a result of the small area of the terminal connections. In a butterfly resonator, however, the inductance and capacitance elements are built as an integral unit in such a manner as to provide a lower minimum inductance, lower losses, and two accessible points across which the maximum resonant impedance developed in the circuit appears. Incorporated in the design is a method of varying the effective inductance by means of eddy-current shielding produced by the rotor plates. The inductance decreases as the capacitance decreases, so that the tuning range is increased.

**28-8. A General Description of Butterfly Resonators.**—Figure 28-8a shows one type of butterfly, called a *true butterfly*, tuned to its lowest

<sup>1</sup> KARPLUS, E., Wide Range Tuned Circuits, *Proc. I.R.E.*, **33**, 426 (1945); KARPLUS, E., The Butterfly Circuit, *General Radio Experimenter*, vol. 19, No. 5, October, 1944; SINCLAIR, D. B., High Frequency Measurements, *Radio-Electronic Engineering* **5** (No. 6) 14 (1945); **6** (No. 1) 11 (1946).

frequency, and Fig. 28-9 shows its equivalent circuit. The capacitance of the resonant circuit consists of the capacitance between one half  $K$  of the rotor, and the adjacent capacitor section  $J$  of the stator, in series

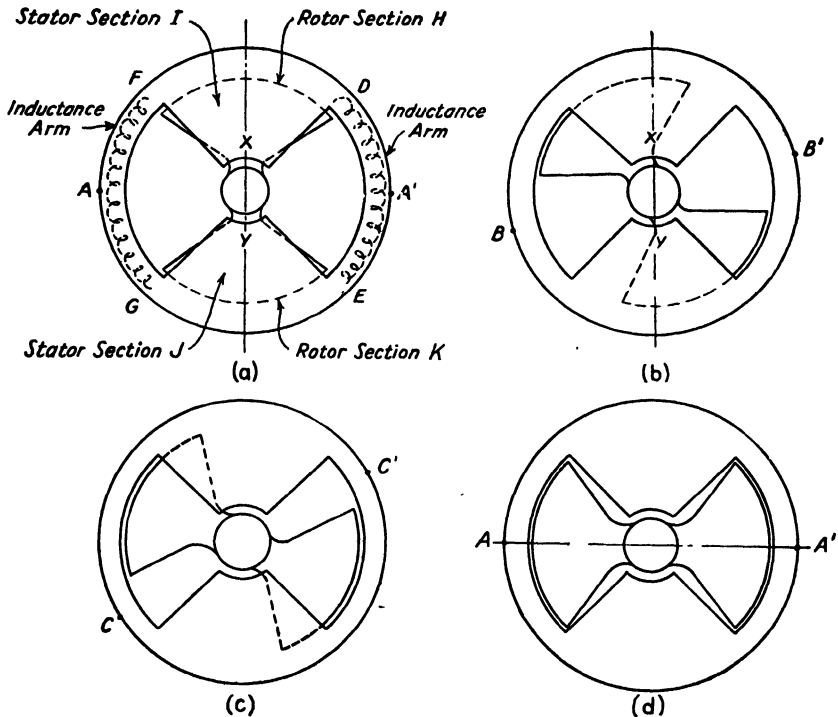


FIG. 28-8.—Variation of the electrical balance points with rotor position in a true butterfly.

with the capacitance between the other half  $H$  of the rotor and the other capacitor section  $I$  of the stator. The inductance is that of the parallel combination of the two inductance arms  $F-G$  and  $D-E$ , which are actually parts of the stator and which complete the circuit between the two capacitor sections  $I$  and  $J$  of the stator. At the lowest resonant frequency, the whole unit shown in Fig. 28-8a is balanced electrically with respect to the line  $AA'$  passing through the center of the rotor and the mid-points of the inductance arms. Therefore the center of the rotor and the mid-points of the inductance ring are all at the same r-f potential. If the butterfly is floating, or ungrounded, and has symmetrical distributed capacitances to ground, as is true in the usual type of operation, these points will be at ground potential.

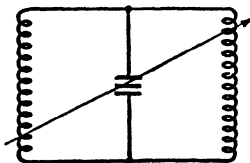


FIG. 28-9.—Approximate equivalent circuit of a true butterfly.

the butterfly is floating, or ungrounded, and has symmetrical distributed capacitances to ground, as is true in the usual type of operation, these points will be at ground potential.

As the resonant frequency is increased by turning the rotor slightly to decrease the capacitance, the rotor plates move into the region containing the magnetic field produced by currents flowing in the inductance arms, as shown in Fig. 28-8*b*. In this area the rotor plates act as an eddy-current shield for the magnetic field and reduce the effective inductance of the arms. Under these conditions the electrical mid-points of the inductance arms, which are at the same r-f potential as the center of the rotor, shift to  $B, B'$ .

Figure 28-8*c* shows the butterfly tuned to a still higher frequency. The rotor plates shield the inductance to a greater extent and therefore have a greater effect on the inductance. At this setting the electrical mid-points of the inductance arms shift to  $C, C'$ .

At the highest resonant frequency, for which the capacitance is a minimum, the rotor plates produce the maximum amount of shielding, as shown in Fig. 28-8*d*. Because of the eddy-current shielding, the magnetic field is confined to the circumferential gaps between the rotor plates and inductance arms and to the radial gaps between the rotor plates and stators. As a result, the inductance is decreased appreciably. At this setting, the electrical circuit is symmetrical again, and the electrical mid-points of the inductance arms return to  $A, A'$ .

The maximum impedance at all frequencies is developed across the points marked  $X$  and  $Y$  in Fig. 28-8*a*. A butterfly is, however, essentially a two-terminal device, as no other point has a fixed potential relative to these points over the tuning range, except the center of the rotor, to which it is difficult to make noise-free connections.

In a butterfly the eddy-current loss is usually much greater than the ohmic loss in the inductance arms. As a result of the increased eddy-current shielding produced by the rotor, the eddy-current loss and, hence, the equivalent series resistance in the circuit increase rapidly as the butterfly is tuned to higher frequencies. In typical butterflies, the decrease in inductance and increase in equivalent series resistance of the circuit are sufficient to keep the resonant impedance approximately constant over the tuning range. The resonant impedance is also roughly proportional to the diameter of the butterfly for units designed for the same low-frequency limit; typical units, with circular-sector rotor plates, as shown in Fig. 28-8, have impedances of the order of 10,000 ohms. The  $Q$  developed by butterflies, however, varies appreciably over the tuning range. The  $Q$  is a maximum at the low-frequency end of the tuning range and decreases as the butterfly is tuned to higher frequencies because the ratio of the effective inductance to the equivalent series resistance decreases with increasing frequency more rapidly than the frequency increases. Typical butterflies have values of  $Q$  lying in the range between 200 and 1000.

In order to increase the tuning range over that obtainable with a single rotor and a single stator plate, butterfly resonators are usually made up of a number of rotor and stator plates, as shown in Fig. 28-12. In most cases, to assure maximum mechanical rigidity, the height of the inductance arm is made the same as the height of the stator-plate stack. A more complete discussion of the effect of increasing the number of plates is presented in Secs. 28-9 and 28-13.

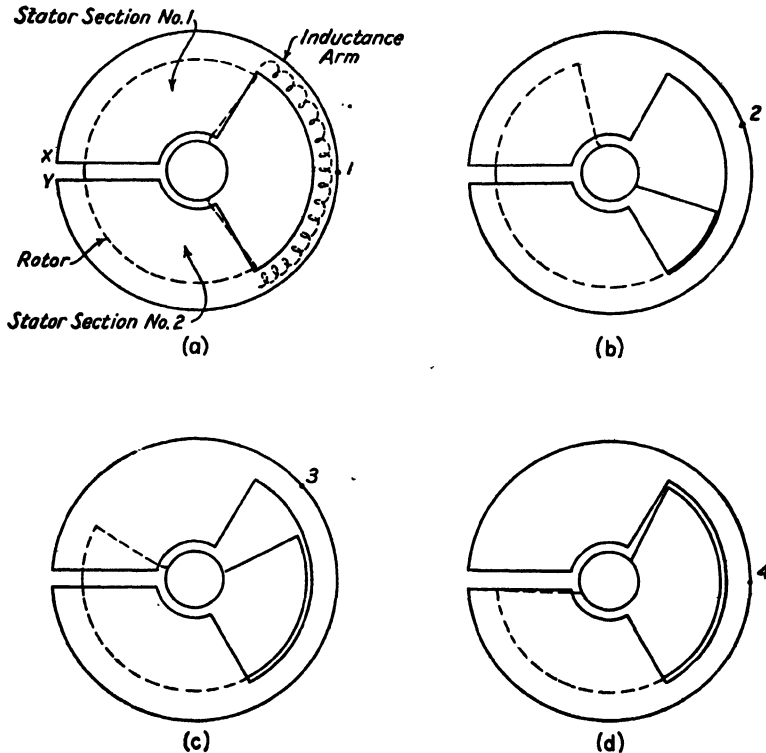


FIG. 28-10.—Variation of electrical balance point with rotor position in a semibutterfly.

Another type of butterfly, called the *semibutterfly*, is shown in Fig. 28-10. This butterfly has only one inductance arm, and in the usual design the rotor turns through 120 deg. When the butterfly is rotated, the inductance is changed by the eddy-current shielding produced by the rotor, as in the true butterfly, but because of the unbalanced capacitances from the rotor to each stator at higher frequencies, the center of the rotor is not balanced with respect to the opposite sides of the stator, except at the lowest resonant frequency. Figures 28-10a, b, c, and d show the position of the rotor and mid-point of the effective inductance at several frequencies. The mid-points are marked 1, 2, 3, and 4, in order of increasing frequency. The maximum resonant impedance at all frequencies is

developed between the opposite capacitor sections of the stator at the points labeled *X* and *Y*.

The semibutterfly has less mechanical and electrical stability than the true butterfly, as the stator plates are not complete rings. Furthermore, the rotor is not electrically balanced with respect to the two capacitor sections of the stator except at the lowest resonant frequency. The rotor must therefore be well insulated from its drive shaft, and care must be taken to prevent series resonances from occurring in the structure between the rotor and ground in the tuning range.

The semibutterfly is, however, usually better suited than the true butterfly to wide-range operation at relatively low frequencies when a

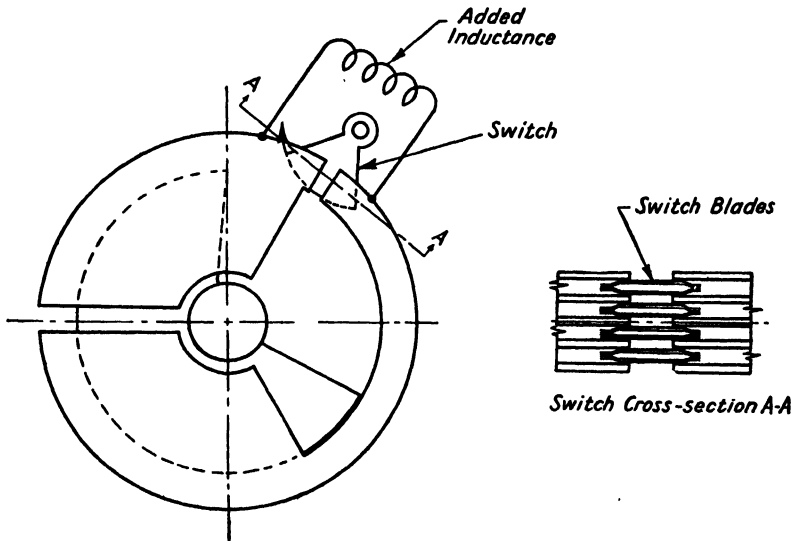


FIG. 28-11.—Semibutterfly with a range switch.

unit of the smallest possible size is required, as it is possible to obtain higher maximum inductance and capacitance in a unit of a given size with a semibutterfly, which has only one inductance arm instead of two in parallel, and stator sections covering 120 deg instead of 90 deg. It is also possible to extend the low-frequency range of a semibutterfly by breaking the inductance arm by means of a low-inductance switch and inserting an external inductance, as shown in Fig. 28-11. Switching is much more difficult with true butterflies as two switches are required.

A semibutterfly is more difficult to construct than a true butterfly as the rotor usually covers 240 deg, as shown in Fig. 28-10, and therefore it cannot be inserted after the stator has been assembled.

The true butterfly is better suited for wide-range operation near the high-frequency end of the frequency range under consideration than the



semibutterfly, as the load, either a tube or crystal, usually has an effective capacitance that is normally of the same order of magnitude as the minimum butterfly capacitance. In order to tune to relatively high frequencies, therefore, the minimum inductance and total minimum capacitance must be small and, if a wide range is desired, the maximum capacitance must be as large as possible. A true butterfly of a given stack height designed for a given minimum inductance is usually larger in diameter than a similar semibutterfly having the same inductance and has approximately the same minimum capacitance. Consequently, the area of the stator and rotor plates can be made greater which, of course, increases the tuning range over that obtainable with a semibutterfly of the same size by increasing the maximum capacitance. Also, the rotor in a typical true butterfly is approximately at ground potential over the tuning range and hence is less likely to be a source of trouble at high frequencies than the unbalanced rotor in a semibutterfly.

**28-9. Butterfly Design.**—The problem of designing a butterfly to cover a specified frequency range is somewhat complicated at the present time by the lack of a simple method of calculating the effective inductance at the high-frequency end of the tuning range. The minimum capacitance can be estimated, but, since the inductance is unknown, the top frequency limit cannot be determined very accurately. The inductance of a true butterfly at the low-frequency end of the range can be calculated from the formula for the inductance of a ring of rectangular cross section by dividing it by 8 to account for the two 90-deg sectors in parallel and multiplying it by an empirical factor of 1.35 to account for the inductance of the capacitor sections of the stator plates and the inductance of the rotor. The resultant formula for the inductance of a true butterfly is<sup>1</sup>

$$\begin{aligned} L &= 1.35 \times \left(\frac{1}{8}\right) \times 0.01257r \left(\ln \frac{36r}{h+w} - 2\right) \\ &= 0.00212r \left(\ln \frac{36r}{h+w} - 2\right) \mu h \end{aligned} \quad (28-4)$$

where  $r$  is the inside radius of the inductance ring, and  $h$  and  $w$  are the height and width of the inductance arm. All lengths are expressed in centimeters. The maximum capacitance can be calculated by conventional means, and, from the values of maximum inductance and capacitance, the low-frequency limit of the tuning range can be calculated fairly accurately.

The ratio of the inductance at the low-frequency end of the range to the inductance at the high-frequency end of the range depends greatly on the size of the butterfly and shape of the plates. In typical units, ratios

<sup>1</sup> KARPLUS, E., *loc. cit.*

ranging from 1.5 to 3.5 are obtained. The highest ratio actually obtained was 4.6 in a butterfly<sup>1</sup> 5 in. in diameter consisting of 14 rotor plates with a  $\frac{1}{16}$ -in. clearance between adjacent stator and rotor plate edges. This unit had a capacitance ratio of 22 and a tuning range from 47 to 470 Mc.

The tuning range of a butterfly of a given type depends upon the number of plates or stack height, upon the outside diameter of the inductance arms, and upon a number of other factors. Two methods of changing the range of a butterfly of a given size are to change the spacing between rotor and stator plates, or to change the number of plates at constant stack height by simultaneously changing the thicknesses of the plates. Usually, however, the minimum practical plate thickness and spacing are used, and these methods are not applicable. The minimum practical spacing between the rotor and stator plates has been found to be about  $\frac{1}{64}$  in. as the mechanical difficulties increase very rapidly with closer spacings. Plate thicknesses of about  $\frac{1}{32}$  in. have also been found to be satisfactory. In the following discussion of the variation in tuning range with stack height and diameter, constant plate thickness and spacing are assumed.

Increasing the number of plates, or stack height, lowers the low-frequency limit rapidly since the maximum capacitance increases more rapidly because of the larger number of plates than the inductance decreases because of the greater height of the inductance arms. However, the upper frequency limit decreases very slowly with increasing stack height, as the minimum capacitance does not increase much more rapidly than the minimum inductance decreases. In fact, when only a few plates are used, the upper frequency limit may increase as the stack height is increased because the minimum inductance decreases more rapidly than the minimum capacitance increases. In general, therefore, increasing the number of plates results in an increase in the tuning range. However, as the stack height is increased, the resonant impedance decreases; also ultimately a point is reached beyond which spurious responses occur in the tuning range (see Sec. 28-13). One or both of these effects place a limit on the stack height for most applications. The unit also becomes more difficult to build as the stack height is increased, because of the larger number of plates and closer tolerances required.

The tuning range of a butterfly also tends to increase proportionately to the diameter because the maximum inductance and capacitance, which determine the low-frequency limit, both increase approximately as the square of the diameter, but the minimum inductance and capacitance, which determine the high-frequency limit, increase slowly with the diameter. Actually if the maximum tuning range free from spurious

<sup>1</sup> *Ibid.*

responses is desired, the optimum diameter is closely related to the top frequency limit and to the plate spacing.

The actual tuning ranges obtainable with butterflies may also be greatly affected by the reactance of the load. In typical cases, however, tuning ratios of 3:1 to 5:1 are usually obtainable in butterfly resonators with typical loads.

The manner in which the resonant frequency varies with angle of rotation in a true butterfly with circular-sector rotor plates similar to the one in Fig. 28-8 is undesirable for many applications, as the rate of change of

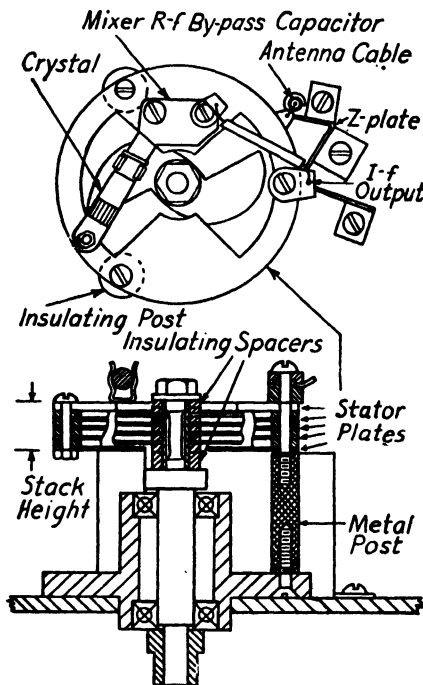


FIG. 28-12.—300- to 1000-Mc true-butterfly preselector.

frequency with rotation over most of the tuning range is very slow except near the upper end of the range, where it increases rapidly. In most applications a semilogarithmic or linear variation in frequency with rotation is desired. Either type of tuning characteristic may be obtained with a true butterfly with circular-sector plates by means of a mechanical compensating device. However, such a device is usually relatively complicated and is a source of added backlash. A simpler solution is to change the shape of the rotor plates to produce the desired frequency variation. The butterfly shown in Fig. 28-12 has rotor plates that produce approximately a logarithmic curve of frequency vs. rotation. A butterfly with shaped rotor plates, however, has a considerably smaller tuning range than a similar butterfly

with circular-sector plates, as the maximum capacitance is less, with the smaller rotor-plate area, and the minimum inductance is larger, as a result of the smaller amount of shielding produced by the rotor at the high-frequency end of the tuning range.

The resonant impedance of a true butterfly with shaped plates is no longer practically constant over the tuning range, but increases as the frequency is increased. Also,  $Q$  does not decrease so rapidly with increasing frequency as in a butterfly with circular-sector rotor plates. The extent of the departure of both resonant impedance and  $Q$  from the characteristics of a butterfly with circular-sector plates depends on the

rotor-plate shape. Therefore a unit designed to cover a specified frequency range with shaped plates is either larger in diameter or greater in height than a unit with circular-sector plates with the same plate thickness and spacing. However, tuning ranges from 3:1 to 5:1 are usually obtainable in units having rotor plates that produce a semilogarithmic variation in frequency with rotation.

The optimum outside diameter of a butterfly depends on many factors, such as the tuning range required, the necessity of the prevention of spurious responses, the impedance of the load, the plate thickness and spacing, the shape of rotor plate, and various mechanical considerations. It is therefore not easy to set up general specifications for the optimum diameter. However, in order to present some information on the order of magnitude of satisfactory diameters for operation at various frequencies, a rough chart of the outside diameter as a function of the top frequency of the tuning range for true butterflies with plates giving a semilogarithmic variation of frequency with rotation is given in Table 28-1. Semibutterfly units have somewhat smaller outside diameters than those given in the chart for true butterflies.

TABLE 28-1.—APPROXIMATE DIAMETERS OF TYPICAL TRUE BUTTERFLIES WITH SEMILOGARITHMIC-FREQUENCY CHARACTERISTICS AS A FUNCTION OF THE UPPER FREQUENCY LIMIT

Upper Frequency Limit, Mc	Approximate Butterfly O.D., In.
300	5½
400	4½
650	3½
1000	2½

**28-10. Butterflies as Radio-frequency Tuners.**—Butterfly circuits possess many characteristics that make them useful as r-f tuners. As mentioned previously, butterflies are best suited for operation at frequencies between about 100 and 1000 Mc. In this frequency range, conventional inductor-capacitor resonators suffer from the difficulties outlined in Sec. 28-7, and, although coaxial-line resonators possess superior electrical characteristics, they are physically large and bulky. At frequencies much lower than 100 Mc, butterflies must be made very large and hence are impractical, since conventional circuits are much smaller and perform satisfactorily. At frequencies much above 1000 Mc the decreasing  $Q$  and increasing number of spurious responses present in units of practical design reduce their usefulness; coaxial-resonant circuits, which at these frequencies are reasonably small, are more desirable. In general, butterfly tuners have the following desirable characteristics:

1. Wide tuning range
2. Absence of sliding contacts

3. Relatively high  $Q$
4. Compact physical size
5. Practically frictionless mechanical drive

As mentioned in Sec. 28-9, tuning ranges covering a 3:1 to 5:1 frequency variation are in general relatively easily obtainable with butterflies.

The only moving element in a butterfly is the rotor, which is insulated from the drive shaft supporting it. In a true butterfly the rotor is approximately at ground potential, and consequently the amount of r-f current flowing through the bearings on the drive shaft is usually negligible. The noise produced by erratic contacts in the bearings when the tuning is changed is therefore also usually negligible. The rotor in a semibutterfly, however, is not at ground potential at all frequencies, and hence better insulation between the rotor and shaft is required to keep the bearing noise at a negligible value.

In coaxial-line resonators, sliding short-circuiting contacts are sometimes used for tuning. This type of contact, however, usually produces noise in the receiver when it is tuned, and the abrasive action on the cylinder walls may in time be a source of trouble. Wide-range coaxial-line resonators with choke plungers or choke joints, which are described in Sec. 28-23 and Chap. 32, do not have sliding contacts, but since they are usually  $\frac{1}{4}$  or  $\frac{1}{2}$  wavelength long at the center of the tuning range, they increase the length of the resonator appreciably and are therefore impractical in the frequency range under consideration.

The unloaded  $Q$  of a butterfly varies appreciably with size and frequency, but in general lies between 200 and 1000. However the unloaded  $Q$  and the  $Q$  of the circuit loaded by a constant resistance *decreases* as the frequency is increased, a variation that is opposite to the variation desired for constant-band-width receivers, since a reduction in selectivity with increasing frequency results.

It has already been pointed out that butterflies are compact in size. A semibutterfly unit covering the frequency range from 100 to 500 Mc is only  $2\frac{1}{2}$  in. in diameter and about 3 in. tall, with the mounting, while a coaxial resonator covering the same frequency range would be about 30 in. long.

In a butterfly, tuning is accomplished by turning the rotor; hence if ball bearings are used in the rotor bearings, the force required to tune the unit can be made very small. The smaller the driving force required, the simpler the drive mechanism required to produce low-backlash tuning. For precise tuning a worm and worm-gear combination can easily be used to obtain a large step down between the knob shaft and the butterfly rotor. Coaxial resonators require a translational motion for tuning,

which in most cases means that a rack and pinion, a lead screw, or linkage mechanism must be used to change the linear motion to rotary motion. If sliding contacts are used, the large driving force required complicates the driving mechanism when precise antbacklash operation is desired.

In general, a tuner used in a tuned r-f amplifier or mixer stage is fed from a low-impedance source, the antenna, and is coupled to a higher impedance source, the grid of a tube or a crystal mixer. The tuner must therefore act also as an impedance transformer. It must have a pass band that is at least as wide as the pass band of the i-f amplifier and an off-frequency attenuation or loss that produces at least the amount of image and harmonic rejection prescribed by the receiver specifications. The maximum usable loaded  $Q$  is determined by the desired width of the pass band, and for any given  $Q$  the image and harmonic rejection can be obtained from the universal curve for a single-tuned circuit given in Fig. 28-2. If the desired attenuation characteristic cannot be obtained from a single-tuned circuit with the specified  $Q$ , it may be possible to use two butterfly circuits in a double-tuned arrangement and hence obtain a greater image and harmonic rejection. However, the design and construction of this type of tuner are much more complicated than those of the single-tuned type.

**28-11. Selectivity and Pass-band Loss.**—In Sec. 28-10 it was mentioned that butterfly resonators have values of unloaded  $Q$  ranging from about 200 to 1000, depending on the design and frequency. These values are less than the  $Q$  of well-designed coaxial resonators, but in many cases, in the frequency range under discussion, wide band width is required in the preselector and, as a result, the loaded  $Q$  must be made relatively low. For instance, if a 2-Mc band width between half-power points is desired over the frequency range from 75 to 300 Mc, the loaded  $Q$  cannot be greater than 37.5 at 75 Mc or greater than 150 at 300 Mc. Consequently, the difference in pass-band loss obtained in using resonators with very high values of  $Q$  and resonators with moderately high values of  $Q$  may be small. The actual pass-band loss of a single-tuned resonator as a function of its loaded and unloaded  $Q$ 's is given by Eq. (28-2) for the case in which the input circuit, usually the antenna, is matched to the preselector with the mixer load connected. Greater pass-band losses will result if the input circuit is mismatched, but the added loss is independent of the relationship between the loaded and unloaded values of  $Q$ .

In Sec. 28-8 it was pointed out that the unloaded  $Q$  of a butterfly decreases slowly as it is tuned to higher frequencies. In most designs the loaded  $Q$  is mainly determined by the equivalent shunt resistance of the antenna and mixer circuits, as a low pass-band loss is desired, and the unloaded  $Q$  is made much larger than the loaded  $Q$ . If the ratio between

the unloaded and the loaded  $Q$  is assumed to be large, the loaded  $Q$  is given by the equation

$$Q = \frac{R_L}{2\pi fL} \quad (28-5)$$

where  $R_L$  is the equivalent resistance of the loads referred to the maximum-impedance points,  $L$  is the inductance of the butterfly, and  $f$  is the frequency. In most cases, the equivalent load resistance can be assumed to be approximately constant over the tuning range (see Sec. 28-12). However,  $L$  decreases relatively slowly with frequency, because of the eddy-current shielding produced by the rotor, and consequently  $Q$  decreases with increasing frequency. Butterflies with shaped plates have a more rapid decrease in  $Q$  with frequency than units with circular-sector plates, since the inductance does not decrease so rapidly. A more uniform loaded  $Q$  could be obtained over the frequency range if the couplings from the input and output circuits to the butterfly were varied with frequency in such a manner that the equivalent  $R_L$  produced between the high-impedance points increased with frequency. Such a change in coupling could possibly be obtained by taking advantage of the change in inductance caused by the rotor, but as yet no attempts have been made to design a unit on this basis.

**28-12. Coupling Methods.**—One of the major difficulties encountered in the design of butterfly tuners is in coupling the input and output circuits to the butterfly in a manner that provides the desired impedance transformation and selectivity between the input and output circuits. In most cases these two circuits should be matched so as to give maximum power transfer and a loaded  $Q$  that produces the required selectivity over the tuning range. Actually, the problem is complicated by the variations with frequency in both input and output loads because of the change in antenna impedance with frequency and the change in mixer impedance with both frequency and local oscillator voltage. In many well-designed systems these variations may be held within reasonable limits. In the following discussion, constant loads will be assumed.

As is shown in Figs. 28-8 and 28-10 and discussed in Sec. 28-8, the only parts of a butterfly that maintain their relative potentials with respect to ground as the butterfly is tuned are the capacitance sections of the stators marked  $X$  and  $Y$  and, in the case of a true butterfly, the center of the rotor. All points on the inductance arms have changing r-f potentials with respect to other parts of the butterfly and ground as the butterfly is tuned. Also, the ratio of the inductance of one segment of an inductance arm to the total inductance varies appreciably as the rotor is turned. It is therefore difficult to couple to the butterfly by direct connection, capacitance coupling, or loops and have the coupling coef-

ficient remain constant over the tuning range. As a result, in units in which a step-up is required from the antenna to the mixer or amplifier stage, the rotor is usually designed to produce only a relatively small amount of eddy-current shielding of the inductance, and the coupling is made near point *D* in Fig. 28-8*a*, where the inductance is the least affected by the rotor. Figure 25-7 roughly illustrates this type of coupling. The antenna is loop coupled to the butterfly, and the output load is a crystal mixer that is connected between one capacitor section of the stator and a point on one of the inductance arms. This coupling system is by no means optimum, as it does not satisfy the conditions required for match-



FIG. 28-13.—75- to 300-Mc semibutterfly preselector.

ing or for optimum  $Q$  over the tuning range, but is a practical compromise that gives fairly good results. Somewhat greater attenuation at frequencies far from resonance could probably be obtained if the mixer were connected on the opposite side of the butterfly from the input loop, as the direct coupling between the antenna and mixer would thus be reduced. Both the antenna and mixer circuits can be loop coupled to the butterfly. For best results the input and output coupling loops should be located on opposite sides of the butterfly.

One method of overcoming the variation in impedance-transformation ratio between the input and output is to use a modified semibutterfly in which the inductance is constant over the tuning range. Such a butterfly is shown in Fig. 28-13. Since the inductance is not decreased as the



resonant frequency is increased in this unit, the maximum tuning range is somewhat less than could be obtained in a standard semibutterfly.

If the off-frequency attenuation is to be made as large as possible, all common impedances between the input and output circuits must be minimized. In an early preselector, Fig. 28-14, the input circuit was

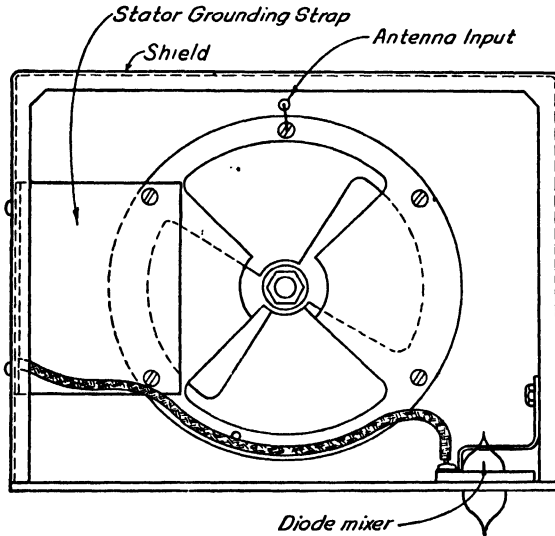


FIG. 28-14.—Early 80- to 300-Mc true-butterfly preselector.

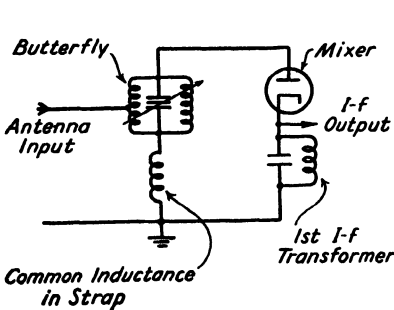


FIG. 28-15.—Equivalent circuit of preselector in Fig. 28-14.

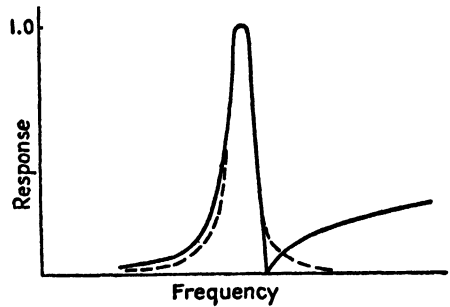


FIG. 28-16.—Selectivity curve of preselector in Fig. 28-14.

connected from the mid-point of the inductance arm to ground, and the mixer was connected from one side of the stator to ground. The opposite stator was grounded by means of an aluminum strap. This strap had a considerable inductance which produced a common impedance in the input and mixer circuits, as shown in the equivalent circuit in Fig. 28-15. The resulting response curve of the preselector is shown in Fig. 28-16. At frequencies below the main butterfly resonance, the relatively large

inductance in series with the butterfly caused the attenuation to be less than that calculated from the  $Q$  of the circuit. At a frequency just above that of the main butterfly resonance frequency, the capacitive reactance of the butterfly resonated with the series inductance of the strap and caused the dip in the response curve shown. At higher frequencies the attenuation became relatively small as the impedance of the combination of the butterfly and strap became relatively large. The performance of this unit was unsatisfactory, as the off-frequency attenuation was much too low. Coupling of this type and other types caused by stray electric and magnetic fields have to be eliminated in order to obtain maximum performance from any preselector.

**28-13. Spurious Responses.**—One undesirable characteristic of some wide-range butterfly resonators for use in preselectors is the presence of spurious responses in the tuning range. Spurious responses are important in preselectors used in superheterodyne receivers as well as in receivers employing the direct-detection principle because mixers in superheterodynes will produce i-f output signals whenever the difference between the frequency of the input signal and any multiple of the local-oscillator frequency is equal to the intermediate frequency. Hence, if the frequencies at which the spurious responses occur are approximately equal to a multiple of the main resonant frequency of the tuner, the attenuation of signals occurring at these frequencies may be very small. The  $Q$  of the circuit in the spurious-response range is approximately of the same order of magnitude as that in the main range, and hence the attenuation may be relatively low over a relatively broad band of frequencies on either side of the spurious resonant frequency.

The most important spurious responses are usually caused by resonances resulting from various current paths through the stacks of rotor and stator plates. In general, their number and amplitudes increase as the stack height is increased. Figure 28-17 shows a plot of the main and spurious responses of a typical true butterfly that has shaped rotor plates and a relatively large stack height. The amplitudes of these responses are appreciably affected by the method of coupling to the butterfly, and the responses usually can be greatly reduced, although not

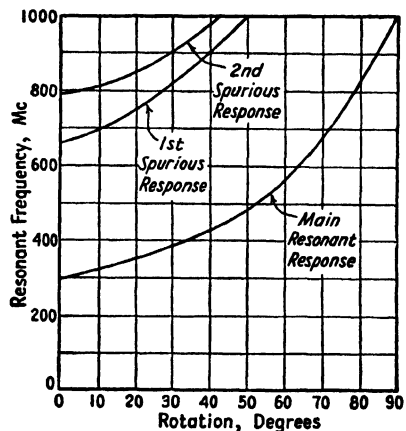


FIG. 28-17.—Spurious modes present in a 300- to 1000-Mc tuner.

completely eliminated, by experimentation with the coupling systems. A more satisfactory method of eliminating these responses is to shift them outside the tuning range and insert a fixed low-pass filter in the input circuit that cuts off at the upper end of the tuning range. The frequency of the spurious responses can be increased by (1) reducing the butterfly stack height with a corresponding increase in the rotor-plate area or butterfly diameter to maintain the desired tuning range, (2) short-circuiting the ends of the rotor plates by means of straps, as shown in Fig. 28-18. The straps are placed in positions in which they do

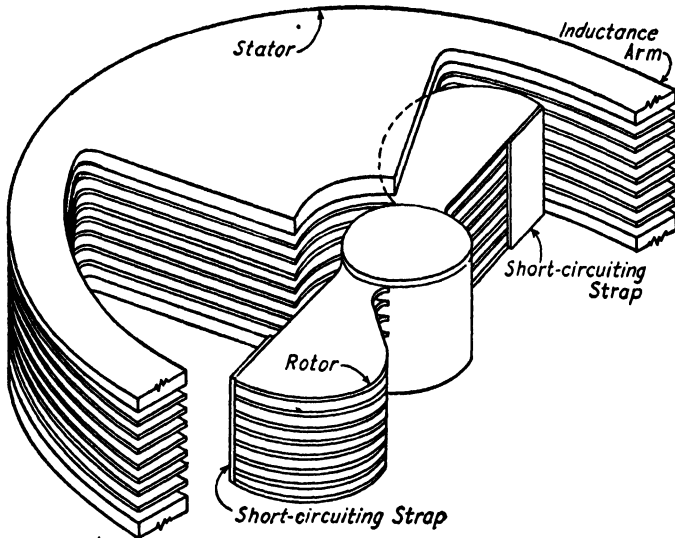


FIG. 28-18.—Butterfly with short-circuiting straps on the rotor plates.

not interfere with the normal 90-deg butterfly rotation required to cover the tuning range.

The spurious responses present in a 300- to 1000-Mc butterfly resonator, the responses of which are plotted in Fig. 28-17, were shifted out of the main-response range by reducing the stack height. The rotor-plate area was increased slightly to maintain the desired tuning range. A sketch of the actual preselector unit with the mixer and input coupling used is shown in Fig. 28-12. In order to find the arrangement that shifted the first spurious response outside the range, the mixer was used as a simple detector, a signal of the same frequency as the upper end of the desired tuning range, 1000 Mc in this case, was fed into the preselector, and the settings of the butterfly were noted at which responses were obtained. The actual main resonant frequencies corresponding to these settings were obtained and the data plotted as a function of number

of rotor plates, as shown in Fig. 28-19. For all stack heights at which the main resonant frequency corresponding to the first spurious response is below the desired low-frequency limit, no spurious responses are present in the desired tuning range.

In this case, 300 Mc was the specified low-frequency limit, and hence stacks having four or fewer rotor plates shift the first spurious response to above 1000 Mc. The curve of minimum resonant frequency shows, however, that the butterfly did not tune quite down to 300 Mc. In order to extend the low-frequency limit to at least 300 Mc, the rotor plate area was increased slightly. This increase had very little effect on the frequencies at which the spurious responses occurred. Figure 28-19 also shows the amplitude of the spurious responses as a function of stack height for the coupling arrangement used. In this case the amplitudes decreased very rapidly with decreasing stack height and were very small for the final design, which had four rotor plates.

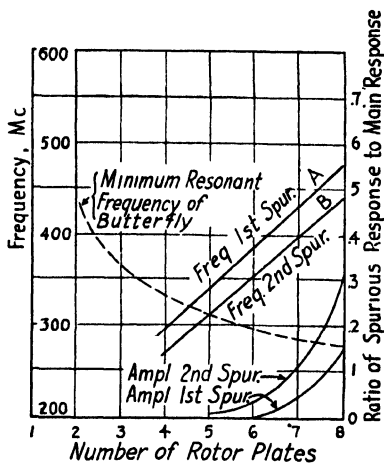


FIG. 28-19.—Amplitude and frequency of spurious responses as a function of stack height: curve A, frequency of main resonance when first spurious response is at 1000 Mc; B, frequency of main resonance when second spurious response is at 1000 Mc.

#### 28-14. Examples of Butterfly Tuner Design.

*Example 1:* Tuner for a superheterodyne receiver.

Specifications:

Frequency range: 75 to 300 Mc

Band width: At least 1 Mc

Use: Tuned mixer circuit

In this case a modified semibutterfly  $4\frac{1}{2}$  in. in diameter was used in which the inductance remained constant over the band in order to obtain as good an impedance match as possible between the input circuit and the tuner over the tuning range. A picture of this unit appears in Fig. 28-13. One capacitor section of the stator was grounded through low-inductance straps in order to keep all common couplings at a minimum. The mixer was connected directly across the maximum-impedance points of the butterfly, since in this position connections could be made with very short leads, and direct coupling between the input circuit and the mixer kept very small. The equivalent resistance of the mixer was made high enough to make the loaded  $Q$  at the low-frequency end of the tun-

ing range the required value for the band width desired. The method of varying the equivalent resistance of the mixer is discussed in Sec. 29-12. In this circuit the inductance was 0.040  $\mu$ h and the maximum capacitance 112  $\mu$ mf. The required effective load resistance  $R_{ah}$  was found from the equation

$$R_{ah} \approx 2\pi f L Q = 2\pi f L \frac{f}{\Delta f}$$

where  $f$  is the lowest operating frequency, 75 Mc, and  $\Delta f$  is the desired band width, 1 Mc. The desired total load resistance calculated from the equation was 1400 ohms. As is evident from the above equation, the loaded  $Q$  of the butterfly with a constant load and constant inductance is inversely proportional to frequency. The  $Q$  at 75 Mc is

$$Q = \frac{f}{\Delta f} = \frac{75}{1} = 75$$

The corresponding loaded  $Q$  at 300 Mc is only 19. This means that if the tuner is used in a superheterodyne receiver having an intermediate frequency of 30 Mc, and the local-oscillator frequency is above the signal frequencies, the image rejection will be 40.5 db at 75 Mc and only 18.3 db at 300 Mc, as determined from Fig. 28-2.

*Example 2: Tuner for a superheterodyne receiver.*

Specifications:

- Frequency range: 300 to 1000 Mc
- Band width: At least 2 Mc
- Use: Tuned mixer circuit

The 2½-in. diameter true butterfly shown in Fig. 28-12, whose spurious response characteristics were discussed in Sec. 28-13, was chosen for this application. In the figure the butterfly is shown tuned to the upper limit of the desired tuning range.

In order to meet the band-width specification, the loaded  $Q$  at 300 Mc, the low-frequency end of the tuning range must be less than

$$Q = \frac{f}{\Delta f} = \frac{300}{2} = 150$$

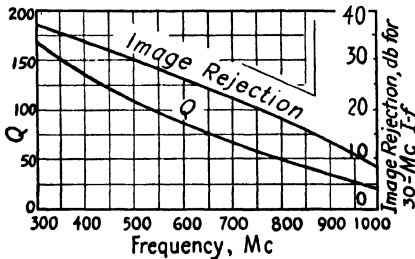


FIG. 28-20.—Loaded  $Q$  and image rejection of the tuner shown in Fig. 28-12.

in the local-oscillator voltage applied to the mixer. Figure 28-20 shows the loaded  $Q$  and the image rejection as a function of frequency for a 30-Mc intermediate frequency.

The butterfly acted as both an impedance transformer and a tunable filter between the antenna input circuit and the crystal mixer. The center conductor

of the antenna cable was directly connected to the butterfly inductance arm, and the outer conductor was connected by means of a low-inductance Z-plate to the center of the inductance arm, as shown in Fig. 28-12. The center of the inductance arm was also connected to ground by a metal post. The Z-plate reduced the self-inductance of the input circuit. The crystal mixer was connected from one stator plate to a tap on the opposite inductance arm, instead of directly across the opposite stator sections, in order to increase the loaded  $Q$  and hence the selectivity of the circuit.

*Example 3:* Tuner for direct-detection receiver.

Frequency range: 100 to 1000 Mc

Since it was not practical to cover this whole frequency range with one butterfly unit, two units were used, each mounted in a separate shielded box. One was a  $4\frac{1}{2}$ -in. true butterfly that tuned from 100 to 400 Mc and the other a  $2\frac{1}{2}$ -in. true butterfly that tuned from 400 to 1000 Mc. The tuning range of the butterflies had to be sacrificed in order to produce a linear frequency variation with rotation, which required the use of plates having only a very small area compared with the maximum obtainable in the size of butterfly used.

Each butterfly had a crystal detector mounted directly across its high-impedance points, and the antenna was directly tapped to the center of the inductance leg. Spurious responses were eliminated by proper adjustment of the coupling. It was found that the spurious responses could be reduced to a very low value if the antenna tap was placed exactly at the center of the stack.

**28-15. Double Butterfly.**—If greater image and harmonic rejection are desired than is obtainable with single butterflies, it is possible to couple two butterflies loosely to form a double-tuned circuit. In this way the image rejection can be increased greatly without reducing the width of the pass band. Very little work has been done along these lines, and no complete model has been built. The two main problems are (1) keeping the two butterflies tuned to the same frequency or frequencies differing by the desired amount over the band, (2) designing a mutual coupling system that will provide the correct coefficient of coupling at each point in the range.

Frequency tracking can be accomplished by bending stator plates on one of the units if the butterflies are mounted either coaxially on the same shaft or side by side with their shafts geared together. If the units are mounted side by side or coaxially on different shafts, tracking can be accomplished by using an adjustable cam system for controlling the relative angular positions of the two shafts.

It probably is possible to design a coupling system that will provide the desired coupling over a fairly wide range by combining both electric and magnetic coupling. However, the changes in inductance caused by the rotor blades complicate this problem.

**28-16. Mechanical Design.**—Most types of butterflies should not be much more difficult to build in production than ordinary variable air capacitors, and the same manufacturing techniques can be applied. In

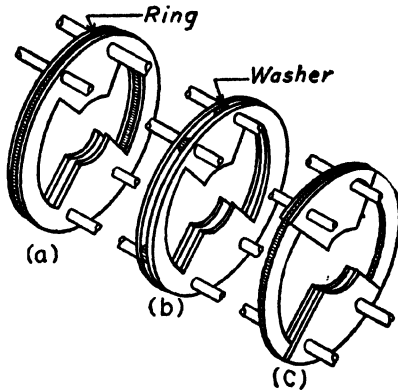


FIG. 28-21.—Three types of butterfly construction.

experimental work, however, it is convenient to build up a unit using alternate plates and spacers, since they can be changed easily. However, in this type of construction, the thicknesses of the plates and spacers must be held to very close tolerances or selective assembly used, as the inaccuracies in thicknesses are cumulative. For experimental purposes three different types of stator construction have been used, and examples of each are shown in Fig. 28-21. The three differ electrically only slightly, type *a* being somewhat superior.

Two types of insulated shafts are shown in Fig. 28-22, one a ceramic shaft and the other a steel shaft with insulating spacers. The type using the steel shaft is the strongest mechanically but has a lower impedance to ground, and in some applications at high frequencies,

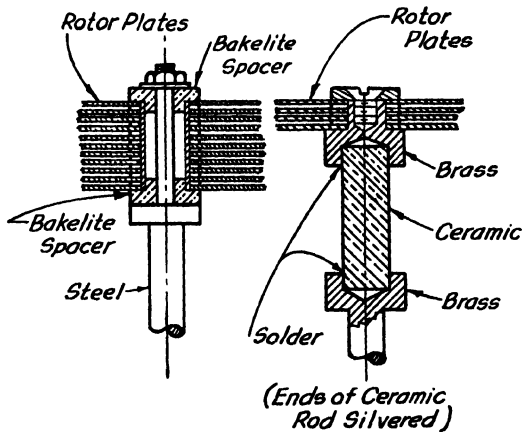


FIG. 28-22.—Two types of insulated rotor shafts.

particularly in semibutterflies, resonances, or even the reactance of the shaft alone, may be a source of trouble. For maximum stability and resettability, the rotor shaft should run in ball bearings. When such high accuracy is not required, other types of bearings are satisfactory.

It has been found very advantageous to mount the entire butterfly unit on a separate casting, as shown in Fig. 28-12, as the entire unit can be assembled and tested before it is mounted in its permanent position. Replacement and servicing also are simplified through the use of this type of construction.

**28-17. The Coaxial Cavity as a Radio-frequency Tuner.**—The resonance properties of short-circuited and open-circuited transmission lines are well known.<sup>1</sup> The theory of resonant coaxial lines will therefore be reviewed only briefly. Figure 28-23 shows the voltage and current distribution along the lines for  $\frac{1}{4}$ -,  $\frac{1}{2}$ -,  $\frac{3}{4}$ -wavelength resonance. In each case the line is short-circuited at the left end. For lines an odd number of quarter wavelengths long, the right end is open-circuited. For lines an even number of quarter wavelengths long, the right end is short-circuited. By a short circuit is meant a termination by an imped-

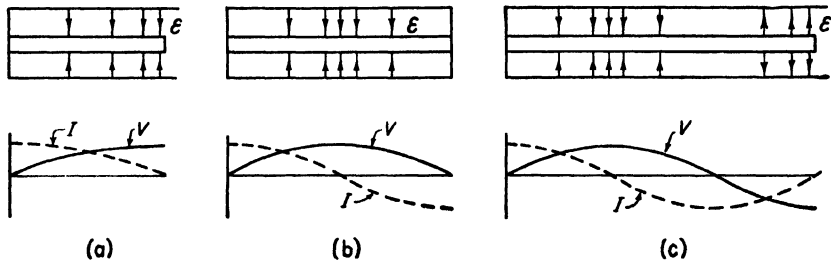


FIG. 28-23.—Approximate voltage and current distribution in (a) a quarter-wave, (b) a half-wave, and (c) a three-quarter-wave resonant coaxial line. The field strength  $\epsilon$  is also indicated.

ance very small in comparison with the characteristic impedance of the line. By an open circuit is meant a termination by an impedance very large in comparison with the characteristic impedance of the line. The frequency of resonance is given by

$$f = \frac{3(10)^{10}n}{4l} \tag{28-6}$$

where  $n$  is the number of quarter wavelengths along the line at the resonant frequency  $f$  and  $l$  is the line length in centimeters. In an r-f tuner, a line is ordinarily used at its lowest possible, or fundamental, resonance, in order to have the greatest possible resonant-frequency separation. With a quarter-wave line, the closest resonant frequencies to the fundamental occur at three, five, seven, etc., times the fundamental frequency. With a half-wave line, they occur at two, three, four, etc., times the fundamental. A quarter-wave resonant line therefore gives greater separation of the higher resonant frequencies from the fundamental.

<sup>1</sup> SLATER, J. C., "Micro-wave Transmission," Chap. 1, McGraw-Hill Book Company, Inc., New York, 1942.



The *unloaded*  $Q$  of a resonant coaxial cavity  $Q'$  is an important consideration in the design of an r-f tuner. As shown by Eq. (28-2), the unloaded  $Q$  of a single resonant cavity must be ten times the  $Q$  of the cavity loaded by the input and output coupled impedances in order that

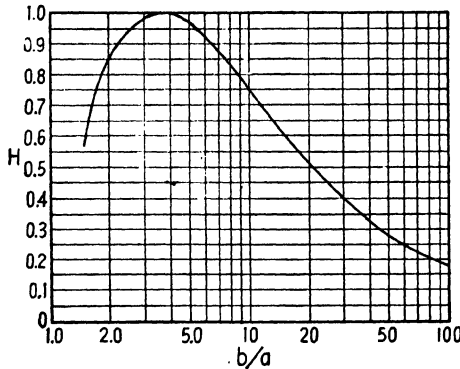


FIG. 28-24.—Factor  $H$  used with Eq. (28-7) in calculating the unloaded  $Q$  of a resonant coaxial line. (From F. E. Terman, "Radio Engineers Handbook," Fig. 53, p. 192.)

the insertion loss of the cavity may not be over 1 db. The following formula gives the theoretical  $Q$  of an unloaded copper coaxial cavity.<sup>1</sup>

$$Q' = 0.0839 \sqrt{f} \cdot bH \tag{28-7}$$

where  $H$  is a factor given by Fig. 28-24,  $f$  is the frequency in cycles per second,  $b$  is the radius of the outer conductor in centimeters. For a

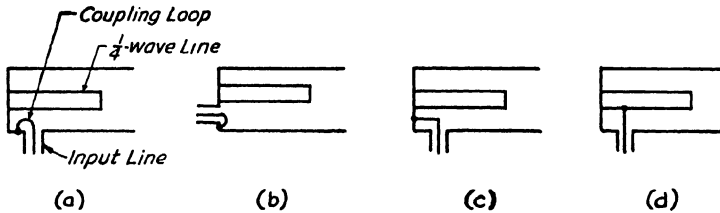


FIG. 28-25.—Magnetic coupling to a coaxial cavity.

cavity made of a *nonmagnetic* metal other than copper,  $Q'$  must be multiplied by the factor  $\sqrt{\sigma/\sigma_c}$ , where  $\sigma_c$  is the conductivity of the copper and  $\sigma$  is the conductivity of the other metal. At a given frequency the unloaded  $Q$  of a coaxial cavity of a given outer radius is a maximum for  $b/a$  equal to 3.6, a ratio that corresponds to a characteristic impedance of 77 ohms. Figure 28-24 indicates, however, that for values of  $b/a$  between 2 and 7.5, the unloaded  $Q$  is reduced by not more than 15 per cent. This range

<sup>1</sup> Equation (28-7) and Fig. 28-24 are taken from Terman, *op. cit.*, p. 192.

in  $b/a$  corresponds to a range in characteristic impedance of 42 to 121 ohms. In designing a coaxial tuner, the ratio of  $b/a$  chosen will depend more on other considerations than on attaining a slight increase in  $Q$ . It should be remembered that Eq. (28-7) assumes the ideal case of pure metal with perfectly smooth walls and neglects losses in the short-circuiting connections required at one or both ends of the cavity. In practice, the unloaded  $Q$  will generally be somewhat less than the value given by Eq. (28-7).

The tuned cavity may be loaded in many ways, some of which are shown in Fig. 28-25. Although a quarter-wave resonant line is used in Fig. 28-25, the coupling method is similar for a line any number of quarter wavelengths long. Since all the examples in Fig. 28-25 use magnetic (or current) coupling, these coupling devices are most effective near the short-circuited, or high-current, end. In electric (or voltage) coupling, shown in Fig. 28-26, the coupling devices are located an odd number of quarter wave-

lengths from a short-circuited end, in a region of intense electric field. Magnetic coupling has been used more extensively than electric coupling.

There is a useful relation between the  $Q$  and the load resistance. The  $Q$  of a resonant circuit or cavity is given by Eq. (28-1). The total stored energy in a resonant coaxial cavity is equal to  $I_1^2 Z_0 n / 8f$ , where  $I_1$  is the rms current at the short-circuited end,  $Z_0$  is the cavity characteristic impedance,  $n$  is the number of quarter wavelengths along the cavity, and  $f$  is the frequency, all expressed in mks units. Therefore

$$Q = \frac{2\pi f I_1^2 Z_0 n}{\text{average power dissipation}} \tag{28-8}$$

If the external loading is to be preponderant over the internal dissipation of the cavity the total loss is  $I^2 R$ , where  $R$  is the equivalent load resistance acting in the resonant cavity, and  $I$  is the current associated with this value of  $R$ . For most kinds of coupling used in coaxial cavities, the manner of specifying the proper current and resistance to be used is a matter of definition. In a high- $Q$  circuit the loading may be assumed to be concentrated at any desired part of the circuit, but the proper value of  $R$ , corresponding to the associated  $I$ , must be used.

Since the loading may be assumed to be anywhere in the cavity, it will be most convenient to assume it to be concentrated at the short-circuited end and to consist of a resistance  $R$ , offered to the total current

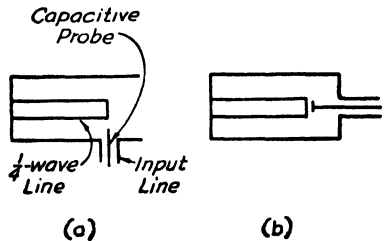


FIG. 28-26.—Electric coupling to a coaxial cavity.

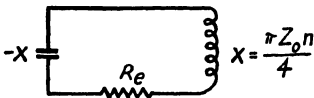
$I_1$  at that part of the coaxial line. Equation (28-8) then becomes

$$Q = \frac{\pi Z_0 n}{4R_e} \tag{28-9}$$

This formula assumes  $Q'$ , the unloaded  $Q$ , to be infinite. If  $Q'$  is not large enough to be ignored, the following exact equation may be used:

$$Q = \frac{\frac{\pi Z_0 n}{4R_e} Q'}{\frac{\pi Z_0 n}{4R_e} + Q'} \tag{28-10}$$

Equation (28-9) provides several useful and basic facts about loaded



$$Q = X / R_e$$

FIG. 28-27.—Approximate equivalent circuit for a resonant coaxial cavity loaded by an equivalent resistance  $R_e$  in series with the short-circuited end of the cavity.  $Q = X/R_e$ .

cavities. (1) The loaded  $Q$  is proportional to the number of quarter wavelengths in the cavity. (2) The loaded  $Q$  is proportional to the characteristic impedance of the cavity. (3) The  $Q$  is inversely proportional to the equivalent load resistance in series with the maximum current  $I_1$ . All these parameters may be used, therefore, in obtaining the desired  $Q$  and, hence, the desired band width.

A useful equivalent circuit may now be deduced from Eq. (28-9). In terms of the resonant circuit shown in Fig. 28-27,  $Q = X/R_e$ . Comparison with Eq. (28-9) shows that, as far as the loading of the cavity is concerned, the coaxial cavity is equivalent at resonance to an inductance  $L = \pi Z_0 n / 4\omega$  in series with a capacitance  $C = 4 / \omega \pi Z_0 n$  and the equivalent load resistance  $R_e$ .

When the cavity is used as a tuner, two distinct coupling devices are needed, one for the ingoing signal, the other for the outgoing signal (Fig. 28-28). If their equivalent resistances, referred to the maximum current  $I_1$ , are  $R_{e1}$  and  $R_{e2}$ , the total loading is given by the sum of these resistances. In other words,  $R_e = R_{e1} + R_{e2}$  must be used in Eq. (28-9) and Fig. 28-27. If  $R_{e1}$  is the equivalent generator impedance and  $R_{e2}$  the equivalent load impedance, these resistances must be equal for a perfect match in the single cavity tuner.

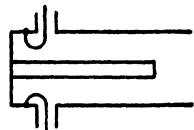


FIG. 28-28.—A coaxial cavity having an input loop and an output loop.

Loop coupling is generally used in single-cavity tuners. As shown in Fig. 28-28, the input and output loops should be separated as far as possible so that direct magnetic coupling between them is negligible. If the loops are located on opposite sides of the coaxial center conductor,

the direct mutual coupling will usually be sufficiently small. A perfect match at the resonant frequency may always be obtained if the input and output loops have the same size and shape and are located at points of equal intensity. Usually, the effect of self-inductance of the coupling loops is merely to shift the resonant frequency slightly.

**28-18. Coupling Problems in a Coaxial Cavity.**—In practice the cut-and-try method of adjusting the coupling loops has been found to give the desired tuner characteristics quite readily. The universal response curves of Secs. 28-4 to 28-6 (Figs. 28-4 to 28-7) serve as one valuable guide; the following derivation will serve as another.

Let the resonant cavity and coupling loop of Fig. 28-29a be represented by the equivalent circuit of Fig. 28-29b. The equivalent generator driving the loop has an internal voltage  $E$  and an internal resistance  $R_g$ . The mutual impedance between the parallel resonant circuit and the coupling loop may be calculated from the following equation:

$$Z_M = \frac{E}{I_1} \quad (28-11)$$

where  $E$  is the emf induced in the open-circuited loop by the field due to the current  $I_1$  at the short-circuited end of the line. This emf is equal to  $jA\mu_0\omega\mathcal{H}$ , where  $A$  is the loop area,  $\mu_0 = 4\pi(10)^{-7}$  henry per meter,  $\omega$  is the angular frequency, and  $\mathcal{H}$  is the mean value of the magnetic field passing through the loop at right angles to the plane of the loop, expressed in mks units. For an ideal resonant coaxial line, in which end effects and other field disturbances are neglected, the magnetic field at any point determined by the radius  $r$  and the electrical length  $\theta = 2\pi fx/v$  at resonance (see Fig. 28-29a) is given by

$$\mathcal{H} = \frac{I_1}{2\pi r} \cos \theta \quad (28-12)$$

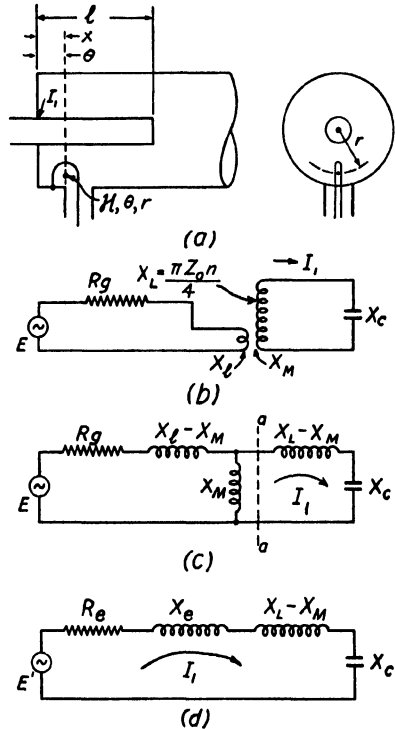


FIG. 28-29.—A coaxial cavity loaded by a single loop. Several forms of the equivalent circuit for this cavity are shown in (b), (c), and (d).

Therefore

$$Z_M = j \frac{A\mu_0\omega \cos \theta}{2\pi r} \quad (28-13)$$

or

$$X_M = \frac{A\mu_0 f \cos \theta}{r} \quad (28-14)$$

where  $r$  and  $\theta$  are the coordinates of the effective center of the loop. The equivalent inductive reactance of the cavity at resonance, referred to  $I_1$ , was shown in Sec. 28-17 to be independent of frequency, and is equal to

$$X_L = \frac{\pi Z_0 n}{4}$$

The circuit of Fig. 28-29*b* is equivalent at all frequencies to that of Fig. 28-29*c*. This circuit is in turn equivalent at a *single* frequency to that of Fig. 28-29*d*, where  $E'$ ,  $R_e$ , and  $X_e$  are determined by Thevenin's theorem from the part of the circuit to the left of the dashed line  $a-a$  in Fig. 28-29*c*. We may assume circuit 28-29*d* to be an accurate representation of 28-29*c* over a narrow frequency band. The circuit  $Q$  may now be easily calculated as the total inductive reactance at resonance divided by  $R_e$ . Although  $X_e$  and  $X_M$  will have a slight effect on the resonant frequency of the circuit, they are usually small enough to be neglected in calculating the loaded  $Q$  of the cavity. By applying Thevenin's theorem,  $R_e$  is found to equal  $(X_M)^2/R_0$ , for small  $X_i$  and  $X_M$ . The circuit  $Q$  for a coaxial tuner loaded by one loop may therefore be expressed as

$$Q = \left( \frac{\pi Z_0 n}{4} \right) \left( \frac{r^2 R_0}{A^2 \mu_0^2 f^2 \cos^2 \theta} \right) \quad (28-15)$$

For a *single-cavity matched tuner*, two loops are used. The effective series resistance offered to the current  $I_1$  is equal to  $2R_e$ , and therefore the  $Q$  may be expressed as

$$Q = \left( \frac{\pi Z_0 n}{8} \right) \left( \frac{r^2 R_0}{A^2 \mu_0^2 f^2 \cos^2 \theta} \right) \quad (28-16)$$

Since the 3-db band width  $\Delta f$  is equal to  $f/Q$  for a single-cavity tuner, we may write the band width as

$$\Delta f = \frac{8A^2 \mu_0^2 f^3 \cos^2 \theta}{\pi Z_0 n r^2 R_0} \quad (28-17)$$

The last equation (expressed in mks units) gives, subject to the assumptions made in its derivation, the band width of a single coaxial-cavity tuner loaded by equal input and output loops projecting into the cavity at points of equal field strength. A number of valuable deductions

may be gained from this equation: (1) If the loop is small enough so that it can be considered to be entirely at the short-circuited end of the cavity, the band width increases as the cube of the frequency. (2) The variation with frequency of the band width depends only on the product

$$f^3 \cos^2 \theta = f^3 \cos^2 (2\pi f x/v),$$

which can be made to vary with frequency in many ways, as shown in Fig. 28-30. (3) For a given location of the loops, the band width varies as the square of their areas, and inversely as the square of the radii of their effective center points. (4) For a given set of loops and a given

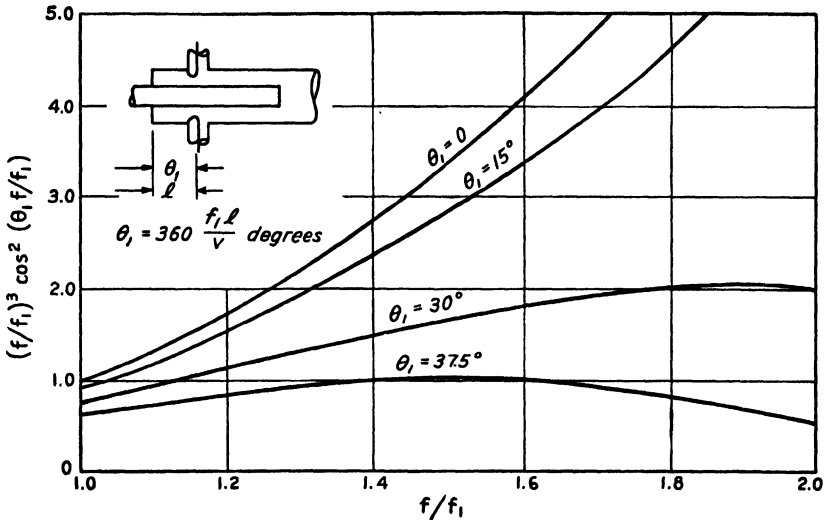


FIG. 28-30.—Variation of band width with frequency for a single coaxial tuner. The curves show effect of spacing of loop from short-circuited end of cavity.

cavity outer diameter, the band width varies inversely as the characteristic impedance of the coaxial cavity.

Although a number of important assumptions were made in the derivation of the band-width formula, this formula will apply roughly to most practical coaxial-cavity tuners loaded by loops, and the deductions obtained from the formula will provide valuable guideposts in the empirical design of single-cavity coaxial tuners.

In actual practice, a certain amount of electric coupling will be combined with the magnetic coupling of the loop. This is due to the fact that the loop projects into the cavity and some electric field lines will terminate on the loop. If the loop is large, the amount of electric coupling may be quite appreciable. If the loop is small, however, and is located at the short-circuit point in the cavity, there will be negligible electric field near the loop and hence negligible electric coupling.

**28-19. Coupling-loop Construction.**—The total inductance of a coupling loop is equal to the mutual inductance between the loop and the

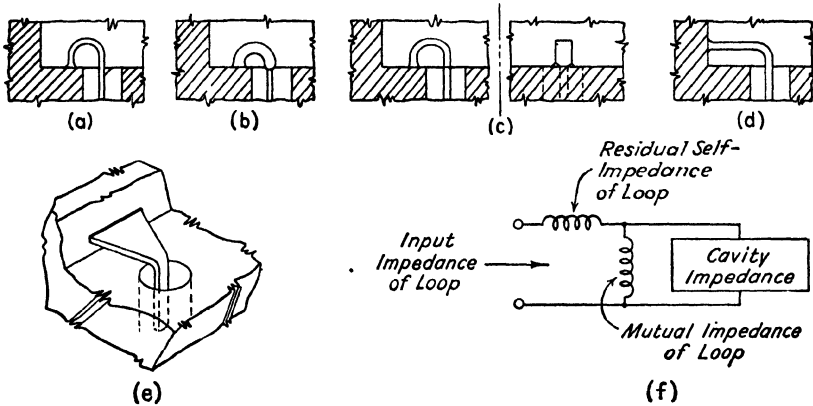


FIG. 28-31.—(a) A simple coupling loop; (b), (c), (d), and (e) more complex types of loops; (f) equivalent circuit of the loop and cavity.

cavity plus the residual self-inductance of the loop (Fig. 28-31f). The cavity will tune out the self-inductance of the loop at the over-all resonant frequency, but, since the cavity must be detuned slightly from its unloaded resonant frequency in order to counteract the loop self-reactance, the tuning curve will be affected. In certain tuners, such as three-cavity tuners, in which tracking of the cavities is a serious problem, it is desirable to make the self-inductance of the loop as small as possible. Several ways of doing this will be discussed.

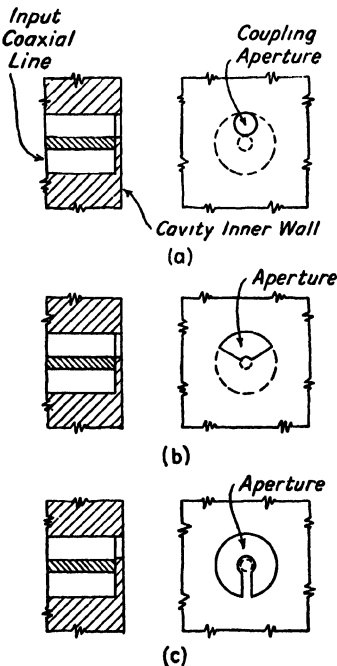


FIG. 28-32.—Aperture type of coaxial-line-to-cavity coupler.

and a cavity. This type has almost zero self-inductance and, in this

Figure 28-31a shows an ordinary coupling loop. By using heavier wire as in Fig. 28-31b, or by using flat strip as in Fig. 28-31c, the self-inductance will be reduced. By using the corner of the cavity, as in Fig. 28-31d, the self-inductance may be reduced still more. A fan-shaped loop as in Fig. 28-31e provides still less self-inductance.

In Fig. 28-32 is shown an aperture type of coupling between a coaxial line

respect, is far superior to those of Fig. 28-31. It has the further advantage that the structure is flush with the cavity wall and, hence, has a minimum effect on the cavity field pattern and tuning curve. Because of these properties, this type of coupling has been found very useful in three-cavity tuners (see Fig. 28-41).

**28-20. Short-circuiting Devices.**—In the discussion of resonant coaxial cavities, a good short circuit between the inner and outer conductors was assumed at one or both ends of the cavity. The practical problem of attaining an acceptable short circuit is complicated by several factors: (1) In the odd-quarter-wavelength line, the short circuit must not interfere with the tuning motion of the inner conductor. (2) In the even-quarter-wavelength line, although one short circuit may be obtained by a rigid soldered joint, the other must be provided by a *freely moving* conducting plunger. This plunger must provide a very low-impedance path between the inner conductor and the outer conductor. (3) In a wide-tuning-range receiver, a very large number of mechanical tuning cycles must be expected during the life of the receiver. The short-circuiting joints must not wear appreciably during this time. (4) For most receiver tuning applications it is important to prevent tuning noise caused by a poorly designed short-circuiting joint. (5) The friction in the tuning mechanism must be small so that the mechanical drive may be easily built without excessive backlash. (6) The loss in the short-circuiting device must remain very low during the life of the receiver. The loss generally increases with wear.

Three basic types of short-circuiting joints have been used at the Radio Research Laboratory. These are the *metal-to-metal*, or *finger joint*; the *high-capacitance*, or *low-impedance joint*; and the *choke joint*. They will be discussed in the following sections.

**28-21. The Metal-to-metal Joint.**—The *metal-to-metal joint* is illustrated in Fig. 28-33. For best results, the fingers should extend as far as possible, up to  $\frac{1}{4}$  wavelength, from the plate to which they are attached. Since the cavity current is a maximum at the plate, and zero  $\frac{1}{4}$  wavelength from it, the use of fingers  $\frac{1}{4}$  wavelength long places the actual finger contacts at a point of lower current along the cavity wall, with the result that losses and tuning noise are less than if the finger contacts were very short. In practice, the fingers will generally have to be somewhat shorter than  $\frac{1}{4}$  wavelength even at the highest frequency in the tuning range, and therefore a really good compromise on finger length is not possible over the entire range. In general, finger contacts have thus far proved unsuccessful in wide-range receivers from the standpoints of noise, wear, and friction.

**28-22. Low-impedance Joint.**—The *low-impedance short-circuiting joint* has worked successfully in single-cavity tuners. In this type of



joint, shown in Fig. 28-34, the center conductor is supported by a non-metallic bushing, since a metallic bushing would short-circuit the low-

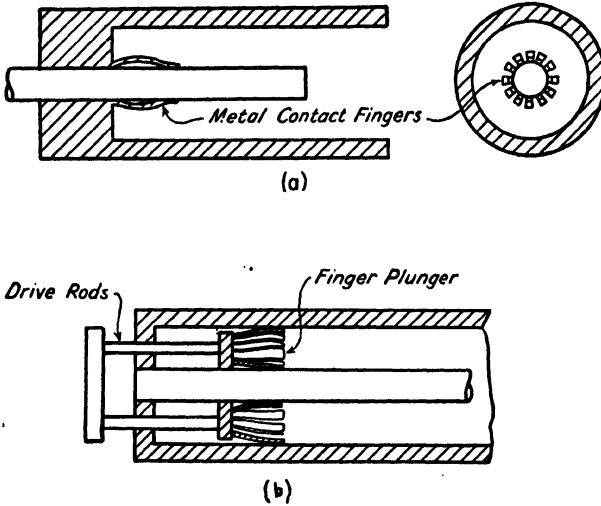


FIG. 28-33.—Finger short-circuiting joint: (a) contact to movable center conductor; (b) contact to fixed inner and outer conductors by movable finger plunger.

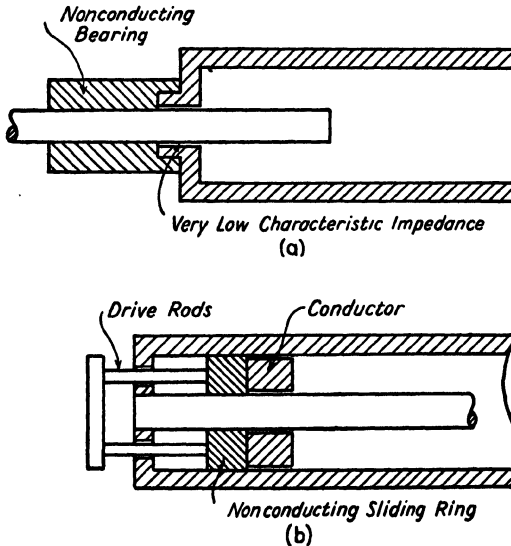


FIG. 28-34.—A short-circuit path through a low-impedance line: (a) movable center conductor; (b) movable short circuit.

impedance line and would cause considerable tuning noise and probably introduce appreciable loss. The coaxial cavity is terminated by the input impedance of this low-impedance line, which itself is terminated by virtu-

ally an infinite impedance. Since an open-circuited line has an input reactance equal to  $-jZ_0 \cot(2\pi l/\lambda)$ , the input impedance of this short-circuiting section will be zero when its length is  $\frac{1}{4}$  wavelength and infinite when its length is zero or any number of half wavelengths. For best results, therefore, the length of this line should be  $\frac{1}{4}$  wavelength at the average frequency of the tuning range. For example, for a tuning range from 1000 to 3000 Mc, the average frequency is 2000 Mc, and therefore the length of the low-impedance line should be  $\frac{1}{4}$  wavelength at that frequency. The reactance formula shows that for this case the input reactance of the short-circuiting line will be just equal to its characteristic impedance at the extreme edges of the band and less everywhere between. Since clearance between the inner and outer conductors may perhaps be as small as 0.005 in., the characteristic impedance for a line  $\frac{1}{2}$  in. in diameter can be made as low as about 1 ohm. This provides a good short-circuit for the usual single-cavity tuner, and good results are obtainable over even a wider range of wavelengths, or for a short-circuiting line somewhat less than  $\frac{1}{4}$  wavelength long at the highest frequency. If the length of the line is less than  $\frac{1}{8}$  wavelength at the highest frequency in the tuning range, the low-impedance line may be thought of as a large lumped capacitance.

Although satisfactory for most single-cavity applications, this low-impedance joint has the disadvantage that signals can leak through it into or out of the cavity. This might result in undesired pickup of strong fields in the vicinity of the receiver. With two or more coupled cavities with ganged tuning motion, this simple type of short-circuiting joint has the further disadvantage that it provides an uncontrolled alternate coupling path between the cavities. Because of the possibility of resonance in the ganging mechanism, this type of joint has not proved to be satisfactory in multiple-cavity tuners.

**28-23. The Choke Joint.**—The most satisfactory short-circuiting device from all standpoints except added complexity is the double- $Z_0$  section, also known as the *choke joint*. Figure 28-35 shows two choke joints, one a short-circuiting joint to the center conductor, the other a choke plunger that provides low-impedance paths to both the inner and outer conductors. The operation and design of this type of joint are covered in detail in Chap. 32 on coaxial oscillators. For that use, the choke-joint plungers required are often so large that they are subject to higher mode resonances of the waveguide type, as explained in that chapter. These may cause excessive loss, pass-band distortion, and tuning-curve kinks. None of these higher modes will resonate in the tuning range, however, if the maximum circumference of each part of the choke joint does not exceed approximately  $\frac{9}{10}$  wavelength at highest operating frequency. Since this condition can usually be met readily

in tuners, the design of a choke plunger for a tuner is a much simpler problem than for an oscillator. If necessary, the circumference limitation can often be exceeded to some extent, as is explained quantitatively in Chap. 32.

The choke joint provides a low-impedance short-circuiting path over a very wide frequency band. It can be designed to work very well over a

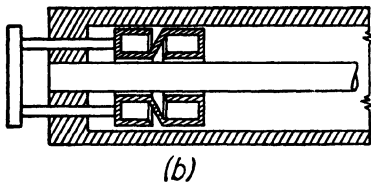
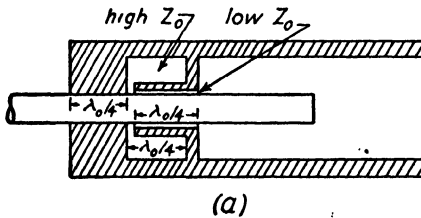


FIG. 28-35.—The choke joint in a coaxial-line cavity: (a) a low-impedance short-circuiting joint to the center conductor; (b) a double choke-joint plunger.

5:1 or 6:1 tuning range. Since up to now the requirement has been for tuners with only about a 2:1 range, the design problem becomes very simple.

The choke joint may be designed as follows. At the average frequency of the tuning range, the low-impedance and high-impedance sections of line are each made  $\frac{1}{4}$  wavelength long. The characteristic impedance of the low-impedance line should be made as small as possible, and the characteristic impedance of the high-impedance line should be made as high as possible. Mechanical-construction problems will provide the limitations on these values.

The working-model sketches in the following sections will provide a further guide. For exact design, Chap. 32 should be consulted.

**28-24. Spurious Responses in Coaxial Cavities.**—It was pointed out in Sec. 28-17 that a quarter-wave resonant coaxial cavity will have higher resonances at odd multiples of the fundamental frequency and that a half-wave resonant coaxial cavity will have higher resonances at all multiples of the fundamental frequency. Besides these usual responses, a coaxial line can also have waveguide-mode resonances, which can cause spurious tuner responses. This phenomenon is described in Chap. 32. The cutoff frequency of the lowest possible waveguide mode occurs very nearly at the frequency at which the average circumference in the coaxial cavity is equal to a space wavelength, *i.e.*, at which the space wavelength in centimeters is equal to  $\pi(a + b)$ , where  $a$  and  $b$  are the radii of the inner and the outer conductor, respectively, in centimeters. Spurious responses due to these higher order transmission modes will therefore not occur below this frequency, and it is usually a simple matter to dimension the tuner cavity so that these spurious responses will occur above the tuning range of the cavity.

**28-25. Coupling between Coaxial Cavities.**—In multiple-cavity tuners, it is necessary to provide a mutual reactance of proper magnitude between adjacent cavities in order that energy can be transferred from one to the other. The effect of the magnitude of this coupling reactance has been explained in Secs. 28-5 and 28-6. Loops and apertures have proved to be practical coupling devices between resonant cavities (see

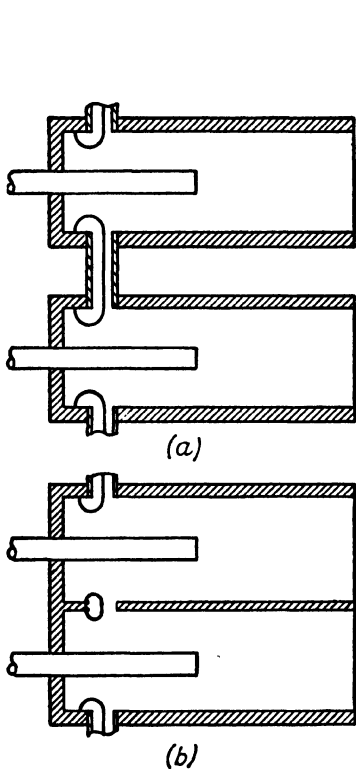


FIG. 28-36.—Loop coupling between two coaxial cavities: (a) connection through a coaxial line; (b) connection through a line of minimum possible length.

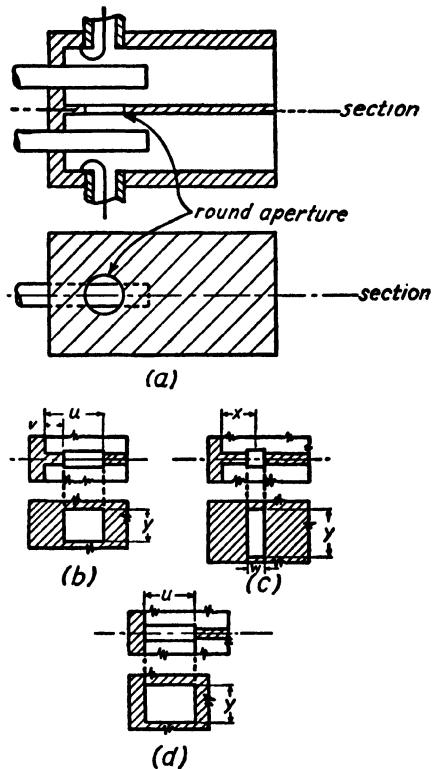


FIG. 28-37.—Aperture coupling between two coaxial cavities. Various aperture shapes are shown in (a), (b), (c), and (d).

Figs. 28-36 and 28-37). Two loops and a length of connecting line are shown in Fig. 28-36a. For use over a wide tuning range, the connecting line must be very short compared with  $\frac{1}{4}$  wavelength at the highest frequency. The two cavities are better made with a thin adjacent wall, as in Fig. 28-36b, a design that permits the use of a connecting line of negligible length between the cavities. The variation of the mutual reactance with frequency is similar to that for the input loop, discussed

in Sec. 28-18 above. Therefore, if constant percentage band width is desired, the loop must not be located quite at the end of the cavity.

Apertures have been found to be preferable to loops in coupling microwave cavities together. Aperture coupling, also known as *iris*, *orifice*, or *waveguide coupling*, consists merely of an opening of simple shape in the thin wall between the cavities. Some of the more useful variants of this type of coupling are shown in Fig. 28-37. In addition to simple round and rectangular apertures, two important special cases of the rectangular hole are illustrated. These are (1) a narrow transverse slot, and (2) a rectangular hole commencing at the short-circuited end of the cavity (*i.e.*, the dimension  $v$  equals zero). All these apertures behave very similarly. Their length or width must be a small fraction of a wavelength in order to prevent resonance effects. Experience has shown that the degree of coupling that they provide depends mainly upon their transverse width and that the variation of coupling with frequency depends mainly upon the location of their approximate centers with respect to the end of the cavity. The variation of coupling with frequency is similar to that for loops.

Examples of the design of tuners having aperture coupling will be presented in Secs. 28-27 and 28-28. The design of a particular aperture for a two- or three-cavity tuner is readily carried out if several basic properties of aperture coupling are kept in mind. (1) Increasing the aperture dimension in the direction transverse to the cavity axis has a very large effect on the coupling reactance, and hence on the band width, and the effect is *approximately equal* at all frequencies in the tuning range. (2) Increasing the distance from the short-circuited end of the cavity to the center of the aperture will decrease the band width at the high end of the frequency range more than at the low end. (3) Increasing the length of the aperture in the direction of the axis of the cavity, without at the same time shifting the center of the aperture, will have a relatively small effect, compared with the other changes, but will tend to increase the band width at the low end of the range more than at the high end. These rules should be regarded as only a rough guide, since in some cases the coupling characteristics may be affected in a somewhat different manner.

It should be pointed out that the loop coupling of Fig. 28-36*b* is really loop coupling combined with some aperture coupling. In some cases, a combination of aperture and loop coupling may be useful.

**28-26. Design of Single-cavity Coaxial Tuners.**—The single-cavity tuner consists merely of a resonant coaxial cavity and input and output loops. The cavity may be made  $\frac{1}{4}$ ,  $\frac{1}{2}$ ,  $\frac{3}{4}$  wavelength long, depending upon the frequency and the amount of tuning motion required and

whether the close spurious responses of the longer cavities will cause any trouble in the particular receiver.

The loops may be designed by using the principles and approximate formulas of Sec. 28-18. They should be located in such positions with respect to the end of the cavity that the desired variation of band width with frequency is attained. If the input and output impedances for the tuner are equal, the loops should have the same size and shape and should be similarly located. If these impedances are unequal, as will generally be true when the output connects directly to a detector, the loops must also be of unequal size so that each loop will cause the same value of *effective* load resistance  $R_e$  to be presented to the maximum cavity current. This adjustment is easily carried out experimentally by merely

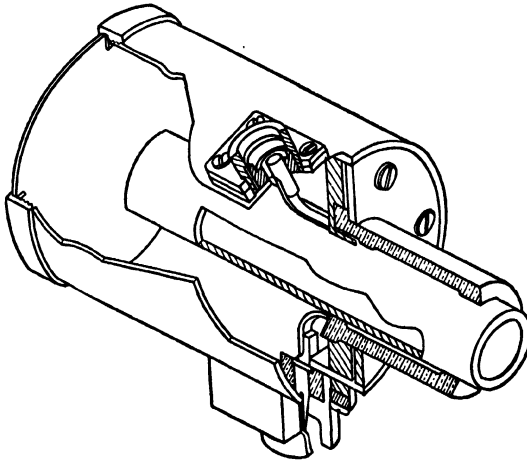


FIG. 28-38.—Single-cavity quarter-wave tuner.

varying the size of one of the loops until maximum signal response is attained.

An example of a coaxial single-cavity quarter-wave tuner for use with a 1000- to 3000-Mc direct-detection type of receiver is shown in Fig. 28-38. The shape of the response curve is, of course, very nearly that of the universal response curves of Figs. 28-2 and 28-4.

**28-27. Design of Two-cavity Coaxial Tuners.**—The two-cavity tuner has one more parameter than the single-cavity tuner. This is the coupling, or mutual, reactance between the cavities. The design of two-cavity coaxial tuners has thus far been largely empirical. The guesswork is aided, however, by the universal pass-band curves of Fig. 28-5 and by the rough rules given for the various kinds of couplings in Secs. 28-18, 28-19, and 28-25.

The universal response curves indicate that, for optimum flatness of pass-band response and minimum insertion loss, the degree of coupling should be maintained approximately equal to, or slightly greater than, critical coupling throughout the tuning range. The main effects of the output, input, and intermediate couplings can be illustrated by a single example. First assume a condition of critical coupling. Then increasing the coupling between the two cavities will increase the band width and at the same time cause two peaks to appear and the midband loss to

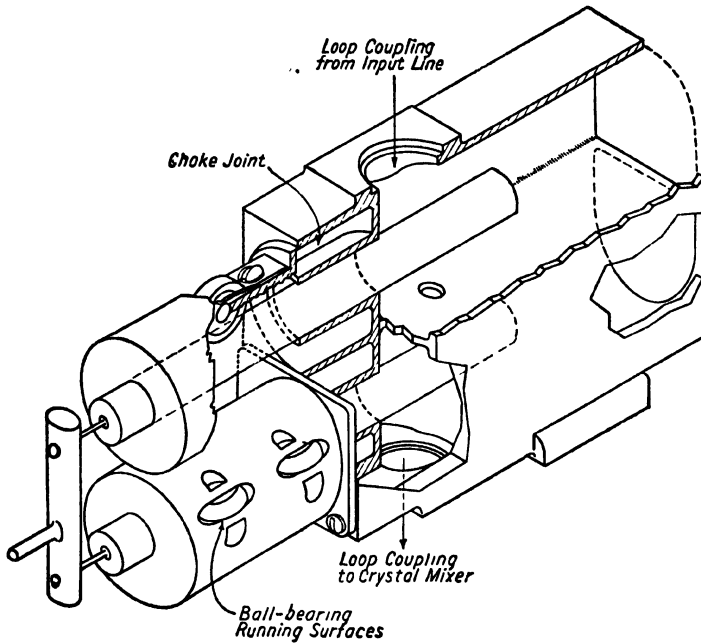


FIG. 28-39.—Two-cavity quarter-wave tuner.

increase. Increasing the input and output couplings, *i.e.*, decreasing the cavity  $Q$ 's, will flatten the pass-band-response curve but have less effect on the band width.

For best pass-band response, the  $Q$  of the two cavities should be approximately equal. If the input and output terminal impedances are equal, and the input and output coupling loops are made identical, the cavity  $Q$ 's will also be equal. In a receiver, however, the crystal or vacuum-tube detector or mixer will connect directly to the output loop of one of the cavities. Since the impedance of this load will in general be different from that of the input line, an output loop of different size may be required in order to make the cavity  $Q$ 's equal.

A two-cavity quarter-wave tuner is shown in Fig. 28-39 and a half-wave resonant tuner in Fig. 28-40. Both of these tuners are for the 2000- to 4000-Mc range. They both have approximately the response corresponding to critical coupling and a band width that varies from about 25 to 55 Mc.

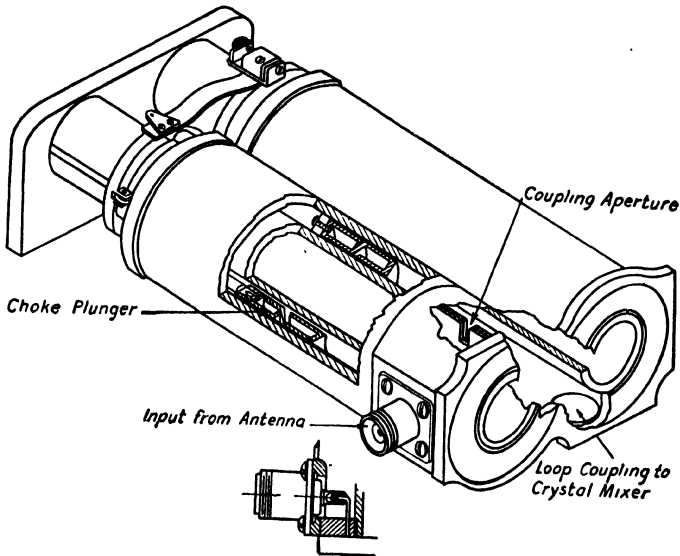


FIG. 28-40.—Two-cavity half-wave tuner.

**28-28. Design of Three-cavity Coaxial Tuners.**—The *three-cavity* tuner differs from the two-cavity tuner in the addition of a center cavity and the presence of two intermediate coupling reactances instead of one. The three-cavity tuner does not have any additional parameters, however, since the cavities may be made identical and the intermediate couplings equal. As far as the number of independent parameters is concerned, therefore, the design of a three-cavity tuner is no more complicated than the design of a two-cavity tuner. There is, however, another important factor that makes the three-cavity design difficult. This is the problem of making the center cavity track perfectly with the outer cavities. Perfect tracking requires identical tuning curves for the three cavities. Under this condition, direct mechanical ganging of the three cavities is possible. Perfect tracking of the two-cavity tuner is achieved merely by making the cavities identical and their input and output loading loops approximately equal. With the three-cavity tuner, this procedure guarantees only that the outer pair of cavities will track, while the center cavity may have a somewhat different tuning curve. This is caused by two factors. (1) Each cavity must tune out not only



its own reactance but also the self-reactances of its coupling loops and apertures. These reactances will in general have values for the center cavity different from those for the outer ones. (2) Any extraneous discontinuities, such as that presented by loops and apertures, will affect the field distribution and, hence, the tuning curve of a resonant cavity.

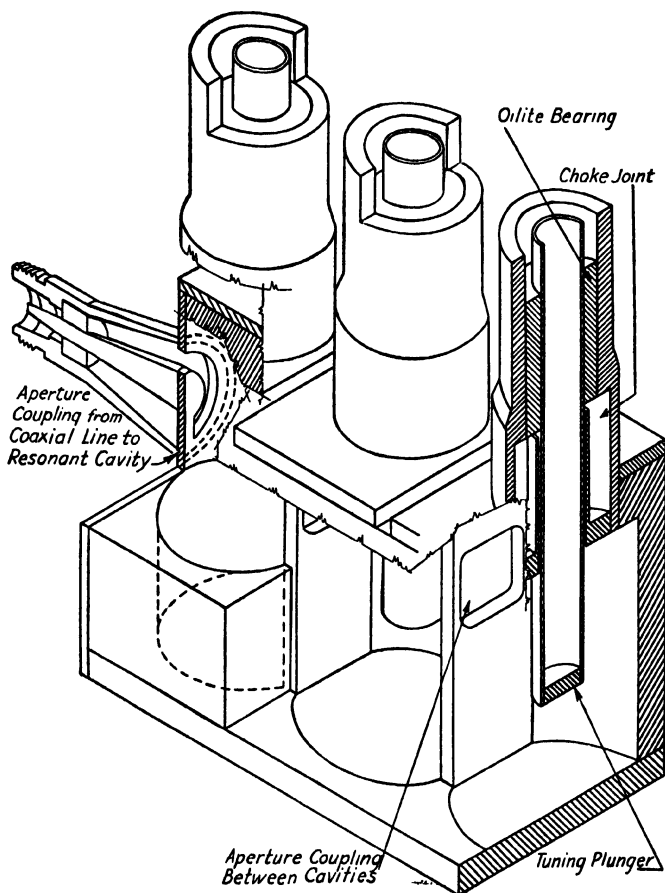


FIG. 28-41.—Three-cavity quarter-wave tuner.

Such discontinuities will in general have values for the center cavity different from those for the outer ones. It is therefore necessary (1) to make the self-reactances and the field-discontinuity effects of the coupling elements negligible, or (2) to make them compensate each other over the tuning range, or (3) to introduce some sort of compensating element. Of these three tracking methods, the first has proved practical and is the only one used thus far.

It has been found that aperture coupling through thin walls provides a mutual reactance with very low self-reactance, even when the aperture opening is quite large. Ordinary loop coupling, on the other hand, usually has considerable self-reactance. Consequently, aperture coupling (see Figs. 28-32 and 28-37) has proved to be preferable to loop coupling in three-cavity tuners.

Figure 28-41 shows a sketch of a three-cavity tuner working on the quarter-wave resonance for the 2000- to 4000-Mc tuning range. The measured pass-band response is almost perfectly flat throughout the range, and the 3-db width varies from 31 Mc at the low end to 48 Mc at the high end.

**28-29. Rectangular-waveguide Cavity.**—The relatively large size and high  $Q$  of waveguide cavities make them useful at the higher frequencies. Figure 28-42 shows a resonant cavity in the shape of a hollow rectangular prism with conducting walls. This cavity may be analyzed as a length of rectangular waveguide short-circuited at both ends. Such a cavity has an infinite number of resonant frequencies. The *free-space* wavelengths at which the cavity is resonant are given by

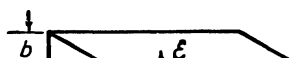


FIG. 28-42.—Rectangular waveguide cavity.

$$\lambda_{res} = \frac{2}{\sqrt{\left(\frac{m}{a}\right)^2 + \left(\frac{n}{b}\right)^2 + \left(\frac{p}{c}\right)^2}} \quad (28-18)$$

where  $m$ ,  $n$ ,  $p$  are positive integers (one of which may be zero). The integers  $m$ ,  $n$ , and  $p$  are equal to the number of half-period variations of the field along the dimensions  $a$ ,  $b$ , and  $c$ , respectively.

When the cavity is used as a tuner, the particular resonant frequency chosen should be the lowest possible one for the cavity dimensions, *i.e.*, it should be the fundamental or lowest order resonance, and it should be separated as much as possible from the higher order resonances. The lowest possible resonant frequency is that of the 1,0,1 resonance mode. The occurrence and separation of the next higher modes depends upon the cavity shape. By making  $b$  fairly small, all  $m,n,p$  resonance frequencies for  $n$  equal to or greater than one can be made considerably higher than the fundamental resonant frequency. Only the  $m,0,p$  modes are then important. The curves corresponding to Eq. (28-18) are plotted for the first few  $m,0,p$  modes in Fig. 28-43 with free-space wavelength  $\lambda$  and the dimension  $c$  as variables. All  $m,0,p$  modes have the electric-field vector in the  $b$  direction as shown in Fig. 28-42. Since  $n = 0$  there are no field variations in this direction.

The separation between the fundamental mode and the next higher mode may be increased further by the proper location of the exciting voltage. Figure 28-43a shows a thin waveguide cavity which may be tuned by a short-circuiting plunger that varies the length  $c$  and thus the resonant frequency, as indicated by Eq. (28-18) and Fig. 28-43b. If a thin cavity is fed in one corner as in Fig. 28-44a, the maximum tuning

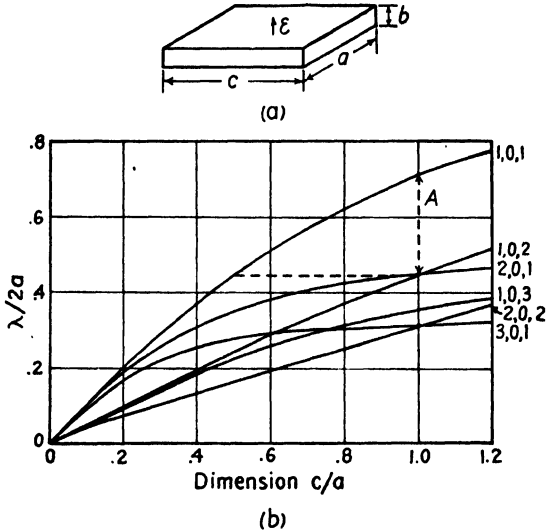


FIG. 28-43.—Tuning curves for the first few  $TE_{m,0,p}$  modes. A indicates tuning range on the  $TE_{1,0,1}$  mode that is free from multiple resonances, with an unsymmetrical feed.

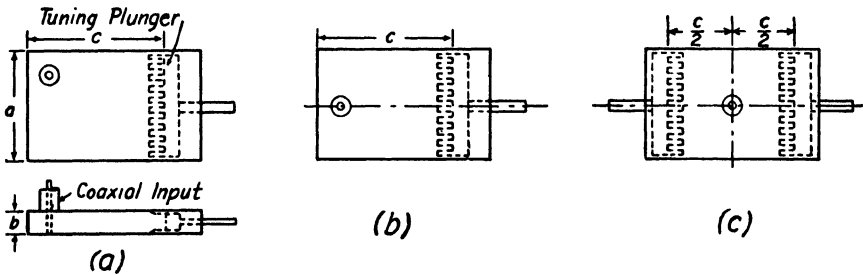


FIG. 28-44.—Rectangular waveguide cavity fed by a coaxial line: (a) unsymmetrical feed; the (b) symmetrical with respect to one axis; (c) symmetrical with respect to two axes.

range possible on the 1,0,1 mode resonance without overlapping of the 1,0,2 or 2,0,1 modes is 1.55:1 (see Fig. 28-43). By using a feed symmetrical with one axis of the cavity (Fig. 28-44b), the range may be increased to 1.75:1, since the 2,0,1 mode will not be set up and the 3,0,1 and 1,0,2 modes are the next ones to cause trouble. By using a balanced feed symmetrical with both axes and keeping this symmetry by tuning two sides of the cavity simultaneously (Fig. 24-44c), the range may be

increased to 2.2:1, since no even-order modes will be set up and overlapping of the 1,0,3 and 3,0,1 modes is therefore the limiting factor. Another possible method of increasing the tuning range for a single response is to place a discontinuity in the cavity in such a manner that it will have the effect of increasing the slope of the tuning curve (wavelength-vs.-plunger position) of the fundamental mode with respect to

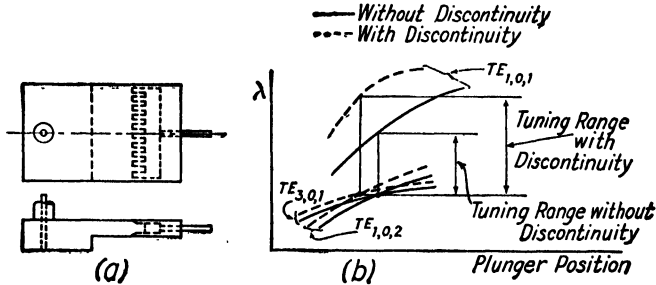


FIG. 28-45.—A rectangular-waveguide cavity having a discontinuity in the height. This construction gives an increased tuning range free of multiple responses.

that of the second-order mode. An example of this is given in Fig. 28-45, where the range was increased from 1.75:1 to 1.9:1 by this scheme.

The waveguide cavity may be used as a tuner, as shown in Fig. 28-46. One coaxial line is the input line, and the other the output line. The outer conductors contact the upper surface of the cavity, and the inner conductors the lower.

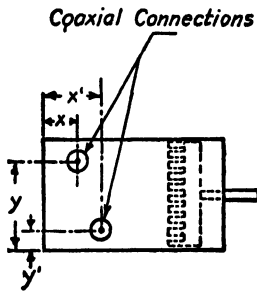


FIG. 28-46.—A rectangular-waveguide-cavity tuner or detector.

In a thin cavity the coupling is principally due to the magnetic field alone. If one of the coaxial lines is replaced by a crystal making r-f contact with the top and bottom of the cavity, a tuned detector results. Impedance matching is accomplished by varying the position of the coaxial-line connection. The closer a connection is to the center of the cavity, the higher is the impedance presented by the cavity. If one coaxial-line connection is located at point  $x, y$  (Fig. 28-46) and the other at point  $x', y'$ , then at the 1,0,1 resonant frequency the coaxial-line impedances  $Z_0$  and  $Z_0'$  should be related as follows for a perfect match:

$$\frac{Z_0}{\sin^2\left(\frac{2\pi x}{\lambda_{res}}\right) \sin^2\left(\frac{2\pi y}{\lambda_{res}}\right)} = \frac{Z_0'}{\sin^2\left(\frac{2\pi x'}{\lambda_{res}}\right) \sin^2\left(\frac{2\pi y'}{\lambda_{res}}\right)} \tag{28-19}$$

The loaded  $Q$  of the cavity is made large by having the coaxial connections very near the edge of the cavity. It is made small by moving the connections toward the center of the cavity.

The coaxial connections should be as far apart as is practical, in order to minimize direct mutual coupling between them. The effect of this coupling is to permit a small amount of signal to be transmitted at all frequencies.

At a given band width, the off-band rejection may be increased by coupling together two or more waveguide cavities, as shown in Fig. 28-47.

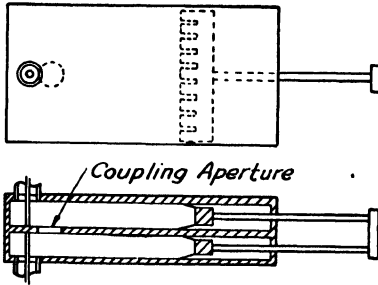


FIG. 28-47.—A method of coupling together two rectangular-waveguide cavities.

### 28-30. "Loaded" Waveguide Cavity.

—In the last section a waveguide cavity was described that is tuned by changing the cavity length. In this section another method of tuning a waveguide cavity will be presented. Figure 28-48 shows a rectangular-waveguide cavity having a conducting rod projecting inward parallel to the  $E$  field. Such a cavity is known as a *loaded* cavity. Due to

the intense magnetic field around the rod, and to the intense electric field between the end of the rod and the bottom of the cavity, the resonant frequency of the cavity is lower than for the same cavity without the rod. The higher resonant modes, however, are affected to a less degree, and hence a large tuning range free of multiple responses is available.

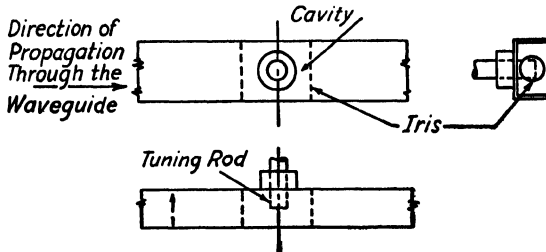


FIG. 28-48.—Loaded waveguide cavity having waveguide terminations.

The maximum frequency in the tuning range is obtained when the rod is completely withdrawn. This frequency may be calculated from Eq. (28-18). As the rod is inserted farther and farther into the cavity, the resonant frequency decreases. The resonant frequency approaches zero as the gap between the rod and the bottom of the cavity is made vanishingly small. In practice, a 2:1, or greater, tuning range is easily obtainable.

Figure 28-48 shows a metal-to-metal bearing contact between the tuning rod and the cavity wall. Such a contact is likely to be noisy

and lossy. The types of contacts shown in Figs. 28-34 and 28-35 for coaxial cavities are suitable for use with the loaded waveguide cavity. The choke-joint type of Fig. 28-35a is to be preferred.

The cavity of Fig. 28-48 is shown coupled to input and output waveguide lines by means of irises. One type of inductive iris is shown, but almost any other iris shape may be used. Loop coupling to a coaxial

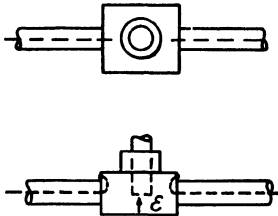


FIG. 28-49.—Loaded waveguide cavity coupled to coaxial lines by means of loops.

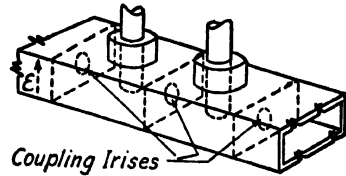


FIG. 28-50.—Two loaded waveguide cavities coupled by means of irises.

line is also possible, as shown in Fig. 28-49. It is of interest to note that the cavity of Fig. 28-49 resembles a short large-diameter coaxial-line cavity. Actually there is a smooth transition between the properties of a waveguide cavity and a coaxial-line cavity as the length-to-diameter ratio is varied from small to large values.

Figure 28-50 shows the manner in which two or more cavities may be coupled together by apertures. As in coaxial cavities, the location of the

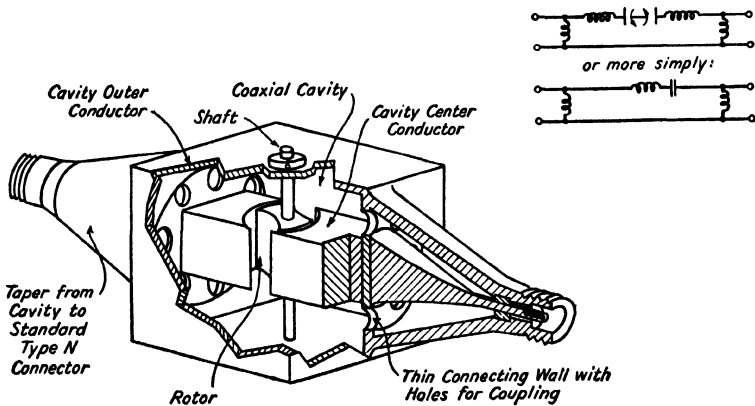


FIG. 28-51.—A rotary-tuned coaxial cavity having shunt-inductance coupling.

apertures may be used to control the variation of coupling over the tuning range.

**28-31. Rotary-tuned Coaxial Cavity.**—The tuner of Fig. 28-51 is a coaxial cavity with a capacitance rotor symmetrically located at the center. The rotor-shaft bearings are at a point of negligible r-f current and, therefore, cause no tuning noise. The coaxial input and output

lines are coupled through a low shunt reactance, the equivalent circuit being approximately as shown in Fig. 28-51. The shunt reactances may be inductive or capacitive. A shunt inductance can be simply a thin short-circuiting plate containing holes, as in Fig. 28-51. A cavity having capacitance coupling is sketched in Fig. 28-52.

The minimum resonant frequency occurs when the rotor is fully engaged, *i.e.*, when the capacitance is a maximum. This resonant fre-

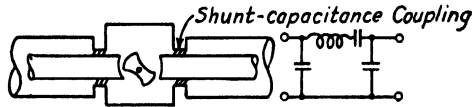


FIG. 28-52.—A rotary-tuned coaxial cavity having shunt-capacitance coupling.

quency is given approximately by

$$f = \frac{1}{2\pi} \sqrt{\frac{3(10)^{10}}{lZ_0C}} \quad \text{cps} \quad (28-20)$$

where  $l$  is one-half of the cavity length in centimeters,  $C$  is the maximum capacitance in farads between the rotor and one of the center-conductor end faces, and  $Z_0$  is the characteristic impedance of the coaxial cavity. The maximum resonant frequency occurs at a frequency somewhat less than that for which the length of the cavity is  $\frac{1}{2}$  wavelength from coupling plate to coupling plate. An experimental model, which was

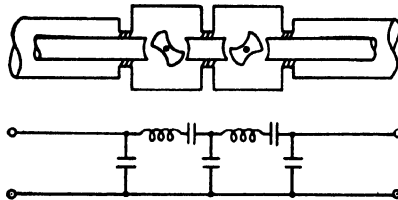


FIG. 28-53.—Two rotary-tuned coaxial cavities coupled by shunt capacitances.

built in a cubical cavity 2 in. on a side, had a tuning range from 650 Mc to slightly over 2000 Mc.

Two or more rotary-tuned coaxial cavities may be coupled together by inductances or capacitances, as shown in Fig. 28-53.

**28-32. Rotary-tuned Waveguide Cavity.**—The waveguide tuner shown in Fig. 28-54 is in principle similar to that of Sec. 28-30. In this tuner, however, the tuning is accomplished by a rotary motion. In one position of the rotor the capacitance between the top and bottom of the waveguide cavity is maximum; in a position at 90 deg to the first the capacitance is minimum. The minimum frequency in the tuning range is obtained for the former position, the maximum frequency for the latter.

As in the rotary-tuned coaxial cavity of Sec. 28-31, the drive-shaft bearings pass through the cavity walls at points of negligible r-f current and, hence, cause negligible tuning noise.

Coupling to the input and output waveguide lines is easily accomplished by means of irises. Since the field pattern in the cavity changes with the position of the rotor, a large variety of curves of coupling impedance vs. frequency may be obtained by locating the coupling apertures in the irises at different positions in the vertical direction. A method of providing the rotary-tuned waveguide cavity with coaxial terminations

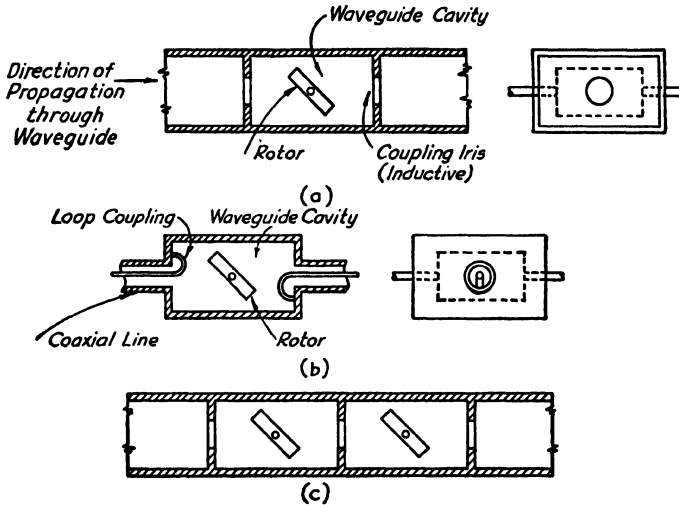


FIG. 28-54.—Rotary-tuned waveguide cavity: (a) cavity coupled by irises to waveguide lines; (b) cavity coupled by loops to coaxial lines; (c) two cavities coupled to each other and to waveguide lines by irises.

is shown in Fig. 28-54b. Figure 28-54c shows how two or more cavities may be coupled together by irises.

The maximum frequency in the tuning range is somewhat less than that for the rectangular waveguide cavity with the rotor removed. The minimum frequency is somewhat greater than the cutoff frequency of the waveguide to which the cavity is coupled (Fig. 28-54a).

A tuner such as that of Fig. 28-54a is very easily constructed but has a limited tuning range. In order to increase the tuning range, a construction like that of Fig. 28-55 may be used. In this tuner the rotor and the cavity walls are specially shaped to give an increased maximum capacitance.

Two experimental models similar to that of Fig. 28-55 were built. The first, a single-cavity tuner, had a tuning range from 2160 to 3980 Mc (1.85:1); the second, consisting of two coupled cavities, had a useful



tuning range from 2300 to 3400 Mc (1.48:1). In the latter tuner, it was possible to adjust the size and location of the three coupling irises so that the tuner was almost exactly critically coupled throughout the tuning

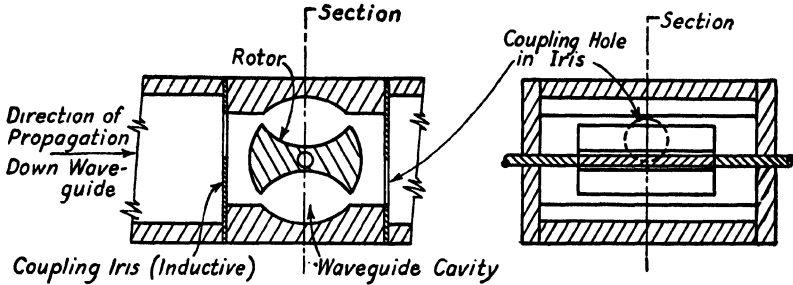


FIG. 28-55.—A wide-range rotary-waveguide-tuner design.

range. This condition of coupling provides maximum flatness of pass-band response and minimum over-all pass-band loss. The band width varied between 26 and 38 Mc in the tuning range.

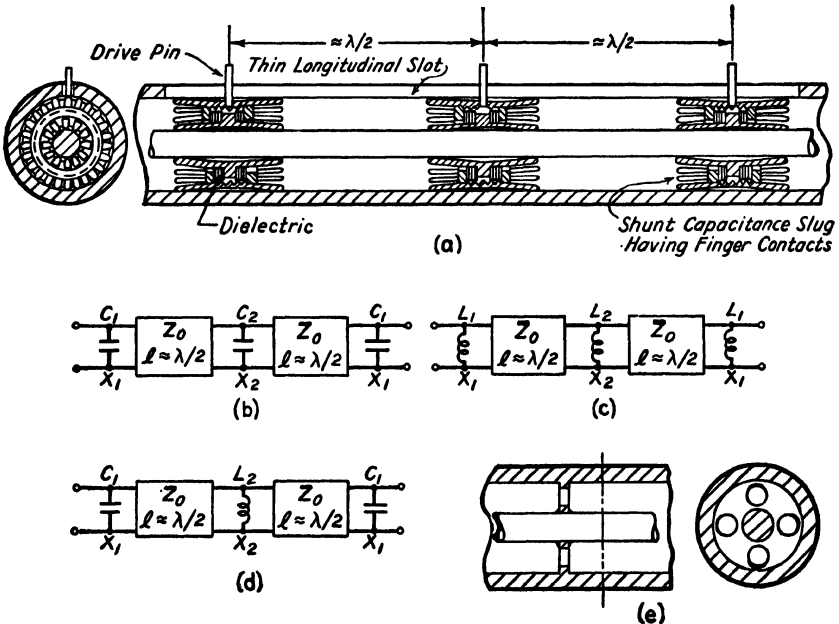


FIG. 28-56.—(a) Movable slug tuner; (b), (c), and (d) equivalent circuits; (e) shunt inductance.

**28-33. Movable Slug Coaxial Tuner.**—Figure 28-56a shows a two-circuit tuner constructed in a straight length of coaxial line. This tuner is seen to consist of a coaxial line having three shunt capacitances spaced

approximately  $\frac{1}{2}$  wavelength apart. Tuning is accomplished by moving the outer capacitance slugs by means of drive pins projecting through a slot. The circuit representation of this construction is shown in Fig. 28-56*b*.

Instead of shunt capacitances, shunt inductances might also be used, as shown in Fig. 28-56*c*; or both types of reactances might be used, as in Fig. 28-56*d*. A method of constructing a suitably small shunt inductance is shown in Fig. 28-56*e*.

The design equations for this two-circuit tuner are

$$X_1 = \sqrt{\left(\frac{\pi Z_0 R}{2p}\right) \left(\frac{\Delta f}{f}\right)} \quad (28-21)$$

$$X_2 = \left(\frac{k}{k_c}\right) \left(\frac{X_1^2}{R}\right) \quad (28-22)$$

where  $X_1$  and  $X_2$  are the shunt reactances (either capacitive or inductive),  $Z_0$  is the characteristic impedance of the tuner line,  $R$  is the terminal load resistance (usually set equal to  $Z_0$ ),  $\Delta f/f$  is the band-width ratio measured at the 3-db-down points,  $k/k_c$  is the ratio of actual coupling to critical coupling between the two circuits, and  $p$  is a number related to  $k/k_c$  and to the midband dip. Illustrative values are given in Table 28-2.<sup>1</sup>

TABLE 28-2

Midband dip, db	$k/k_c$	$p$
0	1	1.4
2	2	2.6

When shunt capacitances are used, it has been found that this tuner may be designed to give very closely the desired band width and response shape. A model similar to that of Fig. 28-56*a*, with ganged tuning, covered the 2000- to 4000-Mc range. In another model the outer capacitance slugs consisted of concentric rings suspended in air so as to eliminate tuning noise. The principal application of this type of tuner may prove to be as a semifixed narrow-band filter in fixed-frequency systems.

<sup>1</sup> The values in this table are taken from the curves in Fig. 28-5. Additional values may be obtained from these curves if desired.

## CHAPTER 29

### DETECTORS AND MIXERS

BY R. A. SODERMAN

**29-1. Introduction.**—In both superheterodyne and direct-detection types of wide-range radar-intercept receivers operating at frequencies above about 100 Mc, the first detector or mixer usually assumes an importance much greater than it does in receivers operating at lower frequencies, as generally the first mixer or detector is not preceded by r-f amplifier stages. Consequently, the mixer or detector gain or loss and the noise generated in the stage have a very large effect on the signal-to-noise ratio in the receiver output and on the over-all receiver noise figure  $F$ , as defined in Sec. 25-6, which, in well-designed receivers, determines the maximum sensitivity.

At frequencies up to about 1500 Mc, the addition of r-f amplifier stages using the best tubes commercially available at the present time, such as the type 2C40 lighthouse triode, would increase the maximum sensitivity of superheterodyne radar-intercept receivers by increasing the signal-to-noise ratio in the receiver output and would also make the mixer characteristics of less importance. At frequencies above about 1500 Mc, however, the addition of r-f amplifier stages, using commercially available tubes, actually would decrease the signal-to-noise ratio in the receiver output, since the added gain obtained would not be sufficient to compensate for the added noise generated by the tubes. In general, r-f amplifiers were not used in most wide-range radar intercept receivers even in the frequency range between 100 and 1500 Mc, because of their complexity and the more difficult tracking problems involved. Usually, adequate sensitivity for radar-interception applications could be obtained without using r-f amplification.

If high-sensitivity receivers are desired, superheterodynes are generally used in preference to direct-detection receivers because of the inherent insensitivity of low-level detectors and the consequent large amount of r-f amplification required to increase the sensitivity to a value comparable with the sensitivity of a superheterodyne without r-f amplifier stages. In general, therefore, r-f amplifiers are not used in high-frequency direct-detection receivers.

As a result of the gain of the r-f amplifier stages in conventional low-frequency receivers using r-f amplifiers, the input impedance of the

mixer or detector is relatively unimportant as far as the signal-to-noise ratio is concerned, since the mixer has very little effect on the signal-to-noise ratio in the receiver output. In v-h-f wide-range receivers, on the other hand, where the mixer is the first stage, and hence very important, the input impedance and variations in the input impedance with frequency may have a large effect on the receiver sensitivity and selectivity. The reason for this is the difficulty of designing simple transformers for use between the antenna and mixer circuits to provide the required impedance transformation for maximum signal-to-noise ratio and the desired selectivity over the whole tuning range.

The choice of the intermediate frequency for a wide-range radar-intercept receiver is more complicated than for a conventional low-frequency superhetrodyne receiver for two reasons:

1. The wide receiver pass bands and the lack of selective r-f amplifiers limit the selectivity of the r-f input circuit and usually make it necessary to use very high intermediate frequencies in order to obtain adequate image rejection. Since the amount of noise generated by the i-f amplifier increases as the intermediate frequency is increased, however, the signal-to-noise ratio tends to decrease with increasing intermediate frequency.

2. The most commonly used high-frequency mixer, the crystal rectifier,<sup>1</sup> has a noise spectrum in which the amplitude of the noise decreases with increasing frequency up to a certain point, beyond which the noise generated remains practically constant. As a result of these two opposing factors, the choice of the intermediate frequency is usually a compromise between selectivity and sensitivity.

The second-detector stage in high-frequency superheterodyne receivers usually differs slightly in operating frequency and band width from those used in conventional low-frequency receivers. In most wide-range radar-intercept receivers, an intermediate frequency lying above 30 Mc and a video band width greater than 1 Mc are used.

As at lower frequencies, detectors are used also to measure r-f voltages for the calibration of signal generators, for the measurement of impedances by the slotted-line method, and for simple monitoring of signal levels. Since the same types of detectors are used for r-f voltmeters as for mixers and detectors, a brief discussion of high-frequency voltage-measuring and monitoring devices is included in this chapter.

<sup>1</sup> No appreciable amount of work was carried out at the Radio Research Laboratory on crystal research, and consequently most of the information contained in this chapter on crystal theory is the result of the work of other laboratories and is included here for completeness. A much more exhaustive treatment of crystals appears in "Crystal Rectifiers," Radiation Laboratory Series, Vol. 15, McGraw-Hill Book Company, Inc., New York (in press).

**29-2. Types of Mixers and Detectors.**—At frequencies above 100 Mc the most common types of mixers and detectors used are triodes, diodes, and crystal rectifiers. In general, the use of multigrid tubes is avoided, since the amount of noise generated increases very rapidly with the number of tube elements. The development of modern high-frequency crystal rectifiers was carried to a high state of perfection during the war, and there are on the market relatively stable units mounted in small cartridges with sealed adjustments, as shown in Fig. 29-1.

At frequencies up to about 500 Mc, triodes such as the type-2C40 lighthouse tube may sometimes be used as mixers in broad-band receivers

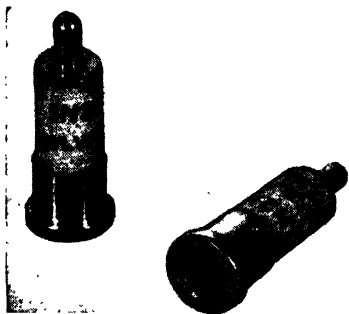


Fig. 29-1.—Type-1N21-B crystal rectifiers.

in spite of the relatively large amount of noise they generate, since the relatively high conversion gains produced usually make it possible to obtain approximately the same or possibly a higher signal-to-noise ratio than if a diode or crystal mixer were used. Because of transit-time effects, however, the conversion gain obtainable from a triode mixer stage with a given tube decreases and the amount of noise generated increases, as the frequency is increased. Above 500 Mc, crystal and

some diode mixers, in spite of their conversion loss, are appreciably superior to any triode mixers now available because of the relatively small amount of noise generated.

Because of the smaller amount of noise generated by crystals, they are slightly superior electrically to diodes as mixers even at relatively low frequencies. Their use becomes increasingly desirable as the frequency is increased, since the conversion loss of diode mixers as the result of transit-time effects increases at high frequencies more rapidly than does the conversion loss of typical crystal mixers. Transit-time effects are negligible in crystals, but other effects, which are discussed in following sections, tend to increase the conversion loss at very high frequencies. The conversion efficiency of commercially available crystals remains relatively constant up to much higher frequencies than that of any diode now available. In fact, the conversion loss of type-1N26 crystals is relatively low even at 23,000 Mc.

Triodes, diodes, and crystal rectifiers are used also as low-level detectors in direct-detection receivers and have roughly the same relative variations in performance with operating frequency as when they are used as mixers, except that the general sensitivity level is much lower, and crystals are appreciably superior to diodes at all frequencies.

**29-3. Crystal Rectifiers.**—Modern crystal rectifiers are similar to early crystal rectifiers in that they consist of a crystal embedded in a fusible metal and a “cat whisker” of thin tungsten wire that touches the surface of the crystal, as shown in Fig. 29-2. The wire forms one terminal of the rectifier and the fusible metal the other. The crystal is one of a class of semiconducting materials such as silicon, germanium, galena, or iron pyrites, whose surface or barrier layers between the metal contact and the crystal body exhibit a nonlinear resistance to the flow of current. In general, the resistance to flow of current in one direction is much greater than to the flow of current in the opposite direction. Consequently, if an alternating voltage is applied across the terminals, a rectifying action will occur. For small voltages the resistance to the flow of current in the low-resistance or *front* direction decreases rapidly as the applied voltage is increased. The rate of decrease of the front resistance with applied voltage decreases, however, as the voltage becomes relatively large and a constant value of resistance is approached. This effect is explained by the constant resistance, called the *spreading resistance*, of the body of the semiconducting crystal. Since the spreading resistance is in series with the nonlinear barrier resistance, the front resistance cannot become less than the spreading resistance, which is normally between 10 and 200 ohms in typical crystals. The back resistance is very great for small applied voltages and remains relatively large up to moderately large back voltages. At still greater voltages the back resistance tends to decrease relatively rapidly. The voltage at which the back resistance begins to decrease materially depends on the type of crystal material and the adjustment. The back resistance of a typical 1N21B silicon crystal, which is one of the types generally used as high-frequency mixers, on the average starts to decrease appreciably at back voltages above about 3 volts. However, certain types of germanium crystals can be adjusted to have very high back resistances for voltages up to 50 or 100 volts or even more. The simplified equivalent circuit of a crystal is shown in Fig. 29-3, in which the barrier resistance is labeled  $R_b$  and the spreading resistance  $R_s$ , and Fig. 29-4 shows typical current-voltage characteristics of silicon and germanium crystals.

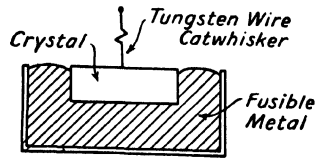


FIG. 29-2.—Sketch of a crystal rectifier.

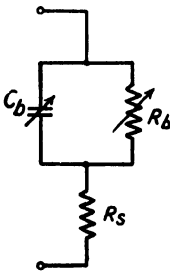


FIG. 29-3.—Simplified equivalent circuit of a crystal rectifier.

A small capacitance  $C_b$ , which exists across the barrier layers between the end of the tungsten wire and the crystal body, effectively shunts the

nonlinear resistance  $R_b$ , as shown in Fig. 29-3. The magnitude of the capacitance varies somewhat with applied voltage and frequency, but in the following discussion it will be assumed to be constant. The reactive current flowing through the capacitance also flows through the spreading resistance and causes a power loss and voltage drop that effectively decreases the voltage applied across the rectifying barrier, and thus reduces the rectifying efficiency of the crystal. Since the reactive current increases with increasing frequency, the rectification efficiency decreases as the frequency increases. In order to increase the frequency at which the reactance of the capacitance becomes low enough to have an appreciable effect on the rectification efficiency, the area of the contacting point of the cat whisker is reduced to decrease thereby the

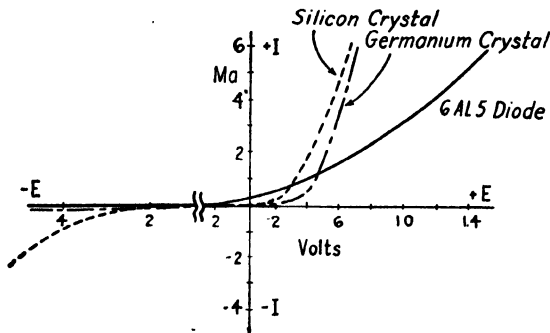


Fig. 29-4.—Typical crystal current-voltage characteristics.

capacitance  $C_b$ . The maximum power input a crystal can stand without being permanently damaged decreases with the area of contact, however, and therefore the contact area is not made any smaller than necessary to prevent the capacitance from having an appreciable effect at the highest frequency for which the crystal was designed. Type-1N21B crystals, which are designed for operation at frequencies up to about 3500 Mc, have barrier capacitances of the order of  $0.3 \mu\text{mf}$ , and crystals designed for operation at high frequencies have smaller barrier capacitances.

**29-4. Crystal-mixer Circuits.**—As is well known, if two signals of different frequencies are applied to a circuit having a nonlinear resistance characteristic, a mixing action will occur and the output will contain components having the same frequencies as the two input signals, components having frequencies equal to the sum and difference of the two input frequencies, and possibly higher order components.<sup>1</sup> In most super-

<sup>1</sup> TERMAN, F. E., "Radio Engineers' Handbook," p. 567, McGraw-Hill Book Company, Inc., 1943. REICH, H. J., "Theory and Applications of Electron Tubes," 2d ed., p. 314, McGraw-Hill Book Company, Inc., 1944.

heterodyne receivers, the received signal is heterodyned with a large signal from a local oscillator and the difference frequency amplified by the i-f amplifier.

A typical high-frequency mixer circuit and its simplified equivalent circuit are shown in Figs. 29-5 and 29-6. The antenna circuit is usually connected to the mixer through a broad-band transformer or a preselector, in order to provide the desired match for maximum sensitivity between the antenna and mixer. The local-oscillator input may be connected

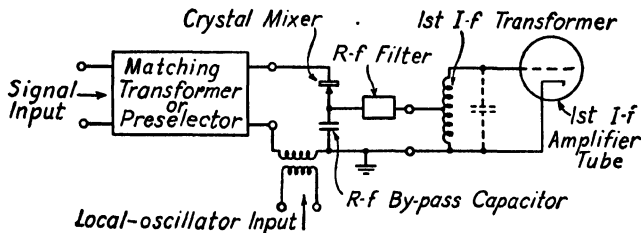


FIG. 29-5.—A typical high-frequency mixer circuit.

either in series or parallel with the signal input. If it is connected in series, the local-oscillator circuit usually should present a low impedance to signal-frequency currents in order to prevent absorption of a large portion of the signal power or increasing the complexity of the matching problem. If the local-oscillator signal is connected in parallel with the mixer, the local-oscillator circuit should present a high impedance to signal-frequency currents for the same reasons as outlined above. Furthermore, when the local oscillator is series connected, the effective impedance of the signal source in series with the local oscillator should usually be small compared to the mixer impedance, at the local-oscillator frequency, as the local-oscillator power requirements, amount of local-oscillator power radiated by the antenna, and broad-band coupling difficulties between the local oscillator and mixer thus usually are minimized. In parallel connections, the impedance should be high.

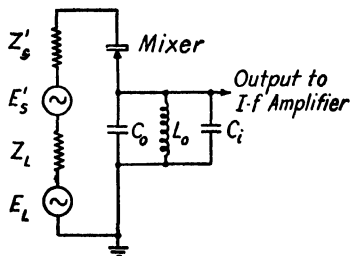


FIG. 29-6.—Simplified equivalent circuit of the mixer shown in Fig. 29-5.

The i-f output voltage in the circuit of Fig. 29-6 is developed across the r-f by-pass capacitor  $C_o$ , which in conjunction with the effective capacitance of the first i-f stage  $C_i$  and with the inductance of the first i-f transformer  $L_o$  forms a parallel resonant circuit at the intermediate frequency. This circuit should present a low impedance to all high-frequency components of current. Consequently, in many cases, an r-f



filter is inserted between the r-f by-pass capacitor and the i-f transformer to prevent high-frequency resonances from occurring in this circuit in the receiver tuning range.

**29-5. Crystal-mixer Characteristics.**—The performance of a crystal mixer is usually specified in terms of its effective conversion loss and effective noise temperature as a function of frequency. The *conversion loss*  $L$  of a crystal mixer, which in this case includes the matching transformer between the antenna and crystal circuits, is defined as the ratio of the maximum available signal-power input, *i.e.*, the power input if the mixer is matched to the antenna circuit, to the maximum available i-f power output, *i.e.*, the power output produced when the i-f load is matched to the output impedance of the mixer. Consequently, if the mixer is not matched to the antenna, the conversion loss will be greater than if it were matched, since the actual power input to the mixer is less than the maximum available power. As can be seen from the preceding discussion, the conversion loss  $L$  actually includes both the loss due to mismatches and dissipation between the antenna circuit and the crystal and the actual conversion loss in the crystal.

The excess noise produced by the mixer over the Johnson noise, which would be generated by a resistance equal to the i-f output resistance of the mixer, is specified by assigning to the output resistance a fictitious noise temperature such that this resistance would produce the amount of noise actually generated by the mixer. A *noise-temperature factor*  $t$ , sometimes called the *output noise ratio*, is defined as the ratio of the fictitious temperature of the output resistance to the room temperature. It can be determined from the expression

$$t = \frac{\text{actual noise power generated by the mixer}}{\text{noise power generated at room temperature by a resistance equal to the mixer output resistance}} \quad (29-1)$$

For a perfect mixer,  $t = 1$ , but in typical crystal mixers,  $t$  varies from slightly greater than 1 to about 3.

Since both the conversion loss and the noise temperature vary with local-oscillator power (see Sec. 29-7), these characteristics are specified at a given local-oscillator power input.

By means of the following equation, the over-all noise figure  $F_r$  of a receiver can be calculated from the mixer conversion loss  $L$ , the noise-temperature ratio  $t$ , and the noise figure  $F_i$  of an i-f amplifier, expressed as a ratio:

$$F_r = L(F_i + t - 1) \quad (29-2)$$

or

$$F_r \text{ (db)} = 10 \log_{10} L(F_i + t - 1) \quad (29-3)$$

If a receiver is composed of an i-f amplifier having a noise figure of 3.16, or 5 db, and a crystal mixer having a noise-temperature ratio  $t$  of 2 and a conversion loss  $L$  of 4, the over-all noise figure of the receiver will be

$$F_r = L(F_i + t - 1) = 4(3.16 + 2 - 1) = 16.64, \text{ or } 12.2 \text{ db}$$

In other words, the actual sensitivity will be 12.2 db less than the maximum theoretical sensitivity obtainable with a perfect receiver.

Most standard mixer crystals were designed for use in radar systems operating over very narrow frequency bands. Consequently, the characteristics of a standard crystal are defined in terms of the performance at a certain frequency of a certain type of mixer with the crystal in question inserted, used with a certain type of matching transformer, and a specified i-f load resistance, usually 400 ohms. The local-oscillator power input used for these tests varies from 0.5 to 1.0 mw for different types of crystals. The matching transformer is designed to match an average crystal to an antenna input circuit having a standard impedance, and therefore the conversion loss  $L$  of a crystal, measured in the mixer, is affected by deviations from the average input and output impedance.

Table 29-1 gives the specifications of several types of standard crystals defined in the manner just described. The noise figure  $F_r$  included in the table is the noise figure of a receiver composed of the mixer and an i-f amplifier having a noise figure of 3.16, or 5 db.

TABLE 29-1.—STANDARD CRYSTAL-MIXER CHARACTERISTICS

Frequency of measurement, Mc	Least sensitivity	Medium sensitivity	Greater sensitivity
3100	1N21 (obsolete) $L < 8.5$ db $t < 4$ $F_r < 16.4$ db	1N21A $L < 7.5$ db $t < 3$ $F_r < 14.6$ db	1N21B $L < 6.5$ db $t < 2$ $F_r < 12.7$ db
9375	1N23 $L < 10$ db $t < 3$ $F_r < 17.1$ db	1N23A $L < 8$ db $t < 2.7$ $F_r < 14.9$ db	1N23B $L < 6.5$ db $t < 2.7$ $F_r < 13.4$ db
25,000	.....	1N26 $L < 8.5$ db $t < 2.5$ $F_r < 15.2$ db	

$L$  = conversion loss, decibels  
 $t$  = effective crystal-temperature ratio  
 $F_r$  = noise figure of receiver assuming that  $F_i = 5$  db

In the design of wide-range matching transformers, of either the tuned or the untuned type, it is important to know the crystal input impedance as a function of frequency. The general trends are discussed in Sec. 29-6, but the actual impedance at high frequencies depends to a large extent on the type of mounting used and, consequently, is usually measured at the input of the mixer under consideration. The effective input resistance is roughly of the order of 300 ohms for crystals operating around 3000 Mc and is somewhat less for crystals operating at higher frequencies. The output resistance of crystals usually varies from about 200 to 600 ohms.

**29-6. Radio-frequency Impedance Considerations.**—As pointed out by E. W. Herold,<sup>1</sup> there is an optimum relationship between the actual mixer input resistance and the effective resistance of the antenna circuit as viewed from the mixer terminals. In triode mixers this relationship is not the same as that producing maximum power transfer, since the noise generated by electronic loading in the grid circuit is much greater than that produced by a resistance equal to the input resistance of the tube. Therefore, if the noise generated in the mixer plate circuit is neglected, the over-all signal-to-noise ratio is greater if the antenna circuit is coupled so that the effective antenna resistance across the mixer terminals is lower than the input resistance of the tube. However, the effective noise voltage of the plate circuit and following amplifier stages referred to the mixer grid circuit is independent of the resistance in the

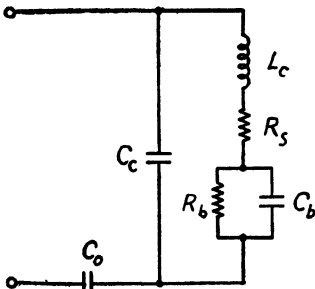


FIG. 29-7.—An approximate equivalent circuit of a crystal mixer.

grid circuit. Since the effective signal voltage applied to the grid decreases as the mismatch is increased, if the noise generated in the grid circuit could be neglected, the signal-to-noise ratio would decrease from a maximum under matched conditions, as the degree of mismatch is increased. When both the grid and equivalent plate noise are considered, however, the over-all signal-to-noise ratio will increase to a maximum as the effective antenna resistance is decreased by mismatching and will then decrease again as a result of plate noise. The improvement in signal-to-noise ratio obtainable and the optimum mismatch depend on the relative magnitudes of the grid noise and the effective plate noise.

In a diode or crystal mixer, the relation between the input noise, similar to the grid noise in a triode, and the effective output noise, similar

<sup>1</sup> HEROLD, E. W., An Analysis of Signal-to-noise Ratio of U-h-f Receivers, *RCA Rev.*, 6, 302-331 (1942).

to the plate noise, is more obscure, but because of the relatively large conversion loss, the effective output noise referred to the input circuit is usually much larger than the input noise. Therefore, the maximum signal-to-noise ratio occurs approximately when the antenna circuit is *matched* to the mixer.

In order to match the antenna to the mixer, a transformer must be designed that will provide the desired resistance step-up, tune out all reactance, and have the desired band width. The design of a tunable or broad-band transformer for wide-range operation may be difficult owing to the complicated reactance network in the crystal. Figure 29-7 shows an approximate equivalent circuit of a crystal mixer. As is evident from the diagram, the mixer has series and parallel resonances. The exact frequencies at which these resonances occur depend on the type of crystal and the mounting structure. The first resonance in standard high-frequency crystals in typical mountings is above 3000 Mc.

**29-7. Effect of Changes in the Local-oscillator Power Input on Mixer Performance.**—The conversion loss, noise temperature, and input and output impedances are all affected by changes in the local-oscillator input to the crystal. The conversion loss with no local-oscillator power input is infinite but decreases rapidly as the local-oscillator power is increased. As local-oscillator power input is increased further, a point is reached beyond which the rate of decrease in conversion loss begins to taper off and gradually approaches a minimum value. For even larger local-oscillator power inputs, the conversion loss begins to increase again, because of the decrease in back resistance for large applied voltages. In typical crystals, the conversion loss decreases very slowly for local-oscillator power inputs producing rectified crystal currents from about 0.3 to 2.0 ma or greater. An approximate curve of the variation in conversion loss with local-oscillator power input, as indicated by the rectified crystal current produced, is shown in Fig. 29-8.

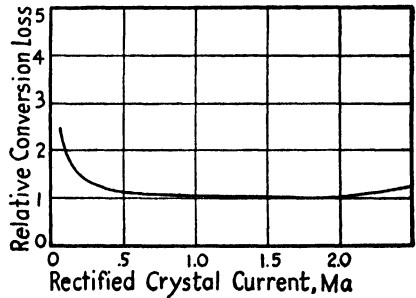


FIG. 29-8.—Variation in conversion loss with local-oscillator power input for a typical crystal mixer. The local-oscillator power input is indicated in terms of the rectified current produced by the mixer.

The effective noise temperature increases as local-oscillator power input is increased. The increase results from the increasing amount of local-oscillator noise applied to the crystal (see Sec. 29-11) and the increasing amount of noise actually generated in the crystal because of the increasing back voltage. The noise output due to local-oscillator

noise is approximately proportional to the local-oscillator power input. but the noise generated in the crystal increases slowly with local-oscillator power for small local-oscillator power inputs, and very rapidly for relatively large local-oscillator powers.

In typical cases, the increase in noise with local-oscillator power roughly offsets the decrease in conversion loss over wide ranges of local-oscillator power inputs, and this results in a fairly constant noise figure for large variations in local-oscillator power. Actually, with typical crystals, the noise figure is usually constant within about 1 db for variations in local-oscillator power producing rectified crystal currents between about 0.3 and 1.5 ma.

The variations in effective input and output resistance with local-oscillator power input at high frequencies depends on the various reactance elements in the mixer circuit (see Sec. 29-6). At low frequencies, however, both the input and the output resistances are relatively high for low local-oscillator power inputs, but decrease rapidly as the local-oscillator power is increased. The rate of reduction in input and output resistance decreases as the power is increased, and for relatively large power the resistance decreases relatively slowly. Over the range of local-oscillator power input used in typical mixers, the input and output resistances do not vary rapidly with local-oscillator power. At high frequencies the effective input impedances may be greatly affected by the circuit reactances, but the same general effects are generally produced.

**29-8. Local-oscillator Coupling Problems.**—As mentioned in Sec. 29-4, the local oscillator should be coupled to the mixer in such a manner that a sufficient amount of local-oscillator power is fed into the crystal and that the local-oscillator coupling does not upset the impedance match between the mixer and the antenna circuit or absorb an appreciable amount of signal power. Actually in many wide-range receivers it has not been possible to fulfill both of these conditions without increasing the complexity of the receiver appreciably, and, as a result, compromises have been made.

In receivers using butterfly oscillators and preselectors, direct magnetic coupling between oscillator and preselector butterflies has been found to give good results when the intermediate frequency or the difference in frequency between the signal and the local oscillator is relatively high compared with the signal frequencies. Since, when this is true, the local-oscillator resonator is appreciably detuned from the preselector resonator frequency, the mutual loading and frequency-pulling difficulties are usually small. A tuner using butterfly resonators with magnetic coupling between the local oscillator and the preselector has been constructed that operates satisfactorily over a frequency range from 70 to 300 Mc with a 30-Mc intermediate frequency. Another butterfly pre-

selector using magnetic coupling but operating on the second harmonic of the local-oscillator frequency performs satisfactorily over the frequency range from 300 to 1000 Mc with a 30-Mc intermediate frequency.

In higher frequency wide-range preselectors using coaxial tuners, the local oscillator is usually coupled to the mixer through a coaxial transmission line. Excessive variations in local-oscillator power input to the crystal may then be caused by improper termination of the line from the local oscillator to the mixer. In fact, the standing-wave ratio on the line may become high enough to overload the oscillator and cause it to cease oscillating at some frequencies. It is usually difficult to devise a coupling network that will match the line to the mixer over wide frequency ranges without interfering with the signal-circuit relations. The standing-wave ratio may, however, be reduced to a reasonable value

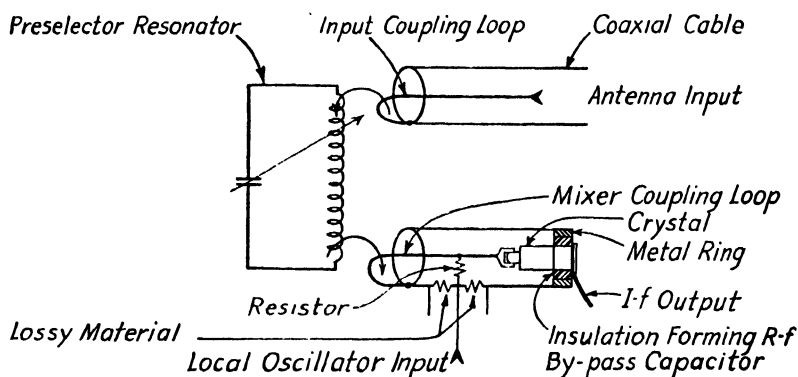


FIG. 29-9.—A schematic diagram of a preselector and mixer using direct coupling between the local oscillator and mixer.

by inserting small pieces of lossy material, such as Polyiron, in each end of the line. The pieces are proportioned to introduce a loss that keeps the standing-wave ratio within reasonable limits but does not attenuate the local-oscillator output unreasonably.

One method of connecting the local oscillator to the mixer is shown in Fig. 29-9. The center conductor of the line from the local oscillator is connected through a resistor to the center conductor of the line between the preselector coupling loop and the crystal. The resistor, which should be large compared with the impedance of the line between the coupling loop and crystal but not so large that it is effectively by-passed by its own capacitance, is used to prevent the local-oscillator line from absorbing an appreciable amount of power or upsetting the impedance relations in the signal circuit. In a mixer described more fully in Sec. 29-15, satisfactory operation over the frequency range from 2000 to 4000 Mc is obtained with a 500-ohm  $\frac{1}{2}$ -watt carbon resistor.

Another method of coupling the local oscillator to the mixer is actually to couple it through the preselector cavity. The local-oscillator line is connected to an additional loop or probe in the tuner near the loop feeding the mixer. The coupling between the two loops transfers the local-oscillator power to the mixer. In this method, however, the cavity is not tuned to the local-oscillator frequency but to the signal frequency, and consequently the coefficient of coupling is small. A schematic diagram of this type of coupling is shown in Fig. 29-10. The same precautions with respect to signal-power loss and local-oscillator mismatch must be observed as in the first method. A disadvantage of this type of coupling is that the coupling of the local-oscillator circuit is much greater to the signal-input circuit than to the mixer circuit, since the tuner is resonant at the signal frequency. When the available local-oscillator power is

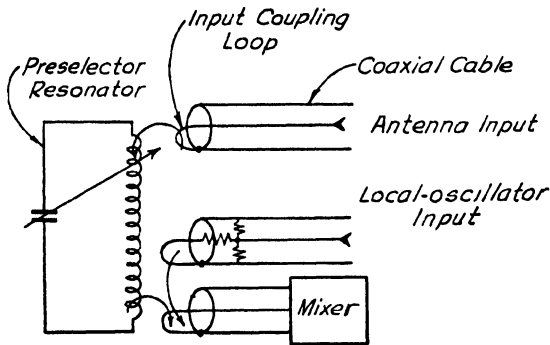


FIG. 29-10.—A schematic diagram of a preselector and mixer using inductive coupling between the local oscillator and mixer.

very low, difficulty may therefore be encountered in obtaining a sufficient amount of local-oscillator power in the mixer circuit without causing an excessive signal-power loss. This effect may be overcome if a nondissipative coupling network is used between the local oscillator and preselector, and in many cases it is possible to design a simple nondissipative network that produces satisfactory results over wide frequency ranges.

One method of coupling the local oscillator to the crystal mixer in waveguide mixers is to connect the coaxial line from the oscillator directly in series with the mixer, as shown in Fig. 29-11. The impedance presented by the line in series with the crystal should be low to both r-f and i-f currents. Since the local oscillator is not tuned to the signal frequency, the impedance of the coupling loop terminating the line in the local-oscillator cavity is low if the loop is very small. Hence the desired low impedance can be approximated by making the line very short by mounting the mixer and local oscillator very close together.

**29-9. Termination of Waveguide in Broad-band Untuned Waveguide Mixers.**—In untuned waveguide mixers, the crystal is usually mounted directly across the waveguide, as shown in Fig. 29-11. However, the end of the waveguide is rarely left open, as the loss in signal power at high frequencies due to radiation from the open end is relatively large and the stray-field pickup may be serious. For narrow-band operation, the end of the waveguide may be closed, or short-circuited, with the distance between mixer and end of the waveguide adjusted to approximately a quarter of a guide wavelength in the section of waveguide beyond the mixer. The terminating section then acts as a high-impedance shunt across the crystal. This method of terminating the waveguide is not satisfactory for very broad-band mixers, however, since the length of waveguide beyond the mixers cannot be fixed at a value that presents a high shunting impedance over wide frequency bands. If a short section is used, the impedance may be very low at the low-frequency end of the band; if a long section is used, resonances occurring when the length is half a guide wavelength effectively produce a short circuit across the mixer.

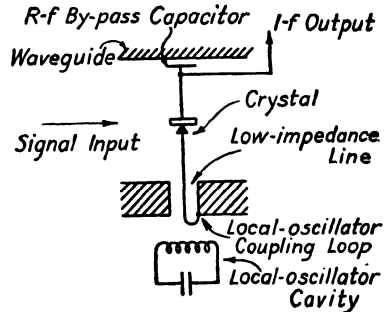


FIG. 29-11.—Equivalent circuit of a crystal mixer in a waveguide.

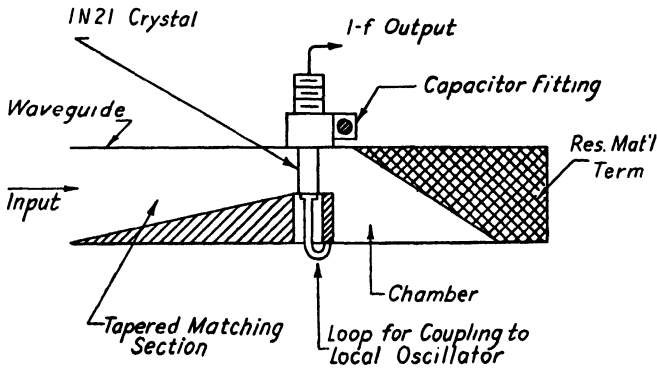


FIG. 29-12.—Sketch of a step mixer.

One method of achieving a broad-band termination is to use between the mixer and the short-circuited end of the guide a short section of waveguide that has a much higher characteristic impedance than the input waveguide. A small tapered piece of lossy material, such as cloth or bakelite coated with resistive material is inserted into the end of the terminating waveguide section to reduce the amplitude of the wave



reflected from the short circuit. Consequently, the shunting impedance across the mixer is approximately equal to the characteristic impedance of the terminating section over the whole frequency band. Through the use of a simple matching transformer it is usually possible roughly to match a crystal to the antenna input waveguide over very wide frequency bands. An example of this type of mixer, called a *step mixer*, is shown in Fig. 29-12.

**29-10. Crystal Characteristics Affecting Conversion Loss at High Frequencies.**—As pointed out in Sec. 29-3, the capacitance across the barrier layer in a crystal causes a reactive component of current to flow through the spreading resistance. The conversion efficiency decreases rapidly when the reactive current becomes appreciable. Crystal mixers for operation near 3300 Mc, such as the type 1N21B, have barrier capacitances that are small enough to cause only a slight decrease in conversion efficiency up to this frequency. Type-1N23B crystals have smaller barrier capacitances than the type 1N21B and may therefore be operated at frequencies up to about 10,000 Mc before the conversion efficiency begins to decrease rapidly. 1N26 crystals, which have still smaller capacitances, may be operated efficiently up to about 25,000 Mc.

**29-11. The Optimum Intermediate Frequency from Noise Considerations.**—In the choice of an optimum intermediate frequency for the greatest signal-to-noise ratio, the variations in noise output with frequency from both the crystal mixer and i-f amplifier must be considered. In general, the noise figure of an i-f amplifier increases as the frequency is increased (see Sec. 33-4). Therefore the lower the intermediate frequency, the more sensitive the receiver can be made if the noise output of the mixer remains constant.

The noise output from a practical mixer can be divided into two parts. One part is the actual noise generated in the crystal, which is indicated by means of the noise temperature of the output resistance. The other part is converted noise from the local oscillator. The magnitude of the noise generated by the crystal is not independent of the intermediate frequency but reaches very high values at low frequencies and decreases rapidly with increasing frequency up to about 10 or 15 Mc, beyond which it assumes a constant value. The noise temperature for various crystals given in Table 29-1 is measured at a frequency at which the actual crystal noise has reached a constant value and does not take into consideration converted noise from the local oscillator. The local oscillator produces noise voltages on either side of the carrier, the spectrum of which, in negative-grid oscillators, is determined by the  $Q$  of the oscillator resonator, as shown in Fig. 29-13. The noise components, which differ from the carrier frequency by an amount equal to the intermediate frequency, mix with the carrier in the crystal and produce noise

in the output. The amplitude of this noise is proportional to the local-oscillator power. It is evident from Fig. 29-13 that the higher the intermediate frequency, the smaller will be the noise produced in the *i*-acceptance band by this source. The spectrum of the noise produced by reflex-klystron oscillators is usually determined not only by the cavity *Q* but also by the setting of the reflector voltage. In general, reflex klystron oscillators produce a greater amount of noise than do negative grid tubes. For instance, at 3000 Mc typical negative-grid oscillators produce a negligible amount of noise for intermediate frequencies above 15 Mc, but some reflex klystrons produce an appreciable

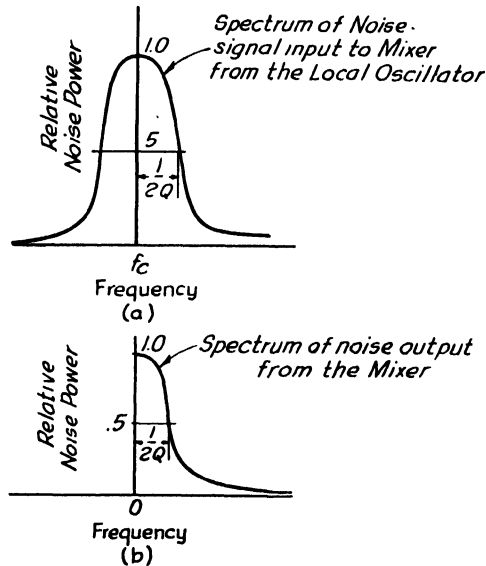


FIG. 29-13.—Spectrum of local-oscillator noise from a negative-grid oscillator.

amount of noise up to about 30 Mc. Consequently, for maximum signal-to-noise ratio in the receiver output in this frequency range, the intermediate frequency should be roughly between 15 and 30 Mc, depending on the type of local oscillator used. At 25,000 Mc, reflex-klystron local oscillators produce sufficient noise to raise the noise-temperature factor of the output resistance to a value of 2 to 15 even with an intermediate frequency of 60 Mc. Consequently, a higher intermediate frequency is desirable for maximum sensitivity at this frequency, possibly around 120 Mc. Magic *T*, and other types of balanced mixers in which the local-oscillator noise is balanced out, have not been adapted for use in wide-range receivers as yet.

**29-12. Effect of Bias on Crystal-mixer Performance.**—The most desirable location of the mixer in butterfly resonators and some other types of tunable transformers and preselectors is directly across high-

impedance points. Since the mixer loads the oscillator heavily in this position and causes the selectivity of the preselector to be poor, the mixer input resistance should be as high as possible. The mixer input

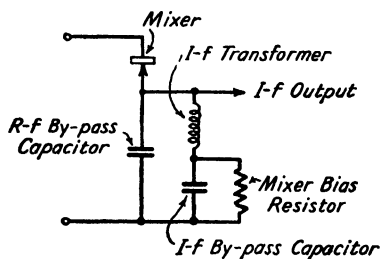


FIG. 29-14.—Schematic diagram of a mixer using back bias.

resistance, and consequently the preselector selectivity, can be increased by applying a bias in the back direction. If a resistance is placed in the d-c circuit, as shown in Fig. 29-14, the crystal will produce its own back bias. The amount of bias can be controlled by the size of the resistance. The input and output resistances increase, and in general the conversion loss decreases slightly, with increasing

back bias. However, the noise generated rises rapidly, and the over-all noise figure increases, with increasing bias. Under some circumstances it may be desirable to sacrifice sensitivity for increased input resistance.

**29-13. Harmonic Mixing.**—In a superheterodyne receiver, spurious responses can be produced whenever the difference between any integral multiple of the local-oscillator frequency and any integral multiple of the signal frequency is equal to the intermediate frequency [see Eqs. (25-10) and (25-11)]. Although these higher order responses are usually undesirable, the multiple 2, 3, or 4 of the local-oscillator frequency may be used in some wide-range receivers, in order that the oscillator can operate at lower frequencies and cover a much wider signal range than would be possible if the receiver operated on the oscillator fundamental. The objection to this method of operation is that a larger number of spurious responses are produced, since the separation between adjacent multiples of the local-oscillator frequency is smaller than if the fundamental local-oscillator frequency were used.

Too much emphasis cannot be placed on the fact that mixing at multiples of the local-oscillator frequency takes place even when the local-oscillator signal contains no harmonics, as this point is often overlooked.

Spurious responses obtained from heterodyning of the fundamental or multiples of the local-oscillator frequency with multiples of the signal frequency are usually negligible unless the signal voltage is large, but they may be very objectionable in receivers having little or no selectivity in the preselector, particularly with pulsed signals.

A mixer having a large back bias usually has less difference in conversion loss on various multiples of the local-oscillator frequency than does a mixer with zero bias. Consequently, a mixer with zero bias is usually preferable from the standpoint of spurious responses resulting from mixing of signals with multiples of the local-oscillator frequency.

**29-14. Diode Mixers.**—As discussed in Sec. 29-2, diodes are slightly inferior in noise figure to crystal mixers even at low frequencies and become increasingly less desirable at higher frequencies. However, diodes are usually much more rugged mechanically and can withstand much greater overloads than crystals. Consequently, they are preferred for some relatively low-frequency mixers but usually are not used at frequencies above about 500 or 1000 Mc.

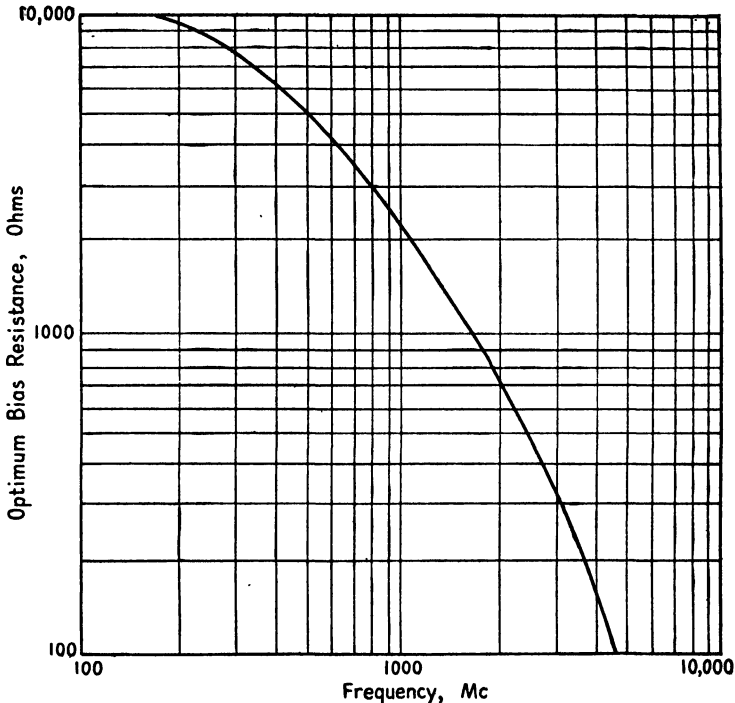


FIG. 29-15.—Variation in optimum bias resistance with frequency for a British high-frequency diode.

The actual circuits and methods of operation of diode mixers are similar to those of crystal mixers except that the mechanics of rectification is different, the input and output resistances are higher, and heater connections must be made. The decrease in conversion efficiency at high frequencies is mainly the result of transit-time effects, rather than of capacitance as in a crystal. In a diode the noise generated does not increase rapidly as the back bias is increased, and consequently the overall noise figure may be improved by providing a back bias. The optimum size of the resistor used for producing the self-bias decreases as the operating frequency is increased. A curve showing the variation in optimum bias resistance with frequency for a u-h-f British diode is given

in Fig. 29-15. As in a crystal, the input resistance increases as the back bias is increased.

### 29-15. Examples of Crystal and Diode Mixers.

*Example 1:* In Fig. 30-1 is shown a plug-in tuner for a superheterodyne receiver that covers the frequency range from 75 to 300 Mc. Both the oscillator and the preselector resonators are butterflies, and a diode mixer is mounted directly across the high-impedance points of the preselector butterfly. The preselector acts both as a band-pass filter and as the matching transformer between the mixer and the antenna circuit, which connects to a tap on the inductance arm, as shown. In the design of this tuner there were several reasons for choosing a diode as the mixer. The main one was that the most desirable place to connect the mixer is directly across the high-impedance points of the resonator,

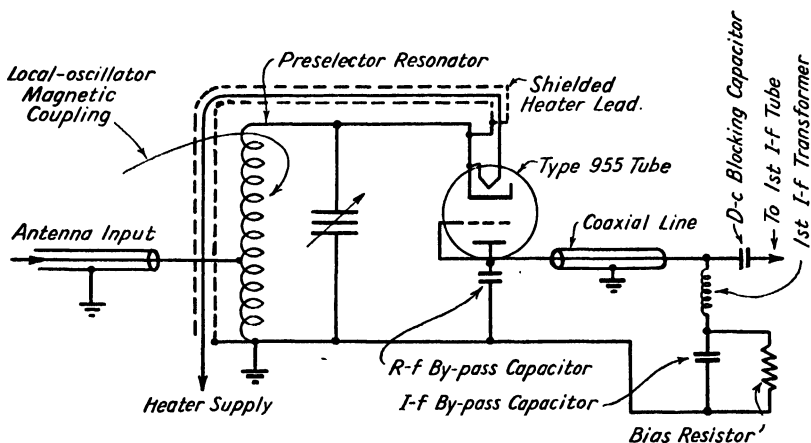


FIG. 29-16.—Schematic diagram of a diode mixer operating from 70 to 300 Mc.

since in this position the leads can be kept short and stray direct coupling between the antenna and mixer circuits kept at a minimum. In this position the mixer loads the tuner very heavily and has a large effect on the selectivity, which was of prime importance in the application for which this mixer was designed. Since a higher input resistance can be obtained with a diode than with a crystal, a type-955 acorn triode connected as a diode was used, in spite of its somewhat higher noise figure. Actually, a 15,000-ohm self-biasing resistor was connected in the d-c circuit of the mixer, as shown in the schematic diagram of Fig. 29-16. The self-biasing resistor increases both the input resistance and the noise figure of the mixer. The local-oscillator power is coupled to the mixer by magnetic coupling between the two butterflies, and, since the intermediate frequency is 30 Mc, no apparent difficulties are encountered in absorption of signal power by the local oscillator or in the oscillator loading caused by the mixer. The ungrounded heater lead is shielded and brought to r-f ground potential by running it along the inductance arm to ground, as shown in Fig. 30-1.

*Example 2:* In Fig. 29-9 is shown a mixer used in a superheterodyne receiver covering the range from 2000 to 4000 Mc. The tuner consists of two critically

coupled coaxial resonators. The mixer, which is a 1N21B crystal, is loop coupled to one cavity. The local oscillator is coupled to the mixer through a coaxial line tapped across the line joining the preselector cavity coupling loop and the crystal. The position of this tap is adjusted to give most uniform crystal current throughout the tuning range of the receiver. A 500-ohm series resistor is connected between the center conductor of the oscillator line and the center conductor of the signal-input line to prevent the local-oscillator line from absorbing a large amount of signal power, or from introducing appreciable reflection in the line between the preselector cavity and the crystal.

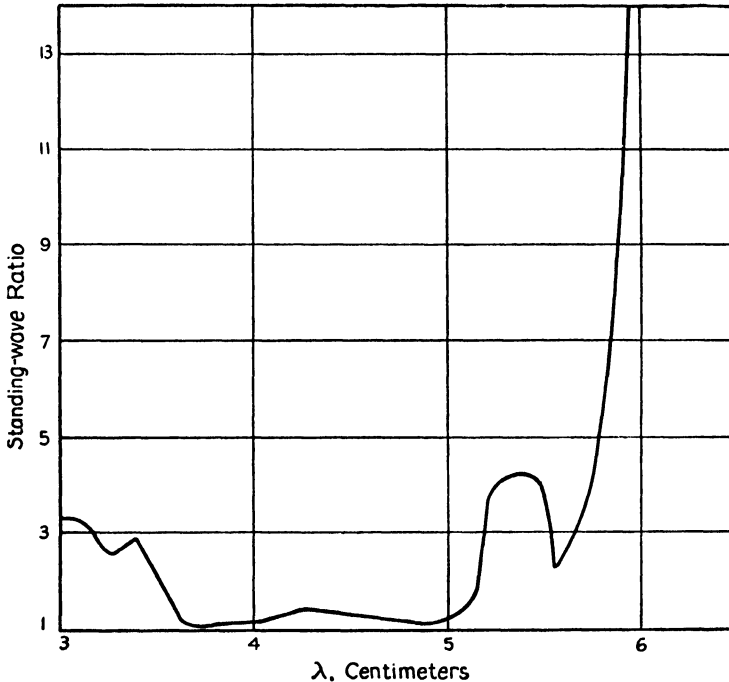


FIG. 29-17.—Standing-wave ratio as a function of wavelength for a step mixer similar to the one shown in Fig. 29-12, operating from 5000 to 10,000 Mc.

*Example 3:* In Fig. 29-12 is shown a sketch of an untuned waveguide mixer operating over the frequency range from 5000 to 10,000 Mc or from 3 to 6 cm. A tapered section of waveguide is used as a broad-band matching transformer between the antenna input waveguide and the crystal mixer. The mixer, a 1N23B crystal, is mounted across the narrow end of the tapered guide and is followed by a section of higher impedance which is approximately terminated by a wedge-shaped strip of bakelite coated with resistive material and which shunts the crystal with a relatively high impedance over the whole frequency range. The top end of the crystal is connected to the waveguide through an r-f by-pass capacitor across which the i-f output is developed. Local-oscillator power is coupled to the mixer from an adjacent local oscillator through a short length of low-impedance line that is connected in series with the crystal.

The mixer is fairly well matched to the antenna input waveguide over the operating frequency range, as can be seen from the plot of standing-wave ratio in the antenna waveguide as a function of frequency shown in Fig. 29-17. It is presumed that the rise in standing-wave ratio at the low-frequency end of the tuning range is a result of approach to the cutoff frequency of the guide. Figure

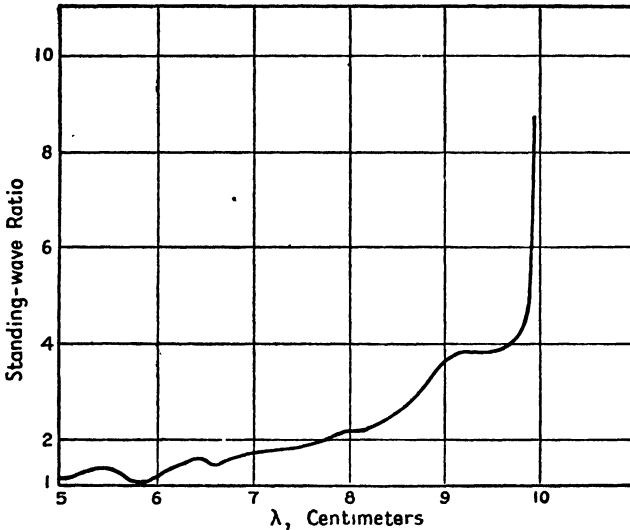


Fig. 29-18.—Standing-wave ratio as a function of wavelength for a step mixer similar to the one shown in Fig. 29-12, operating from 3000 to 6000 Mc.

29-18 shows the standing-wave ratio obtained from a similar mixer designed to operate from 3000 to 6000 Mc.

**29-16. Low-level Direct Detection at High Frequencies.**—Low-level direct detectors are essentially low-sensitivity devices and consequently have a limited usefulness. The low sensitivity is a result of the inherent

low rectification efficiency of all types of rectifiers with small applied voltages.

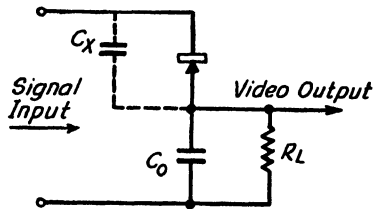


Fig. 29-19.—Schematic diagram of a typical low-level detector.

Basically a low-level detector consists of a rectifying unit such as a crystal or diode in series with an r-f bypass capacitor that is usually shunted by a resistor, as shown in Fig. 29-19. The rectified voltage appearing across the capacitor when a signal is applied across

the input terminals is proportional to the instantaneous peak amplitude of the r-f voltage applied, if the rectification efficiency is constant for various r-f voltage levels. Consequently, the amplitude of the rectified voltage follows the envelope of the input signal if the time constant of the RC circuit is short enough to allow the voltage to follow the modulating

frequencies. In most very low-level detectors, however, the rectification efficiency is not independent of the applied voltage. For example, the crystal has a "square-law" characteristic, and the output voltage is proportional to the r-f power input. Consequently, the modulation envelope will be distorted in the output. Since pulsed signals were received in most applications of radar-intercept receivers, the variation in rectification efficiency produced no distortion.

**29-17. Diode and Crystal Low-level Detectors.**—At very low signal levels the rectification efficiency depends on the slope of the current-voltage curve near zero voltage when the signal frequency is low. The larger the second derivative  $d^2i/de^2$  of the curve near the origin, the greater is the efficiency. In general, crystal rectifiers have a much greater rate of change of current with voltage than diodes at very low voltages and consequently have much higher efficiencies. Typical curves of current vs. voltage for crystals and diodes have been shown in Fig. 29-4. In a diode, because of the emission velocity of the electrons and the contact potential, a negative voltage is required to reduce the current to zero, and consequently the rate of change of voltage near zero is relatively small. The detection efficiency is consequently low. Furthermore, as a result of the low applied voltages, transit-time effects become serious in diodes at relatively low frequencies and reduce the rectification efficiency. Crystals do not suffer from transit-time effects, but at high frequencies the shunting effect of the capacitance across the barrier layer reduces the rectification efficiency in the same manner as it does in crystal mixers. Since the barrier resistance of crystals is much higher when they are used as low-level detectors than when they are used as mixers, the effect of the capacitance is greater. In general, crystals rather than diodes are normally used in high-frequency direct-detection receivers because of their greater detection efficiency. Therefore only crystal detectors will be discussed in the following sections.

**29-18. Equivalent Circuit of a Low-level Crystal Detector.**—At very low levels the rectification efficiency of a crystal is very low, and as a result, changes in the output circuit have very little effect on the input impedance. The detector may therefore be represented, as shown in Fig. 29-20, by a four-terminal network (reactive elements are neglected in this circuit) which consists of a constant resistance  $R_i$ , shunted across the input r-f terminals, and a video output circuit composed of a constant-current generator  $I_o$  and an output resistance  $R_o$ . At signal-input levels up to several microwatts, the crystal operates in a square-law region, and both the input and output resistances are approximately equal and independent of input power. The resistance is approximately equal to the reciprocal of the slope of the current-voltage curve, shown in Fig. 29-4, at zero voltage. The magnitude of this resistance varies between



crystals but normally is of the order of several thousand ohms. At higher levels, the crystal gradually approaches a linear characteristic, and the input and output resistances decrease rapidly. The “square-law” region is usually of most importance as the maximum sensitivity of the receiver is ordinarily determined by the crystal characteristics in this region.

In the square-law region, the output rectified current is proportional to the power input, and the proportionality factor  $b$  relating them when the output circuit is short-circuited is defined by the relation

$$b = \frac{P_s}{I_{sc}^2} \tag{29-4}$$

where  $P_s$  is the r-f power input in watts and  $I_{sc}$  is the direct current in amperes, produced with the output circuit short-circuited. The current

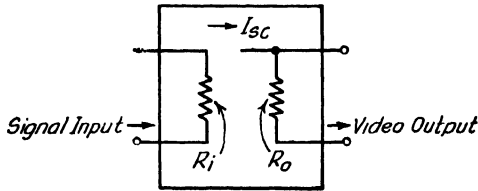


FIG. 29-20.—Four-terminal-network equivalent of a low-level crystal detector.

produced by the constant-current generator in Fig. 29-20 is, therefore,  $I_{sc} = P_s/b$  and the output voltage,  $E_o = \frac{P_s}{b} R_o$ . In the case of a pulsed signal,  $P_s$  and  $E_o$  are the values at the crest of the pulse. The output for a sinusoidally modulated signal can easily be calculated.

For high-frequency modulation the effective time constant of the resistance-capacitance circuit consisting of the r-f by-pass capacitance  $C_o$ , the total capacitance  $C$  across the crystal at the modulation frequencies, the load resistance  $R_L$ , and the back resistance  $R_b$  of the crystal must be made short enough so that the circuit can follow the modulation. In most applications the load resistance can be made infinite, as the charge leaks off the total by-pass capacitance through the back resistance of the crystal, which is approximately equal to  $R_o$ , rapidly enough to follow the modulation.

**29-19. Noise in Low-level Crystal Detectors.**—In general the limiting sensitivity of a direct-detection receiver, like that of a superheterodyne receiver, is determined by the signal-to-noise ratio in the output. The noise produced in a crystal detector is primarily of two types:

1. Johnson noise, which is a result of thermal fluctuations in the crystal output resistance.
2. Converted noise from incidental d-c or r-f sources.

In a crystal operating without bias at low levels, the Johnson noise is greatly predominant. The power generated by this source is

$$P_n = 4KTB \tag{29-5}$$

where  $K$  is Boltzmann's constant,  $T$  the absolute temperature in degrees Kelvin, and  $B$  the integrated band width of the receiver in cycles.

When extraneous high-level r-f or d-c voltages are applied to the crystal, a large amount of additional noise, called *converted noise*, is also produced. For instance, if the crystal is biased with 0.5 ma of current flowing in the forward direction, the equivalent temperature of the output resistance of the crystal  $T$  in Eq. (29-5) rises to about 1000 times its normal value in the 1-kc region of the noise spectrum. For biases in the backward direction, the noise is much greater and varies approximately as the square of the bias current. Measurements at 0.01-ma back-bias current show equivalent noise temperatures 100,000 times the normal value in the 1-kc region of the noise spectrum. The noise generated also increases rapidly when large r-f voltages are applied. Converted noise from either r-f or d-c sources has a frequency spectrum with a maximum at low frequencies and decreasing practically inversely with frequency at higher frequencies. Since the receiver sensitivity is usually limited by the noise generated in the detector, all extraneous r-f or d-c sources should be isolated from the detector to keep the generated noise at minimum. If this is impractical, the amplifiers should have as high a low-frequency cutoff as possible, in order to eliminate the large-amplitude low-frequency noise voltages.

**29-20. Direct-detection Receiver Sensitivity.**—As in superheterodyne receivers, the signal-to-noise ratio in the output limits the sensitivity of a direct-detection receiver. Since, in general, the detection efficiency is very low, the noise input from the antenna can be neglected in the output of the detector, as the antenna noise is far overshadowed by the crystal noise. Actually, the video-amplifier stage following the detector also generates noise (see Sec. 33-4). The noise generated by the video amplifier can be accounted for by placing a fictitious noise-generating resistance  $R_A$  in series with the grid of the first stage, as shown in Fig. 29-21. In type-6AC7 tubes,  $R_A$  is approximately 1200 ohms.

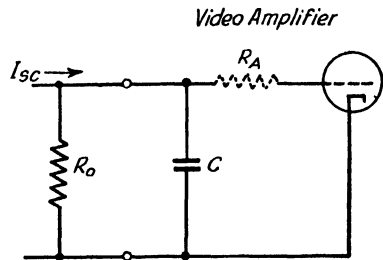


FIG. 29-21.—Equivalent circuit of a low-level detector.

Under the assumption that the converted noise is very small and can be neglected, the total equivalent rms noise voltage  $\bar{N}$  produced at the

grid of the first video stage is the sum of the noise voltages generated by the crystal and the amplifier.

$$\bar{N}^2 = 4KTB(R_A + R_o) \quad (29-6)$$

where  $R_A$  is the equivalent noise-generating resistance in the grid of the first video stage and  $R_o$  is the output resistance of the crystal. The peak signal voltage  $E_o$ , appearing at the grid of the first video stage for a pulsed signal whose power at the crest of the pulse is  $P_s$ , is

$$E_o = \frac{P_s}{b} R_o \quad (29-7)$$

Therefore the peak signal-to-rms noise ratio is

$$\frac{E_o}{\bar{N}} = \frac{\frac{P_s}{b} R_o}{\sqrt{4KTB(R_A + R_o)}} = \frac{P_s}{\sqrt{4KTB}} \cdot \frac{R_o}{b \sqrt{R_A + R_o}} \quad (29-8)$$

The pulsed-signal input power that produces a receiver output voltage of peak value equal to the rms noise voltage is then

$$P_s = \sqrt{4KTB} \cdot \frac{b}{R_o} \sqrt{R_A + R_o} \quad (29-9)$$

The factor  $R_o/(b \sqrt{R_A + R_o})$  is called the *figure of merit* of the receiver. The minimum detectable signal is inversely proportional to the figure of

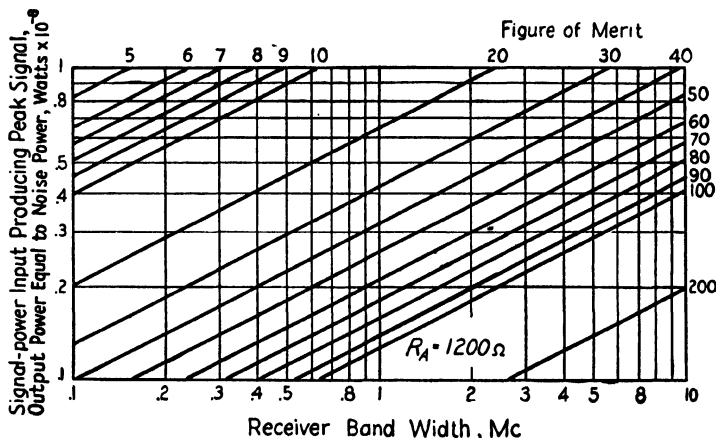


FIG. 29-22.—Peak-pulsed signal-power input required to produce a peak output-voltage pulse equal in amplitude to the rms noise voltage as a function of the figure of merit of a low-level detector.

merit. Figure 29-22 is a chart showing the relationship between receiver band width and signal-power input for pulsed signals producing a signal in the output whose peak power is equal to the rms noise power, for various figures of merit. The equivalent noise resistance  $R_A$  of the video amplifier

is assumed to have a value of 1200 ohms. For a sinusoidally modulated signal, the input power should be divided by  $m\sqrt{2}$ , where  $m$  is the modulation coefficient, to obtain the carrier power required to produce a modulation-frequency output signal whose rms voltage is equal to the rms noise voltage.

The rectification factor  $b$  increases with increasing frequency, because of the capacitance effect described in Sec. 29-17. Therefore it must be known at the operating frequency if the sensitivity is to be calculated. It can be measured by supplying the crystal with a known amount of r-f power and measuring the rectified current. Type-1N32 crystals have figures of merit of approximately 100 for  $R_A = 1200$  ohms and a video output resistance  $R_o$  varying from about 5000 to 20,000 ohms at frequencies of about 3000 Mc. Type-1N21B crystals have figures of merit and resistances varying from 60 to 200 and from 1000 to 15,000 ohms, respectively, under the same conditions. Type-1N31 crystals have a figure of merit greater than 55 with  $R_A = 1200$  ohms and a video output resistance between 6000 and 24,000 ohms at 10,000 Mc.

**29-21. Input Impedance of a Low-level Detector.**—Since the detector must be matched to the antenna circuit for maximum sensitivity, the variations in the input impedance of the detector with frequency are very important in wide-range receivers, since they affect the design of the matching transformer. The actual crystal input and output resistances are approximately equal to the reciprocal of the slope of the current-voltage curve at zero voltage; the actual impedance developed across the terminals may depend to a great extent on the reactances in the circuit. The equivalent circuit of a crystal detector is similar to the circuit of a crystal mixer, shown in Fig. 29-7. As a result of the complicated nature of the circuit, it is usually difficult at high frequencies to design very wide-range fixed transformers or tuned transformers requiring only a single tuning adjustment to provide the desired match, and consequently in most practical cases compromises are made.

In one detector, a type-1N21B crystal became series-resonant at about 3500 Mc and had a  $Q$  between 5 and 10. However, the actual resonant frequencies obtained in practice depended largely on the type of mounting of the detector.

### 29-22. Examples of Wide-band Direct Detectors.

*Example 1:* In one direct-detection receiver covering the frequency range from 100 to 1000 Mc, two butterfly tuners and two crystal detectors were used. One butterfly tuned over the range from 100 to 400 Mc, and the other from 400 to 1000 Mc. Type-1N27 crystals were used as detectors and mounted directly across the high-impedance points of the butterflies. A somewhat more detailed description appears in Sec. 28-15.

*Example 2:* Several high-frequency wide-range direct-detection receivers using tunable coaxial resonators as preselectors were built. The crystal detector and antenna circuits were magnetically coupled to the resonator, and the video output was obtained across the r-f by-pass capacitor in series with the crystal. The tuner acted both as a filter and as a transformer. Units covering frequency ranges of 1000 to 3500 Mc, 3000 to 6500 Mc, and 6000 to 10,000 Mc were constructed.

**29-23. Second Detectors.**—The design of second detectors for use with the broad-band high-frequency r-f amplifiers used in radar-intercept receivers is very similar to that of conventional second detectors. The main differences are that low load resistances must be used, since the modulation frequencies are very high, and that a much lower detection efficiency is obtained than in narrow-band receivers. The carrier frequency is usually between 30 and 200 Mc. In order to keep the efficiency as high as possible, the i-f by-pass capacitance in series with the detector is usually made small because, for the same circuit time constant, the load resistance can be made larger with a smaller capacitance. This cannot be carried too far, however, as the i-f by-pass capacitance and internal capacitance across the detector form a capacitance voltage divider across the input circuit. In typical circuits, i-f by-pass capacitances of about 10 or 20  $\mu\mu\text{f}$  are used, and second-detector losses of about 10 db are usually obtained with a 4-Mc pass band and a 6H6 diode.

The type-6AL5 double diode is one of the best high-frequency second detectors, because of its low front or conducting resistance and low capacitance. A current-voltage characteristic of a type-6AL5 diode is plotted in Fig. 29-4.

It will be noted in Fig. 29-4 that germanium crystals have lower front resistances and capacitances than diodes and also very high back resistances over a range of back voltage extending to high values that make it possible to obtain higher detection efficiencies and less capacitance loading of the output i-f transformer than with a diode. Also the unit is small, and no heater connections are required. The type-IN34 germanium crystal has been designed for second-detector applications and can withstand back voltages of 50 volts or greater without suffering damage, since the back resistance remains high.

**29-24. Crystals as Measuring Devices.**—At high frequencies, crystal detectors are very useful for indicating the relative magnitudes of applied r-f voltages<sup>1</sup> and are used in measuring the standing-wave ratio in slotted lines, in monitoring the output of oscillators, and, at relatively low frequencies, in actually measuring r-f voltages. The rectified short-circuit

<sup>1</sup> PETERSON, A., Vacuum Tube and Crystal Rectifiers as Galvanometers and Voltmeters at Ultra High Frequencies, *General Radio Experimenter*, 19, No. 12, 1-7 (May, 1945).

current produced by a crystal may be used as an indication of the applied signal, but usually the open-circuit d-c voltage produced across the r-f by-pass capacitor is used. At low voltages, the output voltage is proportional to the square of the input voltage; at voltages above about 0.05 volts, it becomes almost directly proportional to the applied voltage. At very large applied voltages, the rectified voltage tends to depart from the linear relation, as shown in Fig. 29-23, because of the decrease in back resistance. The voltage level at which this occurs varies between crystals. Type-1N34 germanium crystals are linear up to very high voltages but have poor high-frequency characteristics because the barrier capacitance is high. Their rectification efficiency tends to drop at frequencies above about 100 Mc.

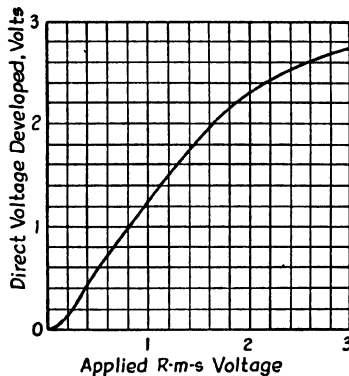


FIG. 29-23.—Rectified output voltage as a function of rms applied voltage for a typical type-1N21B crystal.

Because of their low barrier capacitance, silicon crystals, such as the 1N21B, have much better high-frequency characteristics. The rectified voltage produced for a given input voltage tends to increase with frequency, because of the effect of the series-resonant circuit formed by the barrier capacitance and the cat-whisker inductance. The voltage reaches a maximum at series resonance and decreases at higher frequencies. Type-1N21B crystals usually are resonant at around 3500 Mc in typical mountings, although the actual resonant frequency of the detector when used in a circuit depends on the additional circuit reactances. In typical applications, relatively accurate measurements of voltage can be obtained at frequencies up to about 2000 Mc. Other types of crystals have higher resonant frequencies and therefore can be used at even higher frequencies. In spite of the resonance effects, crystals are commonly used as an indication of relative voltage at frequencies even above the series-resonant frequency.

## CHAPTER 30

### LOCAL OSCILLATORS: I

BY R. A. SODERMAN, W. H. HUGGINS, AND F. J. KAMPHOEFNER

#### GENERAL CONSIDERATIONS AND BUTTERFLY OSCILLATORS

**30-1. General Requirements.**—An oscillator suitable for use in a superheterodyne receiver must at all times satisfy the following requirements as it is tuned throughout its operating range:

1. There must be no abrupt *jumps* or discontinuities in the frequency variation with tuning.
2. There must be no *erratic* discontinuities in the amplitude of oscillation.
3. The r-f power delivered to the mixer must be adequate to assure proper conversion in the mixer.
4. The relation between the tuning drive and oscillation frequency must be simple and without irregularity.

The first requirement must obviously prevail if the receiver is to give *complete* coverage within the tuning range. Usually, a sudden change in the mode of operation or the excitation of a parasitic resonance is responsible for a frequency discontinuity, although sometimes an erratic metallic contact will also produce this effect. The elimination of all parasitic resonances (and their attendant frequency irregularities) throughout the tuning range constitutes the major problem in the design of wide-range microwave oscillators.

The second requirement simply states that there must be no “tuning noise.” The tuning operation of any wide-range oscillator requires that the frequency-selective parts of the oscillator be varied mechanically. This in turn often involves friction or wiping contacts through which r-f currents must pass. The rather erratic variation of resistance at these contacts can loss modulate the oscillator and produce tuning noise. The obvious remedy for this difficulty is to prevent currents from passing through such erratic contacts by using balanced circuits or suitable chokes and filters. Unfortunately, isolating filters may in themselves contribute parasitic resonances, which also may be very difficult to eliminate.

To meet the third requirement, the oscillator must be built around a tube potentially capable of delivering, throughout the tuning range,

power in excess of that actually required by the mixer. This is necessary because lossy padding is often introduced to reduce the coupling between the oscillator and signal circuits, and this increases the oscillator power requirements. In a typical 3-cm-band oscillator, an output power of not less than 10 to 15 mw has been found adequate. Of course, even though the tube is capable of developing the necessary power, there is still the problem of obtaining with an untuned output circuit sufficiently uniform coupling over the tuning range. The output coupling may excite or exhibit parasitic resonances and, hence, must be designed with the first two requirements in mind. Some of the factors that must be considered are discussed in this chapter and in Chap. 32.

Fortunately, it has been found that the fourth requirement will automatically be satisfied if the first and second requirements are met. This is because tuning irregularities are almost always due to the presence of other resonances in the circuit. The importance of this requirement should be emphasized if other tunable devices, such as a preselector, are to be tracked with the oscillator. It is apparent that an irregular tuning characteristic would be next to impossible to track.

Chapters 30 to 32 on local oscillators are therefore concerned primarily with *techniques* and circuits that may be utilized to satisfy the first two requirements listed above. Detailed descriptions of actual oscillators and their design peculiarities will be given where it is desirable to illustrate the basic phenomena under discussion. It may appear, at first reading, that the discussion in Chap. 32 of parasitic resonances in coaxial cavities and plungers is unnecessarily detailed. When it is realized, however, that the suppression and control of parasitic resonances constitutes the major problem in the design of wide-range microwave oscillators and other tunable microwave circuits, it becomes apparent that this emphasis is justified. If these parasitic resonances are to be combated in a logical manner, the factors that determine their excitation and resonant frequencies must be understood.

**30-2. Survey of Oscillator Types.**—The local oscillator suitable for use in a search receiver of the type described in Chap. 25 should still satisfy the requirements mentioned in the preceding section even after thousands of tuning operations. This imposes a rather severe mechanical limitation in that sliding contacts should be avoided. Hence, the oscillator types to be described are those that are capable of withstanding a large number of tuning operations without developing noise and without change in calibration.

At frequencies less than 1000 Mc, the butterfly oscillator is the most attractive. The resonator in these oscillators is compact and sufficiently like a lumped coil-capacitor combination so that higher frequency circuit resonances are usually outside the oscillator range, and the problem of



mode interference does not arise. Furthermore, the resonator gives extremely wide-range tuning without sliding contacts.

At frequencies greater than 1000 Mc, coaxial-cavity oscillators become of practical size. However, the use of short-circuited coaxial-line sections in extending the oscillation range of triode tubes presents several problems not encountered in the butterfly oscillator.

1. While a butterfly resonator ordinarily yields a resonant impedance sufficient to support oscillation at only one frequency within its tuning range for each setting, a coaxial-line resonator can often resonate at two or more frequencies within a 3:1 range. Hence, oscillation at an undesired frequency may occur, and the problem of mode interference in a coaxial resonator may be much more severe than for a butterfly resonator having the same tuning ratio.

2. With present-day triodes, it has been found that the necessary impedances between tube elements required for oscillation cannot be maintained over a wide tuning range with a single variable circuit at frequencies much greater than 1000 Mc. To extend the operating frequency beyond the maximum obtainable with a single circuit, two tuned circuits are required. This introduces the complication that both resonators must be tuned and tracked together. Although the necessity of tuning two variable elements in triode oscillators is mechanically objectionable, the fact that two elements must be adjusted to obtain oscillations may be used to prevent oscillation at undesired frequencies. By proper design, mode interference can be avoided throughout a tuning range of 3:1 or more.

3. The coaxial-line resonator must be tuned with a short circuit that does not involve sliding contacts if excessive power loss, erratic electrical variations, and mechanical wear are to be avoided. Chapter 32 deals with the problems that may be encountered in designing noncontacting short circuits that are effective over a frequency ratio as great as 5:1.

TABLE 30-1.—TUNING RANGES OF TYPICAL WIDE-RANGE LOCAL OSCILLATORS

Tube	Type	Resonator(s)	$N$ ,* cycles	Tuning range	$k$ Mc
9002 or 955.....	Triode	Butterfly	...	100-500 Mc	0.1-0.5
6F4 and 703A...	Triode	Butterfly	...	450-1100 Mc	0.45-1.1
2C40 (light-house).....	Triode	Two, $3\lambda/4$ coaxial	...	10-30 cm	3.0-1.0
2K28.....	Reflex klystron	$\lambda/4$ coaxial	$1\frac{3}{4}$	11-25 cm	2.7-1.2
		$3\lambda/4$ coaxial	$2\frac{3}{4}$	6.8-14 cm	4.4-2.2
2K48.....	Reflex klystron	$\lambda/4$ coaxial	$1\frac{3}{4}$	5.3-10.5 cm	5.7-2.9
		$3\lambda/4$ coaxial	$2\frac{3}{4}$	3.5-6.0 cm	8.6-5.0
		$3\lambda/4$ coaxial	$3\frac{3}{4}$	2.8-4.55 cm	10.7-6.6
2K49.....	Reflex klystron	$\lambda/4$ coaxial	$1\frac{3}{4}$	4.3-7.9 cm	7.0-3.8
		$3\lambda/4$ coaxial	$2\frac{3}{4}$	3.1-5.0 cm	9.7-6.0
		$3\lambda/4$ coaxial	$3\frac{3}{4}$	2.6-3.8 cm	11.5-7.9

\*  $N$  refers to the number of transit-time cycles for the different repeller ranges.

At frequencies above 1500 Mc, coaxial-cavity oscillators employing the reflex klystron are the most satisfactory. The two principal advantages of reflex tubes over triodes are that only a single resonant circuit is required, the feedback being inherent in the tube, and that the selection of the desired resonator mode of operation may be accomplished electrically through control of the applied repeller voltage.

A summary showing representative oscillator and tube types together with typical tuning ranges is given in Table 30-1.

The remainder of this chapter deals with the specific problems involved in the design of the butterfly type of oscillator. Chapters 31 and 32 are concerned primarily with the design of wide-range oscillators employing a reflex klystron in a single coaxial-line resonator. For specific information on the design of triode oscillators incorporating two coaxial-line resonators, the reader is referred to Chap. 15. Much of the information included in Chap. 32 is applicable to coaxial-line-resonator design in general.

**30-3. Butterflies as Resonators for Wide-range Oscillators.**—In the frequency range between 100 and 1000 Mc, one of the most practical types of wide-range low-power oscillators consists of the combination of a negative-grid triode tube and a butterfly resonator.<sup>1</sup> As pointed out in Chap. 28, conventional coil and capacitor resonant circuits are unsatisfactory for wide-range operation at the higher frequencies principally because large self-inductance and high losses arise from improper current feed to the capacitor stack. The self-inductance of the capacitor limits the highest resonant frequency and also makes it very difficult to make connections to the points across which the maximum impedance is developed. Coaxial-line resonators designed for use in this band have many desirable electrical features, but are physically very large and bulky compared with butterfly resonators designed for the same frequency range. A resonant line operating on its quarter-wavelength mode, for instance, is about 30 in. long at 100 Mc.<sup>2</sup>

A general description of butterfly resonators has been presented in Chap. 28. However, a few characteristics that are important in oscillator circuits are restated below:

1. Butterflies require no sliding contacts carrying r-f or direct current. The only movable element in a butterfly is the rotor, which is mounted on an insulated shaft. Since a butterfly is normally operated floating with respect to ground, the voltages with respect to ground of certain important parts of the butterfly are

<sup>1</sup> KARPLUS, E., The Butterfly Circuit, *General Radio Experimenter*, **19**, No. 5 (October, 1944); Wide-range Tuned Circuits, *Proc. I.R.E.*, **33**, 426 (1945); SINCLAIR, D. B., High-frequency Measurements, *Radio-electronic Engineering*, **5**, No. 6, 14 (December, 1945); **6**, No. 1, 11 (January, 1946).

<sup>2</sup> The capacitive loading at the tube may shorten this length considerably, however.

determined by the distributed capacitance of the butterfly to ground. In true butterflies, the symmetrical type used in the oscillator shown in Fig. 30-1, the capacitances to ground of the butterfly itself are symmetrical, and, if no unbalanced external reactances are added, the center of the rotor will be approximately at ground potential. Therefore the r-f current flowing through the capacitance across the rotor insulator and through the ball bearings to ground is very small,

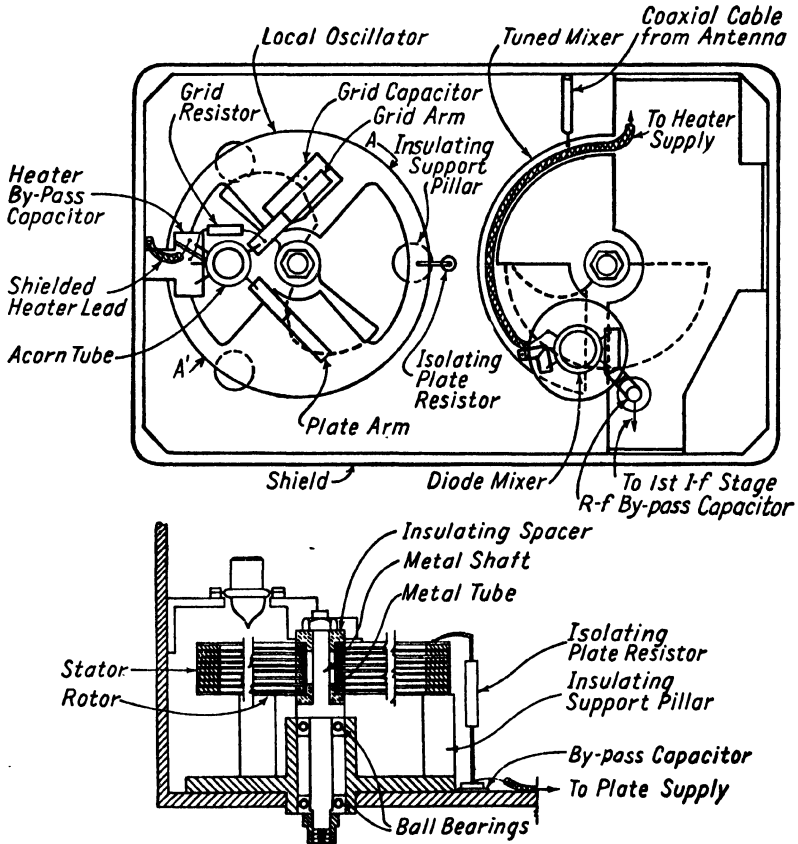


Fig. 30-1.—Local oscillator and preselector assembly.

and the amount of noise modulation of the r-f voltage that occurs as the rotor is turned is negligible. In the semibutterfly of the unsymmetrical type shown in Fig. 30-9, the unit is balanced at its lowest frequency but is unbalanced at all other frequencies. As a result, the rotor is not at ground potential over most of the tuning range, and a very low capacitance between the rotor and its mounting shaft is required to keep the r-f current flowing through the ball bearings at a small value.

2. Butterfly circuits have very wide tuning ranges. The actual range obtainable depends on the physical size of the unit, the size and shape of the capacitor

plates, the spacing between the adjacent capacitor plates, and the effective shunting reactance of the load and oscillator tube. Units have been built covering a frequency range of 10:1, but in typical oscillator circuits tuning ranges varying from 3:1 to 5:1 can usually be attained without switching.

3. Butterfly circuits have a relatively high  $Q$  and a resonant impedance that is sufficient to support oscillation with most low-power triodes. In the frequency range under discussion typical butterflies have an unloaded  $Q$  ranging between 200 and 1000 and a resonant impedance of the order of magnitude of 10,000 ohms.

4. The points across which the maximum impedance is developed at resonance are readily accessible and remain fixed over the tuning range. Low-inductance connections can easily be made to tubes or other elements from these points.

5. Butterflies are mechanically easy to tune, as only a simple rotary motion is required, whereas, in coaxial-line resonators a translational motion is required for tuning. In the latter, therefore, a lead screw, rack and pinion, or linkage system must be used to change the rotary dial motion to linear motion. Furthermore, the static and dynamic friction of a butterfly tuning mechanism can be made very small if ball bearings are used, and very smooth precise tuning can be obtained with only a very small amount of backlash. In coaxial or parallel-wire resonant lines having sliding contacts, both the static and dynamic friction are much greater than in butterfly circuits, and, in many cases, the plunger tends to move in small jumps.

**30-4. Oscillator Circuits.**—In a superheterodyne receiver in which single-dial tuning is desired, the local oscillator should have only a single

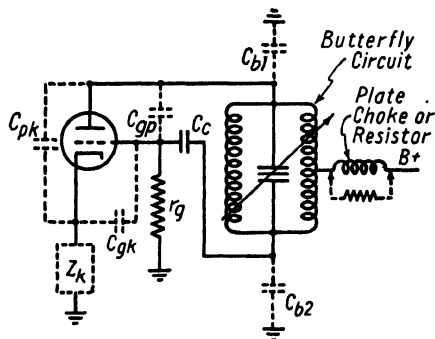


FIG. 30-2.—Schematic diagram of butterfly oscillator.

tuning adjustment, since any additional adjustments require a tracking mechanism, which increases the complexity and cost of the unit. An oscillator consisting of a butterfly resonator and a triode tube connected in a modified Colpitts circuit<sup>1</sup> in which the interelectrode capacitances of the tube form the main feedback network meets this requirement. In an oscillator of this type, the butterfly is connected between the plate

<sup>1</sup> Classified as a Class I oscillator in Chap. 14.

and the grid of the tube as shown in the schematic diagram, Fig. 30-2, and the frequency of oscillation is controlled by turning the butterfly rotor. A sketch of such an oscillator is shown in Fig. 30-1.

A simplified equivalent circuit of this oscillator is illustrated in Fig. 30-3, and Fig. 30-4 shows the same circuit with the oscillator tube replaced by its equivalent circuit. If linear operation of the tube is assumed, the general equation for oscillation of this circuit is

$$\frac{Z_G(\mu + 1) + Z_B}{Z_P + Z_B + Z_G} = -\frac{r_p}{Z_P} \quad (30-1)$$

where  $Z_P$  is the total impedance both internal and external to the tube connected between the plate and the cathode,  $Z_G$  is the total impedance between the grid and the cathode,  $Z_B$  is the total impedance between the

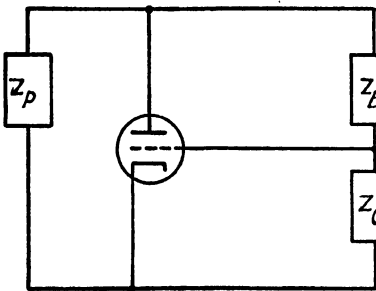


FIG. 30-3.—Generalized circuit of triode oscillators.

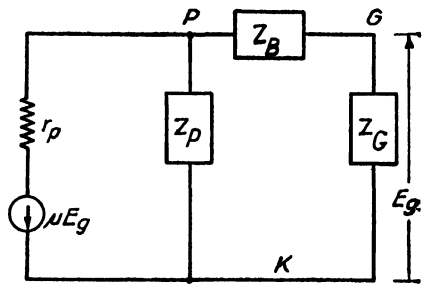


FIG. 30-4.—Equivalent circuit of triode oscillators.

plate and the grid which includes the butterfly impedance, and  $r_p$  and  $\mu$  are the plate resistance and amplification factor, respectively, of the triode. Under normal steady-state operating conditions, the oscillator does not operate in a linear region but as Class C.<sup>1</sup> However, linear conditions are approximated when the oscillations first start building up, and Eq. (30-1) is useful since it indicates whether oscillations will occur under a given set of conditions.

If all the circuit elements are pure reactances, the conditions for oscillation become

$$\mu X_G = X_P \quad (30-2)$$

$$X_P + X_B + X_G = 0 \quad (30-3)$$

Equation (30-2) shows that for oscillation the plate-to-cathode and grid-to-cathode reactances must have the same sign, *i.e.*, they must both be inductive or both capacitive. The magnitude of the grid-to-cathode reactance must be equal to the magnitude of the plate-to-cathode

<sup>1</sup> For this class of operation the general equation for oscillation is still valid if the effective values of  $r_p$  and  $\mu$  are used.

reactance divided by the amplification factor  $\mu$  for steady-state linear operation. However, since it is desired to have the oscillation build up to a point where the oscillator operates as Class C, the feedback and hence the grid reactance is made greater than this value. Since the sum of the plate-to-cathode, grid-to-cathode, and plate-to-grid reactances must be zero, the sign of the reactance between the plate and grid must be opposite to that of the reactance between the plate and cathode or grid and cathode. In fact

$$X_B = - (1 + \mu)X_G = - \left(1 + \frac{1}{\mu}\right)X_P \quad (30-4)$$

Equation (30-3) shows that the three reactances  $X_G$ ,  $X_P$ , and  $X_B$  must form a series-resonant circuit at the oscillating frequency.

In the schematic diagram shown in Fig. 30-2, if the cathode is allowed to *float* with respect to ground, *i.e.*, if  $Z_k = \infty$ , the ratio of the r-f grid voltage to the r-f plate voltage is determined by the tube interelectrode capacitances, and the reactance of the grid-to-cathode capacitance must be equal to or larger than that specified by Eq. (30-2) in order for oscillation to occur. Therefore, if the circuit elements have no losses, the ratio of the grid-to-cathode interelectrode capacitance to the plate-to-cathode interelectrode capacitance must be equal to or less than  $\mu$ . In the practical case, the losses are not zero,  $Z_k$  is not infinite, and the oscillation equations become more complex than Eqs. (30-2) and (30-3). However, similar equations can be derived by equating the real and imaginary parts of Eq. (30-1) with the actual impedances inserted. From these equations it is found that the feedback must be greater than that specified by Eq. (30-2), and, in practice, an interelectrode-capacitance ratio of approximate unity usually produces the best results for wide-range operation.

**30-5. Butterfly Design.**—The requirements for a butterfly for use in an oscillator circuit are very similar to those for r-f tuners, and in general the design information given in Chap. 28 for butterfly tuners is applicable to butterfly oscillators. However, in oscillators the presence of spurious modes in the tuning range usually does not affect the performance, since the oscillators tend to operate on the dominant or fundamental mode. The shunt impedance of the butterfly at resonance is important in oscillator applications and should be kept high for best results. If this impedance becomes too low at any point in the operating band, oscillations will cease. The magnitude of the minimum shunt impedance that will sustain oscillation depends on the tube constants, the feedback, and the losses in the oscillator circuit. If all the constants are known, the minimum shunt impedance for oscillation can be computed from Eq. (30-1),

but usually in high-frequency wide-range oscillators the circuit is so complex that an experimental solution must be obtained.

Butterfly circuits ordinarily do not develop very high resonance impedances because of the low ratio of inductance to capacitance. The resonance impedance  $R_{s,h}$  of a butterfly can be calculated from the equation

$$R_{s,h} \approx \frac{(2\pi fL)^2}{R_s} = \frac{L}{C} \quad (30-5)$$

where  $L$  is the effective butterfly inductance,  $C$  the butterfly capacitance,  $f$  the resonant frequency, and  $R_s$  the effective series resistance. In a butterfly with circular-sector rotor plates, as shown in Fig. 28-8, the inductance decreases appreciably as the butterfly is tuned to higher frequencies. The effective series resistance is mainly determined by the loss caused by eddy currents in the rotor plates, which are responsible for the inductance decrease. In butterflies with circular-sector rotor plates, the changes in inductance and effective resistance balance the capacitance changes, so that the resonant impedance remains practically constant over the tuning range. In typical butterflies, the impedance developed is of the order of magnitude of 10,000 ohms.

In many oscillators it is desirable to have approximately a linear or logarithmic frequency variation with butterfly rotation. To achieve either characteristic, the rotor plates must be specially shaped. For instance, plates similar to the type shown in Fig. 30-1 may be used. The shape given the rotor plates reduces their effective area and results in a lower maximum capacitance and a smaller change in inductance over the tuning range than is obtained in a similar butterfly having circular-sector rotor plates. A butterfly having these shaped plates must therefore be larger in diameter, have a larger number of plates, or have closer spacing between plates than does a unit with circular-sector plates covering the same tuning range.

The impedance produced by butterflies having shaped plates varies appreciably over the tuning range. It is a minimum at the low-frequency end of the tuning range and increases as the circuit is tuned to higher frequencies, because the eddy-current shielding produced by the rotor plates does not increase the losses or decrease the effective inductance rapidly enough to offset the decrease in capacitance. The smaller the relative rotor plate area is, the larger is the variation in impedance produced. However, for a butterfly of a given diameter with a given number of rotor plates with the same plate spacing, the impedance at a given frequency is greater in a unit having shaped plates than in one having circular-sector plates, but the unit having shaped plates will not

tune to so low or so high a frequency as the unit with circular-sector plates.

In the design of wide-range butterflies using shaped plates, the balance between stack height and butterfly diameter must be carefully considered. For a butterfly of a given diameter, an increase in the stack height (*i.e.*, the number of rotor and stator plates) will decrease the low-frequency limit and increase the tuning ratio. However, this change will also reduce the resonant impedance developed at any given frequency. In fact, for two butterflies of a given diameter, one with circular-sector plates and the other with a sufficiently large number of shaped plates to cover the same frequency range and consequently a greater stack height, the butterfly having the circular-sector plates will develop the largest impedance at the low-frequency end of the tuning range, because of its higher  $L/C$  ratio. The maximum stack height that can be used in butterfly oscillators with shaped plates is the height at which the developed impedance is just great enough to sustain oscillation at the low-frequency end of the tuning range. In order to design an oscillator having the same frequency variation with rotation that will oscillate at still lower frequencies, a butterfly of larger diameter should be used, as it develops higher impedances due to its larger  $L/C$  ratio.

✓ One method of obtaining a wide-range butterfly oscillator that is very small in size is to use very close plate spacing. However, a minimum spacing of about 0.015 in. has been found to be a practical limit, as the manufacturing difficulties increase rapidly with closer spacing.

In general, with shaped plates, the smaller the ratio of the actual area of one rotor plate to the area of a circular-sector plate having the same maximum radius, the larger the size of butterfly required for a given frequency range.

It has been found that aluminum can be used for the rings and plates of the butterfly for frequencies up to about 400 Mc, but at higher frequencies better operation has been obtained from butterflies fabricated from silver-plated brass.

✓ To keep the effective plate- and grid-lead inductance at a minimum, the oscillator tube should be mounted as close as possible to the high-impedance points on the butterfly and connections made between the tube and butterfly by means of short low-inductance straps or bars. Figures 30-1, 30-9, and 30-10 show typical mounting methods for true and semibutterflies.

**30-6. Grid-blocking Capacitor and Resistor Considerations.**—The series inductance of the grid-blocking capacitor  $C_g$  connected between the grid and butterfly, as shown in Fig. 30-2, adds to the effective lead inductance in the grid connection and is a potential source of trouble at high frequencies. In order to keep this inductance at a minimum, the grid



capacitor is usually made an integral part of the junction of the grid arm and the butterfly, as shown in Fig. 30-1. The capacitance of this capacitor affects the high-frequency limit of the tuning range and the potential of the cathode with respect to ground, as it is effectively in series with the grid and the other tube elements. If the capacitance is reduced, the high-frequency limit will be increased, although the amplitude of oscillation may decrease.

The grid resistor is usually connected from grid to cathode or from grid to ground. Since it acts as a load on the oscillator in either position, the resistance should be no smaller than necessary. A choke may be connected in series with the resistor if the loading is too severe.

The values of the grid capacitor and resistor must be chosen so that the time constant  $RC$  will be less than the value that causes the oscillator to "motorboat" at any setting of the butterfly.

**30-7. Plate-supply Connections.**—As already mentioned, the butterfly circuit is usually allowed to float with respect to ground. To prevent the plate-supply connection from disturbing the butterfly balance with respect to ground and thus affecting the feedback relations, this connection is made near the point on the butterfly which is, on the average, closest to ground potential. In both the true and semibutterflies the connection is usually made at the mid-point of the inductance arm, as shown in Figs. 30-1 and 30-9. However, as this point does not remain exactly at ground potential throughout the tuning range, an isolating impedance should be inserted between the plate-supply lead and the butterfly. A by-pass to ground should be provided at the plate-supply end of the isolating impedance, as shown in Fig. 30-1, to prevent resonances in the plate-supply circuit from affecting the performance of the oscillator. A carbon resistor is usually the best isolating impedance as it has no high- $Q$  resonances and yields a fairly constant impedance over the frequency band. The use of a resistor may, however, prevent the starting of oscillation at the low-frequency end of the tuning range. This is a result of the limitation by the resistor of the maximum plate current and hence of the transconductance, which may not be great enough, when the circuit is in a nonoscillating condition, to overcome the combined effect of the butterfly loss and large grid loss at zero bias and allow oscillations to build up. The voltage drop and power loss in the resistor also may be objectionable. If a choke is used, the best results are usually obtained when it is self-resonant below the lowest operating frequency and, hence, is capacitive in the tuning range. Sometimes, however, in very wide-range oscillators it may be necessary to make the choke resonant in the lower part of the operating band in order to increase its impedance level throughout the tuning range. The choke must then be carefully oriented with respect to the magnetic field of the butterfly to

minimize the coupling between the choke and butterfly. Even with fairly small couplings the choke may load the oscillator sufficiently at the resonant frequency of the choke to stop the oscillator and cause a *hole* in the tuning range.

Coupling of the butterfly to supply leads, which may form parasitic resonant circuits, must be prevented, and usually it is desirable to use shielded leads with the shields grounded every few inches and the ends of all leads well by-passed to ground.

**30-8. Sources of Holes.**—As a result of the complicated nature of the butterfly resonator and impedances associated with the oscillator tube, it is sometimes difficult to determine the reasons for regions of nonoscillation or *holes* in the tuning range. Spurious resonances associated with the cathode-lead inductance, external leads between grid or plate and cathode, the plate-supply choke, or other leads and chokes in the oscillator enclosure may all act to cause either a jump in oscillator frequency or, more likely, a cessation of oscillation in the vicinity of resonance known as a *hole*. Oscillations will also cease should either the resonant impedance of the butterfly or the feedback become too small. Actually, there is a great deal of interaction between all parts of the circuit: a spurious resonance may greatly alter the feedback or the resonator impedance; magnetic and capacitive couplings may exist between various circuit elements. Hence, in actual practice, some holes may have to be removed by trial-and-error methods. However, in spite of the many sources of trouble, oscillators that will operate over a reasonable tuning range of say 3:1 or even 5:1 can usually be constructed without excessive difficulty if the precautions outlined in this chapter are observed.

**30-9. Effect of Cathode-lead Inductance.**—In conventional tubes the cathode impedance is not zero, even if the cathode terminals on the tube are directly grounded, because of the inductance of the lead from the cathode element in the envelope. If the cathode terminal is directly grounded or isolated from ground by a finite impedance, the cathode impedance will affect the feedback and operating frequency because it is common to the grid and plate circuits, as may be seen in Fig. 30-5. Actually the cathode-lead inductance in combination with the tube capacitances and butterfly capacitances to ground produces resonances in the *effective* feedback circuits between plate and cathode and grid and cathode, which cause holes if they occur in the tuning range of the oscilla-

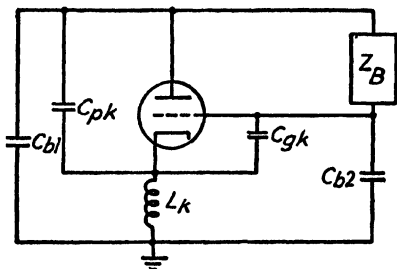


FIG. 30-5.—Equivalent circuit including cathode-lead inductance.

tor. In typical oscillators incorporating type-955 or 9002 triodes with the cathode terminal directly grounded, a broad hole in the vicinity of 450 Mc is apparently caused by the cathode-lead inductance.

To eliminate the effect of the cathode-lead inductance, the cathode should float with respect to ground. Practically, however, it is impossible to obtain an infinite impedance from the cathode to ground over a broad frequency band and still make the low-resistance d-c and a-c connections to the cathode and heater.

It has been found experimentally that the insertion of a choke coil between the cathode terminal and ground shifts the hole to a lower frequency, as would be expected on the basis of the preceding theory. It usually is possible to design a choke, resonant near the low-frequency end of the range, that will shift the hole outside the operating band. The choke must have a small enough effective capacitance near the high-frequency end of the band to prevent the effective choke capacitance and actual cathode-lead inductance in the tube from forming a series-resonant circuit. It is usually also desirable to shunt the choke with a resistance of the order of magnitude of 10,000 ohms in order to reduce the  $Q$  of the circuit. In most cases a hole caused by the cathode-lead inductance can be removed by experimenting with the design of the choke and the value of the shunting resistance.

It also has been found experimentally that the hole around 450 Mc usually can be removed by connecting the cathode to ground through a series resistance that evidently reduces the  $Q$  of the feedback circuits at their resonant frequencies. If a resistor of the proper value is used, the  $Q$  of the feedback circuits usually can be reduced to a value where they no longer stop the oscillations. A small coil, resonant at a frequency above the operating range, is wound around the resistor to provide a low-resistance path for the heater supply and cathode currents. A resistance of approximately 500 ohms has been found to give good results in typical butterfly oscillators using type-955 and 9002 tubes.

In the preceding discussion only a single cathode connection has been mentioned. Actually two connections are required; one for the common cathode and filament lead and one for the other filament lead. The added impedances discussed in the preceding paragraphs must be inserted in both of these leads.

**30-10. High-frequency Limitations.**—As the frequency is increased, the plate- and grid-lead inductances and interelectrode capacitances become more important parts of the resonant circuit. Finally, at some frequency they will form a complete parallel-resonant circuit when the plate and grid terminals are short-circuited. The equivalent circuit under these conditions is shown in Fig. 30-6. The frequency at which

this internal tube resonance occurs is called the *natural resonant frequency* of the tube.

In the schematic diagram of Fig. 30-6, the leads from the tube elements are replaced by lumped inductances. Actually, however, the plate and grid leads form a transmission line with distributed parameters, and resonances can occur at frequencies above the natural resonant frequency of the tube with the transmission line operating on higher order modes.

As pointed out in Sec. 30-4, at low frequencies the effects of lead inductances can be neglected and the feedback circuits external to the tube, shown in Fig. 30-5, are essentially pure capacitances shunting the tube interelectrode capacitances. The required conditions for oscillation can therefore easily be maintained over a wide band. As the natural resonant frequency of the tube is approached, however, the inductances in the cathode, plate, and grid leads modify the external feedback circuit, and eventually Eq. (30-2) is no longer satisfied and oscillation ceases. In typical butterfly oscillators continuous oscillation over wide-frequency ranges can be produced up to frequencies that are about 70 to 80 per cent of the natural resonant frequency of the tube. Oscillations can be produced at still higher frequencies, even above the natural resonant frequency of the tube if the feedback is adjusted properly, but it is impossible to maintain the required feedback for oscillation under these conditions over any appreciable frequency range with fixed feedback circuits. Therefore operation at these frequencies is impractical in oscillators having only a single tuning adjustment.

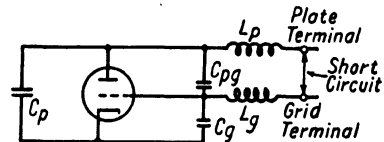


FIG. 30-6.—Approximate equivalent circuit of a triode tube for oscillations at its natural resonant frequency.

**30-11. Stability.**—In superheterodyne receivers, the accuracy with which the frequency of a received signal can be determined is largely a function of the stability of the oscillator, the accuracy with which the dial can be read, and the resetting errors in the mechanism connecting the oscillator and the calibrated dial. The resetting and dial-reading errors can be made very small through the use of a well-designed mechanical drive and a large dial. In the limiting case, therefore, the inherent stability of the oscillator determines the calibration accuracy of the receiver.

In a butterfly oscillator operating near the natural resonant frequency of the oscillator tube, the frequency stability of the oscillator for changes in voltage depends not only on the  $Q$  of the resonant circuit but also to a large extent on changes in the effective interelectrode capacit-

ances and losses of the tube, which forms a major part of the tuned circuit at these frequencies. Changes in plate or filament voltage affect the effective interelectrode capacitances as a result of thermal expansion and variation in space charge. An increase in plate voltage usually increases the frequency, while an increase in filament voltage usually lowers the frequency. These two effects tend to compensate when the line voltage is changed, but the effect of the plate-voltage variation usually predominates. Consequently, the frequency stability of oscillators operating near the natural resonant frequency of the tube is determined mainly by the characteristics of the tube. At frequencies where tube capacitance is a less important part of the tuned circuit, the  $Q$  and temperature coefficient of the resonant circuit become more important, and the stability is much greater. Greater stability could be obtained by using looser coupling between the tube and the butterfly. However, the load impedance would thereby be reduced, causing the efficiency and power output to decrease and possibly causing the oscillations to stop in some regions of the tuning range. In typical circuits, the frequency change near the high-frequency end of the tuning range is approximately  $\pm 0.1$  per cent for a  $\pm 10$  per cent change in line voltage.

The amount of frequency modulation present in the output of the local oscillator is important in many cases as it effectively frequency modulates all i-f signals produced by the mixer. The two main sources of frequency modulation are a-c ripple on the plate-supply voltage and the magnetic field caused by the a-c heater. The amount of frequency modulation resulting from the ripple on the plate-supply voltage is determined by the dynamic stability of the oscillator. In the low-frequency portion of the tuning range where the stability is great, very little frequency modulation is produced by a given ripple voltage, but near the high-frequency end of the tuning range, the stability is much poorer, and hence a greater amount of frequency modulation is produced by the same ripple voltage. In both cases, the amount of frequency modulation produced is less than that predicted from the static stability factor as the temperature of the tube elements cannot follow the ripple frequency.

The amount of frequency modulation caused by the filaments or heaters depends on the oscillator stability and the type of filament or heater. In general, less ripple is produced by heater-type tubes than by filament-type tubes, because of the smaller amount of electric and magnetic modulation of the electron stream produced by the former.

In well-designed and well-constructed butterfly oscillators, the percentage variation in frequency with temperature over the part of the tuning range where the butterfly is the major part of the tuned circuit is of the same order of magnitude as the coefficient of expansion of the metal used for the butterfly plates. In most cases the metal is brass,

which produces a frequency variation of about 0.004 per cent per degree centigrade of temperature change. The rotor and stator supports must be designed to have equal changes in height with temperature, or much larger frequency variations may result. Furthermore, if one or more rotor plates is badly aligned, *i.e.*, if it is much closer to one stator plate than to the other, large variations of frequency with temperature can be produced because of the more rapid change in capacitance with spacing between the plates that are close together. Therefore, for greatest temperature stability, the plate alignment should be very good.

Another important effect is the change in calibration caused by replacing the oscillator tube. In circuits in which the tube capacitances comprise an important part of the capacitance across the resonator at the high-frequency end of the tuning range, this error can be very great. In some butterfly oscillators, variations as great as  $\pm 2$  per cent have been obtained between tubes. The magnitude of this error decreases very rapidly as the frequency is decreased, however, and in the middle and lower portions of the tuning range, the calibration is usually practically independent of the tube.

From the above discussion, it is evident that the over-all frequency accuracy obtainable depends largely on the ratio of the effective tube capacitances to the total capacitance across the resonant circuit. At frequencies where the effective tube capacitance is negligible compared with other capacitances, calibration accuracies of about  $\pm 0.25$  per cent can be obtained for operation over a temperature range from  $-55$  to  $+85^{\circ}\text{C}$  and a  $\pm 10$  per cent variation in line voltage. At higher frequencies, where the effective tube capacitance is important, larger errors will be obtained mainly as a result of the variation between tubes.

**30-12. Output-coupling Methods.**—The problem of coupling a fairly uniform amount of power from the butterfly local oscillator to the mixer in wide-range receivers is complicated by the variations in the amplitude of oscillation and in the electric and magnetic field caused by the rotor over the tuning range. The field variation is discussed in Sec. 28-12. In most local-oscillator applications, the power requirements are not large, and relatively large variations in the local-oscillator power fed into the mixer do not affect the performance of the receiver appreciably. Hence, the oscillator and coupling system should be designed to produce a voltage across the mixer which does not vary over the tuning range beyond the limits between which the mixer performance remains practically constant.

In most receivers using butterfly local oscillators, either loop coupling or direct magnetic coupling between the oscillator butterfly and mixer butterfly is used. When loop coupling is used, the loop should be located near the part of the inductance arm where the inductance changes the

least. This is at point *A* in Fig. 30-1 in a true butterfly and at point *B* in Fig. 30-9 in a semibutterfly. The loop is usually connected directly or by means of a coaxial transmission line to the mixer. When simple magnetic coupling is used between the oscillator and mixer, the two butterflies are located side by side with their inductance arms adjacent, as shown in Fig. 30-1. The amount of coupling can be varied by adjusting the spacing between the butterflies or partly shielding them from each other. This method of coupling is generally used only when the intermediate frequency is relatively high. The difficulties encountered in mutual loading and frequency pulling of the two circuits may be great when a low intermediate frequency is used and both circuits are tuned very close to the same frequency.

**30-13. Butterfly Oscillator Efficiency.**—It can be seen from the discussion in Secs. 30-4, 30-9, and 30-12 that at high frequencies it is practically impossible to achieve high efficiencies over wide frequency ranges with butterflies, because of the large variations in feedback and effective load with frequency. The power output can be increased at one frequency by inserting the proper external feedback reactances between plate and cathode or between grid and cathode in order to provide the feedback required for most efficient operation, but the efficiency at other frequencies will usually be reduced as a result. In order to prevent the cessation of oscillation at frequencies at which the magnitude of the feedback decreases radically, the nominal feedback is made very large and the efficiency is consequently low. For wide-range operation a feedback ratio of approximately 1:1 has been found to be desirable. In other words, a grid-to-cathode capacitance equal to the plate-to-cathode capacitance usually produces the most satisfactory results.

**30-14. Oscillator Tubes.**—Most high-frequency triode tubes having a grid-to-cathode and plate-to-cathode capacitance ratio of about unity operate well with butterfly resonators. Table 30-2 gives a partial list of tubes that are adaptable for use with butterfly resonators, grouped according to their approximate highest operating frequency when used in these circuits. The pentodes listed are usually connected as triodes.

The type-955 tubes have natural resonant frequencies of about 700 Mc and can be made to oscillate with butterfly circuits over wide-frequency ranges up to about 500 Mc. They also have grid and plate terminals that are located close together and a cathode connection on the opposite side of the envelope, which facilitates mounting on butterflies. Figure 30-1 shows a type-955 triode mounted on a butterfly. The input power required for operation is low, about 2.5 watts, and sufficient r-f power is produced for local-oscillator applications.

The type-6F4 acorn triode is a very useful tube for operation at frequencies up to about 1100 Mc. It also is a low-power tube with a

grid-to-cathode and plate-to-cathode capacitance ratio near unity and performs very well with butterfly circuits. Its natural resonant frequency is about 1500 Mc.

TABLE 30-2.—PARTIAL LIST OF TUBE TYPES ADAPTABLE FOR USE WITH BUTTERFLY RESONATORS

Types	Highest operating frequency	
	Approx. 500 Mc	Approx. 1000 Mc
Acorn.....	955 ✓ 958	6F4
Miniature.....	9002' ✓ 6AG5 6C4 6J4 6J6 6AK5	
Doorknob.....	WE316A	WE368A WE703A
Disk seal or lighthouse.....	....	2C40 2C43

The type-9002 miniature tube is electrically similar to the 955 and also has physical characteristics that make it very adaptable to butterfly circuits. Other miniature tubes, such as the 6AG5, 6AK5, 6C4, and 6J4 have natural resonant frequencies between 500 and 600 Mc and oscillate up to about 75 per cent of their resonant frequency when used with butterfly circuits. The 6C4 is a relatively high-power tube, having a plate dissipation of 5 watts. The 6J6, a double-triode miniature type, which has a natural resonant frequency of about 700 Mc, is also used with butterfly circuits.

The doorknob tubes are tubes of much higher power than any of the previously mentioned types and have plate-dissipation ratings of about 25 watts. However, they also have high-current low-voltage filament circuits, requiring adjustment of the filament current to the minimum value giving satisfactory operation, if maximum tube life is desired. The optimum filament current varies between tubes and with age, which is an undesirable feature for receiver local oscillators where a minimum number of adjustments is desired.

The disk-seal or lighthouse tubes listed, the 2C40 and 2C43, are relatively high-power tubes. The actual plate dissipation depends on the amount of external cooling provided at the plate connection. In



most circuits, however, the dissipation is usually greater than 6 watts. These tubes were designed for use in grounded-grid circuits using coaxial cavities between plate and grid and between grid and cathode. The original plan was to obtain feedback through coupling circuits between the two cavities, and the interelectrode capacitances were not designed to be used as feedback circuits. As a result the grid-to-cathode capacitance is much greater than the plate-to-cathode capacitance. When the tube is used with butterflies at high frequencies, the feedback produced by the interelectrode capacitances is usually insufficient to support oscillation over wide frequency ranges. An external capacitance can be connected between plate and cathode to increase the feedback, but in all the designs tried up to the present time satisfactory performance at frequencies approaching the natural resonant frequency has not been obtained. Either because the resonant frequency of the external paths cannot be made sufficiently high or the cathode inductance is too large, the addition of an external feedback capacitance considerably lowers the high-frequency limit that can be reached. A network can be designed that will produce oscillations over a narrow range at higher frequencies, but no satisfactory broad-band feedback circuit has been found that will allow the circuit to oscillate at frequencies above about 750 Mc, in spite of the fact that the natural resonant frequency of the tube is about 1800 Mc.

### 30-15. Examples of Butterfly Local Oscillators.

*Example 1* (Fig. 30-1).

Frequency range: 100 to 350 Mc

Use: Local oscillator in a superheterodyne receiver using a diode mixer with a butterfly as a tunable r-f filter

In this oscillator, a true butterfly (4½ in. in diameter) was chosen for the tuned circuit instead of a semibutterfly because of its greater stability and simpler fabrication. The butterfly consisted of a stack of seven rotor and eight stator plates made from aluminum to reduce the weight and save the silver-plating operation required if the plates are fabricated from brass. A type-955 acorn triode was used as an oscillator tube with its plate and grid terminals connected to the butterfly by low-inductance arms.

The rotor plates were designed to provide a semilogarithmic frequency variation with rotation and a relatively high resonant impedance at the low frequencies. Because of the relatively low operating frequencies, no resonances were encountered in the feedback networks, and it was possible to ground the cathode directly by means of a low-inductance bar. A 25- $\mu\text{f}$  grid capacitor and a 25,000-ohm grid resistor were used. The plate supply was connected to the butterfly through a 10,000-ohm isolating resistor. As the plate-supply voltage was higher than the tube rating, the isolating element also served as a voltage-dropping resistor.

Radio-frequency power was transferred to the tuned mixer by magnetic

coupling between the inductance arms of two adjacent butterflies, as shown in Fig. 30-1. A 30-Mc intermediate frequency was used, resulting in a 30-Mc difference between the tuning of the oscillator and preselector butterflies.

Although only a 100- to 350-Mc tuning range was desired, this oscillator operated satisfactorily from 93 Mc to about 400 Mc, providing an ample tuning margin.

*Example 2 (Fig. 30-7).*

Frequency range: 100 to 500 Mc

Use: Local oscillator in a superheterodyne receiver using an untuned crystal mixer.

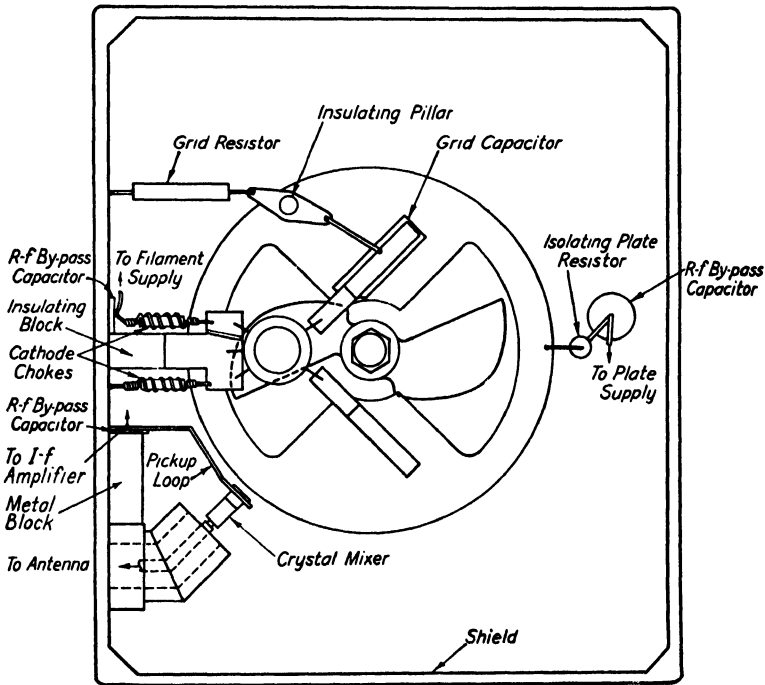


FIG. 30-7.—100- to 500-Mc oscillator assembly.

This oscillator was similar to the one described in Example 1, using a type-955 acorn triode tube, but because of the increased range required the stack was increased to 10 stator plates and 9 rotor plates, and silver-plated brass was substituted for aluminum.

In this oscillator, difficulty was encountered from lead inductances above 400 Mc when the cathode was grounded. To eliminate holes or serious dips in the output, the cathode feedback circuit was damped by inserting 500-ohm resistors between the cathode and heater terminals and ground. The end of one resistor was grounded through an r-f by-pass capacitor as this lead supplied the heater voltage to the tube and could not be directly grounded. The resistors

were shunted by coils consisting of several spaced turns of wire, wound directly on the outside of the resistors. The coils presented a low resistance to the direct and low-frequency alternating currents, but a high impedance to the r-f currents.

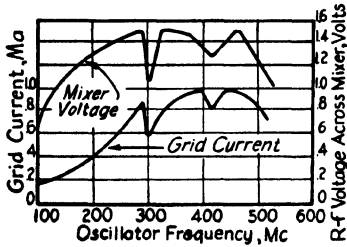


FIG. 30-8.—Variation of oscillator output with tuning in a wide-range oscillator.

The crystal mixer was coupled to the oscillator by means of a loop, as shown. Figure 30-8 shows the variation in grid current and voltage produced across the crystal as a function of frequency. The dip in output around 300 Mc is due to the butterfly circuit, while the dip around 425 Mc is a result of the resonance caused by the cathode-lead inductance and not completely eliminated by the cathode resistors. However, these dips do not have any noticeable effect on the curve of frequency variation with butterfly rotation and hence are not objectionable. The graph illustrates the typical rather wide variation in output obtained in very wide-range butterfly oscillators.

frequency variation with butterfly rotation and hence are not objectionable. The graph illustrates the typical rather wide variation in output obtained in very wide-range butterfly oscillators.

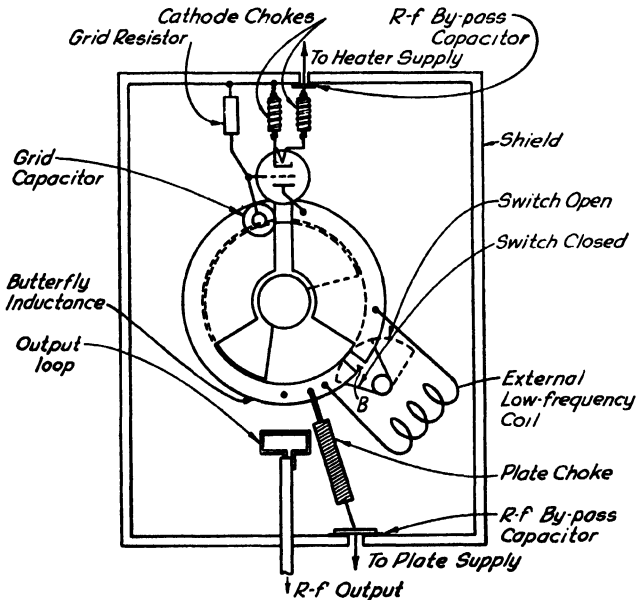


FIG. 30-9.—40- to 500-Mc oscillator assembly.

**Example 3 (Fig. 30-9).**

Frequency range: 40 to 500 Mc

Use: This unit was designed as a test oscillator but could be used as a local oscillator in a receiver.

This oscillator makes use of a semibutterfly  $2\frac{1}{2}$  in. in diameter consisting of nine 120-deg stator and eight 240-deg rotor plates with a switch in the inductance arm, as shown. The function of the switch is to add a large external inductance to the butterfly and hence lower the operating frequency. The low-frequency range is from 40 to 115 Mc, and the high-frequency range from 115 to 500 Mc. In the high-frequency range, the rotor produces an appreciable shielding of the inductance, resulting in approximately a 2:1 change in effective inductance over the tuning range. The tube used is a type-9002 miniature triode, the plate and grid of which are connected to the high-impedance points on the butterfly. The rotor is supported by, but is well insulated from, a steel shaft. A grounding strap is required on the top of the supporting shaft to shift the frequency of series resonance to ground of the circuit formed by the capacitance from the rotor to the shaft and the inductance of the shaft to ground. Damping resistors are used in the cathode and filament leads, as in Example 2. The plate supply is connected to the butterfly through a choke that is self-resonant at 65 Mc. In order to keep a high impedance level at the high-frequency end of the range, the self-resonant frequency of the choke was not reduced below the operating range. The high impedance was required because a relatively large r-f voltage appeared across the choke at high frequencies as a result of the change in ground point on the inductance arm as the inductance was changed.

Power was extracted from the butterfly by means of a loop that coupled to the butterfly inductance in the high-frequency range and to the external inductance in the low-frequency range.

*Example 4* (Fig. 30-10).

Frequency range: 450 to 1050 Mc

Use: Signal generator or local oscillator.

This oscillator makes use of a type-703A doorknob triode tube and a true-butterfly resonant circuit. The butterfly is  $2\frac{1}{2}$  in. in diameter and has three rotor and four stator plates. The plate and grid prongs of the tube are connected across the high-impedance points of the butterfly as shown. The grid capacitor is built in and has a capacitance of about  $4\ \mu\mu\text{f}$ .

A 10,000-ohm grid resistor is connected directly from the grid terminal to ground, and the plate supply is isolated from the butterfly by means of a choke wound on a resistor that is resonant below the operating band. Filament power is supplied through an  $L$  bracket made of two separate conductors by-passed to each other and grounded through r-f by-pass capacitors. Feedback problems were encountered in this oscillator due to resonances caused by the inductance of the  $L$  bracket and cathode leads in combination with the tube capacitances and stray capacitances of the butterfly to ground, which caused a hole at approximately 500 Mc. An approximate equivalent circuit is drawn in Fig. 30-11. If the  $L$  bracket is grounded to the wall of the shield at point  $A$  in Fig. 30-10 or 30-11, the frequency at which the hole occurs increases to about 650 Mc. It has been found that if a resistor of the proper value is placed between point  $A$  and ground, the hole can be removed, leaving only a minor dip in output. The resistance is in parallel with the inductance  $L_{K2}$  and damps the resonances. For its maximum amount of damping, the resistance should be approximately equal

to the inductive reactance at the feedback-circuit resonant frequency. The inductance  $L_{K2}$  is roughly  $0.03 \mu\text{h}$ , which has a reactance of 110 ohms at 600 Mc,

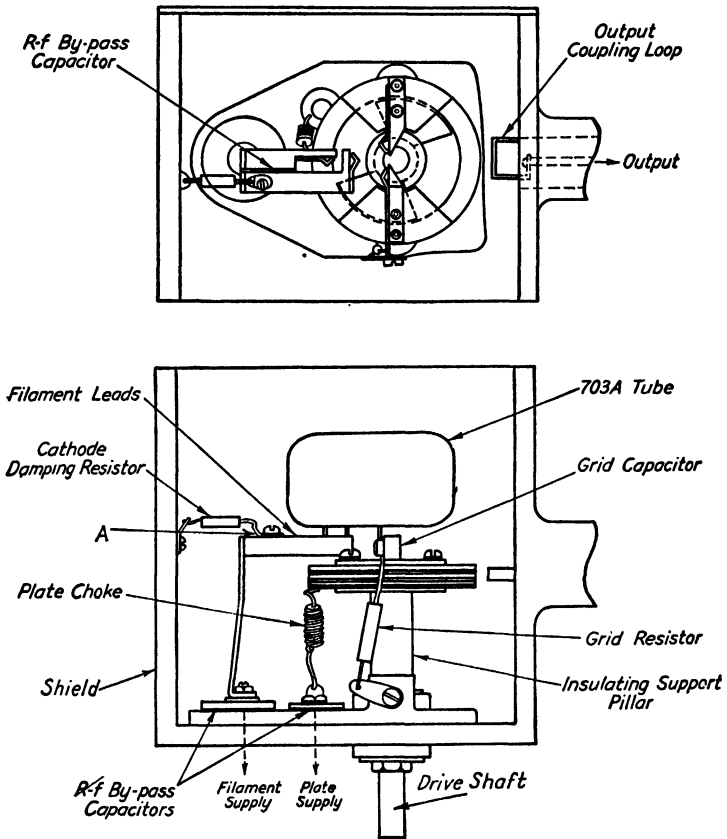


FIG. 30-10.—Doorknob oscillator assembly (tube removed in the upper view).

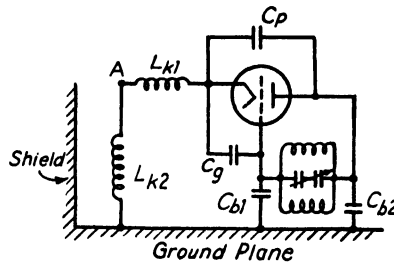


FIG. 30-11.—Equivalent circuit of doorknob oscillator.

and hence a resistance of about 110 ohms should be optimum. Experimentally, a resistance of 150 ohms has been found to produce the best results. Its value checks quite well with the above reasoning.

In a signal generator using this oscillator, power was extracted by means of a loop coupled to one inductance arm of the butterfly, as shown in Fig. 30-10. The output power delivered to a fixed 50-ohm load resistor without matching transformers varied from about 200 mw to more than 1 watt over the tuning range.

### 30-16. Mechanical Tracking of Oscillator with Preselector and Dial.

To obtain a single-dial tuning control in a superheterodyne receiver incorporating a preselector (r-f tuner), it is necessary that some mechanical system be devised that will at all times maintain the proper relationship between the preselector and local-oscillator tuning adjustments. Furthermore, to allow for slight differences between manufactured units, as well as variations due to differences in local-oscillator tubes, the mechanical system must be adjustable to some extent.

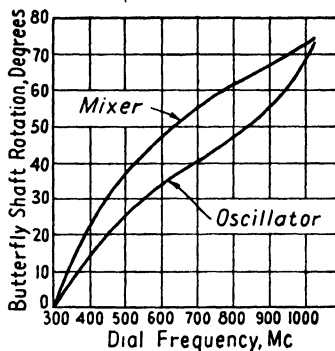


FIG. 30-12.—Mixer and oscillator tuning characteristics.

A satisfactory method of tracking the preselector with the local oscillator may best be illustrated by referring to a typical receiver in which this problem is encountered. Figure 25-7 shows the r-f section of a 300- to 1000-Mc receiver in which the oscillator and preselector butterfly resonators follow radically different laws of required shaft rotation vs. frequency, as shown in Fig. 30-12.

Figure 30-13 shows a cam-linkage system that can be used to track the preselector properly with the local oscillator. The tuning-knob shaft is connected to the main drive shaft by a set of spring-loaded reduction gears which also drive the calibrated tuning dial. The motion of the main drive shaft is transmitted to the butterfly rotor shaft of the oscillator through a worm and worm wheel having a 20:1 reduction. The motion of the oscillator butterfly is then transmitted to the preselector butterfly by a series of cams and linkages.

Within this linkage system, a pair of rollers operates between a peculiarly shaped cam and an adjustable track formed from stainless-steel strips laminated for flexibility. The shape of the cam was com-

puted from the data of Fig. 30-12, so that in conjunction with the linkage characteristic the proper relative motion of the mixer and oscillator butterflies would be obtained. The cam is cut to give the average compensation required of the system. To compensate for minor differences between units, the contour of the flexible track may be shifted by means of the nine front-panel adjusting screws. A pointer attached to the roller and extending through the panel shows which screw should be adjusted for a particular dial setting.

The tuning-dial calibration of this system is nonlinear since the dial rotation is linearly related to the rotation of the oscillator butterfly rotor. (This is not true if the plates are cut for straight-line-frequency opera-

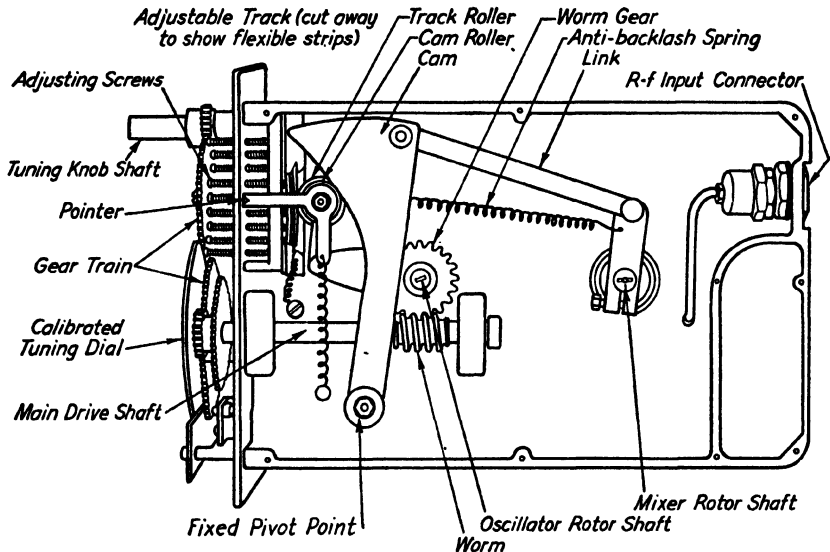


FIG. 30-13.— Typical adjustable tracking system.

tion). Obviously, a second cam system similar to that just discussed could be inserted between the tuning dial and the oscillator butterfly in such a way as to give a linear dial calibration. Not only is such a dial easier to read, but it would also make possible the use of a counter mechanism attached directly to the tuning-knob shaft to indicate the frequency directly.

It is apparent that the cam-linkage system described can easily be adapted to give a translatory motion such as that required for tuning coaxial-line resonators.

When used with a reflex oscillator, a linear-frequency dial drive is doubly useful. Since the required repeller voltage of a reflex klystron varies linearly with the frequency, the dial drive is a convenient motion for driving a linear repeller-voltage control (see Sec. 31-12).

## CHAPTER 31

### LOCAL OSCILLATORS: II

#### REFLEX-KLYSTRON OSCILLATORS

BY W. H. HUGGINS, R. O. PETRICH, AND J. W. KEARNEY

**31-1. Introduction.**—A method of treating oscillator behavior that is particularly applicable to the reflex oscillator has been presented by J. R. Pierce.<sup>1</sup> The method is based upon the consideration that the *total* admittance between two nodes (junctions) in a circuit is zero for any natural oscillation of the circuit.<sup>2</sup> Thus, suppose that the complete circuit connecting two nodes is split into two parts, as shown in Fig. 31-1. There will be associated with each part of the circuit self-admittances  $Y_1$  and  $Y_2$ , respectively. (These are the admittances of each part as measured with the remaining part disconnected and short-circuited.) In general, transfer or mutual admittances  $Y_{12}$  and  $Y_{21}$  will also be present. Each of these represents the ratio of short-circuit current in one circuit to the voltage applied to the other and, for triode oscillators, will generally depend upon the feedback circuit and grid-to-plate transadmittance of the tube. In any case, the condition for oscillation at any frequency is that the total admittance at that frequency must be zero. That is,

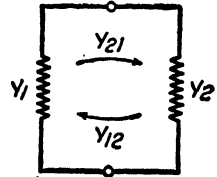


FIG. 31-1.—Circuit corresponding to Eq. (31-1).

$$Y_1 + Y_2 + Y_{21} + Y_{12} = 0 \tag{31-1}$$

For a reflex tube, however, the feedback is inherent in the tube itself, and if we let the two junctions correspond to the two bunching grids or orifices forming the interaction gap of the tube, the total admittance between these grids may be separated into the admittance  $Y_e$ , due to the r-f variations in the electron stream passing between the grids, and the remaining admittance, which includes the “cold” admittance of the tube and the external admittance of the resonant circuit connected to the tube. If the cold admittance of the tube is included in the circuit admittance  $Y_e$ , the condition for oscillation is that

$$Y_e + Y_c = 0 \tag{31-2}$$

<sup>1</sup> PIERCE, J. R., *Reflex Oscillators*, *Proc. I.R.E.*, **33**, 112 (1945).

<sup>2</sup> SCHELKUNOFF, S. A., “Electromagnetic Waves,” p. 229, D. Van Nostrand Company, Inc., New York, 1943.



Note that since there is no coupling between the circuit and the electron stream other than through the connection of these at the interaction gap, the mutual admittances  $Y_{21}$  and  $Y_{12}$  are zero.

The theory of reflex-oscillator performance, in the light of Eq. (31-2), resolves itself into a study of the factors that control  $Y_o$  and  $Y_c$ . Oscillations may occur whenever the electronic admittance is the negative of the circuit admittance. The reflex oscillator is particularly useful for illustrating many of the phenomena that must be considered in designing coaxial cavities tunable over a wide range, because the reflex tube is self-contained. External feedback circuits are, therefore, not required, and it is possible to break the oscillator theory into two parts: that dealing with the resonator, and that dealing with the active part of the oscillator—the electron beam in the tube. For this reason, most of the resonator theory concerned with parasitic resonances, mode separation, and noncontacting plungers in coaxial lines is presented in a subsequent chapter. This chapter is concerned with reflex-oscillator behavior without restriction as to the type of resonator to be used.

**31-2. The Electronic Admittance.**—Figure 31-2 shows the essential structure of a modern reflex oscillator. It consists of an electron gun that directs an electron stream through an interaction gap defined by two grids or orifices maintained at a potential  $V_0$  positive with respect to the cathode. The resonator in conjunction with the self-capacitance of the grids presents a very high shunt impedance, *i.e.*, a very small induced current in it is capable of developing a very large voltage across the gap. After passing through the grids, the electron stream enters a negative-field region produced by a repeller electrode maintained at a potential  $V_R$  negative with respect to the cathode. This negative field reverses the motion of the electrons, and they are reflected back through the gap toward the cathode. Each of the grids will intercept only a fraction of the total beam current, so the electrons that have been reflected back into the cathode space may, under certain conditions, again reverse their direction and cross the gap three or more times. In the simple theory only two traverses of the gap are considered, however.

Assume that an r-f voltage, of amplitude  $V$ , exists across the interaction gap of the resonator. This r-f voltage will modulate the velocity with which the electrons enter the repeller space. The faster moving electrons penetrate farther than the slower moving electrons, with the result that the electrons that are reflected back through the gap do not return in a uniform stream but instead cross the gap in bunches. If the bunches cross the gap when the r-f voltage is such as to oppose their motion, the *average* velocity of the electrons will be decreased, and energy equal to the decrease in kinetic energy of the electrons will be delivered to the electromagnetic field of the oscillation in the resonator. If this

energy is delivered at a rate equal to the total power loss of the resonator, the oscillation will be self-sustaining.

The mechanism whereby the electron bunches transfer their energy to the resonator is one of currents induced through variation of the electron charge within the gap.<sup>1</sup> Obviously, the degree to which the electrons are bunched is dependent upon the r-f voltage obtaining across the interaction gap. For small voltages, in fact, the ratio of the induced current, arising as a result of the bunching, to the gap voltage that causes the bunching is nearly constant. This ratio is the *electronic admittance*. Although the r-f voltage varies sinusoidally with time, the induced cur-

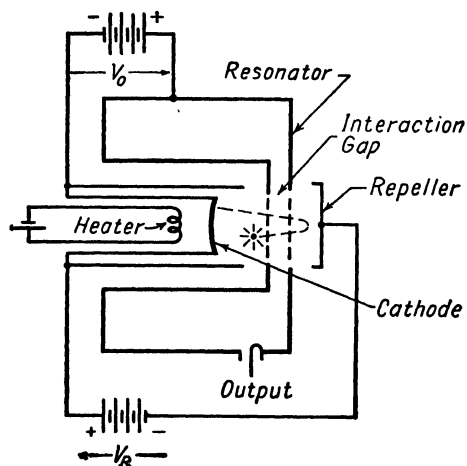


FIG. 31-2.—A modern reflex oscillator.

rent is periodic but may be extremely nonsinusoidal in wave shape.<sup>2</sup> Hence, in defining the electronic admittance, the fundamental sinusoidal component of current is implied.

As the amplitude of the r-f voltage is increased, the induced current becomes more and more distorted, and eventually the fundamental-frequency component of the current decreases through zero. The electronic admittance is therefore a function of the amplitude of oscillation as well as of the frequency, tube geometry, and voltages  $V_0$  and  $V_R$  applied to the resonator and repeller, respectively. The principal effects of each of these factors may be adequately explained by the simple transit-time theory, which assumes that the r-f voltage is small compared with the accelerating voltages and ignores, among other things, diffusion of the electrons due to space-charge repulsion and multiple-

<sup>1</sup> RAMO, SIMON, Currents Induced by Electron Motion, *Proc. I.R.E.*, **27**, 584 (1939).

<sup>2</sup> BLACK, L. S., and P. L. MORTON, Current and Power in Velocity-modulation Tubes, *Proc. I.R.E.* **32**, 477 (1944).

transit effects. Derivations of standard expressions relating these factors may be found in the literature.<sup>1</sup> If

$I_0$  = beam current

$V_0$  = accelerating voltage (cathode to cavity)

$V_R$  = negative repeller voltage

$V$  = peak r-f voltage across gap

$\beta$  = beam coupling coefficient (ratio of amplitude of the velocity modulation produced by the gap, expressed in volts, to the r-f gap voltage)

$N$  = number of r-f cycles during reflex transit time (for oscillation  $N \approx n + \frac{3}{4}$ ,  $n$  any positive integer including zero)

$J_1(X)$  = first-order Bessel function

the electronic admittance is

$$Y_e = \frac{2I_0\beta}{V} J_1\left(\frac{\beta\pi NV}{V_0}\right) j e^{-j2\pi N} \quad (31-3)$$

The magnitude of this admittance is  $|Y_e| = \frac{2I_0\beta}{V} J_1\left(\frac{\beta\pi NV}{V_0}\right)$ , and its phase angle is  $\pi/2 - 2\pi N$ . The admittance will be a pure negative conductance whenever the phase angle is an odd multiple of  $\pi$  or whenever  $N = n + \frac{3}{4}$ . The largest negative value of this conductance will occur as  $V$  approaches zero. The magnitude then becomes

$$G_e = -\frac{I_0\beta^2\pi N}{V_0} = -G_0\beta^2\pi N \quad (31-4)$$

where  $G_0 = I_0/V_0$  is called the *d-c beam conductance*.  $G_e$  may be considered to be the *small-signal electronic conductance*. In terms of  $G_e$ , the magnitude of the electronic admittance for large  $V$  may be written

$$|Y_e| = -2G_e \frac{J_1(X)}{X} \quad (31-5)$$

where the transit-time parameter  $X$  is given by  $X = \beta\pi N \frac{V}{V_0}$ . Figure 31-3 shows how  $|Y_e|$  varies with the relative amplitude of the bunching voltage. Actually, the assumption is made in deriving Eq. (31-3) that  $V \ll V_0$ . Hence Eq. (31-5) will hold approximately for larger values of  $N$ , but it is probably in error for  $N = 1\frac{3}{4}$ , and surely in error for  $N = \frac{3}{4}$ , because to obtain a small  $N$ ,  $V$  must be large.

The preceding discussion has expressed the electronic admittance in terms of the transit-time cycles  $N$ . It is more important to know how  $Y_e$  varies with  $V_R$ . If a uniform repeller field is assumed, the reflex

<sup>1</sup> PIERCE, *loc. cit.*

transit time  $\tau_0$  will be proportional to the velocity with which the electron enters the retarding field and inversely proportional to the intensity of that field. Hence,

$$\tau_0 = K \frac{\sqrt{V_0}}{V_0 + V_R} \tag{31-6}$$

where  $K$  is a constant depending upon the tube geometry and electron constants. The number of r-f cycles  $N$  that elapse is given simply by the product of the frequency  $f$  and the reflex transit time, or

$$N = fK \frac{\sqrt{V_0}}{V_0 + V_R} \tag{31-7}$$

Usually, over a given repeller range of operation,  $N$  is fixed (e.g.,  $N \approx 1\frac{3}{4}$ ) so that, as the frequency of operation is changed, the repeller voltage must also be varied. Therefore

$$V_R = \frac{K \sqrt{V_0}}{N} f - V_0 \tag{31-8}$$

It can be seen from Eq. (31-8) that for a fixed resonator voltage  $V_0$  the ideal relation between  $f$  and  $V_R$  is linear. Furthermore, when  $V_R < V_0$ , a decrease in  $V_0$  will allow a decrease in frequency. This effect may be used to advantage in extending the low-frequency limit of a given repeller range.

The low-frequency limit of any given repeller range is determined in some measure by the repeller voltage at which repeller current begins. The velocity modulation imposed upon the electron stream produces some fast-moving electrons that will strike the repeller if  $V_R$  is less than  $\beta V$ . The resulting repeller current is undesirable in that it introduces an internal-regulation problem into the design of the repeller-voltage source. Furthermore, emission of gas and secondary electrons from the repeller may shorten tube life and produce a loss of r-f power.

An important aspect of the idealized electronic admittance is that its phase angle is dependent only on  $N$ , which in turn is a function of the repeller voltage. Hence, as  $N$  is increased by decreasing  $V_R$  from a very large value toward zero, the *small-signal* electronic admittance for a given

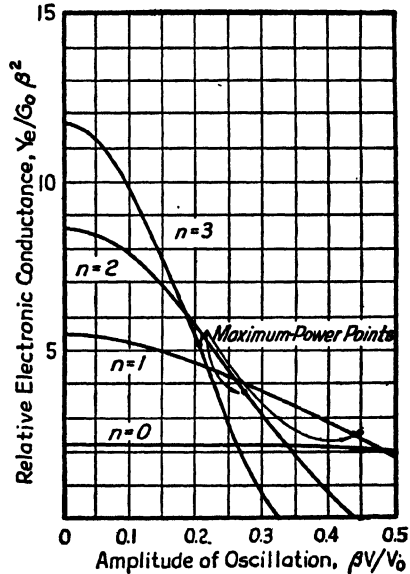


FIG. 31-3.—Electronic conductance as a function of amplitude of oscillation.

frequency moves in an ever-increasing spiral, as illustrated in Fig. 31-4.

A few comments as to the limitations and significance of Eq. (31-8) should be made at this point. First, it will be apparent with a little consideration that for a small r-f voltage the bunches will tend to form around those electrons which are passing through the interaction gap at the instant the gap voltage is zero and decreasing. For the bunch to deliver its maximum energy to the resonator, it must return through the gap when the gap voltage offers maximum opposition. That will be three-quarters of a cycle plus any integral number of cycles later. Hence for oscillation,  $N = \frac{3}{4} + n$ .

Second, for a given repeller voltage (and hence for a given transit time  $\tau_0$ ), the frequencies of optimum oscillation in the various repeller ranges

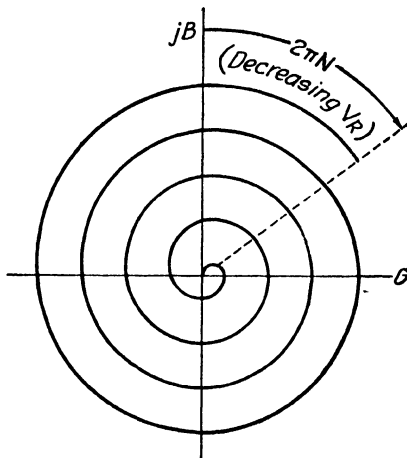


FIG. 31-4.—Electronic admittance as a function of transit angle and repeller voltage.

will always be related by the simple formula  $f = N/\tau_0$ . This relation holds even for tubes that do not have the uniform fields assumed in setting up Eq. (31-8). Hence, in specifying the characteristics of a given reflex klystron, the relation between repeller voltage  $V_R$  and transit time  $\tau_0$  is of fundamental importance. Since  $\tau_0$ ,  $N$ , and  $\lambda$  are related by the equation  $c\tau_0 = N\lambda$  (where  $c$  is the velocity of light), the repeller voltage will be a function of  $N\lambda$ . The relation will be most nearly linear if  $V_R$  is expressed as a function of  $1/N\lambda$ . Experimental data expressing this relationship have been plotted in Fig. 31-5 for

several types of reflex tubes. Notice that the empirical linear equations which may be used to approximate these curves differ considerably with respect to the  $V_0$  term from the ideal Eq. (31-8).

**31-3. Power Stability.**—The selection of the particular repeller range (corresponding to  $n$  equal to 1, 2, etc.) to be used in a reflex oscillator depends primarily upon the frequency range over which the oscillator is to operate. In a wide-range oscillator incorporating a given tube, there is usually only one repeller range that will cover the desired frequency range. In narrow-range oscillators, however, several repeller ranges might be used, and choice of the particular repeller range then depends upon other factors, such as power output, stability, electrical tuning, and resonator mode interference. It will be shown that the repeller

ranges corresponding to the larger values of  $n$  possess a greater inherent stability but a smaller power output.

For a steady oscillating condition, the electronic conductance must be the negative of the circuit conductance. The power developed by the

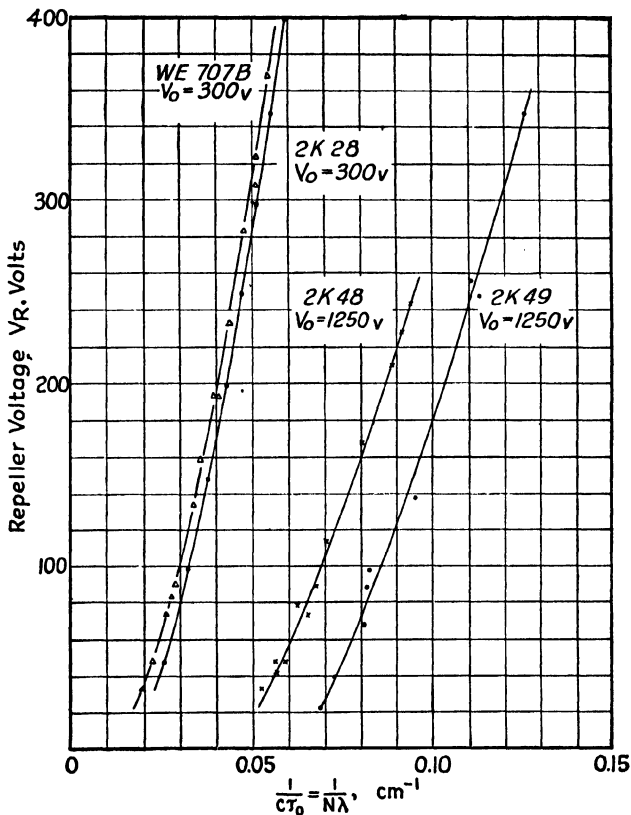


FIG. 31-5.—Repeller characteristics of typical reflex tubes.

electron stream will be, in terms of Eq. (31-5),

$$\begin{aligned}
 P &= Y_e \frac{V^2}{2} & (31-9) \\
 &= \frac{I_0 V_0}{\pi N} J_1(X) \cdot X
 \end{aligned}$$

It may be shown by differentiating Eq. (31-9) that the maximum power will be delivered by the electron stream when the transit-time parameter  $X = 2.40$ , or when

$$\frac{\beta V}{V_0} = \frac{0.764}{N} \tag{31-10}$$

Points corresponding to this optimum amplitude of oscillation have been marked with a dot on the curves of Fig. 31-3. The maximum power developed at these points, as found by setting  $X = 2.40$  in Eq. (31-9), is

$$P_{\max} = \frac{0.398I_0V_0}{N} \quad (31-11)$$

Although experimental power values are usually only a fraction of those predicted by Eq. (31-11), the above simple theory does show that the maximum power varies inversely with the number of transit-time cycles  $N$  and is proportional to the beam power  $I_0V_0$ .

While maximum power output is obtainable for small  $N$ , maximum stability is usually obtained for larger  $N$ . To illustrate, let us assume that the circuit conductance is 2.5 in the normalized units of Fig. 31-3. The amplitude of oscillation would then be 0.43 for  $N = 1\frac{3}{4}$  and 0.325 for  $N = 2\frac{3}{4}$ . If the oscillator load were increased to give a circuit conductance of, say, 3.5, the amplitude of the oscillation would be 0.34 for  $N = 1\frac{3}{4}$  and 0.285 for  $N = 2\frac{3}{4}$ . Hence, the *relative* change in oscillation amplitude for a given change in load is less for the larger  $N$ . Furthermore, unless the circuit admittance were less than 2.4, it would be impossible to obtain oscillations for  $N = \frac{3}{4}$ . Oscillations in the  $\frac{3}{4}$ -cycle range may be obtained in very low-loss cavities, but they are so extremely unstable and susceptible to slight changes in circuit loading that this range has not been found of practical value.

The total r-f power loss may be divided between that occurring in the tube and that in the external resonator and load. The latter losses will be considered later. The tube power losses are largely due to the glass dielectric seal between the bunching grids and to the resistance loss in the grids themselves. At low frequencies there exists a high electric field in the vicinity of the glass seal, and the dielectric loss in the glass may represent a large part of the total circuit loss. In the design of some tubes an effort is made to dimension the tube in such a manner that a voltage minimum occurs in the vicinity of the glass seal at the high-frequency limit of operation. This compensates to some extent for the decrease in the coupling coefficient  $\beta$  at the higher frequencies.<sup>1</sup>

Variations from the foregoing simple transit-time theory may be expected. The current  $I_0$  is the effective beam current which, depending

<sup>1</sup> The velocity modulation of the beam resulting from a given r-f voltage will always be decreased if the gap voltage changes appreciably during the time required for an electron to traverse the gap. Hence, the beam coupling coefficient  $\beta$  may be expected to decrease at the higher frequencies since frequency is proportional to the transit angle  $\theta_1$  of the electrons across the gap. The relation is  $\beta = \frac{\sin(\theta_1/2)}{\theta_1/2}$ , and usual design results in a gap-transit angle  $\theta_1$  (in electrical radians) such that  $\beta$  is about 0.5 to 0.9.

upon the geometrical openness of the grids and the focusing of the beam, may be appreciably less than the total cathode current. Furthermore, the presence of an r-f oscillation produces a decrease in the average velocity of the reflected electrons that have returned into the cathode region, and the beam focusing will therefore be altered because of modification of the space-charge distribution with oscillation. Also, some fraction of the beam electrons may be expected to cross the gap three or more times. The phase angle as well as the bunching of the electrons that make this third crossing will be a critical function of the voltages on the tube and the amplitude of oscillation. Hence, the electronic admittance may possess marked irregularities not accounted for by the simple theory. These effects will be discussed later in connection with electronic hysteresis.

**31-4. Frequency Stability.**—An idea of the voltage stability may be gained by differentiating the logarithm of Eq. (31-8)

$$\frac{df}{f} = \frac{dV_0 + dV_R}{V_0 + V_R} - \frac{1}{2} \frac{dV_0}{V_0} \quad (31-12)$$

The operating frequency will be substantially independent of slight changes in the cavity voltage  $\Delta V_0$  if the power supplies are compensated so that the repeller voltage changes by a proportional amount  $\Delta V_R$  where

$$\Delta V_R = \frac{(V_0 - V_R)}{2V_0} \Delta V_0 \quad (31-13)$$

This relation should hold for tubes having uniform repeller fields. The compensation of tubes having bucket-shaped repellers may be accomplished experimentally.

Of course, physical changes such as thermal expansion of the grids may also affect the operating frequency. Compensation of effects of this kind must be included in the design of the tube, and little can be done with a tube already developed other than to provide proper cooling. However, ambient temperature effects may be compensated by controlling the thermal expansion of the tuning mechanism, and fixed-frequency oscillators may be frequency stabilized by coupling to stabilizing cavities and discriminator circuits.

**31-5. The Resonator Admittance.**—The admittance of any reactive two-terminal admittor such as the circuit seen by the electron stream may be approximated to any desired accuracy by the series of parallel-resonant circuits shown in Fig. 31-6. The elements  $L_0$  and  $C_0$  will be present if the circuit admittance is zero at infinite and zero frequencies, respectively, while the  $n$ th parallel-resonant circuit produces an admittance zero at  $\omega_n = 1/\sqrt{L_n C_n}$ .



In a wide-range oscillator, an effort is made to employ a resonator that gives an antiresonance widely separated in frequency from all other spurious resonances. Hence, for frequencies in the immediate vicinity of the desired resonance, the resonator will behave substantially as a simple parallel-resonant circuit, the total impedance of all other elements in Fig. 31-6 being negligible compared with that of the antiresonant element. Furthermore, the effect of a small amount of dissipation may be included by shunting the antiresonant element with a conductance. Therefore, in the absence of near-by spurious resonances, any resonator will behave substantially as the simple circuit shown in Fig. 31-7. The results will be most useful if they are expressed in terms of indexes such

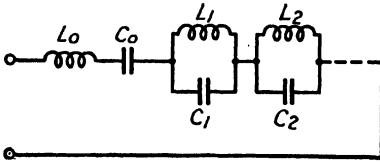


Fig. 31-6.—General reactance network.

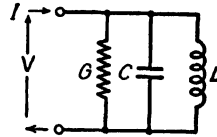


Fig. 31-7.—Equivalent circuit of resonator.

as characteristic impedance  $K$ , resonant radian frequency  $\bar{\omega}$ , figure of merit  $Q$ , and frequency-deviation factor  $\delta$ . The admittance of the circuit of Fig. 31-7 is simply

$$Y_o \approx \frac{1}{K} \left( \frac{1}{Q} + j2\delta \right) \tag{31-14}$$

where

$$K = \sqrt{\frac{L}{C}}, \quad Q = \bar{\omega} \frac{C}{G}, \quad \bar{\omega} = \sqrt{\frac{1}{LC}}, \quad \omega = (1 + \delta) \bar{\omega}$$

It is possible to normalize the above equation by introducing new units of voltage and current such that

$$\begin{aligned} \text{Unit voltage} &= \sqrt{K} \quad \text{volts} \\ \text{Unit current} &= \frac{1}{\sqrt{K}} \quad \text{amp} \end{aligned}$$

Note that this change of units leaves the power invariant. In terms of these new units the circuit admittance is (small letters will be used for normalized values)

$$y \approx \frac{1}{Q} + j2\delta \tag{31-15}$$

Thus, in the vicinity of a simple antiresonance where  $\delta$  is small, the admittance of the resonator will vary as illustrated in Fig. 31-8, which shows that, for a limited frequency range near antiresonance, the conductance  $g$

is constant, independent of frequency. The admittance is shown at frequency intervals differing by 0.125 per cent. The validity of the approximations leading to the straight-line admittance variation should be mentioned. If the admittance of Fig. 31-8 were produced by a cavity resonator that had a  $Q$  of 133, the small section shown would approximate the arc of a large admittance circle having its center roughly at  $g = 65$ . Apparently, even for a frequency range much greater than that considered in Fig. 31-8, for practical purposes the admittance variation will still be linear.

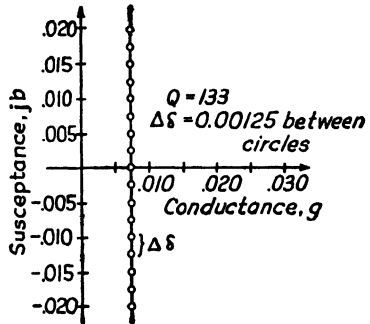


FIG. 31-8.—Typical resonator-admittance variation near antiresonance.

**31-6. Electronic Tuning.**—Since all simple resonators will ordinarily behave as illustrated in Fig. 31-8, we are now able to discuss the behavior of a reflex oscillator, even though the exact type of resonator is not specified.

A useful property of the reflex klystron is that the phase angle, and hence the susceptive component of the electronic admittance, is a function of the repeller voltage. This susceptance, which may be of either sign, is in shunt across the resonator and exerts a tuning effect. The shift in frequency resulting from maximum variation of this susceptance may be several tens of megacycles in a typical 10-cm-band oscillator. This effect may be utilized to produce frequency modulation or stabilization of the oscillator.

Since for oscillation,  $Y_e = -Y_c$ , we superimpose the curve of Fig. 31-8 upon the negative of that of Fig. 31-4.<sup>1</sup> For a fixed repeller voltage the electronic admittance is relatively slow changing with respect to frequency but is a function of  $V$ , the amplitude of the r-f oscillation, according to the curves of Fig. 31-3. The circuit admittance, on the other hand, is independent of the amplitude of oscillation but is a rapidly changing function of frequency. Hence, the intersection of the  $-Y_e$  line with the  $Y_c$  line gives both amplitude and frequency of the oscillation. This is illustrated in Fig. 31-9, where the  $-Y_e$  line for a repeller voltage in the  $N = 2\frac{3}{4}$  range together with  $Y_c$  lines for an unloaded and loaded resonator are shown.

As stated in Sec. 31-2, the admittance spiral shown in Fig. 31-9 represents the *maximum* value of  $-Y_e$ , which corresponds to zero amplitude of oscillation ( $V = 0$ ). As the amplitude is increased from zero,

<sup>1</sup> PIERCE, *loc. cit.*

the entire spiral pattern decreases in size, and hence the beam negative admittance decreases, according to Eq. (31-5), until its conductive component becomes equal to the conductance of the specific load in question. Steady-state equilibrium is thus possible only when this maximum  $-Y_e$  spiral sector for a specific repeller range lies to the right

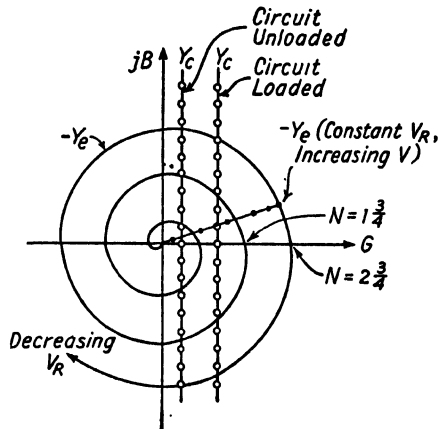


FIG. 31-9.—Admittance plot illustrating electronic tuning.

of the load line,  $Y_c$ . Several interesting conclusions can be drawn from Fig. 31-9.

1. With regard to the change in frequency obtainable with repeller voltage variation, it is to be noted that the maximum electronic tuning effect for a given r-f voltage  $V$  is obtained when the number of transit-time cycles  $N$  is large. Thus, in Fig. 31-9, the maximum electronic tuning is nearly twice as great for  $N = 2\frac{3}{4}$  as for  $N = 1\frac{3}{4}$ .

2. Oscillations may occur for any repeller voltage within a certain range of values. The center of each oscillating range is approximately the voltage for which  $-Y_e$  is real and positive. The electrical tuning resulting from a slight shift in repeller voltage about this point will be greater for the loaded than for the unloaded resonator.<sup>1</sup> Thus, as usual, a low- $Q$  resonator is found to be more easily frequency modulated than one of higher  $Q$ .

3. As the repeller voltage is decreased from a large (negative) value, there will occur several voltage ranges over which oscillations may take place. However, as may be shown by differentiating Eq. (31-7), the angular velocity  $dN/dV_R$  of the  $-Y_e$  line increases as  $V_R$  decreases, and hence the voltage ranges for oscillation become very narrow. This makes the repeller-voltage tracking problem more difficult for the range corresponding to larger values of  $N$ .

<sup>1</sup> Note that in Fig. 31-9 the spacing between points on the  $Y_e$  loci represents equal frequency increments.

**31-7. Oscilloscopic Techniques.**—The usual resonator is capable of resonating simultaneously at several frequencies within the operating range of a given reflex tube. The desired frequency may ordinarily be obtained by proper adjustment of the repeller voltage. However, when such separation cannot be effected, “mode interference” results. Also, parasitic resonances in the circuit may produce slight jumps in frequency or marked reduction in power output over exceedingly narrow parts of the tuning range, and electronic hysteresis may be present. The most satisfactory method of detecting these defects is by visual presentation of oscillator behavior on a cathode-ray oscilloscope.

A crystal voltmeter may be coupled to the resonator to give an indication of the oscillation amplitude. Furthermore, an alternating-voltage source may be connected in series with the repeller voltage supply in such a way that the instantaneous repeller voltage may be cyclically swept over its entire normal operating range. If, then, the crystal voltmeter is connected to the vertical amplifier of the oscilloscope and the repeller voltage is applied to the horizontal amplifier, a trace similar to that of Fig. 31-10 may be obtained.

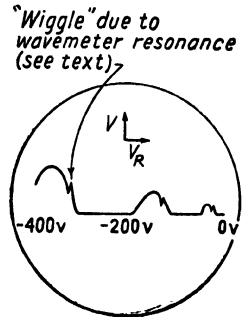


FIG. 31-10.—Oscilloscopic presentation of repeller ranges.

A little experience with a particular type of reflex tube usually enables one to tell almost at a glance the  $N$ -range for each oscillation. Thus, for the trace of Fig. 31-10, the oscillation at the extreme left is probably the  $N = 1\frac{3}{4}$ -cycle range, the next range to the right  $N = 2\frac{3}{4}$ -cycle, etc.

As the resonator is tuned to a higher frequency, the oscillating ranges in Fig. 31-10 all shift toward the left since, by Eq. (31-8), a greater repeller voltage is required for oscillation at a higher frequency (on a given repeller range). In fact, as has already been mentioned, the repeller voltage in a given  $N$ -range is roughly proportional to the frequency, and hence the horizontal position of any given oscillation range gives a rough indication of the oscillating frequency.

The electrical tuning occurring over each repeller range may easily be measured. If a resonant-type wavemeter is coupled loosely into the r-f line between the resonator and the crystal voltmeter, a little wiggle, as shown in Fig. 31-10, will be produced in the crystal output whenever the wavemeter resonates. If the tuning of the wavemeter is varied slightly, this wiggle will move across the range traces, thus showing that the oscillation frequency does actually change with the repeller voltage.

The horizontal sweep of the cathode-ray trace shown in Fig. 31-10 may be calibrated in volts, and the oscillating voltage ranges may be read directly. By observing these voltage ranges at various oscillating

wavelengths, a repeller voltage vs. wavelength characteristic can be constructed such as that shown in Fig. 31-11. Although the general shape of the repeller ranges shown in Fig. 31-11 is determined by the tube characteristics alone, the width and short-wavelength limits of each of the ranges are necessarily dependent on the losses of the resonator. Thus, for example, while the particular resonator used in obtaining the data of Fig. 31-11 did not allow oscillations at wavelengths less than 6 cm, other resonators have been developed that have allowed oscillations at

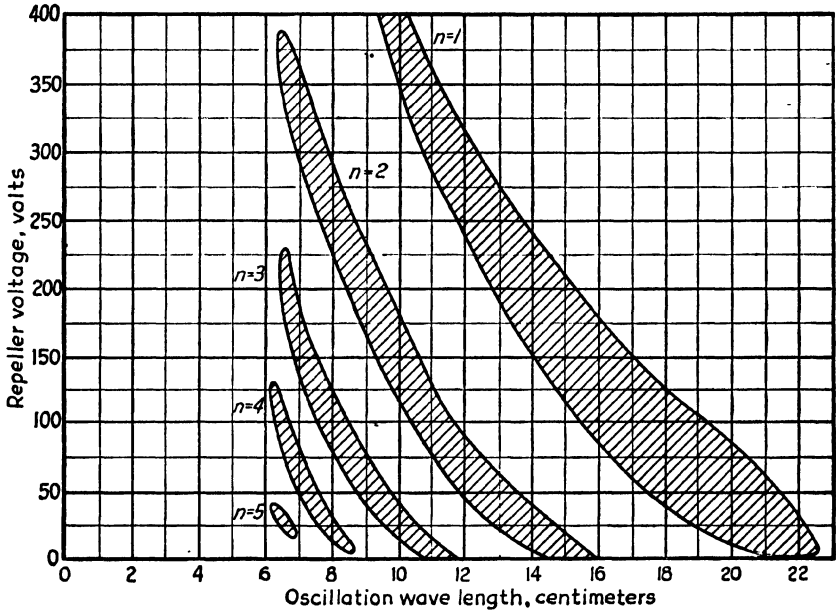


FIG. 31-11.—Repeller characteristic of 2K28 tube.

wavelengths as short as 5 cm on the  $N = 4\frac{3}{4}$ -cycle range with this tube. Note also that the typical oscilloscope trace of Fig. 31-10 would be obtained at about 10 cm for a tube having the characteristics of Fig. 31-11.

**31-8. Electronic Multiple Transits and Hysteresis.**—In some types of reflex tubes such as the 2K48 and 2K49, multiple-transit effects may be particularly pronounced. The total number of cycles that have elapsed between the first and third transits of the gap is several times the number  $N$  between the first and second traverses. Thus, the total electronic admittance roughly consists of the sum of several terms of the form  $J_1(x)/x$ , and the variation of the admittance with the amplitude of oscillation probably appears as sketched in Fig. 31-12.

Of course, the relative phase of the third-transit electronic admittance with respect to the main (or second-transit) admittance will be a critical function of tube voltages. For simplicity, these admittances were assumed to be in phase in constructing Fig. 31-12. Because of this

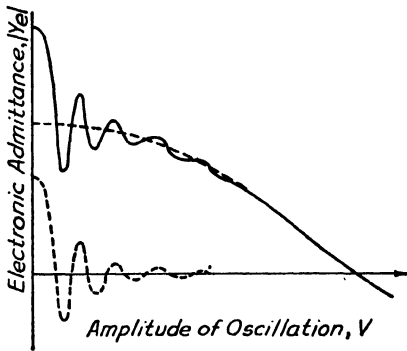


FIG. 31-12.—Effect of multiple transits upon electronic admittance.

steplike variation in the electronic admittance, the amplitude of oscillation may vary with repeller voltage, as shown in Fig. 31-13. As one would expect from examina-

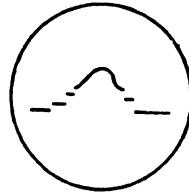


FIG. 31-13.—Typical effect of multiple transits on oscilloscopic presentation.

tion of Figs. 31-12 and 31-13, the effect of multiple transits is most marked when the circuit loading is large and the amplitude of oscillation is small.

Another electronic effect, closely related to that of multiple transits, is that known as *electronic hysteresis*. By using the oscilloscopic technique

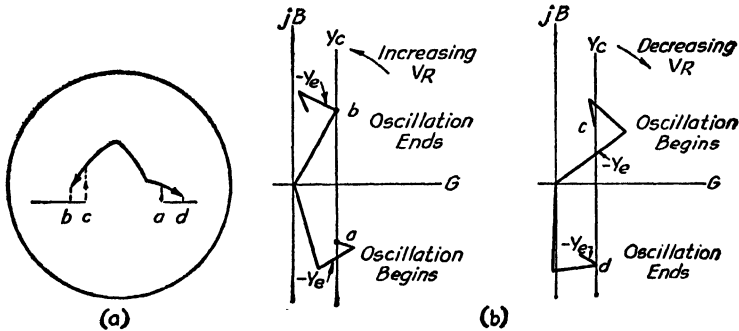


FIG. 31-14.—Effect of multiple transits upon electronic admittance: (a) Oscilloscopic presentation; (b) the electronic-admittance  $(-Y_e)$  characteristic at fixed repeller voltages  $a$ ,  $b$ ,  $c$ , and  $d$  as r-f amplitude  $V$  varies.

previously described, one may observe this effect while sweeping the repeller voltage through the range for which oscillations ordinarily occur. If electronic hysteresis is present, the repeller voltages at which oscillations begin and end will be greater with increasing repeller-voltage than with decreasing voltage. As shown in Fig. 31-14, this phenomenon may be explained if it is assumed that abrupt changes in the *phase* of the

electronic admittance occur with changes in the amplitude of the r-f oscillation. The result of such changes in phase is to cause violent bends in the electronic admittance characteristic. If it is kept in mind that the end of the  $-Y_c$  curves shown in Fig. 31-14 corresponds to the electronic admittance for an oscillation just beginning, *i.e.*, of zero amplitude, it is apparent that oscillations cannot commence until the *end* of the  $-Y_c$  line crosses to the right of the  $Y_c$  line.

Such hysteresis effects are not particularly serious once the tube is oscillating on a given repeller range, because oscillations will continue, provided  $V_R$  remains anywhere within that range. However, hysteresis can be extremely undesirable whenever the operational requirements are such that a nonoscillating tube must be brought into oscillation through adjustment of the repeller voltage from outside to within the oscillating range. Under this condition, *the effective width of the repeller range may be decreased as much as 70 per cent by severe electronic hysteresis.* This feature is particularly serious when repeller-voltage modulation of the tube is used, or when the power supplies of an automatically tracked oscillator must be turned off and on during periods of operational use.

**31-9. Harmonic-frequency Generation.**—Inasmuch as the electron-beam bunching of a reflex klystron is distinctly nonsinusoidal, the beam induces harmonic components in addition to the fundamental component of current across the gap. The “forced” oscillations set up by these harmonic components are normally very small, but in some measurement work they may not be negligible, and an output filter must be used if a serious error is to be avoided.

The use of a reflex oscillator as a harmonic generator has not been experimentally investigated, but, theoretically, if the resonator were simultaneously antiresonant at both fundamental and harmonic frequencies, a considerable amount of harmonic energy could be abstracted from the beam. Advantages that might be expected of such an oscillator are as follows:

1. Harmonic frequencies may be obtained from a low-frequency low-voltage tube.
2. The inherent stability of the harmonic-frequency oscillation should be excellent. That is, loading at the harmonic frequency could not “kill” the oscillation, and change in frequency with load tuning should be slight, if present at all.

Intermodulation effects due to the extremely nonlinear action of transit-time phenomena have also been observed. For example, at certain critical points within the tuning range of the oscillator, a cavity will often resonate simultaneously at frequencies that are exactly in the ratio of 2:3. If the repeller voltage is adjusted for the lower of these two

frequencies, power output may be obtained at the higher frequency, even though the repeller voltage is not correct for operation at that frequency. It is believed that this behavior is due to intermodulation effects producing a *subharmonic* of the main transit-time frequency. Similar effects may be noticed if the resonator is simultaneously resonant at frequencies having the ratio of 3:4, etc.

**31-10. Effect of Parasitic Resonances.**—Chapter 32 will be chiefly concerned with parasitic resonances that may exist in a coaxial-cavity resonator. It has been found that, insofar as the tube operation is concerned, any parasitic resonance acts upon the resonator in a manner similar to that of the loosely coupled secondary circuit on the primary circuit of Fig. 31-15.

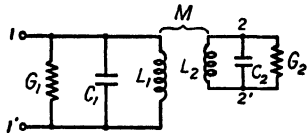


FIG. 31-15.—Equivalent circuit for effect of parasitic resonance

It is well known that the effect of a coupled circuit is to alter the input admittance of the primary circuit. This effect will, in general, be greater the higher the figure of merit  $Q_2$  of the secondary circuit, the greater the coefficient of coupling  $k$ , and the closer the operating frequency to the resonant frequency  $\bar{\omega}_2$  of the secondary circuit. In fact, if a secondary frequency-deviation factor  $\delta_2$  is defined by the relation

$$\omega = (1 + \delta_2)\bar{\omega}_2 \tag{31-16}$$

the conductive and susceptive components of the admittance  $Y_c$  presented by the primary resonant circuit will be

$$\left. \begin{aligned} G_{in} &= \frac{1}{K} \left[ \frac{1}{Q_1} + \frac{k^2 Q_2}{1 + (2\delta_2 Q_2)^2} \right] \\ B_{in} &= \frac{1}{K} \left[ 2\delta_1 - \frac{k^2 Q_2}{1 + (2\delta_2 Q_2)^2} \cdot (2\delta_2 Q_2) \right] \end{aligned} \right\} \tag{31-17}$$

The first terms of Eq. (31-17) are the values that were shown in Eq. (31-14) to exist for a simple resonator. The second terms inside the brackets therefore represent the change in resonator admittance arising from a parasitic resonance. The effect of the parasitic resonance is always (1) to *increase* the circuit conductance, (2) to *oppose* the usual increase in circuit susceptance with increasing frequency. The relative effect of the parasitic resonance is determined by the coupling  $k$  between the desirable resonance and the parasitic resonance and by the figure of merit  $Q_2$  of the latter. If  $k \ll 1/Q_2$ , the parasitic resonance may have negligible effect. If  $k > 1/Q_2$ , the parasitic resonance introduces a loop into the  $Y_c$  locus. When  $k = 1/Q_2$  the loop becomes a cusp. These three conditions are illustrated in Figs. 31-16 and 31-17. The same



resonator constants used in Fig. 31-8 have been assumed in calculating these figures.

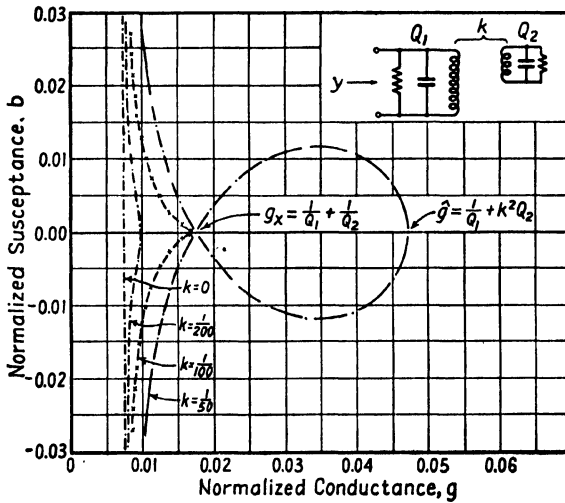


FIG. 31-16.—Effect of parasitic resonance on circuit admittance. Coupling varied.  $Q_1 = 133$ ,  $Q_2 = 100$ ,  $\delta_1 = \delta_2$ , and  $\Delta\delta = 0.00125$  between points.

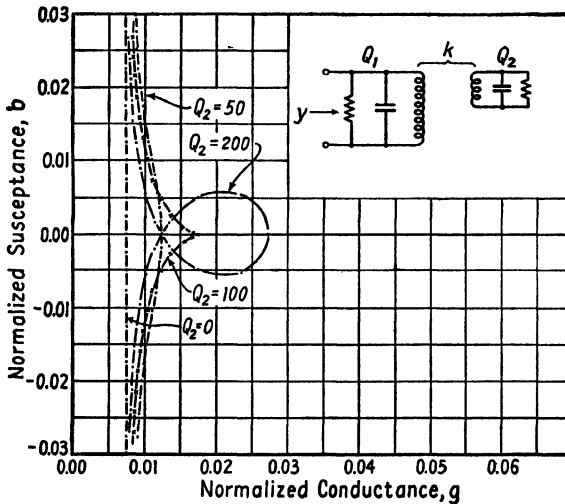


FIG. 31-17.—Effect of parasitic resonance on circuit admittance. Parasitic  $Q$  varied.  $Q_1 = 133$ ,  $\delta_1 = \delta_2$ ,  $k = 0.01$ ,  $\Delta\delta = 0.00125$  between points.

It is assumed that the resonant frequencies of both circuits are the same, the frequencies at which the loop crosses the conductance axis may be calculated by equating  $B_{in}$  to zero. This gives

$$\hat{\delta} = 0$$

and

$$\delta_s = \pm \frac{1}{2} \sqrt{k^2 - \frac{1}{Q_2^2}} \tag{31-18}$$

The conductances at those frequencies for which the susceptance is zero are found to be, respectively,

$$g = \frac{1}{Q_1} + k^2 Q_2$$

and

$$g_s = \frac{1}{Q_1} + \frac{1}{Q_2} \quad \left( \text{exists only if } k > \frac{1}{Q_2} \right) \tag{31-19}$$

It will be noted that the *maximum conductance*  $g$  at the extreme right of the loop increases by an increment proportional to  $k^2$ , whereas the *cross-over conductance*  $g_s$  is independent of  $k$ . Thus, the size of the loop is a sensitive function of  $k$ , much more so, at least, than of  $Q_2$ .

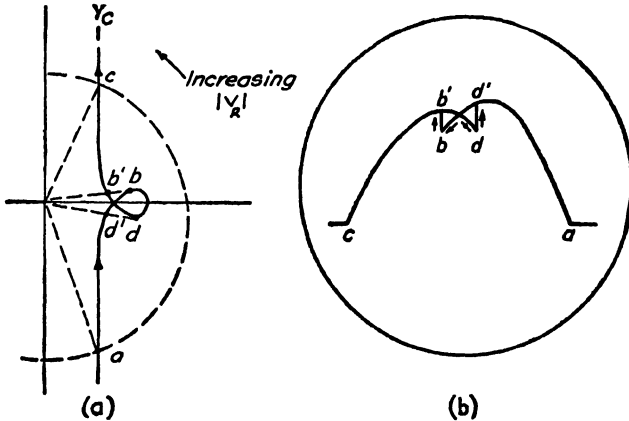


FIG. 31-18.—Diagrams showing effect of parasitic resonance.

Equations (31-17) also show that the change in admittance resulting from the parasitic resonance is a function only of the frequency deviation  $\delta_2$  from the resonant frequency of the parasitic resonance and is independent of  $\delta_1$ , the frequency deviation from the resonant frequency of the main resonator. Hence, as the frequency of oscillation is varied by tuning the resonator (*i.e.*, the 1-1' circuit of Fig. 31-15), the loop of Fig. 31-16 is displaced vertically but is not changed in shape. If tuning of the resonator also affects the resonant frequency of the parasitic resonance, the actual motion of the admittance locus with tuning may be calculated by first determining the proper functional relationship between  $\delta_1$  and  $\delta_2$  from mode-plot data.

The presence of a loop or bulge in the circuit admittance curve is most easily detected by the cathode-ray-oscilloscope technique described in Sec. 31-7. Again the negative of the electronic admittance characteristic is superimposed upon the circuit admittance. Figure 31-18a shows this superposition with  $-Y_e$  lines drawn for several different repeller voltages, and Fig. 31-18b shows the corresponding oscilloscopic trace. For increasing  $V_R$ , oscillations commence at voltage  $a$ . The frequency of oscillation gradually increases until voltage  $b$  is reached. At this point the oscillator frequency suddenly jumps from that corresponding to  $b$  to that of  $b'$ . A similar discontinuity at a slightly different repeller voltage, as at  $d$  to  $d'$ , occurs with decreasing repeller voltage. These jumps in frequency may be measured with a wavemeter, although usually the amplitude of oscillation changes sufficiently to make the discontinuity clearly visible, as illustrated in Fig. 31-18b.

It should be mentioned that, although three intersections of  $Y_e$  with  $-Y_e$  are possible in the vicinity of the loop, only two of these intersections represent stable operating points. Over the part of the loop from  $b$  to  $d$ , the susceptance *decreases* with frequency. J. R. Pierce has shown in an unpublished report that an "oscillation will be stable if, at the intersection of  $-Y_e$  with  $Y_e$ , the direction of change of  $-Y_e$  with increasing voltage lies counterclockwise from the direction of change of  $Y_e$  with increasing frequency."<sup>1</sup> Over the section of the loop extending from  $b$  to  $d$  this condition is not satisfied; a diminishing oscillation will encounter an ever-increasing transient circuit conductance, and stable oscillations cannot result.

<sup>1</sup> This criterion is based upon the consideration that, for dynamic stability, after an initial increase  $dV$  in the amplitude of oscillation (resulting from a brief *momentary* decrease in load, let us say), the oscillation must decay to its original value. An oscillation whose amplitude is decaying slowly according to the exponential factor  $e^{-\omega t}$  may be considered as a *steady-state* oscillation having a complex frequency  $\omega + j\mu$ . Therefore, for stability, an increase in the amplitude of oscillation should result in a positive imaginary increment in frequency. For steady-state oscillations (both for real and complex frequencies),

$$Y_e + Y_c = 0$$

and

$$\frac{dY_e}{dV} dV + \frac{dY_c}{d\omega} d\omega = 0$$

Hence

$$d\omega = - \left( \frac{\frac{dY_e}{dV}}{\frac{dY_c}{d\omega}} \right) dV$$

and in order that the imaginary part of  $d\omega$  be positive, the criterion for stability as stated by Pierce must be satisfied.

Figure 31-18 represents the condition for which  $k > 1/Q_2$ . Such an admittance loop cannot be tolerated because oscillations at frequencies lying between  $b$  and  $d$  will be skipped. In fact, the jump in frequency at the crossover point of the loop is, by Eq. (31-18),

$$\Delta\delta = \sqrt{k^2 - \frac{1}{Q_2^2}} \quad (31-20)$$

It is of interest to note that  $\Delta\delta$  can be measured with a selective wave-meter; so if  $Q_2$  is measured or calculated by conventional methods, Eq. (31-20) provides an experimental method of determining  $k$ .

A jump in frequency will not be present if  $k < 1/Q_2$ . Hence, to eliminate the undesirable effects of a parasitic resonance, it is necessary first to reduce the coupling to as small a value as possible and then decrease  $Q_2$  (if necessary) until  $Q_2 < 1/k$ . The maximum conductance  $g_{\max}$  would for this condition occur when  $1/Q_2 = k$  and, by Eq. (31-19),

$$g_{\max} = \frac{1}{Q_1} + k \quad (31-21)$$

Equation (31-21) permits us to determine the maximum tolerable parasitic-resonance coupling. Suppose, for example, that negative electronic conductance of 100  $\mu\text{mhos}$  is available for neutralizing circuit losses in a coaxial-cavity oscillator ( $Z_0 = 40$  ohms) operating on  $3\lambda/4$  cavity mode and with a 2K28 reflex tube. It may be shown that if  $n$  is the number of quarter wavelengths in a coaxial line of characteristic impedance  $Z_0$ , the equivalent lumped circuit of Fig. 31-15 will have a characteristic impedance

$$K = \frac{4}{n\pi} Z_0 \quad (31-22)$$

Since  $g_{\max}$  in Eq. (31-21) is expressed in normalized units, the "unnormlized" electronic conductance required for neutralizing the circuit loss represented by Eq. (31-21) will be  $G_e = g_{\max}/K$ . To estimate the maximum coupling that may be tolerated, we shall assume that the entire circuit loss is due to the parasitic resonance, *i.e.*,  $Q_1 = \infty$ . Then, by Eqs. (31-21) and (31-22), if the resonator conductance is to be less than 100  $\mu\text{mhos}$ , the coupling coefficient  $k$  of the parasitic resonance must be less than 0.0017, and the  $Q$ -factor of the parasitic resonance would have to be less than 590 if a frequency discontinuity were to be avoided.

In view of this typical, extremely small threshold coupling coefficient of 0.0017, it is apparent that in a reflex oscillator that requires a large circuit  $Q$  for proper operation almost any parasitic resonance presents a serious problem. Experience has shown this to be all too true. Irregu-

larities and asymmetries in tube or cavity can often produce a coefficient of coupling sufficiently great to excite these resonances. For example, it has been estimated that the maximum allowable eccentricity of a choke plunger in a typical coaxial cavity is less than 0.002 in. if undesirable coupling with the  $TE_{1,1}$  cavity mode is to be prevented. Such mechanical tolerances are not practicable, and other means of controlling this resonance are described in Chap. 32.

**31-11. Power-supply Requirements.**—A major consideration in receiver design is the frequency stability of the local oscillator. In receivers utilizing cavity-type reflex-klystron oscillators, there are three principal causes for instability: an imperfect mechanical drive on the oscillator tuner, variations in ambient temperature of the oscillator tube and cavity, and variations in oscillator voltages. Only the last of these three causes will be discussed in this section.

Three general types of voltage variation cause instability in the frequency of reflex tubes:

1. Nonperiodic, usually slow-time, shifts in frequency resulting from poor long-period regulation of cavity and repeller voltage supplies
2. Ripple-frequency frequency modulation resulting from insufficient filtering of cathode and repeller voltages
3. Power-line-frequency frequency modulation resulting from the magnetic field produced by the alternating current in the cathode heater.

The last difficulty is in most cases not serious because it is the usual practice to use noninductive heaters.<sup>1</sup> If necessary, it can be eliminated by using direct heater current. The discussion will therefore be directed toward the cavity and repeller voltage-supply requirements.

Before power-supply specifications can be determined, it is necessary that the allowable frequency modulation and drift due to voltage variations be specified. The allowable frequency shift due to voltage variations can be obtained only after mechanical-drive features and temperature effects have been studied. The over-all tolerable frequency shift is determined largely by the receiver i-f band width and is much greater than the allowable frequency modulation, which must be limited to a small value if it is not to have a very bad effect on the presentation of the received signal. We shall assume that these two factors, maximum allowable frequency shift and maximum allowable frequency modulation, have been determined. In the discussion of power-supply design considerations the following symbols will be used:

<sup>1</sup> Some difficulty due to heater-current modulation has been observed in development models of the 2K48 and 2K49 tubes, however, and all a-c magnetic fields at the electron gun of any reflex klystron must be avoided.

- $\Delta f_1$ , percentage drift in frequency caused by slow nonperiodic voltage variations, *i.e.*, by improper voltage regulation
- $\Delta f_2$ , percentage deviation of frequency caused by ripple-frequency voltage variation
- $V_R$ , negative repeller voltage with respect to cathode
- $V_0$ , cavity voltage with respect to cathode
- $\Delta V_R$ , percentage change in repeller voltage,  $V_R$
- $\Delta V_0$ , percentage change in cavity voltage,  $V_0$
- $I_0$ , beam current
- $VR$ , percentage voltage regulation
- $\rho$ , ripple factor

The effect of repeller voltage variations may be expressed in terms of the ratios  $\Delta f_1/\Delta V_R$  and  $\Delta f_2/\Delta V_R$ . These are equal and may be determined experimentally by the method of Sec. 31-7 by measuring the electronic tuning. From the discussion presented in Sec. 31-6, it is apparent that the ratio will depend upon the particular repeller range employed; so experimental measurements should be made at representative points throughout the tuning range of the oscillator.

Variation in the cavity voltage produces not only an electronic tuning effect, but also a mechanical tuning effect in that the thermal expansion resulting from the variation in power dissipated at the tube electrodes may alter the capacitance of the interaction gap. The 2K28 has been

TABLE 31-1.—POWER-SUPPLY REGULATION AND RIPPLE FACTOR FOR REFLEX OSCILLATORS

Tube type	2K28	2K48 and 2K49
Repeller range.....	$N = 2\frac{3}{4}$	$N = 3\frac{3}{4}$
Resonator mode.....	$3\lambda/4$	$3\lambda/4$
Tuning range, <i>k</i> Mc.....	2 to 4	7 to 10
Maximum allowable $\Delta f_1$ .....	$\pm 0.05\%$	$\pm 0.02\%$
Maximum allowable $\Delta f_2$ .....	$\pm 0.005\%$	$\pm 0.002\%$
$\Delta f_1/\Delta V_R$ and $\Delta f_2/\Delta V_R$ .....	0.025 max	0.008 max
$\Delta f_1/\Delta V_0$ and $\Delta f_2/\Delta V_0$ .....	0.0125 max	0.033 max
Maximum allowable $VR$ of $V_R$ supply.....	$\pm 1\%$	$\pm 1.25\%$
Maximum allowable $VR$ of $V_0$ supply.....	$\pm 2\%$	$\pm 0.3\%$
Cavity voltage $V_0$ , volts.....	$300 \pm 6$	$1250 \pm 4$
Repeller voltage $V_R$ , volts.....	$-30 \pm 0.3$ to $-300 \pm 3$	$-50 \pm 0.6$ to $-400 \pm 5$
Cathode current, ma.....	35 to 40	16-20
Maximum allowable $\rho$ of $V_R$ supply.....	0.07%	0.09%
Maximum allowable $\rho$ of $V_0$ supply.....	0.14%	0.5%

compensated in its internal design for this thermal change. The effect of cavity-voltage changes is related to the effect of repeller-voltage changes by Eq. (31-13). In other tubes, such as the developmental models of the 2K48 and 2K49, the thermal frequency drift resulting from a change in cavity voltage may be much larger than any electronic effect and, for this reason, a cavity-voltage supply must have excellent regulation, even though a fairly large ripple voltage may be tolerated.

Table 31-1 gives typical ripple and regulation factors for the 2K28 and 2K48 tubes when used as local oscillators for receivers incorporating panoramic presentation.

**31-12. Repeller-voltage Tracking Systems.**—In order to provide a single tuning adjustment for a reflex-klystron oscillator, the repeller voltage must be tracked with the cavity tuning. The requirements for such a voltage-tracking system for use with the typical reflex tubes considered are as follows:

1. It must be capable of tracking some predetermined voltage curve within approximately plus or minus 5 volts throughout the range.
2. It must have adequate end-point adjustment to compensate for variations in tubes.
3. The voltage source should present a low impedance, since the repeller may draw up to 1½-ma current on low repeller voltages.
4. It should have low-wear operation for rapid and frequent sweeping.
5. For use with some tubes it must be sufficiently insulated so that it can operate at 1200 to 1500 volts below ground.

This section describes several types of tracking systems capable of satisfying most or all of the requirements listed above.

*Nonlinear-gear Tracking System.*—The voltage to the repeller may be applied from the center tap of a linear voltage divider connected across

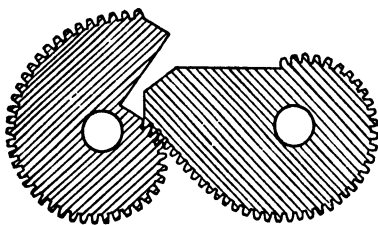


FIG. 31-19.—Nonlinear gears.

a regulated supply and driven by a set of nonlinear gears cut to provide the proper tracking voltage for the particular repeller-voltage range used. The gears may be driven from the mechanical drive that tunes the cavity. A single tuning adjustment for the oscillator is thus provided. A set of gears of this type is shown in Fig. 31-19 and a typical schematic diagram of the electrical circuit in Fig. 31-20. The end-point adjustments are made with  $R_2$  at the high-frequency end and  $R_3$  at the low-frequency end of the tuning range. If it is necessary to operate over a frequency range in which two repeller-voltage ranges must be used, two voltage

dividers may be ganged together and a microswitch provided to switch from one to the other in changing ranges.

This system is very satisfactory for use in applications where rapid and frequent sweeping of the oscillator is not necessary, and the wear on the voltage divider is negligible. The system is simple and compact and uses standard voltage dividers, and the gears may be adapted to production.

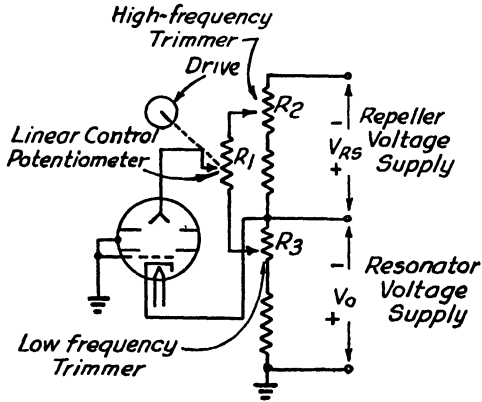


FIG. 31-20.—Schematic diagram of a typical circuit for use with nonlinear gears.

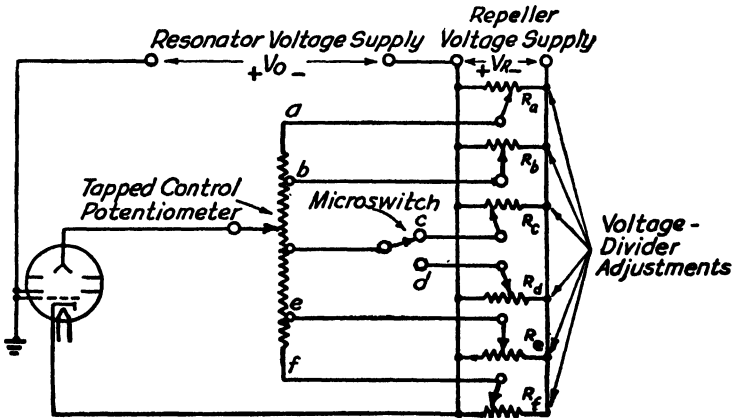


FIG. 31-21.—Tapped-voltage-divider tracking circuit.

It has the disadvantage that, in order that the voltage source should have a low-impedance, the bleeder current must be fairly large, and considerable power is dissipated in the voltage divider. Furthermore, it is necessary to provide high-voltage insulation between the voltage divider and the gears.

*Tapped-voltage-divider Tracking System.*—A tapped voltage divider and resistance network may be used to accomplish the same purpose as a standard linear voltage divider driven by nonlinear gears. A circuit



diagram of this type of voltage divider and resistance network is shown in Fig. 31-21, and a set of curves showing the method of tracking is given in Fig. 31-22. The voltage-divider resistance network consists of a linear-taper tapped voltage divider connected to a resistance network so that any desired voltage may be set up at any specified tap. The curve produced by this method is a succession of straight lines of varying

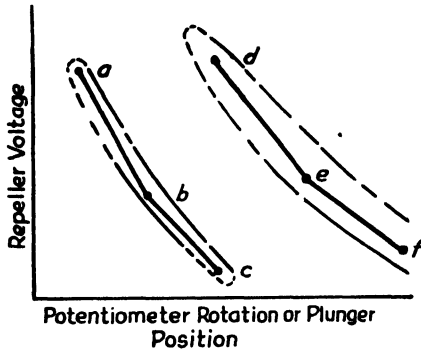


FIG. 31-22.—Method of tracking tapped voltage divider.

slopes, the number of lines being one less than the number of taps. Tracking adjustments are made with  $R_a$ ,  $R_b$ ,  $R_c$ , etc., set at the points indicated on the curve. By means of a microswitch that switches from one range to the other at the desired point, this circuit also provides for tracking when two repeller-voltage ranges are used.

This system satisfies the same requirements as the system using nonlinear gears, but has the disadvantage that it requires the use of a special nonstandard voltage divider. The alignment problem for accurate tracking is more difficult since all the adjustments are interdependent.

*Tapered-voltage-divider Tracking System.*—A voltage divider may be tapered so that its curve of output vs. rotation approximates the required tracking curve. It may be connected in exactly the same manner as the voltage divider with nonlinear gears and will have the same electrical and mechanical characteristics. The disadvantage of this system over one using nonlinear gears is that a nonstandard voltage divider must be used, thus making replacement difficult.

*Tube-characteristic Tracking System.*—Another method for tracking a nonlinear curve with a linear voltage divider is to develop the repeller voltage across a resistor in series with a triode whose characteristics are made a function of a linearly varying resistor in series with the cathode. A circuit of this type is shown in Fig. 31-23, in which  $R_1$  is the variable voltage divider,  $R_2$  is the resistor across which the repeller voltage is developed, and  $R_3$  and  $R_4$  are voltage dividers for making the end-point adjustments at the high- and low-frequency ends, respectively.

By choosing a tube with the proper characteristics, accurate tracking may be accomplished with a system of this type. Like other voltage-divider-controlled systems, it is not well adapted to rapid and frequent sweeping because of wear on the voltage divider. It also presents a source of high impedance and may cause trouble at low repeller voltages

when repeller current is drawn. For application to some tubes, the whole system must operate at large voltages below ground.

*Variable-transformer Tracking System.*—A voltage-tracking system may be built using a stabilized a-c source that is controlled by a variable transformer, amplified to the desired level, rectified, filtered, and applied to the repeller. A block diagram of such a system is shown in Fig. 31-24. The regulated a-c source may be a stabilized a-f RC oscillator, the out-

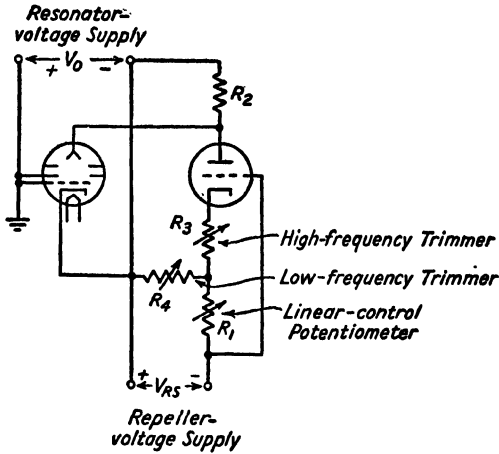


FIG. 31-23.—Tracking system using characteristic of triode.

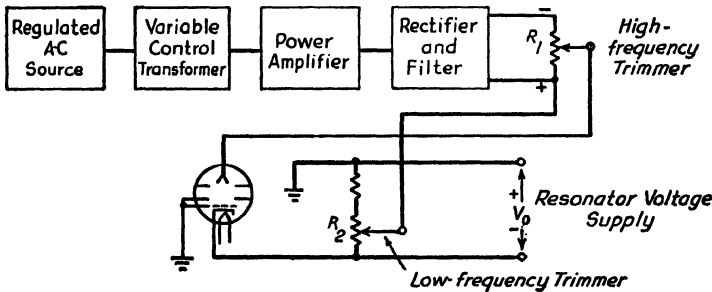


FIG. 31-24.—Variable-transformer tracking system.

put of which is fed into a selsyn which is used as the variable transformer. The selsyn may be used as the controlling element because the straight-line portion of its curve of output vs. rotation closely approximates the curve of repeller voltage vs. frequency for the oscillator on the desired mode. The selsyn is geared directly to a straight-line-frequency dial, and the cavity is tuned by a mechanical drive employing a cam system for changing from straight-line-frequency rotation to the desired longitudinal movement. In aligning this voltage-tracking system, the correct

portion of the selsyn curve is determined and adjusted permanently. The end-point adjustments to compensate for variations in tubes are made with  $R_1$  at the high-frequency end and with  $R_2$  at the low-frequency end of the range.

This system meets all the requirements given at the beginning of this section. It may be made virtually free from backlash, the wear is very low, and it is well adapted to rapid and frequent sweeping. Although this system is very good electrically, it is more complicated and of larger size and weight than those previously described. The  $RC$  oscillator and amplifier must be highly stabilized, and the supply voltage to them must be well regulated. However, multiple-range tracking with this system could easily be accomplished by combining in appropriate resistance networks the output voltages from the three-phase windings of the selsyn transformer.

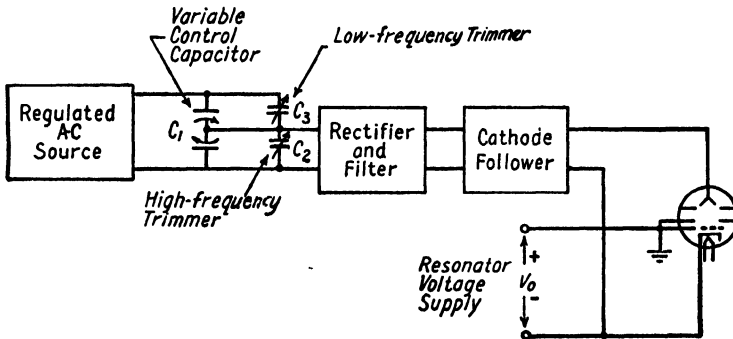


FIG. 31-25.—Capacitance-divider tracking system.

*Capacitance-divider Tracking System.*—A capacitance divider may be used in a system similar to that using a variable transformer. A regulated a-c source is fed to the capacitance divider, the output of which is rectified, filtered, fed to a cathode follower, and applied to the repeller. A block diagram of such a system is shown in Fig. 31-25. In this figure, the double-stator capacitor  $C_1$  is used as the capacitance divider by feeding the regulated a-c source across the two stators and obtaining the output between the rotor and one stator. Although particularly accurate alignment is possible by correct shaping of the capacitor plates, some curves can be followed closely enough by using a standard straight-line capacitance capacitor. The end-point adjustments of the tracking curve are made by adjusting the trimmers  $C_2$  and  $C_3$  at the high- and low-frequency ends, respectively.

For best operation, the capacitance divider should operate into a constant high-impedance load, while the repeller supply should be of fairly low impedance to minimize the effect of repeller current drawn on

low reflector voltages. To satisfy these requirements, a heavily loaded cathode-follower stage with a high input impedance is connected to the output of the rectifier.

The characteristics of this system are very similar to those of the variable-transformer type except that this system is somewhat smaller in size and weight. It is good electrically, and, since it has very low wear, it may be adapted to rapid and frequent sweeping.

## CHAPTER 32

### LOCAL OSCILLATORS: III

#### WIDE-RANGE COAXIAL-LINE RESONATORS

BY W. H. HUGGINS, H. M. ZEIDLER, AND L. A. MANNING

**32-1. Introductory Summary.**—This chapter deals with factors controlling the design of a coaxial-line resonator<sup>1</sup> that must be tunable over a wide frequency range in the microwave region. Because it requires but a single resonator, the reflex-klystron oscillator has been used in this chapter to illustrate the general problems of mode interference, parasitic resonances, etc., which may occur in a coaxial resonator having a non-contacting plunger (tuning element). It should be emphasized that those parts of this chapter which are concerned with parasitic resonance, mode separation, and noncontacting plungers in coaxial-line sections have direct application to the design of other microwave equipment incorporating coaxial-line sections such as tunable filters and preselectors, wave traps, and multiple-resonator oscillators.

**32-2. Circular Coaxial Resonators.**—Of the various resonators that may be used in wide-range microwave oscillators, the type that is formed from a short-circuited section of circular coaxial line offers the most attractive electrical and mechanical properties.

From the electrical standpoint, a short-circuited coaxial-line section forms an excellent resonator, for the following reasons:

1. It is self-enclosed and therefore does not radiate energy, as would an unshielded circuit such as a parallel line.
2. It possesses a *TEM* mode resonance, which by proper selection of conductor diameters may be widely separated in frequency from most of the higher order parasitic resonances that occur in all microwave resonators.
3. Many microwave vacuum tubes are of a circularly symmetrical construction and, hence, are excellently suited for use in a coaxial resonator.
4. Because the tuning device, or plunger, may be of fixed shape, it is practicable to incorporate into it transmission-line sections that will simulate a short circuit over a given tuning range without requiring actual metallic contact.
5. A linear relation exists between plunger displacement and the resonant wavelength.

<sup>1</sup> For brevity, the more exact term *coaxial-line resonator* may hereafter be shortened to *coaxial resonator*.

Obvious mechanical advantages of a coaxial resonator are its simplicity and the ease with which circularly symmetrical parts may be produced on a machine lathe.

**32-3. Summary of Basic Wave Types.**—Detailed mathematical treatments of the wave types possible in a coaxial resonator may be found in other references<sup>1</sup> and will not be presented here. In order that we may be explicit in the discussion of the resonance phenomena, however, it will be advantageous to describe certain basic wave types that are encountered in coaxial resonators.

*Transverse-electromagnetic Waves (TEM).*—These waves contain neither electric nor magnetic field in the axial direction of propagation. They are the usual *transmission-line* waves and are sometimes referred to as the *dominant* or *principal waves* because they can be propagated at frequencies lower than that required by the other (waveguide) types listed below. It is this type of wave that is mainly utilized in a wide-range coaxial resonator to present a high impedance to the electron beam of the reflex tube.

*Transverse-electric Waves (TE).*—These waves have a component of magnetic field but no electric field in the axial direction. Most of the parasitic resonances encountered in a coaxial resonator are due to waves of this type. None of these waves is of any use in a coaxial electron tube—all are parasites in the worst sense.

*Transverse-magnetic Waves (TM).*—These waves have a component of electric field but no magnetic field in the axial direction. The particular *TM* waves that exhibit circular symmetry account for the distortion and bending of the field at the tube end of the resonator. If the resonator diameter is sufficiently large (compared with a wavelength), the *TM* wave set up by this discontinuity may be propagated and may produce parasitic resonances that can limit the high-frequency tuning range of a given resonator.

We shall now examine each of these wave types more carefully and attempt to describe with sketches the approximate spatial distribution of the electric and magnetic fields associated with the standing waves of each type. To avoid confusion in these sketches, only the electric field or the magnetic field will be shown at one time. It will be possible to deduce the other field as well as the surface currents and charges if it is kept in mind that, for standing waves in a resonator formed of perfect conductors, the following five rules apply:

<sup>1</sup> See, for instance, RAMO, SIMON, and J. R. WHINNERY, "Fields and Waves in Modern Radio," John Wiley & Sons, Inc., New York, 1944; SCHELKUNOFF, S. A., "Electromagnetic Waves," Chap. 10, D. Van Nostrand Company, Inc., New York, 1943.

1. Electric-field lines, when closed by the conductor surface upon which they terminate, form closed paths that must encompass a changing magnetic field.
2. Electric-field lines that terminate on a conductor are normal to the conductor at the surface and must induce thereon a bound charge proportional at every point to the electric-field intensity.
3. Magnetic-field lines always form continuous closed paths that must surround either a conduction current or a displacement current (changing electric field).
4. The current flow in the conductor surfaces may be obtained from the electric-field distribution. By 2, above, the surface current must flow toward (or away from) regions of high surface charge density. The time of maximum current flow will precede the time of maximum positive charge accumulation by 90 electrical degrees.
5. The magnetic field at the surface of the conductor is everywhere tangential to that surface. Furthermore, it is *at all times* proportional in magnitude and directed at right angles to the surface current density. Since, by rule 4, the surface currents are in time quadrature with the electric field, it is apparent that the magnetic and electric fields in a resonator are also in time quadrature.

**32-4. Transverse-electromagnetic (TEM) Mode.**—The transverse-electromagnetic mode is the ordinary transmission-line mode and is characterized by magnetic- and electric-field distributions in the transverse plane which are identical with those obtained for the static cases.

It is assumed that the coaxial conductors are short-circuited by an end plate that gives rise to a perfect standing wave, as shown in Fig. 32-1. From ordinary transmission-line theory, the voltage of the inner conductor with respect to the outer at a distance  $x$  from the end plate is  $V = -V_{\max} \sin 2\pi x/\lambda_g$  where  $\lambda_g$  is the wavelength of the standing wave in the resonator. By rules 2 and 4 of Sec. 32-3 the conductor current is easily shown to be circumferentially uniform and directed entirely axially. The axial current density is indicated graphically in Fig. 32-1 by the thickness of the shaded portion of the conductor walls, and the inner conductor current flowing in the direction of the end cap is

$$I = jI_{\max} \cos \frac{2\pi x}{\lambda_g}$$

The impedance between conductors at any point  $x$  looking toward the end plate will then be

$$Z_{i,n} = \frac{V}{I} = j \frac{V_{\max}}{I_{\max}} \tan \frac{2\pi x}{\lambda_g} \quad (32-1)$$

The ratio  $V_{\max}/I_{\max}$  for the *TEM* mode is independent of frequency and depends only upon the relative line proportions. It is equal to the *characteristic impedance*  $Z_0$ , and for a coaxial line having inner and outer

radii  $a$  and  $b$ , respectively,

$$Z_0 = 60 \ln \frac{b}{a} = 138 \log_{10} \frac{b}{a} \tag{32-2}$$

Also, if  $c$  is the velocity of light in the dielectric medium, we may set  $\beta = 2\pi f/c = 2\pi/\lambda_g$ , where  $\beta$  is the *propagation phase constant*. Equation (32-1) may therefore be expressed as

$$Z_{in} = jZ_0 \tan \beta x \tag{32-3}$$

This expression is, of course, a familiar part of the usual transmission-

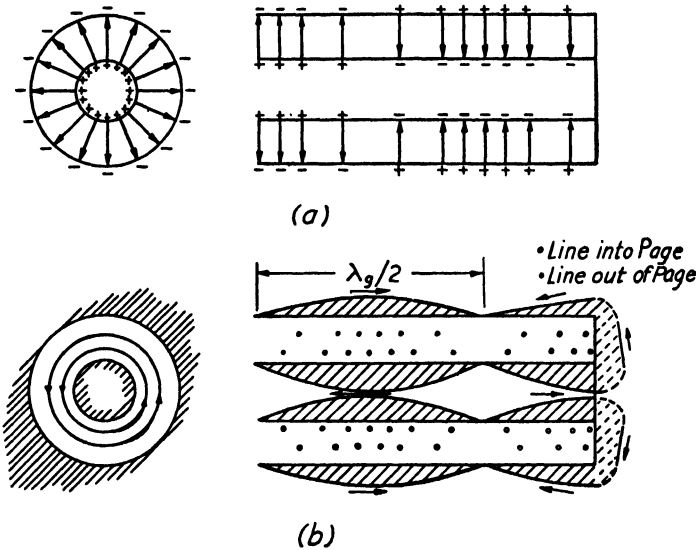


FIG. 32-1.—*TEM* field distribution: (a) electric field and surface charge; (b) magnetic field and surface current. Width of shaded portion proportional to current density in plane of page.

line theory. Equation (26-15) may be used to calculate the input impedance when the line section is terminated in an impedance  $Z_R$ .

The determination of the maximum impedance that may be developed by a lossy coaxial line will be found in other references.<sup>1,2</sup>

**32-5. Transverse Electric (TE) Modes.**—The *TE modes* are characterized by an electric field that lies entirely in the transverse plane but that has both circumferential and radial components. Subscripts are used to designate a particular *TE* mode. Thus, the  $TE_{0,m}$  wave is a circular electric wave of order  $m$ ;  $m$  is one greater than the number of

<sup>1</sup> TERMAN, F. E., Resonant Lines in Radio Circuits, *Elect. Engr.*, **53**, 1046 (1934).

<sup>2</sup> For an analysis of a capacitance-loaded lossy line, see L. S. Nergaard and Bernard Salzberg, Resonant Impedance of Transmission Lines, *Proc. I.R.E.*, **27**, 579-583 (1939).



cylinders upon which the electric vector vanishes, excluding the coaxial conductors. The  $TE_{n,m}$  ( $n \neq 0$ ) waves are noncircular waves;  $n$  is the number of axial planes upon which the circumferential component of the electric vector vanishes, and  $m$  is one greater than the number of cylinders upon which the radial component of the electric vector vanishes.

The most common  $TE$  wave possesses an electric vector that vanishes upon only one nodal plane and upon no cylinders. This is the  $TE_{1,1}$  wave, the field of which is sketched in Fig. 32-2. Two significant facts should be noted about this wave. First, circumferential as well as axial

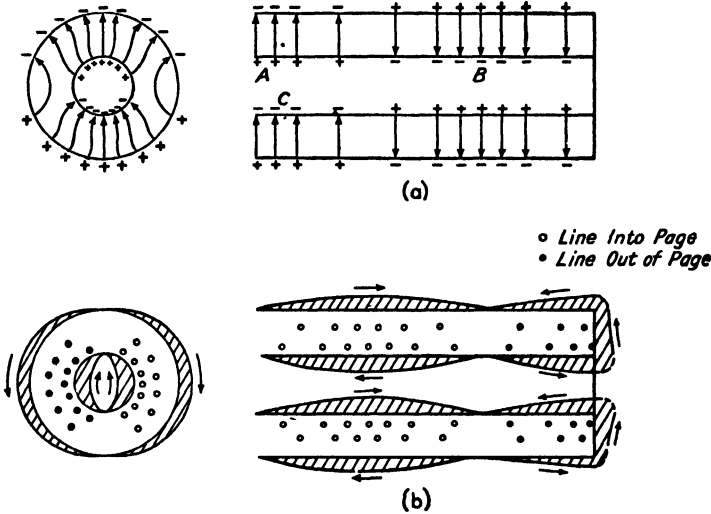


FIG. 32-2.— $TE_{1,1}$  field distribution: (a) electric field and surface charge; (b) magnetic field and surface current. Width of shaded portion proportional to current density in plane of page.

currents exist, and bound charges of opposite sign reside diametrically opposite each other on the same conductor, as, for example, at  $A$  and  $C$ . As long as the circumferential distance between these charges is considerably greater than the free-space wavelength, the current flow is mostly axial. At longer wavelengths, however, the conductor surface acts as an inductive short circuit between the charges of opposite sign on that surface with the result that, for wavelengths greater than some critical wavelength, the wave is attenuated and no standing waves can result. The *guide wavelength*  $\lambda_g$  is always greater than the free-space wavelength  $\lambda$  and may be expressed in terms of the *critical* or *cutoff* wavelength  $\lambda_c$  by the relation

$$\lambda_g = \frac{\lambda}{\sqrt{1 - \left(\frac{\lambda}{\lambda_c}\right)^2}} \tag{32-4}$$

where, for the  $TE_{1,1}$  mode,  $\lambda_c$  is equal to the mean circumference of the coaxial line.<sup>1</sup>

The second fact which should be noted is that, at free-space wavelengths only slightly shorter than  $\lambda_c$ , the guide wavelength may become very great. Since the spacing between the bound charges on opposite sides of the same conductor (as at  $A$  and  $C$ ) is then much less than the axial distance between unlike charges (as from  $A$  to  $B$ ), most of the current flow is circumferential, and the *axial* component of current becomes zero as the cutoff wavelength is approached. If we define the characteristic impedance  $Z_0$  as the ratio of the maximum *transverse* voltage to the maximum *axial* current,<sup>2</sup> it is apparent that the characteristic impedance will become infinite at cutoff. In fact, it may be written as

$$Z_0 = \frac{Z_0'}{\sqrt{1 - \left(\frac{\lambda}{\lambda_c}\right)^2}} \quad (32-5)$$

where  $Z_0'$  is the ratio of maximum transverse voltage to maximum axial current at infinite frequency.

Other  $TE_{n,m}$  modes are also possible. The free-space cutoff wavelength for these modes is roughly (for  $n \neq 0$ )

$$\lambda_c = \frac{1}{\sqrt{\left[\frac{m-1}{2(b-a)}\right]^2 + \left(\frac{n}{2\pi c}\right)^2}} \quad (32-6)$$

where  $b$  and  $a$  are the outer and inner radii, respectively, and  $c$  is the mean radius,  $c = (a + b)/2$ . This equation is based upon an approximation that is valid only when  $b$  and  $a$  are nearly equal. However, it may be applied with reasonable accuracy to the dominant  $TE$  and  $TM$  waves and will be used here to illustrate *roughly* the relative cutoff wavelengths of the various waves. For a fairly typical case  $b = 2a$ , and if we let the mean circumference be unity, *i.e.*,  $2\pi c = 1$ , then  $a = 0.10609$ ,  $b = 0.21219$ ,  $c = 0.1595$ , and Table 32-1 may be calculated.

Examination of this table shows that the cutoff wavelengths of wave types exhibiting radial variations, *i.e.*,  $m > 1$ , are shorter than those of waves having no radial variations. Since the shortest wavelength at which it has been found practicable to operate a coaxial-line resonator is

<sup>1</sup> See KIRKMAN, R. A., and M. KLINE, The Transverse Electric Modes in Coaxial Cavities, *Proc. I.R.E.*, **34**, 14-17 (1946) and the discussion of this paper by W. H. Huggins to be published in the *Proc. I.R.E.*, in 1947.

<sup>2</sup> Since the *total* axial current in any  $TE$  wave is zero, it is necessary to choose some quantity such as a partial current, partial bound charge, or maximum stored energy in the resonator as representative of the axial current. These definitions all differ by a numerical factor. To choose  $Z_0'$  so that it coincides with the  $TEM$  characteristic impedance is adequate for the purpose at hand.

TABLE 32-1.—COMPARISON OF APPROXIMATE CUTOFF WAVELENGTHS FOR *TE* AND *TM* MODES  
 [Values for  $b = 2a$ , as calculated from Eq. (32-6)]

<i>n</i>	<i>m</i> for <i>TE</i> <sub><i>n,m</i></sub> wave ( <i>n</i> ≠ 0)		
	1	2	3
0		0.212	0.106
1	1.00	0.208	0.106
2	0.50	0.195	0.104
3	0.33	0.180	0.101
	—	1	2
<i>m</i> for <i>TM</i> <sub><i>n,m</i></sub> and <i>TE</i> <sub>0,<i>m</i></sub> waves (for <i>TE</i> <sub>0,<i>m</i></sub> waves use <i>n</i> = 1).			

somewhat greater than half the mean circumference of the coaxial line, only the *TEM*, *TE*<sub>1,1</sub> and (possibly) *TE*<sub>2,1</sub> modes can ordinarily resonate and are of immediate importance to us.

**32-6. Transverse Magnetic (TM) Modes.**—The *TM* modes are characterized by a magnetic field that lies entirely in the transverse plane but that has both circumferential and radial components. Subscripts are used to designate a particular *TM* mode. Thus, the *TM*<sub>0,*m*</sub> wave is a circular magnetic wave of order *m*; *m* is one greater than the number of cylinders to which the electric vector is normal, excluding the coaxial conductors. The *TM*<sub>*n,m*</sub> (*n* ≠ 0) waves are noncircular waves; *n* is the number of axial planes upon which the circumferential component of the magnetic vector vanishes, and *m* is one greater than the number of cylinders upon which the radial component of the magnetic vector vanishes, excluding the coaxial conductors.

Each of these *TM* waves also exhibits a cutoff wavelength that may be found approximately by using in Eq. (32-6) a value for *m* that is one greater than that defined above with the restriction that no *TM* wave is possible when *m* = 0 (see Table 32-1). Hence, the *dominant TM mode* is that in which the magnetic field is circularly symmetric but vanishes at one cylindrical surface lying between the inner and outer conductors. It is designated as the *TM*<sub>0,1</sub> mode and has a cutoff wavelength approximately equal to the *difference* in *diameters* between the outer and inner coaxial conductors. Unlike the *TE*<sub>1,1</sub> mode, for which the cutoff wavelength is at least twice as great as that of all other *TE* modes, the cutoff wavelength of the *TM*<sub>0,1</sub> mode may be only slightly greater than that of the *TM*<sub>1,1</sub>, *TM*<sub>2,1</sub> etc., modes.<sup>1</sup>

<sup>1</sup> For a plot of cutoff wavelengths of some higher order *TM* waves in coaxial lines, see Ramo and Whinnery, *op. cit.*, Sec. 9.02.

Just as for the  $TE$  modes, the wavelength  $\lambda_g$  of the standing wave, given by Eq. (32-4), is greater than the free-space wavelength  $\lambda$ . It is also possible to speak of the characteristic impedance of a  $TM$  mode as being a quantity proportional to the ratio of the maximum transverse voltage to the maximum axial current. By rule 5 of Sec. 32-3 it is apparent that *all conduction current must be axial*. There is, however, some question as to the meaning of transverse voltage since in any transverse plane the radial component of electric-field intensity reverses sign so

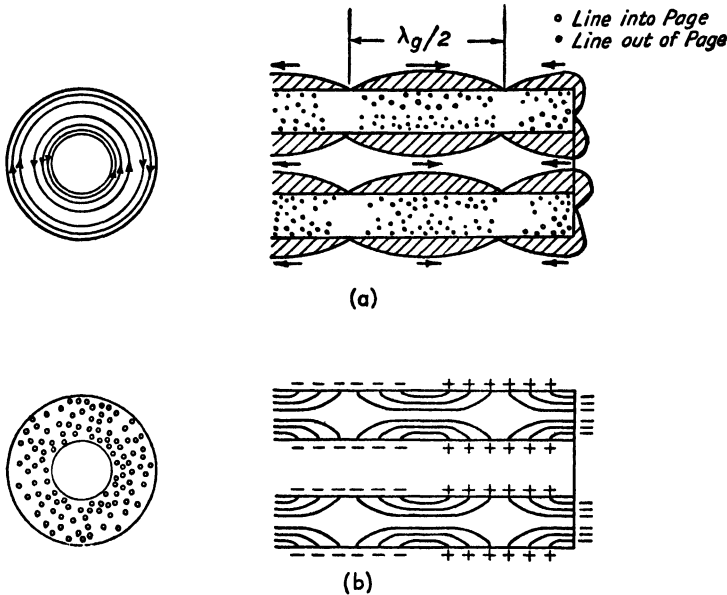


FIG. 32-3.— $TM_{0,1}$  field distribution: (a) magnetic field and surface currents; (b) electric field and surface charge. Width of shaded portion proportional to current density in plane of page.

that its integral between the inner and outer conductors is always zero. Nevertheless, regardless of what representative quantity proportional to the radial electric field is used, the characteristic impedance  $Z_0$  will be a function of the wavelength according to the relation

$$Z_0 = Z_0' \sqrt{1 - \left(\frac{\lambda}{\lambda_c}\right)^2} \tag{32-7}$$

where  $Z_0'$  is again the characteristic impedance at infinite frequency. That is, the characteristic impedance of a  $TM$  wave becomes zero at the cutoff wavelength. The physical explanation for this fact is that as the guide wavelength  $\lambda_g$  becomes very great, practically all the voltage induced by the magnetic field is used in establishing the *axial* component of electric field, the *radial* component of electric field thus approaching zero at cutoff.

**32-7. Adaptation of Coaxial Resonators to Typical Reflex Tubes.**

The 2K48<sup>1</sup> and 2K49 reflex klystrons have been especially designed for use in a coaxial cavity by making the inner conductor an integral part of the tube. The 2K28 tube, although it was designed especially for mounting in a rectangular waveguide resonator, can also be adapted to a coaxial resonator by using suitable clamping fingers to connect the tube to the inner conductor of the resonator.

Three different local oscillators utilizing coaxial-cavity resonators with noncontacting plungers are shown in Fig. 32-4. The small oscillator at the left incorporates a 2K48 tube and can be tuned from 6600 to 10,700 Mc. The oscillator in the middle uses a 2K28 tube and can be tuned from 2200 to 4200 Mc. The large oscillator at the right also uses a 2K28 tube and is tunable from 1200 to 2700 Mc.

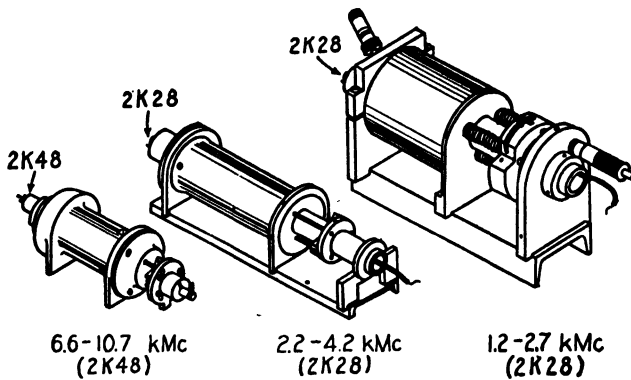


Fig. 32-4.—Typical coaxial-resonator reflex oscillators.

In each of these oscillators, the noncontacting plunger is fastened to a rigid carriage supported by six ball bearings that ride against the coaxial surfaces. Since this construction eliminates practically all mechanical wear, these oscillators should perform properly after hundreds of thousands of tuning operations.

Figure 32-5 shows an exploded view of the 2K48 oscillator. The inner conductor of the coaxial resonator is an integral part of the 2K48 tube, and the repeller terminal is supported at the end of this conductor by a suitable porcelain insulator. The inner conductor is clamped into rigid alignment with the plunger and outer conductor by means of a V block which when in place, as shown in Fig. 32-6, may be tightened by a screw that projects on the outside of the cavity. The slots in the plunger and the lossy material are required to suppress parasitic resonances, as will be explained later.

<sup>1</sup> CLARK, J. W., and A. L. SAMUEL, A Wide-tuning-range Microwave Oscillator Tube, *Proc. I.R.E.*, **35**, 81 (1947).

The 2K28 tube was not designed expressly for use in a coaxial resonator. It was adapted to the 2200- to 4200-Mc oscillator, by using "clip-on" finger rings for increasing the diameter of the tube flange that

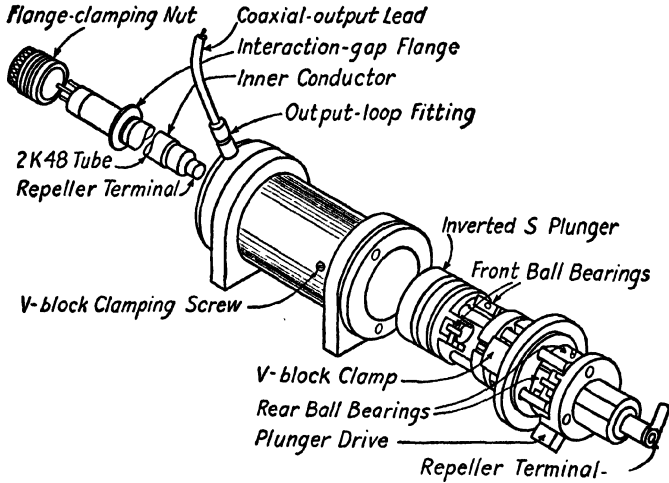


FIG. 32-5.—Exploded view of 6.6- to 10.7-kMc oscillator.

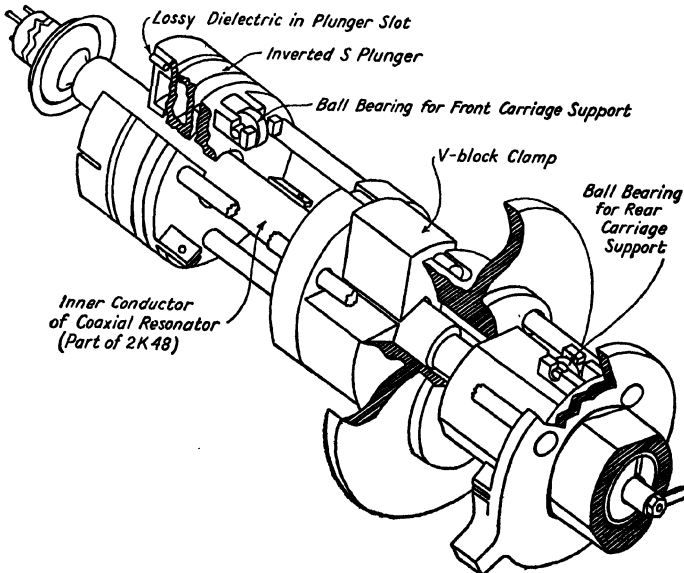


FIG. 32-6.—Sectioned view of plunger, carriage, and V-block clamping 2K48 tube in position.

connects to the outer cavity and incorporating the "collet" fingers shown in Fig. 32-7 for gripping the tube flange that connects to the inner conductor. The collet fingers are an important design point in this oscil-

lator because they permit the use of a small ( $1\frac{5}{16}$  in. diameter) inner conductor to place the  $TE_{1,1}$  resonance (see Sec. 32-22) outside the high-frequency end of the tuning range.

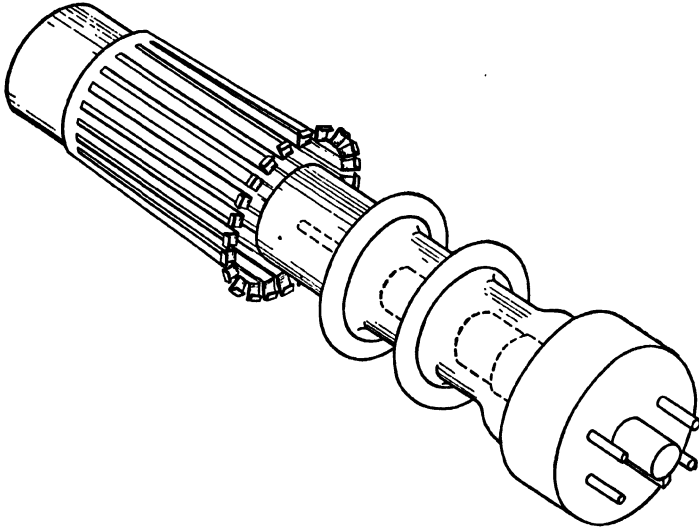


FIG. 32-7.—Collet fingers for clamping 2K28 tube to a small inner conductor of coaxial resonator.

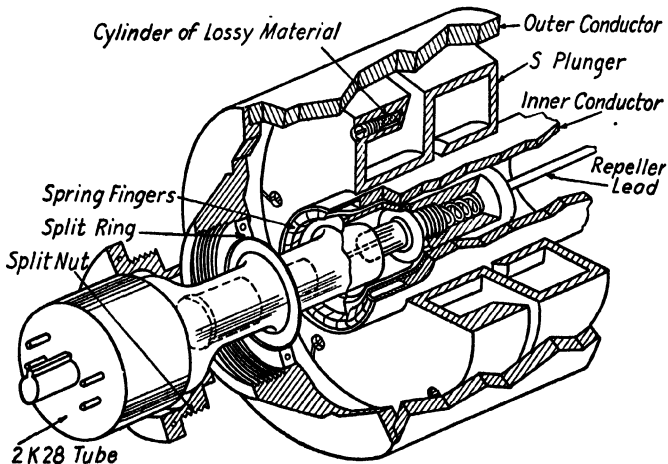


FIG. 32-8.—Method of fastening 2K28 tube flanges in outer and inner conductors of a large coaxial resonator.

A partial cutaway view of the 1200- to 2700-Mc oscillator is shown in Fig. 32-8. Unlike the other two oscillators, which utilize resonators  $\frac{3}{4}$  wavelength long, this oscillator employs a quarter-wave resonator. Hence, the actual motion required of the plunger to tune the oscillator

over its range is less than that required by the 2200- to 4200-Mc oscillator. For the same reason, a much greater fraction of the cavity is occupied by the plunger. A split-nut split-ring combination is used to clamp the outer flange of the tube to the outer conductor. Spring fingers distributed around the inside end of the inner conductor make contact to the other flange on the tube. A spring clip automatically connects to the reflector pin when the 2K28 is inserted.

Each of the oscillators described in this section is tuned by moving the plunger and thus changing the effective length of the short-circuited coaxial-line section that controls the wavelength of oscillation. The factors that determine the relation between the length of the resonator and the resonant wavelengths will be considered in the following sections.

**32-8. Condition for Oscillation.**—The reflex tube is connected to the coaxial line by means of an appropriate end cap which, together with the tube, closes off the open end of the coaxial line and forms the resonator, as shown in Fig. 32-9. If we define the *corner admittance*  $Y_i$  as the admittance presented to the coaxial line by the end cap and tube, natural oscillations can occur when the input admittance  $Y$  of the coaxial line is such that  $Y_i + Y = 0$  (see Sec. 31-1). When the reflex tube is oscillating, the amplitude of oscillation will be such that the negative-conductance component of  $Y_i$  just equals the positive conductance presented by the coaxial-line section, and the frequency of oscillation will be such that  $B_i$ , the susceptance component of  $Y_i$ , is the negative of the coaxial-line susceptance  $B$ . Hence, for resonance, the line length  $l$  must be related to the corner susceptance  $B_i$  and line characteristic impedance  $Z_0$  by the equation

$$l = \frac{\lambda}{2\pi} \operatorname{ctn}^{-1} B_i Z_0 \quad (32-8)$$

Of, course, the corner admittance will be influenced by the electronic admittance of the tube. However, the effect of the electron stream can at most produce only a slight affect on  $B_i$ , and the effect of the electronic admittance may usually be neglected.

**32-9. Equivalent Corner Length.**—The corner susceptance  $B_i$  is an extremely complex function of wavelength. Certain equivalent circuits may be used to represent this susceptance at wavelength long compared with corner dimensions, but at best the corner must be treated in a qualitative and semiempirical way. First, however, let us note that

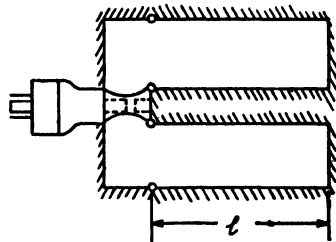


FIG. 32-9.—Division of resonator into corner and coaxial line.



if a coaxial line is terminated in a perfect open circuit (*i.e.*,  $B_t = 0$ ) resonance will occur by Eq. (32-8) whenever,  $l = (2k - 1)\lambda/4$ , in which  $k$  is an integer. Because of this fact, it is conventional to consider a resonator as operating on quarter-wave ( $k = 1$ ), three-quarter-wave ( $k = 2$ ), etc., resonator modes even though the tube and corner may be far from an "open" circuit.

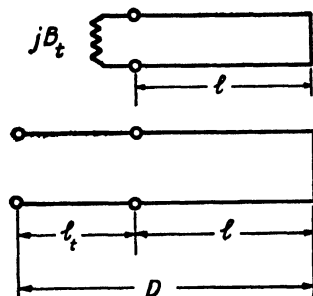


FIG. 32-10.—Equivalent length of corner susceptance.

as the corner. This equivalent length is

$$l_i = \frac{\lambda}{2\pi} \tan^{-1} (B_t Z_0) \quad (32-9)$$

and resonance will obtain when

$$D = l + l_i = (2k - 1) \frac{\lambda}{4} \quad (32-10)$$

or when

$$l = \left[ \frac{2k - 1}{4} - \frac{1}{2\pi} \tan^{-1} (B_t Z_0) \right] \lambda \quad (32-11)$$

### 32-10. Effect of Inductive and Capacitive Corner Terminations.

Equation (32-11) may be used to calculate the tuning curves, provided that the corner susceptance  $B_t$  is known a priori as a function of wavelength. On the other hand, if Eq. (32-8) is rearranged slightly, it may be used to calculate the corner susceptance  $B_t$  from experimental tuning curves relating  $l$  and  $\lambda$ . In order to illustrate the general effect of the corner susceptance, we shall now consider the two most simple terminations, *viz.*, a perfect capacitor and a perfect inductor.

At very low frequencies the corner susceptance  $B_t$  should be primarily that of the tube, which at these low frequencies behaves as a simple capacitance  $C$ . Hence

$$B_t Z_0 = \omega C Z_0 = 2\pi \frac{C}{\tilde{C}} \cdot \frac{1}{\lambda} \quad (32-12)$$

where  $\tilde{C}$  is the distributed capacitance per unit length of the coaxial line. If  $\lambda_0$  is defined as the wavelength for which  $B_t = 1/Z_0$ , Eq. (32-9) may

be written as

$$l_t = \frac{\lambda}{2\pi} \tan^{-1} \frac{\lambda_0}{\lambda} \tag{32-13}$$

and, when  $\lambda > \lambda_0$ ,

$$l_t \approx \frac{\lambda_0}{2\pi} \tag{32-14}$$

Equation (32-14) shows that at long wavelengths (where  $B_t < 1/Z_0$ ) a simple capacitance termination acts as an open-circuited coaxial line

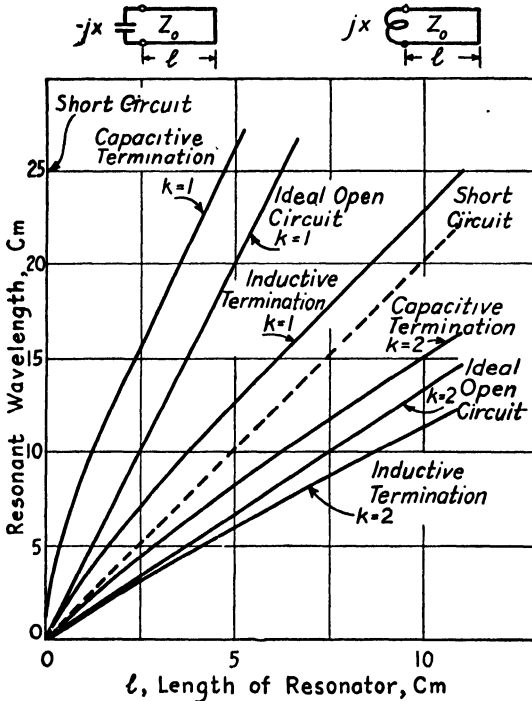


FIG. 32-11.—Tuning curves for coaxial resonator terminated in a simple lumped reactor. Inductance and capacitance chosen so that  $|X| = Z_0$  at  $\lambda_0 = 10$  cm.

of constant length  $\lambda_0/2\pi$ . This effect is illustrated in Fig. 32-11, which shows tuning curves as calculated from Eq. (32-11). Values on the three-quarter-wave tuning curves ( $k = 2$ ) are obtained at any given wavelength  $\lambda$  by adding  $\lambda/2$  to the value of  $l$  on the corresponding quarter-wave ( $k = 1$ ) tuning curve.

Figure 32-11 also shows the calculated tuning curve for a constant-inductance termination. Here, for wavelengths greater than  $\lambda_0$ , the inductance acts essentially as a *short-circuited* coaxial line of constant length  $\lambda_0/2\pi$  where  $\lambda_0$  is the wavelength at which the inductive reactance is equal to the characteristic impedance of the coaxial line. It should be

noted that the slope of this tuning curve (for  $k = 1$ ) is always less than four, whereas with a capacitance termination the slope is always greater than four. Furthermore, for any given cavity length, the *ratio* of the wavelengths on the quarter- and three-quarter-wave tuning curves is greater than three for capacitive termination and less than three for inductive termination. The ratio between the resonant wavelengths of these modes is important in controlling the *TEM* mode interference to be discussed in Sec. 32-15.<sup>1</sup>

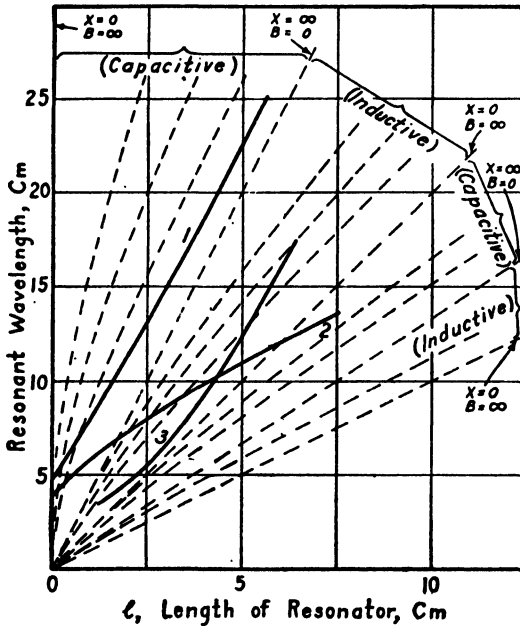


FIG. 32-12.—Physical realizability of tuning curves. Curves (1) and (2) are realizable. Curve (3) violates Foster reactance theorem.

**32-11. Physical Realizability of  $\lambda$ -D Tuning Characteristic.**—It might appear at first glance that the curves in Fig. 32-11 are extremely hypothetical and would offer little information regarding the behavior obtained with the much more complicated corner susceptance occurring in a microwave resonator. Actually, however, if it is assumed that the corner susceptance obeys Foster's reactance (susceptance) theorem, it follows that at a given frequency the corner susceptance will always increase more rapidly with increasing frequency than will the susceptance of the equivalent *simple* capacitance or inductance.<sup>2</sup> Hence,

<sup>1</sup> See also, SUTRO, P. J., Theory of Mode Separation in a Coaxial Oscillator, *Proc. I.R.E.*, **34**, 960 (1946).

<sup>2</sup> Stated mathematically this relation for lumped networks is  $dB/d\omega \geq |B|/\omega$  or  $dX/d\omega \geq |X|/\omega$ . Notice that this relation is more restricted than the relation

physically realizable tuning curves will always cross the dotted family in Fig. 32-12 (obtained for all possible values of fixed  $L$  or  $C$ ) with a slope that is less than the slope of the dotted family at the point of intersection.

By examining a particular tuning curve when superimposed upon the dotted family of Fig. 32-12, the behavior of the corresponding corner-reactance function can be deduced. As an illustration, the corner-reactance function corresponding to the tuning curve 1 is essentially capacitive and has zero reactance at a wavelength of 4.8 cm. Similarly, the corner reactance corresponding to curve 2 is essentially capacitive at

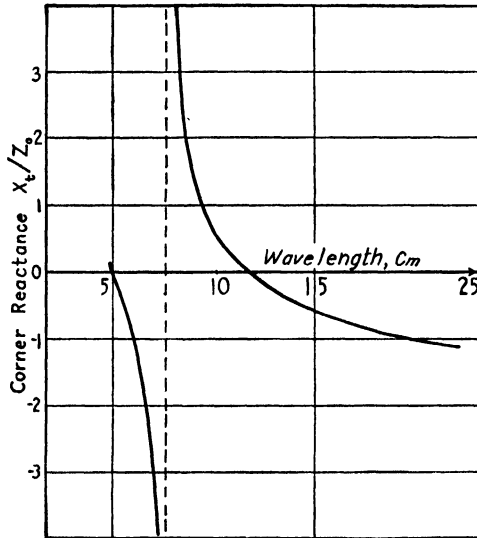


FIG. 32-13.—Corner reactance for tuning curve (2) of Fig. 32-12.

long wavelengths, and at shorter wavelengths varies as shown in Fig. 32-13. The slope of the reactance characteristic in this figure is always negative because it is plotted against wavelength instead of frequency.

**32-12. Effect of Cavity Dimensions.**—Because the dimensions of a given klystron are fixed, a change in the diameters of the coaxial resonator will produce a change in the  $\lambda$ - $D$  tuning curves. The type of distortion that may be expected to result from a change in resonator diameters is illustrated in Fig. 32-14. These curves illustrate two things: (1) They show the effect of increasing the characteristic impedance of the resonator (from 37 to 50 ohms) by increasing the diameter of the outer conductor.

$dB/d\omega > 0$  which is ordinarily given. For proof, see H. W. Bode "Network Analysis and Feedback Amplifier Design," p. 181, D. Van Nostrand Company, Inc., 1945. Also for an extension of Foster's reactance theorem to a lossless resonator, see W. R. MacLean, The Reactance Theorem for a Resonator, *Proc. I.R.E.*, **33**, 541 (1945).

(2) They show the effect of a bulge or discontinuity at the tube end of the inner conductor. In calculating the curves of Fig. 32-14, an equivalent circuit was used for the tube and corner. Considerations involved in establishing an equivalent circuit are as follows:

1. The capacitance of the interaction gap and glass seal of the reflex tube is represented in Fig. 32-14 by the capacitor  $C_1$ .
2. The displacement current flowing through  $C_1$  sets up a magnetic field surrounding the interaction gap inside the tube and the corner space. The effect of this magnetic field is equivalent to an inductance in series with the tube capacitance. This inductance may be broken into two components, that due to the magnetic field inside the reflex tube, and that due to the magnetic field

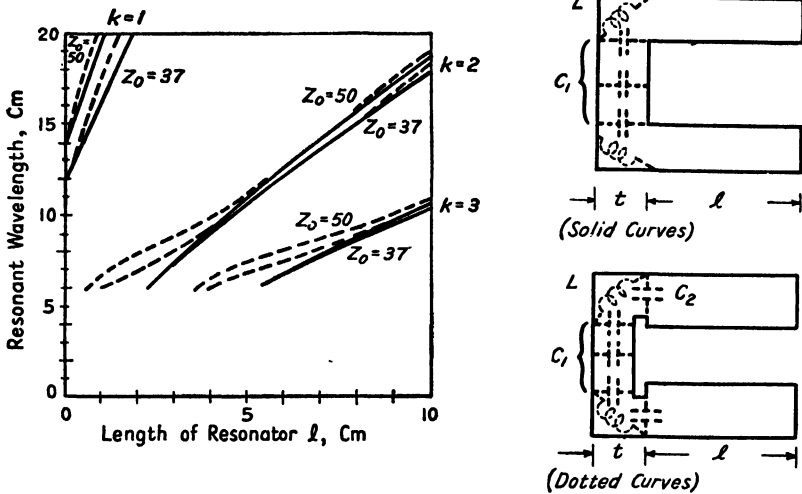


FIG. 32-14.—Tuning curves illustrating effects of increasing outer diameter of resonator and of discontinuity at tube end of inner conductor. Curves calculated for 2K28 tube with  $t = 1$  cm,  $C_1 = 3\mu\text{f}$ ,  $C_2 = 1.5\mu\text{f}$ ,  $L = Z_0 t/c$ .

outside the tube, in the corner of the resonator itself. If the thickness  $t$  of the corner section is electrically small, the corner and tube inductances may be calculated using ordinary d-c inductance formulas. If then the division between tube and corner is assumed to coincide with the surface of the inner conductor, the reactance of the corner will be equal to the inductive reactance of a short-circuited length  $t$  of coaxial line, or  $jX = jZ_0 \tan 2\pi t/\lambda \approx jZ_0 2\pi t/\lambda$ .

The internal inductance of the reflex tube depends upon the geometry of the interaction-gap electrodes. In low-voltage tubes (such as the 2K28) in which the interaction-gap grids have a relatively large diameter, this internal inductance is small and the tube ordinarily behaves as a capacitance. In high-voltage tubes (such as the 2K48 and 2K49), however, in which the interaction gap is formed of small-diameter nipples, the internal inductance may be so great that the tube behaves substantially as an inductance throughout its operating range. Since the calculations of Fig. 32-14 were made for a 2K28 tube, this internal induct-

ance component was ignored for simplicity. Obviously, the internal inductance could be included in the calculations if, for example, it were desired to make a more accurate estimate of the short-wavelength tuning limit on the quarter-wave ( $k = 1$ ) resonator mode.

3. At the discontinuity where the inner conductor of the coaxial line connects to the flange of the reflex tube, a concentration of electric flux will occur. The effect of this field distortion is, to a certain extent, equivalent to a capacitance  $C_2$  shunted across the resonator.<sup>1</sup> This discontinuity capacitance will be markedly increased if the diameter of the inner conductor is increased by fingers that grip the tube flange, such as those illustrated in Fig. 32-7. The tuning curves of Fig. 32-14 exaggerate the effect of this discontinuity capacitance, since it was ignored completely in calculating the solid tuning curves and arbitrarily assigned a large value (one-half the tube capacitance) in calculating the dotted curves.

The data of Fig. 32-14 illustrate several important design factors: (1) It should be noted that the short-wavelength limit of the quarter-wave mode ( $k = 1$ ) is increased when the outer diameter of the cavity is increased. (2) Perhaps, more important, however, from the standpoint of *TEM*-mode interference (to be discussed in Sec. 32-15) is the fact that the tuning curves are *raised* by different amounts on the  $k = 1$ ,  $k = 2$ , and  $k = 3$  modes at any given resonator length  $l$ .

The discontinuity capacitance  $C_2$  is an extremely important design factor. (1) It will be observed that, at a given cavity length, the changes in oscillation wavelengths resulting from this discontinuity capacitance on the  $k = 1$ , 2, and 3 resonator modes are all different. Hence, the *TEM*-mode interference, to be discussed in Sec. 32-15, will be altered by this discontinuity either for better or for worse, depending upon the relative positions of the interfering modes. (2) The finger bulge affects the tuning curve of the  $TE_{1,1}$  parasitic resonance (see Sec. 32-22) as well as that of the *TEM* mode. Experience has shown that if this parasitic resonance is to be moved to as short a wavelength as possible the diameter and *length* of the finger bulge must be reduced to as small dimensions as practical mechanically. The collet type of gripping fingers shown in Fig. 32-7 seems to be the best in this respect.

**32-13. Effect of Plunger Reactance.**—One other source of tuning-curve distortion is that due to the reactance of the plunger. In the preceding discussion it was assumed that the plunger presented a pure short circuit to the coaxial line. Actually, the plunger ordinarily presents a small reactance  $X_p$  which alters the resonant wavelength of the resonator. The distortion may best be visualized by introducing the concept of *equivalent length*  $l_p$  of the plunger. This length is that

<sup>1</sup> For a related analysis of discontinuity susceptances, see J. R. Whinnery and H. W. Jamieson, *Coaxial-Line Discontinuities*, *Proc. I.R.E.*, **32**, 695-709 (1944).

of a section of short-circuited coaxial line that will have the same input reactance as the plunger,

$$l_p = \frac{\lambda}{2\pi} \tan^{-1} \frac{X_p}{Z_0} \quad (32-15)$$

The condition for resonance then, in terms of the equivalent plunger and corner lengths  $l_p$  and  $l_i$ , respectively, and length  $l$  of coaxial line, is

$$l_i + l + l_p = (2k - 1) \frac{\lambda}{4} \quad (32-16)$$

Hence, the effect of plunger reactance on any of the tuning curves already given may be obtained simply by subtracting  $l_p$  from the  $l$  value as calculated for a perfect short circuit.

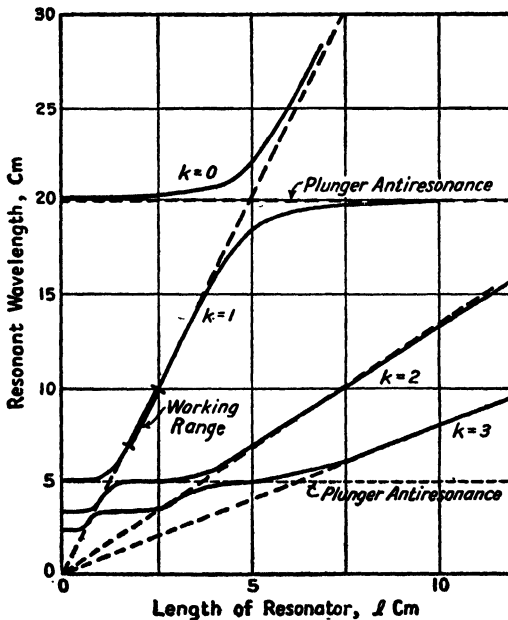


FIG. 32-15.—Distortion of tuning curves due to plunger reactance. Assumptions: open-circuited cavity ( $B_i = 0$ ); S-type plunger, design wavelength at 8 cm; antiresonances at 20 and 5 cm.

Although a detailed discussion of plunger behavior will be presented in the latter part of this chapter, the type of tuning-curve distortion due to the plunger reactance should be mentioned here. It is illustrated in Fig. 32-15, which shows tuning curves for a noncontacting plunger designed to operate at wavelengths near 8 cm. For purposes of illustration, the tuning-curve distortion was exaggerated in this instance by assuming a comparatively narrow-range plunger having antiresonances at 5 and 20 cm. In more usual wide-range plungers, the ratio between

the two antiresonant wavelengths bracketing the tuning range would likely be about 10:1, and the distortion due to the plunger would be considerably less pronounced than that shown in Fig. 32-15.

One interesting result of the plunger reactance is the  $k = 0$  mode shown in Fig. 32-15. This resonance occurs at wavelengths much greater than the design wavelength of the plunger and results when the coaxial-line sections of the plunger effectively become part of the main coaxial line. It will be noted that for small values of  $l$  the resonant wavelength is practically independent of cavity length. On the other hand, the near-horizontal parts of the tuning curves will usually represent inoperative regions because the plunger resistance may become relatively great when the plunger is antiresonant. (The plunger resistance is discussed in Sec. 32-34.)

### 32-14. Repeller-voltage-vs.-cavity-length Tuning Characteristics.

It has generally been found most useful to analyze wide-range reflex-oscillator behavior on the basis of the experimental relationship between the plunger position and the repeller voltages at which oscillation occurs (see Sec. 31-7). By this method, the various afflictions peculiar to reflex oscillators such as holes, parasitic resonance, and electronic hysteresis are easily detected. The same oscillographic technique may be applied in studying the important problem of mode interference now to be discussed in detail.

If the repeller-voltage ranges over which oscillations occur are plotted as a function of plunger position, a *mode plot* is obtained. This mode plot resembles the typical repeller characteristic of Fig. 31-10, which shows the repeller-voltage ranges for oscillation as a function of wavelength. The mode plot is complicated, however, by the fact that a coaxial resonator of equivalent length  $D$  can resonate whenever

$$D = (2k - 1) \frac{\lambda}{4}$$

Hence the mode plot is a superposition of the repeller ranges obtaining for each of the resonator modes, ( $k = 1, 2, 3$ , etc.), and to identify completely each oscillation mode it is necessary to specify both the repeller range and the resonator mode. The mode designation will hereafter be expressed by the number pair  $(k, n)$  where the first integer  $k$  designates the resonator mode, and the second integer  $n$  designates the repeller range (transit cycles  $N = n + \frac{3}{4}$ ). A typical experimental mode plot is shown in Fig. 32-16.

Fortunately, it is possible to make certain generalizations concerning the behavior of any reflex klystron (regardless of its repeller characteristic) if the assumption is made that the equivalent corner length  $l_c$  is



constant, irrespective of plunger position. The conclusions based on this idealized resonator may then be adjusted to account for differences

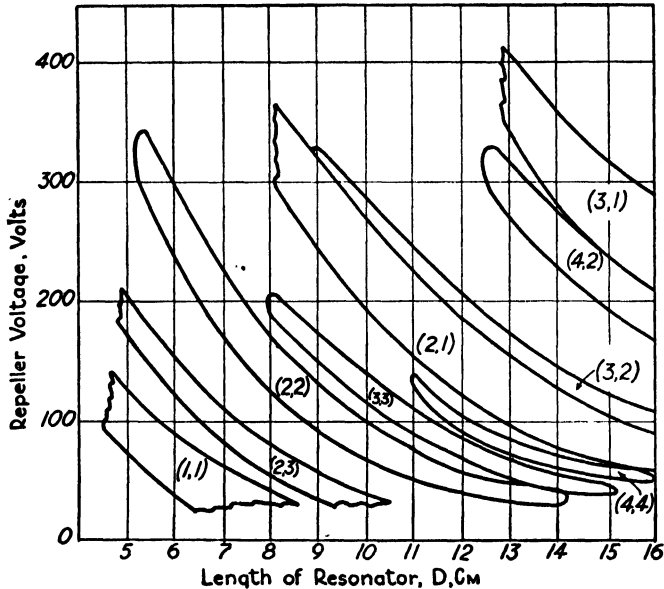


FIG. 32-16.—Mode plot of WE 707B klystron in a coaxial resonator, Coaxial resonator diameters: outer conductor, 2 in., inner conductor,  $\frac{1}{16}$  in.

obtained in the tuning of an actual resonator. To demonstrate these generalizations, we shall first define

$\tau$  = reflex transit time, seconds

$c$  = velocity of light, centimeters per seconds

$N = (n + \frac{3}{4})$  = number of r-f cycles during reflex transit;  $n$  is zero or any positive integer

$D$  = equivalent cavity length, centimeters

$\lambda$  = wavelength of oscillation, centimeters

Just as the unit *light-year* has been used by astronomers to express great distances, so also it is convenient to use the unit *light-centimeter*, *i.e.*, the time it takes light to travel 1 cm, to express the extremely short reflex transit *time*. It follows that

$$c\tau = N\lambda \quad (32-17)$$

Since the left side of Eq. (32-17) is independent of the oscillator tuning and depends only upon the electrode voltage applied to the reflex tube (see Fig. 31-5), it is apparent that the various wavelengths of optimum oscillation that may be obtained for any given repeller voltage are all related by the values of  $N$  corresponding to  $n = 0, 1, 2$ , etc. Hence, the

problem of mode interference is basically *independent* of the repeller characteristic of the reflex klystron.<sup>1</sup>

To include the various cavity modes in the analysis, it is noted that in a coaxial resonator  $\lambda = 4D/(2k - 1)$  and hence

$$c\tau = N\lambda = \left(\frac{4n + 3}{2k - 1}\right) D \tag{32-18}$$

Equation (32-18) expresses the relation between the transit time and the equivalent resonator length that must obtain for operation on any

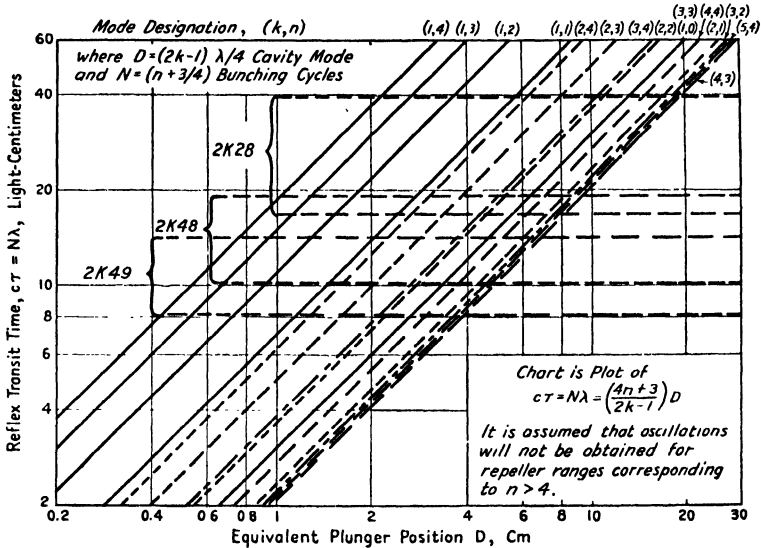


FIG. 32-17.—Universal mode chart for a reflex klystron in a linear resonator.

mode (k, n). This equation is plotted in Fig. 32-17. It is assumed that oscillations will not be obtained for repeller ranges corresponding to  $n > 4$ .

In applying the universal mode chart of Fig. 32-17 to a specific oscillator, the following limitations are imposed upon the ordinate and abscissa values. First, the reflex transit time is a function of the repeller voltage, as shown in Fig. 31-5, and, if proper focusing and bunching is to obtain, the useful range over which the transit time may be varied depends upon the klystron construction. The ratio of maximum to minimum obtainable transit times is ordinarily about 2:1. The

<sup>1</sup> Actually, however, even though mode interference *potentially* exists, satisfactory operation may often be obtained if the interfering mode is so recessive to the desired mode of operation. To this extent, the repeller characteristics *do* enter into the mode-interference problem.

transit-time ranges for three different reflex klystrons are also indicated in Fig. 32-17.

Second, permissible values of  $D$  can never be less than  $l_i$ , the equivalent length of the tube and corner. Hence, to be physically obtainable, the desired mode must lie to the right of  $D = l_i$  and within the transit-time bracket corresponding to the reflex tube being used. Although the wavelength of oscillation does not appear explicitly in Fig. 32-17, it is readily obtained by dividing the transit time  $c\tau$  by the number of reflex transit cycles  $N = n + \frac{3}{4}$  for the mode under consideration.

**32-15. TEM-mode Interference.**—When any two modes of Figs. 32-16 or 32-17 are nearly superposed, there exists a coincidence of repeller voltage and resonator tuning conditions for the generation of oscillations at two frequencies. This phenomenon is termed *mode interference* and gives rise to a major problem in the design of microwave reflex oscillators.

Of special significance is the fact that *in an idealized resonator* the adjacent modes are essentially parallel—they may overlap, partially or fully, and may converge at the lower repeller voltages, *but they may never intersect*. Mode crossover can occur only when the tube corner or plunger introduces a nonlinear distortion into the  $\lambda$ - $D$  tuning characteristics of the resonator. Since all oscillation modes correspond to the same value of  $\tau$  at a given repeller voltage, all are distorted in an identical manner by a nonlinear relation between  $\tau$  and  $V_R$ . Hence, the nonintersection condition is independent of the configuration of the repeller field. That is, although a change in the construction of the interaction gap of the klystron would probably alter the mode interference because it would change the  $\lambda$ - $D$  tuning characteristics, a change in only the repeller structure could *not basically* alter the mode interference (see footnote to Sec. 32-14).

It was mentioned in Sec. 32-12 that the klystron tube possesses an internal inductance as well as a capacitance. If the effective  $L/C$  ratio of the reflex tube is less than that of the coaxial line, it will be called a *low-impedance* tube. A resonator incorporating a low-impedance tube will behave as if it were capacitively loaded in that the slopes of the  $\lambda$ - $D$  tuning characteristics will be somewhat greater than for an ideal resonator and the ratio between frequencies of oscillation on, say, the  $k = 1$  and the  $k = 2$  modes will be greater than 3.

If the effective  $L/C$  ratio of the reflex tube is equal to that of the coaxial line, it will be called a *matched-impedance* tube. The  $\lambda$ - $D$  tuning characteristics of a resonator incorporating a matched-impedance tube should agree quite closely with those of an ideal resonator.

If the interaction-gap electrodes are long and of small diameter, so that the internal tube inductance is large and the gap capacitance small, the effective  $L/C$  ratio of the tube may be considerably larger than that

of the coaxial line. Such a tube will be called a *high-impedance* tube. A resonator incorporating a high-impedance tube will behave as if it were inductively loaded in that both the slopes of the  $\lambda$ - $D$  tuning characteristics and the ratios between the resonant frequencies on the various cavity modes will be somewhat less than the corresponding values for a matched-impedance tube.

**32-16. Desirable Modes and Ranges.**—From an inspection of the universal mode chart shown in Fig. 32-17, one can conclude that certain modes should be less susceptible to mode interference than others. Of course, if the reflex klystron has already been designed, it may not be possible to use a preferred mode to cover a given tuning range. If both tube and resonator design can be developed simultaneously, however, or if there is a choice of several different reflex klystrons, an effort should be made to utilize one of the several preferred modes shown in Table 32-2.

*Preferred Cavity Modes.*—If the tube and, hence, the equivalent corner length  $l_c$  are sufficiently small so that the desired tuning range can be covered on the  $k = 1$  (quarter-wave) resonator mode, not only can *TEM*-mode interference be eliminated, but also the *TE*<sub>1,1</sub> parasitic resonances in the cavity and plunger may be largely eliminated or avoided (*cf.* Sec. 32-21). Hence, this restriction in size is extremely desirable and should be achieved, where possible, in spite of manufacturing and constructional difficulties.

The  $k = 2$  (three-quarter-wave) resonator mode possesses two advantages over the  $k = 1$  mode: (1) The resonant wavelength is less affected by changes in tube capacitance or undesirable plunger movement, and, hence, the stability and accuracy of the tuning calibration is inherently greater. (2) The tuning range of the  $k = 2$  mode extends to shorter wavelengths than that of the  $k = 1$  mode. The disadvantages of operation on the  $k = 2$  resonator mode are twofold. *TEM* mode interference with other modes is more likely; parasitic *TE* resonances can occur in a three-quarter-wave resonator that cannot possibly occur in a quarter-wave resonator.

*Preferred Repeller Ranges.*—The factors that determine the choice of repeller range are the power output, stability, and tuning ratio. It has been shown in Sec. 31-3 that the largest output power is developed for the ranges corresponding to the smaller values of  $n$ , and, because of the relatively great width of these small- $n$  repeller ranges, the repeller voltage adjustment is not critical. On the other hand, the small- $n$  ranges not only possess small electronic conductances, but they are also subject to instability arising from multiple-transit effects and electronic hysteresis.

The large- $n$  repeller ranges are much more stable (within limits)

TABLE 32-2.—PREFERRED OSCILLATION MODES IN WIDE-RANGE REFLEX OSCILLATORS

Mode ( $k, n$ )	Interfering modes			Other properties
	Low- $Z$ tube	Matched- $Z$ tube	High- $Z$ tube	
(1, 2)	.....	....	....	Completely free of all serious mode interference. Large tuning ratio with excellent stability and reasonable power output. However, repeller design and physical-size limitations of existing reflex klystrons are such that this mode can be used only over lowest part of frequency range
(2, 3)	.....	....	(1, 1)	Mode interference with Mode (1, 1) may be partly eliminated by use of a mode suppressor described in Sec. 32-19. High operating frequency is usually obtainable on this mode, although tuning ratio is usually less than 2:1
(2, 4)	.....	(1, 1)	(1, 1)	Low power output. Narrow repeller-voltage adjustment. Small tuning ratio. May be used to provide oscillations at frequencies higher than those obtainable on Mode (2, 3). Will require a mode suppressor to eliminate Mode (1, 1) interference, as noted
(2, 2)	(3, 4)	(3, 4)	(3, 4)  (3, 3)	Potentially interfering Mode (3, 4) is usually recessive to more vigorous Mode (2, 2). Hence interference seldom occurs in c-w operation, but may occur in pulsed operation or under heavy loading of the oscillator. Interference with Mode (3, 3) may occur at low frequencies. Possesses large tuning ratio
(1, 1)	(2, 4)	(2, 4)	(2, 4)  (2, 3)	Potential interference with recessive Mode (2, 4) throughout tuning range; usually not bothersome in c-w operation and under light loading. Mode (2, 3) is usually recessive to more vigorous Mode (1, 1) but may give interference at high frequencies because of poor stability of $n = 1$ repeller range

but only at the expense of reduced power output. Furthermore, usual tube design is such that for operation on the large- $n$  repeller ranges, the frequency is so high that the electron transit angle across the interaction gap becomes appreciable and the beam-coupling coefficient  $\beta$  [see Eq. (31-4)] rapidly diminishes with increasing  $n$ . Hence, the tuning-ratio

possible on the larger  $n$  ranges is reduced, and operation on repeller ranges larger than  $n = 4$  is usually impossible.

Because of the limitations just discussed, the preferred repeller ranges are those corresponding to  $n = 1, 2,$  and  $3$ . Both the  $n = 1$  and  $n = 2$  ranges produce reasonable output power and offer a large tuning ratio. In some tubes, such as the 2K48, rather severe electronic hysteresis may occur on the  $n = 1$  range, however (see Sec. 31-8). The  $n = 2$  and  $n = 3$  ranges are usually quite stable, but the tuning ratio of the  $n = 3$  range in present-day klystrons is somewhat less than that of the smaller- $n$  ranges.

**32-17. Elimination of TEM-mode Interference.**—It has been shown in the preceding sections that the *TEM*-mode interference is determined primarily by the  $\lambda$ - $D$  tuning characteristics of the resonator. Hence, the factors that influence the  $\lambda$ - $D$  tuning characteristics are necessarily those which must be controlled to eliminate or avoid *TEM*-mode interference.

From the viewpoint of this section, the data of Table 32-2 present a first-class conundrum—the electronic engineer designs his tube with a small interaction-gap capacitance to secure better efficiency, but the resulting high-impedance tube is subject to increased *TEM*-mode interference. Furthermore, as shown in Sec. 32-22, the  $TE_{1,1}$  parasitic resonance occurs at a longer wavelength when the interaction-gap capacitance is decreased, and, as a result, the high-frequency limit of the tuning range may be decreased.

The simplest way of avoiding the most serious *TEM*-mode interference is, therefore, to make the characteristic impedance of the coaxial resonator as large as possible compared with the characteristic impedance  $\sqrt{L/C}$  of the klystron tube. However, since the largest permissible diameter of the outer coaxial conductor must be limited to a fairly small value if parasitic *TM* and *TE* resonances are to be avoided (see Sec. 32-22), and since the diameter of the inner coaxial conductor must be larger than some value fixed either by tube dimensions or maximum tolerable circuit loss, it is usually impossible to obtain a resonator characteristic impedance much in excess of 50 ohms. Hence, the most *useful* reflex tube is one having a characteristic impedance of about 50 ohms or less.

It was also mentioned in Sec. 32-13 that the  $\lambda$ - $D$  characteristics are distorted by the reactance of a noncontacting plunger. As is apparent from Fig. 32-15, however, this tuning-curve distortion is similar to that obtained with a high-impedance tube in that the relative separation of the cavity modes is decreased, and it is undesirable in all cases of practical importance because it will aggravate any incipient mode interference.

When it is not possible to achieve adequate clearance between modes through control of cavity characteristic impedance, the distortion neces-

sary to prevent mode interference may be introduced into the  $\lambda$ - $D$  tuning curves by the use of a coaxial "stub" such as that shown in Fig. 32-18. Because of its function, this supplementary line section has been called a *mode suppressor*. A mode suppressor of this type may be required to eliminate Mode (1, 1) interference in oscillators operating on Mode (2, 3). The various design factors will now be considered in detail.

Mode interference occurs in a reflex oscillator if conditions are such that oscillations are possible at *either* of two frequencies  $f_1$  or  $f_2$  for the *same* repeller voltage and resonator tuning. Let it now be assumed that an oscillator possessing mode interference is modified by an additional coaxial-line section of length  $l_s$  introduced in series with the outer coaxial conductor, as shown in Fig. 32-18. The equivalent circuit is shown in Fig. 32-19. If the electrical length of the series section is such

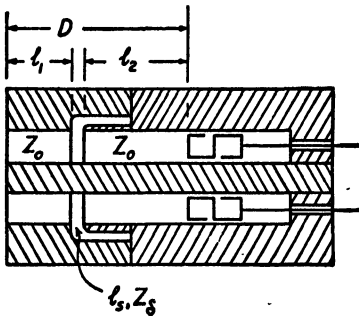


Fig. 32-18.—Mode-suppressor cavity.

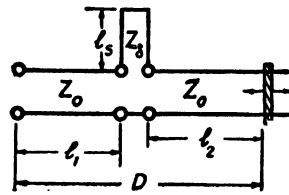


Fig. 32-19.—Equivalent circuit of Fig. 32-18.

that its reactance is zero at the desired frequency  $f_2$ , the effective length of the cavity will not be changed, and hence the frequency of oscillation will remain unaltered.

If the reactance of the series section at the interfering frequency  $f_1$  is appreciable with respect to the characteristic impedance of the resonator and if the series section is not inserted at a current null, the resonant frequency of the system will be shifted from  $f_1$  to some new frequency  $f_3$ . For oscillations to occur at  $f_3$ , a different repeller voltage is required. If the change in required repeller voltage is great enough, the two modes are effectively separated, and mode interference is eliminated *for that particular resonator-tuning position*. The shift in the modes may result in interference between  $f_2$  and  $f_3$  over some *other portion* of the tuning range, however.

**32-18. General Analysis of TEM-mode Suppressor.**—The type of  $\lambda$ - $D$  tuning characteristic distortion produced by a mode suppressor may be best analyzed in terms of the equivalent circuit shown in Fig. 32-19. In this equivalent circuit, the coaxial section of length  $l_1$  includes the

equivalent length  $l_c$  of the corner and tube. The calculated results for simplicity are based upon the assumption that  $l_1$  is constant. If experimental data of the variation of  $l_c$  with  $\lambda$  are available, it is apparent that this corner-effect distortion could be included in the analysis with but little additional complication.

If any lossless system is arbitrarily broken into two parts, the sum of the reactances presented by each of these parts must be equal to zero for

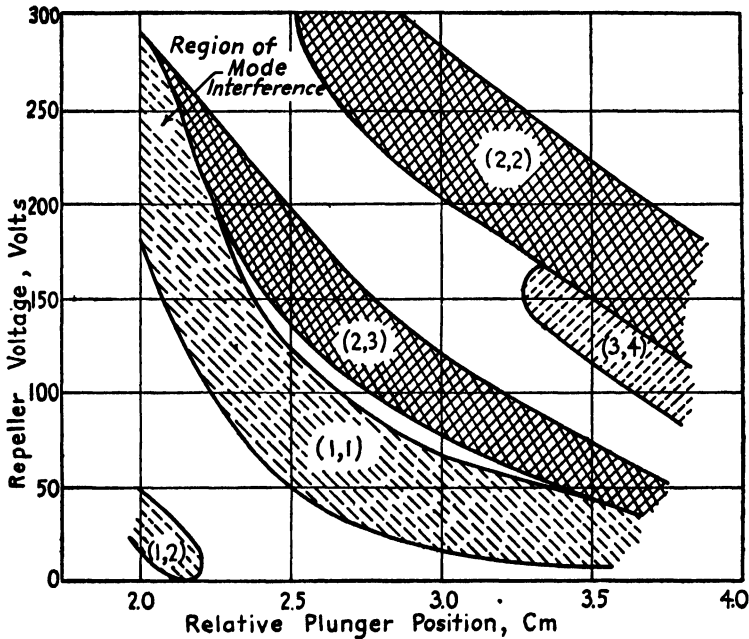


FIG. 32-20.—Mode plot of 2K48 oscillator without mode suppressor.

resonance. Hence, at the junction  $x$  of the three line sections  $l_1$ ,  $l_2$ , and  $l_s$ , the resonance condition is that

$$Z_1 + (Z_s + Z_2) = 0 \tag{32-19}$$

or, in terms of the usual reactance expressions for open-circuited and short-circuited transmission lines,

$$-Z_0 \operatorname{ctn} \frac{2\pi l_1}{\lambda} + \left( Z_s \tan \frac{2\pi l_s}{\lambda} + Z_0 \tan \frac{2\pi l_2}{\lambda} \right) = 0 \tag{32-20}$$

Equation (32-20) may be solved for  $l_2$  and, since  $D = l_1 + l_2$ , the equation relating  $\lambda$  and  $D$  is

$$D = l_1 + \frac{\lambda}{2\pi} \tan^{-1} \left( \operatorname{ctn} \frac{2\pi l_1}{\lambda} - \frac{Z_s}{Z_0} \tan \frac{2\pi l_s}{\lambda} \right) \tag{32-21}$$



Except in the vicinity of the antiresonant wavelength  $\lambda_\infty$  of the series section, the magnitude of the second term in the bracket is relatively small in the practical cavity, and the tuning equation reduces to the simple linear form normally encountered. In the region of the antiresonant wavelength  $\lambda_\infty$  of the series section, however, the second term in the bracket becomes predominant and introduces a distortion component into the tuning curves of the oscillator.

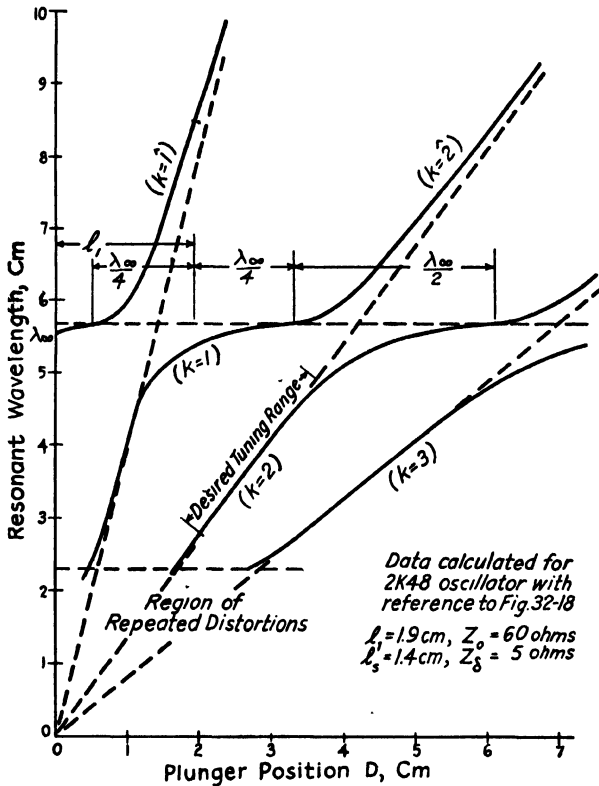


Fig. 32-21.—Distortion of  $\lambda$ - $D$  tuning curves produced by mode suppressor.

The design of a mode suppressor involves so many factors, such as cavity size, tube loading, and parasitic resonances, that it constitutes a major problem in itself. For this reason no exact general treatment is possible here. There are, nevertheless, a number of design criteria that apply rather generally, and these may best be illustrated by discussing a particular mode-suppressor resonator.

The smallest oscillator shown in Fig. 32-4 uses a 2K48 tube and tunes from 6600 to 10,700 Mc on Mode (2, 3). Because of the large outer diameter of the coaxial resonator, a  $TM_{0,1}$  resonance distorts the  $k = 2$  tuning

curve in such a manner as to cause severe interference with Mode (1,1). This mode interference is illustrated in Fig. 32-20. (The tuning-curve distortion arising from  $TM_{0,1}$  corner resonance is discussed in Sec. 32-23.)

The theoretical tuning curves for this particular oscillator as calculated from Eq. (32-21) are shown in Fig. 32-21. The effect of the mode suppressor is to distort the idealized (dotted) tuning curves very markedly at wavelengths near that at which the suppressor becomes antiresonant. In fact, the mode suppressor produces a discontinuity in the tuning curves. For the lossless case, there is a discontinuity in  $D$  of  $\lambda_{\infty}/2$  at the wavelength  $\lambda_{\infty}$ . The upper segments of the tuning curves will be designated by a  $k$  value with circumflex.

The hypothetical joining of adjacent branches of tuning curves occurs because the circuit dissipation was ignored. In an actual oscillator the resistance component of the mode-suppressor impedance is sufficiently large to reduce the  $Q$  of the resonator greatly at wavelengths near  $\lambda_{\infty}$ . Because of the greatly increased power loss, it is consequently impossible to obtain oscillations at wavelengths near  $\lambda_{\infty}$ . The actual width of the nonoscillation region depends upon the electronic conductance available to neutralize the resonator losses, and a wider region of nonoscillation may therefore be expected on the repeller ranges of smaller  $n$ .

It is possible to predict the  $V_R$ - $D$  characteristics corresponding to the tuning curves of Fig. 32-21 by cross-plotting against a  $V_R$ - $\lambda$  range plot for the 2K48 klystron (similar to that shown in Fig. 31-11). A mode plot calculated in this way is shown in Fig. 32-22. Also shown in the same figure is the actual mode plot as determined experimentally.

Comparison of Fig. 32-22 with Fig. 32-20 shows that the mode suppressor has succeeded in clearing Mode (2, 3) of virtually all interference with Mode (1, 1). The interference that remains is practically coincident with the normal high-frequency limit of Mode (2, 3), and so is of little consequence. There are several discrepancies between the calculated and experimental plots which should be explained.

1. The calculated curves are based on a matched-impedance tube. Since the 2K48 is a high-impedance tube, the  $k = 2$  modes should be shifted to the left with respect to the  $k = 1$  modes. This effect tends to produce interference between the ( $\hat{1}$ , 1) and (2, 3) modes.

2. The reversal of the slope of the modes at short cavity lengths is due to the proximity effect of the plunger across the mode-suppressor gap.

3. In a hypothetical lossless resonator, Modes (1,  $n$ ) would be joined with Modes ( $\hat{2}$ ,  $n$ ), as shown by the dotted lines in the calculated curves of Fig. 32-22, and severe mode interference could result. Fortunately, however, in an actual oscillator, the increased circuit loss at wavelengths near  $\lambda_{\infty}$  produces regions of nonoscillation in the interfering modes so that mode interference is prevented.

4. It is of interest to note that because of the double-valued tuning curves, a mode may actually interfere with itself (such as Modes (2, 2) and  $(\hat{2}, 2)$ ).

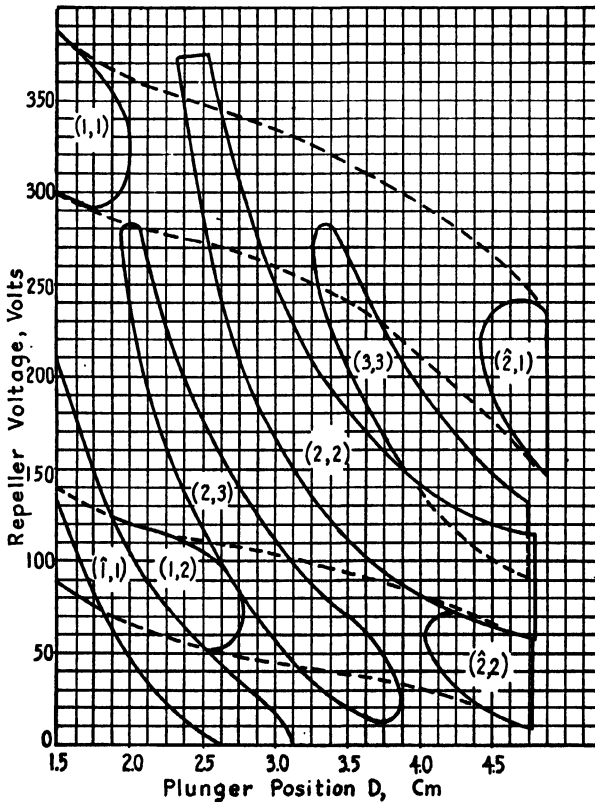
**32-19. Design of the  $k = 1$  Mode-suppressor Section.**—The design of the suppressor for Mode (1, 1) may be based on the following considerations:

1. The mode suppressor should not appreciably distort the tuning curve of the desired mode if  $k = 3$  mode interference and a reduction in resonator  $Q$  are to be avoided. It is seen that the tuning curves of Fig. 32-21 satisfy this principle.

2. The antiresonant wavelength  $\lambda_\infty$  should be the largest value that will provide Mode (1, 1) clearance at the high-frequency limit of Mode (2, 3).

3. The characteristic impedance  $Z_0$  of the suppressor must be great enough to provide adequate clearance of the Mode (1, 1) at the longer wavelengths.

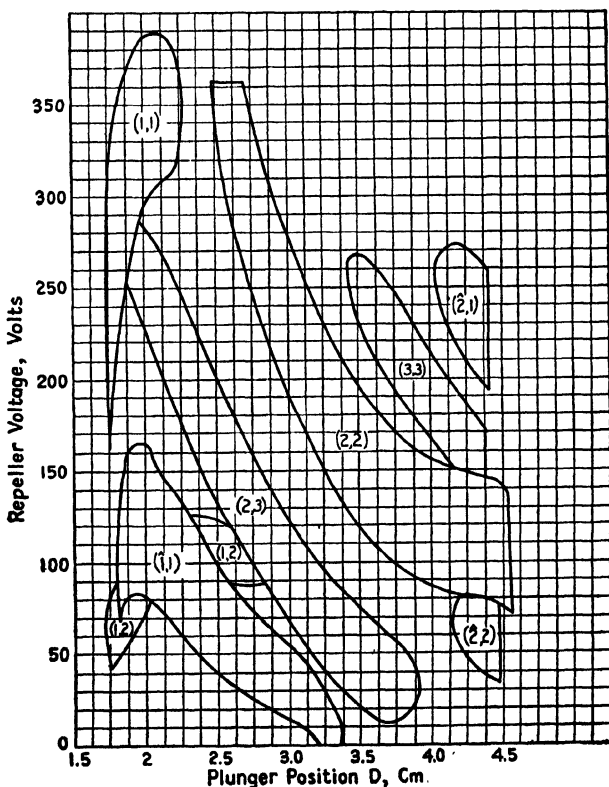
Because the mode suppressor ideally becomes resonant at  $\lambda_\infty$  and also at  $\lambda_\infty/3$ , a ratio of 3:1, the first requirement listed above may usually be satisfied if the desired tuning ratio is not appreciably greater than 2:1.



(a)  
FIG. 32-22.—Agreement between calculated and experimental mode

It is apparent that a more elaborate suppressor section could be used. For example, in the event that mode interference could not be eliminated over the entire tuning range with a single suppressor section, it might be possible to incorporate a second suppressor that is antiresonant at a longer wavelength. It would be necessary, however, to design the two sections to provide overlapping regions of nonoscillation for the repeller ranges involved. Interference would otherwise result at the wavelength where the reactances of the two sections are equal and opposite. Or, if the first and second antiresonant frequencies of the mode suppressor must be separated by a ratio either greater or less than 3:1, a compound-line section (see Sec. 32-28) might be used.

**32-20. Parasitic Circumferential Resonances of the Suppressor Section.**—The mode suppressor of Fig. 32-18 can support parasitic resonances that may result in oscillator holes or frequency discontinuities, as described in Sec. 31-10. The method of controlling these resonances will now be discussed.



(b)

plots for mode-suppressor cavity: (a) calculated, (b) experimental.

These parasitic resonances are due to waves propagated circumferentially around the suppressor section. For propagation in this direction there exists a guide wavelength  $\lambda_g$  that may be approximated with reasonable accuracy by assuming that the suppressor section shown in Fig. 32-18 is the *right half* of a rectangular waveguide that has been bent around in a circle and joined to itself. The cutoff or critical wavelength  $\lambda_c$  for propagation around this guide is twice the width of the guide or  $\lambda_c = 4l_s$ . Circumferential resonances will occur whenever the mean circumference  $C$  of the suppressor section is an integral multiple  $n$  of the guide wavelength  $\lambda_g$ , Eq. (32-4).

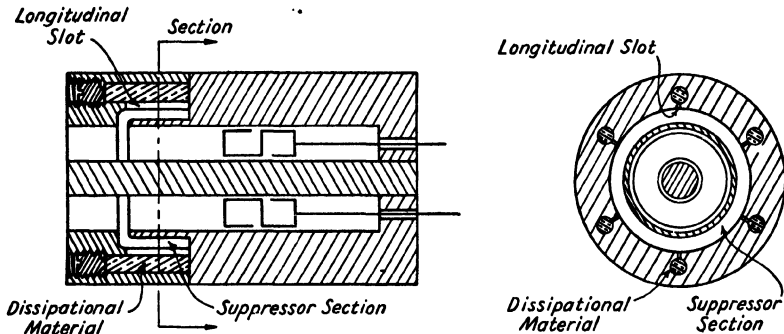


FIG. 32-23.--Mode-suppressor cavity with dissipational suppression of parasitic resonances in the suppressor section.

If the parasitic-resonance wavelength is denoted by  $\lambda_s$ ,

$$C = n\lambda_g = \frac{n\lambda_s}{\sqrt{1 - \left(\frac{\lambda_s}{4l_s}\right)^2}} \quad (32-22)$$

Solving Eq. (32-22) for  $\lambda_s$ ,<sup>1</sup> gives

$$\lambda_s = \frac{C}{\sqrt{n^2 + \left(\frac{C}{4l_s}\right)^2}}, \quad n = 1, 2, \text{ etc.} \quad (32-23)$$

These parasitic resonances may be suppressed by slotting the mode-suppressor section, as shown in Fig. 32-23. The *TEM* field does not penetrate through the slots into the lossy material, and the *TEM* per-

<sup>1</sup> A more rigorous analysis of these resonances may be based upon the fact that these *circumferential* resonances are equivalent to *TE*<sub>*n*,1</sub> antiresonances in the coaxial stub. The *TE*<sub>*n*,1</sub> wave is cut off in the main cavity, and hence the cavity presents an *inductive* termination to the mode-suppressor section. The actual resonant wavelengths will, therefore, be slightly less than those calculated from Eq. (32-23).

formance is, therefore, practically unchanged. The lossy material does, however, affect the circumferential resonances because the circumferential currents must flow across the slots, and the effective  $Q$  of the parasitic resonance may be greatly reduced by this method of selective loading.

It was shown in Sec. 31-10 that the effect of a parasitic resonance depends upon its  $Q$  and upon its coefficient of coupling  $k$  with the  $TEM$  mode. To avoid a frequency discontinuity, the product  $Qk$  must be less than unity, and, to avoid excess loading, the coupling must be extremely small.

Unfortunately, it has been found that the coupling coefficient to the one-cycle resonance ( $n = 1$ ) is quite large because all cavity *eccentricities*, such as that of the plunger or tube, contribute *strongly* to the excitation of this one-cycle resonance. The loading effect on the  $TEM$  resonance is usually so excessive that a hole results.

On the other hand, simple eccentricities produce only a slight coupling to the *multiple-cycle* resonances ( $n > 1$ ). The product  $Qk$  for these multiple-cycle resonances can, therefore, be decreased sufficiently below unity by means of the method illustrated in Fig. 32-23 practically to eliminate the effect of these multiple-cycle resonances on the  $TEM$  mode. However, an abrupt irregularity, such as a coupling loop or probe, near the mode suppressor, may increase the excitation of the multiple-cycle resonance sufficiently to cause a hole.

**32-21. Parasitic TE and TM Modes.**—If the transverse dimensions of the resonator are comparable to the wavelength, resonant modes other than the  $TEM$  types considered in Sec. 32-8 may exist in the resonator. If the oscillator is to function properly throughout its tuning range, the resonator must be so designed that the wavelengths of *all* parasitic resonances occurring in the main resonator<sup>1</sup> lie outside the tuning range of the oscillator. The factors that control the wavelengths at which these parasitic resonances occur will be discussed in the following sections.

**32-22. TE Parasitic Resonances.**—The  $TE_{1,1}$  resonance is the most common of the cavity parasitic resonances because it can occur at the longest wavelength. The other  $TE$  resonances are similar in behavior but not so common. Since the wavelength at which the cavity is resonant for any  $TE$  mode is a function of the tuning of the resonator,  $TE$  tuning curves exist that resemble in some ways the  $TEM$  tuning characteristics of Sec. 32-8. Two important differences exist, however.

<sup>1</sup> Parasitic resonances in supplementary parts of the resonator, such as the non-contacting plunger or the mode suppressor, which occur at wavelengths within the tuning range of the oscillator may sometimes be tolerated. Experience has shown, however, that it is impossible to control satisfactorily over a wide tuning range parasitic resonances occurring in the main resonator and that such resonances are usually disastrous.

1. The wavelength  $\lambda_g$  of a  $TE$  mode in the coaxial-line section is greater than the free-space wavelength  $\lambda$ , and it becomes infinite at the cutoff wavelength  $\lambda_c$ . (see Eq. 32-4). Hence, a parasitic resonance is possible only at wavelengths less than  $\lambda_c$ , regardless of the length of the resonator.<sup>1</sup>

2. The second important distinction between  $TEM$  and  $TE$  resonances in a coaxial resonator has to do with the effective termination presented to the coaxial line by the tube and its corner. For the  $TEM$  mode, this termination is equivalently an *open circuit* so that resonance obtains when the resonator is effectively  $\frac{1}{2}, \frac{3}{4}$ , etc., wavelength long; for the  $TE$  modes, on the other hand, the corner termination is equivalently a *short circuit*, and resonance is obtained when the

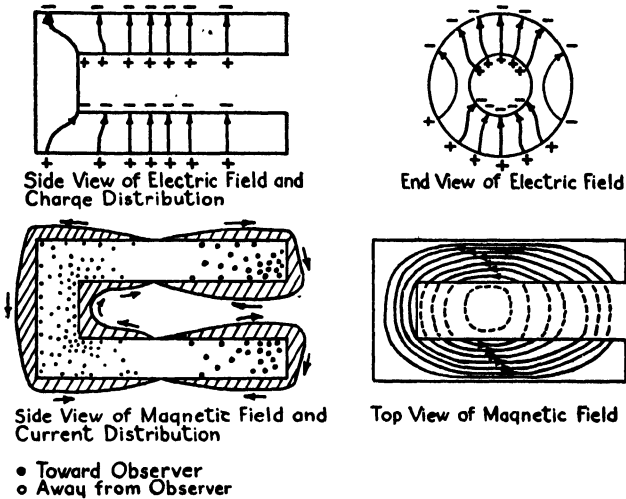


FIG. 32-24.—Sketch of  $TE_{1,1}$  fields in a coaxial resonator.

resonator is effectively  $\frac{1}{2}, 1$ , etc., wavelength long. Hence, the condition for resonance of any  $TE_{n,1}$  mode is simply

$$D = k \frac{\lambda_g}{2} \tag{32-24}$$

where  $D$  is the total equivalent length of the resonator and is equal to the sum of the equivalent corner length  $l_c$ , the length of the coaxial line  $l$ , and the equivalent plunger length  $l_p$ , and  $k$  is an integer designating the order of the mode.

For the  $TE_{1,1}$  mode, the equivalent length of the corner is roughly equal to the mean distance around the corner to the axis of the tube. Measurements made on a properly *slotted* plunger have shown that the slotted plunger presents approximately the same impedance to the  $TE_{1,1}$  wave as to the  $TEM$  wave. Hence the equivalent plunger length  $l_p$  is negligibly small.

<sup>1</sup> In certain rare cases, the corner and tube loading may be such as to produce in effect a parasitic resonance at a wavelength somewhat greater than  $\lambda_c$ .

The field configurations of a  $TE_{1,1}$  resonance in a coaxial resonator are shown in Fig. 32-24. These field sketches were drawn using the five rules of Sec. 32-2 as a guide. The following peculiarities of this  $TE_{1,1}$  resonance should be noted:

1. There can be *no* electric field at the axis of the tube gap. Since the electric field above the axis is directed in the opposite direction to that below, the fields effectively neutralize each other at the axis. Because of this effect, the cavity is effectively short-circuited at the axis of the gap.

2. Because of 1, there is practically no electric field across most of the gap of the reflex tube. Large variations in gap capacitance will therefore produce only a slight effect on the  $TE_{1,1}$  resonant wavelength.

3. The resonator acts as if it were short-circuited to the  $TE_{1,1}$  mode because, as shown in Fig. 32-24, the charges simply surge between top and bottom surfaces of the *same* conductor. Axial current across the tube gap is, therefore, not required.

Since the guide wavelength is  $\lambda_g = \frac{\lambda}{\sqrt{1 - (\lambda/\lambda_c)^2}}$ , Eq. (32-24) may be solved for  $\lambda$  to give

$$\lambda = \frac{1}{\sqrt{\left(\frac{k}{2D}\right)^2 + \left(\frac{1}{\lambda_c}\right)^2}} \quad (32-25)$$

Tuning curves calculated from this equation are shown in Fig. 32-25. If it is assumed that the equivalent lengths of the corner to the  $TEM$  and  $TE$  waves are identical, the intersections of the  $TEM$  tuning curves (also shown in Fig. 32-25) with the  $TE$  tuning curves give the theoretical wavelengths at which parasitic resonances may be expected to cause trouble. In oscillators using the 2K28 tube the agreement between these theoretical values and the values actually measured has been quite close. In other oscillators where the  $TEM$  tuning curves differ from those given in Fig. 32-25, the agreement has not been so good. If the distortion of the  $TEM$  curves is considered, more accurate estimates may obviously be made.

It is of considerable importance that  $TE_{1,1}$  interference is not possible on the quarter-wave ( $k = 1$ )  $TEM$  mode. If the three-quarter-wave ( $k = 2$ )  $TEM$  mode is to be utilized, the  $TE_{1,1}$  interference wavelength at  $\lambda = 0.75 \lambda_c$  must be moved outside the tuning range, preferably on the short-wavelength end. Two methods may be used to decrease this wavelength. (1) The diameters of the coaxial conductors may be decreased in order to decrease  $\lambda_c$  and hence the interfering wavelength. (2) The  $TEM$  tuning curves may be moved toward the left and raised. From the data of Fig. 32-11, it is apparent that an *increase in tube*



capacitance will shift the TEM curves to the left and thus decrease the  $TE_{1,1}$  interference wavelength. (Note that this is exactly opposite to the usual effect of an increase in capacitance on resonant wavelengths.)

This effect has produced some surprising results. For example, the 7-to 14-cm oscillator shown in Fig. 32-4, using the ordinary 2K28 tube,

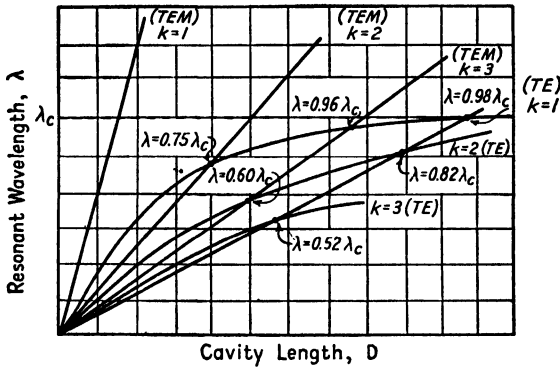


FIG. 32-25.—Tuning curves showing points of simultaneous TEM- and TE-mode resonance.

was observed to have a  $TE_{1,1}$  interference at a wavelength of 6.8 cm. When a special tube identical to the 2K28 in exterior dimensions but with a gap capacitance only about two-thirds as large (the intention in so reducing the capacitance was apparently to improve the short-wavelength performance of the tube) was inserted in the resonator, the  $TE_{1,1}$

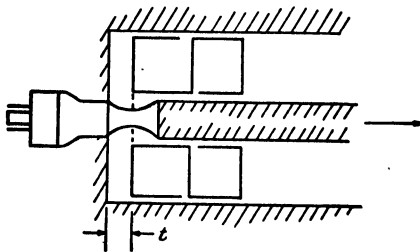


FIG. 32-26.—Resonator condition for radial-line resonance.

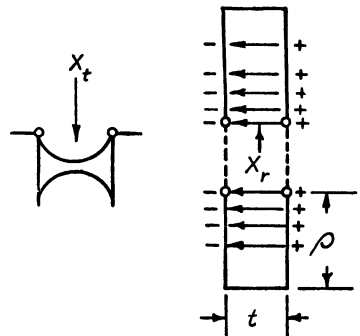


FIG. 32-27.—Division of resonator into tube and radial-line section.

interference moved to a wavelength of 7.8 cm. It would not have been possible to design a resonator to cover the 7- to 14-cm tuning range with this special tube. Hence, a certain amount of tube capacitance may be invaluable in extending the high-frequency range of a given resonator, and the low-capacitance tube may be inferior to a tube having greater capacitance. (For other disadvantages of a low-capacitance tube, see Sec. 32-15.)

**32-23. TM Parasitic Resonances.**—In the foregoing discussion, all interaction between the *TEM* and *TE* modes was ignored. If the resonator and all parts associated with it were perfectly symmetrical, there would be no coupling between the *TEM* and *TE<sub>n,1</sub>* modes. However, a

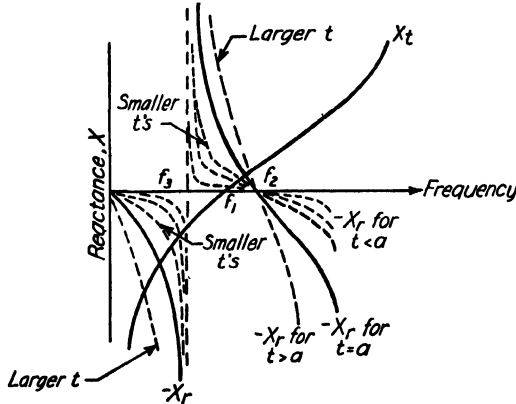
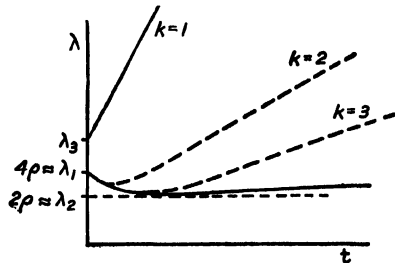


FIG. 32-28.—Plot of tube and radial-line reactances as a function of frequency for various thicknesses *t* of radial line.

*radial-line* (*TM<sub>0,1</sub>*) resonance may sometimes be set up *in the corner* at somewhat longer wavelengths. Since this radial-line corner resonance may restrict the high-frequency limits of all cavity modes, it deserves further comment. When the cavity length *t* is very short, as shown in Fig. 32-26, it may be considered as a radial line, as shown in Fig. 32-27. When the distance  $\rho$  is approximately  $\frac{1}{4}$  wavelength, this radial-line section becomes antiresonant. The reactance  $X_r$ , presented by the radial line is proportional to its thickness. Hence, for various values of *t*, the negative ( $-X_r$ ) of this reactance would vary with frequency, as shown in Fig. 32-28.



Also plotted in Fig. 32-28 is the reactance  $X_t$  presented by the tube.

FIG. 32-29.—Typical tuning curves as affected by *TM<sub>0,1</sub>* resonance.

By usual theory, oscillations will be obtained when  $X_t = -X_r$ , and hence each intersection of these curves gives the operating frequency for a particular value of *t*. There are *two* intersections for *each* *t*; along one branch  $\lambda$  increases with *t* (this branch corresponds to the regular quarter-wave mode), and along the other branch  $\lambda$  decreases with *t*.

The  $k = 2, 3$ , etc., modes degenerate into the latter short-wavelength branch, as shown in Fig. 32-29. A tapered corner might be used if it

were necessary to increase the high-frequency limit, or the outer diameter could be decreased in order to shorten the radial line.

**32-24. Output-coupling Methods.**—The use of small probes or loops inserted into a cavity resonator to couple the field of the electromagnetic oscillation therein with an external circuit has been discussed in Chap. 9 and elsewhere.<sup>1</sup> However, there are certain requirements peculiar to a local oscillator for use in a superheterodyne that must be tuned over a wide range, and these deserve further discussion here.

1. Although the coupling need not give maximum possible power output, it is necessary that adequate power be delivered to the crystal mixer to assure proper conversion throughout the tuning range. Ordinarily, power variations within the tuning range having a maximum power of four or five times the minimum power may be tolerated.

2. To avoid unnecessary complications, the coupling should be fixed and should not require mechanical adjustment with oscillator tuning. The loop or probe must therefore be inserted into the resonator at such a point that no nulls occur within the tuning range.

A loop couples primarily with the magnetic field in the resonator, and its position in the resonator for optimum coupling is obviously at a point of maximum surface current. A loop placed at the face of the plunger may always be used to give a substantially uniform coupling over a tuning ratio as great as 5:1. However, in a local oscillator that must undergo thousands of tuning operations, the mechanical and electrical complications involved in incorporating the coupling loop and flexible output coaxial line into the movable plunger system are so great that this method has not been used.<sup>2</sup>

Likewise, since a probe couples primarily with the electric field, optimum probe coupling will be obtained when the probe is located at a point of maximum electric-field intensity. The electric field will always be a maximum at the interaction gap of the reflex klystron, but obviously no coupling probe can be inserted at that point. If the oscillator is operating at a low frequency so that the equivalent length of the tube is less than  $\frac{1}{4}$  wavelength, a probe inserted as close to the interaction gap as possible might be used to give adequate coupling.

It is often found, however, that the equivalent length of the tube exceeds  $\frac{1}{4}$  wavelength. For example, with a 2K28 reflex klystron operat-

<sup>1</sup> Terman, F. E., "Radio Engineers' Handbook," pp. 271-272, McGraw-Hill Book Company, Inc., New York, 1943.

<sup>2</sup> At the high-frequency limit of the tuning range, where the length of the cavity may become very small, the fields may be so distorted that optimum coupling is not obtained at the face of the plunger. The coupling will ordinarily be adequate, however.

ing at a wavelength of 8.5 cm, the first quarter wavelength of the oscillation lies within the space bounded by the tube flanges. Obviously, some other position in the resonator at which an electric field obtains must be selected for probe coupling.

Output coupling to a quarter-wave resonator ( $k = 1$ ) may therefore be obtained through either a loop in the plunger or a probe near the interaction gap of the tube. Output coupling to a three-quarter-wave resonator ( $k = 2$ ) may be obtained at the same points when possible. In addition, optimum coupling may be obtained by a loop inserted at a point  $\frac{1}{2}$  wavelength in front of the plunger, or by a probe inserted at a point  $\frac{1}{4}$  wavelength in front of the plunger. However, if the probe or loop is placed at a fixed point in the resonator wall, its position will deviate from that for optimum coupling as the resonator is tuned through its operating range. We shall now determine the best average position for a loop or probe in a  $\frac{3}{4}$ -wavelength resonator.

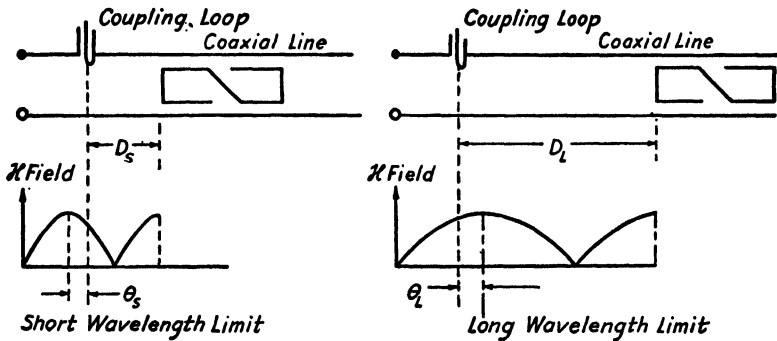


FIG. 32-30.—Plunger-loop relations.

**32-25. Optimum Position of a Fixed Loop in  $\frac{3}{4}$ -wavelength Resonator.**—The points of maximum magnetic field intensity in a three-quarter-wave resonator occur at the plunger and  $\frac{1}{2}$  wavelength in front of the plunger. A loop inserted into the resonator wall at a point  $\frac{1}{2}$  wavelength ahead of the plunger for a given wavelength of operation will be closer to the plunger electrically when the resonator is tuned to a shorter wavelength and farther from the plunger electrically when the resonator is tuned to a longer wavelength of oscillation. We shall specify, then, that the best position of the loop will be that for which the deviation in electrical degrees from the positions for optimum coupling shall be equal and opposite at the short- and long-wavelength limits of the tuning range. With reference to Fig. 32-30, the following parameters are defined:

$\lambda_s, \lambda_L$  = short- and long-wavelength limits of the tuning range of the oscillator

$\theta_s, \theta_L$  = number of electrical degrees deviation from the position of optimum loop coupling at the short- and long-wavelength limits of the tuning range

$D_s, D_L$  = position of the plunger relative to the loop at the short- and long-wavelength limits of the tuning range.

$\rho$  = tuning ratio,  $\lambda_L/\lambda_s$

These parameters are related as follows for loop coupling:

$$D_s = \frac{\lambda_s}{2} - \lambda_s \left( \frac{\theta_s}{360} \right) \quad (32-26)$$

$$D_L = \frac{\lambda_L}{2} + \lambda_L \left( \frac{\theta_L}{360} \right) \quad (32-27)$$

and if it is assumed that the electrical deviations from position of optimum loop coupling are equal

$$\theta_L = \theta_s = \theta_m$$

The total distance of plunger travel may then be expressed in terms of Eqs. (32-26) and (32-27) as

$$D_L - D_s = \frac{\lambda_L - \lambda_s}{2} + \frac{\theta_m}{360} (\lambda_L + \lambda_s) \quad (32-28)$$

If, the experimental  $\lambda$ - $D$  tuning characteristic is available for the resonator in question, values of  $D$  corresponding to the long- and short-wavelength limits of operation may be placed in Eq. (32-28) and the resulting equation solved for  $\theta$ . This value of  $\theta$ , when substituted into either Eq. (32-26) or Eq. (32-27) will give the best position for the loop.

It is interesting that if the  $\lambda$ - $D$  tuning characteristics are assumed to be those of an *idealized* three-quarter-wave resonator, then

$$D_L - D_s = \left(\frac{3}{4}\right)(\lambda_L - \lambda_s)$$

and the electrical deviation  $\theta_m$  from optimum coupling position may be expressed in terms of the tuning-ratio factor  $\rho$  as

$$\theta_m = 90 \frac{\rho - 1}{\rho + 1} \quad (32-29)$$

A similar analysis may be made for a probe inserted into the resonator at an average position which is 90 electrical degrees ahead of the plunger. It will be found that the electrical deviation from optimum coupling position may be expressed in terms of the tuning ratio by

$$\theta_s = 180 \frac{\rho - 1}{\rho + 1} \quad (32-30)$$

It is apparent that the simple probe is inferior to the loop as a broad-band coupling device because the point of maximum electric-field intensity moves at a speed twice that of the point of maximum magnetic-field intensity. Figure 32-31 shows that for a 2:1 tuning range, loop coupling suffers a 30-deg deviation, whereas that of probe coupling would be 60 deg. The corresponding reductions in power output would be 25 and 75 per cent, respectively, at the limits of the 2:1 tuning range.

The foregoing discussion has ignored the effect of the change in frequency on the coupling and also variations in amplitude of oscillation with frequency. Since these depend upon the particular characteristics of the loop and reflex klystron used, the ignoring of these effects seems justified. In the final design, these and other effects, such as field distortion due to the corner, may require that the position of the coupling loop be shifted to accentuate one portion of the tuning range.

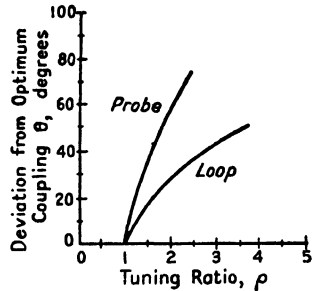


FIG. 32-31.—Loop and probe coupling characteristics.

**32-26. Combination Loop-probe Methods.**—In some microwave oscillators in which the resonator design requirements have led to the use of an outer cavity diameter that is relatively large compared with operating wavelength, it may be impossible to place a loop at the optimum position.

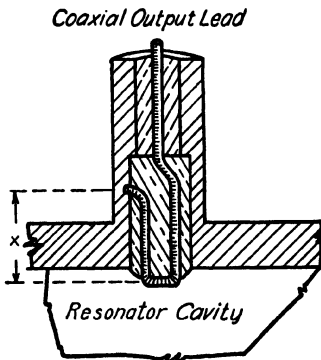


FIG. 32-32.—Composite probe-loop coupling system.

In that event, a composite loop-probe system such as that sketched in Fig. 32-32 must be used. At wavelengths where the section X becomes approximately  $\frac{1}{4}$  wavelength, this section refers a high impedance to the tip of the loop, and the system operates essentially as a probe. When X is approximately  $\frac{1}{2}$  wavelength, a low impedance is referred to the tip of the loop, and the coupling becomes essentially magnetic. By incorporating capacitance plates on the tip of the loop and by controlling the loop area, satisfactory characteristics can usually be achieved over a

tuning ratio of at least 2:1. Notice that the angular position of the loop in the cavity is of importance, since rotating the loop 180 deg will reverse the phase of the magnetic excitation but will leave the electric excitation unchanged.

**32-27. General Consideration of Noncontacting Plunger Design.**

The remainder of Chap. 32 is concerned with *plungers* that may be inserted into coaxial lines to simulate the effect of a short circuit at (or near) the face of the plunger.

A short-circuiting ring with fingers to make a sliding metallic contact between the inner and outer coaxial conductors is a common device for tuning a coaxial cavity. For use in power oscillators that are ordinarily tuned a limited number of times during the life of the equipment, this simple device is probably satisfactory. But for use in the local oscillator of a search receiver, which may be subjected to millions of tuning operations, a simple finger plunger has the following shortcomings:

1. To assure good electrical contact, the fingers must assert a reasonable pressure against the cavity surfaces. No materials having suitable electrical properties are known which will resist the mechanical wear resulting from indefinitely repeated tuning operations.

2. The contact resistance between the fingers and the cavity surfaces varies erratically with tuning, particularly when mechanical wear is appreciable and particles of corroded metal and dirt may come between the sliding surfaces. The variation in contact resistance with tuning affects the output of the oscillator and produces a "finger" noise in the output of the receiver which is very objectionable.

3. As the fingers wear, the tuning calibration of the oscillator will change slightly. Furthermore, a mechanical "hysteresis" due to buckling of the fingers from the sliding friction may also occur.

The remainder of this chapter describes noncontacting plungers which, over a wide operating range, produce less loss than the ordinary finger plunger, are perfectly "quiet" in tuning, and may be tuned a number of times limited only by the life of the carriage that supports the plunger. The resonant plungers may be used safely in low-power oscillators, but, for use in high-power oscillators, the possibility of dielectric breakdown due to the intense electric field at certain points within the plunger structure must be kept in mind. The problem of internal arc-over should be investigated if noncontacting plungers are to be used in high-power circuits.

Actually, it is not necessary that the plunger present a perfect short circuit. It is necessary only that the plunger produce a negligible power loss—it may accept energy during half of the r-f cycle, provided that it returns essentially all the energy during the remaining half cycle. Stated in another way, ideally the plunger impedance presented to the cavity must be a pure reactance. The effect on the cavity of a plunger reactance  $jX_p$ , measured at the face of the plunger, is identical to the effect of an ideal short circuit located  $\theta_p$  electrical degrees behind the plunger

face. If the characteristic impedance of the cavity is  $Z_0$ , we have

$$\theta_p = \tan^{-1} \frac{X_p}{Z_0} \quad (32-31)$$

If  $|X_p| \ll Z_0$ , the equivalent length  $\theta_p$  of the plunger is very small and, for practical purposes, the plunger may be considered as presenting a short circuit at its face.

Another point of view that is especially useful is that the plunger acts as a filter section whose function is to isolate the front of the cavity from the rear. Obviously, for proper operation, the filter should present a very large insertion loss, and hence the filter should operate well within the stop band. This point of view is useful in expressing the plunger resistance component that arises from energy leaking past the plunger. Thus, it is possible to express the plunger input resistance  $R_p$  in decibels below the characteristic impedance  $Z_0$  of the resonator by means of the formula

$$L = 10 \log_{10} \frac{R_p}{Z_0} \quad (32-32)$$

The quantity  $L$  may be interpreted as the amount in decibels by which the power extracted by the plunger is less than the power that would pass down the coaxial line if it were of infinite length.

The mechanical problem of maintaining uniform concentricity of the plunger within the coaxial cavity is not a simple one. In fact, for proper operation, the clearance between the plunger and the cavity walls must be kept very small (0.010 in. being a common clearance). It is important that sporadic contact of the plunger with the cavity does not occur. Such contact can destroy the resonant properties of the plunger, and the sudden irregular changes in plunger impedance may cause sudden jumps in the resonant frequency or produce sufficient power loss to prevent oscillations. Furthermore, if certain parasitic resonances are to be prevented, it is important that the plunger be kept concentric within close limits.

In general, any type of physical contact between the front sections of the plunger and the cavity is undesirable. This includes contact with dielectric surfaces as well as metallic fingers. The British have found that a sliding dielectric surface can pick up metallic particles and become as noisy as a sliding-finger contact. However, if the plunger were to be used in a low- $Q$  cavity, slight changes in plunger loss might be negligible compared with the total cavity loss, and dielectric support or even a finger-type plunger might be used satisfactorily.

We shall now consider the various types of noncontacting plungers that will simulate a short circuit in a coaxial cavity. In analyzing these



plungers, it will be possible to apply to the coaxial-line section the usual transmission-line techniques. The following assumptions will be made to simplify the analysis and reduce the number of design parameters:

1. The discontinuity capacitances<sup>1</sup> are negligible.
2. The thickness of the plunger walls is negligible.
3. The thickness of each low-impedance gap is negligible compared with main cavity dimensions.
4. The rear of the cavity is terminated in its characteristic impedance. This is equivalent to assuming that the coaxial cavity is semiinfinite in length.

The first assumption will be justified later when it is shown experimentally that discontinuity effects simply shift those characteristics which are functions of wavelength to a slightly longer wavelength. The second and third assumptions give results that are too optimistic, but here again, a reasonable margin may be allowed to compensate for this error. The fourth assumption is essential, for otherwise the impedance presented to the rear of the plunger by the rear cavity would be a function of plunger position, and it would be impossible to give plunger characteristics independent of the cavity characteristics.

**32-28. Compound-line Section.**—Before discussing the various types of noncontacting plungers, it will be informative to consider the behavior of the compound-line section shown in Fig. 32-33. Compound lines of this type may be used as mode-suppressor sections. Furthermore, the reactance characteristics of noncontacting plungers will be found to resemble those of the compound-line section.

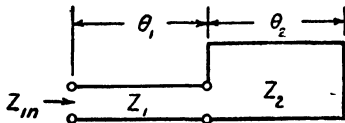


FIG. 32-33.—Compound-line section.

An expression for the input impedance is perhaps most easily obtained by replacing the second line section by a line having characteristic impedance  $Z_1$  and an electrical length  $\theta_2'$  so chosen as to present the same reactance to the first line section as the actual line. This equivalent length is

$$\theta_2' = \tan^{-1} \left( \frac{Z_2}{Z_1} \tan \theta_2 \right) \quad (32-33)$$

In terms of this equivalent length, the input impedance is simply

$$Z_{in} = jZ_1 \tan (\theta_1 + \theta_2') \quad (32-34)$$

If  $m = Z_2/Z_1$ , optional forms for Eq. (32-34) are

$$\begin{aligned} Z_{in} &= jZ_1 \tan [\theta_1 + \tan^{-1} (m \tan \theta_2)] \\ &= jZ_1 \frac{\tan \theta_1 + m \tan \theta_2}{1 - m \tan \theta_1 \tan \theta_2} \end{aligned} \quad (32-35)$$

<sup>1</sup> WHINNERY and JAMIESON, *loc. cit.*

For the particular case where  $\theta_1 = \theta_2$  and  $m > 1$ , the input impedance varies with the electrical length or frequency, as shown in Fig. 32-34.

The important characteristic of the compound-line section is that the poles and zeros of the impedance function are no longer equally spaced as they would be for a short-circuited line of uniform characteristic impedance. For the particular characteristic shown in Fig. 32-14, there is a large range about the 90-deg point where the input impedance changes comparatively slowly. In fact, in this range, the first term in the denominator of Eq. (32-35) may be neglected, and an approximate expression for the input reactance is

$$X_{in} \approx -Z_1 \left( \text{ctn } \theta_1 + \frac{1}{m} \text{ctn } \theta_2 \right) \tag{32-36}$$

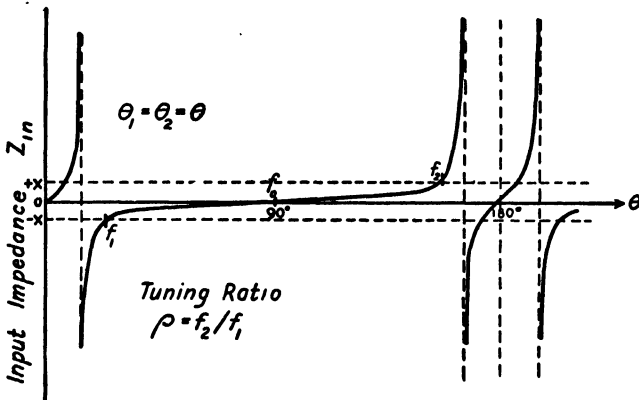


FIG. 32-34.—Input impedance of compound-line section for  $m > 1$ .

For very large values of  $m$ , it is apparent that the input reactance is approximately that of an open-circuited line of length  $\theta_1$  and characteristic impedance  $Z_1$ . The superiority of the compound-line section over a simple open-circuited line is that the former is completely enclosed, and hence the losses may be kept very small, whereas a simple open-circuited line is actually terminated in a discontinuity impedance that may have a large loss component due to radiation, coupling to external fields, etc.

The compound-line section may be used to present a broad-band "short circuit." If the maximum allowable impedance  $|X|$  of this short circuit occurs at the extremes,  $f_1$  and  $f_2$  of the tuning range (see Fig. 32-34), we may define the tuning ratio  $\rho$  as

$$\rho = \frac{f_2}{f_1} \tag{32-37}$$

It can be shown that the tuning ratio will be a maximum when  $\theta_1 = \theta_2$ . This is a rather important result springing from what we shall call the

*principle of equal design lengths.* It can be demonstrated for the compound-line section by either maximizing the analytic expression for  $\rho$  with respect to the ratio  $\theta_2/\theta_1$ , or minimizing all the derivatives of Eq. (32-36) at the frequency  $f_0$ . In either case, it will be found that the maximum tuning ratio will be obtained when  $\theta_1 = \theta_2$ .

The principle of equal design lengths may appear to contradict the "stagger-tuned" principle that has been so successfully applied to broadband coupling circuits, etc. The important distinction between the two

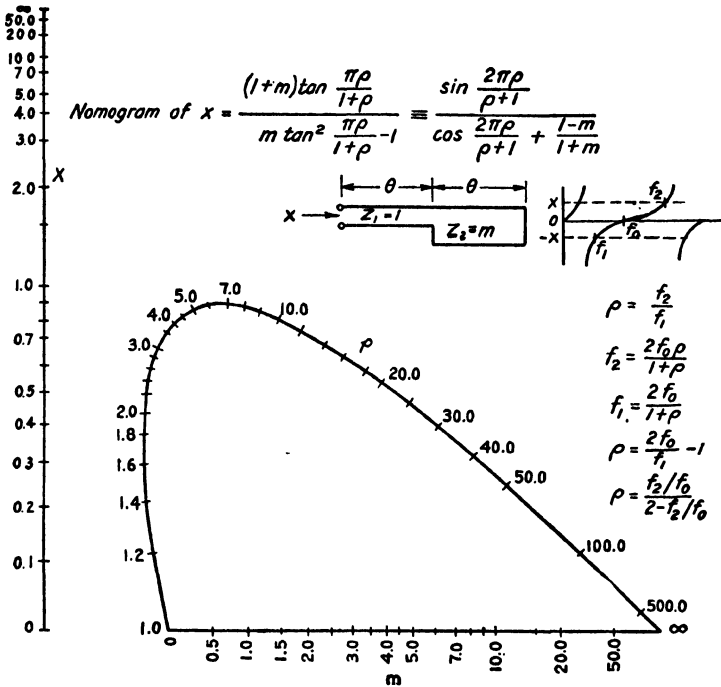


FIG. 32-35.—Nomogram of tuning ratio  $\rho$  of compound-line section.

is that the first principle applies to purely reactive circuits, whereas the latter principle applies to lossy circuits in which the circuit behavior is greatly modified by the resistance loadings.

To simplify impedance calculations of the compound-line section, the nomogram of Fig. 32-35 was prepared. This nomogram enables one to determine quickly the maximum tuning range for any particular impedance ratio  $m$  and input reactance level  $x$ . Observe that  $x$  has been normalized with respect to the characteristic impedance  $Z_1$ . This nomogram also gives the frequencies at antiresonance simply by setting  $x = \infty$ . For the optimum compound-line section in which  $\theta_1 = \theta_2 = \theta$ , the input impedance as expressed by Eq. (32-35) may be written as

$$\begin{aligned}
 Z_{in} &= jZ_1 \tan 2\theta \left( \frac{1}{1 + \frac{K_r}{\cos 2\theta}} \right) \\
 &= jZ_1 \frac{\sin 2\theta}{\cos 2\theta + K_r}
 \end{aligned}
 \tag{32-38}$$

where  $K_r$  is analogous to the reflection coefficient at the discontinuity in the line,

$$K_r = \frac{Z_1 - Z_2}{Z_1 + Z_2} = \frac{1 - m}{1 + m}
 \tag{32-39}$$

**32-29. Basic Noncontacting Plunger Types: Capacitance Plunger.**

The simplest noncontacting plunger is probably a simple cylindrical ring filling most of the space between the inner and outer conductors, as shown in the cross section of Fig. 32-36. This type will be called a *capacitance plunger* because capacitance effects are predominant.

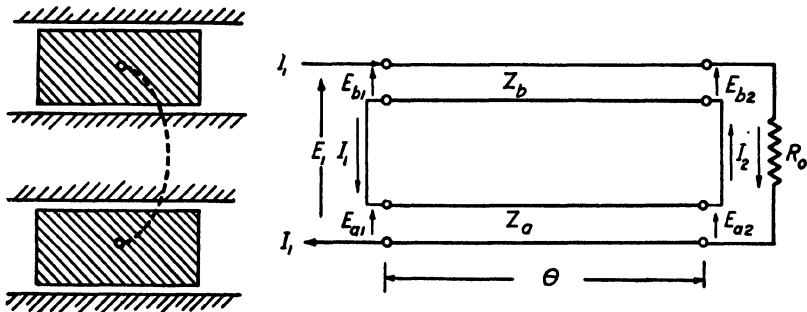


FIG. 32-36.—Capacitance plunger and equivalent circuit.

In the equivalent circuit, the transmission lines having characteristic impedances  $Z_a$  and  $Z_b$  are those formed by the inner and outer coaxial gaps of the plunger. The impedances of the front and rear faces are zero, and the rear of the cavity is assumed to present its characteristic impedance  $R_0$  to the plunger.

It should be noted that equal and opposite currents are assumed to flow on the two coaxial surfaces of each of these transmission lines. It may at first appear that this assumption is not justified since, if a *direct* voltage were applied to the cavity, it is obvious that direct current would flow along the cavity walls but *not* over the plunger surfaces, as is indicated in the equivalent circuit. However, if the effective skin depth is small compared with the plunger dimension, this assumption is justified for the following reason: For small skin depths, there can be no magnetic field inside the metallic plunger, and hence the integral of the magnetic-field intensity around a path such as the dotted one of Fig. 32-36 must be zero. By Biot-Savart's law, the total current flowing through

the surface bounded by this path must also be zero, and the current over the inner surface of the plunger must be exactly equal and opposite to that over the inner conductor. A similar argument may be applied to the outer gap, and the assumption of current equality in the equivalent circuit is thus justified.

There are six variables in this equivalent network:  $I_1$ ,  $I_2$ ,  $E_{b1}$ ,  $E_{b2}$ ,  $E_{a1}$ , and  $E_{a2}$ . They are related by the following six equations based on the usual lossless transmission-line theory:

$$E_{b1} = \cos \theta E_{b2} + jZ_b \sin \theta I_2 \quad (32-40)$$

$$I_1 = \frac{j}{Z_b} \sin \theta E_{b2} + \cos \theta I_2 \quad (32-41)$$

$$E_{a1} = \cos \theta E_{a2} + jZ_a \sin \theta I_2 \quad (32-42)$$

$$I_1 = \frac{j}{Z_a} \sin \theta E_{a2} + \cos \theta I_2 \quad (32-43)$$

$$E_1 = E_{b1} + E_{a1} \quad (32-44)$$

$$R_0 I_2 = E_{b2} + E_{a2} \quad (32-45)$$

These equations may be solved for the ratio  $E_1/I_1$ , which, by definition, is the *input impedance*  $Z_p$  of the plunger. If it is assumed that

$$Z_a = Z_b = Z_0,$$

and if the *plunger-gap parameter*  $m = R_0/2Z_0$  is introduced, the normalized plunger input impedance as derived from Eqs. (32-40) through (32-45) is

$$\frac{Z_p}{R_0} = \frac{1 + \frac{j\Psi}{m}}{1 + jm\Psi} \quad (32-46)$$

where  $\Psi = \tan \theta$ .

The resistive and reactive components of the plunger input impedance given by Eq. (32-46) are

$$\frac{R_p}{R_0} + j \frac{X_p}{R_0} = \frac{1 + \Psi^2}{1 + m^2\Psi^2} - j \frac{\left(m - \frac{1}{m}\right)\Psi}{1 + m^2\Psi^2} \quad (32-47)$$

*It must be emphasized here that the resistive component in Eq. (32-47) is but one of two components forming the total input resistance. The derivation of Eq. (32-47) ignores the power losses in the plunger itself. Hence, the resistance term in Eq. (32-47) represents that due only to the rear-cavity loss (i.e., in  $R_0$ ), and it must be augmented by an additional resistance component arising from the internal losses of the plunger.*

When  $\Psi > 1$  and  $m \gg 1$ ,

$$Z_p \approx \frac{R_0}{m^2} - j \frac{R_0}{m\Psi} \quad (32-48)$$

and hence if the plunger length is selected so that it is 90 deg at the mid-frequency  $f_0$ , the input resistance is substantially constant and the input reactance varies as the cotangent of the electrical length.

The input resistance (due to rear-cavity loss) for a typical plunger ( $m = 18.6$ ) is shown in Fig. 32-37 as a function of the electrical length of the plunger. The resistance is expressed in decibels below  $R_0$ , as explained in Sec. 32-37. The function has been plotted only for the interval  $0 \leq \theta \leq 90^\circ$  because it is symmetrical about  $\theta = 90^\circ$ .

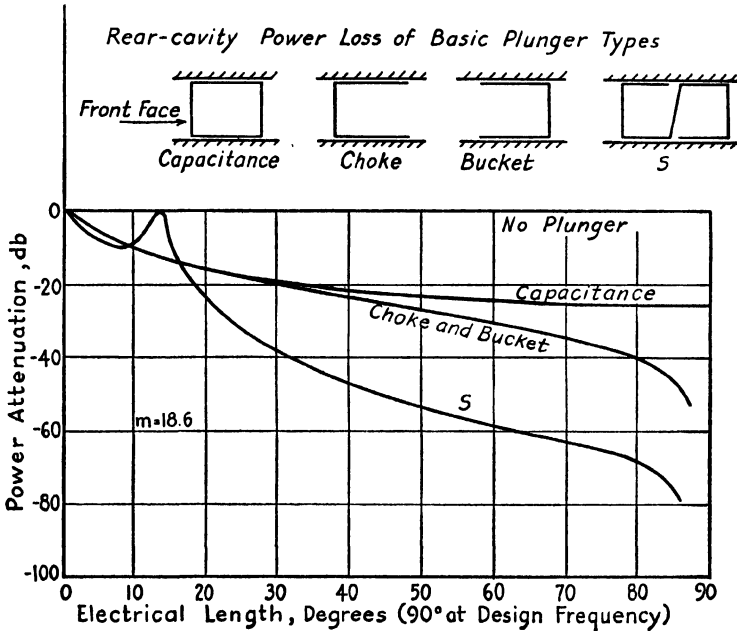


FIG. 32-37.—Rear-cavity power loss of basic plunger types.

**32-30. Choke and Bucket Plungers.**—If the rear part of the capacitance plunger is cut away, a *choke plunger* is formed (see Fig. 32-37). This type of plunger offers greater rear-cavity isolation than the simple capacitance plunger and is mechanically superior because of its lighter weight. The analysis proceeds exactly as for the capacitance plunger except that in Eq. (32-45)

$$(R_0 + Z_s)I_2 = E_{b2} + E_{a2} \tag{32-49}$$

where  $Z_s$  is the impedance of the short-circuited line section cut into the rear of the plunger. If the plunger walls are made negligibly thin,  $Z_s \approx jR_0\Psi$  and

$$\frac{Z_p}{R_0} = \frac{1 + j\left(1 + \frac{1}{m}\right)\Psi}{(1 - m\Psi^2) + jm\Psi} \quad (32-50)$$

At frequencies near the design frequency, where  $\Psi \gg 1$ , the impedance of this groove will be much greater than  $R_0$ , and hence the total impedance  $R_0 + Z_p$  is largely reactive (*i.e.*, of low power factor). This produces a marked decrease in rear-cavity loss, and consequently the input resistance decreases rapidly as  $\Psi \rightarrow \infty$  (or  $\theta \rightarrow 90$ ). This effect is also shown in Fig. 32-37.

Another method of decreasing the input resistance is to cut out the front face of the capacitance plunger in order to form what we shall call a *bucket plunger*. This type of plunger is also superior to the capacitance plunger in that both resistance and reactance are markedly decreased near  $\theta = 90$  deg. The impedance at the input of the low-impedance gaps is obviously the same as that of the capacitance plunger. However, this impedance acts in the cavity at a point about  $\theta$  deg ahead of the effective plunger face. The current is reduced by a factor of  $\cos \theta$ , and hence the *equivalent* resistance at the (new) plunger face is also reduced. The input impedance of the bucket plunger is

$$\frac{Z_p}{R_0} = \frac{1 + j\frac{1}{m}\Psi}{\left[1 + \left(1 + \frac{1}{m}\right)\Psi^2\right] + j[(m-1)\Psi + m\Psi^3]} \quad (32-51)$$

Surprisingly, the input resistance of the bucket plunger is found to be equal (within slide-rule accuracy) to the input resistance of the choke plunger (see Fig. 32-37).

It can be shown that the rear-cavity loss obtained with a capacitance plunger is dangerously large, particularly if the resonator is to be used with a reflex klystron. The occurrence of rear-cavity resonances may easily increase the power absorption by many times. It is desirable, therefore, as will be shown later, that the rear-cavity loss be less than -45 db. The only practical method of obtaining this large attenuation is to combine two of the basic plunger types just considered into a two-section plunger.

**32-31. S and Z Plungers.**—The best wide-range two-section plunger is that formed by placing a bucket section immediately back of a choke section. The forward section and rear sections may be joined in three different ways, as shown in Fig. 32-38, all of which are equivalent electrically. For any of these *S* plungers

$$\frac{Z_p}{R_0} = \frac{[1 - (1 + 2m)\Psi^2] + j\left(2 + \frac{2}{m}\right)\Psi}{[1 - (1 + 2m)\Psi^2] + j2m(1 - m\Psi^2)\Psi} \quad (32-52)$$

Similar analyses may be made for other combinations of the choke and bucket sections. The calculated rear-cavity losses are presented in Fig. 32-39. It is noted that the *S* plunger produces a large attenuation over the widest frequency range but that both the double-bucket and

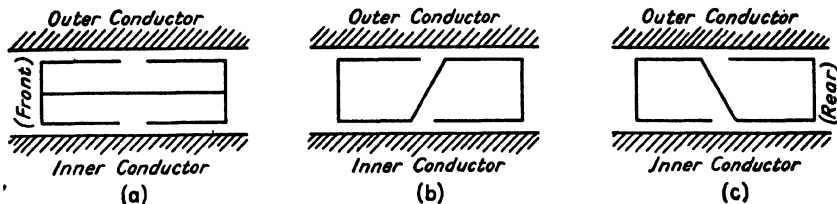


FIG. 32-38.—Equivalent forms of *S* plungers.

double-choke plungers offer a higher attenuation for  $60^\circ < \theta < 120^\circ$ . This would appear to indicate that the latter plungers would be superior to the *S* plunger if the tuning ratio were less than 2:1. It will presently be shown, however, that the *internal* plunger losses far exceed the rear-cavity losses in this range, and hence this “superiority” is of doubtful significance.

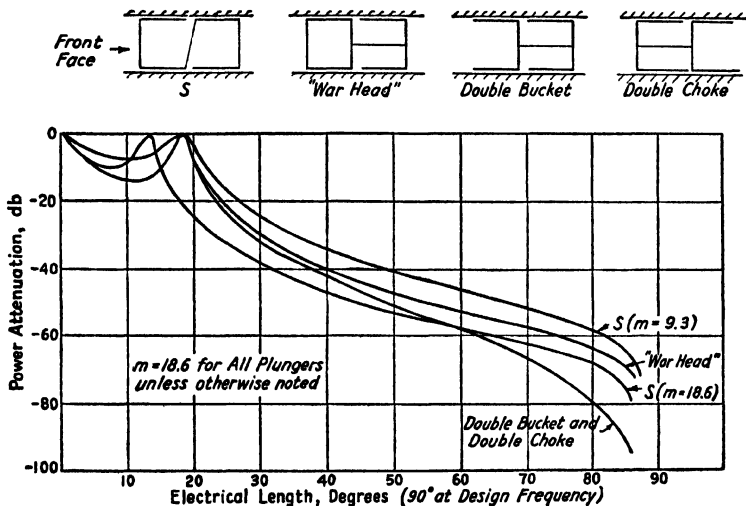


FIG. 32-39.—Rear-cavity power loss of basic plunger types.

With the exception of the bucket-faced plungers, the reactances of all types over the normal operating range are about the same. These reactances are compared in Fig. 32-40. Here again, since the curves have odd symmetry about  $\theta = 90$  deg, only half of the complete characteristic is given.

One important peculiarity of any of the double-section plungers shown in Figs. 32-38 and 32-39 is the antiresonance that occurs for a small  $\psi$ .



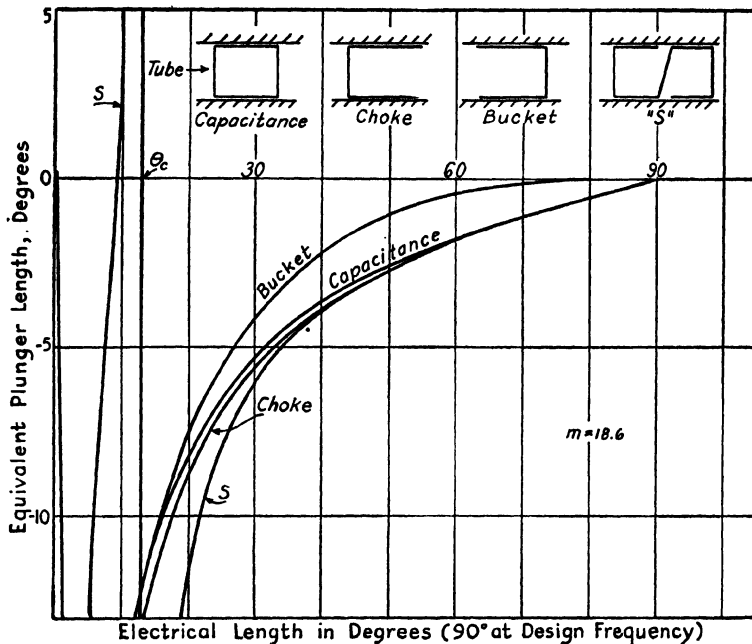


FIG. 32-40.—Input reactance of basic plunger types.

Thus, in the terminology of Fig. 32-41, the following approximations may be derived for the *S* plunger, provided  $m \gg 1$ :

$$\left. \begin{aligned}
 \theta_a &= \frac{1}{\sqrt{3m}} \quad \text{radians}, & L_a &= 10 \log_{10} \left( 1 + \frac{16m}{27} \right) \\
 \theta_b &= \frac{1}{\sqrt{2m}} \quad \text{radians}, & L_b &= 10 \log_{10} \left( \frac{m}{2} \right) \\
 \theta_c &= \frac{1}{\sqrt{m}} \quad \text{radians}, & L_c &= 0
 \end{aligned} \right\} \quad (32-53)$$

The point  $\theta_c$  is at the center of the antiresonance for which  $jX_p = 0$ .

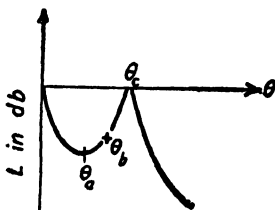


FIG. 32-41.—Rear-cavity power loss of *S* plunger near antiresonance.

**32-32. Measurement of Plunger Reactance.**

—It has not been possible to measure the rear-cavity power loss. However, a reasonable experimental check has been obtained on the plunger reactance as calculated for a typical *S* plunger. A comparison of calculated with experimental plunger reactance values is given in Fig. 32-42. The conclusion that may be drawn from these data is that discontinuity capacitance effectively causes the plunger to resonate when  $\theta \approx 80$  deg instead of  $\theta = 90$  deg.

the plunger to resonate when  $\theta \approx 80$  deg instead of  $\theta = 90$  deg.

Hence, the plunger should be shortened electrically to compensate for the effect of this capacitance. (In fact, although the plunger used in obtaining the data of Fig. 32-42 was designed so that  $\theta = 90$  deg at  $\lambda = 7$  cm, it

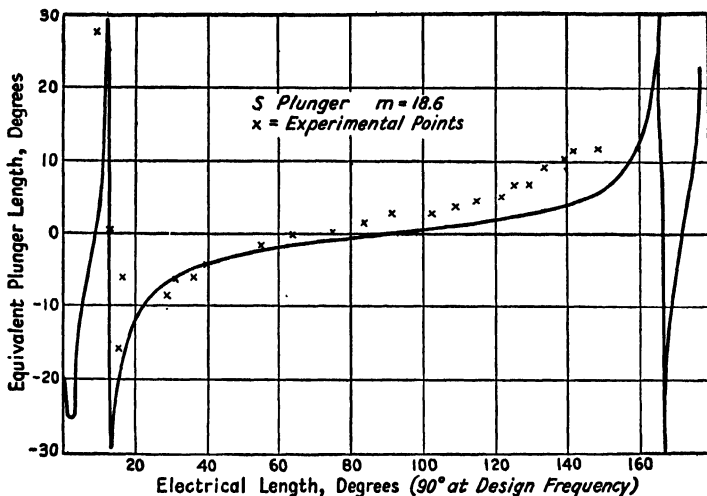


FIG. 32-42.—Comparison of experimental vs. calculated plunger reactances.

was used successfully in a cavity tuning from 7 to 14 cm.) The experimental values shown in Fig. 32-42 were calculated from resonance data of an actual coaxial cavity shown in Fig. 32-43.

Cavity resonance would occur ideally when the cavity length  $d$  is any multiple of  $\frac{1}{2}$  wavelength. Since the plunger presents an equivalent length  $l_p$ , however, actual resonance occurs when

$$d_1 = \lambda/2 - l_p, \quad d_2 = \lambda - l_p, \\ d_3 = 3\lambda/2 - l_p.$$

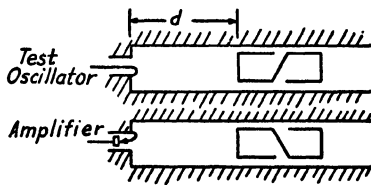


FIG. 32-43.—Plunger tester.

By making accurate measurements on any two  $d$ 's,  $l_p$  can be calculated. A more accurate, average value for  $l_p$  can be obtained if  $d_1, d_2, \dots, d_n$  are measured. Then

$$l_p = \frac{1}{2} \frac{n+1}{n-1} (d_n - d_1) - \frac{\sum_1^n d_i}{n} \tag{32-54}$$

Obviously, Eq. (32-54) gives  $l_p$  in the same units as the  $d$ 's.

Incidentally, the same technique may be used to measure the equivalent length of the plunger for higher order  $TE$  modes. It has been found

that, when the plunger is slotted, the impedance to the  $TE_{1,1}$  mode, at least, is nearly the same as to the dominant  $TEM$  mode.

**32-33. Internal Power Loss of Plunger.**—It has already been mentioned that the total plunger input resistance consists of two components: that due to energy leaking by the plunger into the rear cavity, and that due to the power loss inside the plunger itself. Rear-cavity power losses have already been considered. In this section, the internal loss of the plunger will be investigated.<sup>1</sup>

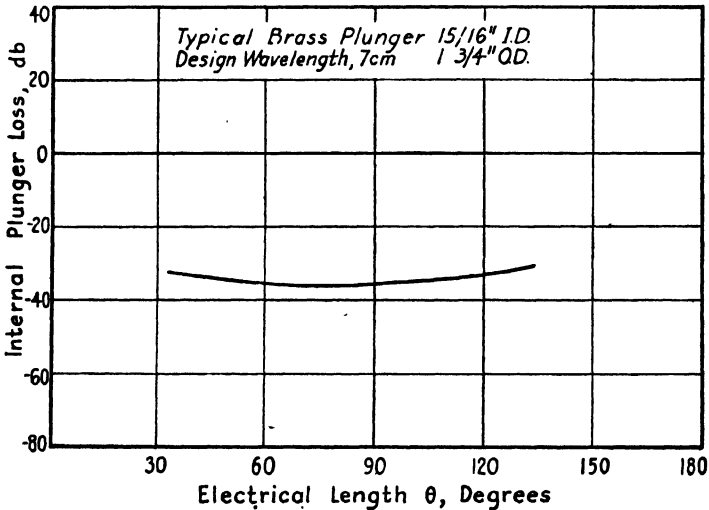


FIG. 32-41. ---Internal plunger loss.

All the flat-faced plungers shown in Fig. 32-39 behave within their normal operating range as if they were a compound-line section. If  $l$  is the length of each line section and  $\lambda_g$  is the circumference of the low-impedance coaxial gap, an approximate expression for the input resistance of a compound-line section in terms of the surface resistivity  $R_s$  can be shown to be approximately

$$R_{in} \approx R_s \frac{l}{\lambda_g} \left(1 + \frac{1}{m^2}\right) \left(1 + \frac{1}{\Psi^2}\right) \quad (32-55)$$

where, as before,  $m = Z_2/Z_1$  and  $\Psi = \tan \theta$ .

For a typical plunger, there are two gaps of circumference  $\lambda_a$  and  $\lambda_b$ , and the terms containing  $m^2$  may be neglected. The internal plunger

<sup>1</sup> A more accurate analysis than this of Secs. 32-33 and 32-34 is given by HUGGINS, W. H., Broad-band Noncontacting Short Circuits for Coaxial Lines, *Proc. I.R.E.* (to be published).

input resistance may, therefore, be approximated by

$$R_{in} \approx R_s l \left( \frac{1}{\lambda_a} + \frac{1}{\lambda_b} \right) \frac{1}{\sin^2 \theta} \quad (32-56)$$

For a typical brass plunger designed for maximum rear-cavity attenuation at 7 cm,  $\lambda_a = 7.60$  cm,  $\lambda_b = 13.9$  cm,  $l = 1.7$  cm,  $Z_0$  of main cavity = 37.2 ohms,  $R_s = 0.087/\sqrt{\lambda}$ , and the internal loss is

$$\begin{aligned} L_i &= 10 \log_{10} \frac{R_{in}}{Z_0} \\ &\approx -30.9 - 5 \log_{10} \lambda - 20 \log_{10} \sin \theta \end{aligned} \quad (32-57)$$

This internal loss is plotted in Fig. 32-44. Most important is the fact that it changes relatively slowly with  $\lambda$ . In fact, because of the compressive effect of the logarithmic scale, it is found that the internal losses of most brass or silver-plated plungers may be taken as  $-35$  db throughout their operating range.

The outstanding point of the preceding discussion is that *the internal plunger loss cannot be reduced much below  $-35$  db*. This, incidentally, is about equal to the loss that would occur if the plunger were replaced by another half-wavelength of cavity perfectly short-circuited at the far end.

**32-34. Total Power Loss of Plunger.**—The total input resistance of the plunger is determined by the *total* plunger loss. It is evident that, provided both losses are small, a slight internal loss should not noticeably affect the rear-cavity attenuation, and likewise a little power leakage into the rear cavity should not change the internal loss. The actual plunger input resistance may, therefore, be considered as the sum of two resistances, one due to the internal loss, and the other arising from the rear-cavity loss.

Hence, we may state that for practical purposes, *the total plunger loss  $L$  is equal to either the rear-cavity or the internal loss, whichever is greater*. (It must be realized that  $L$  must be considered algebraically: the greater loss has a smaller  $L$ , numerically.) The error in combining losses in this way does not exceed 3 db, the error when the loss components are equal.

We shall now set up a criterion for selecting the plunger-gap ratio  $m$ . The internal plunger loss is substantially independent of  $m$ , but it may be shown that the rear-cavity loss varies inversely as  $m^4$  for a double-section plunger. Obviously, very small plunger gaps present severe mechanical problems of alignment and manufacture, and it would be very helpful if some criterion could be set up for determining the largest plunger gap that would still give satisfactory electrical performance. Of course, one would always be free to use a gap smaller than this, if doing so would not produce mechanical complications.

Because the internal plunger loss remains fixed at about  $-35$  db, little is gained by decreasing the rear-cavity loss much below this value. Hence, the plunger should be designed so that the rear-cavity loss is less than  $-35$  db over the tuning range by the least possible amount. If the rear cavity is terminated so that rear-cavity resonances cannot occur, it should be satisfactory to select a gap ratio  $m$  such that the rear-cavity loss is equal to  $-35$  db at the extremes of the tuning range. If the design is such that mild rear-cavity resonances can occur, it seems very unlikely that they would increase the rear-cavity loss by much more than 10 db

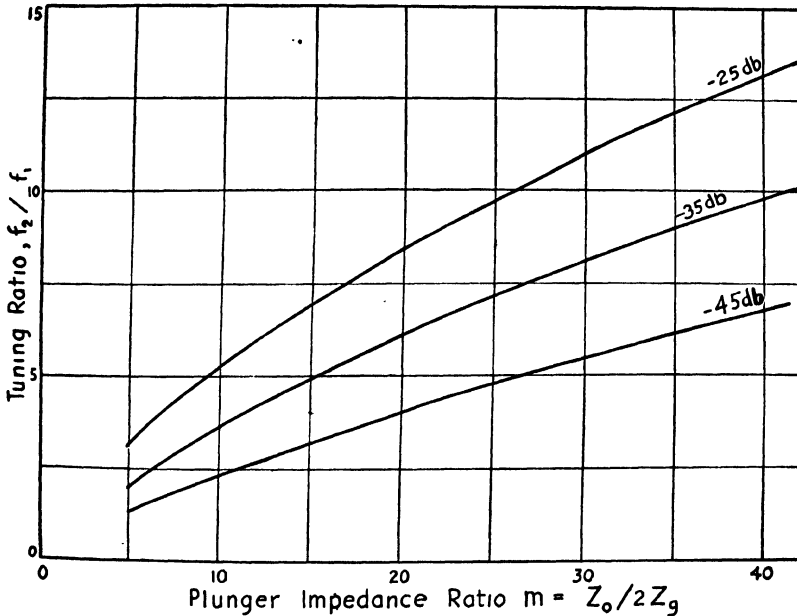


Fig. 32-45.—Tuning ratio of  $S$  plunger for  $-25$ ,  $-35$ , and  $-45$ -db rear-cavity losses as a function of plunger-gap impedance ratio  $m$ .

and, in this case, a rear-cavity attenuation of at least 45 db (in the absence of resonances) should be provided over the tuning range.

Design data calculated for the  $S$  plunger are shown in Fig. 32-45. These curves give the tuning ratios, as limited by  $-25$ -,  $-35$ -, and  $-45$ -db rear-cavity losses, as a function of the plunger-gap ratio  $m$ . In using these curves, an  $m$  value should be selected that will give a tuning ratio somewhat greater than that actually required. Furthermore, if the inner and outer gap impedances differ, the  $Z_0$  appearing in  $m = Z_0/2Z_g$  should be the *greater* of the two characteristic impedances.

The preceding discussion shows the futility of using more than two resonant sections in the plunger. Although plungers having three or more sections would provide very high rear-cavity attenuation and would

allow a somewhat larger plunger gap (if the tuning ratio were sufficiently small), these advantages would be offset by the added length and weight of the plunger. Furthermore, for each section added, a new antiresonance would be introduced and the tuning range might actually be narrowed. It may be concluded, therefore, that *nothing is gained by using more than two sections in a plunger.*

**32-35. Permissible Plunger Loss in Reflex Oscillators.**—It has been pointed out that the power loss in a typical plunger cannot be reduced much below  $-35$  db, and a design procedure has been suggested for assuring a loss that does not appreciably exceed this figure. This section will cover the determination of the largest power loss for which a reflex klystron may be expected to sustain oscillations.

It is easily shown that the input conductance of a coaxial resonator having a characteristic impedance  $Z_0$  and resonating on mode  $k$  is approximately related to the resonator  $Q$  by

$$G_{in} = \frac{(2k - 1)\pi}{4Z_0Q} \quad (32-58)$$

But for oscillation,  $|G_e| \geq G_{in}$ , where the electronic conductance  $|G_e|$  is defined in Sec. 31-2. Therefore, the resonator  $Q$  must satisfy the inequality

$$Q \geq \frac{(2k - 1)\pi}{4Z_0|G_e|} = \frac{(2k - 1)}{4Z_0G_0\beta^2N} \quad (32-59)$$

where  $G_0$  is the d-c beam conductance,  $N$  the number of reflex transit cycles, and  $\beta$  the beam-coupling coefficient.

The minimum  $Q$  value satisfying Eq. (32-59) corresponds to the greatest load for which oscillations can still occur. This extinction  $Q_e$  value may be determined experimentally by increasing the circuit loss with a *frequency-insensitive* load until the threshold of oscillation obtained. Then, with the tube inoperative and the loading unchanged, the  $Q_e$  of the cavity may be measured by the usual detuning methods employing an external source of r-f power.

We shall next determine the maximum plunger resistance that would give the extinction  $Q_e$  under the assumption that all the loss is caused by the plunger. We note that  $G_{in} = R_p/Z_0^2$  and use Eq. (32-58) to obtain the relation

$$\frac{R_p}{Z_0} < \frac{(2k - 1)\pi}{4Q_e} \quad (32-60)$$

where an inequality has been used to emphasize the fact that other than plunger losses also exist in the oscillator. That these other losses alone are usually not sufficient to bring the cavity  $Q$  near extinction is proved experimentally by the fact that considerable external loading of the cavity may usually be tolerated without stoppage of oscillation.

An expression for the maximum permissible plunger resistance directly in terms of beam current, instead of in terms of experimentally determined  $Q_e$ 's, is obtained by substituting Eq. (32-59) into Eq. (32-60).

$$\frac{R_p}{Z_0} < \pi Z_0 G_0 \beta^2 N \quad (32-61)$$

Critical "maximum" plunger-loss values may, therefore, be given

$$L = -10 \log \frac{4Q_e}{(2k-1)\pi} = 10 \log \pi Z_0 G_0 \beta^2 N \quad (32-62)$$

It is not necessary that the extinction  $Q$  be known with great precision; because of the large rate of change of plunger input resistance with frequency, a roughly specified value of critical resistance accurately specifies the working range of the plunger. Thus an error of 100 per cent in determining a critical value of  $R_p$  produces an error in  $L$  of about 3 db out of 25 or 30 db.

The critical value of  $L$  in a typical case may be found for a 2K28 tube with  $G_0 = 0.02/300$ ,  $\beta = 0.5$ ,  $N = 2.75$ , and  $Z_0 = 37.5$ . With these values,  $L = -23$  db.

In another oscillator using a 2K48 tube,  $Z_0 = 37$ ,  $G_0 = 0.015/1000$ ,  $\beta = 1$ ,  $N = \frac{7}{4}$ , and  $L = -25.2$  db. For the same oscillator, an experimental extinction  $Q_e$  of about 700 was obtained on the  $k = 2$  cavity mode. The corresponding value of  $L$  is  $-24.7$  db.

It appears, then, that the plunger loss must never exceed a value corresponding to roughly  $-25$  db if reflex oscillator holes are to be avoided. This value is further evidence corroborating the wisdom of designing the plunger so as to produce a rear-cavity attenuation greater than 45 db over the tuning range. For a plunger so designed, rear-cavity resonances would have to increase the rear-cavity loss more than one hundred times to "kill" the oscillator. It is believed that this is a reasonable safety margin and that, for such a plunger, rear-cavity effects will not cause trouble.

**32-36. Parasitic Resonances in a Noncontacting Plunger.**—It is unfortunate that all the noncontacting plungers discussed in the preceding sections are subject to parasitic resonances at sufficiently short wavelengths. These resonances are caused by waves propagated circumferentially around the small gaps between the plunger and the outer and inner conductors of the coaxial resonator. A detailed analysis of these plunger resonances is beyond the scope of this book.<sup>1</sup> However, both experiment and theory indicate that for an *unslotted S* plunger:

<sup>1</sup> HUGGINS, W. H., Parasitic Resonances in the Unslotted *S*-type Plunger, *Proc. I.R.E.* (to be published); Control of Parasitic Resonances in the *S*-type Plunger, *Proc. I.R.E.* (to be published).

1. A one-cycle circumferential resonance will occur at a wavelength a few per cent less than the mean circumference of the outer plunger gap.
2. Another one-cycle resonance will occur at a wavelength roughly 10 per cent less than the mean circumference of the outer plunger gap.
3. Two resonances, one at a wavelength a few per cent greater and the other at a wavelength a few per cent less than the mean circumference of the inner gap, will also occur.
4. The slightest eccentricity or tilting of the plunger will produce a *strong* coupling between the normal *TEM* field and the *one-cycle* circumferential resonances. It is impractical to maintain the plunger sufficiently concentric to prevent excitation of these parasitic resonances.
5. On the other hand, *multiple-cycle* circumferential resonances are only *slightly* coupled to the normal *TEM* field by a marked plunger eccentricity.

It was shown in Sec. 31-10 that parasitic resonances that are but slightly coupled to the dominant mode may be eliminated by adding sufficient dissipation to the parasitic circuit. In view of the fact that the coupling between the one-cycle parasitic resonances and the *TEM* field cannot reliably be reduced to a value sufficiently small to avoid holes or frequency discontinuities, it is apparent that

1. The one-cycle resonances must be moved to wavelengths outside the tuning range of the plunger.
2. A method of reducing the *Q* of the multiple-cycle parasitic resonances that remain within the tuning range must be employed that will not at the same time appreciably increase the plunger resistance presented to the normal *TEM* field.

The plunger and cavity surfaces may be considered as forming a "parallel-strip" transmission line which has been bent around and closed upon itself. Obviously, the resonant wavelength of this "transmission ring" may be increased by increasing either the capacitance or the inductance per unit length of the strip. Thus, if the gap were filled with a dielectric material having a relative dielectric constant  $\epsilon$ , the parasitic resonant wavelength would be increased in the ratio  $\sqrt{\epsilon}$ . While this method might have some application, it possesses two disadvantages: (1) a sliding contact would of necessity exist between the dielectric material and the conductor; (2) all dielectric materials produce a power loss that would increase the input resistance of the plunger.

A better method of increasing the wavelength at which the one-cycle resonances occur is to slot the plunger axially, as shown in Fig. 32-6 and Fig. 32-46, which shows the plunger used in the 2.2 to 4.2-kMc oscillator of Fig. 32-4. The effect of such slots is to add reactances in series with the transmission ring and thus increase the equivalent electrical circumferences. As an example, the one-cycle circumferential resonances in the inner gap of the plunger shown in Fig. 32-46 occurred



at an average wavelength of 7.8 cm. After slotting with five slots, the one-cycle resonances moved to about 20 cm, which was well outside the desired tuning range (7 to 14 cm). Multiple-cycle resonances may remain within the tuning range, but, since the coupling to these resonances is slight, they may be suppressed satisfactorily by placing a lossy dielectric in the slots.

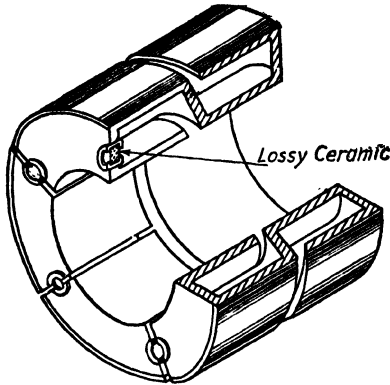


FIG. 32-46.—Slotted plunger showing method of loading slots.

The positioning of this lossy material should be such as not to couple appreciably with the normal *TEM* field. In the plunger of Fig. 32-46, small slugs of powdered-iron ceramic (Magicore) are bridged across the slots in the face of the plunger. In the plunger of Fig. 32-6 ordinary pencil lead was placed *inside* the slot. With this arrangement, the lossy material is shielded from the dominant *TEM* field, but the parasitic field penetrates the slot into the lossy material because of the circumferential component of current (or, equivalently, because of the axial component of magnetic field).

The best method of slotting a particular plunger in the last analysis

The best method of slotting a particular plunger in the last analysis

TABLE 32-3.—CHART SHOWING WAVELENGTH OF SLOT RESONANCES FOR 7- to 14-CM PLUNGER SIMILAR TO THAT OF FIG. 32-46

Plunger Type	Number of Slots	Width of Slots	Resonant Wavelength of Slots, Cm												
			5	6	7	8	9	10	11	12	13	14	15		
S*	—	—													
S	—	—													
S	3	1/64"													
S	3	1/32"													
S	3	1/16"													
S	5	1/64"													
S	5	1/32"													
S	5	1/16"													
Z	—	—													
Z	3	1/64"													
Z	3	1/32"													
Z	3	1/16"													
Z	5	1/64"													
Z	5	1/32"													
Z	5	1/16"													
Z	6	1/32"													

\*Plunger Was Eccentric

must be determined by trial and error. However, a slot-resonance theory, based on the analogy with a series-loaded transmission ring, shows that ordinarily

1. The fewest possible number of slots should be used.
2. An odd number of slots is preferable to an even number.
3. The *Z* or inverted-*S* plunger is superior to the British *S* plunger.

These conclusions are in agreement with the experimental results of Table 32-3 which shows the wavelengths within the 7 to 14-cm tuning range of the plunger of Fig. 32-46 at which parasitic resonances occurred as a function of the number of slots, slot width, and plunger type. Unlike all other plungers, the five-slot, *Z* plunger has only one resonance within the tuning range. (This is a three-cycle resonance. The one- and two-cycle resonances occur at 20 and 18.1 cm, respectively.) Hence, this plunger was used in preference to the others. This does not mean, however, that a five-slot *Z* plunger is the best in all cases.

Great care must be exercised during the manufacture and slotting of these plungers. If one of the sectors should become bent ever so slightly, the resulting irregularity in the plunger gap may increase the excitation of certain of the multiple-cycle resonances sufficiently to cause holes and frequency discontinuities.

## CHAPTER 33

### INTERMEDIATE-FREQUENCY AMPLIFIERS

BY M. T. LEBENBAUM

**33-1. Introduction.**—The type of i-f amplifier used in a wide-range tunable receiver is of a somewhat specialized nature, and certain factors of importance to the designer of amplifiers for use in other types of receivers may be neglected while others become of major significance. Those to be discussed in this chapter come under the general classification of wide-band high-gain amplifiers. By wide band is meant band widths of at least 1 to 2 Mc extending to at least 20 to 30 Mc. By high gain is meant gains of the order of 80 to 115 db.

From these specifications, certain conclusions may be drawn immediately. With large band width required, the gain per stage will be much less than, for instance, in a broadcast receiver i-f amplifier. Stage gains greater than 30 db are seldom encountered. It is thus obvious that the best possible tube must be used if the total number of stages employed to obtain the desired result is to be reasonable. The greater the amplification necessary, the more important the “merit” of the tube becomes. It is well at this point to establish a basic concept that will be used throughout to measure the merit of a given tube and also the merit of the amplifier stage or stages including the coupling network.

This factor of merit is known as the *gain-band-width* product. As will be shown in Sec. 33-9, the center-frequency voltage amplification  $G$  times the 3-db band width  $BW$  for a single stage of amplification using a pentode tube and a single-tuned coupling network is given by the expression

$$G \times BW = \frac{g_m}{2\pi C}$$

which is a constant for a given tube and network and is independent of center frequency. Here  $g_m$  is the tube transconductance in micromhos and  $C$  is the total capacitance in micromicrofarads associated with the tuned circuit, including tube, socket, and wiring capacitances. The band width  $BW$  and also the product  $G \times BW$  are expressed in megacycles. For instance, if 6AK5 pentodes are used,  $C$  is about 11  $\mu\mu\text{f}$ , and  $g_m$  is approximately 4500  $\mu\text{mhos}$ . The gain-band-width product for this case is 65.2 Mc. This means that for a given band width the avail-

able gain using a single-tuned coupling network is fixed. For a band width of 10 Mc, the gain of the stage is  $65.2/10$ , or 6.52. For 5 Mc, this would be 13.0. The  $G \times BW$  product is obviously, then, a useful figure to compare the relative merit of two types of tubes. The larger the product, the greater is the gain obtainable for a given band width, or the greater the band width for a given gain. This product is also useful in comparing types of coupling networks, using the single-tuned network as a reference. For a given tube, various coupling networks will give different gain-band-width products, the more complex networks usually giving larger factors.

The tubes most commonly used in i-f amplifiers at this writing are the 6AC7 and the 6AK5, the latter being used almost exclusively at the present time. The 6AC7 with  $g_m$  of 7500  $\mu\text{mhos}$  and  $C$  of 25  $\mu\text{mf}$  has a  $G \times BW$  product of 47.8 Mc. The 6AK5, as mentioned above, has a  $G \times BW$  product of 65.2, although it has a lower  $g_m$ . The latter point is important. Because the merit of the amplifier stage is inversely proportional to the capacitance associated with the tuned network, it is common to use only the tube, socket, and wiring capacitances as the total tuning capacitance; the lower this capacitance can be made, the larger the  $G \times BW$  product will be. The 6AK5 has the added advantage that it is a miniature tube and is physically easier to handle in the circuits used.

**33-2. Choice of Intermediate Frequency.**—The ultimate in a tunable receiver is a single-dial single-signal receiver. This means ganging of the local oscillator, mixer, and preselector circuits. In order to obtain a single-signal receiver it is necessary to remove all image and harmonic responses, or at least to reduce them to a large extent. Any reasonable amount of preselection will be adequate to take care of the harmonic responses. Image rejection is much more difficult to obtain. With ordinary preselector circuits, rejection increases with increased spacing between the true response and the image, a fact that calls for as high an intermediate frequency as is reasonably attainable. But the noise figure of the amplifier becomes worse with increasing frequency. Furthermore, the ganging problem tends to increase in complexity when the local oscillator and preselector circuits are widely different in frequency, especially at lower radio frequencies. The final choice of the intermediate frequency is therefore one of compromise between the desired image-rejection ratio, on the one hand, and the desired sensitivity and the mechanical complexity that may be tolerated in the ganging of the r-f circuits, on the other.

The design of i-f amplifiers for use in wide-range receivers differs in several important respects from that used in fixed-frequency receivers, such as for most radar applications. The most widely used intermediate

frequency in radar receivers is 30 Mc. Initially, this value was chosen as a convenient one, without too great a justification.<sup>1</sup> Subsequent studies have proved that the choice was well taken; the 30-Mc i-f amplifier has no outstanding advantages over higher or lower frequency amplifiers, but at the same time, it suffers no major disadvantages. It gives adequate image spacing for radar purposes, allows sufficient ratio of intermediate to video frequencies for the separation of i-f components from the video-amplifier frequencies, and with available tubes gives good signal-to-noise ratio. It is relatively simple to manufacture and keep aligned in the field, especially in view of later circuit developments. In special cases where very great (i-f and video) band widths are required, and the problem of separation of the two is complicated, higher intermediate frequencies have been used. There is a tendency, however, to standardize on the 30-Mc figure because of the deterioration in signal-to-noise ratio and the increasing difficulty of manufacture and field servicing as the frequency increases.

The considerations involved in the choice of the intermediate frequency for the wide-tuning-range receiver are somewhat different. Preselection becomes of paramount importance, if a "single-signal" receiver is to be built, and, as a corollary, image spacing becomes a determining factor in image rejection. The early receivers designed to cover a wide band in the u-h-f range had tunable mixers, but these mixers were *not* ganged to the local oscillator. Therefore, regardless of the intermediate frequency, no image rejection was possible. As a result, the intermediate frequency chosen was one about which most was known, *viz.*, 30 Mc. But as techniques improved, ganging of mixer and oscillator was incorporated, and later ganged preselection ahead of the mixer. These advances have been necessarily paralleled by a change in intermediate frequency in order to achieve the greatest possible image rejection and thus to approach the ideal single-dial single-signal receiver. In a recent receiver covering the frequency range from 2000 to 4000 Mc, a 200-Mc i-f amplifier was employed which, with the ganged preselector used, gave an image-rejection ratio greater than 50 db.

The actual choice of intermediate frequency from the standpoint of image rejection must be made on the basis of the selectivity of the r-f circuits preceding the i-f amplifier. From the r-f selectivity curve, the desired image spacing for a given image rejection may be chosen, and the intermediate frequency required will be equal to one-half of this spacing times the oscillator harmonic utilized.

**33-3. Band Width and Selectivity Characteristics.**—The band-width and selectivity characteristics of the i-f amplifier are determined by

<sup>1</sup> FINK, DONALD G., "Radar Engineering," p. 267, McGraw-Hill Book Company, Inc., New York, 1947.

several considerations. First, the band width must be sufficiently wide to accept satisfactorily the intelligence being transmitted and sufficiently uniform throughout the acceptance band to reproduce this intelligence with the desired fidelity. For example, the band width required for a television amplifier is proportional to the number of picture elements transmitted, so that high definition requires large band widths. For reception of pulse transmissions, the situation is somewhat complicated by the variety of presentation methods, but for most purposes, a band width in megacycles equal to  $1.2/T$ , where  $T$  is the pulse length in microseconds, gives optimum signal-to-noise ratio. This consideration—adequate reproduction of the transmitted intelligence—sets the minimum band width necessary.

Second comes the problem of locating a signal that may be intermittent, as in pulsed transmission, or may be directionally radiated and sweeping in azimuth at the same time. One must then consider the probability that the receiver may be tuned through the frequency of the desired signal without producing a response. This is especially true in the higher frequency ranges for the following reason. In a tunable receiver, it is desirable to obtain the widest possible tuning range in each band. The r-f circuits usually employed limit this to about a 2- or 3-to-1 frequency range regardless of where the band is placed in the spectrum. In the higher frequency ranges, then, more megacycles are included between the upper and lower frequency limits, and in order to maintain the same probability of intercepting a given signal, it is necessary to increase the i-f band width as the r-f band is raised. In the frequency range up to about 1000 Mc, a 4-Mc band width has proved adequate from the probability standpoint. From 1000 to 3000 Mc, 10 Mc is a fair compromise, and above this, 20 Mc has been used. A third consideration is local-oscillator stability. The band must be sufficiently wide so that change of the local-oscillator frequency with time under the conditions of operation of the equipment will not cause the i-f output of the mixer to drift out of the acceptance band of the i-f amplifier.

It should be noted that the smallest band width consistent with these considerations should be used, as the noise figure of the amplifier deteriorates with increase in band width (see Sec. 33-4).

The selectivity characteristic desired is influenced by three factors: (1) the band width, (2) rejection to frequencies outside the pass band, and (3) transient response. The band width is fairly universally defined as the so-called 3-db band width. This band width  $\Delta f$  is that included between the two extreme half-power or 3-db points, using maximum gain as a reference level, with the qualification that, if the gain characteristic exhibits peaks, no dip shall be more than 3 db lower than any peak. The rejection for off-band frequencies is not so simply defined. Broad-

cast receiver practice is to define this rejection in terms of a figure called *adjacent-channel rejection ratio*. This figure is the ratio of the ordinates of the selectivity curve for the resonant frequency and another frequency differing from the resonant frequency by one channel width. It is difficult to apply this to the receivers under consideration for several reasons, the most important of which is the fact that there is no fixed "channel" width one can use for calculating the ratio. The r-f band covered is so large that many types of radio services are encountered, and even the channel used for the same service varies in width with the portion of the spectrum used. For this reason, another figure defining off-band rejection must be found. One that has proved useful is called the *60-to-6-db band-width ratio*. It is the ratio of the band widths at 60 db down from maximum gain to that at 6 db down. A figure of 2.5 has been used in specifications for military communications receivers; at the higher radio frequencies, a figure of 4 is considered adequate. Since wide ranges in the input signal level are often encountered, it is important that the off-band rejection, sometimes called *skirt selectivity*, be as high as possible in order to prevent strong signals close to the pass band from producing a response in the receiver.

Transient response, again, is determined by the service for which the receiver is used. If one is concerned with the steady-state operation, covering a large range of frequencies, it is better to have a gain characteristic with small dips and covering a wide band. If, on the other hand, good transient response is required, as in television, then the flat-topped curve is bad because it means overshoots. From a transient consideration, the rounded selectivity curve of synchronous single-tuned circuits<sup>1</sup> is best, and a compromise must be made between the desired transient response, skirt selectivity required, and gain-band-width products available with various types of couplings. For many applications, however, the flat-topped selectivity curve may be used with good results, and it will be the shape of curve considered for types of couplings other than synchronous single-tuning, because of the relatively simple mathematics involved.

**33-4. Noise in Intermediate-frequency Amplifiers.**—The general considerations of receiver noise and noise figure have been treated in Sec. 25-6. The noise generated in the crystal mixer has been discussed in Sec. 29-5. There are, however, additional sources of noise generated in the i-f amplifier that can have an appreciable effect on the over-all noise figure of the receiver.

It is well known that, since a current flow is a movement of discrete charges rather than the flow of a continuous "fluid," the random arrival

<sup>1</sup> The term *synchronous tuning* is used to designate a series of circuits tuned to the same frequency.

of these charges on a tube element, called *shot effect*, as well as the random division of the total space current between elements in multielement tubes, known as *partition effect*, produces noise in the circuit associated with this element. The rms fluctuation current, for example, from a temperature-limited diode, measured over a frequency band  $\Delta f$ , is given by<sup>1</sup>

$$I_n^2 = 2eI_{dc} \Delta f = 3.18 \times 10^{-19} I_{dc} \Delta f \tag{33-1}$$

where  $e$  = electron charge =  $1.59 \times 10^{-19}$  coulomb

$I_{dc}$  = direct diode current, amperes

$\Delta f$  = band width measured in cycles per second for which  $I_n$  is the rms noise current

The study of this noise has been extensive,<sup>2</sup> and the results can be presented in usable form. The conventional method of representation of this noise is to assume that the tube is noise free and that the noise in the plate circuit arises from the presence of a constant-voltage noise generator in series with the grid (see Fig. 33-1). The mean square voltage of this noise generator as given by Eq. (25-1) is  $E_n^2 = 4KTR_{eq} \Delta f$ , where  $R_{eq}$  is a fictitious resistance at room temperature of such value that if shunted across the input of a noise-free tube the noise current in the plate circuit is the same as that for the noisy tube with short-circuited input.<sup>3</sup> The equivalent noise resistance for triode amplifiers is then given by the equation<sup>4</sup>

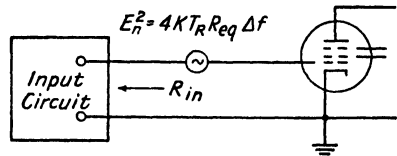


FIG. 33-1.—Circuit for inclusion of the effects of shot and partition noise.

$$R_{eq} = \frac{2.5}{g_m} \tag{33-2}$$

<sup>1</sup> SCHOTTKY, W., Spontaneous Current Fluctuations in Various Conductors, *Ann. d. Physik*, **57**, 541 (1918).

<sup>2</sup> A series of papers in the *RCA Review* under the title "Fluctuation Noise in Space-charge-limited Currents at Moderately High Frequencies" contains considerable information on the subject. They are Part I, B. J. Thompson, General Survey, **4**, 269 (1940); Part II, D. O. North, Diodes and Negative Grid Triodes, **4**, 441 (1940); **5**, 106 (1940); Part III, D. O. North, Multicollectors, **5**, 244 (1940); Part IV, B. J. Thompson and D. O. North, Fluctuations Caused by Collision Ionization, **5**, 371 (1941); Part V, W. A. Harris, Fluctuations in Vacuum Tube Amplifiers and Input Systems, **5**, 505 (1941); **6**, 114 (1941).

<sup>3</sup> Some Aspects of Radio Reception at Ultra High Frequency, Part II, L. Malter, Admittances and Fluctuation Noise of Tubes and Circuits, *Proc. I.R.E.*, **31**, 499 (1943).

<sup>4</sup> HARRIS, *loc. cit.*



and for pentode amplifiers by

$$R_{eq} = \frac{I_b}{I_b + I_{c2}} \left( \frac{2.5}{g_m} + \frac{20I_{c2}}{g_m^2} \right) \tag{33-3}$$

where  $g_m$  = grid-plate transconductance

$I_b$  = average plate current

$I_{c2}$  = average screen-grid current

At moderately high frequencies, this type of noise, *i.e.*, shot and partition noise, constitutes the major contribution of the tube to the total noise. At frequencies at which this is true, the noise figure of an amplifier stage is given by

$$F = 1 + \frac{R_{eq}}{R_{in}} \tag{33-4}$$

where  $R_{eq}$  is defined as above and  $R_{in}$  is the impedance looking from the grid toward the input terminals, as shown in Fig. 33-1. At 30 Mc

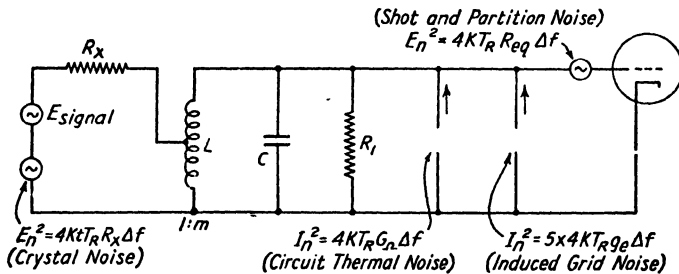


FIG. 33-2.—Complete equivalent circuit of input to first stage.

using both 6AK5's and 6AC7's, the measured noise figures check closely with those calculated from the above expressions; at 60 Mc, experimental results show that the formula still holds quite accurately for the 6AK5, but the figure is low for the 6AC7, and the deviation between theoretical and experimental results increases as the frequency is raised above 60 Mc.

North and Ferris<sup>1</sup> have indicated the probable source of the additional noise. They state that random variations in space current will induce current fluctuations in the control-grid circuit, giving rise to grid-voltage fluctuations proportional to the total input impedance (tube and circuit) and, for small transit angles, proportional to frequency. The results for oxide-coated cathodes show that the noise is equivalent to the thermal noise of a resistor of a value equal to the electronic loading of the grid circuit and at a temperature about five times room temperature. Fur-

<sup>1</sup> NORTH, D. O., and W. R. FERRIS, Fluctuations Induced in Vacuum-tube Grids at High Frequencies, *Proc. I.R.E.*, **29**, 49 (1941). Additional data are presented by G. E. Valley, in "Microwave Receivers," Radiation Laboratory Technical Series, Vol. 23, Chap. 4, McGraw-Hill Book Company, Inc., New York, 1946.

thermore, this work shows that, to a first approximation, induced grid noise may be added to the plate noise referred to the grid as though they were independent sources of noise.<sup>1</sup>

The equivalent circuit of the input to the i-f amplifier may then be drawn as in Fig. 33-2. The notation is

$T_r$  = room temperature, degrees Kelvin

$t$  = factor to give equivalent crystal temperature (see Sec. 29-5)

$R_x$  = i-f impedance of the crystal mixer

$R_{e,q}$  = equivalent noise resistance of the tube as defined above

$g_{\Omega}$  = input conductance due to circuit and leads

$g_e$  = input conductance due to electronic loading

$R_1 = 1/(g_{\Omega} + g_e)$

$\Delta f$  = band width of input circuit as defined in Eq. (25-7)<sup>2</sup>

It is common practice to use the transformed crystal impedance as the load on the first grid, the transformation being such that the band width of the input circuit is that desired. Then,  $R_1$  consists only of losses in the  $LC$  tuned circuit, plus lead and tube losses. The transformer may be, and usually is, a more complex circuit than that shown, in order that the maximum voltage gain be realized. That this is important, and also that a limit of desirable step-up exists, may be seen by consideration of the equivalent circuit.

First, neglecting the constant-current noise sources and considering only the shot noise, it is evident that the higher the voltage gain realized in the transformer between crystal and grid, up to the point at which an impedance match is obtained between  $R_x$  and  $R_1$ , the better the noise figure will be. This may also be seen from Eq. (33-4), where  $R_{in}$  increases with increase in step-up ratio. Under normal conditions,  $R_1$  is sufficiently high that the matched-impedance limitation on desirable transformation ratio is seldom reached before band-width considerations become the controlling factor. Second, when the constant-current noise sources are taken into account, it may be seen that the higher the input impedance of the tube, the larger the contributions these sources will make. The exact input impedance at which these sources become important depends on the frequency and the type of tube used. For the 6AK5 pentode at 30 Mc, the impedance for minimum noise figure (neglecting band-width considerations) is of the order of 10,000 to 12,000 ohms, decreasing to

<sup>1</sup> Work has been carried out that enables one to take into account the effect of induced grid fluctuations at higher frequencies, but that is beyond the scope of this chapter. See VALLEY, *loc. cit.*; and HEROLD, E. W., *An Analysis of the Signal-to-Noise Ratio of Ultra-high Frequency Receivers*, *RCA Rev.*, **6**, 320 (1942).

<sup>2</sup> For practical multistage amplifiers, this so-called *noise band width* is the same as the 3-db band width defined in Sec. 25-6.

about 500 ohms at 200 Mc. It is obvious, then, that band-width considerations will limit the step-up ratio at 30 Mc, for with ordinary input circuits 2000 ohms represents the required load for an amplifier of 6-Mc band width, and that under these conditions induced fluctuation noise is not too important. At higher frequencies, however, increasing importance of this source of noise may cause it, rather than band-width considerations, to limit the allowable step-up ratio in the input transformer.

The effect of grid-fluctuation noise is usually of second order. However, as tubes are developed that have reduced  $R_{eq}$ , and especially as new input circuits utilizing the much lower  $R_{eq}$  available with triode operation are devised,<sup>1</sup> the second-order effects become primary effects.

Certain other sources of noise exist but are of relatively small importance. Positive ion current to the control grid has a "shot" effect associated with it, producing a noise that may be represented by an equivalent resistance similar to that used with shot effect in the plate circuit:<sup>2</sup>

$$R_{eq} = 19.3I_g(Z_g)^2 \quad (33-5)$$

where  $I_g$  is the grid current in amperes and  $Z_g$  is the absolute value of the external circuit impedance connected between grid and cathode. Other sources include secondary emission and reflection of electrons from a virtual cathode.

It has been assumed thus far that all the noise developed in the i-f amplifier which contributes to the over-all noise figure comes from the first tube. This is very accurate for reasonably high stage gains; if stage gains are low, it is simple to include the effect of additional noise by use of the following formula:

$$F_{12} = F_1 + \frac{F_2 - 1}{g_1} \quad (33-6)$$

where  $F_{12}$  is the combined noise figure of two stages,  $F_1$  and  $F_2$  being the individual-stage noise figures, and  $g_1$  being the power gain of the first stage.

**33-5. Input Admittance of Vacuum Tubes.**—The input admittance of vacuum tubes used in i-f amplifiers is often of sufficient magnitude to affect seriously the amplifier performance if its presence is neglected. The literature dealing with the subject is extensive, and only the general results will be presented here, and the manner in which these affect the design problem pointed out.

<sup>1</sup> VALLEY, *loc. cit.*; VALLEY, G. E., and H. WALLMAN, "Vacuum Tube Amplifiers," Radiation Laboratory Series, Vol. 18, Chap. 18, McGraw-Hill Book Company, Inc., New York, (in press).

<sup>2</sup> TERMAN, F. E., "Radio Engineers Handbook," p. 316, McGraw-Hill Book Company, Inc., New York, 1943.

The input resistance can be due to four causes:<sup>1</sup>

1. Leakage current between the grid and other electrodes
2. Electronic and positive ion current due to grid collection or emission of electrons or ions
3. Coupling between the grid and any other electrode, the circuit of which contains an impedance of appreciable magnitude at the input frequency
4. Transit time of the electrons between cathode and grid

The input capacitance is also dependent on four factors:

1. The grid size and proximity to other electrodes at ground potential at the operating frequency
2. Space charge, which is equivalent to a reduced distance between cathode and grid
3. Coupling between the grid and any other electrode, the circuit of which has an impedance of appreciable magnitude at the operating frequency
4. Transit time of the electrons

In wide-band amplifiers, the impedance of the coupling network in the pass band is low compared with that ordinarily encountered in broadcast

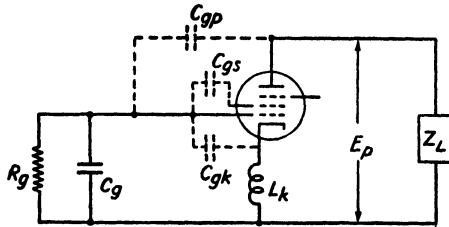


FIG. 33-3.—Equivalent circuit showing interelectrode coupling.

receiver i-f amplifiers or similar narrow-band applications. For this reason, certain effects may be neglected, and others, which are negligible in low-frequency narrow-band work, become major factors. At the present time, the great majority of wide-band i-f amplifiers have frequencies between 15 and 200 Mc, the largest groups being at 30 and 60 Mc. In this range, the largest part of the conductive portion of the input admittance of the tube is due to the coupling between the grid and other electrodes and to transit time of electrons, the former effect predominating at the frequencies and band widths under discussion.

To a first approximation, the resistive and capacitive components of the input admittance, as shown in Fig. 33-3, due to grid-plate capacitive coupling are given by the following formulas:

<sup>1</sup> STURLEY, K. R., "Radio Receiver Design," pp. 37-54, John Wiley & Sons, Inc., New York, 1943, presents a general discussion of causes of input admittance of vacuum tubes and a fairly complete discussion of that due to coupling between the grid and other electrodes.

$$R_o = - \frac{1}{A \sin \theta} \frac{\omega C_{gp}}{\omega C_{gp}} \quad (33-7)$$

$$C_o = C_{gp}(1 + A \cos \theta)^1 \quad (33-8)$$

where  $C_{gp}$  = grid-plate tube capacitance

$A$  = ratio of voltage developed across the load impedance in the plate circuit to the applied signal

$\theta$  = angle by which the voltage across the load impedance leads the equivalent voltage acting in the plate circuit

From Eq. (33-7), it may be seen that the resistive part of the input admittance may be either positive or negative depending on the phase angle of the load impedance  $Z_l$  and, therefore, may lead to regeneration of such a degree that oscillations occur. It may be shown that the gain of a single stage is limited by this condition to<sup>2</sup>

$$\text{Max gain} = \sqrt{\frac{g_m}{\pi f C_{gp}}} \quad (33-9)$$

where  $f$  is measured in cycles per second,  $g_m$  in mhos, and  $C_{gp}$  in farads. The actual allowable gain must be considerably less than this value, since regenerative effects must be kept small to prevent variation of selectivity with  $g_m$ .

A second source of input loading which can assume appreciable proportions is that due to inductance in the cathode lead. The input resistance resulting from this source is given by<sup>3</sup>

$$R_o = \frac{1}{\omega^2 g_m L_k C_{gk}} \quad (33-10)$$

where  $R_o$  = input resistance due to cathode-lead-inductance loading

$L_k$  = cathode lead inductance, henrys

$\omega$  =  $2\pi f$

$g_m$  = tube transconductance, mhos

$C_{gk}$  = grid-cathode tube capacitance, farads

<sup>1</sup> To obtain total input capacitance,  $C_{gk}$  and  $C_{gs}$  must be added to Eq. (33-8), where  $C_{gk}$  is the grid-cathode tube capacitance and  $C_{gs}$  is the grid-screen tube capacitance.

<sup>2</sup> A discussion of this condition as it applies to one, two, and three stages of amplification is given by B. J. Thompson, *Oscillation in Tuned Radio-frequency Amplifiers*, *Proc. I. R. E.*, 421 (1931).

<sup>3</sup> STRUTT, M. J. O., and A. VAN DER ZIEL, The Causes for the Increase of the Admittance of Modern High-frequency Amplifier Tubes on Short Waves, *Proc. I. R. E.*, 26, 1011 (1938).

For a 6AK5 tube operating at 200 Mc, this loading resistance may be as low as 1000 ohms unless proper precautions are taken. It has been found advisable when operating at frequencies where this loading is important to use a cathode by-pass condenser that is in approximate series resonance with the lead inductance. Care must be taken that this resonance is at a higher frequency than the operating frequency; otherwise the input resistance from this source will be negative. Other methods have been suggested for the neutralization of this loading where high- $Q$  input circuits are desired.<sup>1</sup> However, because only wide-band amplifiers involving relatively low values of  $Q$  are under consideration, approximate methods of neutralization, such as the resonance method suggested above, are sufficient to decrease the input admittance to such a value that it plays no adverse part in the loading of the input circuit. It is also of interest to note that this input loading is in the nature of a degenerative feedback affecting both signal and noise equally and, as such, does not enter into the noise calculations.<sup>2</sup>

Although the loading due to transit time is an important consideration from the noise standpoint, it is not very serious as a source of resistive load because of the heavy loading required to obtain the band widths under consideration. Ferris has shown that the loading due to the transit time of the electrons between cathode and grid is<sup>3</sup>

$$R_o = \frac{1}{kg_m f^2 \tau^2} \quad (33-11)$$

where  $g_m$  = tube transconductance

$f$  = frequency

$\tau$  = time required for the electron to travel from cathode to grid

$k$  = a constant determined by grid and plate voltages and by the ratio of transit times from cathode to grid and grid to plate

It is important to note that the effect increases as the square of the frequency, so that the transit-time loading may become of interest if the intermediate frequencies are pushed higher; but with present frequencies and tubes, its effect on the input loading is small compared with grid-plate feedback and cathode-lead-inductance loading.

The loading from the other sources mentioned—leakage current between the grid and other electrodes, and electronic and positive ion current due to grid collection or emission of electrons or ions—is practi-

<sup>1</sup> FREEMAN, R. L., Input Conductance Neutralization, *Electronics*, **12**, 22 (1938).

<sup>2</sup> STRUTT, M. J. O., and A. VAN DER ZIEL, Methods for the Compensation of the Effects of Shot Noise in Tubes and Associated Circuits, *Physica*, **8**, 1 (1941).

<sup>3</sup> FERRIS, W. R., Input Resistance of Vacuum Tubes as Ultra-high-frequency Amplifiers, *Proc. I. R. E.*, **24**, 82 (1936).

cally negligible under ordinary conditions encountered in wide-band amplifiers.

The input capacitance, mentioned above, is composed of the so-called *cold* capacitance, the capacitance between the grid and the grounded electrodes such as cathode and screen when no space current is present; an increase in the cold capacitance caused by the presence of space charge when the tube is conducting, which has the effect of a reduced distance between grid and cathode and is a function of the space current; and a reflected reactance caused by coupling between the grid and any other electrode, the circuit of which has an impedance of appreciable magnitude at the operating frequency. The latter component of the total capacitance usually results almost entirely from the coupling between grid and plate, see Eq. (33-8), and is also a function of the gain of the tube. A variation in input capacitance is obviously encountered with variation in gain, and various methods have been devised to neutralize this change.<sup>1</sup> These methods involve a loss in gain, which is serious in wide-band high-gain amplifiers where stage gain is usually low and a large number of tubes are required to obtain the desired over-all gain. In addition, because of the low-stage gain, the percentage variation of total input capacitance is relatively small with variation in gain. It is not common, therefore, to attempt to compensate for the change in capacitance in these amplifiers.

**33-6. Gain.**—As mentioned in Sec. 25-5, the receiver sensitivity is limited by receiver noise, and for good performance, this noise must be amplified so as to give sufficient output for the type of use for which the receiver is designed. If signals down to noise level are to be detected adequately, it is necessary to raise the noise to a level sufficient to produce linear operation of the second detector. The minimum level at which the usual second detectors operate linearly is about  $\frac{1}{2}$  to 1 volt. This also is a convenient input level for the various types of presentation circuits.

From the information presented in Sec. 25-6, 29-5, and 33-4, it is possible to make rough calculations as to the total noise power present at the grid of the first tube for a given band width and frequency. From the noise power and input impedance at the first grid, it is possible to calculate the rms noise voltage that must be amplified to the desired level at the second detector, and therefore the total required gain can be determined. For purposes of this calculation, it is safe to neglect the effect of transit-time noise for all ordinary cases, as this assumption will

<sup>1</sup> FREEMAN, R. L., Use of Feedback to Compensate for Vacuum-tube Input-capacitance Variations with Grid Bias, *Proc. I. R. E.*, **26**, 1360 (1938); FARRINGTON, J. F., Compensation of Vacuum Tube Input Capacitance Variation by Bias Potential Control, *R. M. A. Eng.*, **4**, 13 (1937).

result in a required gain figure that is slightly greater than actually needed.

**33-7. General Serviceability and Tube-constant Variations.**—The designer of any electronic equipment is always faced with the problem of utilizing commercially available components that may be interchanged without seriously affecting performance and of putting these components together in such manner that maximum ease of servicing is attained. A high degree of conformity of techniques has been developed through the necessity of military standardization that may well be carried into commercial practice. For example, two tubes are used almost exclusively in the type of amplifiers under consideration, the 6AC7 and 6AK5. Numerous miniature components have been developed which are being widely used with excellent results.

One of the more significant advances has been in the development of the so-called *button and feed-through capacitors* (see Fig. 33-18). These find numerous applications in this work because of their small size and low inductance and are excellent for use in decoupling circuits. Improvements in the characteristics of all miniature components have been made, so that a wide variety is available. These small components aid in lowering stray capacitances to ground, a reduction that is equivalent to an effective increase in gain band-width product.

The variation in transconductance and capacitances from tube to tube also presents special problems to the designer. For example, the manufacturer's tolerances for the 6AK5 are as follows:

$g_m$ .....	3500-6500 $\mu\text{mhos}$
$C_{pk}$ .....	3.4-4.4 $\mu\mu\text{f}$
$C_{pb}$ .....	2.45-3.25 $\mu\mu\text{f}$

If an amplifier is to be constructed that will operate satisfactorily, independent of the tube changes, the necessary gain must be obtained with minimum- $g_m$  tubes, yet the amplifier must show no regenerative tendencies with high- $g_m$  tubes. This imposes severe restrictions on the designer, especially in the construction of high-gain multistage amplifiers; for the additional gain when shifting from low to high  $g_m$  tubes can be of the order of 5.5 db per stage. In addition to handling the increased  $g_m$  from tube to tube under the same operating conditions, it is also necessary to handle  $g_m$  changes due to power-supply variations. Although the i-f amplifier is often operated from a regulated power supply, checks for regeneration are made at plate voltages 50 per cent greater than the operating voltage. It is interesting to note that the variation of  $g_m$  between tubes is considerably less if cathode bias is used rather than fixed bias. The problem of building a stable amplifier with unse-



lected tubes demands the utmost care in physical layout and electrical decoupling.

In addition, the variation of capacitance from tube to tube must be considered if fixed-tuned coils are used in the interstage coupling network. Fortunately, although the allowable variation of  $C_{gk} + C_{gp}$  in 6AK5's is  $\pm 0.9 \mu\mu\text{f}$ , it has been found that 90 per cent of the tubes have variations of only  $\pm 0.45 \mu\mu\text{f}$ . Even this variation becomes of importance when intermediate frequencies greater than 60 Mc are employed. At 30 Mc, fixed-tuned coils are used to a large extent for wide-band i-f amplifiers, but if narrow bands with steep "skirts" are necessary, detuning with variation of tube capacitances becomes sufficiently important so that tunable coils are required.

Good physical layout is a somewhat nebulous term. It depends on so many variable factors that it is only possible to speak in generalities. In Sec. 33-13 there is presented a discussion of physical factors affecting regeneration that might well come in this section. The electrical and physical design are closely allied, and it has been found from experience that good electrical design results in a good mechanical layout. An example of the use of miniature components in a layout that provided both ease of servicing and good electrical characteristics is shown in Fig. 33-18.

**33-8. Interstage Coupling Methods.**—The network used as coupling between amplifier tubes determines the selectivity characteristic of the amplifier and, in conjunction with the amplifier tube, also determines the gain. In general, the voltage amplification of an amplifier stage as a function of frequency may be expressed by

$$\text{Gain} = g_m Z(\omega) \quad (33-12)$$

where  $g_m$  is tube transconductance and  $Z(\omega)$  the transfer impedance of the interstage network as a function of frequency.

If this function is plotted, the resulting curve is the selectivity characteristic of the single stage, the over-all characteristic being obtained by multiplying the gain functions of the various stages. In the next three sections, some of the common coupling networks are discussed and their relative advantages and disadvantages evaluated.

**33-9. Single-tuned Coupling.**—The simplest coupling method used in wide-band i-f amplifier construction is the single-tuned network, *i.e.*, each interstage coupling network consists of a single inductance and single capacitance (usually the tube plus stray capacitance) in parallel, damped by the appropriate resistance load, and the successive interstage networks are all resonant at the same frequency. The advantages of such a "synchronous" single-tuned amplifier are

1. Simplicity of design and construction
2. Ease of initial and field alignment
3. Good transient response
4. Relative freedom from critical loading and tuning.

The disadvantages of this type of amplifier for wide-band high-gain applications are

1. Number of stages restrictive for band widths greater than 2 to 3 Mc
2. Impracticability or impossibility of obtaining necessary gain for band widths greater than 4 Mc
3. Low "skirt" selectivity

It is of interest to consider in some detail this type of coupling in order to develop the basic set of values that may be used as a reference for evaluating more complex coupling schemes. The essential components of a single-tuned stage are shown in Fig. 33-4, in which the d-c returns are neglected. The notation is as follows:

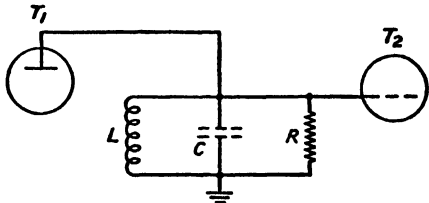


FIG. 33-4.—Elements of a single-tuned coupling network.

$$C_T = C_{inputT_2} + C_{outputT_1} + C_{strays}$$

$R$  = damping resistance including effects of plate resistance of  $T_1$ , input resistance of  $T_2$ , and shunt resistance of  $L$  and  $C$ , as well as of the damping resistor itself

$L$  = inductance to resonate with  $C_T$  at  $\omega_0 = 1/\sqrt{LC_T}$

The voltage-gain function for this network from grid of  $T_1$  to grid of  $T_2$  is

$$\text{Gain} = g_m Z(\omega) = g_m \frac{R}{1 + jQ \left( \frac{\omega}{\omega_0} - \frac{\omega_0}{\omega} \right)} \tag{33-13}$$

where  $g_m$  = tube transconductance

$$Q = \omega_0 RC_T$$

$$\omega = 2\pi f$$

For values of  $\omega$  close to  $\omega_0$ , this reduces to

$$\text{Gain} = g_m \frac{R}{1 + j2RC_T(\omega - \omega_0)} \tag{33-14}$$

Equation (33-13) is the exact form of the gain function, displaying geometric symmetry, while Eq. (33-14), the approximate form, may be used for circuits the band width of which is small compared with

the resonant frequency, *i.e.*, high- $Q$  circuits, and displays arithmetic symmetry.

In Eqs. (33-13) and (33-14), the half-power points occur when  $Q \left( \frac{\omega}{\omega_0} - \frac{\omega_0}{\omega} \right) = \pm 1$  and  $2RC(\omega - \omega_0) = \pm 1$ , respectively. In both cases, this gives

$$\Delta f = \frac{1}{2\pi RC} \quad (33-15)$$

an equation that incidentally shows that the band width for a given interstage capacitance and damping resistor is independent of center frequency. Also, since  $Q = \omega_0 RC = 2\pi f_0 RC$

$$Q = \frac{f_0}{\Delta f} \quad (33-16)$$

If we now multiply Eqs. (33-13) and (33-15) or (33-14) and (33-15) for  $\omega = \omega_0$ , we find that the resulting product is a constant.

$$\text{Gain} \times \text{band width} = \frac{g_m}{2\pi C_T} \quad (33-17)$$

The value of this constant is indicative of the merit of the stage. If the product is large, then, for a given band width a relatively larger gain may be obtainable. It also shows that gain and band width are inseparable; one can be increased by a sacrifice in the other, but the product of the two for a single-tuned stage is a constant dependent only on the tube transconductance and the total interstage capacitance.

When a number of identical single-tuned amplifier stages are connected in cascade, the over-all selectivity function becomes the product of the individual selectivity functions. This reduces to

$$\text{Over-all band width} = (\text{one-stage band width}) \times \sqrt{2^{1/n} - 1} \quad (33-18)$$

where  $n$  is the number of tuned circuits. The value of the expression  $\sqrt{2^{1/n} - 1}$  as a function of  $n$  is shown in the lower curve of Fig. 33-5. It is obvious from the curve that, as the number of stages is increased, the band width of the individual stages must increase rapidly in order to maintain the same over-all band width. The series of curves of Fig. 33-6 shows the available gain for a given band width as a function of the number of stages for the two most commonly used tubes, the 6AC7 and the 6AK5. It may be seen that for relatively narrow band widths a single-tuned amplifier will give high gain for a reasonable number of tubes; but as the band width increases beyond .4 Mc, it is not only impractical but often impossible to obtain the necessary gain, since the over-all gain actually becomes less with additional stages. This is shown

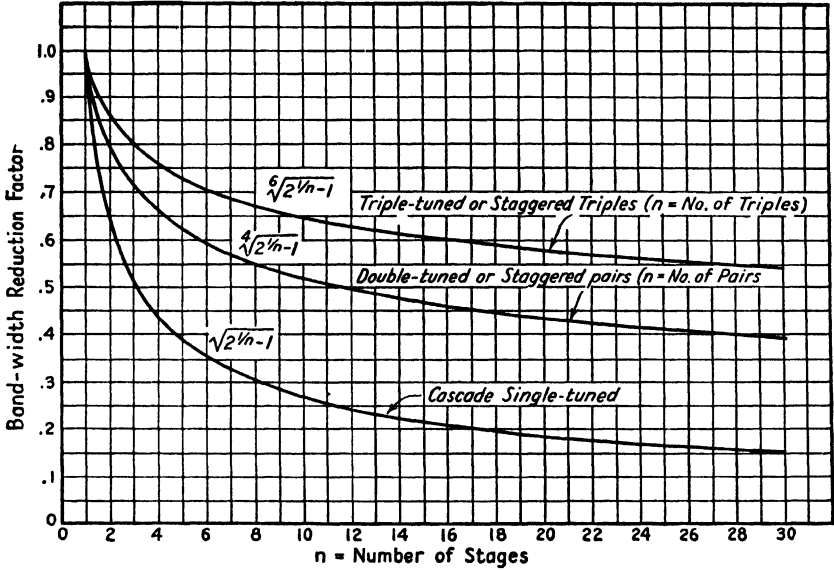


FIG. 33-5.--Band-width reduction factor for various types of coupling networks as a function of the number of cascaded stages.

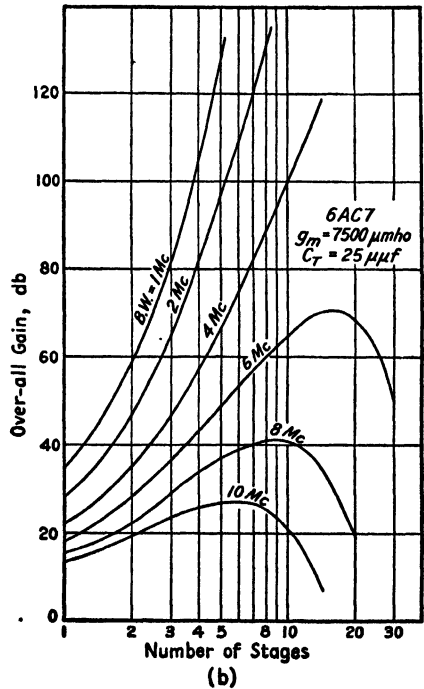
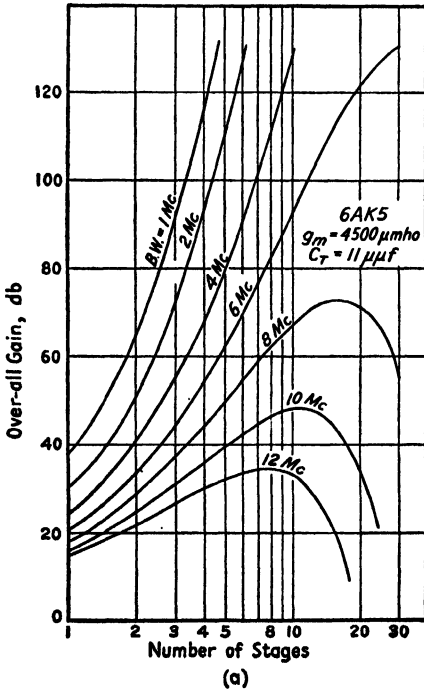


FIG. 33-6.—Available gain for a given over-all band width plotted as a function of the number of synchronous single-tuned stages employed.

with greater emphasis by replotting the results in the form of Fig. 33-7, determining for a given gain the maximum band width obtainable, regardless of the number of stages. This limitation is a serious one, for high gain and wide band together are necessary in i-f amplifiers for the type of receiver under consideration. A gain of 100 db is commonly needed, and the maximum band width theoretically obtainable, with the best tube now in production, the 6AK5, is only 6.9 Mc, which for many applications is inadequate. In addition, the ridiculous number of 23 stages is needed to accomplish even that result.

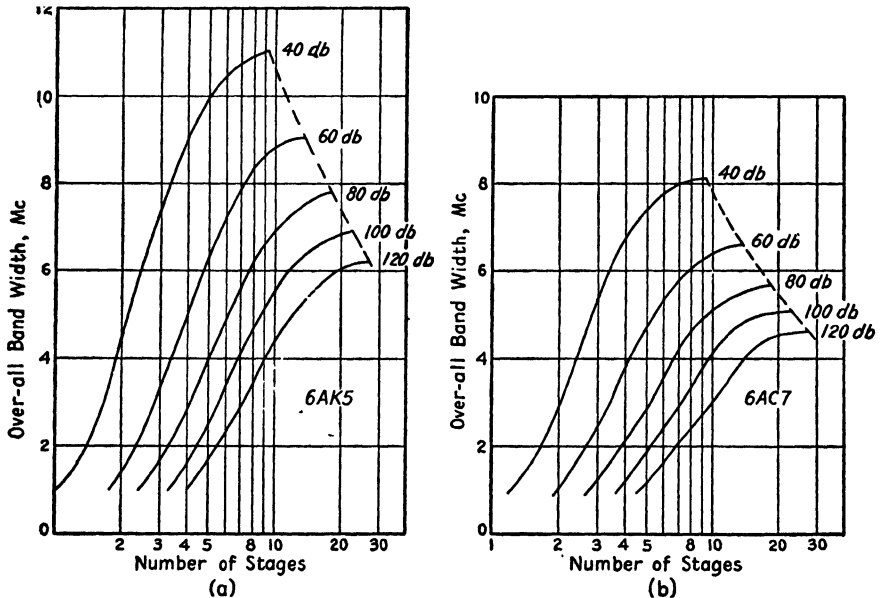


FIG. 33-7.—Available band width for a given gain plotted as a function of the number of synchronous single-tuned stages employed. The dotted curve connects the points of maximum band width attainable with a given over-all gain, regardless of the number of stages used.

The skirt selectivity of an amplifier using synchronous single-tuned circuits, as defined by the 60:6-db ratio, is not high. A typical amplifier using 6AC7 tubes has five single-tuned stages, each of band width slightly greater than 5 Mc centered at 30 Mc. A gain of approximately 90 db with a 3-db over-all band width of 2 Mc was realized, but the 60:6-db ratio was 8.9.

**33-10. Multituned Coupling Networks.**—The single-tuned amplifier attains simplicity at the sacrifice of certain desirable characteristics. If one is willing to sacrifice this simplicity, advantages may be gained. Traditionally, the next step is to use the double-tuned coupling network; two tuned circuits are coupled by any one of a number of methods, the

result being a greater gain per stage, flatter response in the pass band, and steeper skirts; in addition, the over-all band width goes down more slowly as identical stages are cascaded, as shown in Fig. 33-5. The disadvantages are, of course, more elements in the coupling network, more tuning adjustments, which unfortunately are not independent of each other, and a transient response with larger overshoots than for the single-tuned amplifier, especially when the circuits are overcoupled.

The more common methods of coupling using multituned networks are covered extensively in the literature.<sup>1</sup> A form that has been found useful in wide-band amplifiers converts the ordinary transformer-coupled circuit to its equivalent  $\pi$  or  $T$ . Since the derivation is based on the transformer-coupled case, a few basic relations of this circuit are given here. The circuit and notation are shown in Fig. 33-8. At the fre-

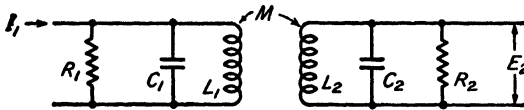


FIG. 33-8.—Equivalent circuit for a double-tuned mutually coupled interstage network.

quencies commonly used, *i.e.*, 30 Mc and above,  $C_1$  and  $C_2$  consist of the tube and stray capacitances associated with the output and input circuits, respectively. The condition of transitional coupling<sup>2</sup> results in the so-called *flat-topped* selectivity curve. While this is not necessarily the ideal curve,<sup>3</sup> it is by far the most feasible to handle mathematically and is the characteristic usually used in design work. The ordinary condition of loading is with equal  $Q$ 's in the primary and secondary, for this condition is the least critical of alignment and least sensitive to tube changes. More gain may be obtained by loading on one side only, but except for the input circuit to the first i-f stage where the crystal impedance is transformed to the proper grid impedance, this form of loading is rarely used.

<sup>1</sup> AIKEN, C. B., Two-mesh Tuned Coupled Circuit Filters, *Proc. I.R.E.*, **25**, 230; 672 (1937); TERMAN, F. E., "Radio Engineers' Handbook," pp. 151-164, McGraw-Hill Book Company, Inc., New York, 1943; STURLEY, K. R., "Radio Receiver Design," pp. 137-148, John Wiley & Sons, Inc., New York, 1943.

<sup>2</sup> Aiken defines transitional coupling as that coupling for which the transition from a single-peaked to two-peaked selectivity characteristic takes place. A more general definition, which is not limited to only two coupled circuits, is that transitional coupling exists when

$$\frac{dZ_{12}}{df} = \frac{d^2Z_{12}}{df^2} = \frac{d^3Z_{12}}{df^3} = 0$$

where  $Z_{12}$  is the transfer impedance of the coupling network. The frequency  $f_0$ , where this occurs is defined as the center frequency.

<sup>3</sup> See Sec. 33-3.

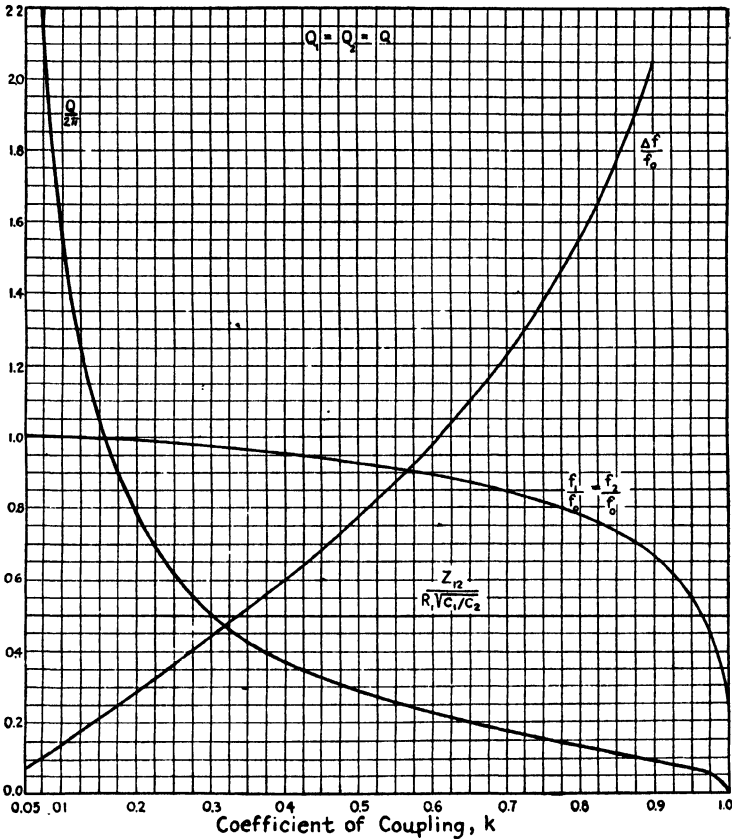


FIG. 33-9.—Design curves for determining the constants of a transitionally coupled double-tuned coupling network for the case of equal primary and secondary  $Q$ 's.

Figures 33-9 and 33-10 result from an exact analysis of transitional coupling for the double-tuned circuit of Fig. 33-8.<sup>1</sup> The notation is

$$Z_{12}(f) = \text{magnitude of the transfer impedance} = \left| \frac{E_2}{I_1} \right|$$

$$k = \text{coefficient of coupling} = \frac{|M|}{\sqrt{L_1 L_2}}$$

$$f_0 = \text{center frequency, defined by } \frac{dZ_{12}}{df} = \frac{d^2 Z_{12}}{df^2} = \frac{d^3 Z_{12}}{df^3} = 0$$

$$f_1 = \text{primary frequency} = \frac{1}{2\pi \sqrt{L_1 C_1}}$$

$$f_2 = \text{secondary frequency} = \frac{1}{2\pi \sqrt{L_2 C_2}}$$

<sup>1</sup>The following curves and example are from an unpublished report of C. P. Gadsden, Radiation Laboratory, Massachusetts Institute of Technology.

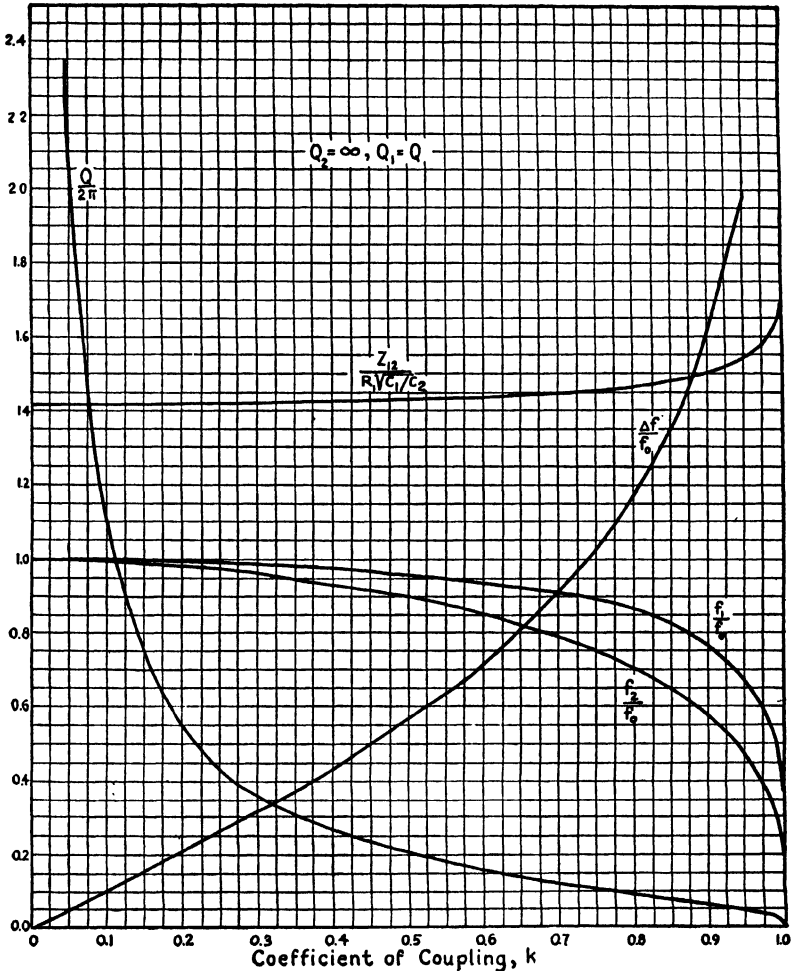


FIG. 33-10.—Design curves for determining the constants of a transitionally coupled double-tuned coupling network loaded on one side only.

$$Q_1 = \text{primary } Q = 2\pi f_1 R_1 C_1; \quad Q_2 = \text{secondary } Q = 2\pi f_2 R_2 C_2$$

$$\Delta f = \text{band width between 3-db points of a single stage}$$

$$G \times BW = g_m Z_{12}(f_0) \times \Delta f$$

The use of these curves is straightforward. Figure 33-9 is for the case of equal  $Q$ 's and Fig. 33-10 for loading on one side only. As an example of the use of the curves, suppose that four stages of transitionally coupled double-tuned circuits are to be cascaded to give an over-all band width of 10 Mc centered at 30 Mc. From Fig. 33-5, the band-width reduction factor is 0.67, so that the band width of the individual stages must be  $10/0.67 = 15$  Mc. Assume  $C_1 = 4 \mu\mu\text{f}$  and  $C_2 = 8 \mu\mu\text{f}$  (approximate



values for the 6AK5) and equal primary and secondary loading. Then  $\Delta f/f_0 = 1\frac{5}{30} = 0.5$ , and from the curves for this value,

$$k = 0.337$$

$$\frac{Q}{2\pi} = f_0 R_1 C_1 = f_0 R_2 C_2 = 0.450$$

$$\frac{f_1}{f_0} = \frac{f_2}{f_0} = 0.967$$

and

$$\frac{Z_{12}}{R_1 \sqrt{\frac{C_1}{C_2}}} = 0.50$$

Then

$$R_1 = \frac{0.45}{30 \times 10^6 \times 4 \times 10^{-12}} = 3750 \quad \text{ohms}$$

$$R_2 = \frac{C_1}{C_2} R_1 = 1875 \quad \text{ohms}$$

$$f_1 = f_2 = 0.967 \times 30 = 29 \quad \text{Mc}$$

$$Z_{12} = 0.5 \times 3750 \sqrt{\frac{4}{8}} = 1325 \quad \text{ohms}$$

From the latter figure, the gain-band-width product is 89 Mc (assuming  $g_m = 4500 \mu\text{mhos}$ ), which means a stage gain of  $89/15 = 5.9$ , whereas

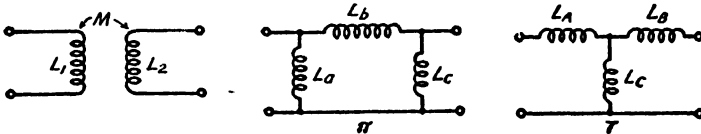


Fig. 33-11.—Equivalent circuits for the case of double-tuned coupling networks.

a single-tuned circuit of the same band width working between the same capacitances would have a product of 59.6 Mc or a stage gain of 4.0. In addition, four single-tuned stages in cascade would give an over-all band width of 6.5 Mc, as compared with 10 Mc.

This form of the double-tuned circuit is somewhat difficult to handle at these frequencies with respect to adjusting for proper  $k$ . By converting the mutually coupled system to its equivalent  $\pi$ - or T-form, each element of the network becomes a physical self-inductance. The conversion formulas are as follows, using the notation of Fig. 33-11:

$$\left. \begin{aligned} L_a &= \frac{L_1 L_2 - M^2}{L_2 - M} \\ L_b &= \frac{L_1 L_2 - M^2}{M} \\ L_c &= \frac{L_1 L_2 - M^2}{L_1 - M} \end{aligned} \right\} \quad (33-19)$$

$$\left. \begin{aligned} L_A &= L_1 - M \\ L_B &= L_2 - M \\ L_C &= M \end{aligned} \right\} \quad (33-20)$$

It is important in the use of these equivalents to reduce the mutual coupling between the inductive elements to a minimum. One coil form used in the equivalent  $\pi$ -section network is shown in Fig. 33-12. The three inductances are wound on the same form with short-circuited turns separating them. These short-circuited turns reduce the mutual coupling between inductances to a negligible quantity and, in addition, serve as lead supports. In the receiver illustrated in Fig. 25-6, the T equivalent is used; the structure employed is shown in Fig. 33-13. In this receiver the i-f amplifier had a band width of 4 Mc centered at 30 Mc and a gain, including the second detector, of approximately 90 db.

In general, the double-tuned circuit has a gain-band-width product of  $\sqrt{2} \times \frac{g_m}{2\pi C_T}$  where  $C_T = C_1 + C_2$

(see Fig. 33-8) and  $C_1 = C_2$ . If  $C_1 \neq C_2$ , this factor is increased in the ratio  $(C_1 + C_2)/2\sqrt{C_1 C_2}$

This advantage over the single-tuned circuit is often of importance where large band widths are required and stage gain is low.

If more than two tuning elements are employed, the selectivity characteristic becomes more nearly square, the skirt selectivity becoming greater as a consequence, and the gain-band-width factor increases. Since the selectivity characteristic is more nearly square, the over-all band width decreases even more slowly as stages are cascaded, as shown in the top curve of Fig. 33-5 for the triple-tuned case. The greater complexity, however, makes the addition of tuning elements impractical, and few applications have been made.

As already mentioned, one of the disadvantages of double tuning is the difficulty in alignment. Normally, this must be done stage by stage, and is a tedious procedure, even with the aid of a "wobulated" or sweeping-frequency signal generator.

An interesting method of aligning double-tuned i-f amplifiers that aids in rapid and simple field alignment is described here. Practically no test equipment or skill is necessary to align the amplifier, only a communications receiver of the proper frequency range, and sometimes an ordinary a-c voltmeter. This method is useful, however, only when a number of identical i-f amplifiers are to be aligned and only when these

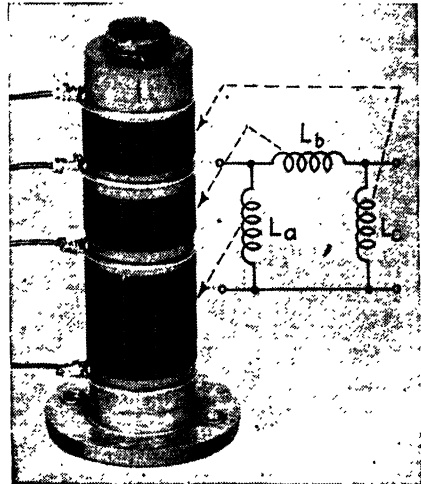


FIG. 33-12.—A coil form for a  $\pi$ -section coupling network.

amplifiers have been properly designed in the first place. Furthermore, the method applies to field or production-line alignment, and not to the laboratory design problem.

To explain the principle of operation, one first assumes two signal sources feeding into the amplifier and a selective output meter tuned to the difference frequency between the signal sources and connected following a detector; one may then adjust the tuning and coupling of one interstage transformer for maximum output. When this condition is reached, the product of the responses of the *stage being tuned* at the two frequencies of the signal sources has been maximized. If the signal frequencies are correctly chosen and the interstage network has been properly

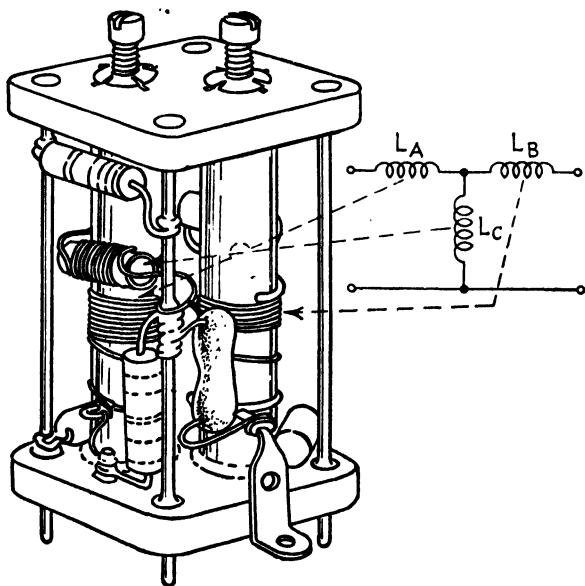


Fig. 33-13.—A coil form for a T-section coupling network.

designed, *i.e.*, if the variable elements are adjustable over a range large enough to include the proper value, and if the damping is correct, the resultant response curve may be shown to be of optimum shape. Random noise in the *i-f* stage, if of sufficient magnitude to give a measurable output from the second detector, will perform the same function as the two signals assumed. If receiver noise is not sufficient, a noise source may be connected to the input. For example, if the response curve is double-peaked and the selective device tuned to this peak separation, then all beats obtained from the noise components of frequency difference equal to this separation will add in the output. Those components actually at the proper peak frequencies will produce the predominant products.

The receiver second detector, then, produces the beats, the video

amplifier removes i-f components, and the communications receiver provides the selective amplifier and output meter; if no output meter is available on the receiver, an ordinary a-c voltmeter of practically any type plugged in the audio jack or across the output transformer will suffice. For a given type of i-f amplifier, it is necessary to determine the proper frequency setting of the selective device in order to obtain an optimum selectivity characteristic. As mentioned above, for a double-peaked curve, a setting equal to the desired peak separation is usually a good approximation, and a few trials of settings slightly above or below this value should produce a value that may be used in aligning all other i-f amplifiers of the same design.

For instance for the double-peaked response, it was pointed out that the proper setting is that for the peak separation rather than the desired 3-db band width; the relation between these must be determined. The setting is usually about three-fourths of the desired band width; for a particular amplifier with a band width of 4 Mc, a setting of 2.8 Mc gave the proper shape, as shown in Fig. 33-14. The order in which the stages are tuned has no effect on the final selectivity curve, except where feedback across the plate-grid path is appreciable.

**33-11. Stagger Tuning.**<sup>1</sup>—One of the most significant contributions in the field of wide-band high-gain i-f amplifiers has been the refinement and development of the theory of stagger tuning. Although the basic concepts were published some years ago,<sup>2</sup> there had been until recently only very limited applications in this country. Within the last few years the theory has been independently developed in this country, and extensive applications have been made. The method of stagger tuning provides the best solution to the construction of practical i-f amplifiers with high gain and wide bands. Although stagger tuning may be applied to amplifiers using multituned coupling networks in order to increase the gain-band-width product, its real value is in its application to the single-tuned amplifier.

<sup>1</sup> This section is condensed from unpublished material by H. Wallman of Radiation Laboratory. A complete discussion of the theory and application of stagger tuning, including a bibliography, is given by Valley and Wallman, *op. cit.*, Chap. 6.

<sup>2</sup> BUTTERWORTH, S., On the Theory of Filter Amplifiers, *Wireless Eng.*, 7, 536-541 (1930); SCHIENEMANN, R., Tragerfrequenzverstärker grosser Bandbreite mit gegeneinander verstimmteten Einzelkreisen, *Telegraphen-Fernsprech-Funk und Fernseh-Technik*. January, 1939, pp. 1-7.

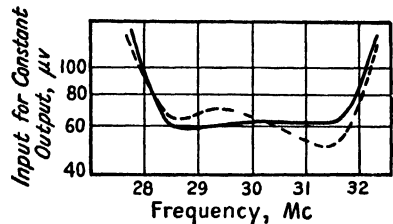


FIG. 33-14.—Response curves for an i-f amplifier showing the results of the noise method of alignment: dashed line, response of amplifier as received from factory; solid line, response after realignment by noise method.

As pointed out in Sec. 33-9, the greatest advantage of the single-tuned amplifier is in its simplicity of manufacture and ease of alignment. The disadvantages are brought out by Figs. 33-6 and 33-7; when wide band and high gain together are necessary, cascade single-tuning not only involves an unreasonable number of tubes but often fails entirely to achieve the desired result. The most desirable system of coupling would be one that retained the simplicity of the single-tuned network but that had a greater gain-band-width product and greater skirt selectivity. By suitably staggering in frequency and adjusting the  $Q$ 's of the single-tuned circuits, this system can be approached. It is conceivable that the design specifications might be such that an additional increase in gain-band-width product over that available with stagger tuning would be needed to make an amplifier possible, *i.e.*, with band widths of 75 or 100 Mc. But for the designer of the type of wide-band high-gain i-f amplifiers with which this book deals, *i.e.*, with bands from 2 or 3 to 20 or 30 Mc wide and gains of 80 to 115 db, the stagger-tuning method is the most practical because of its outstanding simplicity and economy.

The advantages of stagger tuning are of two types: (1) The mechanical simplicity of construction of the cascade single-tuned amplifier is retained, and to a great extent, the simplicity of alignment. (2) The improved gain-band-width product and skirt selectivity increase the attainable band width to a point where one may successfully utilize single-tuned coupling networks for most present-day wide-band high-gain applications. A few examples may show this more clearly than would a theoretical discussion.

The simplest case of stagger tuning is the staggered pair. First, let us express the gain-band-width product in units of  $g_m/2\pi C_T$  and call this the *gain-band-width factor*. The gain-band-width factor for a single-tuned stage will, therefore, be unity. If two single-tuned circuits of a given band width have resonance peaks staggered by an amount equal to their band width, the resultant band width will be  $\sqrt{2}$  times as great as that of each individual circuit, the over-all selectivity function will be in both absolute value and phase that of a transitionally coupled double-tuned circuit, and the gain-band-width factor, *viz.*, the *individual stage-gain times over-all band width*, for the *combination* will be 1. From the curves of Fig. 33-5 for cascaded single-tuned stages, we find that if these two stages were tuned to the same frequency the stage-gain times over-all band-width factor would be only 0.644, so that the staggered pair represents an improvement of  $1/0.644$  or 1.55. The advantages are obvious. Since the staggered pair has the same selectivity curve as that of the transitionally coupled double-tuned circuit, the over-all band width goes down less rapidly when the pairs are cascaded than when synchronous single-tuned stages are cascaded. This may be seen from the curve of

Fig. 33-5 for the transitionally coupled double-tuned amplifier, if one remembers that each *pair* of stages in the stagger-tuned amplifier corresponds to one double-tuned stage. In a six-stage amplifier, for example, three staggered pairs will have *twice* the band width for the same gain as six synchronous stages. This improvement has been made with only one sacrifice in simplicity: the alignment must be made in two steps instead of one, but no additional elements have been added. To some extent, however, the noncriticalness of the synchronous tuning is lost.

If one is willing to use three settings of the signal generator when aligning the amplifier, further increase in the gain-band-width factor may be made. If three stages are properly loaded and staggered, the over-all selectivity function will be in both phase and absolute value that of a transitionally coupled triple-tuned circuit, and the stage-gain times over-all band-width factor will be 1. Since the factor for three synchronous stages is 0.51 (Fig. 33-5), the staggered triple is superior by a ratio of  $1/0.51$ , or 1.96.

This staggering may be carried to any number of stages, depending only on the extent to which one is willing to sacrifice simplicity for improved characteristics. This sacrifice is not very great as it entails only the tuning of a circuit to an additional frequency, and each adjustment is independent of all others.

**33-12. Design of a Stagger-tuned Amplifier.**—The design of a stagger-tuned amplifier is extremely simple. Figures 33-15 and 33-16 contain all the necessary information to design i-f amplifiers using staggered pairs and staggered triples. The method is best demonstrated by an example.

An amplifier is to be built using 6AK5's with a band width of 12 Mc, centered at 30 Mc and with a gain of approximately 110 db. A trial-and-error method is needed to determine the number of stages required, but little experience is necessary to make a fairly close first approximation. For the particular requirements stated above, about five staggered pairs would be a reasonable starting point. From Fig. 33-5, or from the expression for the band-width reduction factor,<sup>1</sup> the band width per pair is calculated.

$$\begin{aligned} \text{Band width per pair} &= (\text{over-all band width}) \times 1.1 \sqrt[4]{n} = 12 \times 1.1 \sqrt[4]{5} \\ &= 12 \times 1.1 \times 1.495 = 18 \quad \text{Mc} \end{aligned}$$

<sup>1</sup> The general form of this band-width reduction factor (see Eq. 33-18) is

$$\sqrt[m]{2^{1/n} - 1}$$

where  $m$  = the number of tuned circuits in the interstage network

$n$  = number of cascaded stages

For single tuning,  $m = 1$ ; double-tuning,  $m = 2$ ; etc.

Approximate forms for the band-width reduction factor for  $n > 4$  are for single tuning  $1/(1.2 \sqrt{n})$ , for double-tuning (or staggered pairs where  $n$  = number of pairs)  $1/(1.1 \sqrt[4]{n})$ , and for triple tuning (or staggered triples where  $n$  = number of triples)  $1/(1.06 \sqrt[3]{n})$ .

For the 6AK5 with  $g_m$  of 4500  $\mu\text{mhos}$  and  $C_T$  of 11  $\mu\text{mf}$ , the gain-bandwidth product is  $(4500 \times 10^{-6}) / (2\pi \times 11 \times 10^{-12}) = 65.2 \text{ Mc}$ . Therefore, since the stage-gain times pair-band width for a staggered pair is equal to  $g_m / 2\pi C_T$ , the mean stage gain is  $65.2 / 18 = 3.62$ , or 11.2 db.

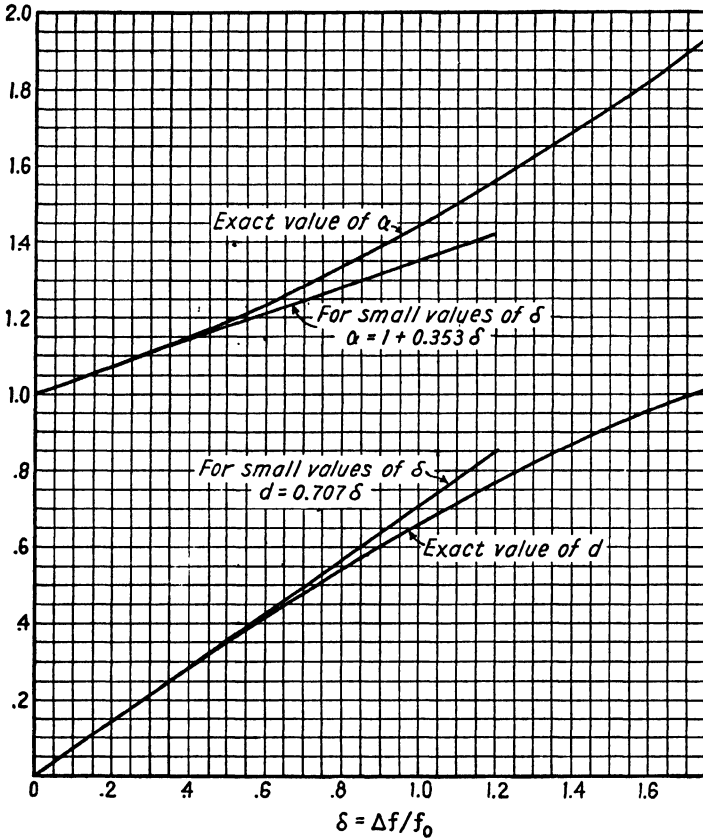


FIG. 33-15.—Curves for determination of the dissipation factor  $d$  and the stagger factor  $\alpha$  for staggered pairs: (1) an exact staggered pair of stage gain  $G$  has as great an over-all band width  $\Delta f$  as one single-tuned stage of gain  $G$ , i.e.,  $G \Delta f = g_m / 2\pi C$ ; (2) an exact staggered pair of over-all band width  $\Delta f$ , (geometrically) centered at  $f_0$  consists of two single-tuned stages of dissipation factor  $d (= 1/Q)$ , staggered at  $f_0 \alpha$  and  $f_0 / \alpha$  where  $d$  is given in the lower curve and  $\alpha$  in the upper curve, as functions of  $\delta = \Delta f / f_0$ ; (3) an amplifier made up of  $n$  pairs has  $1 / (1.1 \sqrt{n})$  the band width of one pair.

For 10 stages, the over-all gain would be  $10 \times 11.2$ , or 112 db. Since this fulfills the requirements, the circuit constants are next determined. From Fig. 33-15,  $\alpha$  and  $d$  are determined for  $\delta = \Delta f / f_0 = 1/30 = 0.60$

$$\alpha = 1.24 \quad \text{and} \quad d = 0.41$$

then, since

$$d = \frac{1}{Q}, \quad Q = \frac{1}{0.42} = 2.44$$

$$f_1 = \alpha f_0 = 1.24 \times 30 = 37.2 \quad \text{Mc}$$

$$f_2 = \frac{f_0}{\alpha} = \frac{30}{1.24} = 24.2 \quad \text{Mc}$$

$$R_1 = \frac{2.44}{2\pi \times 37.2 \times 11 \times 10^{-6}} = 950 \quad \text{ohms}$$

$$R_2 = \frac{2.44}{2\pi \times 24.2 \times 11 \times 10^{-6}} = 1460 \quad \text{ohms}$$

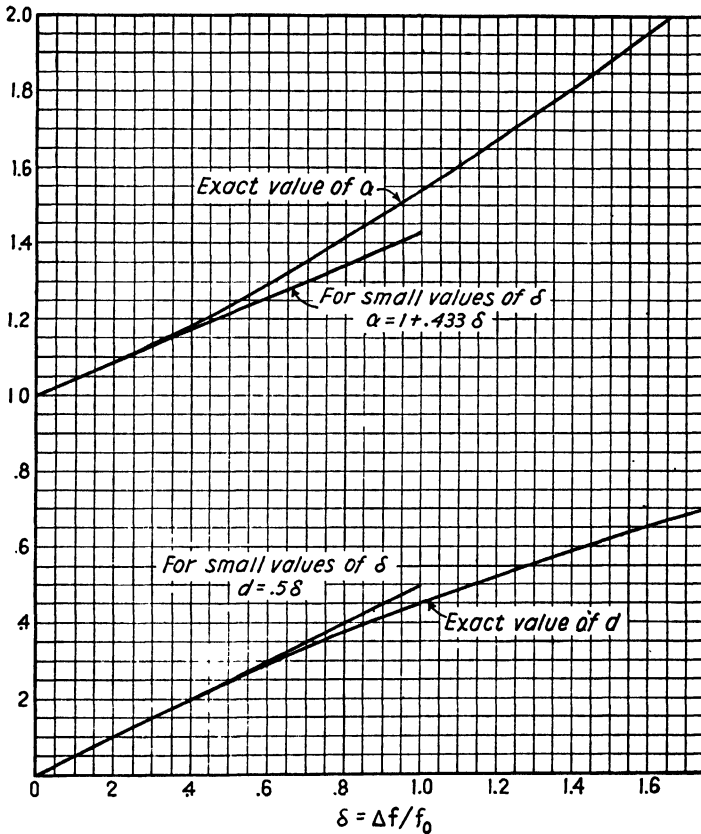


FIG. 33-16.—Curves for determination of the dissipation factor  $d$  and the stagger factor  $\alpha$  for staggered triples: (1) an exact staggered triple of stage gain  $C$  has as great an overall band width  $\Delta f$  as one single-tuned stage of gain  $G$ , i.e.,  $G \Delta f = g_m / 2\pi C$ ; (2) an exact staggered triple of over-all band width  $\Delta f$ , (geometrically) centered at  $f_0$  consists of two single-tuned stages of dissipation factor  $d$ , staggered at  $f_0\alpha$  and  $f_0/\alpha$  and one single-tuned stage of dissipation factor  $\delta$  centered at  $f_0$ , where  $d$  is given in the lower curve and  $\alpha$  in the upper curve as functions of  $\delta = \Delta / f_0$ ; (3) an amplifier made up of  $n$  triples has  $1/(1.06\sqrt[n]{n})$  the band width of one triple.

The amplifier would then consist of five sets of staggered pairs, each pair made up of one stage tuned to 37.2 Mc damped with 950 ohms and one stage tuned to 24.2 Mc damped with 1460 ohms. The important



point to note is that the damping resistors are not the only loads on the tuned circuits. Tube input and coil resistance contribute to some extent to the total damping, and some experimenting must be done to determine the proper resistor size. What is important is that the tuned circuits shall have the proper selectivity. The next higher resistor to the calculated values of  $R_1$  and  $R_2$  in the 5 per cent preferred series will be a good approximation at 30 Mc. Table 33-1 may be used to calculate loading due to the grid-plate-capacitance path, which is usually the largest source of tube input loading if cathode lead inductance has been properly compensated (see Sec. 33-5).

TABLE 33-1

	$\Delta g^*$ Multiply $A_0' C_{gp} \omega$ by	$\Delta C^*$ Multiply $A_0' C_{gp}$ by
Staggered triples:		
1. Side followed by side.....	0.267	0.077
2. Center followed by side .....	0.433	0.25
3. Side followed by center.....	0.495	0.572
Staggered pairs:		
1. Side followed by side.....	0.400	0.200
2. Center followed by side (input circuit).....	0.500	0.500
3. Side followed by center (output circuit)....	Values depend on band width of center stage and must be calculated for the individual case	

- \*  $C_{gp}$  = plate-grid capacitance, farads
- $\omega$  = resonant frequency of grid circuit
- $\Delta g$  = conductive component of fed-back grid admittance
- $\Delta C$  = shunt capacitive component fed-back into grid
- $A_0' = g_m R_L$ , where  $R_L$  is load resistance

NOTE: When the plate circuit is higher in frequency than the grid circuit,  $\Delta g$  is negative.

If it is necessary to keep the number of tubes to a minimum, the higher gain-band-width product of a staggered triple may be utilized. Here the mean stage gain times band width of *three* stages is equal to  $g_m/2\pi C_r$ , and three staggered triples, consisting of a total of 9 tubes, will probably give as good or better results than the 10 stages arranged in pairs. The calculations follow:

For three triples to have an over-all band width of 12 Mc, each triple must have a band width of  $12 \times 1.06 \sqrt[3]{3}$ , or 15.2 Mc. From Fig. 33-16 the triple consists of two stages of dissipation factor  $d$  staggered at  $\alpha f_0$  and  $f_0/\alpha$  and one stage of dissipation factor  $\delta$  centered at  $f_0$ . Then

$$\delta = \frac{\Delta f}{f_0} = \frac{15.2}{30} = 0.507$$

From the curves

$$d = 0.245 \quad \text{and} \quad \alpha = 1.24$$

Then

$$f_1 = \frac{30}{1.24} = 24.2 \quad \text{Mc}$$

$$f_2 = 30 \times 1.24 = 37.2 \quad \text{Mc}$$

$$f_3 = f_0 = 30 \quad \text{Mc}$$

$$R_1 = \frac{10^6}{0.245 \times 2\pi \times 24.2 \times 11} = 2440 \quad \text{ohms}$$

$$R_2 = \frac{10^6}{0.245 \times 2\pi \times 37.2 \times 11} = 1590 \quad \text{ohms}$$

$$R_3 = \frac{10^6}{0.507 \times 2\pi \times 30 \times 11} = 950 \quad \text{ohms}$$

The gain per stage is  $65.2/15.2 = 4.32$ , or 12.7 db, which for nine stages gives a total gain of 115 db:

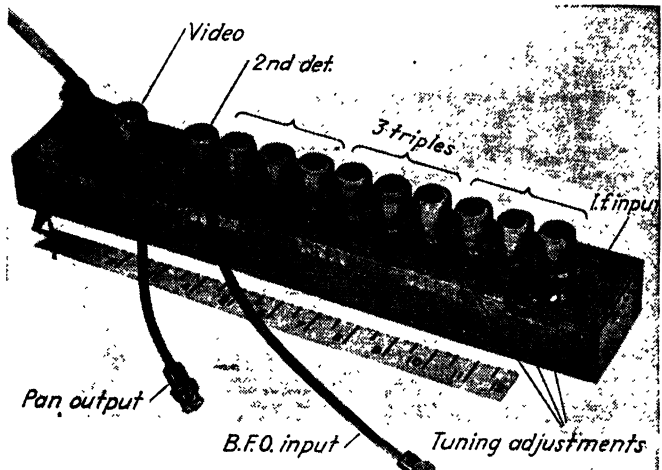


FIG. 33-17.—Assembly of the main-amplifier section of a 200-Mc i-f amplifier 20 Mc wide.

It will be noticed that the  $Q$ 's of the circuits tuned to  $f_1$  and  $f_2$  are higher than for the staggered pair. As the number of stages staggered increases, the  $Q$ 's go up and the circuits become more critical to changes in tube parameters and accuracy of loading, the penalty paid for an increase in stage-gain-over-all band-width product. Almost all actual i-f amplifier requirements may be met using staggered pairs, or at the most staggered triples.

An actual application of staggered triples is shown in Fig. 33-17; Fig. 33-18 shows the bottom of the amplifier with the cover removed. This amplifier, is 20 Mc wide centered at 200 Mc, using 6AK5's. The

over-all response curve is shown in Fig. 33-19. The main amplifier consists of nine stages, arranged in three triples. The gain of the amplifier, including a preamplifier containing another triple, is about

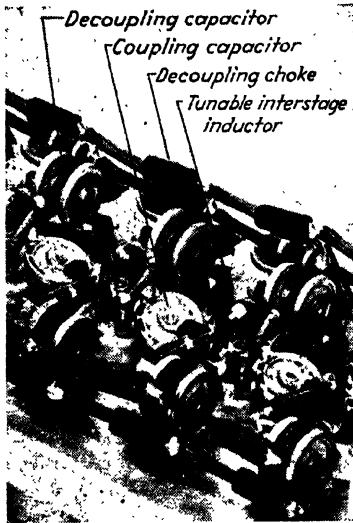


FIG. 33-18.—A section of the 200-Mc amplifier showing constructional details.

95 db. Because it is difficult to determine directly the exact effects of tube and coil loading at 200 Mc, the damping was done experimentally with the circuits tuned to the calculated stagger frequencies. The subsequent models were loaded with the resistor values obtained from the experimental version and exhibited substantially similar characteristics. The 60:6-db band-width ratio for this amplifier was about 2.

The advantages of stagger tuning are obvious from the previous discussion. The multituned coupling scheme has a slight superiority in gain-band-width factor for the same number of tuning elements over the stagger-tuning method, *i.e.* double tuning as compared with staggered pairs, triple tuning with staggered triples, etc. The complexity of the multituned coupling network, however, increases so rapidly beyond

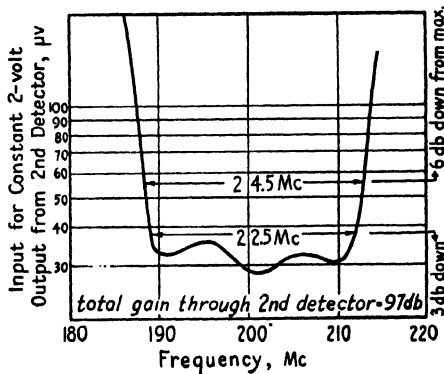


FIG. 33-19.—Response curve of the i-f amplifier of Fig. 33-17.

double tuning that very few practical applications have been made at the intermediate frequencies under discussion. Therefore, the extreme simplicity of design and construction of the stagger-tuned amplifier, coupled with its superiority over the double-tuned amplifier when *three*

or more circuits are staggered, dictates its use for most applications in wide-band high-gain amplifiers.

**33-13. Regeneration.**—Regeneration in high-gain amplifiers has always been a serious problem to the designer. The usual sources of regeneration are

1. Coupling between stages through stray electromagnetic and electrostatic fields
2. Coupling between stages through common impedances
3. Feedback through interelectrode capacitances

Couplings of these types are undesirable, since they distort the selectivity characteristic and, in some cases, cause oscillation. Furthermore, since some effects are functions of operating conditions, the selectivity characteristic will change with variation of supply voltages, setting of gain control, etc.

Although normally one thinks of the inductance in the tuned circuit as the largest source of stray fields that give rise to undesirable induced voltages in adjacent circuits, this is true only at relatively low frequencies. As frequency increases, two effects modify this condition: (1) The size and inductance of the coils decrease rapidly, and thus the field strength at a given distance from the coil becomes smaller. (2) The radiation from any length of straight lead increases. At the frequencies being discussed, if reasonable care is given to the placing of the coils physically in the circuit so as to minimize direct coupling between tuned circuits, regeneration from this source is not important as compared with coupling due to radiation from leads. The first axiom of proper physical layout is: *Keep lead lengths to an absolute minimum.* This may sound trite and has been stated many times before, but it cannot be emphasized too strongly. A second factor that is closely tied in with the "minimum-lead-length" axiom has to do with by-passing; low-inductance by-passing aids greatly in reduction of regeneration. The development of feed-through and button capacitors has been of help in reducing lead inductance between components and their r-f grounding points. An example of the use of button capacitors for by-passing is shown in Fig. 33-18, which shows a section of the 200-Mc i-f amplifier. No interstage shielding was necessary, and there was no trouble with regenerative tendencies. Minimum difficulty will be experienced if the circuit elements are so handled that they perform in the circuit as the lumped constants called for in the schematic diagram. Load resistors should be purely resistive with as little series inductance in leads as possible, by-passes should be purely capacitive, etc.

At low frequencies it is usual to employ a common voltage bus for all stages, each individual stage being separately decoupled from this bus by

means of resistance-capacitance filters. This means that the low-level stages must be decoupled by an amount greater than the over-all amplifier gain if serious regeneration is to be avoided. In high-gain amplifiers, such as those under consideration, this can be a very difficult problem. A much more effective system of supplying voltage to the tubes is that using so-called *series decoupling*. In this method, each stage is fed from one section of a series decoupling network, as shown in Fig. 33-20. Each section need supply only sufficient attenuation to prevent regeneration between *adjacent* stages. If two adjacent stages are successfully decoupled, there will be no trouble from regeneration from this source regardless of over-all gain. The actual impedance  $Z$  in Fig. 33-20 depends on the frequency being amplified and the particular tube element supplied by the network. It is clear that at low frequencies and high-stage gains this method is not practical, because the size of inductance required for  $Z$  would be impractical and would probably be a serious

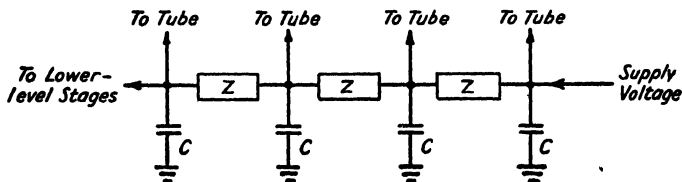


FIG. 33-20.—Schematic diagram of a series decoupling network.

source of stray fields. If resistance were used instead of inductance, the cumulative voltage drop would be excessive. As the intermediate frequency is raised above 15 or 20 Mc, and wide bands are required, the series decoupling method becomes practical. Lower stage gains make it possible to obtain sufficient attenuation per section with resistors of relatively low value as series elements and 500- or 1000- $\mu\text{f}$  button capacitors as shunt elements. In the heater supply, the impedance must have a very low resistance. Here 0.2- $\mu\text{h}$  chokes have proved satisfactory, and the voltage drop when feeding 10 stages has not been excessive. If the loss is too great, the heater chain (or for that matter, any other supply) may be fed from the center. In the 200-Mc i-f amplifier mentioned in Sec. 33-12, a standard decoupling network of a 0.2- $\mu\text{h}$  choke and a 500- $\mu\text{f}$  button capacitor was used, as shown in Fig. 33-18 except in the a-v-c bus, where 47-ohm  $\frac{1}{2}$ -watt resistors were alternated with the chokes. The series decoupling method has been used on a variety of i-f amplifiers of varying band widths and at frequencies of 30 Mc and higher and has been so universally satisfactory that it is considered a standard practice.

When r-f currents flow in the chassis between stages of different level, undesired couplings will result in the same manner as with common impedances in the power supply. If normal care is exercised in choice

of grounding points, trouble should not be encountered. By normal care is meant ensuring that grounding points are chosen so that r-f currents of a given signal level flow only in the interstage section handling that level and do not flow between sections of different levels.

The third source of undesired coupling mentioned, feedback through interelectrode capacitances, has been discussed in some detail in Sec. 33-5. This regeneration, or degeneration, is undesirable, not only because it may cause serious distortion of the selectivity characteristic, but because its effect is a function of the transconductance. It cannot be eliminated except by neutralization, which is difficult to handle with wide bands and because of the physical complexity added by the neutralizing circuit. The only solution is to limit stage gains so that when  $g_m$  is maximum the amount of regeneration is acceptable, and to control the gain in such a manner that the variation is held to a minimum, as described in the next section.

**33-14. Gain Control.**—The most common method of gain control is by variation of the transconductance of the tube. This can be accomplished by several means: variation of plate voltage, variation of the d-c voltage on the control grid, and addition of resistance in series with the cathode. Plate-voltage variation is seldom used because it lowers the amplifier overload capacity. The other two methods have both been extensively employed, and are both satisfactory, although the cathode-resistance method has the advantage that variations in tubes are to some extent minimized at low  $g_m$  by the effective negative feedback of the cathode resistor at zero frequency, *i.e.*, for direct current. The actual method to be used depends largely on which is the more physically feasible in a particular case.

The main problem in gain control is to minimize variation in the shape of the selectivity characteristic with change in gain setting. If all interstage networks are identical, as in synchronous single tuning, no choice is available but to limit the stage gain to the extent that variation in  $g_m$  causes variation in band shape to be held within permissible limits. This can be a severe limitation, especially at high intermediate frequencies. If the stages are nonidentical, however, as in stagger-tuned amplifiers, the stages are affected in varying degrees by the plate-grid feedback (see Table 33-1). It is possible, then, to select the stages on which the gain control operates, so that only those least affected by feedback are varied. For example, the gain control on the 200-Mc amplifier mentioned in Sec. 33-12 acted only on the tubes the plate circuits of which were tuned to the high- and low-stagger frequencies.

In order to handle a wide range of input signal levels without overload, it is desirable to use gain control in the stages closest to the input. Since gain control is accomplished by varying the tube operating point, how-

ever, the noise figure of the amplifier may be adversely affected if the gain control acts on the *first* tube; unless it is necessary to handle an extremely wide range of input signal levels, it is usually placed elsewhere.

**33-15. Automatic Gain Control.**—As in most receivers, there is often need for an automatic gain control in order to accept signals of widely different strengths without continual manipulation of a manual control. The ordinary methods of a-g-c depending on simple rectification of the i-f signal and the use of this “average” voltage to adjust the receiver gain are well known.<sup>1</sup> These usually depend on the fact that the time-constant of the gain control circuit is made sufficiently long so that the derived voltage will not follow the modulation frequencies but only a relatively slow change in the carrier level. In some types of transmissions, however, the rectified i-f signal may not be proportional to carrier level, as in television, or the ratio of peak-to-average signal may be so large as to make it impractical to use the average to control the receiver gain, as in pulse reception.

In television, the average signal is proportional to the general level of the scene illumination, which may change slowly over a long period of time, and which bears no relation to the carrier level. It is obvious that a successful a-g-c system must operate on a portion of the signal that is proportional to the carrier strength. The tips of the synchronizing pulses, or the blanking level, represent two such parts of the signal, and the derivation of the a-g-c-voltage becomes a problem of building a peak-reading device.

A portion of the video signal is therefore fed to a “pulse stretcher” (see Sec. 34-4). Often an audio output system is incorporated in the receiver which may use a stretched output (as in a receiver for the detection of pulse signals), and the first stage of stretching may be designed to furnish this output as well as to supply voltage to the a-g-c circuit. In order to control the gain automatically over a wide range of input signal levels, the a-g-c system must be capable of supplying to the stages being controlled a bias voltage that is many times that actually required, and so further amplification is required before the final stretching that produces this voltage. The decay time constant of the last stretcher depends on the actual application, but if the gain is to be kept reasonably constant it must be at least several times the period between pulses.

<sup>1</sup> See, for example, TERMAN F. E., “Radio Engineers Handbook,” pp. 553-566 McGraw-Hill Book Company, Inc., New York, 1943; REICH, H. J., “Theory and Applications of Electron Tubes,” 2d ed., p. 236, McGraw-Hill Book Company, Inc., New York, 1944.

## CHAPTER 34

### RECEIVER OUTPUT CIRCUITS

By R. R. BUSS, J. D. NOE, C. B. CLARK, AND H. E. OVERACKER

Following the detection process, in which the modulation is recovered from the r-f signal, this modulation must be conveyed to appropriate devices for presentation to the observer. These devices may be ear-phones, cathode-ray oscilloscopes, modulation analyzing devices, or automatic or semiautomatic recorders. Means for conveying the energy from the detector to these output devices, with proper amplification and control of the amplification, as well as the devices themselves, will be discussed in the sections to follow. Also to be discussed in the following sections are panoramic display devices, which logically are grouped with the presentation devices, though working elements may precede or incorporate the detection process.

**34-1. Video Output.**—One of the requirements of a search receiver used for the reception and analysis of pulse signals is its ability to determine the type of transmission. The type of transmission is determined by means of measurement on the received signal to determine characteristics such as pulse length, pulse repetition frequency, and lobing characteristics. The measurement of such quantities requires that the signal be faithfully reproduced. The requirements are more stringent<sup>1</sup> than, for example, for a radar receiver, since the radar receiver can be tailored to fit its own system, while the more general search receiver must be able to reproduce characteristics of any system. Furthermore, other functions must be served by the search receiver, such as aural presentation of the signal, its panoramic presentation on the face of an oscilloscope as a function of frequency, or use of the receiver in conjunction with direction-finding equipment or recorders.

**34-2. Band Width of Video Amplifiers.**—Video-frequency circuits for pulse-analysis work must have a band width in megacycles of uniform response at least as great as the reciprocal of the pulse length in microseconds. The band width should be of the order of twice this minimum value or greater if the pulse is to approximate its original shape. Phase-shift characteristics are fully as important as the amplitude characteristic,

<sup>1</sup> A wider range of characteristics must be accommodated for measurements on an arbitrary signal, but accuracy of wave form can be less than where precision ranging is required. See Sec. 25.



since phase distortion will change the pulse shape, particularly on its leading and trailing edges. In general, requirements similar to those for television amplifiers apply, except that low-frequency response is not nearly so important in pulse analysis. In panoramic-presentation circuits, low-frequency phase distortion is important and must be kept to a minimum. This is discussed further in the section on panoramic presentation.

**34-3. Control of Gain in Video Amplifiers.**—With wide-band video amplifiers, the problems of varying the video gain without changing the fidelity of response of the amplifier are such that in many instances no provision for video gain control is made, control being effected at the r-f or i-f level. However, if the video gain must be varied, it must be accomplished at a low-impedance level, the control must be capacitance

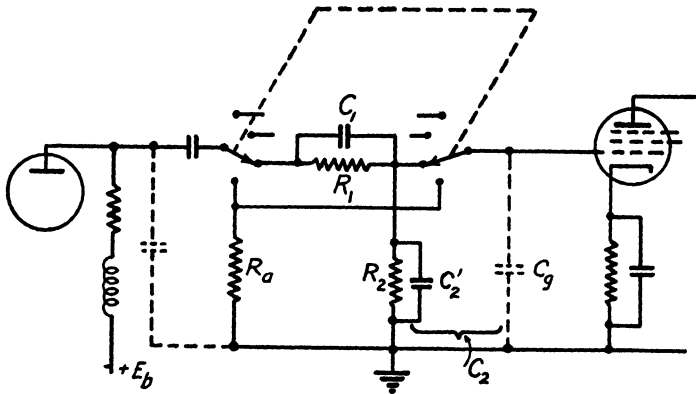


FIG. 34-1.—Step-switch video gain control.

compensated, or the control must be accomplished by varying a tube characteristic. Otherwise the width of the pass band will not be independent of the control position.

Capacitance compensation is best accomplished with a step-switch type of control in which each switch position can be independently compensated, as in Fig. 34-1, but such a control will not allow a continuous gain variation. Each switch position has a resistance-capacitance network of the form indicated in Fig. 34-1. The attenuation voltage ratio of each position is equal to the particular value of

$$\frac{R_2}{R_1 + R_2}$$

at that position. To keep the total impedance independent of attenuator setting, and to keep the attenuation ratio independent of frequency, the resistances and capacitances indicated in Fig. 34-1 are chosen so that

$$R_1 + R_2 = R_a = \text{constant} \tag{34-1}$$

and

$$R_1 C_1 = R_2 C_2 = \text{constant} \quad (34-2)$$

The capacitance  $C_2$  is composed of the added capacitance  $C_2'$  and the tube and wiring capacitance  $C_o$  of the input circuit to the succeeding stage. If  $C_2 = C_o$ , *i.e.*, if  $C_2' = 0$ , when  $R_1 = 0$  (no attenuation), then for any other setting of the attenuator

$$C_1 = \frac{R_1 + R_2}{R_1} C_o = \frac{R_2}{R_1} C_o \quad (34-3)$$

and

$$C_2' = \frac{R_1}{R_2} C_o \quad (34-4)$$

When continuous gain control is obtained by means of a voltage divider similar to those used in a-f circuits, the effect of the capacitance  $C_o$  (Fig. 34-2) at high video frequencies depends on the impedance seen by  $C_o$  looking back into the control circuit. This impedance depends on the setting of the voltage divider and has a maximum value of

$$\frac{R_L + R_i}{4}$$

at the setting for which  $aR_L = (R_L + R_i)/2$ . Accordingly, at this maximum impedance setting, the effect of the capacitance  $C_o$  on the frequency response and phase shift of the video amplifier is greatest. High-frequency considerations are thus based on a design using the impedance value obtained at this maximum-impedance setting of the gain control. The resistance  $R_i$  of Fig. 34-2 is the effective resistance seen by the voltage divider  $R_L$  looking back into the tube, and for a cathode-coupled amplifier  $R_i$  is the parallel combination of  $r_p/(1 + \mu)$  and any external resistance (such as  $R_K$  in Fig. 34-2b) other than the voltage divider  $R_L$ .<sup>1</sup> The symbols  $r_p$  and  $\mu$  are the plate resistance and amplification factor of the tube, respectively. For  $R_i$  greater than  $R_L$ , the maximum phase shift and drop in response at any frequency occur at the maximum gain setting because this setting gives the highest impedance of the source feeding  $C_o$ . With the voltage divider  $R_L$  directly connected into the cathode circuit as in Fig. 34-2a, the direct component of current flowing through the tube and voltage divider causes a direct voltage to appear at the adjustable arm of the voltage divider, the magnitude of the direct voltage depending on the gain setting. Even if the direct voltage is blocked from the next tube by a blocking capacitor and fixed grid resistor, a transient voltage will be applied to the next tube each time the voltage-

<sup>1</sup> See, for example, TERMAN, F. E., "Radio Engineer's Handbook," pp. 429-431, McGraw-Hill Book Company, Inc., 1943.

divider setting is changed. The circuit of Fig. 34-2b will eliminate complications from the direct-voltage change, but for good low-frequency response the blocking condenser  $C_c$  must be very large.<sup>1</sup>

Gain control can also be achieved by varying the transconductance of an amplifier tube by means similar to those used in i-f or r-f amplifiers, *i.e.*, varying grid bias, screen voltage, or plate voltage. An amplifier of this type will not handle a wide range of attenuation, and it will handle only a few volts of signal at its input terminals without distortion. For further discussion of this type of gain control, see Chap. 33.

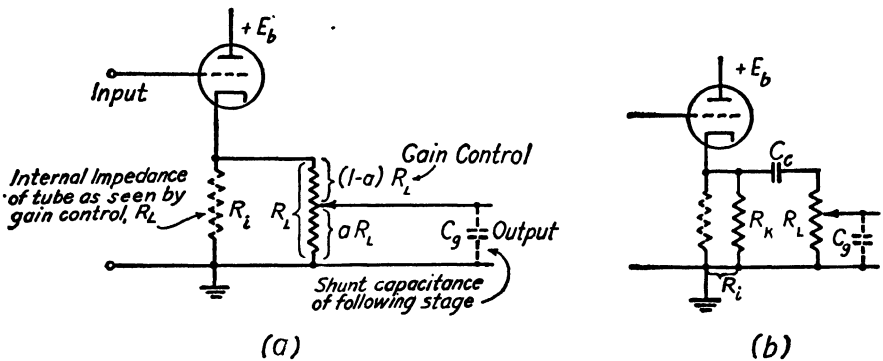


FIG. 34-2.—Continuously variable video gain control.

**34-4. Measurement Problems.**—To be significant, frequency- and phase-response characteristics of the video amplifier of a receiver must include the characteristics of the detector. The ideal method of over-all measurement is to apply to the input of the detector the appropriate known i-f or r-f signal, modulated to a known degree by the desired video frequency, the output impedance of the signal generator being adjusted to equal the effective impedance of the normal circuit as seen by the detector. Often, however, a signal generator suitable for this type of measurement is not available. The response of the video amplifier only is then measured by applying a video-frequency signal to the input of the first amplifier stage following the detector and correcting the results by including the calculated effects of the detector load impedance.<sup>2</sup>

**34-5. Video Output-coupling Circuits.**—Video output-coupling circuits differ from voltage-amplifier circuits in that the primary objective is power developed in a load impedance rather than voltage across a capacitance. Usually, the power must be transmitted some distance by means of a cable or transmission line, and, because of the wide frequency band involved, matching transformers cannot be used. If voltage output rather than power output is desired, but if it must be transmitted some

<sup>1</sup> Terman, *op. cit.*

<sup>2</sup> Terman, *op. cit.*, p. 561.

distance, the problem again reduces to an actual power-amplifier problem, because to transmit the required band width over a cable or transmission line requires proper termination of the line, and to maintain the voltage across the line requires power in the termination.

Since matching transformers cannot be used in most cases, and the load impedance is determined by other considerations, the required power output determines a lower limit to the current-carrying capacity of the output power-amplifier vacuum tube, and it makes no difference as far as power output is concerned whether the load is connected in the plate circuit or in the cathode circuit of the power amplifier.<sup>1</sup> Since this is so, cathode-coupled amplifiers are almost always used because, compared with the plate-coupled amplifier, the cathode-coupled amplifier has several advantages:

1. One of the load terminals may be grounded.
2. The source impedance presented by the tube to the load is low as a result of negative feedback. The tube may therefore be readily matched to a transmission line (for the reduction of reflection), and the amplifier has better amplitude and phase characteristics at high frequencies.
3. As a result of negative-feedback action, nonlinear distortion is lower.
4. As a result of negative-feedback action, the input impedance is higher.

In many cases video amplifiers are called upon to handle signals that are nonsymmetrical about their average values, such as pulses. In such

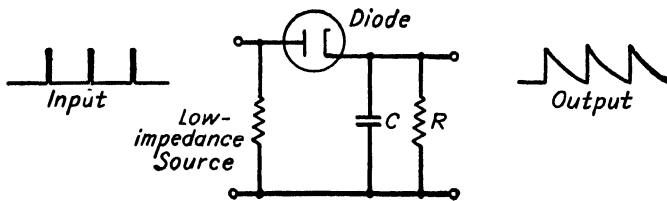


FIG. 34-3.—Diode pulse-stretcher circuit.

cases the power output obtainable is affected by the polarity of the signal. For example, the peak plate-current swing resulting from a negative input pulse is limited by the d-c plate current of the tube, whereas that resulting from a positive input pulse is limited only by the plate voltage and the peak emission capabilities of the tube.

**34-6. Pulse Stretchers.**—In ordinary radio receivers such as those used in communications work, the detector output is usually amplified by an audio amplifier and then applied to phones to produce an aural indication of the presence of a signal. However, since the strength of the signal heard in the phones is proportional to the average *audio* power delivered by the detector, receiver sensitivity is considerably reduced

<sup>1</sup> Terman, *op. cit.*

when pulsed signals are being received. These have low average power, and only a small part of this power is in the a-f range. Similarly, when presentation is made by means of a cathode-ray tube display, and it is not required that exact pulse shape be retained, design of the deflection amplifiers is simplified and contrast of the signal indication against background conditions is enhanced if the proportion of energy of the lower frequency components of recurrent pulses is increased relative to the original distribution. To achieve this effect, a *pulse-stretcher* or *pulse-expander* circuit, such as shown in Fig. 34-3, is often used in receivers used for the reception of pulsed signals.

In this circuit the diode conducts only for the duration of each input pulse, charging the capacitor  $C$  nearly to the peak pulse voltage. The capacitor is then slowly discharged through the resistor  $R$ . The form of the resulting output wave form is shown in Fig. 34-3. Under the assumption that the capacitor  $C$  is charged on each pulse to the peak value of the input pulse voltage, the ratio of the amplitudes of the lower frequency components of a short rectangular input pulse after stretching to the amplitudes of the corresponding components before stretching is approximately<sup>1</sup>

<sup>1</sup> Equation (34-5) is derived as follows:

The rectangular pulses are expressible as a Fourier series

$$y = E_0 \left[ k + \frac{2}{\pi} \left( \sin k\pi \cos x + \frac{1}{2} \sin 2k\pi \cos 2x + \dots + \frac{1}{n} \sin nk\pi \cos nx + \dots \right) \right]$$

where  $x = 2\pi ft$

For very short pulses ( $k \ll 1$ ),  $\sin nk\pi \rightarrow nk\pi$  and the series becomes

$$y = E_0(k + 2k \cos x + 2k \cos 2x + \dots)$$

This expression is accurate to within 2 per cent for harmonics of order lower than  $1/10k$ . Thus, the amplitude of these harmonics is  $2kE_0$  where  $E_0$  is the peak value of the square pulse.

For the stretched pulses, it is assumed that the pulse decays exponentially in accordance with the relation  $y = E_0 e^{-(1/RC)t} = E_0 e^{-ax}$  until the succeeding pulse, when the voltage has a value  $E_0 e^{-1/RCR}$  but is again abruptly raised to  $E_0$ . Here  $t$  is the time in seconds following any incoming pulse, and  $a = \frac{1}{2\pi fCR}$ . As a Fourier series, this becomes

$$y = A_0/2 + A_1 \cos x + A_2 \cos 2x + \dots + A_n \cos nx + \dots \\ + B_1 \sin x + B_2 \sin 2x + \dots + B_n \sin nx + \dots$$

where

$$A_n = \frac{E_0}{\pi} \frac{a}{a^2 + n^2} (1 - e^{-2a\pi})$$

and

$$B_n = \frac{E_0}{\pi} \frac{n}{a^2 + n^2} (1 - e^{-2a\pi})$$

The amplitude of each harmonic is

$$\frac{\text{Harmonic amplitude after stretching}}{\text{Harmonic amplitude before stretching}} = \frac{1}{k} \left[ \frac{1 - e^{-\frac{1}{fCR}}}{\sqrt{4\pi^2 n^2 + \left(\frac{1}{fCR}\right)^2}} \right] \quad (34-5)$$

where  $e = 2.718 \dots$

$k = \frac{\text{length of the rectangular pulses}}{\text{repetition period of the pulses}} = \text{duty cycle of the pulses}$   
 $n = 1, 2, 3, 4, \text{ etc.}, \text{ giving the order of the harmonic, } n f$   
 $f = \text{repetition frequency of the recurrent pulses, pulses per second}$   
 $R \text{ and } C \text{ are given in Fig. 34-3}$

*Example:* Assume a 1- $\mu$ sec pulse input with a repetition rate of 1000 pulses per second ( $k = 10^{-3}$ ), and for the time constant of the stretching circuit a value of  $CR = 10^{-3}$  (giving a decay to approximately 37 per cent of peak value in the interval between pulses). These conditions give nearly a hundredfold theoretical increase in amplitude of the fundamental or first harmonic of the repetition frequency.

Examination of Eq. (34-5) shows that for large values of  $n$  the amplitudes of the harmonics fall off approximately as  $1/n$ . For  $n = 1$ , the ratio given by Eq. (34-5) has a broad maximum for values of  $fCR$  in the vicinity of 0.35, with less than 3-db variation for values of  $fCR$  between approximately 0.15 and 1.00.

Actually, because of the effects of diode resistance, source impedance, etc., the amount of improvement indicated by Eq. (34-5) cannot be achieved in actual practice, particularly at low-signal levels where it is most needed. Improvements in audio power output of the order of 6 to 20 db, however, can be achieved over that possible with the amplifier input directly connected to the driving source, the exact amount depending on the applied voltage. For best performance, both the diode resistance and the impedance of the driving source should be small compared with the capacitor reactance at a frequency in megacycles equal to the reciprocal of the length in microseconds of the shortest pulse to be

$$E_n = \sqrt{A_n^2 + B_n^2} = \frac{E_0}{\pi \sqrt{a^2 + n^2}} (1 - e^{-2a\pi})$$

the ratio of similar harmonics then becomes

$$\frac{\text{Harmonic amplitude after stretching}}{\text{Harmonic amplitude before stretching}} = \frac{E_0(1 - e^{-2a\pi})}{\pi \sqrt{a^2 + n^2}} = \frac{(1 - e^{-2a\pi})}{2k\pi \sqrt{a^2 + n^2}} = \frac{1 - e^{-2a\pi}}{k \sqrt{(2\pi a)^2 + (2\pi n)^2}}$$

Resubstituting  $a = 1/2\pi fCR$  and rearranging then gives Eq. (34-5).

stretched. For this reason, the  $RC$  circuit is usually proportioned with as high a resistance and as low a capacitance as possible. The maximum value of this resistance is usually limited by the input impedance of the following amplifier stage and the fact that high-impedance circuits are extremely susceptible to hum pickup. The time constant of the  $RC$  circuit is governed by the maximum pulse-repetition frequency handled, as may be seen from examination of Eq. (34-5). A typical circuit would use a 1000- $\mu\text{f}$  capacitor and a 1-megohm resistance ( $RC = 10^{-3}$ ,  $fCR = 0.35$  at a repetition frequency of 350 pulses per second).

The pulse-stretcher circuit is also useful in connection with cathode-ray-tube circuits used for measuring pulse-repetition frequency and with direction-finding systems intended for use with pulsed signals. In both these applications the function of the pulse stretcher is to increase the writing time of the cathode-ray-tube beam and, therefore, to increase the intensity of the signal seen on the tube face.

Another application of the pulse-stretching technique is in the operation of meter-type signal-strength circuits. Modifications of the circuit are sometimes employed to increase the average power of pulsed signals sufficiently to operate a d-c meter for indicating relative signal strength.

**34-7. Panoramic Presentation.**—Panoramic presentation is the visual display, usually on the screen of a cathode-ray tube, of receiver response as a function of the frequency setting of the receiver. It is useful in searching for signals whose frequency is unknown, in determining accurately the frequency of a known signal, in setting a controlled local signal to that of an incoming signal, whether for measuring purposes or otherwise, or in making a spectrum analysis of the output of a transmitter or other signal source.

There are two approaches to the problem of panoramic presentation, depending on the purpose for which the receiver is intended. The first approach is to sweep rapidly through the i-f pass band of a superheterodyne receiver, and thus present panoramically a selected narrow band of the range of frequencies to which the receiver can be tuned. The second approach is to sweep through all or part of the primary tuning range of a receiver, usually by sweeping the local oscillator of a superheterodyne, and thus present panoramically a wide band of frequencies. Narrow-band panoramic presentation by sweeping the primary acceptance band of the receiver through a narrow range is possible but is not so satisfactory as the presentation of the i-f acceptance band (see Sec. 34-8). Direct-detection receivers can be arranged for panoramic presentation but, in general, are unsatisfactory because of the difficulty of making the tuning sufficiently frequency selective. In any form of panoramic presentation, the variable tuning elements must be very carefully designed to reduce or eliminate sliding contacts in order to avoid the

noise associated with such contacts. The troubles associated with sliding contacts necessitate the use of tuning elements with nonsliding contacts and, therefore, because of the difficulty of obtaining wide tuning ranges with the latter, tend to limit the frequency range through which it is possible to sweep.

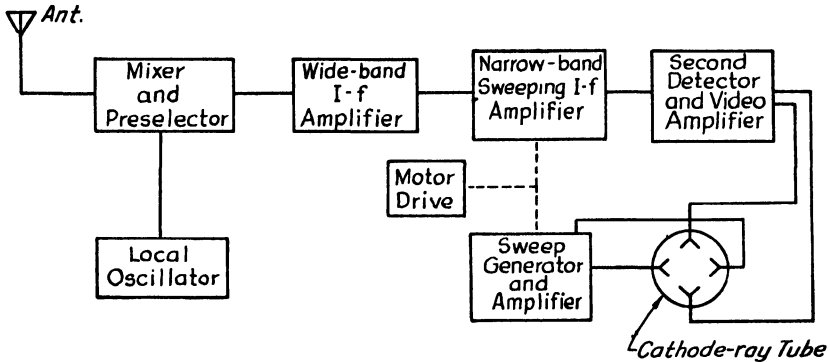


FIG. 34-4.—Superheterodyne receiver with panoramic presentation using a sweeping narrow-band i-f stage.

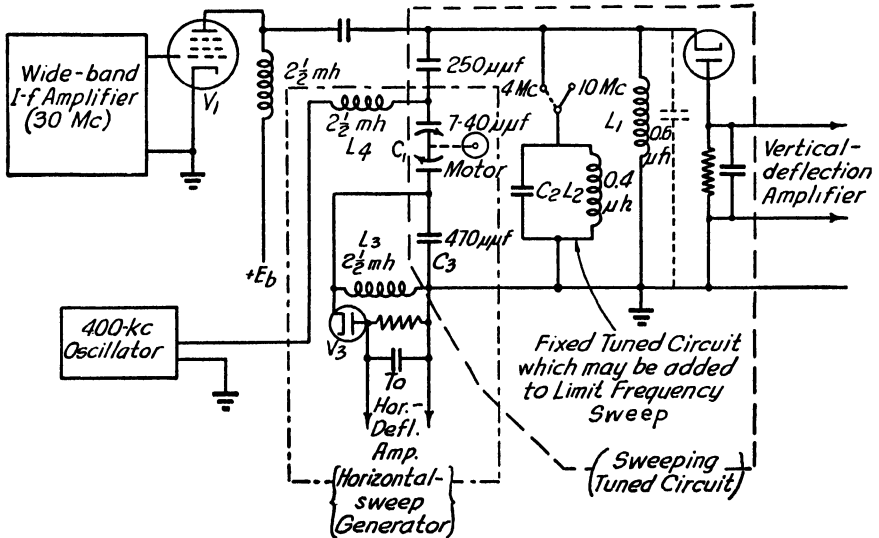


FIG. 34-5.—Details of sweeping narrow-band i-f amplifier and means for obtaining horizontal-deflection voltage.

A block diagram of one type of narrow-band panoramic receiver is shown in Fig. 34-4. In this receiver, a sharply tuned i-f amplifier stage is swept through the broader i-f pass band of the receiver. Figure 34-5 shows circuit details of a portion of a panoramic-display unit to be used with receivers having a 30-Mc i-f amplifier. The motor-driven sweeping



tuned circuit  $L_1C_1$  gives a 10-Mc sweep, but, by adding the fixed-tuned circuit  $L_2C_2$  in shunt with  $L_1C_1$ , the swept band width is reduced to 4 Mc for use with the receiver of Fig. 25-5. The center frequency of  $L_1C_1$  is adjusted by varying the inductance  $L_1$ , and after  $L_1C_1$  is adjusted, the center frequency of the combination of  $L_1C_1$  and  $L_2C_2$  is adjusted by varying  $L_2$ .

The detected output of the sweeping i-f amplifier is further amplified and applied to the vertical deflection plates of an oscilloscope, and a voltage dependent on the position of the motor-driven tuning capacitor is applied to the horizontal-deflection plates. Thus the cathode-ray tube shows the receiver output as a function of the frequency to which the sweeping circuit is tuned. The horizontal sweep voltage can conveniently be obtained, as shown in Fig. 34-5, by using the same rotating variable capacitor that tunes the i-f circuit as one element of a voltage divider in a circuit fed by a constant voltage from an audio or super-sonic oscillator (the 400-kc oscillator of Fig. 34-5). The choke  $L_4$  prevents the 400-kc oscillator from affecting the tuning of the i-f amplifier. The circuit  $L_3C_3$  is the second element of the voltage divider of which  $C_1$  is the first element, and the voltage appearing across this element  $L_3C_3$  is rectified, amplified, and applied to the horizontal-deflection plates of the cathode-ray tube to produce a voltage dependent only on the position of the capacitor. The horizontal deflection obtained in this manner is thus independent of sweep speed. By careful attention to phase distortion in the horizontal-deflection amplifiers (see Sec. 34-10), it is possible to make the relation between horizontal position and the frequency as plotted on the face of the cathode-ray tube independent of the direction of spot travel. It is then possible to use both forward and return traces on the oscilloscope, whereas otherwise it is necessary to blank the return trace to prevent a double image. By utilizing both traces there is no loss of signal during a blanking interval, no blanking circuit is required, and spot intensification during reception of a signal is simplified since it can be achieved with a simple differentiating circuit consisting of a small-time-constant  $RC$  network operating on the amplitude of the signal output from the sweeping i-f amplifier and the subsequent detector. Such a differentiating circuit with a blanked return trace would intensify the portion of the incoming signal where the amplitude is increasing, but reduce the intensity of the portion where the amplitude is falling. With the unblanked return trace, the opposite side of the signal response is intensified on the return trace, giving the effect of an over-all uniform intensification.

An alternative method to that of Fig. 34-4 is to use a double-conversion superheterodyne in which the first i-f amplifier has the desired band width and the second local oscillator is swept over the required band

to convert any signal within the original i-f band to the frequency of a fixed narrow-band second i-f amplifier. A block diagram of such a circuit is shown in Fig. 34-6. This method is often more satisfactory than that of Fig. 34-4 for swept band widths of the order of 20 Mc or less.

The second local oscillator may be tuned mechanically by a motor-driven tuning capacitor, or electronically by reactance-tube techniques. For swept band widths of less than 10 Mc, the electronically tuned oscillator has the advantages over the mechanically tuned oscillator of simplicity and ease of control of sweep speed and deviation. It is less stable and more critical in its operation except when the swept band widths are small. With present techniques, 10 Mc (regardless of center frequency) is roughly the maximum frequency sweep directly obtainable

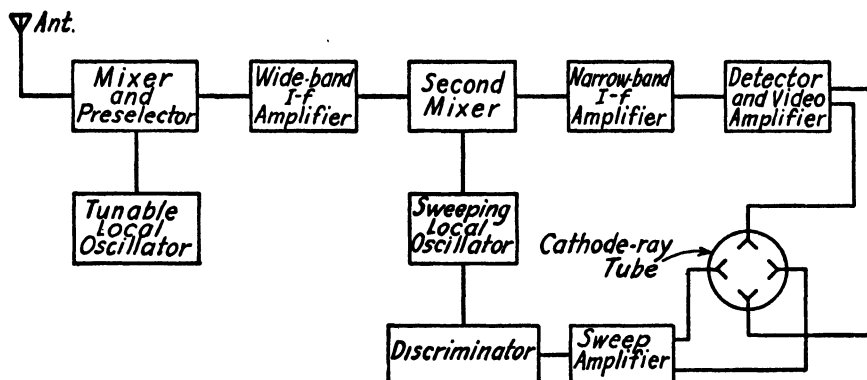


FIG. 34-6.—Superheterodyne receiver with panoramic presentation using a sweeping second local oscillator.

electronically, and the large frequency sweeps are quite critical with respect to vacuum-tube variations, ease of adjustment, and uniformity of oscillator amplitude. Accordingly, swept band widths of 10 Mc or greater are usually obtained by mechanical tuning, increasing-frequency and decreasing-frequency sweeps being superposed in the presentation on the oscilloscope. The discriminator<sup>1</sup> indicated on Fig. 34-6 will give a horizontal-deflection sweep voltage that depends only on the frequency of the oscillator. Such a system of obtaining sweep voltage can be used with either mechanically or electronically tuned sweeping local oscillators. The voltage controlling the reactance tube of an electronically tuned oscillator can be used for the horizontal sweep if desired, but for wide-band sweep the discriminator will give an output more linearly related to frequency.

**34-8. Spurious Responses.**—Panoramic presentation of the i-f acceptance band of a receiver is of great value as a means of recognizing

<sup>1</sup> Terman, *op. cit.*, p. 586.

images and some other common spurious responses. For example, suppose that for the desired signal frequency  $f_d$  the first local oscillator frequency  $f_a$  is higher than the signal frequency by the frequency  $f_i$  of the first i-f amplifier. There will also be response to a second signal  $f_u$ , which is  $f_i$  cps higher in frequency than the local oscillator. Thus, for the desired signal

$$f_i = f_a - f_d$$

and for the undesired frequency

$$f_i = f_u - f_a$$

If the local oscillator frequency is changed to  $f_a + \Delta f_a$ , there will be corresponding shifts in the two intermediate frequencies. For the desired frequency

$$f'_i = (f_a + \Delta f_a) - f_d = f_i + \Delta f_a$$

and for the undesired frequency,

$$f''_i = f_u - (f_a + \Delta f_a) = f_i - \Delta f_a$$

Thus, for the example cited, tuning the local oscillator to a slightly higher frequency results in a slightly higher i-f output for the desired signal and a slightly lower i-f output for the undesired signal, and such a distinction is readily apparent on the panoramic presentation. The undesired response can be ignored in favor of the desired response simply by correlating the direction of travel of the panoramic indication with the direction of turning the main tuning control. Harmonic responses, while not so apparent as images, can be distinguished by their higher rate of travel across the panoramic indicator.

When the double-superheterodyne method with a sweeping second local oscillator is used to obtain panoramic presentation, certain relations between the frequencies of the two i-f amplifiers and the maximum amount of the frequency sweep must be satisfied if unnecessary spurious responses are to be avoided. Because of its nonlinear action, the second mixer generates intermodulation output components, the frequencies of which are equal to the sum and difference of the signal frequency and the second-local-oscillator frequency.<sup>1</sup> The frequency of the second local oscillator is adjusted so that the difference frequency is equal to the second intermediate frequency, and the desired response is obtained. Higher order intermodulation components are, however, also generated by the second mixer. The frequencies of these components are equal to the sums and differences of integral multiples of the signal and second-local-oscillator frequencies. If the frequencies of any of these higher

<sup>1</sup> See, for instance, REICH, H. J., "Theory and Applications of Electron Tubes," 2d ed., Sec. 3-23, McGraw-Hill Book Company, Inc., New York, 1944.

order components having appreciable amplitude should fall within the pass band of the second i-f amplifier, a spurious response will appear on the panoramic indicator. Such responses can be avoided by satisfying the following relations: with the second-local-oscillator frequency above  $f_1$ ,

$$f_2 \neq \frac{(n - m)f_1 + (n + m)x}{m \pm 1} \tag{34-6}$$

and with the second-local-oscillator frequency below  $f_1$ ,

$$f_2 \neq \frac{(m - n)f_1 - (m + n)x}{m \pm 1} \tag{34-7}$$

where  $f_1$  = center frequency of the first (wide-band) i-f amplifier

$f_2$  = center frequency of the second (narrow-band) i-f amplifier

$n$  = order of the multiple of the first intermediate frequency

$m$  = order of the multiple of the second local oscillator

$$-a \leq x \leq a$$

$a$  = maximum deviation of the second local oscillator from its center frequency, assumed equal to half the band width of the first i-f amplifier

$f_1, f_2,$  and  $a$  can be in any similar units of frequency

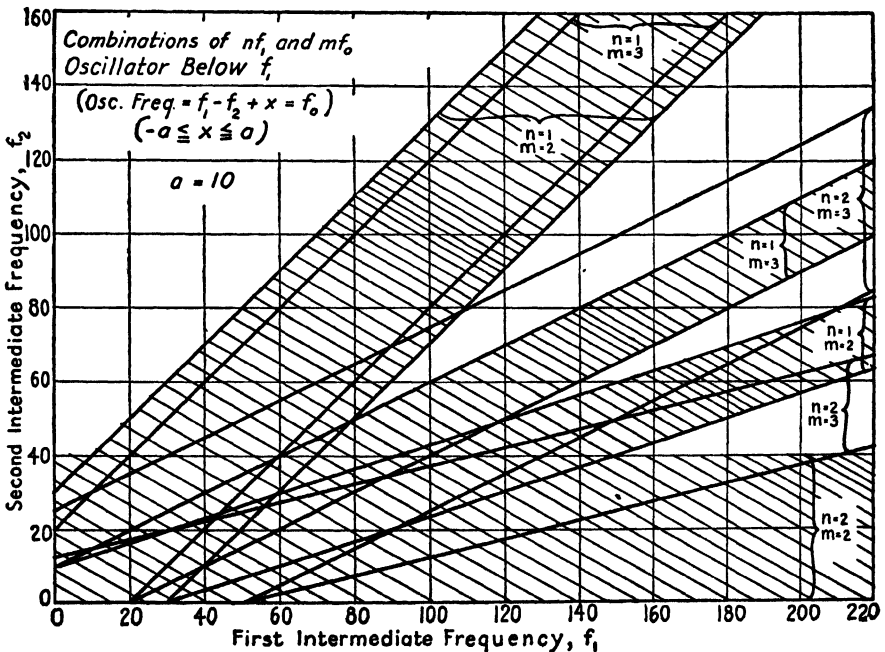


FIG. 34-7.—Diagram illustrating how frequencies of local oscillator and i-f amplifiers can be chosen to avoid interference ( $f_2$  below  $f_1$ ).

The inequality signs indicate that  $f_2$  must not be located anywhere within the frequency regions covered by the right-hand member of the inequality expression. The  $\pm$  sign in the denominator of the right-hand member indicates that two separate regions exist corresponding to  $(m + 1)$  and  $(m - 1)$ . This is true since a difference frequency of  $-f_2$  will cause a spurious response, because  $-f_2$  is the same as  $+f_2$  with a reversal of phase, and the inequality expressions as written are based on the use of positive values for  $f_1, f_2, n, m,$  and  $a$ .

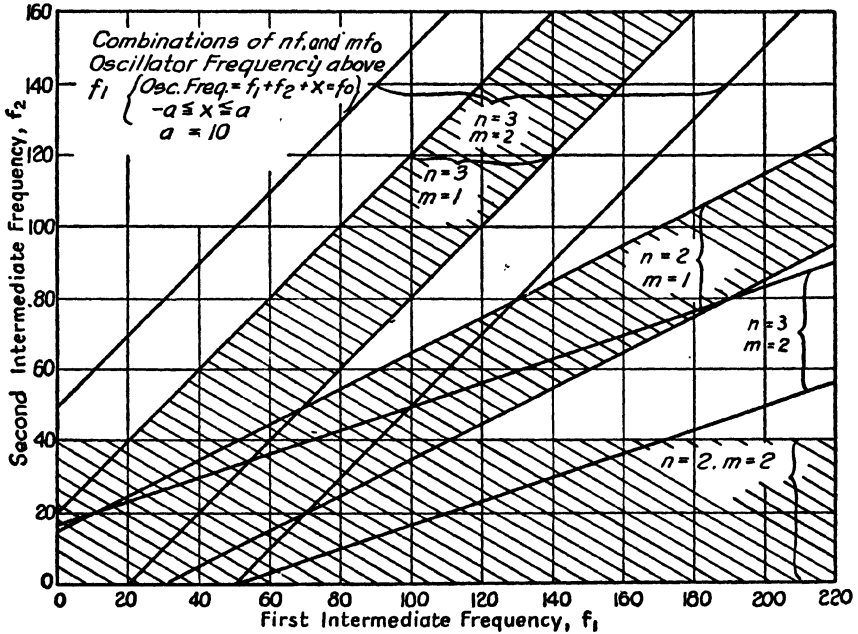


FIG. 34-8.—Diagram illustrating how frequencies of local oscillator and i-f amplifiers can be chosen to avoid interference ( $f_0$  above  $f_1$ ).

It has been found in practice that no trouble is experienced from spurious responses caused by intermodulation components, the frequency of which is equal to the sum or difference of the second or higher order multiple of the  $f_1$  signal frequency and the third or higher order multiple of the second-local-oscillator frequency. The panoramic indicator has insufficient sensitivity to be affected by these high-order intermodulation products, which have small amplitude. Any intermodulation component of lower order, however, will cause trouble if its frequency falls within the pass band of the second i-f amplifier.

The conditions expressed by the inequality relations are shown graphically in Figs. 34-7 and 34-8, where the crosshatched regions indicate values of  $f_2$  for which spurious responses are likely to occur. The

orders  $m$  and  $n$  of the multiples of the second-local-oscillator frequency and of the intermediate frequency associated with possible spurious responses are also indicated. Lines are drawn for the  $m = 2$ ,  $n = 3$ , and for the  $m = 3$ ,  $n = 2$  combinations, but the area between is not cross-hatched, since normally no trouble is encountered. The figures are drawn for  $a = 10$ . For smaller deviations, the interference strips are proportionally narrower.

*Example:* A panoramic-presentation unit is to be built for a superheterodyne receiver with a first i-f amplifier centered at 200 Mc and having a band width of 20 Mc. Thus,  $f_1 = 200$  and  $a = 10$ . From Fig. 34-7 it can be seen that the second intermediate frequency must be located between 40 and 57 Mc, or between 77 and 90 Mc, or above 110 Mc if a spurious response is not to occur when the second local oscillator is below the first i-f amplifier, and even for most of these ranges possible responses can occur for  $m = 3$ ,  $n = 2$  (e.g., an intermodulation frequency equal to three times the 145-Mc oscillator frequency minus twice the 195-Mc signal frequency, or 45 Mc, which is the second intermediate frequency). In an actual receiver, no trouble with spurious responses was encountered with a 50-Mc second i-f amplifier under the above conditions. Examination of Fig. 34-8 shows that, if in the above example the second local oscillator were placed higher in frequency than the first i-f amplifier, a choice for  $f_2$  of 45 Mc would eliminate interference from all intermodulation products of equal or lower order than those corresponding to  $m = 2$ ,  $n = 3$ . With  $f_1 = 200$  Mc and  $a = 10$  as above, an  $f_2$  of 30 Mc allows a possible spurious response from an intermodulation product whose frequency is the difference between twice the signal frequency and twice the second-local-oscillator frequency, regardless of whether the oscillator is above or below the frequency  $f_1$ . In an actual case, the amplitude of this spurious response was such as to require a change to the 50-Mc amplifier mentioned above.

It is assumed that the second intermediate frequency is lower than the first intermediate frequency. It is desirable for v-h-f operation to keep the first intermediate frequency high in order that an r-f preselector can effectively discriminate against the image response from the first conversion. It is desirable to keep the second intermediate frequency low, since a narrow band width is desired.

For very narrow band widths, such as for use in spectrum-analyzer equipments, a very low-frequency second i-f amplifier is employed, and no attempt is made to eliminate the second-conversion image response. The i-f amplifier is often built using a-f or video-frequency amplifier techniques. Intermodulation products, the frequencies of which are equal to the sums or differences of multiples of the second-local-oscillator frequency, and multiples of the signal in the first i-f amplifier, are all superposed or completely outside the usual pass band of the second i-f amplifier, and so cause no trouble, but, unless a balanced converter is

used or the level of the incoming signal is very low at the second converter or both, direct demodulation of the incoming signal will give a spurious response. Practically, if i-f amplifiers tuned to such low frequency are to be used, the amplification should be kept as small as possible in the first (wide-band) i-f amplifier consistent with selectivity requirements and the signal then built up in the second i-f amplifier to the desired level.

**34-9. Marker Signals for Frequency Indication.**—Where a constant check of exact receiver tuning is required, such as in a television relay-station receiver, the system of Fig. 34-9 could be used to give marker signals on the frequency scale of the panoramic presentation indicating

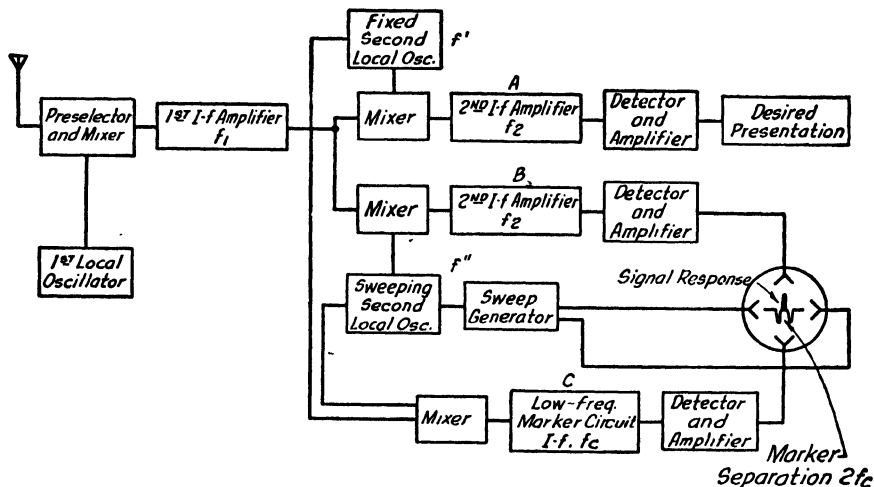


FIG 34-9.—Panoramic marker circuit.

the acceptance band of the normal receiver channel, shown as i-f channel A in Fig. 34-9. Intermediate-frequency channel B has exactly the same center frequency as channel A, but has a narrower band width so that a sharp panoramic presentation is obtained. Intermediate-frequency channel C is of the very low-frequency type discussed at the end of Sec. 34-8 and has a relatively narrow response centered at a frequency  $f_c$  equal to half the band width of channel A. As the sweeping second local oscillator sweeps through the vicinity of the frequency of the fixed second local oscillator, channel C will give two responses corresponding to  $f' - f'' = f_c$  and  $f'' - f' = f_c$ , separated by  $2f_c$  and centered about  $f_2$ . By tuning the receiver so that the signal is "bracketed" between the markers, correct receiver tuning is assured.

**34-10. Phase and Amplitude Response of the Video and Deflection Amplifiers.**—Low-frequency response and phase shift of both vertical- and horizontal-deflection amplifiers are important factors in a cathode-

ray-tube type of panoramic presentation, particularly one with mechanical sweeping of the oscillator or the circuit. With an electronic sweep it is possible to traverse the desired frequency band uniformly in one direction, with a "fly-back" time small compared with the sweep time, so the reverse trace can be blanked out, and amplitude and phase-shift variations merely cause permanent displacement of the traces, for which compensation is relatively simple. However, with mechanical sweeping, the fly-back time cannot be reduced to a small value, so that blanking the reverse sweep results in a loss of approximately half of the reception time of a signal and therefore possibly decreases the information available. By utilizing both forward and return sweeps, it is possible to make use of all the available information, but the deflection obtained in the two directions must be exactly superposed, or little is gained. With a continuous-wave signal input, poor low-frequency response and phase shift

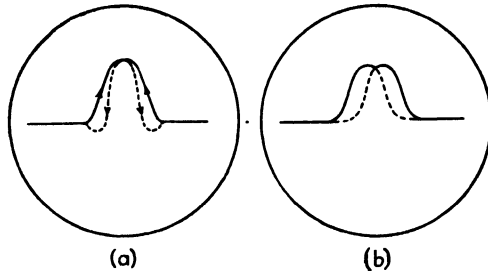


FIG. 34-10.—Effect of poor response and phase characteristics of (a) the vertical amplifier; (b) the horizontal amplifier.

of the vertical amplifier result in a pattern similar to Fig. 34-10a, characterized by overshoot, while poor response and phase characteristics of the horizontal amplifier tend to cause the pattern to be displaced horizontally, as in Fig. 34-10b, because the spot is in different positions for the same frequency on the forward and return traces.

Poor high-frequency response and phase characteristics also affect superposition of the images but, in general, are not so troublesome as low-frequency problems. Low-frequency problems are sufficiently important so that compensation<sup>1</sup> or direct coupling is required.

**34-11. Pulse Stretching and Trace Intensification.**—For most c-w and modulated c-w signals, the writing rate on the cathode-ray tube is sufficiently low so that no particular problems are encountered in obtaining adequate brilliance of the moving spot, but for the usual pulsed signals, the writing rate is too high for adequate brilliance. Thus, panoramic presentation units designed for pulsed-signal reception should incorporate pulse-stretching circuits described in Sec. 34-6 and also have circuits for intensifying the trace during its deflection.

<sup>1</sup> TERMAN, *op. cit.*, p. 414.



**34-12. Recording Circuits and Equipment.**—Under certain conditions it is desirable to have a permanent record of the information obtained by the use of a receiver. Modulation information of particular signals can be recorded on wire or disks by conventional means, or information can be obtained by motion-picture photography of oscilloscope screens. The frequency of received signals as a function of time can be electrically recorded on paper tape, such as Western Union "Teledeltos" facsimile paper. Only the latter recording system is described here.

The recorder is designed about the characteristics of the paper-recording medium employed. This paper is electrochemically darkened when the current density, at a point on its treated surface is made sufficiently high. The paper is sufficiently conducting so that the electrical marking circuit can be completed through the paper from the marking stylus to a backing roller, even though the roller may not be directly behind the marking stylus. If the backing plate or roller is not directly behind the marking stylus, only a slightly higher breakdown voltage is required, since the voltage gradient is high only in the vicinity of the marker stylus where the area involved in current conduction is very small. With the Teledeltos paper, somewhat over 50 volts between the stylus and the backing roller is required to initiate the chemical action that darkens the paper, and for all practical purposes the marking is independent of stylus polarity. Since the paper resistance drops greatly after the action has started, a series current-limiting resistor is required to keep the paper from burning. To obtain the required marking power, a gas-tube circuit is commonly employed, triggered by the detector output produced by the received signal. Two gas tubes, operating in push-pull from an alternating-voltage supply give a continuous recording with good control action. For the recording of modulated continuous waves, application of the detector output of the receiver, through a limiting amplifier, to the control grids of the gas tubes is an effective method. The time duration of the pulses of most pulse-modulated signals is too short for effective recording, however, and some form of pulse stretcher is usually required. In the example of Fig. 34-11 this takes the form of a blocked multivibrator, each incoming pulse causing it to flip from one condition to the other of the two stable conditions; the next pulse then returns it to its original state. Thus, square waves are produced with a fundamental frequency of half the pulse-repetition frequency of the original signal. The initial amplifier tube is run at zero bias to provide a limiting action which increases the effective range of signal amplitudes that will record satisfactorily without gain-control adjustments. This feature is particularly desirable if the operation of the recorder is to be automatic with a wide variety of input signal strengths such as might be encountered under airborne monitoring conditions.

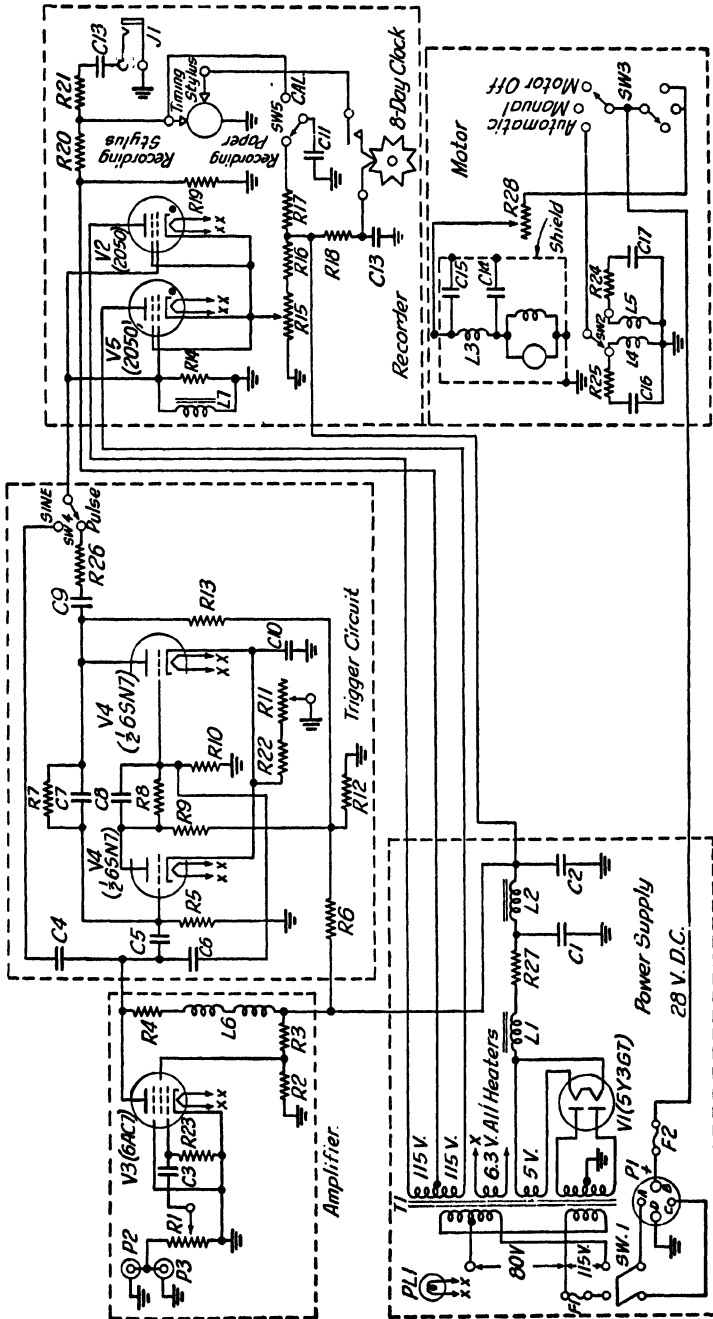


FIG. 34-11.—Schematic diagram of a paper-tape recording system.

In order to indicate the frequency of received signals, the recording stylus is made to move across the tape in synchronism with the frequency sweep. To indicate the time of reception of the signals, the tape can be arranged to advance at a fixed rate of speed, with fixed-interval dots marked along one edge of the tape by means of a fixed stylus and a clock-driven marking circuit. The rate of advance of the tape depends on the frequency with which the traveling marking stylus returns to the same recording position. If the receiver and recorder are varied slowly

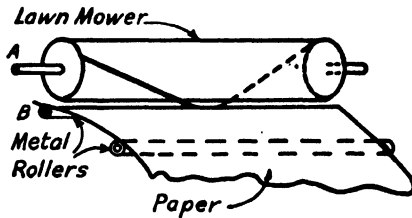


FIG. 34-12.—“Lawn-mower” stylus for high-speed paper-tape recorder. The cylinder has a helical metal ridge on the outside surface and the angular position of the roller is made proportional to the receiver frequency. The recording voltage is applied between shafts *A* and *B*.

over the desired recording band, it is not necessary that the tape travel more than a few inches per hour. However, to obtain the discrimination possible with the “lawn-mower” type of stylus of Fig. 34-12, a more rapid rate of travel of the tape is required. Calibration of the tape corresponding to the frequency setting of the receiver can be accomplished by tuning the receiver to the desired calibrating frequencies

and each time marking the tape by discharging a charged capacitor through the paper. The strip of paper thus calibrated can be cut off and used as a scale to measure the frequency of recorded signals anywhere along the record.

The recorders are built about the characteristics of the paper, but the problems are largely mechanical ones: the tape feed must be of uniform speed and must keep the tape straight; the stylus must in some cases travel alternately back and forth across the paper; the stylus travel must be geared to the receiver tuning. The marking styli must be small to give a clean record, must be hard and wear-resistant, and must have a polished rounded end to minimize soot and dust collection at the tip. Hardened beryllium-copper wire makes a satisfactory stylus. Even tape feed can be accomplished by driving the tape by means of a rubber roller in contact with a metal roller. By individual adjustment of the springs holding the metal and rubber rollers together at each end, the effective operating radius of the rubber roller can be adjusted so that the tape feeds evenly. With a narrow tape, such individual adjustment is not necessary; a prefeed-roller paper guide is sufficient.

**34-13. Pulse Analysis.**—In order to specify completely a voltage pulse, such as might be encountered in the examination of the envelope of the r-f transmissions of a radar, one must determine the maximum amplitude, the duration, and the general shape of the pulse. In addition,

with periodic pulses, the pulse-repetition frequency must be determined.

The duration of a pulse is commonly termed *pulse length* (also called *pulse width*), as suggested by the graphical representation, and is easily defined for purposes of measurement if the pulse is rectangular with infinite slope at its beginning and end. Measurement becomes increasingly difficult, however, as the pulse shape departs from the rectangular, the value obtained being dependent on the particular definition employed. A definition of pulse length for shapes approximating a rectangle, particularly applicable to oscilloscopic examination, is that of the time interval between the points at which the pulse rises and falls through an amplitude 6 db less than the peak amplitude (half-voltage amplitude). For meter presentation, a more suitable definition is the time interval between the points of most rapid rise and fall, particularly as these points are relatively unaffected by the capacitance loading inevitably present in the pulse-handling amplifier circuits.

*Pulse-repetition frequency* (prf) is readily defined as the number of pulses occurring per second.

*Pulse amplitude* is defined as the peak voltage or peak power of the pulse and is expressed in terms of peak volts or peak watts.

In order to measure any one of the three variables—pulse length, amplitude, or repetition frequency—it must first be isolated, *i.e.*, the effect on the measuring apparatus of the other two variables must be eliminated or minimized to the point where they are no longer noticeable. This is quite easy in the determination of pulse-repetition frequency and fairly easy in pulse-amplitude determination. It is relatively difficult, however, for pulse-length determination.

Pulse amplitude is usually measured by peak-voltmeter or oscilloscopic methods, but means for measurement will not be discussed here. The principal methods for measuring pulse length and pulse-repetition frequency are those employing cathode-ray-tube presentation and those using meter presentation. Pulse-repetition frequency is sometimes measured by aural means, but ambiguity is hard to avoid. Representative methods of measurement will be discussed in order to illustrate the principles of each type.

**34-14. Oscilloscopic Measurement of Pulse Length.**—Figure 34-13 shows a method of measuring pulse length and obtaining a visual display of pulse shape. The incoming pulse is amplified for application to the vertical-deflection plates of a cathode-ray tube and is used simultaneously to trigger a saw-tooth voltage generator for the horizontal sweep.<sup>1</sup> Owing to the time that elapses between the arrival of the pulse at the triggering circuit and the beginning of the linear-sweep voltage, some method of phase control must be introduced in order to present all the leading edge

<sup>1</sup> REICH, *op. cit.*, p. 368.

of the pulse on the cathode-ray-tube screen. This may be done either by delaying the pulse until the linear sweep has started, or, in the case of periodic pulses, by delaying the sweep for use in presenting the succeeding pulse. The latter is preferable, if possible, as the phase control may be placed in the sweep circuit, eliminating the possible distortion introduced by a delay line between the signal input and the vertical-deflection plates.

The triggering action of the sweep system of Fig. 34-13 is made relatively independent of pulse amplitude and pulse length by differentiating the pulse to obtain sharp voltage pips from the leading and trailing edges of the pulse, as at *B* in Fig. 34-14 (for the sake of clarity, the rectangular pulse from the flip-flop has not been superposed), and utilizing only the voltage pip from the leading edge of the pulse to trigger the flip-flop circuit or generator of rectangular voltage pulses<sup>1</sup> of Fig. 34-14. The flip-flop then immediately shifts to its second (temporarily)

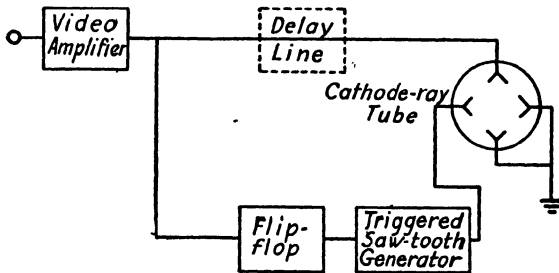


FIG. 34-13.—Pulse display by means of a cathode-ray tube and triggered time base.

stable state and then after a time interval  $t_x$ , controlled largely by the combination of  $(R_1 + R_2)$  and  $C_1$ , returns to its initial stable state, giving the wave form shown at *C* (Fig. 34-14) for each input pulse. By differentiating the wave form at *C* by means of the small-time-constant network  $C_d'R_d'$ , a positive voltage pip and a negative voltage pip are obtainable at *D*, both having essentially constant amplitude. The positive voltage pip occurs nearly simultaneously with the input pulse, and the negative voltage pip has a controllable time delay  $t_x$  with respect to the input pulse.

For recurrent pulses, the negative voltage pulse from the flip-flop of Fig. 34-14 is used to initiate the saw-tooth generator of Fig. 34-13, which then gives a linear-time deflection to the cathode-ray-tube beam. The time delay  $t_x$  is adjusted so that one input pulse causes the start of the cathode-ray sweep just prior to the time of arrival of the succeeding pulse. Calibration of the variable elements  $R_1$  and  $C_1$  (Fig. 34-14) in microseconds allows measurement of pulse length by shifting the pulse

<sup>1</sup> REICH, *op. cit.*, p. 359.

presented on the cathode-ray tube through its own length with respect to an arbitrary point on the screen. Alternatively, the time base can be calibrated. Since the time base on which each pulse is presented is triggered by the preceding pulse, the system is subject to the inaccuracies incurred in making the length of the flip-flop cycle  $t_x$  of the same order of magnitude as the pulse-recurrence period. The inaccuracies can be minimized by returning the grid of  $V_2$  to a positive voltage, as shown in Fig. 34-14, rather than to ground, in order to obtain steeper slope at the point of intersection of the curve of changing grid voltage due to the discharging of capacitor  $C_1$  and the line of critical grid voltage of the tube  $V_2$ . The flip-flop can be made a little more sensitive by applying a differentiated positive pulse to the grid of  $V_1$ , in Fig. 34-14, but in this

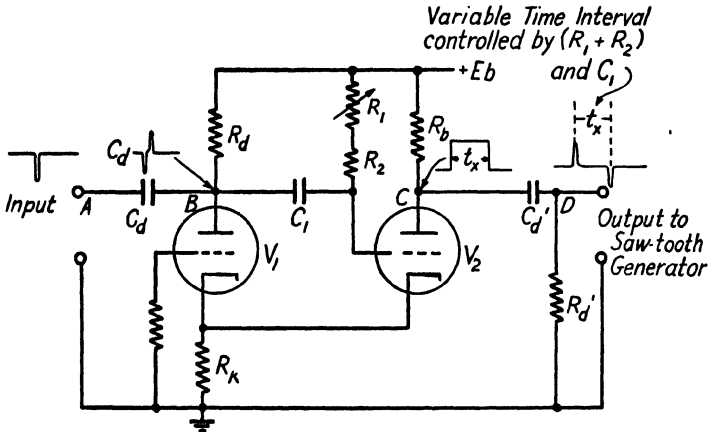


FIG. 34-14.—Flip-flop with RC control of pulse duration.

case trouble may be experienced from the spike from the differentiated trailing edge of the pulse. For aperiodic pulses and transients, the sweep voltage must be triggered by the actual impulse to be displayed, or by some voltage associated with it. When no triggering source is available other than the pulse itself, the pulse may be presented on the cathode-ray tube by placing a delay circuit between the video amplifier and the vertical-deflection plates, as indicated by the dashed block in Fig. 34-13, and initiating the sweep with the leading edge of the pulse. With artificial long lines, delays of the order of several microseconds may be obtained, with little distortion of 1- $\mu$  sec pulses.

For either periodic- or aperiodic-pulse presentation of this type, the flip-flop provides a convenient source of trace-brightening voltage for the cathode-ray tube. This allows adjustment of the intensity control to a point at which the tube is cut off when no sweep voltage is applied, thus preventing the possibility of burning the tube with a stationary spot.

**34-15. Meter Indication of Pulse Length.**—Meter presentation of the length of recurrent pulses requires the elimination or minimization of the effects of amplitude and recurrence frequency on the measuring circuits. The defined pulse length must thus be based on a time quantity suitable for measurement and relatively independent of amplitude and repetition-frequency variations. The most suitable time quantity is that between the points of most rapid rise and fall of the pulse. Pulses originally rectangular become distorted and suffer a time delay in passing through amplifier circuits, which inevitably have band-width restrictions, but the time interval between the points of most rapid rise and fall remains relatively unchanged.

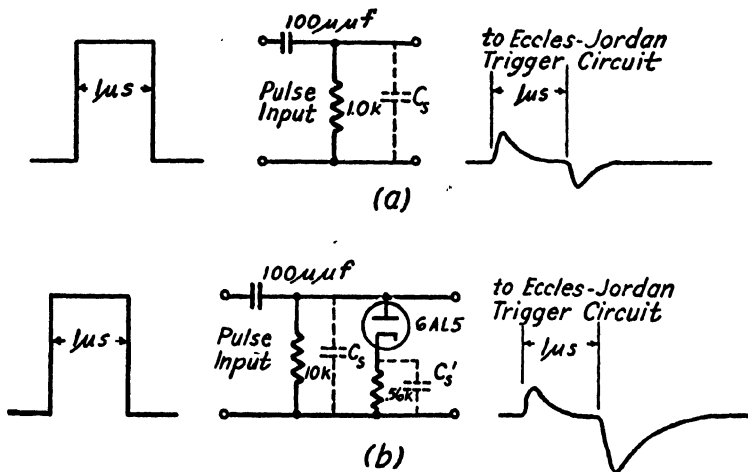


FIG. 34-15.—Differentiator comparison. (a) ordinary differentiator; (b) selective differentiator.

By applying a positive pulse to a differentiator circuit such as that of Fig. 34-15a, a positive and a negative pip are obtained which are separated in time by the length of the applied pulse. If these positive and negative pips are used to turn an Eccles-Jordan trigger circuit<sup>1</sup> on and off, a new pulse can be produced that has an amplitude and shape largely independent of the amplitude, shape, or repetition frequency of the original pulse, except that the length of the new pulse is equal to that of the original. The repetition frequency is likewise unchanged. The inevitable stray capacitances  $C_s$  and  $C_s'$ , in Fig. 34-15, tend to round the leading edges of the positive and negative pips from the differentiator and so make the triggering of the Eccles-Jordan circuit depend on the amplitude of the original input pulse, particularly as the input pulse is

<sup>1</sup> ECCLES, W. H., and F. W. JORDAN, *Radio Rev.*, 1, 143 (1919); REICH, *op. cit.*, p. 353.

itself usually considerably rounded. However, the dependence on amplitude of the time *interval* between turning the Eccles-Jordan circuit on and off is a second-order effect, as may be seen from Fig. 34-16. There the variation with amplitude in the time required to turn the trigger circuit on after onset of the original pulse is counteracted by the nearly equal variation with amplitude in the time required to turn the trigger circuit off after the beginning of decay of the original pulse.

The original pulse shape may be asymmetrical, or asymmetrical noise pulses may be present in the circuit, giving rise to unequal positive and negative pips from the differentiator of Fig. 34-15a. A condition whereby the Eccles-Jordan trigger circuit would be turned on by such a

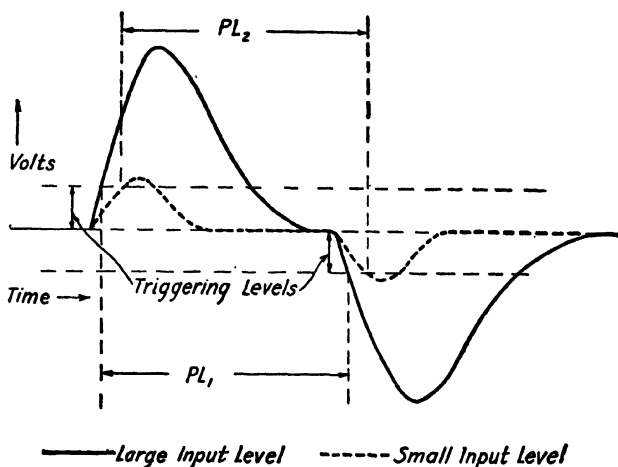


FIG. 34-16.—Variation of indicated pulse length  $PL$  with change of input amplitude.

pulse, but not turned off, would give in effect a pulse to be measured of extremely long duration, and even rare instances of such a large discrepancy might affect adversely the average or indicated value of the desired pulse length. Accordingly the possibility of such an error should be eliminated by emphasizing the negative pip from the trailing edge of the input pulse. This could be done by making the Eccles-Jordan trigger circuit nonsymmetrical, but a preferable method is that shown in Fig. 34-15b, where the effective resistance of the differentiator circuit to the positive and negative pips is different because of the diode action. The resultant unequal action on positive and negative pips destroys to a certain extent the compensating action indicated in Fig. 34-16, except that most pulses have more indefinite trailing than leading edges and, therefore, tend to give too little output from the differentiator on the negative pip. The combination of the usual asymmetrical pulse and the selective differentiator of Fig. 34-15b thus results in a more valid pulse



length of the output pulse from the Eccles-Jordan trigger circuit. Pulse input voltage to the differentiator must be high enough so that power-supply variations have a negligible effect on the indicated pulse length.

The variables of pulse amplitude and shape having been eliminated (the length is still variable, of course), the pulse length can now be measured by means of the circuit of Fig. 34-17 and a peak-reading vacuum-tube voltmeter. The voltage to which the capacitor  $C$  is charged is a function of the  $RC$  product and also of the pulse duration. The peak voltage to which the capacitor charges is then measured by means of a peak-reading voltmeter calibrated directly in microseconds of pulse length. To change scales it is merely necessary to change  $R$  or  $C$ . The problem of measuring the peak voltage of a wave having the shape of that of Fig. 34-17 is a difficult one, because the entire wave has a duration at most of only a few microseconds. The voltmeter must necessarily be a peak voltmeter, because any amplitude quantity other than the peak value of

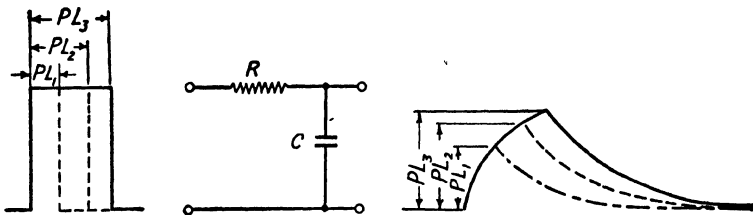


FIG 34-17 — Pulse-length discriminator.

the wave (such as rms or average value) is dependent on the pulse-repetition frequency as well as the pulse length.

To provide a charge in the amount needed by the peak voltmeter circuit requires either many pulses or the use of a pulse lengthener similar to that of Fig. 34-18. The operation is illustrated by the wave forms sketched there and is as follows: When the circuit is in its quiescent condition points  $b$ ,  $c$ , and  $d'$  are at zero or ground potential. Upon arrival of the leading edge of the positive pulse, the potential at  $b$  rises immediately, raising the cathode potential of  $V_3$  and cutting it off, since the potential at  $c$  rises less than at  $b$ .  $C_1$ , however, is small so that it can charge rapidly through the diode  $V_1$ ; so the potential at  $c$  begins to fall immediately. By the time the trailing edge of the pulse comes along, the potential at  $c$  is almost zero again. Meanwhile the pulse has been charging  $C_2$  through the diode  $V_2$  and the resistance  $R_2$  (the capacitor  $C_2$  and the resistor  $R_2$  form the pulse-length sensitive network, which is here combined with the pulse lengthener). When the trailing edge arrives, the potential at  $b$  drops back to ground potential cutting off  $V_2$ . The potential at  $c$ , which is already low, goes negative by nearly the amplitude of the pulse, thus cutting off  $V_1$  and keeping  $V_3$  cut off.

The potential at *c* now rises to zero slowly as  $C_1$  discharges through  $R_1$  and  $R_L$ . When the negative voltage between points *b* and *c* becomes small enough,  $V_3$  conducts, discharging  $C_2$  through  $R_L$  to ground. The result of all this action is that the wave form presented to the voltmeter circuit (connected to the cathode follower at point *d* in Fig. 34-18) is not a peak of relatively short duration as in Fig. 34-17 but is flat as in Fig.

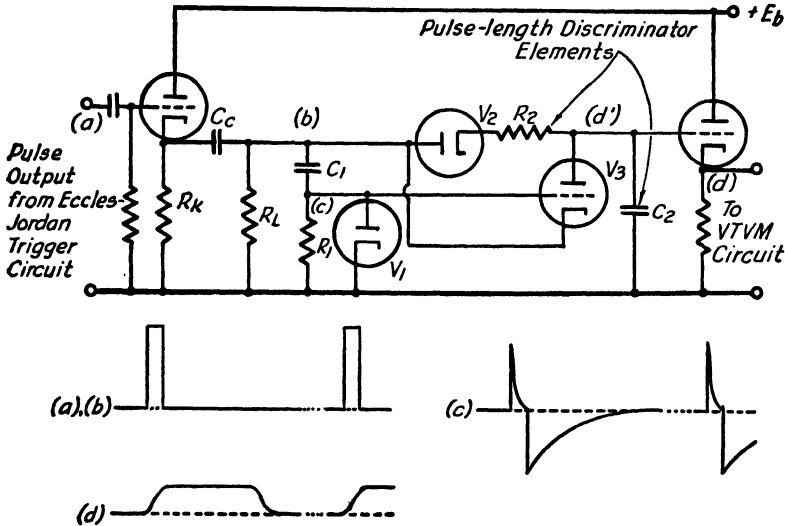


FIG. 34-18.—Pulse lengthener and length discriminator, and pulse forms at points *a*, *b*, *c*, and *d*.

34-18*d*. The amplitude of this new wave form is still proportional to the pulse length, but its duration has been extended, corresponding to a very large amplification of energy.<sup>1</sup> The impedance of the discharging circuit for the capacitor  $C_2$  should be of the same order of magnitude as the charging impedance so that discharge will be complete before the arrival of the next pulse. There is a maximum duty cycle that such a circuit can

<sup>1</sup> Consider a rectangular pulse of amplitude  $V$  volts and length  $w$   $\mu$ sec. If this pulse is impressed upon a fixed resistance, the current, if capacitances are disregarded, is  $V/R$  and the power (usually called *peak power*) is  $V^2/R$ . If this peak power is multiplied by the time of duration of the pulse  $w$ , a quantity is obtained that has the dimensions of energy and is a measure of the energy in the pulse. The term *energy* when applied to a video pulse must be used with some caution, for the energy implied by the video wave shape at some point in nonlinear circuits may not be readily available. This precaution is especially true of the circuit in Fig. 34-18. While the wave shape is the same at point  $d'$  as it is at point  $d$ , the actual available energy content is quite different because of the different circuit impedances involved. At point  $d'$ , current has been sacrificed to maintain voltage; it is the output tube that actually accomplishes the energy amplification in the sense that the energy as determined from the wave shape can be used to excite the meter circuit.

handle. Ordinarily, this limit is approached with systems having a pulse duration greater than approximately  $\frac{1}{2}$  per cent of the interval between pulses.

The use of a pulse-lengthener circuit such as that of Fig. 34-18 makes possible the use of a simple peak voltmeter of the form of Fig. 34-19. The capacitance  $C$  (Fig. 34-19) can be made large enough so that the meter reading will remain substantially constant for a relatively long period of time, yet a short burst of pulses, as from a sweeping radar, is

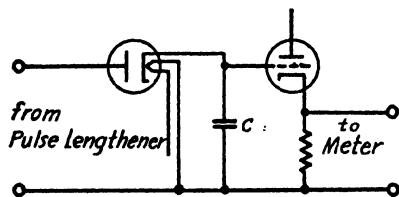


FIG. 34-19.—Simple storage circuit.

sufficient to charge  $C$  to the peak value of the lengthened pulse. To reduce leakage of charge from the capacitor  $C$ , the cathode follower should be operated at a low plate voltage and current to reduce the grid current, and the heater voltage for the diode should be operated below normal to reduce the heater-cathode current.

The heater-cathode current is reduced at first more rapidly than the diode plate-cathode impedance is increased, so that the leakage can be reduced without greatly affecting the diode efficiency. To obtain new readings, provision must be made for periodically short-circuiting capacitor  $C$ .

Another method of determining pulse length employs the principles of the heterodyne wave analyzer, using any suitable communications type of radio receiver. The frequency spectrum of a video pulse is determined and the pulse length therefrom deduced.<sup>1</sup>

**34-16. Oscilloscopic Measurement of Pulse-repetition Frequency.** The repetition frequency of recurrent pulses presented on a cathode-ray



FIG. 34-20.—Cathode-ray-tube patterns in p-r-f measurement.

tube may be determined by applying a sinusoidal voltage of known frequency to the time-axis deflection plates. The frequency of the sinusoidal voltage is varied until it is equal to the pulse-repetition frequency, and a stationary single pulse is obtained on the cathode-ray-tube screen, as shown in Fig. 34-20a. The method is subject to ambiguities, however, for the pattern still shows a single pulse when the frequency of the time-

<sup>1</sup> PETERSON, ARNOLD, *The Communications Receiver as a Wave Analyzer*, *Gen. Radio Experimenter*, 18, No. 8 (1944); STANSEL, F. R., *Some Analyses of Wave Shapes Used in Harmonic Producers*, *Bell Systems Tech. Jour.*, 20, 331-339 (1941).

axis voltage is an integral multiple  $N$  of the repetition frequency. Two pulses are obtained, as in Fig. 34-20*b*, if the time-axis frequency is any odd multiple  $N$  of half the repetition frequency, and in general  $m$  pulses will be obtained if the time-axis frequency has a nonreducible ratio  $N/m$  times the pulse-repetition frequency, so that ambiguities cannot be resolved unless the time-axis frequency is continuously reduced to the lowest frequency that will give a single stationary pulse.

Figures 34-21 and 34-22 illustrate a method helpful in overcoming the ambiguities discussed above by separating the forward and return traces of the base line. The addition of a capacitor  $C$  and a resistor  $R$ , as shown, feeds a portion of the sinusoidal time-base voltage to the vertical-deflec-

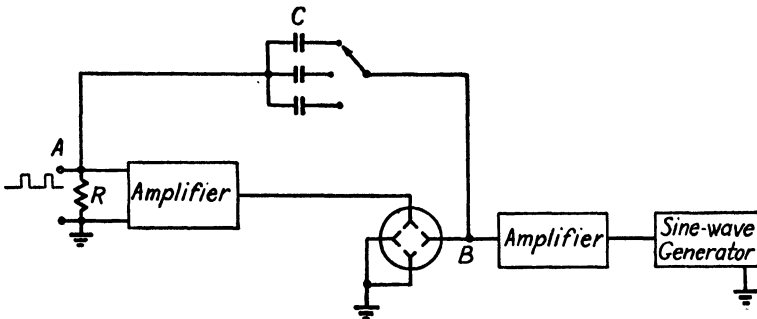


FIG. 34-21.—Block diagram of circuit for elliptical time base.

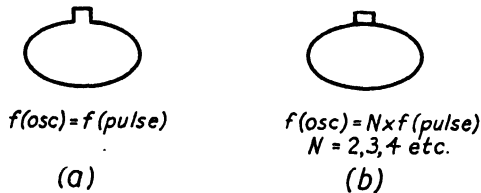


FIG. 34-22.—Cathode-ray-tube patterns in measurement of pulse-repetition frequency.

tion plates in a leading phase with respect to the horizontal-deflection voltage. The result is an elliptical time base rather than a straight line. As may be seen in Fig. 34-22*a*, the open base of the pulse indicates that the time-base frequency is equal to the repetition frequency, whereas a time-base frequency a multiple of the repetition frequency gives a closed-base pulse, as in Fig. 34-22*b*. To minimize the tendency of the pulse voltage to distort the horizontal time axis, the phase-shifted voltage should be obtained from the horizontal-deflection circuit at a high-amplitude level, as at  $B$  in Fig. 34-21, and introduced into the vertical-deflection circuit at a low-amplitude level as at  $A$ . If a wide range of pulse-repetition frequencies is to be investigated, several capacitors may be used with a selector switch, as indicated in Fig. 34-21, since for any one capacitor the ratio of the minor diameter to the major diameter of

the ellipse decreases with increasing frequency. The oscilloscopic method of determining repetition frequency is time-consuming because of the ambiguities, but the method is quite useful for accurate determination of a frequency that is known approximately, or for separation of two or more signals simultaneously present and whose repetition rates differ by as little as one pulse per second or less.

**34-17. Meter Indication of Pulse-repetition Frequency.**—If the recurrent pulses whose repetition frequency is to be measured are available constantly at the meter circuit, an electronic frequency meter<sup>1</sup> will give an accurate repetition-frequency indication. If the pulses are not continuously present as might be the case when receiving the signal from a sweeping radar system, some means of maintaining the meter reading for a period after reception of the pulses is desirable. The measuring circuit must also give a correct reading on only a few received pulses.

The flip-flop circuit of Fig. 34-14 is suitable for removing the effects of pulse length and pulse amplitude, leaving repetition frequency as the only variable. The repetition frequency can then be converted to an

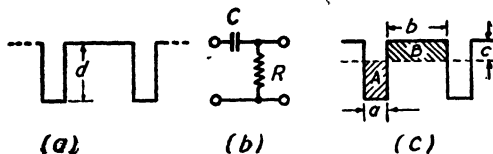


FIG. 34-23.—Pulse-repetition frequency discriminator.

electrical quantity suitable for measurement by the  $RC$  circuit of Fig. 34-23b. Here the input rectangular pulse is negative [such as might be obtained by deriving the output of the flip-flop from the plate of  $V_1$  (Fig. 34-14) instead of from the plate of  $V_2$ ] and has a time duration  $a$  and amplitude  $d$  (Fig. 34-23) which are constant and determined only by the constants of the flip-flop circuit. After the pulse has passed through the  $RC$  circuit, the zero line of voltage is shifted so that for steady-state conditions area  $A$  equals area  $B$  (average voltage = 0). The time  $a$  is constant, and the time  $a + b$  is the pulse-recurrence period, so that as the repetition period decreases (repetition frequency increases) the time  $b$  must decrease, and hence for  $A = B$ ,  $c$  must increase. The amplitude  $c$  is thus directly proportional to pulse-repetition frequency, so that a peak-reading voltmeter using the circuit of Fig. 34-19 can be used to give the desired meter indication of repetition frequency.

The rapidity of response of the network of Fig. 34-23b (*i.e.*, the time required for it to come to equilibrium from a quiescent condition) is a function of the  $RC$  product. If the  $RC$  product is very large, the wave shape (Fig. 34-23c) is square, but the network takes too long to reach

<sup>1</sup> REICH, *op. cit.*, p. 624.

equilibrium conditions. If the  $RC$  product is very small, the wave shape is differentiated and the dependence of the amplitude  $c$  upon frequency becomes a second-order effect; in addition, since the amplitude of each pulse decays exponentially with time, the peak voltmeter reads the peak voltage less accurately than it would if the amplitude remained relatively constant. Accordingly, the  $RC$  product should be the largest value possible that still allows substantially equilibrium conditions to be reached during the shortest expected period of reception of pulses. Figure 34-24 illustrates both the transient before steady-state conditions have been reached and the lack of rectangularity of the pulses after passing through the  $RC$  network.

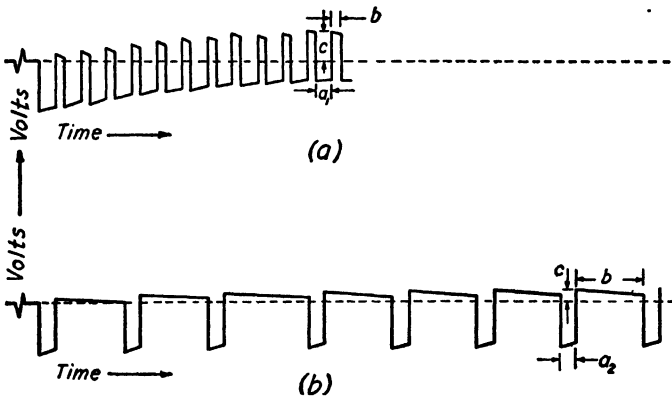


FIG. 34-24.—Transient response of  $RC$  network of Fig. 34-23 to rectangular waves: (a) for a high pulse-repetition frequency; (b) for a low pulse-repetition frequency.

The scale factor of the frequency-measuring circuit can be very simply changed by altering the flip-flop time constant so as to change the time  $a$ , Fig. 34-23, by the desired factor so that the amplitude  $c$  is correspondingly changed. However, the time constant must be chosen so as to ensure that the repetition-frequency meter will read off-scale for all frequencies above the maximum one for which it is calibrated. The flip-flop must, therefore, be able to complete its cycle and again reach equilibrium between pulses up to a frequency slightly greater than twice peak-scale reading. If the flip-flop has not reached equilibrium after operating on one pulse before the next pulse arrives, and the input voltage is marginally low, the flip-flop merely skips the second pulse and operates on the third; *i.e.*, it divides the frequency by 2. It is necessary then, for the frequency at which the circuit skips to be more than twice the full-scale frequency of the meter.

With the above precautions observed, repetition frequency can be measured with an accuracy comparable to that of small indicating instruments, even for a short burst of pulses such as might be received from a sweeping radar system.

## CHAPTER 35

### MEASURING EQUIPMENT FOR RECEIVERS

BY W. B. WHOLEY

**35-1. Test Equipment.**—In preceding sections the problem of testing and aligning wide-range receivers has been discussed, but little mention has been made of the equipment and methods necessary for these tests. Since much of this test equipment is commercially available, and the principles of design well established, only relatively new techniques and equipment such as r-f signal sources, r-f sweep oscillators, and heterodyne frequency meters will be discussed.

Signal sources are needed to supply r-f energy, modulated or unmodulated, for measuring impedance characteristics, noise figures, sensitivity, selectivity, amplifier response, etc. For the measurement of i-f and video responses, lower frequency commercial signal sources are available, so these will not be discussed.

Radio-frequency sweep oscillators can be used for rough and rapid checking of the frequency response of various r-f components, such as mixers, preselectors, and amplifiers. Commercial sweep generators, suitable for i-f amplifier checking, are available for the lower frequencies.

Heterodyne frequency meters are necessary for checking the frequency of receiver local oscillators and for frequency calibration of receivers.

**35-2. Signal Sources.**—Signal sources may be divided into two main groups, *viz.*, *standard signal generators* and *test oscillators*. The basis of each is a stable r-f oscillator accurately calibrated as to frequency, but the test oscillator is simpler in design and has fewer components. Both are modulated.

*Standard Signal Generators.*—Standard signal generators are used for measuring receiver noise figure, sensitivity, selectivity, amplifier response, spurious and image responses, etc. For these purposes a stable r-f oscillator with an accurate frequency calibration is required. The level of the output signal should be accurately calibrated and variable over wide ranges. The value of output impedance is determined by the use for which the signal generator is intended. Since the output voltage or power must be accurately known, the generator must have sufficient shielding to limit leakage to a level very much lower than the desired minimum output. Standard signal generators designed to check

the search receivers previously described should have pulse modulation, which these receivers were designed to receive. Other types of modulation, such as sine-wave amplitude or frequency modulation may also be included, but whether these are feasible or not may be determined by the modulation characteristics of the r-f oscillator. The modulation must be quite versatile, *i.e.*, with sine-wave modulation a large number of frequencies, and with pulse modulation a large number of repetition rates and pulse widths, must be included. A block diagram of a standard signal generator is shown in Fig. 35-1. The components represented in the diagram will be discussed in detail in succeeding sections on oscillators, modulators, and output systems.

**Test Oscillators.**—Test oscillators are a simpler type of generator used as signal sources for aligning preselectors of receivers, for rough performance checks on receivers, and for feeding impedance-measuring lines. This type of service requires a stable r-f oscillator with an accurate frequency calibration, but it does not need to be so well shielded, as the output level of the signal need not be accurately known. A built-in output attenuator, although convenient, is not essential since an external attenuator can be used, nor is it necessary that the attenuator, if included, be accurately calibrated. The type of modulation provided will be dictated by the use for which the test oscillator is intended. For use with impedance-measuring lines the type of modulation should be such as to allow a

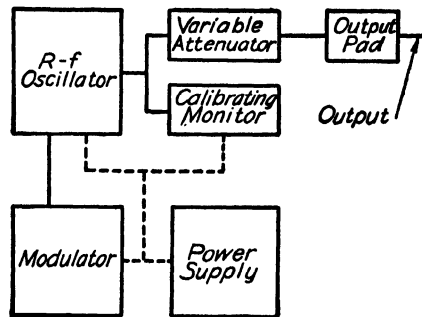


FIG. 35-1.—Block diagram of standard signal generator.

relatively large amount of r-f power output. These high levels of r-f power preclude the use of pulse modulation because of the low duty cycle and limit the types of modulation to sine and square waves. On the other hand, for testing receivers, pulse modulation is advantageous when this is the type of signal that the receivers are designed to receive. As compared with standard signal generators, the modulation characteristics need not be so complete, *i.e.*, in the case of sine waves the modulation can be limited to a few different frequencies and in the case of pulses to a few different repetition rates and pulse lengths. A block diagram for a test oscillator is similar to that of the standard signal generator shown in Fig. 35-1, except that the output pad and the calibrating monitor are omitted.

**35-3. Components of Signal Sources.**—From the foregoing discussion it will be noted that the main components of test oscillators, *viz.*, r-f



oscillators and modulators, are similar to the corresponding components of a standard signal generator. In addition to these two a standard signal generator has two other major components, the output attenuator and the calibrating system. These four components for signal sources will now be discussed in greater detail, and ways of obtaining the desired characteristics will be indicated.

**35-4. Radio-frequency Oscillators.**—The requirements for the r-f oscillator are that it be stable and relatively free of harmonics, and that, for receiver testing, it have a power output of at least 30 mw. Local oscillators designed for receivers usually meet these requirements and have in many cases been used as r-f oscillators in signal generators. Their design is discussed in Chaps. 30, 31, and 32. The oscillators suitable for signal sources can be divided into four groups which are listed below together with the frequency range over which they are generally found useful.

1. Oscillators using miniature or acorn tubes with variable-capacitor *LC* circuits, up to 400 Mc
2. Oscillators using acorn or doorknob tubes with butterfly circuits, 100 to 1000 Mc
3. Oscillators using triodes with line circuits, 100 to 2000 Mc
4. Oscillators using reflex klystrons with external cavities, 1500 to 10,000 Mc

In order to obtain adequate frequency stability for signal-generator purposes with high-frequency oscillators it is necessary to use a well-regulated power supply.

The operating frequency of the oscillator can be indicated by means of either a counter or a dial calibrated directly in frequency and mechanically connected to the oscillator tuning element. Either method is capable of indicating the operating frequency of the oscillator with an error of less than 1 per cent, but the directly calibrated dial is in many cases preferable since the use of counters quite often necessitates calibration curves. With many line oscillators, the tuning is straight-line wavelength, which may be converted to straight-line frequency by the use of a simple cam arrangement. This allows counters to be used to read the frequency directly.

**35-5. Modulators.**—Three main types of modulation are used on signal generators, *viz.*, sine-wave amplitude, pulse amplitude, and frequency modulation. Square-wave modulation can be considered as a special case of pulse modulation. These types will now be considered separately.

*Sine-wave Amplitude Modulation.*—Sine-wave amplitude modulation can be incorporated in signal sources employing triode oscillators. With these oscillators fairly large percentages of modulation, 30 to 50 per

cent, may be obtained before the modulation characteristics of the oscillators become nonlinear, and the amplitude modulation may be obtained without an appreciable amount of frequency modulation. On the other hand, with higher frequency oscillators, such as those using reflex klystrons, it is hard to obtain any degree of amplitude modulation without an appreciable amount of incidental frequency modulation. Therefore, sine-wave modulation is ordinarily not used on these oscillators. Sine-wave modulation when feasible is obtained by plate modulation of the r-f oscillator.

**Frequency Modulation.**—The situation with respect to frequency modulation is almost exactly opposite to that for amplitude modulation. On triode oscillators frequency modulation is usually not used because of the complexity of the circuits necessary to obtain it. On the other hand, rough frequency modulation may be easily obtained in oscillators using reflex klystrons and is usually incorporated in these higher frequency signal generators. Frequency modulation of such oscillators is obtained by applying the modulating voltage to the reflector of the tube, as shown in Fig. 35-2.

**Pulse Modulation.**—Pulse modulators for use in standard signal generators should have the following general characteristics:

1. Variable pulse-repetition rate
2. Variable pulse length
3. Provision for synchronization to externally provided trigger impulses
4. Provision for supplying output trigger impulses
5. Variable delay time between the input or output trigger impulse and the output pulse.

If these signal generators are to be used to check receivers designed to receive radar signals, the variation in pulse-repetition rate, pulse length, and delay time should be approximately 40 to 5000 cps,  $\frac{1}{2}$  to 30  $\mu$ sec, and 3 to 300  $\mu$ sec, respectively. These approximate limits are based on current radar practices and can usually be somewhat modified to suit the requirements in any specific r-f range that the signal generator is to cover.

The foregoing general requirements can be met by means of a pulse generator, of which the block diagram is shown in Fig. 35-3a, and the

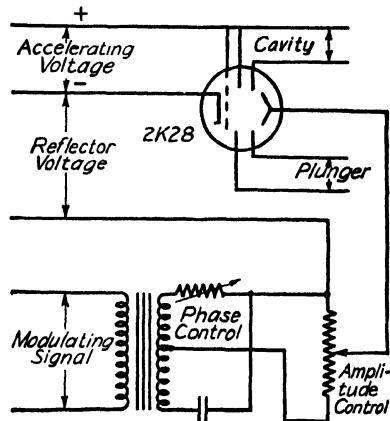


Fig. 35-2.—Circuit for frequency-modulating reflex klystrons.

wave shapes at various points in the circuit in Fig. 35-3b. The circuit shown in block A is for controlling the pulse-repetition frequency. It should be some form of oscillator that will produce an output voltage having steep wave fronts, the frequency of which can be varied and synchronized with a triggering pulse. Oscillators of the relaxation type<sup>1</sup>

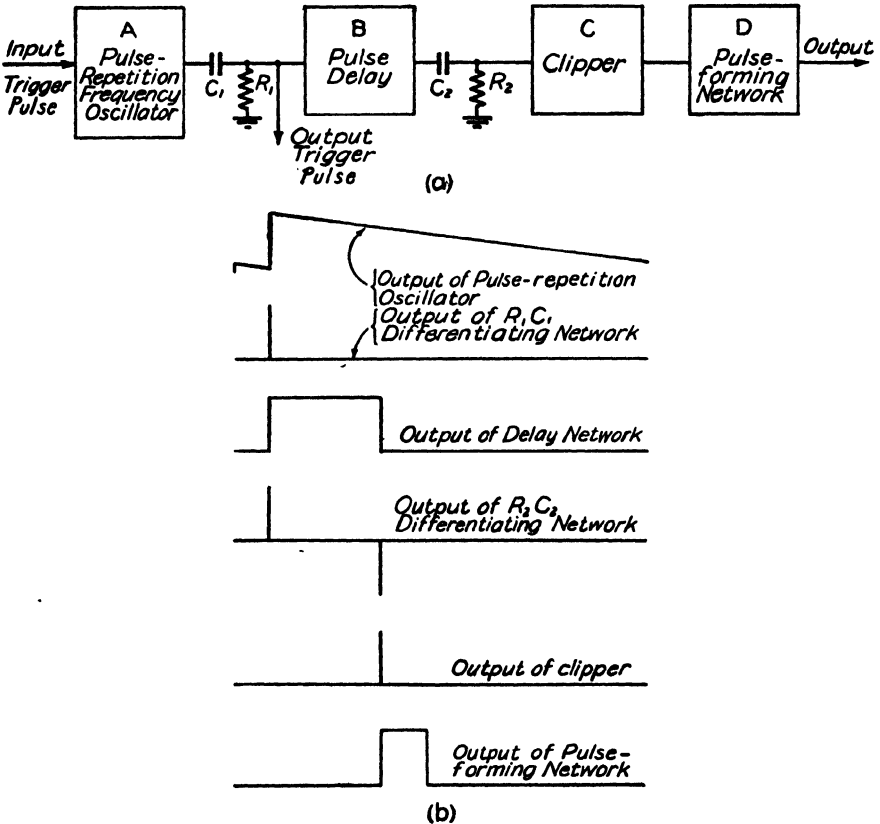


FIG. 35-3.—(a) Block diagram of pulse generator; (b) wave shapes at various points in pulse generator.

will meet these requirements. The output of this circuit is differentiated by means of the resistance-capacitance circuit  $R_1C_1$  to form a sharp trigger impulse, as shown in Fig. 35-3b.

The trigger impulse from the  $R_1C_1$  differentiating network actuates a circuit, shown in Fig. 35-3a as block B, which provides a delay pulse. This pulse-forming circuit can be of the "flip-flop" type<sup>2</sup> with constants

<sup>1</sup> REICH, H. J., "Theory and Applications of Electron Tubes," 2d ed., p 488, McGraw-Hill Book Company, Inc., New York, 1943.

<sup>2</sup> REICH, *op. cit.*, p. 360; PUCKLE, O. S., "Time Bases," p. 36, John Wiley & Sons, Inc., New York, 1943.

so chosen that the length of the output pulse may be varied over the desired range of delay time. The pulse output of this circuit is differentiated by means of a resistance-capacitance circuit  $R_2C_2$  to give two triggering impulses of opposite polarity, one occurring at the leading edge of the pulse, and the other at the trailing edge of the pulse. These two impulses are passed through a rectifying circuit that removes the impulse corresponding to the leading edge of the pulse but allows the other to pass. Thus, the triggering impulse from the rectifying circuit has been delayed with respect to the impulse obtained from the relaxation oscillator by a time equal to the delay-pulse length.

The trigger impulse obtained from the clipping stage can then be used to actuate another flip-flop circuit, shown as block *D* in Fig. 35-3a, which forms the video pulse used to modulate the r-f oscillator. The circuit constants of this flip-flop circuit are chosen so as to give the desired variation of pulse length. In order to obtain rapid rise and decay times and short pulse length, it will be found advantageous to use high-current high  $g_m$  tubes in the pulse-forming circuits.

**35-6. Pulse Modulation of Radio-frequency Oscillators.**—The manner in which the video pulse is applied to the r-f oscillator depends greatly upon the oscillator tube. In applying the pulse to the r-f oscillator, the chief requirement is that the peak value of the r-f pulse output should be the same as the peak value of the c-w output obtained with a d-c voltage equal to the peak value of the video pulse. This is necessary so that the output can be calibrated on continuous wave, for which the average power is relatively high. This calibration can then be used to give an accurate measure of the output when the signal generator is being pulse modulated.

**Pulse Modulation of "Lighthouse" Tubes.**—Oscillators that employ the lighthouse type of triode usually have large capacitances built into them from the plate circuit to ground. Because this large capacitance makes plate modulation with pulses difficult, cathode modulation is used. A method of applying the video pulse to r-f oscillators employing lighthouse tubes is shown in Fig. 35-4. The control and r-f oscillator tubes have a common cathode resistor  $R$ , which is the normal cathode resistor used on the oscillator for c-w operation. The control tube should be a high-current tube, such as the types 6L6, 6Y6, or 6V6. The control tube normally draws sufficient current to bias the oscillator

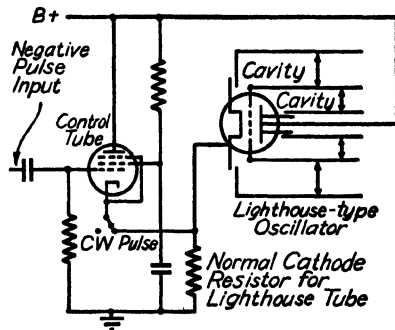


FIG. 35-4.—Circuit for applying pulses to lighthouse-type tubes.



are the same as in c-w operation, and hence the r-f oscillator will operate in the normal manner. Since this method allows the same voltages to be applied to the oscillator tube during the pulse as in c-w operation, it eliminates one of the disadvantages mentioned under reflector pulsing. Since, in this method of modulating the oscillator tube, undesired modes of operation have to be passed through to reach the desired mode, it is necessary that the modulating pulse have rapid rise and decay times so that oscillations cannot build up in these undesired modes.

A better system of modulating reflex klystrons is to apply the pulse to the control grid, but unfortunately in many tubes this electrode is not used or is internally connected to one of the other electrodes. The type-2K28 tube, however, is one in which the control grid is brought out to a separate connection. A circuit for applying the pulse to the control grid is shown in Fig. 35-6. Under normal c-w operation the control grid is connected to the cavity, and if it is made negative with respect to the cavity the r-f tube can be driven into a non-oscillating condition. In pulse modulation a control tube, which should again be a high-current tube, is connected as shown in Fig. 35-6. This control tube will normally draw sufficient current to cause a large enough voltage drop across  $R$  to prevent oscillations. Negative pulses of sufficient magnitude to cut

off the control tube are applied to the control-tube grid. Thus, during the pulse, the voltage drop across  $R$  is zero, normal voltage is applied to the oscillator control grid, and the r-f tube will oscillate in its normal manner. In this method of pulsing, the r-f tube will oscillate in only the desired mode; hence the disadvantage of pulsing through undesired modes is eliminated. The control tube used in control-grid pulsing may be conveniently combined with the pulse-forming flip-flop to eliminate the extra tube.

**35-7. Output Systems.**—In general, the output systems to be discussed pertain to standard signal generators, but they may also be used as auxiliary apparatus with a suitable r-f oscillator. As the block diagram of a standard signal generator (Fig. 35-1) shows, the output system

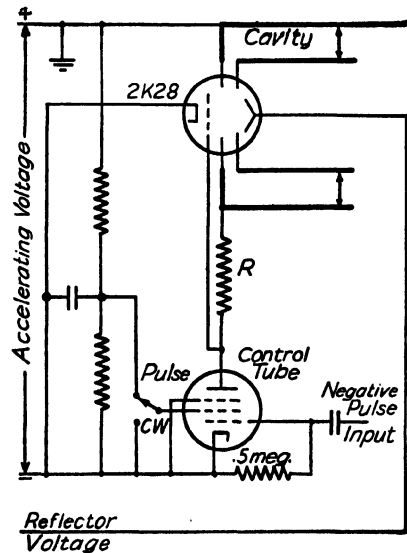


FIG. 35-6.—Control-grid pulse modulation of reflex klystron.

consists of three main parts, *viz.*, the variable attenuator, the attenuation pad, and the reference calibrating system. These may be combined in various ways to make the complete output system.

**35-8. Piston Attenuators.**—One of the most useful types of variable attenuator for use with high-frequency r-f signal generators is the so-called *piston attenuator*.<sup>1</sup> It is well known that for any given waveguide there is a lower frequency limit, called the *cutoff frequency*, below which the attenuation per unit length will be extremely high. Waveguide operated

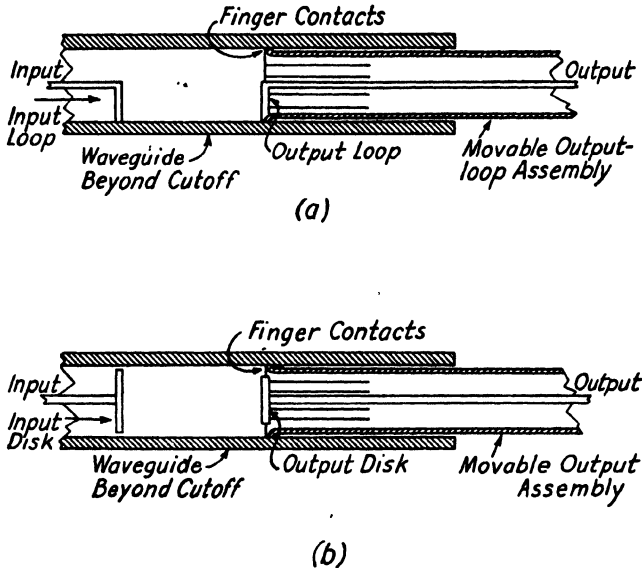


FIG. 35-7.—(a) Piston attenuator using  $TE_{1,1}$  cutoff mode; (b) piston attenuator using  $TM_{0,1}$  cutoff mode.

at frequencies much below cutoff forms the basis of the piston attenuator. Power is fed into a fixed coupling element that excites fields in the guide, and power is coupled out of the guide by means of a movable element that is similar to or identical with the input coupling element. The farther the two elements are separated, the less will be the power coupled out. Two main types of coupling elements are used, *viz.*, loops and disks that excite the  $TE_{1,1}$  and  $TM_{0,1}$  modes, respectively. These attenuators may be made from either rectangular or circular waveguide, but the latter is more generally used for mechanical reasons. Sketches of simple attenuators employing loops and disks for coupling purposes are shown in Fig. 35-7a and 35-7b, respectively.

<sup>1</sup> MONTGOMERY C. G., "Technique of Microwave Measurements," Radiation Laboratory Series, Vol. 11, Chaps. 12 and 13, McGraw-Hill Book Company, Inc., New York, 1947.

It can be shown that the theoretical attenuations for frequencies well beyond cutoff for these two modes<sup>1</sup> are

$$\phi = \frac{54.58}{\lambda_c} \sqrt{1 - \left(\frac{\lambda_c}{\lambda}\right)^2} \quad \text{db per unit length} \quad (35-1)$$

where  $\lambda_c$  = cutoff wavelength  $\begin{cases} \text{for the } TM_{0,1} \text{ mode } \lambda_c = 2.61a \\ \text{for the } TE_{1,1} \text{ mode } \lambda_c = 3.41a \end{cases}$   
 $a$  = radius of guide  
 $\lambda$  = free-space wavelength

The advantage of piston-type attenuators is that a plot of the attenuation in decibels vs. the displacement of the two coupling elements is, except for close spacing of the elements, a straight line, the slope of which is accurately given by the preceding theoretical formulas. Since all quantities in the formulas may be accurately measured, the slope of the curve for either mode may be accurately determined, and hence the attenuator need not be calibrated against another standard attenuator. In regions of close spacing of the coupling elements, the slope is not constant, but varies with displacement. This is caused by the fact that the coupling elements do not excite a single pure mode in the cutoff guide. For example, a loop will excite the desired  $TE_{1,1}$  mode plus some low-level undesired  $TM_{0,1}$  and other higher order modes. These undesired modes attenuate more rapidly than the desired mode and are soon of no consequence. It is in the region where these undesired modes are of significant amplitude that the slope is not constant. The variation of slope with displacement is frequency sensitive, and hence it is impossible to calibrate attenuators that are to be used over a large frequency band in the nonlinear region. As a rough rule the slope will be approximately constant and very close to the theoretical value, if the separation between the coupling elements is greater than the diameter of the tube. In using these attenuators, care should be taken not to operate them in the nonlinear region. Ways of making the slope more nearly constant down to lower attenuation levels are discussed elsewhere.<sup>2</sup>

Theoretically the slope of the calibration curves of piston attenuators varies with frequency, but if they are designed to have a cutoff frequency well above the frequencies at which they are to be used, the variation of attenuation with frequency will be negligible. Hence piston-type attenuators are inherently broad-band devices.

The input and output impedances of piston attenuators are almost entirely reactive and, except in regions of low attenuations, constant over

<sup>1</sup> RAMO, S., and J. R. WHINNERY, "Fields and Waves in Modern Radio," Sec. 9.13, p. 371, John Wiley & Sons, Inc., New York, 1944.

<sup>2</sup> MONTGOMERY, C. G. *op. cit.*, Chap. 3.



the attenuation band. If one of these attenuators is connected to an oscillator through a line whose length is comparable to the wavelength at which the oscillator is operating, the impedance presented to the oscillator coupling element will vary widely over the frequency range. This will have the undesired effect of causing the amount of power coupled into the attenuator from the oscillator also to vary with frequency. There are several ways of minimizing this effect of attenuator loading. One method is by the use of an attenuation pad to terminate the line between the oscillator and attenuator. The loss in the pad lessens the effect that the input impedance of the attenuator has upon the oscillator.

Another method is to shorten the line between the oscillator and attenuator. This type of construction may be carried to a point where the length of line between the oscillator and attenuator coupling elements is zero, but even if the line length is zero the coupling elements themselves will resonate at some frequency and cause trouble. This trouble may be

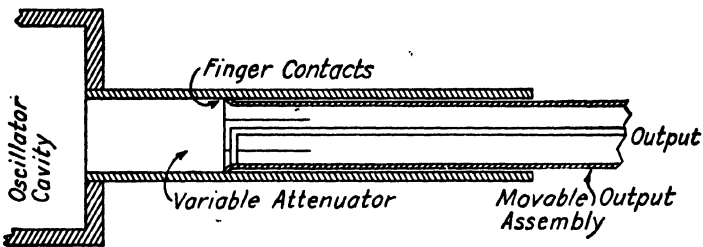


FIG. 35-8.—Method of feeding attenuator directly from cavity.

overcome by removing the input-coupling element entirely and feeding the attenuator directly from the oscillator cavity, as shown in Fig. 35-8.

If piston-type attenuators are to be used at high attenuation levels, of the order of 100 db or greater, it is important to guard against r-f leakage through the low-impedance coaxial line formed by the cutoff waveguide and the loose-fitting adjustable insert that carries the output-coupling element. In order to ensure low leakages, good finger contacts should be used on the insert. Polyiron sleeves placed around the insert will also help to combat this leakage.

**35-9. Attenuation Pads.**—Standard signal generators are required to have a fixed resistive output impedance that is usually low. In line with the present trend, unbalanced coaxial outputs having a resistive output impedance of 50 ohms have been designed for standard signal generators. The following discussion, in which this type of output is considered, is applicable to other types of outputs at other impedance levels. As stated above, the output impedance of a piston attenuator does not meet these requirements, and hence some means of matching must be used

between the variable attenuator and the output. Several methods have been described,<sup>1</sup> but these are essentially narrow band. For broad-band matching a symmetrical attenuator pad having a characteristic impedance of 50 ohms can be inserted in series between the piston attenuator and the output. Without this pad the output impedance is reactive and will vary with frequency, but if an attenuation pad, having an attenuation of 10 db or greater, is used between the attenuator and the output, the source impedance will be very close to 50 ohms and will be resistive.

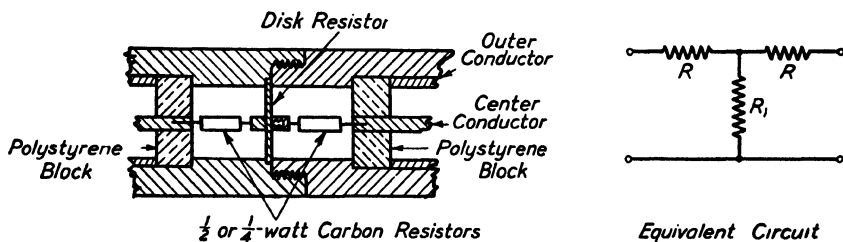


FIG. 35-9.—T attenuation pads. Design formulas:  $R = \frac{10^{\alpha/20} - 1}{10^{\alpha/20} + 1} R_0$ ,  $R_0, R_1 = \frac{R_0^2 - R^2}{2R}$  where  $\alpha$  is the desired attenuation in db,  $R_0$  is the characteristic impedance of the line.

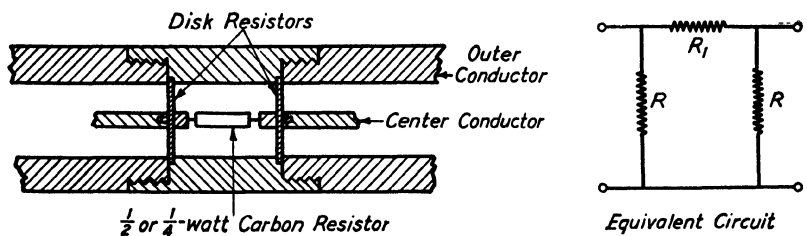


FIG. 35-10.— $\pi$  attenuation pads. Design formulas:  $R = \frac{10^{\alpha/20} + 1}{10^{\alpha/20} - 1} R_0$ ,  $R_1 = \frac{2R_0^2 R}{R^2 - R_0^2}$ , where  $\alpha$  and  $R_0$  are as in Fig. 35-9.

The attenuation pads can be made in several ways. One of the more common types of pads is a length of lossy line such as RG-21/U (nichrome center conductor) or RG-38/U (lossy dielectric). This line should be of sufficient length to give an attenuation of at least 10 db at the frequencies under consideration. Lossy line is easy to use but has the disadvantage that its characteristics change with age; hence the attenuation of these lines must be measured at frequent intervals. It has been found that RG-21/U has more stable characteristics than RG-38/U. Lossy line has no frequency limitations except that at lower frequencies the attenuation per unit length decreases, and it becomes necessary to use greater lengths of line to obtain the desired attenuations.

<sup>1</sup> *Ibid.*

At lower frequencies attenuation pads may be constructed of lumped elements in T- and  $\pi$ -networks. Their construction is shown in Figs. 35-9 and 35-10. The series elements are made of small carbon or metalized resistors, while the shunt elements are made of either small resistors similar to those used in the series elements or commercially available disk resistors. The use of disk resistors causes a smaller discontinuity in the line and hence will allow the use of pads to higher frequencies. Small carbon resistors will serve adequately for the series element for frequencies less than 1000 Mc. If a good grade of metalized resistor is used for the series element, the useful frequency range may be extended up to about 2000 Mc. Because of their construction, they can be used down to very low frequencies.

**35-10. Output Calibration.**—In output systems for standard signal generators there must be some means for measuring or calibrating the output. Signal generators are usually required to have variable outputs

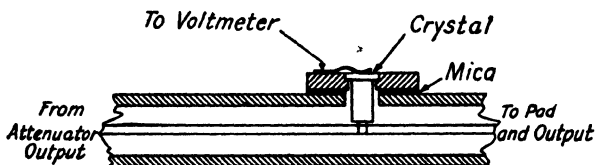


FIG. 35-11.—Calibration of a crystal and voltmeter used to measure the attenuator output.

ranging from  $1 \mu\text{v}$  to about 0.3 volt. This output range is only nominal, depending to a great extent upon the maximum output power that can be obtained from the oscillator, but it serves to indicate the orders of magnitudes involved. Since the measurement of low power or voltage is very difficult, or even impossible with present-day techniques, it has become the standard practice to calibrate the output at the higher levels and then to rely upon the accuracy of the attenuator for lower outputs. This method works very well with piston attenuators as long as they are not operated in the nonlinear region.

A method of calibrating the output is shown in Fig. 35-11. A crystal detector is connected across the output of the attenuator, and its output is measured on a voltmeter circuit. The attenuator is adjusted until a given reference reading is obtained upon the voltmeter, corresponding to a certain output voltage. A movable index is then adjusted so that the reading on the attenuator dial gives the correct output voltage. The attenuator is thereby calibrated at the one relatively high level.

Since crystal detectors can be used only at high levels, this method suffers from the disadvantage that each time the attenuator is calibrated it is necessary to use a high output. It is also impossible to use the detector and voltmeter continuously as a monitor on the oscillator. The

disadvantages can be overcome by monitoring the input power to the attenuator. A bolometer element, for measuring power, is inserted in the attenuator, as shown in Fig. 35-12. The bolometer element is connected to a metering circuit and is used to measure the power density at some fixed point in the cutoff waveguide. The piston attenuator dial can be directly calibrated in output and read opposite a fixed scale, since the power density at any point in the cutoff waveguide varies linearly with distance down the guide. In using this system, the power density in the oscillator cavity is adjusted until a fixed reference reading is obtained upon the power-measuring meter. The value of the attenuated output is then read directly on the attenuator dial which is calibrated from theoretical considerations. The error in the output reading in this method is less than  $\pm 2$  db and can be reduced still further by the use of

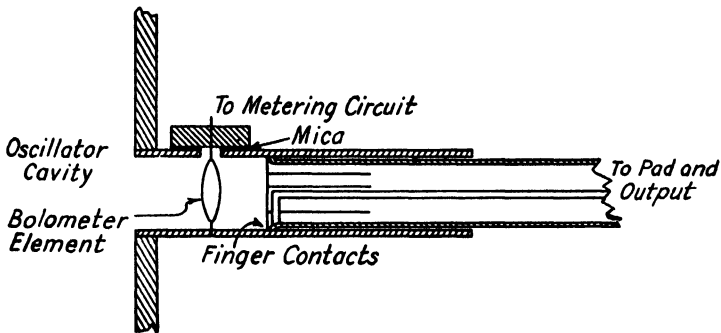


FIG. 35-12. —Method of monitoring input to the attenuator.

output-correction-factor curves. Thus monitoring the input power to the attenuator makes it unnecessary to increase the output to high levels for calibration purposes and also allows the power-measuring circuit to act as a constant monitor on the oscillator.

The main disadvantage of this system is that the power density in the oscillator cavity must be changed in order to standardize the attenuator. This usually requires the adjustment of some electrode voltage on the r-f oscillator tube, which usually affects the operation of the oscillator, especially when it is pulse modulated. With reflex klystrons the pulsing becomes extremely poor if the electrode voltages are not maintained within relatively narrow limits. This disadvantage can be overcome by an arrangement that allows the power-measuring element to be moved along the axis of the waveguide attenuator and by having the position of the power-measuring element control the position of the index opposite which the output attenuator dial is read. This system allows the electrode voltages of the r-f tube to be set at their optimum values and the power-measuring element to be moved in the cutoff guide until it reaches

a position having the power density required for calibration purposes. The mechanical connection between the power-measuring element and the index is arranged so that the output can be read directly from the attenuator dial for all calibrating positions of the power-measuring element. One modified mechanical arrangement for the above method is

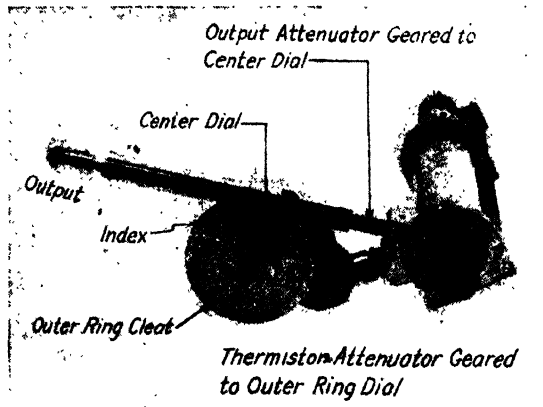


FIG. 35-13.—Modified mechanical arrangement for monitoring attenuator-input power.

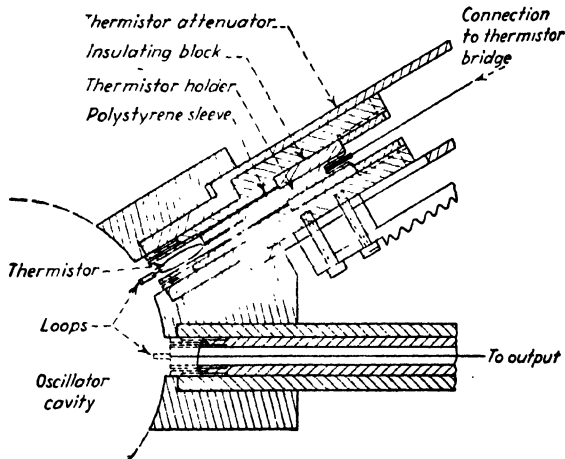


FIG. 35-14.—Detail of attenuator-input monitoring system of Fig. 35-13.

shown in Figs. 35-13 and 35-14. The output attenuator is driven by a rack and pinion. The thermistor monitoring element is mounted in another piston attenuator which is identical with the output attenuator. The thermistor attenuator is driven, through a rack and pinion and a set of gears, by a dial in the form of an outer ring that is concentric with the output attenuator dial. The mechanical linkages are arranged so that both the output and monitor attenuators are moved equal linear

distances for equal angular movements of their respective controls. The inner dial that controls the output attenuator has the desired output scale engraved upon it, while the outer ring that controls the thermistor attenuator has an index line engraved upon it. In use, the thermistor attenuator is adjusted until the metering circuit of the power-measuring element gives a fixed reference reading. The output is then read directly from the attenuator dial opposite the index on the ring. This method assumes that, if it is necessary to change the attenuation on the thermistor attenuator by a given amount in order to keep a standard monitor power level, it will also be necessary to change the output attenuator by an equal amount in order to keep the same output. This system can be made to read the output directly with an error of less than  $\pm 2$  db.

There are several ways in which an output attenuator dial can be calibrated, some of which are

1. In open circuit output volts,  $E$
2. In output voltage across a matched load,  $E_o$
3. In maximum available power output,  $P_o$

If a resistive output impedance of value  $R_o$  is assumed, the relations between the above calibrations are

$$E_o = \frac{E}{2} = \sqrt{R_o P_o} \quad (35-2)$$

$$P_o = \frac{E^2}{4R_o} = \frac{E_o^2}{R_o} \quad (35-3)$$

**35-11. Power Measurement.**—The power-measuring elements generally used are of the bolometer type, the operation of which is based upon change of resistance with temperature. When r-f power is absorbed by a bolometer element, its temperature changes, and hence also its resistance. The resistance change is used as a measure of the r-f power being fed into the element and is usually measured by means of a bridge circuit. Some of the better known types of bolometer elements are Littelfuses, Wollaston wire, lamps, and bead thermistors.

For field service a bolometer element should have the following characteristics: It should be mechanically strong and easily replaceable. For signal-generator use it should be capable of measuring low powers, in the order of 1 mw, without the use of an amplifier. It should be able to withstand a fairly large overload without its characteristics being affected. It should be stable over long periods of time and accurate at widely different temperatures. It should be capable of being used over a large band of frequencies.

Of the bolometer elements listed above, the bead thermistor comes the closest to meeting these requirements. A bead thermistor consists of a

small bead made of metallic oxides and plastic resin, baked together to form a material that has a high negative coefficient of resistance. This bead is enclosed in a glass envelope approximately  $\frac{1}{2}$  in. long and  $\frac{1}{8}$  in. in outer diameter. The two leads to the thermistor are brought out axially from the ends of the structure. When r-f power is absorbed by the thermistor, its temperature rises and its resistance decreases. Thermistors are capable of measuring powers of the order of 1 mw, are rugged, may stand extremely large overloads without damage, and their resistance change is the same function of electrical heating at all frequencies. They are normally operated at d-c resistances varying from 100 to 300 ohms, and since the lead inductance and shunting capacitance of thermistors are very small, this impedance changes very little with frequency. The main disadvantage of thermistors is that they are operated at relatively low temperatures, and hence their characteristics are affected appreciably by changes of ambient temperature.

Littelfuses have been used extensively but are now being more or less replaced by thermistors. Littelfuses are essentially small instrument fuses designed to protect milliammeters. In the sizes used for bolometer elements, they are in effect Wollaston-wire affairs. They are not so

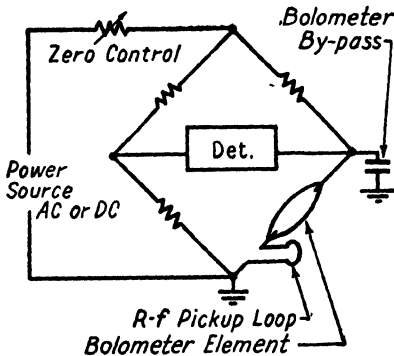


FIG. 35-15.—Elementary thermistor-bridge circuit.

rugged mechanically as thermistors and have approximately one-tenth the sensitivity. They are very susceptible to burnout from overloads. They are normally operated at d-c resistance levels around 200 ohms, but because of their construction they have more shunting capacitance than thermistors, and hence it is harder to obtain broad-band mounts for them. An attempt has been made to overcome this difficulty at the higher frequencies by removing the metal end plates and glass case from the fuse wire and placing the wire directly in the mount, but this results in a rather fragile structure. The main advantage of Littelfuses over thermistors is that they are normally operated at a relatively high temperature, and hence changes of ambient temperature do not affect their characteristics appreciably. Lamps are physically larger than the other types of bolometer elements mentioned, and they usually require very careful matching, especially at the higher frequencies.

The change of resistance in bolometer elements produced by the r-f power is usually measured by means of an a-c or d-c bridge circuit, in which the bolometer element forms one arm. A typical bridge circuit is

shown in Fig. 35-15. These bridges may be of either the unbalanced or the balanced type. In the unbalanced type, the bridge is balanced without the application of any r-f power. The r-f power is then applied to it, and the amount of unbalance, as read on the meter, is used as a measure of the r-f power being fed into the bolometer. In the balanced type the bridge is initially balanced with zero r-f power. The r-f power is then fed into the bolometer and causes the bridge to become unbalanced. The bridge is again balanced by changing the d-c power fed into the bolometer from the bridge supply, and this change of d-c thermistor power is equal to the r-f power. The balanced type of bridge has an advantage over the unbalanced type in that the balanced type of bridge always keeps the thermistor at a constant impedance, a feature that may be required in some applications. On the other hand, the unbalanced type is direct reading and easier to use.

In general, it will be found that certain additions to the basic bridge circuit are necessary with any given type of bolometer element in order to make it useful as a power-measuring device. When using thermistors in balanced bridge circuits the change of thermistor resistance with change in ambient temperature is not detrimental so long as the ambient temperature remains constant during the time that any one reading is being taken. With unbalanced bridges, however, a change of ambient temperature will require a change of bridge power in order to balance the bridge, and this change of bridge power will affect the sensitivity. Several circuits have been developed for compensating for the ambient temperature effects and are described elsewhere.<sup>1</sup>

A disadvantage of Littelfuses is that characteristics vary widely among different fuses, and it is hence necessary to include with the bridge some method for calibrating the bolometer element directly.

It is sometimes desirable to use the thermistor bridge as a wattmeter to measure the power output of transmitters. In this application the thermistor is run at some impedance level between 100 and 300 ohms, whereas the output impedance of the transmitter is usually 50 ohms; hence it is necessary to use a matching transformer between the 50-ohm output of the transmitter and the thermistor. Since the thermistor presents a highly resistive impedance, it can be quite easily matched to the line by means of a taper section to transform the thermistor impedance down to 50 ohms. This system can be made fairly broad band. Since the thermistor needs a d-c return to ground, however, it is necessary to use a tuning stub in the matching section, as shown in Fig. 35-16, and it will be necessary to tune this stub for different frequencies.

A tapered section should be designed for the thermistor, which is operated always at or near some given impedance level. For a more

<sup>1</sup> *Ibid.*



general matching network, a tunable stub and line stretcher, or a double-stub tuner, may be used. Both systems are satisfactory and can be used to match thermistors, operated at any particular impedance in their normal range, to a 50-ohm line. Both methods can be made to cover a 2:1 frequency range or more.

The usual method of adjusting a matching network is to tune the network until maximum output is obtained, under the assumption that at this point the thermistor and matching section present a 50-ohm load to the power source. Hence the thermistor reads the maximum power output  $P_0$  that can be delivered to a 50-ohm load. This assumption is

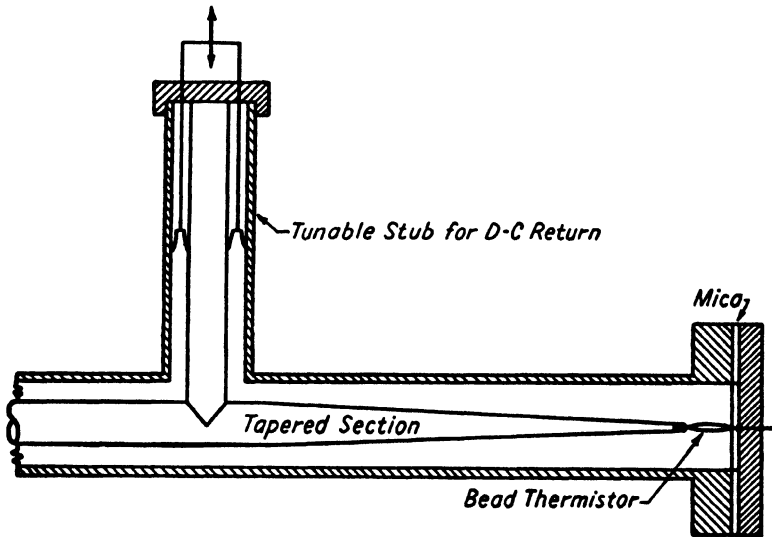


FIG. 35-16.—Taper matching section for thermistors.

valid, provided that the output impedance of the power source itself is 50 ohms. If the output impedance of the power source is not 50 ohms, the matching network will transform the thermistor impedance to the conjugate of the actual output impedance of the power source, and the thermistor will read the maximum power output that can be delivered to this conjugate impedance.

**35-12. Shielding.**—Another problem to be considered with respect to standard signal generators is shielding. The shielding of various circuits should be sufficient to limit the leakage to a value much less than the lowest outputs desired. The shielding problem is fundamentally more difficult at high frequencies than at low frequencies, but fortunately many oscillators designed for high-frequency operation are inherently well shielded. The tuned circuits for these oscillators are usually in the form of coaxial lines, which are in themselves excellent shields. The oscillator

tubes are mounted concentrically in these lines and are thus also well shielded except for their bases. The bases may be shielded by metal tubes mounted on the oscillator structure. The connecting leads to the oscillator tube are then the main remaining source of leakage. The leakage through these leads may be sufficiently reduced by the use of special filter assemblies at the point where they pass through the shield. These filters are constructed and mounted as shown in Fig. 35-17. The filter with the coil is most effective at frequencies below about 3000 Mc, while the one with Polyiron is good for higher frequencies. In order for either of these filters to be effective, it must be mounted in a section of the shield structure itself.

With butterfly and conventional oscillators, the shielding problem is not so simple. Here it is usually accomplished by the use of several

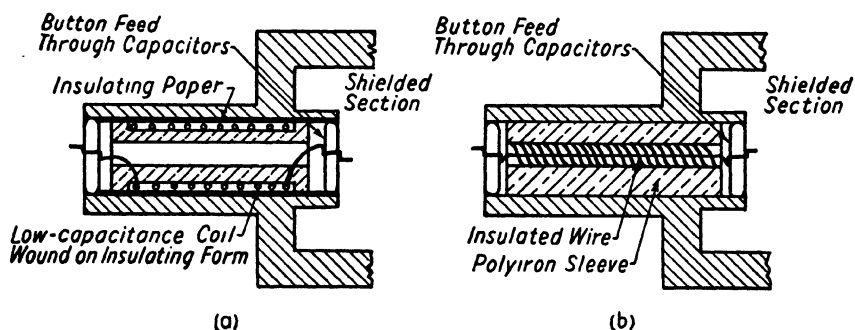


FIG. 35-17.—Line filters.

well-fitted concentric shield cans. The leads are then passed through these shields by means of feed-through capacitors, and a small choke is used in each lead between the shield cans.

In general, it has been found simpler to shield the oscillator and the leads to it, rather than to try to shield the signal generator as a unit. If extremely low leakage is desired, however, it may be found necessary to shield both the oscillator and the complete generator. The shielding of the complete signal generator is done in a conventional manner, by the use of a metal case with a tight-fitting cover. Ventilation and cooling holes should be small, preferably round, and should be covered with a fairly fine-mesh screen. All control shafts extending outside the instrument should be made of some nonmetallic substance.

**35-13. Auxiliary Output Systems.**—It is often desirable to use a test oscillator in conjunction with some external output system to improvise a signal generator.

An external output system that may be used with a test oscillator is shown in Fig. 35-18. Power from the test oscillator is fed through a

piston attenuator into a coaxial-line T junction. The variable attenuator should be calibrated in decibels over its linear range. Both output arms of the T are fed into attenuation pads having the same characteristic impedance and sufficient attenuation (over 10 db) so that the impedance that each output arm of the T junction sees will be the same regardless of the load connected to the output of the pads. Since each output arm of the T sees the same impedance, the power entering the T will split equally between the two outputs. The power output of one of the attenuation pads is fed into a matched load and measured by means of a thermistor bridge, while the output from the other pad is connected to the instrument under test. In use, the variable attenuator is adjusted until a suitable reading, which will be called the *reference output*, can be obtained upon the power-output meter. If the pads have the same

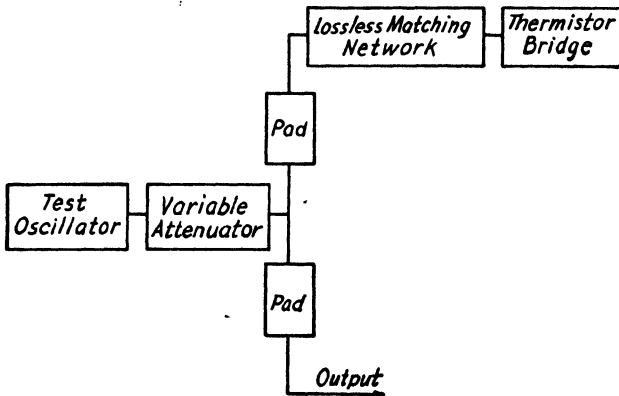


FIG. 35-18.—External output system for use with test oscillators.

attenuation, the power read on the thermistor bridge is then the same as would be delivered from the output connector into a matched load and is, hence, the maximum available power output  $P_o$ . If the pads do not have the same attenuation,  $P_o$  will differ from the power measured on the thermistor bridge by an amount equal to the difference in the attenuation of the two pads. Lower outputs may be obtained by use of the variable attenuator.

The main disadvantage of this type of system is that the power split in the T is very sensitive to load impedances. Because of this fact, the connections to the T should be symmetrical, *i.e.*, the power should be fed into the center arm and the output taken from the two side arms.

There is an inherent 3-db loss of possible output power in the above system, because the power splits equally at the T junction. The various disadvantages and the 3-db loss can be overcome at a slight loss in convenience by the method shown in Fig. 35-19. This system is somewhat similar to the T junction in use, except that the output is first fed into

the power-measuring meter for the setting up of a reference level, and after this reference has been set up the output is switched over to the equipment under test. This system is more sensitive to load impedance.

**35-14. Ultrahigh-frequency Sweep Oscillator.**—A sweep oscillator is a signal source whose output frequency is recurrently swept across some predetermined frequency range. When used in conjunction with an oscilloscope, it is very useful for preliminary studies of r-f amplifiers, mixers, and filters. It eliminates the necessity for running a point-to-point response curve each time a circuit is changed in the device under test. In operation, the output frequency of the generator is swept recurrently across the band of frequencies over which it is desired to obtain the response curve of a piece of equipment. The output of the equipment under test is rectified and applied to the vertical terminals of an oscilloscope, whose horizontal sweep is synchronized with the sweep

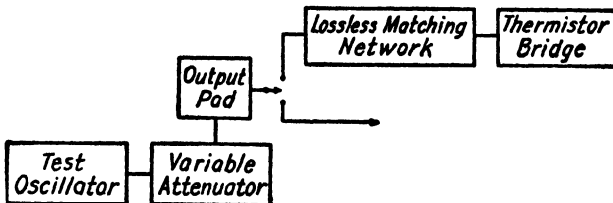


FIG. 35-19.—Alternative output system for use with test oscillators.

of the r-f generator. Thus, the frequency response of the equipment under test is plotted on the oscilloscope screen.

A block diagram of a sweep generator for supplying a varying r-f output frequency and a sweep voltage for an external oscilloscope is shown in Fig. 35-20.<sup>1</sup> This sweep generator will supply a frequency-modulated output with a center frequency that can be tuned from 100 to 1000 Mc and that can be swept over any band of frequencies ranging from 0 to 100 Mc.

A beat-frequency oscillator circuit is employed for producing the r-f signal. The outputs of two 3-cm reflex-klystron oscillator tubes are fed into a common waveguide and mixed in a crystal mixer, and the difference frequency is taken from the output of the crystal. The output frequency can be controlled by the tuning of the oscillator cavities. Frequency modulation is obtained by applying to the reflectors of the klystrons a low-frequency saw-tooth voltage, generated by means of a relaxation oscillator. The output of the relaxation oscillator is amplified and applied to the reflectors of the klystrons through a transformer, which is connected so that the voltages applied to the reflectors are in phase opposition and thus cause the two r-f tubes to change frequency in the opposite

<sup>1</sup> Basic sweep circuit developed at the General Electric Research Laboratory.

directions. The amplitude of the saw-tooth voltage applied to the reflectors may be varied in order to adjust the r-f sweep width. The saw-tooth oscillator also supplies the sweep voltage for an external oscilloscope.

The output from the crystal mixer feeds a coaxial absorption-type wavemeter, the output of which is detected, amplified, and then applied to the vertical plates of the oscilloscope. This will cause a sharp pip on the oscilloscope trace at a point corresponding to the frequency to which the wavemeter is tuned and makes possible the calibration of the oscilloscope trace directly in terms of frequency.

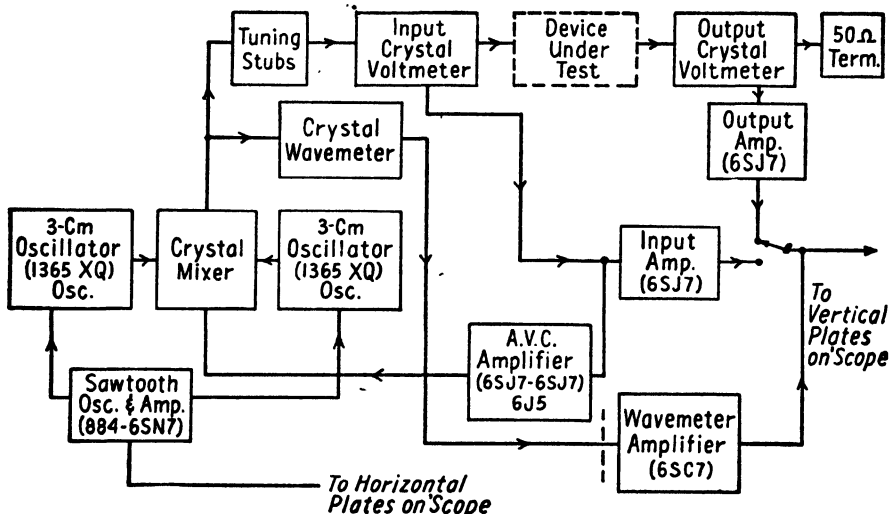


FIG. 35-20.—Block diagram of sweep generator.

The output from the crystal mixer also feeds both the device under test and a crystal voltmeter through a set of tuning stubs. The purpose of the tuning stubs is to make the output from the sweep generator constant over the swept band so that the output from the device under test will truly represent its frequency response. Nevertheless with these tuning stubs alone it will be found very hard to obtain a constant-amplitude r-f signal over the swept band. To overcome this difficulty the output from the crystal voltmeter is amplified, and the amplified output is used to bias the crystal mixer, thus reducing its conversion efficiency on large output signals. Provisions are made for applying the output of the crystal voltmeter to the vertical plates of the oscilloscope. This gives a method of monitoring the r-f signal so that the tuning stubs may be properly adjusted. It will be found necessary to change the tuning of the stubs for different frequencies and for various devices that it is desired to test.

The output from the device under test is detected by another crystal voltmeter, which is similar to the one used on the input side. The detected output signal is then amplified and applied to the vertical plates of the oscilloscope. The trace appearing on the oscilloscope screen is a plot of the frequency response of the equipment under test.

Since the a-v-c voltage applied to the crystal will greatly reduce the variations in the r-f output, but will not completely remove them, a point-by-point response curve should be run for a final accurate check on each piece of equipment.

**35-15. Heterodyne Frequency Meters.**—Heterodyne frequency meters are essentially very stable and accurately calibrated oscillating receivers. A block diagram of a typical heterodyne frequency meter is shown in Fig. 35-21. In this meter the output of a local oscillator is mixed with the signal in an untuned mixer to give an audio beat note that is amplified and used to feed an indicating device, usually a pair of ear-

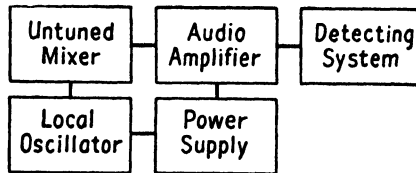


FIG. 35-21.—Block diagram of heterodyne frequency meter.

phones. The advantages of a heterodyne-type frequency meter are that (1) since measurements may be made on harmonics of the local oscillator signal, the range of the frequency is greatly increased; (2) since it has a relatively high sensitivity, it can be loosely coupled to the unknown source.

The chief difference between local oscillators suitable for use in heterodyne frequency meters and those used in receivers is that in the former the frequency must be more accurately known. This is usually accomplished by the use of additional shunting capacitance on the oscillator, which makes it more stable but cuts down the frequency range of the oscillator. An example of this procedure is indicated below. A butterfly oscillator was used in a signal source to cover the frequency range from 40 to 500 Mc. By the addition of shunting capacitance, this frequency range was narrowed to 55 to 250 Mc. This change made the oscillator more stable with respect to variations in oscillator-tube capacitance and brought about a reduction in the frequency-calibration error from  $\pm 1$  per cent on the test oscillator to  $\pm \frac{1}{4}$  per cent on the frequency meter. For still greater accuracy a low-frequency crystal oscillator may be used to provide calibration check points for the local oscillator.



# SUPPLEMENTARY BIBLIOGRAPHY OF RECENT ARTICLES IN THE FIELD

## Chapter 15

- FRANKEL, S., J. J. GLAUBER, and J. P. WALLENSTEIN, A Medium Power Triode for 600 Megacycles, *Proc. I.R.E.*, **34**, 986 (1946).  
JAMIESON, H. W., and J. R. WHINNERY, Power Amplifiers with Disk-seal Tubes, *Proc. I.R.E.*, **34**, 483 (1946).  
SUTRO, P. J., Theory of Mode Separation in a Coaxial Oscillator, *Proc. I.R.E.*, **34**, 960 (1946).

The following reports were recently declassified and are available through the Department of Commerce. They are listed in the Department's Bibliography of Scientific and Industrial Reports.

- PB 2727 COLE, P. A., Measurements on 446 "Light-house" Tubes (Radiation Laboratory Report 413), 1943.  
PB 2772 GARDNER, M. E., Operational Characteristics of 2043 Tubes as Pulsed Oscillators in a Re-entrant Cavity (Radiation Laboratory Report 732), 1945.  
PB 15147 HANSEN, SIEGFRIED, Broad-band Amplification with Grounded Grid Circuits (OSRD Division of Radio Coordination Report 931-8), February, 1944.  
PB 14138 HENKEL, R. L., Operation of RCA A2212 in a Coaxial Cavity Oscillator (Radio Research Laboratory Tech. Memo 411-TM-66).  
PB 13899 HULSTEDE, G. E., A Wide-range Microwave Oscillator (Radio Research Laboratory Report 11), 1943.  
PB 40414 KUPER, J. B. H., *et al.*, Report on Tests of RCA and G. E. Light-house Tubes (Radiation Laboratory Report 61-8), January, 1943.  
PB 15150 LAVOO, N. T., Amplification Characteristics of the L14 with Small Signal Input at 3000 Mc (OSRD Division of Radio Coordination Report 931-12), August, 1944.  
PB 28725 MARKELL, JOHN H., Development of an Experimental Radar Countermeasures Transmitter Employing the LGOON Triode as an Oscillator (Naval Research Laboratory Report R-2432), January, 1945.  
PB 14108 RAMBO, W. R., *et al.*, Test Information on Resnatron Types X-124 and X-139 (Radio Research Laboratory Report 411-126), 1944.  
PB 14179 RAMBO, W. R., and L. D. TUCK, A Triode Oscillator-tripler (Radio Research Laboratory Report 411-116), 1944.  
PB 13921 STEPHENSON, J. G., and R. L. HENKEL, CW Oscillators Using the G. E. ZP-499 Triode in Coaxial Line Circuits (Radio Research Laboratory Report 49), 1943.  
PB 13916 STEPHENSON, J. G., CW Oscillators Using the Experimental G. E. L-3 Triode in Coaxial Line Circuits (Radio Research Laboratory Report 38), 1943.  
PB 14157 STEPHENSON, J. G., and R. L. HENKEL, The G. E. ZP-522 (3C22) Triode as a CW Oscillator and Amplifier in Coaxial Line Circuits (Radio Research Laboratory Report 411-83), March, 1944.



## 1034 SUPPLEMENTARY BIBLIOGRAPHY OF RECENT ARTICLES

- PB 13992 SUTRO, P. J., Theory of Mode Separation in a Coaxial Oscillator (Radio Research Laboratory Report 411-TM-132), 1944.
- PB 14017 SUTRO, P. J., Frequency Bands of Loaded and Unloaded Resonant Sections of Line (Radio Research Laboratory Report 411-TM-85), July, 1944.
- PB 14137 WEBSTER, R. R., and J. G. STEPHENSON, Notes on the Wide Band Modulation of Coaxial Line Oscillators Using Light-house Triodes (Radio Research Laboratory Tech. Memo 411-TM-65), March, 1944.
- PB 14168 WOODS, J. P., and R. O. PETRICH, Wide Band UHF Amplifier (Radio Research Laboratory Report 411-102), September, 1944.

### Chapter 17

- ARTZT, MAURICE, Frequency Modulation of Resistance-capacitance Oscillators, *Proc. I.R.E.*, **32**, 409 (1944).
- BUTLER, F., Reactance-value Frequency Modulator, *Wireless Engineer*, **20**, 539 (1943).
- CHANG, C K., A Frequency Modulated Resistance-capacitance Oscillator, *Proc. I.R.E.*, **31**, 22 (1943).
- HUND AUGUST, "Frequency Modulation," McGraw-Hill Book Company, Inc., New York, 1942
- MARCHAND, M., Fundamental Relationships of F-M Systems, *Communications*, **26**, 56 (1946).
- SHAEFFER, C. F., Frequency Modulator, *Proc. I.R.E.*, **28**, 66 (1940).
- SMITH, JR., A. D., Wide Range Electronic Sweeper, *Communications*, **26**, 24 (1946).
- TRAVIS, CHARLES, Automatic Frequency Control, *Proc. I.R.E.*, **23**, 1125 (1935).

The following reports were recently declassified and are available through the Department of Commerce. They are listed in the Department's Bibliography of Scientific and Industrial Reports.

- PB 15197 HELLER, J. I., Electronic Tuning for Panoramic Reception (OSRD Division of Radio Coordination Report 1138-3), 1944.
- PB 15206 HELLER, J. I., Notes of Factors Affecting the Selection of Values for Use in Phase Net of Reactance Tubes (OSRD Division of Radio Coordination Report 1138-2), 1944.
- PB 15205 HELLER, J. I., Notes on Oscillators in Connection with Electronic Tuning for Panoramic Reception (OSRD Division of Radio Coordination Report 1138), 1944
- PB 14109 KEARNEY, J. W., and W. R. RAMBO, A Common-grid Reactance-tube Circuit at Ultra-high-frequencies (Radio Research Laboratory Tech. Memo 411-TM-40A), 1944.
- PB 14020 KEARNEY, J. W., Reactance Switching: A Method of Producing Wide-band Frequency Modulation (Radio Research Laboratory Tech. Memo 411-TM-90).
- PB 14156 RAMBO, W. R., Class C Operation of Reactance Tubes (Radio Research Laboratory Report 411-82), 1944.
- PB 14146 RAMBO, W. R., A Low-power Spot Jamming Transmitter (Radio Research Laboratory Report 411-TM-76), 1944.
- PB 14108 RAMBO, W. R., Notes on a Common-grid Reactance Tube Circuit (Radio Research Laboratory Tech. Memo 411-TM-40), 1944.
- PB 25470 VITTER, A. L. JR., *et al.*, LCT, 900 Mc/sec FM-CW Magnetron (Radiation Laboratory Report 1005), 1946.
- PB 14137 WEBSTER, R. R., and J. G. STEPHENSON, Notes on the Wide Band Modulation of Coaxial Line Oscillators Using Light-house Triodes (Radio Research Laboratory Tech. Memo 411-TM-65), 1944.

Chapters 18 and 19

- DISHAL, M., Theoretical Gain and Signal-to-noise Ratio Obtained with the Grounded-grid Amplifier at Ultra-high Frequencies, *Proc. I.R.E.*, **32**, 276 (1944).
- DOW, W. G., Equivalent Electrostatic Circuits for Vacuum Tubes, *Proc. I.R.E.*, **28**, 548 (1940); Transit-time Effects in Ultra-high-frequency Class-C Operation, *Proc. I.R.E.*, **35**, 35 (1947).
- HOLLMAN, H. E., Theoretical and Experimental Investigation of Electron Motion in Alternating Fields with the Aid of Ballistic Models, *Proc. I.R.E.*, **29**, 70 (1941).
- JEN, C. K., On the Induced Current and Energy Balance in Electronics, *Proc. I.R.E.*, **29**, 345 (1941); On the Energy Equation in Electronics at Ultra-high Frequencies, *Proc. I.R.E.*, **29**, 464 (1944).
- JONES, M. C., Grounded-grid Radio-frequency Voltage Amplifiers, *Proc. I.R.E.*, **32**, 423 (1944).
- LEHMANN, G. J., and A. R. VALLERINO, Study of Ultra-high-frequency Tubes by Dimensional Analysis, *Proc. I.R.E.*, **33**, 712 (1945).
- LLEWELLYN, F. B., "Electron Inertia Effects," Cambridge University Press, London (in New York, The Macmillan Company), 1941. This book contains a complete bibliography relative to small-signal ultra-high-frequency electron behavior.
- LLEWELLYN, F. B., and L. C. PETERSON, Vacuum-tube Networks, *Proc. I.R.E.*, **32**, 144 (1944).
- RAMO, S., Current Induced by Electron Motion, *Proc. I.R.E.*, **27**, 584 (1939).
- SALISBURY, W. W., The Resnatron, *Electronics*, **19**, 92 (1946).
- SCHADE, H. O., Beam Power Tubes, *Proc. I.R.E.*, **26**, 137 (1938).
- STRONG, C. E., The Inverted Amplifier, *Electronics*, **13**, 14 (1940).
- THOMPSON, B. J., Space-current Flow in Vacuum-tube Structures, *Proc. I.R.E.*, **31**, 485 (1943).
- WANG, CHAO-CHEN, Large-signal High-frequency Electronics of Thermionic Vacuum Tubes, *Proc. I.R.E.*, **29**, 200 (1941).

Chapters 20 to 23

- ASHKIN, A., A High-power Rising-sun Magnetron, *Phys. Rev.*, **69**, 701 (1946).
- BLEWETT, J. P., D. A. WILBUR, and L. D. ROBERTS, Split-anode Magnetrons, *Phys. Rev.*, **70**, 118 (1946).
- FISK, J. B., H. D. HAGSTRUM, and P. L. HARTMAN, The Magnetron as Generator of Centimeter Waves, *Bell System Tech. Jour.*, **25**, 167 (1946).
- GORHAM, J. E., Electron Tubes in World War II, *Proc. I.R.E.*, **35**, 296 (1947).
- HOLLENBERG, A. V., S. MILLMAN, and N. KROLL, One-centimeter Rising-sun Magnetrons with 26 and 38 Cavities, *Phys. Rev.*, **69**, 701 (1946).
- HUNTER, L. P., Energy Build-up in Magnetrons, *Phys. Rev.*, **69**, 700 (1946).
- KROLL, N., and W. E. LAMB, Theory of the Rising-sun Magnetron Anode, *Phys. Rev.*, **69**, 701 (1946).
- LANGMUIR, R. V., and R. B. NELSON, A 10-kw Magnetron with Water-cooled Cathode, *Phys. Rev.*, **70**, 118 (1946).
- MILLMAN, S., and A. NORDSIECK, Development of the Rising-sun Magnetron Anode Structure, *Phys. Rev.*, **69**, 701 (1946).
- PAGE, L., and N. I. ADAMS, Space Charge in Cylindrical Magnetrons, *Phys. Rev.*, **69**, 494 (1946).
- PHILIPS, M., and W. E. LAMB, Space-charge Frequency Dependence of a Magnetron Cavity, *Phys. Rev.*, **69**, 704 (1946).
- POMERANTS, M. A., Magnetron Cathodes, *Proc. I.R.E.*, **34**, 203 (1946).

## 1036 SUPPLEMENTARY BIBLIOGRAPHY OF RECENT ARTICLES

- SCNEIDER, E. G., Radar, *Proc. I.R.E.*, **34**, 526 (1946).  
SONKIN, S., "Crown-of-thorns" Tuning of Magnetrons, *Phys. Rev.*, **69**, 701 (1946).  
WILBUR, D. A., New Magnetron Design for Continuous Operation in the Decimeter Wave Range, *Phys. Rev.*, **70**, 118 (1946).  
WILLSHAW, W. E., and L. RUSHFORD, The High-power Pulsed Magnetron: An Outline of the Mechanism of Operation, *Jour. I.E.E.*, Part IIIA, **93**, 180 (1946).

### Chapters 28 to 30

- CORNELIUS, E. C., Germanium Crystal Diodes, *Electronics*, **19**, 118 (1946).  
FRIIS, H. T., Noise Figures of Radio Receivers, *Proc. I.R.E.*, **32**, 419 (1944).  
GROSS, E. E., Coaxial Butterfly Circuits, *Electronics*, **19**, 156 (1946).  
KARPLUS, E., Components of U-H-F Field Meter, *Electronics*, **19**, 124 (1946).  
MILLER, P. H., Noise Spectrum of Crystal Rectifiers, *Proc. I.R.E.*, **35**, 252 (1947).  
ROBERTS, SHEPARD, Some Considerations Governing Noise Measurements on Crystal Mixers, *Proc. I.R.E.*, **35**, 257 (1947).  
SODERMAN, R. A., A Wide-Range U-H-F Test Oscillator, *Gen. Radio Experimenter* **21**, 4 (1946).  
STEPHENS, W. E., Crystal Rectifiers, *Electronics*, **19**, 112 (1946).

### Chapters 31 and 32

- CLARK, J. W., and A. L. SAMUEL, A Wide-range Microwave Oscillator Tube, *Proc. I.R.E.*, **35**, 81 (1947).  
GINZTON, E. L., and A. E. HARRISON, Reflex-klystron Oscillators, *Proc. I.R.E.*, **34**, 97P (1946).  
HARRISON, A. E., Graphical Methods for Analysis of Velocity-modulation Bunching, *Proc. I.R.E.*, **33**, 20 (1945).  
PIERCE, J. R., Reflex Oscillators, *Proc. I.R.E.*, **33**, 112 (1945).

# INDEX

## A

- Adcock antenna, 210, 221, 222, 298
- Admittance, electronic (*see* Electronic admittance)
- of resonator, 857
- Admittance definition circle, 73
- Ambiguous courses, 295
- Amplifiers, coaxial (*see* Coaxial amplifiers)
- distortion in d-f, 280, 281
  - grounded-grid, 305
  - i-f, 940-976
    - band width of, 942, 943
    - choice of intermediate frequency for, 941
    - coupling methods, interstage, in, 954
    - coupling networks for, band-width reduction factor of, 957
      - multituned, 958
      - single-tuned, 954
    - double-tuned, alignment of, 964
    - gain in, 952
    - gain-band-width factor of, 966
    - gain-band-width product of, 940, 956, 963, 966
    - gain control of, 975, 976
    - miniature components in, 953
    - noise in, 944
      - induced grid, 947
    - noise resistance, equivalent, of, 945
    - partition effect in, 945
    - regeneration in, 973
    - selectivity of, 942
    - selectivity characteristic of, 943
    - series decoupling in, 974
    - shot effect in, 945, 948
    - for spectrum analyzer, 991
    - stagger-tuned, 965
      - advantages of, 972
      - design of, 967
    - staggered pair, 966
    - staggered triple, 967, 970
- Amplifiers, sweeping, 985
- for use in wide-range tunable receivers, 940
  - vacuum tubes used in, input admittance of, 948
    - input capacitance of, 949
    - input resistance of, 949
  - video (*see* Video amplifiers)
- Amplitude modulation, of signal generators, 1010
- (*See also* Oscillators, amplitude-modulated)
- Anode, rising-sun, 500
- Anode cavity of resnatron, 445, 450
- Q of, 460
- Antenna impedance measurements, 36
- Antenna pattern measurements, 46, 52
- Antennas, Adcock, 210, 221, 222, 298
- auxiliary devices for, 192-198
    - (*See also* Switches)
  - balanced, 50
  - broad-band, 1-25
    - band width of, 1
    - parameters that affect, 3
  - beam width of, 23
  - directional, 23
  - impedance compensation of, 10
  - cone (*see* Cone antennas)
  - cone and cylinder, 93-118
  - crossed-Adcock, 302
  - crossed dipole, 300
  - crossed element, phased, 131, 133, 136
  - cylindrical, 101, 110
    - (*See also* Cylinder antennas)
  - for direction finders (*see* Direction-finder antennas)
  - directivity of, 209, 219, 226
  - double-dipole, 299
    - (*See also* Direction-finder antennas)
  - isotropic, 24
  - omnidirectional, 17
  - one-half wavelength long, 221-223
  - primary, 253

- Antennas, radiation patterns of (*see* Radiation patterns)  
 several wavelengths long, 223-225  
 sleeve (*see* Sleeve antennas)  
 slot (*see* Slot antennas)  
 stub, 93, 121  
   triple-stub, 301  
 test, 50  
 turnstile, 131  
 vertical-horizontal, 234
- Aperture, 138, 225  
 collecting, 226, 227  
 collectivity of, 228  
 effect of polarization on, 230  
 effective, 226, 251, 255  
 effectivity of, 228  
 of horn, 142, 143, 146  
 illumination of, 138, 139  
 linear, 220  
 of paraboloid reflector, 163  
 phase distribution in, 164  
 physical, 220, 226, 227  
 reflection by, 5  
 slot antenna as, 171
- Aperture coupling, 497, 782  
 Aperture radiators, 138  
 Apertures, relation between, 228, 231
- Attenuation, in cable, 34  
 in ridge waveguide, 682  
 in waveguide, 677
- Attenuation constant of filters, 694  
 Attenuation pads, 1018  
 Attenuators, piston, 1016  
 Automatic direction finding, 273  
 Automatic gain control, 976  
 Automatic measurement methods, 52  
 A-v-c circuits, 308  
 A-v-c effectiveness, 647  
 Azimuth homing, 299-301
- B**
- Back-heating, 356  
 cathode, 356  
 in magnetrons, 493, 538, 560  
 in resonators, 462  
 in u-h-f oscillators, triode and tetrode, 443
- Back loop, 557  
 Back-lines, 326  
 Balanced antenna, 50  
 Balanced-line measurements, 38
- Balun output transformers, 330-332, 382  
 (*See also* Coupling)
- Baluns, 85-92, 238, 249, 259, 382-385  
 bazooka, 86  
 capacitively coupled, 385  
 conductively coupled, 331, 384  
 in impedance-matching networks, 88  
 inductively coupled, 325, 329, 332, 383  
 performance of, 91  
 type I, 86  
 type II, 87  
 type III, 88, 135
- Band-pass filters, 701, 708, 731, 736  
 Band-pass and high-pass filters, 702, 703, 707
- Band width, of a-m oscillators, 391, 406  
 of antenna, 232  
 of Class C oscillators, 435  
 of i-f amplifiers, 942, 943  
 limitations in, 391  
 3-db, selectivity characteristic of, 943  
 of video amplifiers, 977
- Barrier-layer capacitance of crystals, 799, 817
- Barrier resistance of crystals, 799, 817
- Bazooka, 86
- Beam area of antenna, 230  
 Beam conductance, 852  
 Beam-coupling coefficient, 852, 856, 902  
 Beam tetrode, 452  
 Beam width, of antenna, 23  
 as function of aperture, 146  
 half-power, 219, 223  
 of horn, 151
- Bearing errors of d-f indicators, 288, 292  
 Bearing shift, 236  
 of corner spinner, 251
- Bearings, true, 219
- Bethe hole directional coupler, 600
- Biconical horn, 93, 107  
 Biconical transmission line, 96  
 Bolometer, 31  
 Bolometer bridges, 593  
 Bolometer elements, 1023  
 Bolometer probe, 30
- Broad-band antennas (*see* Antennas, broad-band)
- Bucket plunger, 928
- Bunching of electrons, 445, 850, 864  
 Butterfly design, 754-758, 768  
 frequency variation in, 832  
 plate spacing in, 755, 833

- Butterfly design, shunt impedance in, 831**  
   stack height in, 755, 833  
**Butterfly oscillators, 825, 827-848**  
   cathode-lead inductance in, 835  
   efficiency of, 840  
   examples of, 842  
   frequency modulation in, 838  
   grid-blocking capacitor and resistor in, 833  
   h-f limitations of, 836  
   holes, sources of, in, 835  
   mechanical tracking of, 847  
   oscillator tubes for, 840  
   output-coupling methods for, 839  
   plate-supply connections of, 834  
   stability of, 837  
**Butterfly resonators, 749-769**  
   coupling methods for, 760  
   diameter of, outside, 757  
   double, 767  
   examples of, 765  
   pass-band loss of, 759  
   *Q* of, 751, 759  
   resonant impedance of, 751  
   selectivity of, 759  
   semibutterfly, 752  
   spurious responses in, 763  
   true butterfly, 749  
   as tuners, 757
- C**
- C-rings, 497**  
**Cable, attenuation in, 34**  
**Calorimeter loads, 589, 590**  
**Calorimeter wattmeter, 581**  
   lossy-coaxial-cable, 583  
**Calorimeters, air, 582**  
   quick-response, for large waveguide, 590  
   sloping-guide water-load, 591  
**Capacitance plunger, 925**  
**Capacitance-probe coupling, 385**  
**Capacitors, for coaxial circuits, 367**  
   grid blocking, 833  
   quarter-wave by-pass, 448  
**Carrier frequency of receivers, 628**  
**Cathode back-heating (see Back-heating)**  
**Cathode cavity of resnatron, 445, 447**  
**Cathode chokes, 334**  
**Cathode-coupled amplifiers, 981**  
**Cathode pulsing, 1014**  
**Cathode-ray-tube display, 984**  
**Cathode-ray-tube screens for d-f indicators, 283**  
**Cathodes for magnetrons, 493**  
**Cavity magnetrons (see Magnetrons, cavity)**  
**Cavity modes in reflex oscillators, 901**  
**Cavity oscillators, coaxial, 826**  
   concentric, 359  
**Characteristic impedance, of biconical transmission line, 96**  
   of coaxial lines, 360  
   of cone transmission line, 100  
   of line transformer, 60  
   of oscillator lines, 327  
   of parallel-line oscillators, 327  
   of ridge waveguide, 679  
   of slot antennas, 180-187  
   for *TEM* mode, 880  
   of waveguide, 44, 674  
**Choke joint, 777, 779**  
**Choke plunger, 927**  
**Circles, definition, 54**  
   standing-wave-ratio, 54, 58  
   transformation, 55, 60, 74  
**Circuit efficiency of oscillators, 433**  
**Circularly polarized field, 153**  
**Circularly polarized horns, 153**  
   with dielectric, 156  
**Class B modulators for oscillators, 399**  
**Class C operation of reactance tubes, 418, 419**  
**Class C oscillator, band width of, 435**  
   efficiency of, 433  
   frequency stability of, 435  
   resnatron as, 445  
**Class C oscillators, 433-435**  
**Coaxial amplifiers, construction of, 373**  
   operation of, 358  
   power gain in, 358  
   (See also Coaxial-line circuits)  
**Coaxial-cavity oscillators, 826**  
**Coaxial-cavity resonators (see Resnatron)**  
**Coaxial-cavity tuners (see Tuners)**  
**Coaxial-fed slot, 171**  
**Coaxial-line circuits, 337-375**  
   back-heating in, 356  
   capacitors for, 367  
   characteristics of, 337  
   common cathode, 339  
   common grid, 339, 340, 355  
     analysis of, 411  
   common plate, 339

- Coaxial-line circuits, concentric cavity,  
 cooling of, 359  
 connecting systems in, 364  
 design of, 358  
   mechanical, 370  
 discontinuities in, 713  
 distributed capacitance of, 346  
 grid separation, 339  
 mode interference in, 349  
 mode separation in, 344  
 multiple-mode operation of, 342-344,  
 357  
 multitube, 374  
 output coupling of, 370  
 plungers for, 363  
 $Q$  of, 346  
 trouble shooting in, 371  
 tube and circuit selection for, 359  
 tuning of, 343, 357, 363  
 tuning range of, 349  
 vacuum tubes for, 337
- Coaxial-line resonators, 878-939  
 circular, 878  
 coupling methods for, 916-919  
 modes, preferred, in, 901  
 parasitic resonances in, 909, 911, 915  
 plungers, noncontacting, used in, 920-  
 939  
 (See also Plungers)  
 reflex tubes, adaptation to, 886  
 conditions for oscillation of, 889  
 $TE$  modes in, 879, 881  
 $TEM$  mode in, 879, 880  
 $TEM$ -mode interference in, 900  
 elimination of, 903  
 $TEM$ -mode suppressor, 904-911  
 $TM$  modes in, 879, 884  
 tuning curves for, 891-898, 914  
 physical realizability of, 892
- Coaxial lines, 583-585  
 characteristics of, 337  
 notched, 591  
 with resistive center conductor, 584  
 slotted, 591  
 tapered, 577  
 with water dielectric, 585
- Coaxial measuring line, 29
- Coaxial oscillators, bias for, 356  
 cooling of, 359  
 design of, 358  
 feedback in, 340, 341, 350, 352, 353, 365  
 (See also Coaxial-line circuits)
- Coaxial r-f switches, 194
- Coaxial thermocouple wattmeter, 574
- Coaxial tuning sections, 41
- Coaxial tuning stubs, 42
- Coaxial water-calorimeter wattmeter, 584
- Coefficient of coupling  $k$ , 865
- Coefficient of reflection, 37
- Cold tests, determination of  $Q$  by, 611  
 of resonant systems, 610
- Collectivity, of aperture, 228
- Collector (see Antennas)
- Collet fingers, 887
- Common-cathode circuit, 339
- Common electrode, 322
- Common-grid circuit, 339, 340, 355, 408,  
 415  
 analysis of, 411
- Common-plate circuit, 339
- Commutators, electronic r-f and video,  
 305  
 for homing, 304  
 mechanical r-f, 303, 304, 307  
 mechanical video, 305
- Compound-line section, 922, 924
- Conductance, d-c beam, 852  
 electronic, 869  
 small-signal, 852
- Cone antennas, 3, 93, 94, 102  
 angle of flare of, 4  
 biconical, 93, 107  
 radiation patterns of, 108  
 design of, 105  
 effect of reflectors on, 118  
 impedance of, 93  
 input impedance of, 98, 100  
 patterns of, 101  
 resonances of, first, 100  
 second, 101  
 single-cone, 105  
 stub, 93  
 $TEM$  waves on, 95  
 reflection coefficient of, 104  
 tilted, 108  
 $TM$  waves on, 95
- Cone and cylinder antennas, 93-118
- Cone transmission line, characteristic  
 impedance of, 100
- Conversion loss in crystals, 802, 810
- Co-polymerstyrene, 713
- Corner admittance, 889
- Corner length, equivalent, 889

- Corner reflectors, 129, 223, 245  
 Corner spinner (*see* Direction-finder antennas)  
 Corner susceptance of reflex tube, 889  
 Corner terminations, effect of, 890  
 Coupled-circuit tuners, theory of, 742  
 Coupled circuits, theory of, 742-748  
   three, response curves for, 747, 748, 760  
   two, response curves for, 746  
 Couplers, directional, 594  
 Coupling, to antenna or load, 376  
   aperture, 497, 782  
   balun, 382-385  
     to antennas, 238, 259  
     in parallel-line oscillators, 325, 329-332  
   capacitance-probe, 385, 386  
   capacitive, 379  
   combined probe and loop, 387, 919  
   critical, 742  
   direct, 387  
   inductive, 379  
   iris, 782  
   loop, 377-381  
     in magnetrons, 496  
     in parallel-line oscillators, 325-328  
     in reflex oscillators, 916  
     in tuners, 772  
   orifice, 782  
   probe, 385, 386  
   series output, 389  
   to split-anode magnetrons, 563-565  
   video transformer, 399  
   waveguide, 782  
 Coupling circuits, video output, 980  
 Coupling coefficient, beam, 856  
 Coupling devices, 324  
   requirements for, 376  
 Coupling loops, 599  
   series-tuned, 381  
   untuned, 377  
 Coupling methods, for butterflies, 839  
   interstage, 954  
   power output, 376-390  
   for reflex oscillators, 916  
 Coupling networks, multituned, 958  
   single-tuned, 954  
 Coupling problems in coaxial cavity, 773  
 Cross field, 200, 208  
 Crossed Adcock, 302  
 Crossed dipoles, 301, 302  
 Crossed-element phased antennas, 131, 133, 136  
 Crown-of-thorns tuner, 499  
 Crystal detectors (*see* Detectors)  
 Crystal mixer (*see* Mixers)  
 Crystal r-f voltmeters, 822  
 Crystal rectifiers, barrier-layer capacitance of, 817  
   barrier layers of, 799  
   conversion loss in, 810  
   as measuring devices, 822  
   rectification efficiency of, 800  
   resistance, back, of, 799  
     barrier, 799, 817  
     front, 799  
     spreading, 799  
 Cylinder antennas, 101, 110  
   effect of reflectors on, 118  
   fat, 16  
   input impedance of, 110  
   patterns of, 21, 113, 114  
   for series of 90-deg V, 115  
   resonances of, 111  
  
 D  
 Decoupling, series, 974  
 Deflection amplifiers, 992  
 Design, of butterfly resonators, 831  
   of coaxial oscillators, 358, 370  
   of cone antennas, 105  
   of filters, 685-740  
   of parallel-line oscillators, 332  
   of resonator electrodes, 452  
   of ridge waveguide, 678-681  
   of stagger-tuned amplifier, 967  
   of transformers, 400  
   of triode and tetrode oscillators, 426-444  
 Detector probes, 30-32  
   calibration of, 31  
   with receiver, 31  
   in waveguide, 40  
 Detectors, 816-821  
   crystal, equivalent circuit of, 817  
   noise in, 818  
   diode, transit-time effects in, 817  
   direct, 816  
   wide-band, 821  
   input impedance of, 821  
   low level, 816-821



- Detectors, rectification efficiency of, 817  
 second, 797, 822
- Detectors and mixers, 796-823  
 (*See also* Mixers)
- Detectors and receivers for pattern measurements, 48
- Detectors for u-h-f measurements, 48
- Dielectric materials, 713
- Differentiator, selective, 1001
- Dilectene No. 100, 713
- Diode detectors (*see* Detectors)
- Diode mixers, 813
- Diodes, transit-time effects in, 817
- Dipoles, sleeve, 120, 126  
 bent-, 128
- Direct coupling, 397
- Direct detection at high frequencies, 816
- Direct-detection receivers, 628, 796  
 for pulsed signals, 630  
 sensitivity of, 819  
 tuners for, 741  
 wide-band, 821
- Direction-finder antennas, 218-271  
 Adcock, 210, 221, 222, 298  
 apertures of, 220, 225-231, 251, 255  
 collectivity and effectivity of, 228  
 effect of polarization on, 230  
 relation between, 228, 231  
 band width of, 232  
 beam area of, 230  
 beam width, half power, of, 219, 223  
 bearing deviation of, 235  
 bearing shift of, 236  
 bearing, true, with, 219  
 combination vertical-horizontal, 234, 245, 251  
 directivity of, 209, 219, 226  
 directivity ratio for, 229  
 elevation angle of, 219  
 fixed, 264  
 frequency range of, 233  
 half-wave element, and Adcock array, 237, 238  
 linear, 221  
 with reflector, 222  
 horns as, 223  
 intercept probability of, 268  
 loops as, 220, 221  
 methods of use of, 236  
 octapole, 221  
 one-half wavelength long, 221-223  
 with parabolic reflectors, 223, 253
- Direction-finder antennas, patterns of,  
 effect of reflections on, 210  
 polarization-discrimination ratio of,  
 233  
 power gain of, 226, 228, 271  
 primary, 253  
 response ratio of, 234  
 rotatable, 215, 216  
 rotation speed of, 267  
 several wavelengths long, 223-225  
 spinner auxiliaries for, 246, 256, 257  
 spinners, 236  
 corner-reflector, 223, 245  
 balun coupling of, 238, 259  
 bearing shift of, 251  
 horizontal antenna of, 248  
 r-f relay for, 246, 257  
 vertical antenna of, 247  
 double-loop, 238-245  
 circuit analysis of, 241  
 double parabolic, 253  
 parabolic reflector, 251  
 with horn, 260  
 patterns of, 244, 250, 255  
 testing techniques for, 268  
 line stretcher, use of, in, 271  
 turnstile, 237
- Direction-finder indicators, 215, 272-293  
 asymmetrical patterns on, 276  
 automatic and semiautomatic, 215  
 bearing errors of, 288, 292  
 bearing shift, apparent, due to, 276  
 c-r-t screens for, 283  
 double-line for null-type, 290  
 electrostatic, 277, 284, 285, 289  
 beam modulator for, 279  
 with capacitor scan, 277, 278  
 bearings, simultaneous, by, 277  
 with electronic scan, 285  
 pulse stretcher for, 282  
 restorer circuit for, 279  
 with sine-potentiometer scan, 284  
 with synchro scan, 289  
 time constants of *RC* filter for, 287  
 envelope tracer, 275, 276  
 function of, 272  
 instrument errors of, 292  
 with magnetic scan, 275  
 nonlinear deflections on c-r-t screen of,  
 289  
 presentations by, comparison of, 291  
 pulse, 275, 277

- Direction-finder indicators, radial presentation by, 287  
     bearing errors of, 288  
     sweep circuit for, 288  
     rotating-disk, 273  
     scanning capacitor for, accuracy of, 293  
     sweep circuits for, 285, 288  
     for voice-modulated signals, 275, 284  
 Direction finders, 199–293  
     amplifiers for, 279  
         distortion in, 280, 281  
     automatic, 273  
     Bellini-Tosi, 236  
     cathode-ray, 291  
     microwave, 272  
     null-type, 290, 292  
     pulse analysis and identification with, 280  
     reference bearing for, 292  
     requirements for, above 50 Mc, 202  
     sensitivity of, 276  
     siting by, 203  
     universal, 203  
 Direction finding by homing, 294  
 Direction-finding methods, 204  
     effect of reflections on, 204–208  
     radiation-pressure, 215  
     time-difference, 213  
     for voice-modulated signals, 275, 284  
 Directional antennas, 23  
 Directional characteristic, of antenna, 219  
     (See also Radiation patterns)  
 Directional couplers, 594  
     Bethe hole, 600  
     capacitive-loop, 595  
     two-hole, 599  
 Directivity of antennas, 23, 24, 209, 219, 222, 226  
 Directivity ratio, 229  
 Discontinuities, in coaxial lines, 713  
     in waveguide, 676  
 Discontinuity capacitance, 895  
 Discriminator, 987  
 Disk resistor with voltmeter, 577  
 Distortion in amplifiers, d-f, 280, 281  
 Distributed capacitance of coaxial line, 346  
 Donutron (see Magnetrons, cavity)  
 Double-butterfly tuners, 767  
 Double-dipole wing antenna, 299, 302  
 Double-loop spinner, 238–244  
 Double superheterodyne, 988  
 Doubblers, u-h-f, 374  
 Dummy loads, calorimeter, 589, 590  
     lossy-line, 570  
     oil-immersed, 581  
     resistor-star, 571  
     salt-water, 588  
     sloping-guide water, 571  
     waveguide, 42, 572  
  
 E  
 Eccles-Jordan circuit, 305, 1000  
 Effective aperture, 226, 251, 255  
 Efficiency, of butterfly oscillators, 840  
     of Class C oscillators, 434  
     electronic, of grounded-grid oscillator, 436  
     of split-anode magnetrons, 559, 568  
 Electrode design of resnatron, 452  
 Electron bunching, 445, 850, 864  
 Electron flow in triodes and tetrodes, 437  
 Electron leakage, 508  
 Electronic admittance, 850–854, 857, 859  
 Electronic conductance, 852, 869  
 Electronic efficiency, 434  
     of grounded-grid oscillator, 436  
 Electronic hysteresis, 861–863  
 Electronic scan, 285  
 Electrons, debunching of, in triode oscillators, 439  
 Electrostatic indicator, 277, 284, 285, 289  
 Elevation angle of antenna, 219  
 Elevation homing, 302  
 Elliptical polarization, 199  
 Elliptically polarized field, 153, 158  
 Elpar, 164  
     with horn, 170  
     line focus of, 168  
     patterns for, 170  
 Equivalence principle, 17  
 Equivalent circuits, calculation of parameters of, 617–626  
     of low-level crystal detector, 817  
     of resnatron, 459  
     of resonant systems, 612  
  
 F  
 Feedback, in coaxial oscillators, 340, 341, 350, 352, 353, 365

- Feedback, in coaxial oscillators, inter-electrode, 340  
 in resatron, 463  
*S*-loop, 352  
 wide-range, 353
- Feedback system, external, 341
- Fidelity of receiver, 635, 646
- Figure of merit of receiver, 820
- Filter, *RC*, time constants of, 287
- Filters, transmission-line, 648-740  
 analysis of, methods for, 653-660  
 attenuation constant of, 694  
 band-pass, 701, 708, 731, 736  
 band-pass and high-pass, 702, 703, 707  
 capacitances in, 712  
 cascaded, 685  
 coaxial-line constants of, 653  
 complete, 685  
 design of, 685-740  
 dielectric materials used in, 713  
 half sections for, 652, 696  
 high-pass, 677, 692, 702, 703, 706, 707, 728  
 image impedance of, 649, 651, 694  
 image transfer constant of, 649, 651  
 insertion loss in, 660, 665, 669, 670, 672  
 measurement of, 736  
 nomograms for, 661-662, 685  
 junctions for, 717, 721, 725  
 low-pass, 686, 687, 691, 708, 731  
*m*-derived, 696, 708  
 mechanical construction of, 712  
 mismatched line, loss in, 671  
 parameters of, 649, 652  
 pass-band loss in, 665, 670  
 pass-band response in, 662  
 phase constant of, 694  
 resonant-line, 685, 702  
 ridge waveguide, as circuit element in, 678  
 short-line, 686, 692, 701  
 split-block, 715  
 spurious responses in, 734  
 standing-wave-ratio measurement for, 740  
 stop-band response, 669  
 test methods for, 728, 736  
 theory of, fundamental, 648  
 transforming end sections for, 666  
 types of, 685, 702
- Filters, transmission-line, varying-impedance, 687, 731  
 voltage-current relations in, 648  
 waveguide, 674, 677, 728, 731
- Finger joint, 777
- Finger magnetrons, mode degeneracy in, 551
- Finger noise, 920
- Finger plungers, 363, 920
- Fingers, flexible, 363
- Flare angle of horn, 143, 146, 152
- Focus, line, 168
- Focusing action in resatron, 453
- Foster's reactance theorem, 892
- Frequency, of split-anode magnetrons, 557-558, 568
- Frequency discontinuities, 824
- Frequency measurement, 35
- Frequency meters, electronic, 1006  
 heterodyne, 1008, 1031
- Frequency-modulated oscillators (*see* Oscillators, frequency-modulated)
- Frequency modulation, of butterfly oscillators, 1011  
 of reflex-klystron oscillators, 859  
 of signal generators, 1011  
 (*See also* Oscillators, frequency-modulated)
- Frequency pulling, in butterfly oscillators, 806  
 in magnetrons, 514  
 in split-anode magnetrons, 566-567
- Frequency pushing in magnetrons, 506, 535  
 in split-anode magnetrons, 567  
 in u-h-f oscillators, 429
- Frequency range of antennas, 233
- Frequency stability, of Class C oscillators, 435  
 of reflex oscillators, 870

## G

- Gain, of antenna, 24  
 of i-f amplifiers, 952
- Gain-band-width factor, 966
- Gain-band-width product of i-f amplifiers, 940, 956, 963, 966
- Gain control, automatic, 976  
 continuous, 979  
 in i-f amplifiers, 975  
 in video amplifiers, 978

- Gain requirement, minimum, for receivers, 690
- Gain setting, standard, of receivers, 642
- Germanium crystals, 799
- Grid bias for coaxial oscillators, 356
- Grid-circuit quenching, 356
- Grid emission, 356
- Grid modulation, incidental, 404
  - inphase, 406
  - of resonators, 469
  - of u-h-f oscillators, 401
- Grid-screen  $\mu$ -factor of resonator, 455
- Grid-separation circuit, 339, 459
- Grid warping, 356
- Grounded-grid amplifiers, 305
- Grounded-grid circuits, 459
- Grounded-grid oscillator, electronic efficiency of, 436
- Guide wavelength, 44
- H
- Half sections for filters, 652, 696
- Half-wave element, and Adcock array, 237, 238
  - linear, 221
  - with reflector, 222
- Harmonic-frequency generation in reflex oscillators, 864
- Harmonic responses, 646
- Harmonics, elimination of, 36
- Heterodyne frequency meters, 1008, 1031
- "Heterotone" oscillator, 634
- High-pass filters, 677, 692, 702, 703, 706, 707, 728
- Hole-and-slot magnetrons, 476, 482
- Holes, sources of, 835
  - and trouble shooting, 371
  - in tuning range, of butterfly oscillators, 835
  - of magnetrons, 517
  - in u-h-f oscillators, 316
- Homing, 294-310
  - ambiguous courses in, 295
  - antennas for, 295-302
    - patterns of, 297, 301, 302
    - performance of, 310
  - azimuth, 299-301
  - bearing accuracy with, 294
  - commutators for, 304
  - direction finding by, 294
  - elevation, 302
  - indicators for, 307
  - Homing, polarization, effects of, on, 297
    - universal, 302
- Homing systems, 294-310
  - performance of, 310
- Horns, 8, 138-161
  - aperture of, 142, 143, 146
  - beam width of, 151
    - as function of aperture, 146
  - biconical, 93
    - patterns of, 108
  - circularly polarized, 153, 154, 156, 260, 261
    - with dielectric, 156
    - without dielectric, 154
  - as d-f antennas, 223, 260, 261
  - flare angle of, 143, 146, 152
  - lattice-work, 152
  - measurements of circularity of, 157
  - methods of feeding, 140
  - with parabolic reflectors, 260
  - patterns of, 142, 148, 152
    - polarization, 158
  - phasing section of, 154
  - primary radiators for, 161
    - design and patterns of, 163
  - pyramidal, 145
  - sectoral, 142
  - tapered, 42
- Horns and reflectors, 138-170  
(*See also* Reflectors)
- Huygens' principle, 15-16
- Hysteresis, electronic, 861-863
- I
- I-f amplifier, for spectrum analyzer, 991
  - sweeping, 985
- I-f amplifiers (*see* Amplifiers, i-f)
- Image impedance, 649, 651
- Image rejection, 645, 941
- Image transfer constant, 649, 651
- Images, 988
- Impedance, characteristic (*see* Characteristic impedance)
  - of conical antenna, 93
  - input (*see* Input impedance)
  - of mixers, 804
  - plate modulating, of oscillators, 393
- Impedance characteristics of slot antennas, 180-187
- Impedance compensation, 10, 53-85
  - boundary curves in, use of, 55, 63
  - broad-band, 53

- Impedance compensation, definition circle  
 for, 54  
 admittance, 73  
 impedance-curve transformation, 63  
 by line transformer, 58, 63  
 by networks, 56  
 multielement, 84  
 parallel, 72, 77  
 series, 68  
 single element, 81  
 reflection coefficient, maximum permissible in, 81  
*R-X* diagram, use of, in, 53  
 Smith chart, use of, in, 59, 68  
 standing-wave-ratio circles, use of, in, 58  
 transformation circles, use of, in, 55, 60, 74
- Impedance measurement of antenna, 36  
 Impedance-measuring equipment, 29  
 Indicators, for direction finders, 272-293  
 (*See also* Direction-finder indicators)  
 for homing, 307  
 output, 583, 606, 607
- Inductance, of leads (*see* Lead inductance)  
 of reflex klystron, 894, 900
- Input admittance of vacuum tubes, 948  
 Input capacitance of vacuum tubes, 952  
 Input impedance, of compound-line section, 922  
 of cone antenna, 98, 100  
 of cylindrical radiators, 110  
 of cylindrical-sleeve antenna, 122  
 of detectors, 821  
 of sleeve-stub, 125
- Input resistance of vacuum tubes, 949  
 Insertion-loss, in filters, 660, 665, 669, 670, 672  
 maximum, 672  
 Insertion-loss measurements, 736  
 Insertion-loss nomograms, 661, 662, 685  
 Integrating and bridge circuits, 308  
 Interaction space of magnetrons, 478, 488  
 Interaction time, 440  
 in resonatron, 462  
 Intercept probability of d-f antennas, 268  
 Intermodulation, 864  
 Iris coupling, 782  
 Irises, 171, 676  
 Isotropic antenna, 24
- J
- Joints, rotating, coaxial, 256  
 short-circuiting, 777-780
- Junctions, for filters, 717, 721, 725  
 for ridge waveguide, 723-725  
 tapered-ridge, 725  
 transforming, 721, 725  
 waveguide-to-coaxial, 717, 721, 723-725  
 testing of, 728
- K
- Klystron (*see* Reflex klystrons)  
 Klystron oscillators (*see* Reflex-klystron oscillators)
- L
- L-* and *C*-ring tuning of magnetrons, 528  
*L*-ring resonances in magnetrons, 533  
*L*-ring tuning of magnetrons, 498  
 Lead inductance, effect of, in butterfly oscillators, 835  
 in u-h-f oscillators, 316, 321  
 Lighthouse tubes, pulse modulation of, 1013  
 Line characteristic impedance, 360  
 Line focus, 168  
 Line-to-load connections, 32, 34  
 Line stretchers, 35, 271, 517, 537, 835, 1026  
 Line transformer, 58  
 characteristic impedance of, 60  
 compensation by, 63  
 Littelfuses, 1023  
 Load lamps, 579, 580  
 calibration of, 579  
 gas-filled, 580  
 Loaded *Q*, of magnetron, 534  
 of u-h-f oscillators, 392  
 Loading, transit-time, 951  
 Loads, absorption, 43  
 dummy, 33, 570-574, 577, 581, 588  
 (*See also* Dummy loads)  
 Lobe switching, 295  
 Local oscillators, 824-939  
 butterfly (*see* Butterfly oscillators)  
 butterfly resonators, design of, for, 831  
 circuits for, 801, 829  
 coaxial-cavity, 826

- Local oscillators, coaxial resonators for, 878-939  
 coupling problems in, 806  
 parasitic resonances in, 825  
 reflex-klystron (*see* Reflex-klystron oscillators)  
 tuning noise in, 824  
 tuning ranges of wide-range, 826  
 types of, 825
- Long-line effect, 515
- Loop coupling (*see* Coupling)
- Loops, as d-f antennas, 220-221  
 series-tuned, 325, 377, 379, 381  
 untuned, self-reactance of, 378
- Lossy coaxial lines, 570, 583
- Low-impedance joint, 777
- Low-pass filters, 36, 686, 687, 691, 708, 731
- M
- M*-derived filters, 696, 708
- Magnetic scan indicators, 275
- Magnetic wave, circular, 884
- Magnetron oscillator, 474
- Magnetrons, c-w, 473-525  
 anode, rising-sun, of, 500  
 aperture coupling of, 497  
 back-heating in, 493  
 cathodes for, 493  
 circuit constants of, 486  
 classification of, 474  
 coaxial output for, 496  
 coupling of, 495-497  
 crown-of-thorns tuner for, 499  
 donutron, 477  
 finger or squirrel-cage, 477  
 frequency pulling in, 514  
 frequency pushing in, 506  
 hole-and-slot, 476, 482  
 instability region of, 518  
 interaction space of, 478, 488  
 long-line effect in, 515  
 mechanism of oscillation in, 488  
 mode-jump current in, 495, 504  
 mode separation in, 483  
 as modulated oscillator, 522  
 multicavity, 474  
   electromagnetic field in, 478-485  
   *Q* of, 487  
   neutrode, 475  
   operating characteristics of, 502-525  
   performance of, chart for, 503
- Magnetrons c-w, variations of, with load, 509  
 scaling of, 491  
 slot, 476, 482  
 strapping in, 485  
 vane, 476, 482
- cavity, 526-554  
 back-heating in, 538  
 band-width control of, 536  
 donutron (squirrel-cage), 477, 543  
   mode-*C* operation of, 548  
   mode degeneracy in, 551  
   phase-reversing anode for, 550  
   resonance modes of, 544  
 4J60-to-4J65 low-power, 541  
 frequency pushing in, 535  
*L*- and *C*-ring tuning of, 528  
*L*-ring resonances in, 533  
 line stretcher for, 537  
 loaded *Q* of, 534  
 mode-jump current in, 530  
 model 34, 527  
 multicavity, 474  
 multivane, 526  
 6J21, 530  
   operating characteristics of, 540  
 pulsed, 473  
 split-anode, 474, 560-568  
   back-heating in, 560  
   characteristics of typical, 568  
   circuits for, 555-556  
   cooling of, 558-563  
   efficiency of, 559, 568  
   frequency limits of, 557-558, 568  
   frequency pulling in, 566-567  
   frequency pushing in, 567  
   life of, 562  
   loading of, 563, 567-568  
   mode jumping in, 558-559, 565  
   modulation of, 563, 567-568  
   neutrode, 559  
   performance curves of, 559-561, 565  
   power output of, 559, 568  
   pulsing of, 567  
   shielded oscillator using, 559  
   stabilization of, 561  
   structure of, 557-559  
   theoretical equations for, 562
- Marker signals for panoramic presentation, 992
- Measurement, of antenna impedance, 36  
 of antenna patterns, 46, 52

- Measurement, of frequency, 35
    - of power, 1023-1026
  - Measurement procedure, 36
    - with waveguide, 44-46
  - Measurements, u-h-f, 26-52
    - balanced-line, 38
    - coaxial measuring line for, 29
    - detector probes for, 30
    - detectors and receivers for, 48
    - methods for, automatic, 52
    - signal sources for, 48
    - test antennas for, 50
    - tuning devices for, 35, 41, 42
    - with waveguide, 39, 44-46
  - Measuring devices, crystals as, 822
  - Measuring equipment for receivers (*see* Receiver measuring equipment)
  - Mechanical commutators, r-f, 303, 304
    - video, 305
  - Metal-to-metal joint, 777
  - Mismatch, in tuners, 744
  - Mixers, 800-814
    - crystal, characteristics of, 802
      - circuits of, 800, 804
      - conversion loss in, 805
      - effect of bias on, 811
      - examples of, 814
      - noise output from, 810
      - performance of, 805
      - signal power input of, 802
      - standard, 803
      - in waveguide, 809
    - diode, 813
    - impedance of, 804
    - step, 810
    - waveguide, 809
  - Mode-C operation of magnetron, 548
  - Mode chart, 899
  - Mode degeneracy in finger magnetrons, 551
  - Mode designation, 897
  - Mode interference, in coaxial circuits, 349
    - in reflex oscillators, 861, 897, 900, 903
    - TEM, 900, 903, 904
  - Mode jumping, in magnetrons, 405, 504, 530
    - split-anode, 558, 559, 565
  - Mode plot, 897
  - Mode selection, 431
  - Mode separation, in coaxial circuits, 344
    - in magnetrons, 483
  - Mode suppressor, 904, 908, 922
    - parasitic resonances of, 909
  - Modes, in coaxial resonators, 901
  - Modulation, amplitude (*see* Oscillators, amplitude-modulated)
    - cathode, 402
    - frequency, 1011
    - grid (*see* Oscillators, amplitude-modulated)
    - of magnetron, 522
    - parasitic amplitude, 409, 417
    - of power generators, 313
    - of power oscillators (*see* Oscillators, a-m and f-m)
    - pulse (*see* Pulse modulation)
    - of reactance tubes, 422
    - of resonators, 467-470
    - of signal generators, 1010, 1013
    - of split-anode magnetrons, 563, 567, 568
  - Modulation linearity, 395
  - Modulators, 1010-1015
  - Multiple-mode operation of coaxial oscillators, 342-344, 357
  - Multiple-mode tuning, 343
  - Multiple-transit effects, 862
  - Multitube coaxial circuits, 374
  - Multivane magnetrons, 526
  - Multivibrator, as pulse stretcher, 994
- N
- Neon-tube output indicator, 607
  - Networks for impedance compensation (*see* Impedance compensation)
  - Neutrode, 475, 559
  - Noise, in crystal detectors, 818
    - finger, 920
    - in i-f amplifiers, 944
    - induced grid, 947
    - tuning, 824
  - Noise-band width, 640
  - Noise figure of receiver, 637, 802
  - Noise generator, 638
  - Noise output, from crystals, 810
    - standard, 640
  - Noise resistance, equivalent, 945
  - Noise temperature, 805
  - Noise-temperature factor, 802
  - Noise voltage, thermal, 637
  - Nomograms, insertion-loss, 661, 662, 685
  - Notched coaxial lines, 591

## O

Octapole, 221  
 Orifice coupling, 782  
 Oscillator, concentric-cavity, 359  
 Oscillators, amplitude-modulated, 391-408  
   band width of, 406  
   limitations in, 391  
   cathode modulation of, 402  
   chokes for, 394  
   Class B modulators for, 399  
   coupling in, 397  
   frequency modulation, incidental, of, 396  
   grid modulation of, 401  
   incidental, 404  
   inphase, 406, 408  
   loaded  $Q$  of, 392  
   percentage of modulation of, 406  
   plate and grid modulation of, 403, 405, 406  
   plate impedance of, 393  
   plate modulation of, nonlinearity of, 395  
    $Q$  of, 393  
   transformers, video, for, 399, 400  
   voltage and power relations in, 395  
 coaxial (*see* Coaxial oscillators)  
 coaxial-cavity, 826  
 frequency-modulated, 408-425  
   amplitude modulation, parasitic of, 409, 417  
   common-grid reactance-tube circuit for, 408, 415  
   analysis of, 411  
   phase-splitting network for, 410  
   reactance tubes for, 409  
   Class C operation of, 418, 419  
   modulation of, 422  
   parasitic oscillations in, 415  
   phase relations in, 419  
   plate dissipation in, 419  
   power loss in, 409, 414  
   power relations in, 418  
   simulated impedance of, 411  
   at ultrahigh frequencies, 415  
 "heterotone," 634  
 local (*see* Local oscillators)  
 magnetron, 474  
 reflex-klystron (*see* Reflex-klystron oscillators)

Oscillators, sweep, u-h-f, 1029  
   test, 1009, 1010  
   triode and pentode (*see* Triode and pentode oscillators)  
   triode and tetrode (*see* Triode and tetrode oscillators)  
 Oscilloscopic measurement, of pulse length, 997  
   of p-r-f, 1004  
 Oscilloscopic techniques, 861, 868  
 Output circuits, receiver (*see* Receiver output circuits)  
 Output coupling, to antenna or load, 376  
   of butterfly oscillators, 839  
   of resonatron, 464, 465  
 Output indicators, 583, 606, 607  
 Output transformers for triode and pentode oscillators, 330

## P

Panoramic presentation by receivers, 984-992  
   amplifiers, video and deflection, for, 992  
   with double superheterodyne, 988  
   with i-f amplifier, sweeping, 985  
   marker signals for, 992  
   sliding contacts, effect of, on, 984  
   spurious responses, detection of, by, 987  
 Panoramoscope, 634  
 Paper tape, 994  
   Teledeltos, 994  
 Paraboloid reflectors, primary antenna for, 253  
   effective aperture of, 163  
   for spinners, 223, 253, 260  
 Parallel-line oscillators, 323-332  
   back-lines of, 326  
   characteristic impedance, variable, of, 327  
   with coiled lines, 328  
   design and construction of, 332  
   with helical lines, 330  
   loading of plate and grid lines in, 327  
   shielding of, 332  
   with spiral lines, 328  
   tubes, double-lead, for, 326  
 Parallel networks, 72  
   compensation with, 77  
 Parallel-wire resonator, 556



- Parasitic amplitude modulation, 409, 417
- Parasitic oscillations, in reactance-tube, 415  
 in resonator, 461
- Parasitic resonances, 825, 865, 869  
 in butterfly resonators, 825  
 circumferential, 909-911  
 in coaxial resonators, 909, 911, 915  
 in local oscillators, 825  
 in plungers, 936  
 in reflex-klystron oscillators, 861, 865, 869  
*TE*, 911  
*TM*, 915
- Partition effect, 945
- Pass-band loss, in butterfly resonators, 759  
 in filters, 665, 670
- Pattern measurement of antennas, 46, 48, 52, 297
- Patterns (*see* Radiation patterns)
- Peak voltmeter, 1004
- Pentode oscillators (*see* Triode and pentode oscillators)
- Performance, of baluns, 91  
 of homing systems, 310  
 of magnetrons, 509  
 of mixers, 805  
 of receivers, 635
- Performance chart of magnetron, 503
- Performance curves, of split-anode magnetrons, 559-561, 565
- Phase constant of filters, 694
- Phase distribution in apertures, 164
- Phase front, 204  
 effect of reflections on, 205-208
- Phase-reversing anode for donutron, 550
- Phase-shift constant, 44
- Phase-splitting network, 422
- Phase unbalance, 92
- Phasing section of horn, 154
- Photometers, 579, 580
- Piston attenuators, 1016
- Plate and grid modulation, 403-406
- Plated couples, 576
- Plunger-loop relations, 917
- Plungers for short-circuiting, 363  
 equivalent length of, 895  
 finger, 920  
 flexible-finger, 363  
 noncontacting, 886, 920-939  
 bucket, 928
- Plungers for short-circuiting, noncontacting capacitance, 925  
 choke, 927  
 gap parameter of, 926  
 input resistance of, 921  
 losses in, 929, 932-935  
 parasitic resonances in, 936  
 reactance of, 895, 903, 920, 930  
*S* and *Z*, 928  
 resonant-choke, 363
- Polarization, and cross field, 200, 208  
 effects of, on homing, 297  
 elliptical and circular, 199  
 plane, 199  
 space or ellipsoidal, 201  
 rotating-plane, 200
- Polarization-discrimination ratio of antennas, 233
- Polarization measurements, 157
- Polarization pattern of elliptically polarized wave, 158
- Polystyrene, 713
- Power, determination of, 574  
 maximum attained, 662  
 maximum available, 643  
 required, 311
- Power gain of antennas, 24, 228, 271
- Power generation, 311-315  
 military requirements for, 311-313  
 progress in, 314  
 tube program for, 311
- Power loss, in plungers, 929, 932-935  
 in reactance tubes, 409, 414  
 in tuners, 744
- Power measurement, 1023-1026
- Power-measuring devices, u-h-f, 569-626  
 bolometer bridges as, 593  
 calorimeters as, 582, 590, 591  
 coaxial lines as, 583-585  
 notched, 592  
 slotted, 591  
 coaxial section, tapered, as, 577  
 coupling loop as, 599  
 directional couplers as, 594, 595, 599, 600  
 disk resistor with voltmeter as, 577  
 dummy loads for, 33, 570-574, 581, 588  
 effect of impedance mismatch in, 570  
 load lamps as, 579, 580

- Power-measuring devices,  $\mu$ -h-f, output indicators as, 583, 606, 607  
 photometers as, 579, 580  
 for resonant systems, 610-626  
 ridge waveguide as, 573  
   tapered, 598  
 spectrum analyzers as, 594, 608, 609  
 stub, quarter-wave, as, 574  
 thermistor as, 593  
 thermocouples as, 574-576, 586, 604  
 thermopiles, differential, as, 584  
 wattmeters as, 574, 578, 581-584, 588, 602
- Power output, of split-anode magnetrons, 559, 568
- Power-output coupling methods, (*see* Coupling)
- Power stability, of reflex oscillator, 854
- Power-supply regulation of reflex oscillators, 871
- Preselection, r-f, in superheterodynes, 632
- Primary radiators, for horns, 161, 163  
 for paraboloidal reflectors, 161, 162
- Probe coupling, 385, 386, 916
- Probe-fed slots, 172
- Probe and loop coupling, 387, 919
- Probe voltmeter, 38
- Probes, calibration of, 31  
 detector, 30-32  
 with receiver, 31
- Propagation, of u-h-f waves, 202
- Pulling (*see* Frequency pulling)
- Pulling figure of magnetron, 514
- Pulse amplitude, 997
- Pulse analysis, 996  
 with direction finders, 280
- Pulse length, 997  
 meter indication of, 1000  
 oscilloscopic measurement of, 997
- Pulse modulation, of lighthouse tubes, 1013  
 of reflex klystrons, 1013  
 of signal generators, 1011
- Pulse-repetition frequency, 628, 997  
 meter indication of, 1006  
 oscilloscopic measurement of, 1004
- Pulse signals, characteristics of, 628
- Pulse stretchers, 281, 282, 981, 982, 993, 994, 1002
- Pulse width, 997  
 (*See also* Pulse length)
- Pulsed magnetrons, 473
- Pulsing, cathode, 1014  
 reflector, 1014  
 of split-anode magnetrons, 567
- Pushing (*see* Frequency pushing)
- Q
- Q, of anode cavity, 460  
 of butterfly resonators, 751, 759  
 of coaxial circuits, 346  
 determination of by cold tests, 611  
 of distributed-constant resonant circuit, 744  
 loaded, of magnetrons, 534  
   of u-h-f oscillators, 392  
 of magnetrons, 487  
 of modulated oscillators, 393  
 of multicavity magnetrons, 487
- R
- R-f relay, 246, 257
- R-X diagram, 53
- Radar-intercept receivers (*see* Receivers)
- Radar signals, variations in, 283
- Radiation patterns, 15  
 of Adcock, 222  
 of apertures, 17, 22  
 of biconical antenna, 108  
 of conductors and apertures, 22  
 of cone antennas, 101  
 of corner spinner, 250  
 of crossed dipoles, 301  
 of cylinders, 21  
 of double-dipole wing, 302  
 of elpar antenna, 164, 170  
 of homing antennas, 297, 301, 302  
 of horns, 108, 142, 148, 152  
 of linear dipoles, 113  
 for series of 90-deg V antennas, 115  
 of sleeve dipole, 123, 129  
   with reflector, 130, 131  
 of slot antennas, 172-180  
 of spinners, 255  
 of "split-can" antennas, 191  
 of thin antennas, 19  
 of triple stub, 301  
 of wing dipole, 300
- Reactance of plungers, 895, 903, 920, 930
- Reactance theorem, Foster's, 892
- Reactance tubes, 409  
 modulation of, 422

- Reactance tubes, plate dissipation in, 419  
 power loss in, 409, 414  
 (See also Oscillators, f-m)
- Rear-cavity loss, 926, 928
- Receiver measuring equipment, 1008-1031  
 attenuation pads as, 1018  
 frequency meters, heterodyne, as, 1008  
 modulators as, 1010-1015  
 oscillators, test, as, 1009, 1010  
 piston attenuators as, 1016  
 pulse-modulated oscillators as, 1013  
 signal generators as, 1008  
 output calibration of, 1020-1023  
 output systems for, 1015, 1027  
 shielding of, 1026  
 sweep oscillators as, 1008, 1029
- Receiver output circuits, 977-1007  
 differentiator, selective, for, 1001  
 Eccles-Jordan trigger circuit for, 1000  
 i-f amplifier used in, 991  
 for meter indication of prf, 1006  
 of pulse length, 1000  
 for oscilloscopic measurement, of prf, 1004  
 of pulse length, 997  
 for panoramic presentation, 984-992  
 for pulse analysis, 996  
 pulse stretchers for, 981, 982, 993, 994, 1002  
 for recording, 994-996  
 video amplifiers for, 977-981, 992  
 video output-coupling circuits as, 980
- Receivers, 627-647  
 allowable distortion in, 647  
 carrier frequency of, 628  
 direct-detection, 628, 796  
 for pulsed signals, 630  
 sensitivity of, 819  
 tuners for, 741  
 fidelity of, 635, 646  
 gain requirement, minimum, of, 640  
 gain setting, standard, of, 642  
 noise-band width of, 640  
 noise figure of, 637  
 noise output, standard, of, 640  
 output, maximum, of, 635, 647  
 standard, 641  
 performance of, 635  
 power maximum available, of, 643  
 preselection in, 632
- Receivers, radar-intercept, 796  
 figure of merit of, 820  
 intermediate frequency for, 797  
 noise figure of, 802  
 second-detector stage in, 797  
 second-detectors for, 822  
 sensitivity of, 796  
 radar reception by, 627  
 selectivity of, 635, 645  
 sensitivity of, 635, 636  
 voltage vs. power, 642  
 signal amplification of, 641  
 as spectrum analyzers, 609  
 superheterodyne, 631  
 airborne, 633  
 spurious responses in, 631, 645, 646  
 type of signal received by, 627  
 for u-h-f measurements, 48  
 video-output requirements for, 977  
 of wide tuning range, 627
- Recording circuits, 994-996  
 paper tape for, 994  
 stylus, lawn-mower type, for, 996
- Rectifiers, crystal (see Crystal rectifiers)
- Reflection coefficient, 54, 97  
 maximum permissible, 81  
 of TEM wave on cones, 104
- Reflections, effect of, 204  
 on antenna patterns, 210  
 on phase front, 205-208
- Reflector assemblies, 145, 162
- Reflector pulsing, 1014
- Reflectors, 138, 161  
 corner, 129, 223, 245  
 elpar (elliptical-paraboloid), 164  
 with horn, 170  
 line focus of, 168  
 patterns for, 170  
 narrow grid, 130  
 paraboloid, effective aperture of, 163  
 focal length of, 162  
 primary radiator for, 162  
 design of, 163  
 phase distribution in aperture of, 164  
 shape of, 165
- Reflex-klystron oscillators, 849-877, 879, 901  
 beam-coupling coefficient,  $\beta$ , of, 856  
 cavity modes, preferred, in, 901  
 coefficient of coupling,  $k$ , in, 865  
 condition for oscillation in, 849

- Reflex-klystron oscillators, electron**  
   bunching in, 864  
   electronic admittance of, 850-854, 857, 859  
   electronic conductance in, 869  
   electronic hysteresis in, 861-863  
   electronic tuning of, 859, 861  
   frequency modulation of, 859  
   frequency stability of, 870  
   harmonic-frequency generation in, 864  
   intermodulation in, 864  
   mode interference in, 861, 900, 903  
   multiple transits in, 862  
   oscilloscopic techniques for, 861, 868  
   parasitic resonances in, 861, 865, 869  
   power, maximum, of, 856  
   power stability of, 854  
   power-supply regulation in, 871  
   power-supply requirements of, 870  
   repeller characteristics of, 855, 862  
   repeller current in, 853  
   repeller ranges, preferred, in, 901  
   repeller-voltage tracking of, 860, 872-876  
   resonator admittance of, 857  
   ripple factor in, 871  
   stability, dynamic, of, 868  
   structure of, 850  
   transit-time theory, simple, of, 851  
   tube losses in, 856  
   tuning characteristics of, 897  
   tuning curves of, 906  
**Reflex klystrons, low-impedance, 900**  
   pulse modulation of, 1014  
**Regeneration, 973**  
**Relay-current separator, 257**  
**Resistance of crystals, 799, 817**  
**Resistor star, 571**  
**Resnatron, 312, 445-472**  
   anode cavity of, 445, 450  
     *Q* of, 460  
   anode structures of, 455  
   back-heating in, 462  
   cathode cavity of, 445, 447  
   as Class C oscillator, 445  
   electric-field configuration in, 454  
   electrode design of, 452  
   equivalent circuit of, 459  
   feedback in, 463  
   focusing action in, 453  
   grid-screen  $\mu$ -factor of, 455  
   interaction time in, 462  
**Resnatron, load impedance, optimum, of, 466**  
   modulation of, 467, 469  
   operating data for, 467  
   output coupling of, 464, 465  
   parasitic oscillations in, 461  
   shunt impedance for, 460  
   static characteristics of, 457  
   structural features of, 446  
   transit-time effects in, 461  
   transmitters, 470  
     transmission line for, 466  
   video amplifiers for, 468  
**Resonances of cone antenna, 100, 101**  
   parasitic, 825  
**Resonant circuit, distributed-constant, 744**  
**Resonant frequency of tube, natural, 837**  
**Resonant-line filters, 685, 702**  
**Resonant systems, analysis of, 610-626**  
   calculation of parameters of, 617-626  
   cold tests of, 611  
   constants and parameters of, 611  
   equivalent circuits of, 612  
   *Q* of, determination by cold tests, 611  
   standing-wave diagram for, 615  
**Response curves, for coupled circuits, 746-748**  
   of tuners, 743  
**Response ratio of d-f antennas, 234**  
**Ridge waveguide, 573, 678-684, 723, 726**  
   applications for, 684  
   attenuation in, 682  
   characteristic impedance of, 679  
   as circuit element, 678  
   cutoff frequencies in, 679, 681  
   design curves for, 678  
   design equations for, 681  
   as filter element, 736  
   junctions for, 723-725  
   tapered, 598  
   wavelength of, 675  
**Rieke diagram, 511**  
**Ripple factor of reflex oscillators, 871**  
**Rotary-tuned coaxial cavity, 791**  
**Rotating-plane polarization, 200**  
**Rotation speed, of antennas, 267**
- S**
- S and Z plungers, 928**  
**Salt-water loads, 588**  
**Scaling of magnetrons, 491**

- Scanning capacitor, 216, 278
- Second detectors, 797, 822
- Secondary emission, loading due to, 443
- Sector sweep, 238
- Sectoral horn, 142
- Selectivity, adjacent channel, 645
  - of butterfly resonators, 759
  - of i-f amplifiers, 942
  - of receivers, 635, 645
- Self-reactance of untuned loops, 378
- Semibutterfly, 752
- Sensitivity of receivers, 635, 636
  - voltage vs. power, 642
- Series decoupling, 974
- Shielding of parallel-line oscillators, 332
- Short-circuiting joints, 777-780
- Short-line filters, 686, 692, 701
- Shot effect, 945, 948
- Shotgun oscillator, 375
- Signal amplification of receiver, 641
- Signal generators, 1008
- Signal sources for pattern measurements, 48
- Sleeve antennas, 7, 119-137
  - crossed-element, phased, 131
  - broad-band, 133, 136
  - turnstile, 131
  - cylindrical, input impedance characteristics of, 121, 122
  - dipole, 120, 126
    - bent, 128
    - with corner reflector, 129
    - with narrow-grid reflector, 130
  - patterns of, 123, 129-131
  - end-fed, 119
  - with paraboloidal reflector, 162
  - stub, 120, 121
    - input impedance of, 125
- Slip rings, for spinners, 256
- Sloping-guide water load, 571
- Slot antennas, 10, 171-191
  - as apertures, 171
  - coaxial-line-fed, 171
  - compensated, 187, 188
  - examples of, 188
  - impedance characteristics of, 180-187
  - loaded, 189
  - patterns of, 172-180
    - effect of ground plane on, 174
    - effect of width of slot on, 177
    - of "split-can" antenna, 191
    - of waveguide-fed slot, 176, 179
- Slot antennas, probe-fed, 172
  - reducing size of, 187
  - split-can, 191
  - T-fed, 188
  - waveguide-fed, 171
- Slot magnetrons, 476, 482
- Slotted coaxial lines, 591
- Slotted waveguide sections, 39
- Smith chart, 26-29
  - use of, 37, 59, 68, 511
- Spectrum analyzers, 594, 608, 609
  - i-f amplifier, low frequency, for, 991
- Spinner patterns, 255
- Spinners, 236-264
- Spiral-line oscillator, 328
- Split-anode magnetrons (*see* Magnetrons, split-anode)
- Split-block filters, 715
- Spurious pass bands in tuners, 741
- Spurious responses, in butterfly resonators, 763
  - in coaxial cavities, 780
  - detection of, 987
  - in filters, 702, 734
  - harmonic, 646
  - in superheterodyne, 631, 812
  - i-f break-through, 646
  - image, 645
- Stability, of butterfly oscillator, 837
  - frequency, 857
  - voltage, 857
- Stabilization, of split-anode magnetrons, 561
- Stagger-tuned amplifier, 965
  - advantages of, 972
  - design of, 967
- Stagger tuning, 965
  - advantages of, 972
- Staggered pair, 966
- Staggered triple, 967, 970
- Standard signal generators, 1008
- Standing-wave diagram, 615
- Standing-wave ratio, effect of, 377
  - line-loss correction for, 673
- Standing-wave-ratio circles, 54, 58
- Standing-wave-ratio measurements, 44
- Standing waves in resonator, 879
- Static characteristics of resonator, 457
- Strapping in magnetrons, 485
- Stub antenna, 93, 120, 121, 123
  - quarter-wave, 574
  - tunable, 1026

- Stylus, lawn-mower type, 996  
 Superheterodyne, double, 984-992  
 Superheterodyne receiver, 49, 631, 741  
   airborne, 633  
   double-conversion, 986  
   essential components of, 632  
   harmonic mixing in, 812  
   intermediate frequency, optimum, for, 810  
   signal-to-noise ratio of, 811  
   spurious responses in, 631, 645, 646, 812  
   tuners for, 741  
 Sweep oscillators, 1008, 1029  
 Switches, 192-198  
   coaxial, 194  
     actuator for, 195  
   crossover, 195  
   flat-bladed, 196  
   microwave, 192  
   waveguide, 197  
     actuator for, 198
- T
- Tapered horn, 42  
 Tapered-ridge junction, 725  
 Tapered-ridge waveguide, 598  
 Tapered section for thermistors, 1025  
 $TE_{1,1}$  field distribution, 882  
 $TE_{1,1}$  fields in coaxial resonator, 912  
 $TE$  modes, in coaxial resonators, 879, 881  
   guide wavelength for, 882  
 $TE$  waves, 879  
 Teflon, 713  
 Teledeltos paper, 994  
 $TEM$  mode, 879, 880  
   interference in, 900  
     elimination of, 903  
 $TEM$ -mode suppressor, 904, 911  
   analysis of, 904  
 $TEM$  waves, 879  
   on cone antennas, 95, 104  
 Test antennas, 50  
 Test equipment for receivers, 1008  
 Test methods for h-f filters, 728, 736  
 Test oscillators, 1009  
 Testing techniques for d-f antennas, 268  
 Tetrode, beam (*see* Resnatron)  
 Theory of coupled circuits, 742-748  
 Thermal noise voltage, 637  
 Thermistors, 593, 1023-1026  
 Thermocouples, 574-576, 586, 604  
 Thermopiles, differential, 584  
 Threshold voltage of magnetrons, 504  
 Titanium dioxide, 304, 307, 586, 713  
 $TM$  mode, dominant, 884  
 $TM$  modes in coaxial resonators, 879, 884  
 $TM$  parasitic resonances, 915  
 $TM$  waves, 879  
   on cone antennas, 95  
 Tracking, mechanical, of butterfly oscillators, 847  
 Tracking systems, repeller-voltage, 872-877  
   capacitance-divider, 876  
   nonlinear-gear, 872  
   tapered-voltage-divider, 874  
   tapped-voltage-divider, 873  
   tube-characteristic, 874  
   variable-transformer, 875  
     multiple-range tracking with, 876  
 Transformer, balun (balanced-unbalanced) 330-332, 382  
   (*See also* Baluns)  
   coaxial-line-to-guide, 141  
   line, 58, 60, 63  
   video, 400  
   waveguide, 141  
 Transformers, design of, 400  
 Transforming end sections, in filters, 666  
 Transforming junction, 721, 725  
 Transit angle, 437  
   of Class II oscillator, 319  
 Transit time, 437, 440, 853  
 Transit-time effects, in diodes, 817  
   in resonators, 461  
 Transit-time loading, 951  
 Transit-time parameter, 852  
 Transit-time theory of reflex oscillators, 851, 856  
 Transmission line, biconical, characteristic impedance of, 96  
 Transmission-line filters (*see* Filters)  
 Transmission-line measurements, 26  
 Transmission-line relations, 650  
 Transmission-line waves, 879  
 Transmitters, resnatron, 470  
   transmission line for, 466  
 Transmitting equipment, types and requirements of, 313  
 Triode oscillators, circuits of, 830  
 Triode and pentode oscillators, 316-336  
   analysis of, 318-321  
   cathode chokes, use of, in, 334

- Triode and pentode oscillators, Classes I and II, 318, 319  
 common electrode of, 322  
 coupling for, balun, 325, 329-332  
 loop, 325, 327, 328  
 holes in frequency spectrum of, 316  
 with inductive coupling, 320  
 lead inductance, effect of, in, 316, 320, 321  
 output transformers for, 330  
 parallel-line (*see* Parallel-line oscillators)  
 tubes and circuits for, 322
- Triode and tetrode oscillators, 426-444  
 back-heating in, 443  
 Class C, 433-435  
 band width of, 435  
 electronic efficiency of, 434-435  
 frequency stability of, 435  
 conditions for oscillation of, 427  
 design of, 426  
 efficiency of, 433-440  
 effect of transit time on, 440-443  
 electron flow in, 437  
 equivalent circuit of, 426  
 frequency pushing in, 428  
 grounded-grid, electronic efficiency of, 436-440  
 loading due to secondary emission in, 443  
 mode selection in, 431  
 trend in u-h-f operating conditions of, 444
- Triple-stub antenna, 301
- Trouble shooting in coaxial oscillators, 371
- Tubes, for butterfly oscillators, 840  
 cathode ray, 283, 984  
 for coaxial circuits, 337  
 doorknob, 841  
 double-lead, 326  
 for i-f amplifiers, 948  
 input admittance of, 948  
 input capacitance of, 949, 952  
 miniature, 841  
 reactance, u-h-f, 415  
 resonant frequency of, 837
- Tunable stub and line stretcher, 1026
- Tuners for microwave receivers, 741-795  
 butterflies as, 757  
 coupling methods for, 760  
 (*See also* Butterfly resonators)
- Tuners for microwave receivers, coaxial-cavity, 769-787  
 coupling between cavities in, 781  
 aperture, iris, orifice, or waveguide, 782  
 coupling problems in, 773  
 loop coupling in, 772  
 movable-slug, 794  
 rotary-tuned, 791  
 short-circuiting joints for, 777-780  
 single-cavity, 782  
 spurious responses in, 780  
 three-cavity, 785  
 two-cavity, 783  
 coupled-circuit, theory of, 742-749  
 coupling-loop construction for, 776  
 for direct-detection receivers, 741  
 image frequency in, 741  
 losses in, 744  
 mismatch in, 744  
 response curves for, 743  
 spurious pass bands in, 741  
 for superheterodyne, 741  
 waveguide cavity, 787-791  
 loaded, 790  
 rotary-tuned, 792
- Tuning, of coaxial oscillators, 357  
 electronic, of reflex oscillator, 859  
 multiple-mode, 343
- Tuning characteristics, of coaxial resonators, 892, 897  
 effect of cavity dimensions on, 893  
 effect of plunger reactance on, 895  
 of reflex-klystron oscillators, 892, 897
- Tuning curves, for coaxial resonator, 891  
 physical realizability of, 892  
 for *TEM* and *TE* waves, 913
- Tuning devices for measurements, 35
- Tuning noise, 824
- Tuning range, coaxial-circuit, 349  
 of coaxial line, 361
- Tuning screw, 42
- Tuning sections, coaxial, 41  
 waveguide, 41
- Tuning stubs, coaxial, 42
- Turnstile antenna, 131, 237

## V

- Vacuum tubes (*see* Tubes)
- Vane magnetron, 476, 482
- Vertical-horizontal antennas, 234

- Vertically polarized antenna, 209
- Video amplifiers for receivers, 468, 977-981, 992  
 band width of, 977  
 capacitance compensation in, 978  
 cathode-coupled, 981  
 gain control in, 978, 979  
 measurement problems of, 980  
 phase and amplitude response of, 992  
 phase distortion in, 978
- Video-frequency transformer, 400
- Video output, 977
- Video output-coupling circuits, 980
- Video-transformer coupling, 399
- Voltmeter, crystal, r-f, 822  
 disk resistor, 578  
 peak, 1004  
 probe, 38
- W
- Wattmeter, broad-band monitoring-type, for waveguides, 602  
 calorimeter, 581  
 coaxial-line thermocouple, 574  
 coaxial-line water calorimeter, 584  
 disk-resistor voltmeter, 578  
 gas-filled load-lamp, 581  
 lossy-coaxial-cable calorimeter, 583  
 salt-water calorimeter, 588
- Wave front, 204
- Wave types, basic, 879
- Waveguide, attenuation in, 677  
 below cutoff, 677
- Waveguide, characteristic impedance of, 44, 674  
 as circuit element in filters, 674  
 discontinuities in, 676  
 impedance function for, 674  
 ridge (*see* Ridge waveguide)  
 slotted, 39  
 with tapered ridge, 598  
 wavelength of, 675
- Waveguide cavity, loaded, 790  
 rectangular, 787  
 rotary-tuned, 792
- Waveguide-to-coaxial-line junctions, 717, 721, 723-725  
 testing of, 728
- Waveguide coupling, 782
- Waveguide filters, 674, 677, 728, 731, 736
- Waveguide irises, 676
- Waveguide load, all-metal, 572
- Waveguide measurements, 40, 44-46
- Waveguide mixers, 809
- Waveguide output, 496
- Waveguide switch, 197  
 actuator for, 198
- Waveguide transformer, 141
- Wavemeters as spectrum analyzers, 608
- Waves, principal, 879
- Waves, *TE*, 879
- Waves, *TEM*, 95, 879
- Waves, *TM*, 95, 879
- Waves, transmission-line, 879
- Waves, u-h-f, propagation of, 202
- Wing dipole antenna, 299
- Wollaston wire, 1023









